A Dissertation

by

Michaël BROUTIN

Submitted to the Ecole Nationale des Ponts et Chaussées
in partial fulfillment of the requirements for the Degree of

DOCTOR OF PHILOSOPHY

Major subject: Structures and Materials

Assessment of flexible airfield pavements using Heavy Weight Deflectometers

Development of a FEM dynamical time-domain analysis for the backcalculation of structural properties

Defended on June 11th, 2010 at the LCPC Paris
before a jury composed of:

Committee members:	H. DI BENEDETTO (reviewer)
	F. PFEIFFER (reviewer)
	P. ARGOUL
	D.BRILL
	P. LERAT
	J.M. PIAU
	J.F. SEMBLAT
Supervisor :	M. FREMOND

THESE

présentée pour l'obtention du diplôme de
Docteur de l'Ecole Nationale des Ponts et Chaussées

Spécialité : structures et matériaux

par

Michaël BROUTIN

Evaluation des chaussées souples aéroportuaires à l'aide du déflectomètre à masse tombante (HWD)

Développement d'une méthode d'analyse dynamique temporelle par éléments finis pour le calcul inverse des propriétés structurelles

Soutenue le 11 juin 2010 au LCPC Paris
devant un jury composé de :

Rapporteurs : H. DI BENEDETTO
F. PFEIFFER

Examinateurs : P. ARGOUL
D.BRILL
P. LERAT
J.M. PIAU
J.F. SEMBLAT

Directeur de thèse : M. FREMOND

Acknowledgements

First, I would like to express my gratitude to Prof. Michel Frémond for having accepted to be my supervisor, and to the STAC management for having authorized this work.

I also would like to extend my deepest thanks to Prof. Hervé Di Benedetto, Prof. Friedrich Pfeiffer, Dr. Pierre Argoul, Dr. David Brill, Dr. Patrick Lerat, Dr. Jean-Michel Piau and Prof. Jean-François Semblat for their participation in this dissertation committee. I especially want to thank again Prof. Hervé Di Benedetto and Prof. Friedrich Pfeiffer for having accepted to review the document.

Then I would like to thank all the people who have helped and inspired me during this doctoral study. I cannot enumerate all of them here. Amongst these people, I would like to warmly thank my friends and colleagues Cécile Caron, Jean-Claude Deffieux, Vincent Souque, Régis Bost (STAC), Dominique Guédon (LRPCT), Jean-Michel Simonin, Jean-Michel Piau and Jean-Maurice Balay (LCPC):

Thank you Cécile for our numerous collaborations, your infectious enthusiasm and unfailing good-humour for which you only know the secret. Thank you for having supported and encouraged me in crucial moments. And finally thank you for having worked on the English language of the memoir.

Thank you Jean-Claude for your everyday help, your outspokenness, and for the original experiments we launched together, and for everything you have taught to me since my arrival at the STAC, in all scientific domains.

You both will leave the STAC by the end of the year. I will miss our scientific lively debates, as well as all the numerous good moments spent together.

Thank you Vince for your valuable operational help, for never having hesitated to wake up at 4 a.m. each time I had the good idea to launch experiments.

Thank you Regis for having been present each time I encountered difficulties, whatever it dealt with (the programming, the memoir making up, …). This work would not have been finished on time without your valuable help. Especially thanks for having stood me at my worst moments and for having succeeded in motivating me each time it was necessary, especially in the last weeks.

Thank you Domi for the good moments spent during the construction of the STAC's test facility, and for everything you did on the project. Unfortunately, even though initially planned for that purpose, the instrumentation has not been tested in the frame of the thesis due to cumulative delays induced by construction unconformities. However, this test facility will be the main tool for further improvements of the method developed.

Thank you Jean-Michel (Simonin) for your advices, especially at thesis early times, and for the overview about pavement testing you provided me.

Thank you Jean-Michel (Piau) for the scientific discussions we have had, your valuable help about several points, and for the time you dedicated to me in the last weeks, to debate about the sticking points of the work.

Last but not least, thank you Jean for everything you did for me during the whole thesis period, for having lavishly found time to help me, whatever the hour of the day or even the day of the week, for the numerous receptions you priviledged me in Nantes. Thank you for all fundamental questions you raised (some of them having resulted in perpetual debates still unsolved…), for having allowed me taking some stand back when necessary, and having clarified this work with your valuable advices.

Finally I would like not to forget the colleagues which did not directly work with me, but whose friendship and good-humour indirectly contribute to the work accomplishment. Once more I cannot quote everyone. Thank you to you Anne-Marie, France, Aude, Alain, Jean-Yves without forgetting the old STACiens Cédric, Arnaud and Robert.

Executive summary

The Heavy Weight Deflectometer (HWD) is viewed worldwide as the most appropriate device to assess the bearing capacity of airport pavements. Its principle consists in applying a transient impulsive load simulating the weight effect of an aircraft rolling wheel, onto a stationary load plate placed over the pavement, through a buffer system, and studying the vertical displacements of the pavement surface (deflections) induced by this dynamic loading. The latter are continuously measured during the test by means of geophones placed under the plate and at predetermined locations at the pavement surface. These deflection measurements are used to determine the structural properties of the pavement layers (and optionally other parameters like layer thicknesses but these studies are marginal), by means of a so-called "backcalculation" numerical procedure which consists in 1- choosing a mechanical model for the pavement and 2-identifying the parameters of the model for which theoretical computed deflections fit the experimental data set. Then, forward calculations can be performed to estimate the bearing capacity or the remaining life of the studied structure.

This thesis deals with the assessment of flexible pavement. Geophones are in this case placed beneath the load plate and radially.

Usual processing methods are based on static multilayered elastic models. The only structural properties to be backcalculated are the stiffnesses (Young's moduli) of the different layers. The backcalculations are performed from the pseudo-static deflection bowls. These bowls are reconstituted from the deflection peak values measured by each geophone. As emphasized by several authors, these methods have shown limitations. Actually they use only a few part of available information (peak values), and the static modelling is far from the reality of the test.

The objective of the thesis is to develop an advanced method for the assessment of flexible pavements using HWD tests data. The aim is to achieve a better representation of the observed physical phenomena during dynamic loading and to consider whole available information. Computation of time-related deflections is proposed, relying on a dynamical modelling of applied dynamic loading, and ensuing pavement response.

The main body of the document presents three parts.

The first part describes preliminary studies.

First, the reliability of HWD data for dynamical analysis has been studied, based on the adjunction of external instrumentation to the HWD sensor system, and on crossed tests with other HWD on known test facilities. Then, an experimental repeatability study has been performed. Finally, good linearity of the deformations with applied loading has been demonstrated using experiments conducted on several pavements. Moreover, the occurrence of damping phenomena in the pavement has been emphasized according to gauge signals measured in an instrumented tested pavement. The crossed comparison between theory and practice has also allowed defining a precise experimental protocol for operational test campaigns.

The second part focuses on modelling. The mechanical model is presented first, which allows calculation of displacements and strains in the pavement for a given parameters data set. Then, the developed backcalculation procedure is described, based on this mechanical model. Finally a forward calculation procedure is proposed, which relies 1- on strain calculations using information derived from the backcalculation phase, and 2- on material performances.

A time-domain modelling has been developed. It relies on a 2D axisymmetric finite element dynamical model implemented in the Cesar-LCPC FEM software. According to the preliminary studies, a multilayered isotropic elastic model with damping has been chosen. Load plate modelling is included in the mesh. The model takes into account the applied dynamical load. Three alternative versions of the model have been studied, which differ by the applied dynamical load modelling. First model considers the time-related load imparted to the pavement surface through the plate. In the second model, rubber buffers and the falling mass are included in the mesh and velocity of the dropped mass at impact is imposed at their top. Third alternative version is based on the shock theory. Behaviour laws take into account inertia of materials and structural damping. In Cesar, the only available damping modelling is so far a Rayleigh damping, globally defined at the structure scale. Thus parameters of the model are layer thicknesses (including bedrock depth), material bulk densities and stiffnesses, and structural damping, for the first two alternative models. The third one includes additional parameters which describe the shock laws. The model allows a computation of the theoretical induced time-related surface deflections, for a given set of parameters. A careful study has been carried out to optimize the temporal and spatial discretizations according to the dynamic problem considered.

The backcalculation problem amounts to find a set of parameters resulting in a satisfactory fitting between theoretical and experimental deflection signals. Usual assumption that layers are fully bonded under heavy dynamic load is drawn. Moreover, bulk density ranges are generally quite precisely defined, and layer thicknesses are well-known thanks to ground penetrating radar investigations. In the thesis framework, bedrock depth is independently determined via an advanced existing method using the cut-off frequency of the pavement. The assumption is made that precisions on densities, layer thicknesses and bedrock depth are sufficient so that these parameters can be *a priori* set. Hence the only parameters to be backcalculated are the layer stiffnesses and the structural damping ratio. A thorough study has been performed 1- to investigate the relative influence of the different parameters on the deflection time-histories, 2- to discuss *a posteriori* the relevance of arbitrarily setting some of them, and 3- to establish a criterion to assess if the resulting set of backcalculated parameters is appropriate or not. This study phase relies on the choice of an objective function and a linked target error value. A numerical parametric sensitivity analysis has been performed combined with the results of the aforementioned repeatability tests. This study has allowed 1- proving that the uncertainties on imposed parameters has no significant impact on the backcalculated results, so that the *a priori* hypothesis made is reasonable, and 2- selecting consistent error values with regard to the uncertainties on experimental data and imposed parameters. According to this study, an automated convergence algorithm has been developed for numerical resolution of the backcalculation procedure. This work is based on previous studies led in the frame of several successive supervised training courses where several algorithms have been tested. The retained algorithm consists in a Gauss Newton algorithm including a regularization process. Letting n be the number of parameters to be backcalculated, $n+1$ direct calculations are needed at each algorithm epoch. Its convergence is highlighted on a simulated data set relative to a given pavement structure. It is also shown that robustness of the algorithm is better for dynamic calculations than in the pseudo-static case

which has also been considered. Such a result can be explained by the high overdetermination of the problem when the whole time-histories are considered instead of the peak values only. Conversely, the disadvantage of the dynamic method is that each FEM forward calculation is time consuming, especially in the absence of specific method for calculating the gradients of Gauss Newton algorithm.
A numerical tool has been developed which allows automating the finite elements mesh creation and both backcalculation and forward calculation phases: the so-called PREDIWARE (Pavement Rational Evaluation using Deflections Induced by Falling Weights, for Airfield and Road Engineers) software.

A forward calculation phase is proposed as an illustration of the possible practical use of the backcalculation results. It is performed using the same mechanical model as in the backcalculation phase, taking into account the previously backcalculated parameters. It allows determining the strains generated by a single wheel or a given aircraft landing gear at critical levels in the structure. Thanks to the knowledge of the mechanical material performances (laboratory tests being used to establish the allowable strains versus the number of coverages), and climatic data for temperature corrections, it is then possible to evaluate, amongst other parameters, the conventional bearing capacity of the pavement (in terms of single wheel or considering the whole landing gear assembly), or, for a given traffic mix, the remaining life of the pavement, and if necessary the thickness of a flexible overlay.

The third and last part is dedicated to experimental validation of the proposed numerical method. Several full-scale validations of both backcalculation method and strains determination have been conducted. They consist in test surveys run on 3 well-known pavements, one of them being instrumented. The validation relies on the comparison between backcalculated and laboratory-determined material properties, and on the comparison between theoretically expected strains and gauge measurements, when available.
The method to determine the bedrock depth has been tested on two test facilities, the first one lying over a shallow bedrock (3 m), and the second one over a 12 m deep substratum (theoretical infinite half-space). Results are satisfactory in both cases.
Dynamical backcalculations performed for all test surveys have shown that 1- Good fittings can be found, corresponding to low values of the objective function, with regard to repeatability and sensitivity studies conclusions. 2- However, errors obtained remain much higher than those reached on simulated data. This means that the model is not completely reliable for describing the physical test and can be improved.
Experiment performed on the instrumented pavement has shown a very satisfactory correlation of calculated strains with gage measurements. Nevertheless only one gage profile has been tested, so that this result needs to be confirmed by other experiments.
Comparison between backcalculated and laboratory-determined material properties has emphasized that 1- the dynamical backcalculation provides better results than the pseudo-static one for deep layer moduli determination. Backcalculated values in the dynamical method are close to expected values, 2- numerical moduli found for surface asphalt layers are significantly different from laboratory results, in both dynamic and pseudo-static methods, and 3- damping modelling is not good approximation of the reality. Actually, the contrast between unbound and asphalt materials imply a great difference between mean damping ratios of the different layers, as confirmed in the study by laboratory tests. Moreover, Rayleigh modelling is not representative of the real frequency-dependence of the asphalt materials.

To sum up, the thesis shows that the proposed time-domain dynamical method for HWD data analysis is promising. It especially allows assessing better the behaviour of deeper layers than the pseudo-static method. Robustness of the backcalculation procedure is also largely improved when considering the time-related deflections instead of the peak values only. Nevertheless some discrepancies between numerical and experimental results are observed. They can be due: 1- to an approximate modelling of the damping. The one considered is global Rayleigh damping 2- to a simplifying assumption for asphalt behaviour law. No viscoelastic behaviours are available so far in Cesar-LCPC code. The current modelling is limited to the input of a constant elastic modulus, independent of time, for these materials; and 3- to the quality of asphalt interfaces, which may not be fully bonded, by contrast to the model assumption, also adopted by the main existing calculation softwares. A backcalculation with fully unbonded layers has been performed as an illustration. This issue is to be deepened.

In the light of the thesis, the following improvements of the modelling could be envisaged: 1- implementation of advanced behaviour laws for asphalt materials taking into account a time-dependent modulus. LCPC advanced research, based on the use of the Huet and Sayegh model is in progress. Modelling allows determining the evolution of the secant elastic moduli according to the applied stress path; 2- improvement in the damping modelling, 3 – a better modelling of interfaces, if required. A more thorough examination of the issue of the influence of their bonding on HWD results will be performed to answer this question, and 4- reduction of execution times for the backcalculation phase. Development of a method relying on the self-adjoints theory is in progress, which would allow performing at each calculation step only *2* direct calculations instead of $n+1$.
Further validation phase of the mechanical model will rely on a full-scale validation performed on the STAC's instrumented test facility (located in Bonneuil-sur-Marne, near Paris, France). Test campaigns are expected in spring 2010.
An assessment of the method proposed for the determination of conventional pavement bearing capacity and/or remaining life is also required. In this purpose, a wide-scale study including a regular test survey of given trafficked airfield pavements is planned, coupled with visual inspections.

Keywords:
HWD testing / Dynamical backcalculation / Shock theory / Finite Elements Modeling / Sensitivity analysis / Young's moduli / Damping /Material performances / Pavement bearing capacity / Pavement instrumentation.

Résumé détaillé

Descendant du déflectomètre à boulet du Laboratoire Central des Ponts et Chaussées (LCPC), le Heavy Weight Deflectometer (HWD) est devenu aujourd'hui l'appareil le plus utilisé à l'international pour la détermination de la portance des chaussées aéronautiques. Il est composé d'une masse tombante qui engendre à la surface de la chaussée, par l'intermédiaire d'une plaque rigide et d'un système d'amortissement, un chargement de type impulsionnel, censé simuler le passage d'une roue d'avion. Les déflexions engendrées sont mesurées pendant la période de chargement, au moyen de géophones disposés sous et aux abords de la plaque.

L'analyse de ces déflexions permet de déterminer les propriétés structurelles des différentes couches de chaussée (voire aussi leurs épaisseurs) au moyen d'une procédure d'identification numérique appelée « calcul inverse » qui consiste à : 1 – choisir un modèle mécanique décrivant le comportement de la chaussée sous chargement, et 2 – identifier les paramètres du modèle conduisant au meilleur calage entre les jeux de données numériques et expérimentaux. Un calcul direct peut alors être réalisé, à partir du même modèle mécanique, et en tenant compte des paramètres identifiés, afin d'estimer la capacité portante de la chaussée et/ou sa durée de vie résiduelle.

La thèse s'intéresse à l'évaluation des chaussées souples. Les géophones de mesure sont dans ce cas placés au centre de la plaque de chargement, et radialement.

Les méthodes usuelles d'exploitation des données sont basées sur l'utilisation de modèles élastiques multicouches statiques. Les seuls paramètres structuraux à identifier sont les rigidités (modules d'Young) des différentes couches constitutives. Le calcul inverse est mené à partir de bassins de déflexion pseudo-statiques, reconstitués à partir des déflexions maximales mesurées sur chaque géophone. Les limites de cette méthode ont été soulignées par de nombreux auteurs. D'une part elles n'exploitent qu'une infime part de l'information disponible (valeurs de pic uniquement), et d'autre part elles reposent sur une modélisation statique très éloignée de la réalité de l'essai.

Ainsi, l'objectif de la thèse est de développer une méthode avancée d'évaluation des chaussées souples autorisant une meilleure représentation physique de l'essai et permettant d'exploiter l'ensemble de l'information disponible. Une modélisation dynamique permettant le calcul de l'évolution temporelle des déflexions au cours de l'essai est proposée.

Le corps du document présente trois parties.

La première décrit les études préliminaires.

Tout d'abord, la fiabilité des mesures du HWD en vue d'analyses dynamiques est étudiée, grâce à une analyse spécifique nécessitant la mise en place d'une instrumentation externe en parallèle de la chaîne d'acquisition du HWD, ainsi que grâce à des essais croisés avec d'autres HWD. Ensuite une étude expérimentale de répétabilité est menée. Enfin, la linéarité des déformations par rapport à la charge appliquée est démontrée sur plusieurs sections test, et la présence de phénomènes visqueux dans les matériaux bitumineux mise en évidence d'après la

réponse des capteurs d'une chaussée instrumentée. Parallèlement à ces études spécifiques, un protocole d'essais pour les campagnes de tests opérationnelles est élaboré.
La seconde partie est dédiée à la modélisation. Le modèle mécanique est d'abord présenté ; il permet le calcul des déplacements et des déformations relatives dans la chaussée, pour un jeu de paramètres donné. Dans un second temps, la procédure de calcul inverse développée sur la base de ce modèle est décrite. Enfin, une procédure d'analyse directe est proposée ; elle repose sur 1 – un calcul des déformations relatives critiques dans la chaussée utilisant les résultats de la phase de calcul inverse, et 2 – la connaissance des performances de matériaux.

Une modélisation dynamique dans le domaine temporel est d'abord développée. Elle utilise le code de calcul aux éléments finis CESAR-LCPC et repose sur un maillage 2D axisymétrique. Conformément aux résultats des études préliminaires décrites ci-dessus le modèle choisi est multicouche linéaire élastique avec amortissement. La plaque de chargement est intégrée au maillage. Le modèle tient compte de la nature dynamique de l'effort appliqué. Trois variantes du modèle sont étudiées, qui se distinguent par la modélisation de ce dernier. La première prend en compte l'évolution temporelle de l'effort appliqué, mesuré expérimentalement à l'aide du capteur d'effort intégré à la plaque de chargement. Dans la seconde variante, les tampons amortisseurs et la masse tombante sont inclus dans le maillage, et la sollicitation extérieure est la vitesse initiale imposée à cette dernière. La dernière variante fait appel à la théorie des chocs ; le maillage intègre les tampons. Les lois de comportement tiennent compte de l'inertie des matériaux et d'un amortissement structurel. Le seul amortissement actuellement disponible dans CESAR est un amortissement de Rayleigh, global pour l'ensemble de la structure étudiée. Les seuls paramètres du modèle sont donc, pour les deux premières variantes, les masses volumiques et épaisseurs des couches, leurs rigidités, et le taux d'amortissement. La troisième variante présente des paramètres supplémentaires qui sont ceux de la loi de choc. Le modèle permet de déterminer les évolutions temporelles des déflexions surfaciques résultantes, pour un jeu de paramètres donnés. Une étude minutieuse a permis d'optimiser les discrétisations spatiale et temporelle, pour le modèle dynamique considéré.

Le problème inverse revient alors à trouver un jeu de paramètres qui induise un calage satisfaisant des valeurs numériques sur les données expérimentales. L'hypothèse classique du parfait collage entre les couches sous chargement lourd est retenue. Par ailleurs, la gamme de variation des densités volumiques des matériaux constitutifs est bien connue, de même que les épaisseurs des couches, obtenues à l'aide de campagnes d'investigation au géoradar.

Dans le cadre de la thèse, la profondeur du substratum est déterminée à l'aide d'une méthode avancée, proposée dans la littérature, utilisant la fréquence de résonnance de la structure. L'hypothèse est faite que les précisions sur les densités, les épaisseurs des couches, et la profondeur de substratum sont suffisantes pour que ces paramètres puissent être fixés *a priori*. Les seuls paramètres à identifier sont donc les rigidités des couches et le taux d'amortissement. Une étude approfondie est menée pour 1 – établir l'influence relative des différents paramètres sur les évolutions temporelles des déflexions, 2 – discuter *a posteriori* de la légitimité d'imposer les paramètres précités, et 3 – établir un critère permettant d'évaluer la pertinence d'un jeu de paramètre. Cette étude repose sur le choix d'une fonction objective et d'une erreur cible. Les résultats de l'étude paramétrique sont couplés avec ceux de l'étude de répétabilité expérimentale décrite dans la partie 1. L'étude permet 1 – de démontrer que les incertitudes sur les paramètres imposés *a priori* ne compromettent pas la procédure d'identification, et 2 – de sélectionner une erreur cible cohérente avec les incertitudes tant expérimentales que sur les paramètres imposés. Un algorithme de convergence est développé en fonction de ces enseignements, permettant d'automatiser la résolution numérique de la

phase de calcul inverse. Différents algorithmes ont été testés dans le cadre de plusieurs stages. Il ressort que l'algorithme le mieux adapté au problème est un algorithme de Gauss Newton intégrant une technique de régularisation. Cet algorithme est donc adopté. Selon cette méthode, si *n* est le nombre de paramètres à identifier, *n+1* calculs directs sont requis à chaque étape de l'inversion. La convergence a été démontrée sur un jeu de données simulées correspondant à une structure test. La robustesse de l'algorithme est aussi étudiée. Elle est très bonne, meilleure que dans le cas de la méthode pseudo-statique. Une explication à ce phénomène peut être la grande surdétermination du système lorsque l'ensemble des signaux est considéré, plutôt que les valeurs de pic uniquement. En revanche, la grande faiblesse de la méthode dynamique dans le domaine temporel développée réside dans les temps de calculs très élevés, en particulier en l'absence de méthode spécifique pour calculer les gradients dans l'algorithme de Gauss Newton. Un outil numérique est par ailleurs développé, qui permet l'automatisation du maillage aux éléments finis, et des phases de calcul des deux étapes consécutives du processus : calcul inverse et calcul direct. Il s'agit du logiciel PREDIWARE (Pavement Rational Evaluation using Deflections Induced by Falling Weights, for Airfield and Road Engineers).

Une méthode d'analyse des résultats du calcul inverse est proposée à titre d'illustration. Elle repose sur un calcul direct utilisant le même modèle mécanique, et prenant en compte les paramètres identifiés. Ce calcul permet de déterminer les déformations relatives critiques dans la structure, engendrées par une roue simple isolée (RSI) ou des configurations complexes d'atterrisseurs. A partir de la connaissance des performances mécaniques des matériaux constitutifs (obtenues à l'aide d'essais en laboratoire qui permettent de relier la déformation relative admissible au nombre de cycles de chargements), et de données climatiques pour les corrections en température, il est possible d'évaluer, entre autres paramètres, la capacité portante de la chaussée (en termes de RSI ou bien en considérant les configurations réelles des atterrisseurs), ou bien pour un trafic donné, la durée de vie résiduelle de la chaussée, et au besoin l'épaisseur requise pour un renforcement souple.

La troisième et dernière partie est dédiée à la validation expérimentale de la méthode numérique proposée. Plusieurs expérimentations en vraie grandeur sont menées pour valider les phases de calcul inverse et de calcul de déformations critiques. Les essais sont réalisés sur trois planches de référence, dont l'une est instrumentée. La validation s'appuie d'une part sur la comparaison entre propriétés des matériaux identifiées et mesurées en laboratoire, et d'autre part sur l'exploitation de déformations relatives mesurées sur jauges.

La méthode de détermination de la profondeur de substratum est évaluée sur deux des planches d'essai, la première présentant un substratum peu profond (3 m) et la seconde un substratum à 12 m où le sol est assimilable à un semi-espace infini. Dans les deux cas les résultats sont satisfaisants.

Les calculs inverses effectués sur chacune des planches montrent que 1- un bon calage est obtenu, correspondant à des valeurs d'erreur faibles selon les conclusions des études de répétabilité expérimentale et de sensibilité numérique, mais que 2- les erreurs restent cependant significativement plus élevées que celles obtenues dans le cas de jeux de données simulés, ce qui traduit que le modèle ne reproduit pas tout à fait fidèlement le phénomène physique observé, et peut être amélioré.

L'expérimentation réalisée sur la chaussée instrumentée présente une corrélation satisfaisante entre les déformations relatives calculées et les mesures sur jauges. Cependant un seul profile a été testé, si bien que ces premiers résultats devront être confirmés à grande échelle dans le

futur. La comparaison entre modules élastiques identifiés et mesurés en laboratoire montre quant à elle que 1- la méthode dynamique fournit de meilleurs résultats que la méthode pseudo-statique pour les couches profondes, 2- les valeurs numériques obtenues pour les couches bitumineuses de surface sont quant à elles significativement différentes des valeurs attendues, aussi bien pour la méthode dynamique que pour la méthode pseudo-statique, et 3- la modélisation de l'amortissement est assez éloignée de la réalité. En effet, les essais de laboratoire démontrent un contraste important entre les différents matériaux constitutifs. De plus l'amortissement de Rayleigh lui-même n'est pas représentatif de la dépendance en fréquence réelle.

En résumé, la thèse montre que la méthode dynamique dans le domaine temporel proposée est prometteuse. Elle permet notamment de mieux appréhender le comportement des couches profondes que la méthode pseudo-statique. La robustesse du calcul inverse est aussi largement améliorée par la prise en compte des évolutions temporelles des déflexions plutôt que les seules valeurs maximales. Néanmoins, des divergences entre résultats numériques et expérimentaux subsistent. Elles peuvent provenir : 1- d'une modélisation approximative (Rayleigh global sur l'ensemble de la structure) de l'amortissement, 2- de l'hypothèse simplificatrice du comportement élastique des matériaux bitumineux. Il est actuellement impossible dans CESAR d'introduire de comportements viscoélastiques pour ces derniers. Le modèle développé est limité à la prise en compte pour ces matériaux d'un module élastique, indépendant du temps, et 3- de la qualité des interfaces qui pourraient ne pas être parfaitement collées, contrairement à l'hypothèse retenue ici, et adoptée par défaut dans la plupart des codes de calcul existants. Un calcul inverse avec interfaces parfaitement décollées a été mené en guise d'illustration. Cette question reste à approfondir.

A la lumière des travaux de thèse, les améliorations suivantes pourraient être envisagées : 1- Introduction de lois de comportement avancées pour les matériaux bitumineux avec un module dépendant du temps. Des travaux en cours au LCPC, basés sur un modèle de Huet et Sayegh, permettent de déterminer l'évolution au cours du temps du module sécant en fonction du chemin de contrainte appliqué. 2- Amélioration de la prise en compte de l'amortissement, 3- Approfondissement de la question du collage des interfaces. 4- réduction des temps de calcul pour la phase de calcul inverse. Le développement d'une méthode faisant appel à la théorie des états auto-adjoint est en cours de développement ; cette méthode permettrait de réduire le nombre de calculs directs effectués à chaque étape de $n+1$ à 2.

La poursuite de la phase de validation du modèle mécanique pourra reposer sur l'exploitation des données de la planche instrumentée du STAC (située à Bonneuil-sur-Marne, près de Paris, France). La campagne d'essais doit débuter au printemps 2010.

La méthode proposée à titre d'illustration pour la détermination de la capacité portante et/ou de la durée de vie de la chaussée doit être validée. Une expérimentation à grande échelle basée sur le suivi régulier d'une plateforme couplée à un relevé visuel des dégradations est prévue.

Mots clés :
Tests au HWD / Calculs inverses dynamiques / Théorie des chocs / Modélisation aux éléments finis / Etude de sensibilité / Modules élastiques / Amortissement / Performance des matériaux / Capacité portante d'une chaussée / Chaussées instrumentées.

General introduction

Background and scope of the study

Pavement evaluation usually consists in assessing the surface and structural condition. Surface condition includes all characteristics related to safety and comfort. Structural condition is related to the bearing capacity of the pavement, and traduces the material damage and stiffness evolution. Nowadays structural pavement condition is mainly evaluated on the basis of non destructive testing (NDT) methods combined with visual inspections. Several NDT techniques have been developed.

The historic French non destructive method for determining the bearing capacity of airport pavements is based on the empirical analysis of static plate loads. The test machine involved in this method is called « remorque de portance ». When using this device the method consists in studying the fatigue behaviour (deflections under load and residual deformations) of the pavement-subgrade complex. This method has been made compatible with the CBR design method for flexible pavements.

Besides, rational methods based on dynamic tests have been spreading worldwide in recent years. The STAC acquired in this frame in December 2005 a CarlBro PRI 2100 Heavy Weight Deflectometer (HWD). This non destructive device is today the most commonly used device worldwide. In parallel the STAC has begun to develop its own rational design method.

Its principle consists in applying a transient load to the pavement by dropping a mass from a given height onto a stationary load plate placed over its surface, through a buffer system, and analyzing the ensuing dynamic response of the pavement. The load simulates the loading history associated with the pass of an aircraft rolling wheel. The response of the pavement is assessed through measurement of surface deflections. The latter are continuously measured during the test by means of geophones placed under the plate and at predetermined locations at the pavement surface. Pavement properties are determined by means of a so-called "backcalculation" numerical procedure which consists in choosing a mechanical model for the pavement and identifying the parameters of the model for which theoretical computed deflections fit the experimental data set. Then, forward calculations can be performed to determine critical strains in the structure under specified loads. The latter allow estimating the bearing capacity or the remaining life of the studied structure according to the knowledge of material mechanical performances.

Usual backcalculation procedures involve extracting, for each displacement sensor, the peak deflection from the deflection time-history, to reconstitute a so-called "deflection basin", and matching it through an optimization method to the deflections predicted by a static model of the pavement. In the typical methods, the pavement is idealized as a multilayered isotropic elastic structure, and the only parameters to be backcalculated are the elastic layer moduli, while the layer thicknesses and Poisson's ratio are kept constant.

Nevertheless the pseudo-static backcalculation methods have shown limitations. Actually they neglect damping or inertial effects in the pavement, and take into account only part of the available information. Therefore interest for dynamic analysis has been growing for a few

years. These methods are expected to provide a better estimation of the pavement properties. First the modelling is closer to the studied physical phenomenon. Moreover as the whole time-related deflection can be considered, the system becomes highly overdetermined. Thus the optimization is expected to give more reliable results than in the static case. Finally, the backcalculation process allows backcalculating potentially a greater number of parameters than in static methods. Two types of analysis are possible: the time-domain methods and the frequency-domain methods.

When knowing pavement characteristics, residual bearing capacity and associated remaining life of the pavement can be determined, and if necessary an overlay designed.

Research objectives

The first objective of this research study is to better understand the HWD concept (functioning of the apparatus and principle of data analysis). The second objective consists in elaborating an experimental protocol. Finally it is also intended to develop an advanced method for the assessment of flexible pavements using HWD tests data to overcome the aforementioned limitations of the existing data analysis methods.

First objective has first been achieved in the early months of the thesis period. The second one has required constant comparison between theory and practice. A provisional experimental protocol is provided in appendix 1.3. It may mature in the future with regard to future evolutions in the retained data analysis procedure. Last objective is the object of this memoir.

The main goal is to achieve a better representation of the observed physical phenomena during dynamic loading for both backcalculation and strains determination phases, and to consider the whole available information. A computation of time-related deflections is proposed, relying on a dynamical modelling of applied stresses and ensuing pavement response. Three alternative versions of the model have been studied, which differ by the applied dynamical load modelling. The work includes modelling and experimental validation phases. An automated backcalculation procedure using the established model is also developed for data analysis. Moreover, even if the work focuses on mechanical modelling and associated backcalculation procedure, the evaluation of the pavement performances (residual bearing capacity, remaining life, overlay design) is also addressed.

Organization of work

First a literature review is proposed. An overview of existing methods for structural non destructive testing of pavements is given in the first part. They are classified into three main types: the pavement fatigue analysis methods, the seismic-based methods and the deflection-based methods. The latter are subdivided into several categories, according to the nature of the applied load. The HWD (Fig.0-18) which is the internationally most commonly used device for non destructive airport pavement testing, belongs to one of the latter: the transient load methods. The second part focuses on HWD. The main existing pavement models are described and their respective advantages and shortcomings highlighted. Then backcalculation procedures are examined. Finally forward calculation procedures are discussed, leading to the determination of pavement bearing capacity or remaining life determinations and overlay.

Then, the body of the memoir comprises three parts.

Part 1 describes preliminary studies. First, reliability of HWD data for dynamical analysis is studied, based on the adjunction of external instrumentation to the HWD sensor system, and on crossed tests with other HWD on known test facilities. Then, an experimental repeatability study is performed to determine the precision on HWD time-related signals. Finally, an experiment is conducted in order to assess the linearity of deformations with applied loading, and the occurrence of viscoelastic behaviours in asphalt materials is searched, by studying the response of gauges embedded in an instrumented tested pavement.

Part 2 focuses on modelling. A dynamic time-domain modelling is developed, which relies on a 2D axis-symmetric finite element dynamical model implemented in the Cesar-LCPC FEM software. It takes into account inertia of materials and structural damping. A backcalculation procedure is elaborated, which allows finding the pavement characteristics resulting in a satisfactory fitting between theoretical and experimental signals. A thorough study is conducted to assess if the resulting characteristics set is appropriate or not. This study phase relies on the choice of an objective function and a linked target error. A numerical sensitivity is performed. Its conclusions, combined with information from the aforementioned repeatability experiment, are used to select consistent errors. In the light of these results, an automated convergence algorithm is built for numerical resolution. A tool is also conceived which allows automating the finite elements mesh creation and both backcalculation and forward calculation phases: the PREDIWARE (Pavement Rational Evaluation using Deflections Induced by Falling Weights, for Airfield and Road Engineers) software.

Part 3 is dedicated to the experimental validation of the proposed numerical method. Several full-scale validations of both backcalculation method and strains determination are conducted. They consisted in test surveys run on three well-known pavements, one of them being instrumented. The validation relies on the comparison between backcalculated and laboratory-determined material properties, and on the comparison between theoretically expected strains and gauge measurements, when available.

Introduction générale

Contexte et objet de l'étude

L'évaluation des chaussées consiste classiquement à déterminer leur état surfacique et structurel. L'état de surface inclut toutes les caractéristiques relatives à la sécurité et au confort. L'état structurel est lié à la capacité portante de la chaussée et traduit l'évolution de la rigidité et de l'endommagement du matériau. Sa détermination est essentiellement basée sur des essais non destructifs, combinés avec des inspections visuelles. De nombreuses méthodes d'analyse non destructive existent.

Historiquement la méthode française d'auscultation non destructive repose pour la détermination de la capacité portante des chaussées aéronautiques sur l'analyse empirique de chargements de plaque statiques. La machine impliquée dans cette méthode est la « Remorque de Portance » du STAC. La méthode consiste à étudier la fatigue du complexe chaussée/sol support. Cette méthode a été rendue compatible avec la méthode CBR de dimensionnement relative aux chaussées souples.

Par ailleurs, l'intérêt pour les méthodes rationnelles basées sur l'analyse d'essais dynamiques est apparu à l'échelle internationale depuis quelques années. C'est dans ce cadre que le STAC a acquis en décembre 2005 un Heavy Weight Deflectometer (HWD). Il s'agit d'un modèle CarlBro PRI 2100. Cet appareil d'auscultation non destructive est aujourd'hui le plus utilisé à l'échelle internationale. En parallèle, le STAC a entrepris de développer sa propre méthode rationnelle de dimensionnement.

Son principe consiste à appliquer un chargement transitoire à la surface de la chaussée à l'aide d'une masse tombant d'une hauteur donnée sur une plaque de chargement placée à la surface de la chaussée, et surmontée d'un système de tampons amortisseurs, puis d'analyser la réponse dynamique de la chaussée induite par ce chargement. La sollicitation appliquée est censée simuler l'historique de chargement associé au passage d'une roue d'avion passant à la surface de la chaussée. La réponse est évaluée à l'aide des déflexions de surface, mesurées en continu pendant la durée de l'essai à l'aide de géophones placés sous la plaque ainsi qu'à des distances prédéterminées. Les caractéristiques de la chaussée sont déterminées à l'aide d'une procédure numérique appelée « calcul inverse » qui consiste à choisir un modèle mécanique pour la chaussée et à identifier les paramètres de ce modèle conduisant à un calage satisfaisant entre déflexions numériques et expérimentales. Ensuite, une phase d'analyse directe peut être conduite pour déterminer les contraintes critiques dans la chaussée sous des chargements spécifiés. Ces dernières contraintes permettent d'évaluer la capacité portante de la chaussée étudiée et/ou sa durée de vie résiduelle, à partir de la connaissance des performances mécaniques des matériaux.

Les procédures usuelles de calcul inverse impliquent l'extraction, pour l'historique de déflexion correspondant à chacun des géophones, du pic de déflexion, afin de reconstituer un « bassin de déflexion » expérimental, et de caler, à l'aide d'une méthode d'optimisation, un bassin de déflexion théorique, issu d'une modélisation statique, sur ce bassin expérimental. Typiquement, la chaussée est modélisée par une structure multicouche linéaire élastique, et

les seuls paramètres à rétrocalculer sont les modules élastiques des couches, tandis que les épaisseurs et coefficients de Poisson sont gardés constants.
Néanmoins ces méthodes de calcul inverse pseudo-statiques ont montré leurs limites. En effet, elles négligent l'amortissement ou les effets d'inertie dans la chaussée, et n'exploitent qu'une infime partie de l'information disponible. D'où l'intérêt grandissant pour les méthodes dynamiques. Ces dernières sont supposées fournir une meilleure approximation des caractéristiques de la chaussée. Tout d'abord, la modélisation est plus fidèle au phénomène physique observé. De plus, comme les historiques complets de déflexions peuvent être considérés, le système devient grandement surdéterminé, ce qui a pour double conséquence de permettre d'obtenir *a priori* des résultats plus fiables que dans le cas statique, et d'augmenter le nombre de paramètres à rétrocalculer. Deux types d'analyse sont possibles : dans le domaine temporel, ou bien dans le domaine fréquentiel.

Connaissant les caractéristiques de la chaussée, la capacité portante résiduelle de la chaussée et/ ou la durée de vie résiduelle associée peuvent être déterminées, et un rechargement dimensionné, si nécessaire.

Objectifs des recherches

Le premier objectif des présentes recherches est de mieux appréhender le concept du HWD (fonctionnement de l'appareil et principe d'exploitation des données). Le second objectif consiste à élaborer un protocole expérimental. Enfin, il est ambitionné de développer une méthode avancée d'analyse des données HWD pour les chaussées souples permettant de dépasser les limites des méthodes existantes mentionnées ci-dessus.

Le premier objectif a été réalisé dans les premiers mois de la thèse. Le second, qui a nécessité un aller-retour constant entre théorie et mise en œuvre pratique, a débouché sur le protocole expérimental fourni en annexe 1.3. Ce dernier peut être amené à évoluer au regard des futures évolutions de la méthode d'analyse. Le dernier objectif fait l'objet de ce mémoire.

Le but principal est d'établir une meilleure modélisation du phénomène physique observé durant un chargement dynamique de la chaussée, aussi bien pour la phase de calcul inverse que pour celle de calcul direct, et de considérer l'ensemble de l'information disponible. Un calcul des historiques de déflexion est proposé, qui repose sur une modélisation dynamique de l'effort appliqué et de la réponse induite de la chaussée. Trois versions du modèle ont été étudiées qui diffèrent par la modélisation de l'effort appliqué. Le travail inclut des phases de modélisation et de validation expérimentale. Une procédure de calcul inverse automatisée, utilisant le modèle mécanique établi, est aussi développée. De plus, même si le travail se concentre sur le modèle mécanique et la procédure de calcul inverse associée, l'évaluation des performances de la chaussée (capacité portante résiduelle, durée de vie résiduelle, rechargement) est aussi abordée.

Organisation du travail

Tout d'abord une étude bibliographique est proposée. Un aperçu des méthodes non destructives d'auscultation des chaussées aéronautiques est donné en première partie. Ces méthodes sont classées en trois grandes classes : les méthodes empiriques d'étude de fatigue de la chaussée, les méthodes sismiques, et les méthodes basées sur l'étude des déflexions. Ces dernières sont subdivisées en plusieurs catégories, selon la nature du chargement appliqué. Le

HWD (Fig.0-18) qui est l'appareil d'auscultation non destructive le plus utilisé de par le monde appartient à l'une de ces dernières : les méthodes à chargement impulsionnel. La seconde partie de l'étude bibliographique est consacrée au HWD. Les principaux modèles de chaussée existants sont décrits, et leurs avantages et défauts respectifs soulignés. Ensuite, les procédures de calcul inverse sont examinées. Enfin les données nécessaires à la phase d'analyse directe sont discutées, qui conduisent à la détermination d'une capacité portante et/ou d'une durée de vie résiduelle, voire d'un rechargement.

Le corps du mémoire comprend ensuite trois parties.

La partie 1 décrit les études préliminaires. Tout d'abord la fiabilité des données HWD en vue d'analyses dynamiques est étudiée, à l'aide de la mise en place d'une instrumentation externe, et d'essais croisés avec d'autres HWD sur des structures connues. Ensuite, une expérience de répétabilité est menée afin de déterminer la précision sur les signaux temporels de déflexion. Enfin, une expérience est conduite afin d'évaluer la linéarité des déformations avec l'effort appliqué, et la présence de comportements visqueux dans les matériaux bitumineux est recherchée, en étudiant la réponse de capteurs ancrés dans une chaussée.

La partie 2 se concentre sur la modélisation. Un modèle dynamique dans le domaine temporel est développé. Il repose sur une modélisation aux éléments finis basée sur un maillage 2D axisymétrique. Le code de calcul utilisé est Cesar-LCPC. Le modèle prend en compte les effets d'inertie des matériaux et un amortissement structurel. Une procédure de calcul inverse est élaborée, qui permet de déterminer un jeu de paramètres entraînant un calage satisfaisant entre signaux théoriques et expérimentaux. Une étude approfondie est menée afin de pouvoir évaluer si un jeu de données est approprié ou non. Cette étude repose sur le choix d'une fonction objective et d'une erreur cible liée. Une étude numérique de sensibilité est réalisée. Ses conclusions, combinées avec celles de l'étude de répétabilité précédemment évoquée, sont utilisées afin de choisir de manière cohérente une erreur de minimisation. A la lumière de ces résultats, une procédure de calcul inverse est élaborée. Un outil est aussi conçu afin de permettre l'automatisation des phases de calcul inverse et direct : le logiciel PREDIWARE (Pavement Rational Evaluation using Deflections Induced by Falling Weights, for Airfield and Road Engineers).

La partie 3 est dédiée à la phase de validation expérimentale de la méthode numérique proposée. Plusieurs validations à échelle 1 des phases de calcul inverse et de détermination des contraintes ont été conduites. Elles ont été réalisées sur des chaussées bien connues, dont l'une d'elle est instrumentée. La validation a porté sur les modules rétrocalculés, par comparaison avec les résultats d'essais en laboratoire, et sur les valeurs de déformations relatives, par comparaison des valeurs théoriques avec les résultats de capteurs ancrés, lorsque ces deniers sont disponibles.

Table of contents

List of tables

List of figures

Literature review

1 - Overview of NDT methods for structural evaluation

Background

Regular inspection surveys are necessary in pavement management to anticipate rational policies of maintenance and rehabilitation.

Destructive open cuts may be proposed for performing in-place bearing tests at different levels of the pavement and for taking undisturbed samples for subsequent laboratory testing. However these investigations need a reconstruction phase, are time and cost-consuming. Additionally they raise the question of representativity of the laboratory tests, when unhomogeneous pavement materials are encountered.

Hence interest for non-destructive testing has been growing in the last decades. The rationalization of design methods in the 1960's and 1970's allowed the structural assessment of the bearing capacity of pavements from analysis of surface deformation imparted by a (static or dynamic) load. The two historical main methods for airfield pavement testing were the American Waterways Experiment Station dynamic testing (Fig. 0-17) and the French static STBA trailer (Fig. 0-8) method. Several other non destructive methods have been developed since then.

A general overview of the past, current and potential future non destructive testing apparatus is proposed here, which does not claim to be exhaustive. They are classified into generic methods, corresponding to the type of action imparted to the pavement and related measurement principles. Each method and the corresponding devices are presented and their advantages and shortcomings discussed.

Criteria for assessing the relevance of NDT methods and devices

The relevance of the different devices is ascertained through the following criteria:

a - The test shall represent the effect of the traffic loading weight,
b - The field sampling rate shall be defined to find a compromise between practical feasibility and pavement defect detection,
c - The device shall be appropriate for valuable and straightforward investigations of airfield pavements.

- *a- Representativity of the test against real traffic loading weight effect*

- Rolling wheel representation

The purpose of the Non Destructive Testing (NDT) consists in studying the response of the studied pavement under traffic. Thus, the test shall simulate adequately the effect of the rolling wheel weight. External actions applied by NDT are more or less faithful to this real load effect. Static loads applied by some devices are far from the latter since tests do not excite the dynamic response of the pavement. Devices equipped with stationary dynamic load

plates allow generating actions closer to the observed physical phenomenon. Representativity is still improved with rolling wheel device equipments.

However, the choice of a dynamical external action is not sufficient to warrant that the NDT test is adequately simulating the traffic effect. Actually, as detailed in the second part of this literature review, surface materials present generally frequency-dependent behaviours, whereas the underlying unbound materials display nonlinear behaviours. Thus, to properly study the response of the pavement under traffic using NDT testing, a dynamic loading is needed, the duration and stress amplitude of which shall fall in the range of the real applied weight.

- Load duration

- **Typical strain signal at the bottom of asphalt layer**

The only materials affected by the load duration are asphalt layers which present visco-elastic (or time-dependent) behaviours. The duration under study is the one measured at the bottom of the base asphalt layer. Indeed the failure criterion in asphalt layer is fatigue caused by repeated tensile strain applications at the bottom interface. Fig 0-1 depicts a typical strain gage signal measured at this level, during the pass of a rolling load. This example is extracted from the High Tire Pressure Test (HTPT) experiment, currently in progress in Toulouse Blagnac airport. This program, jointly performed by Airbus, the French Central Laboratory for Civil Works (LCPC), the Toulouse Regional Laboratory for Civil Works (LRPC-T) and the STAC, is aimed to study the influence of an increase in tire pressure on the rutting behaviour of asphalt surface materials. The structure under study presents a 26 cm asphalt layer. On the considered test, a 217 kN load with a 15 bar pressure is applied by the Airbus simulator (Fig. 0-2). Mid-depth temperature in the asphalt layer was 15 °C during the considered test.

A nearly symmetric response is observed. The magnitude asymmetry in the two compressive peaks mainly comes from the delayed relaxation phase due to the material visco-elasticity, and to a lesser extent, to the subgrade drainage conditions.

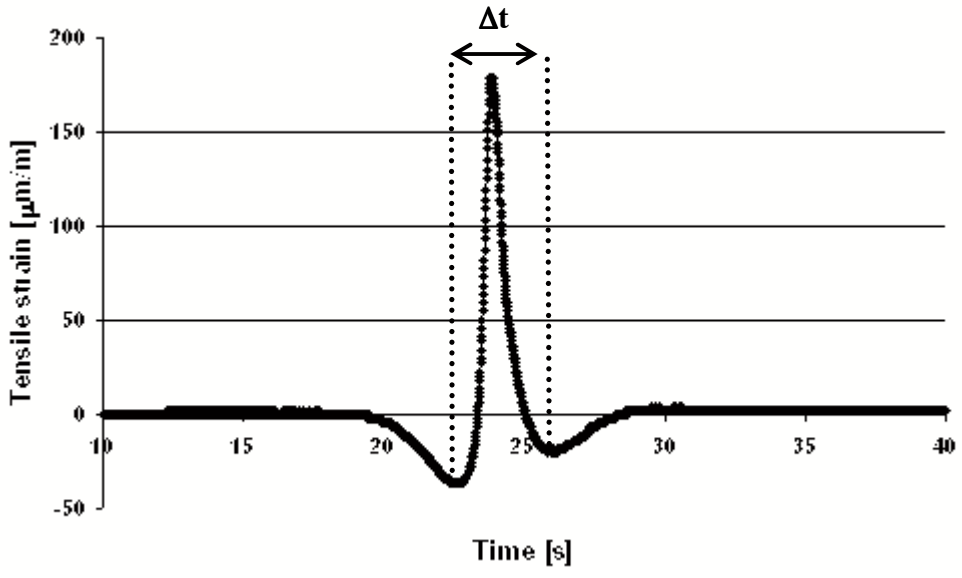

Fig. 0-1 Typical strain gage signal at the bottom of the base asphalt layer

Fig. 0-2 Airbus simulator (Photograph by M. Broutin)

- **Influence of strain duration**

Strain duration may greatly influence the surface layer stiffnesses [Collop,1996] . Hence pavement behaviour may be significantly affected and the further analysis distorted.

- **Relationship between vehicle velocity and stress pulse time**

Except for the specific case of rolling wheel devices for which vehicle velocity is just to be adapted (when possible) to traffic speeds, it is not straightforward to demonstrate that the external action is representative of the traffic, in terms of load duration. Actually, the relationship between vehicle velocity and the resulting surface stress shape and duration on the one hand, and on the other hand between this surface stress and ensuing stress shape and duration at a given depth in the pavement are complex. However these relations are necessary for devices, such as stationary dynamic load plate devices, in order to judge for their relevance.

[Barksdale, 1971] presents a numerical method using a FEM modelling to relate these pieces of information. For this purpose, a principle of superposition has been used, assuming a linear elastic behaviour of the pavement. The influence of material nonlinearity on the results has been shown to be negligible. Wheel is modelled as a circular plate uniformly loaded. Stress at a given point of the pavement is calculated by summing elementary stresses corresponding to the different positions of the plate during its pass. In practice, the load plate remains stationary and the studied pavement point moves. Superposition is made on all points from the point located at the vertical of the load until the last point of the plate influence area, so that a half stress basin is obtained. Signal is assumed to be symmetric.

Note that in Barksdale's study the choice of a static linear elastic model implies that inertia effects and visco-elasticity are not taken into account in the calculation. The effect of principal stress axis rotation is also neglected. This study allows determining the shape and duration of the stress pulse and their variation with depth as a vehicle moves at a constant speed over the pavement surface.

Fig 0-3 and Fig. 0-4 respectively show the evolution of vertical stress in the pavement with depth and the evolution of principal stress in the pavement with vehicle velocity and considered depth.

[Barksdale, 1971] shows that 1- the shape of the stress signal induced at the surface of the pavement is sinusoidal, 2- as for deeper levels the signal shape becomes more triangular, 3- duration of stress signal increases with depth and 4- stress level decreases when vehicle velocity increases.

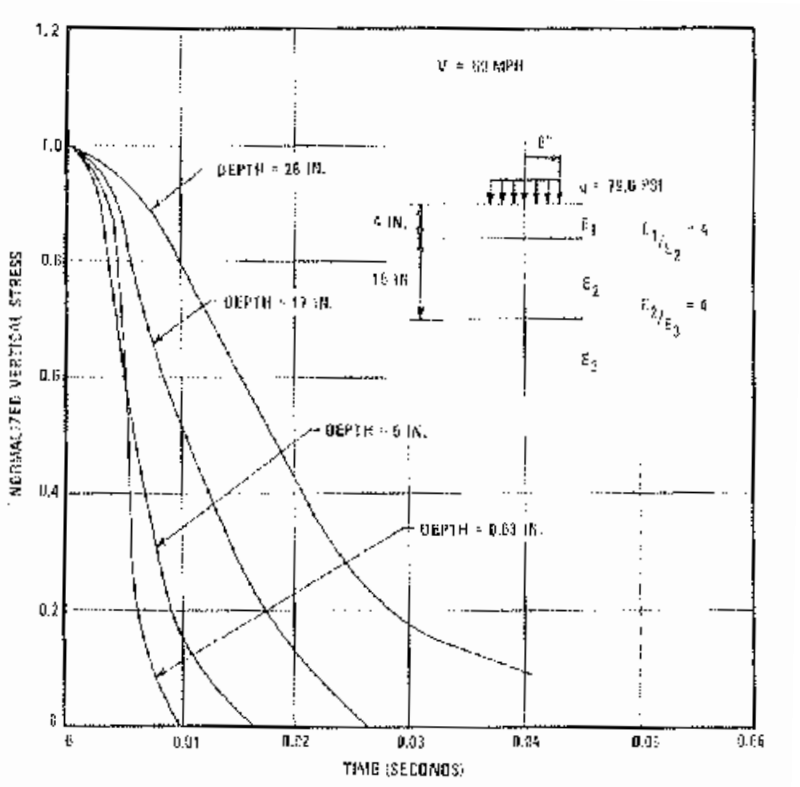

Fig. 0-3 Variation of calculated vertical compressive stress pulse shape with depth, after [Barksdale, 1971]

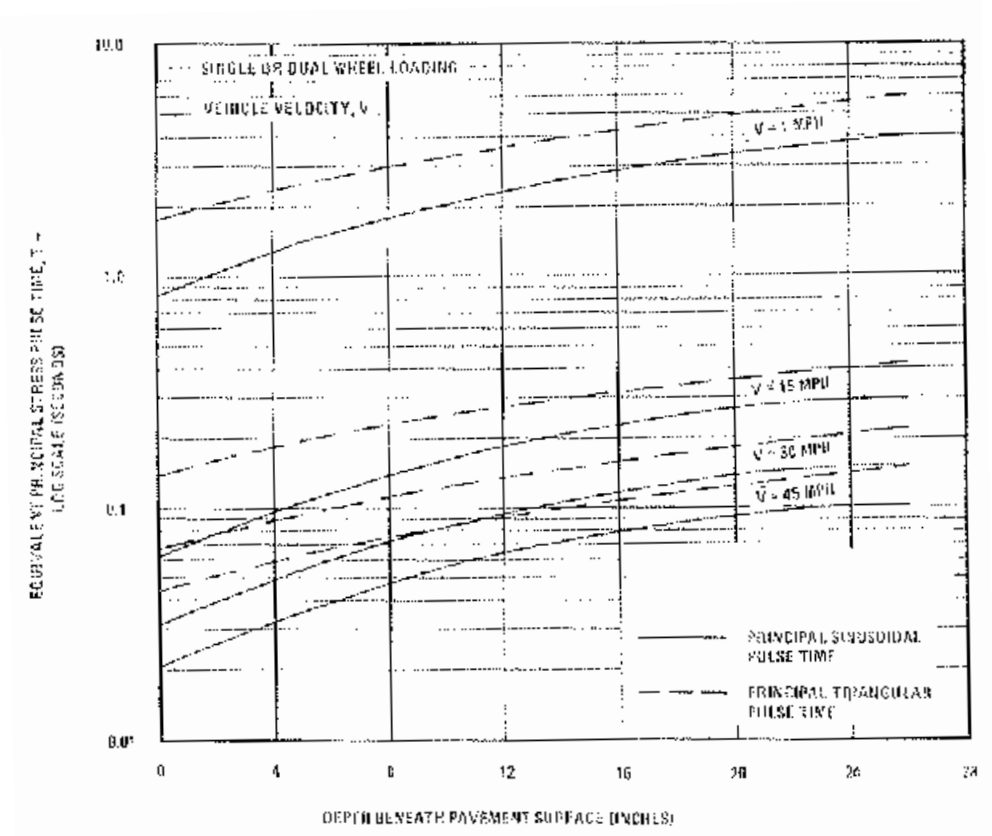

Fig. 0-4 Variation of principal stress pulse time with vehicle velocity and depth, after [Barksdale, 1971]

In addition to this valuable study, it would be interesting to reiterate this kind of numerical study with modern calculation methods, to take into account visco-elastic behaviours and inertia effects, in dynamical FEM modelling with step recovery.

- **Corrections**

If the test is not representative of a real aircraft wheel pass, the subsequent analysis needs to be adjusted so as to take into account material frequency-dependence obtained from laboratory tests. However, the latter are not always available, and they are never representative of in-situ material behaviours. This is the reason why it is imperative to choose tests as representative as possible of the traffic action.

- Load amplitude

Unbound material may present nonlinear behaviours. However, nonlinearity seems to be restricted over a reasonable range of strains [Barksdale, 1971]. Linearity of materials will be examined in this memoir on experimental data from HWD tests. However, as detailed below, some pavement testing methods apply strain fields which do not belong to the strain range associated to real traffic. The influence of nonlinearity becomes in these cases problematical.

- **Corrections**

As for the aforementioned frequency corrections in asphalt material, analysis using linear models shall be corrected based on laboratory tests on unbound materials. Unfortunately, laboratory testing on these materials is even less representative of in-situ materials than for asphalt materials.

b- Representativity of the measurement survey in terms of field test sampling rate

- Continuous vs discrete measurements

Main NDT devices provide discrete information about the pavement structural conditions. A given number of measurement test points is chosen. According to this number, statistically more or less reliable mean values and variances are determined.

However, discrete testing methods do not warrant that critical, or even typical, pavement locations will be tested ([Bay and Stokoe, 1998] or [Simonin et al., 2009]). On the contrary, continuous methods allow the entire pavement to be characterized. Thus, poor, average, and good sections of pavement can rapidly be delineated. Fig. 0-5 well illustrates the phenomenon [Bay and Stokoe, 2008]. In this example reflecting cracking is studied using the so-called RDD device which is a continuous testing device presented hereafter. In the following Δw is a structural index. Outside lane corresponds to a lane presenting no apparent cracking whereas inside lane presents severe reflecting cracking. Very local weak zones (corresponding to reflecting cracks) are delineated (locations 2 and 3). Let us assume that a discrete testing is conducted on the pavement and that no test is performed on locations 2 and 3. Conclusion would be that the red threshold is never reached, and that the structural condition is good.

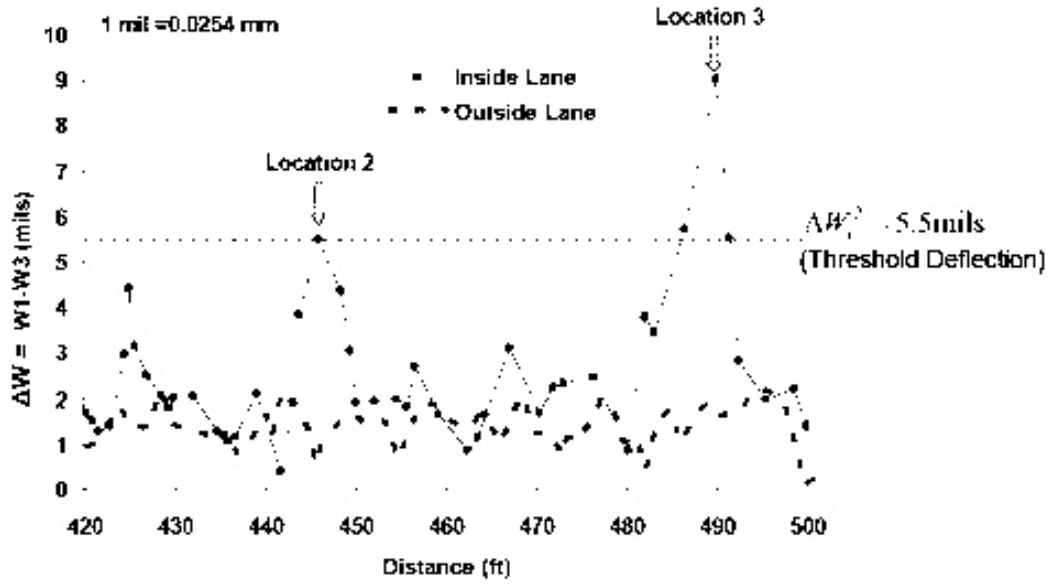

Fig. 0-5 Detection of local distresses in a pavement using continuous testing devices, after [Bay and Stokoe, 2008]

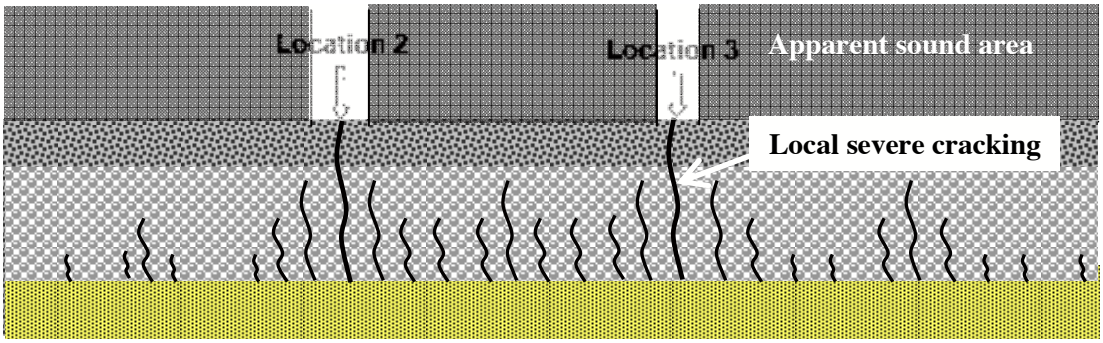

Fig. 0-6 Illustration of discrete damaging of a pavement

Note that discrete tests also raise problems of safety and disturbance for road testing. Nevertheless, this problem is limited on airport pavements.

c- Practical aspects

Different methods and devices are more or less easy to use. Long testing times raise the problem of representative pavement coverage when the spacing between discrete test points is increased.

Main NDT methods

Non destructive testing methods are usually classified into two categories: the seismic-based methods relying on the analysis of low-strain ($< 10^{-6}$) stress waves propagations through the pavement, and the deflection-based methods. The latter consist in studying the magnitude and shape of the surface deflection basins of the pavement under loading. Both methods are used to determine the material properties (in general elastic properties only) of the pavement. These properties are then used to predict the pavement bearing capacity and remaining life. A third type of method, which is a French specificity, is also to be mentioned: it involves the so-called French STBA trailer. This device does not pertain to the deflection-based equipments. It consists in an empirical study of the long-term residual settlement of the pavement-subgrade complex under repeated static plate loads.

For each method, the general measurement principle is described first. Then, the main devices are presented and their respective advantages, limitations and possible improvements are discussed.

Some devices generally dedicated to road testing are also mentioned for their scientific interest, even if their use on airfield pavements is not recommended due to load insufficiency. Nonlinearity may occur in unbound materials, even if the load levels present in the worst cases a 2- to 3- ratio. Above all, these light devices may not be able to affect underlying layers, due to thick upper asphalt layers.

1.1 Assessment of long-term residual settlement method

1.1.1 Principle

The historical method used in France to determine the bearing capacity of airport pavement is based on the empirical analysis of static plate loads. The deflections under load and residual deformations of the pavement-subgrade complex are studied. This method has been made compatible with the CBR design method for flexible pavements. In practice, the studied pavement is subjected to several series of 10 repeated static loading and unloading cycles applied by a hydraulic jack through a loading plate. Settlement is measured simultaneously. An increasing magnitude between the series enables to squeeze the allowable residual settlement, straightlining to 10 000 cycles with a semi-log scale, to a 5 mm consolidation (Fig. 0-7). This criterion may be modified to take into account the pavement age.

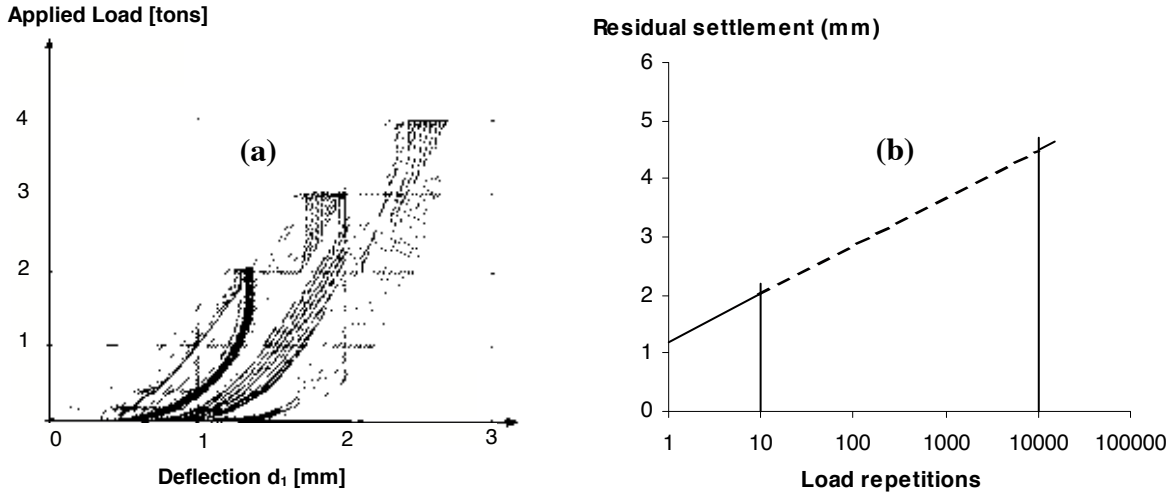

Fig. 0-7 a- Typical load cycles on a flexible pavement, b- Extrapolation of the residual settlement between 10 and 10 000 cycles

1.1.2 Main devices

The test machine involved in this method is called STBA Trailer (in French « Remorque de Portance », Fig. 0-8) [ITAC, 1999], and its unique specimen in the world has been used by STAC since 1973.

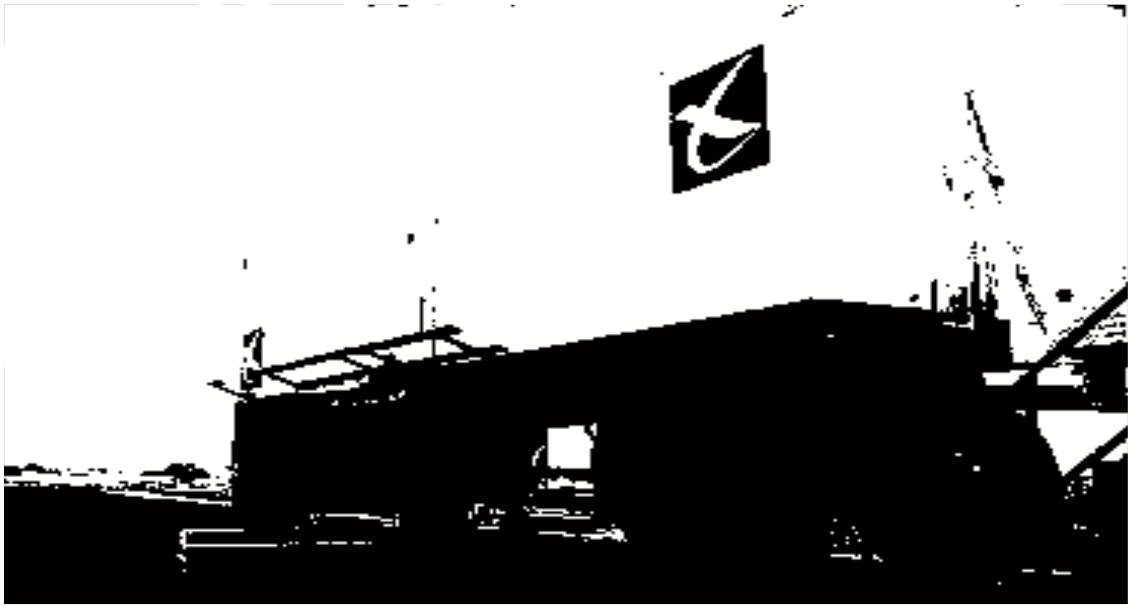

Fig. 0-8 The French STBA Trailer (Source: STAC's database)

1.1.3 Advantages/shortcomings

The French STBA Trailer is the only existing device allowing characterizing directly the fatigue behaviour of the pavement-subgrade complex.

Nevertheless two shortcomings can be mentioned. First fatigue laws are interpolated between 10 and 10 000 load cycles what is debatable. Then, in the case of thick asphalt layers, and especially for high temperatures, creep phenomena may interfere with the test result, leading to a problematical distinction between creep and residual settlement for the measured deformation.

Moreover the device provides discrete measurements of the pavement structural condition. An additional drawback is linked to a heavy operational protocol. Each measurement lasts about 40 min. This test duration limits the number of test points performed on the studied structure.

1.2 Seismic-based methods

1.2.1 Principle

a - Measurement principle

The analysis of surface waves allows evaluating pavement shear moduli, and the layer thicknesses in multilayered structures, by taking advantage of the dispersive nature of the Rayleigh waves. Interpretation relies on three main scientific reviews. 1- shear waves velocity

in materials is directly linked to their stiffness ; 2- body shear wave velocities and phase velocities of surface Rayleigh waves are mathematically related ; and finally 3- Rayleigh waves are dispersive (their phase velocity V_R depends on the frequency f) and their penetration depth depends on the wavelength λ.
Waves are generated over the pavement surface and the propagation of surface waves is analyzed. Then dispersion curves giving shear waves velocity as a function of depth can be constructed based on the aforementioned reviews. Backcalculation of the material moduli use these dispersion curves.

b - Further developments related to functioning

In an elastic half-space a load impact generates two types of body waves: compression or primary (P) waves, shear or secondary (S) waves. Surface Rayleigh (R) waves result from the interaction between the two body waves types. Interest for the R-Waves in propagation analysis comes from their energy. In an isotropic homogeneous infinite half-space R waves represent 67% of the propagated energy, S-waves 26% and P-waves only 7% [Abraham et al., 1997]. But at surface, geometrical decrease in the body waves are proportional to $1/r^2$ (with r the distance to the source) and only $1/\sqrt{r}$ for R waves. This explains why the R-waves are easy to generate and measure.

The measurement principle consists (Fig. 0-9) in measuring the R-wave velocity using receivers positioned at several radial distances from the source. [Hildebrand, 2002] specifies that accelerometers are generally used for short distances and geophones far from the source. The following rule: $\lambda / 4 \leq d_1$ and $\lambda / 16 \leq d_2 - d_1 \leq \lambda$, with λ the wavelength and d_1 and d_2 the distances to the receivers, is recommended in [Abraham et al., 1997].

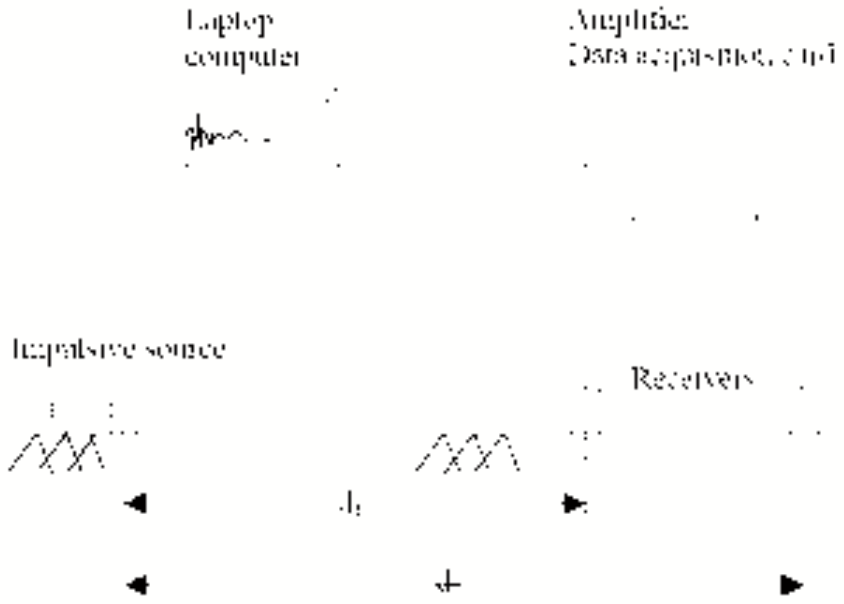

Fig. 0-9 Surface Wave analysis system, after [Hildebrand, 2002]

For a selected *f* frequency, relationship between the phase difference ϕ and elapsed time between receivers is provided by:

$$t(f) = \frac{\varphi(f)}{2\pi f} \quad \textbf{(0-1)}$$

And the Rayleigh velocity by

$$V_R = \frac{d_2 - d_1}{t(f)} \quad \textbf{(0-2)}$$

Finally the wavelength is calculated writing:

$$\lambda = \frac{V_R}{f} \quad \textbf{(0-3)}$$

Numerous relationship linking V_R and V_S are proposed in the literature.
[Roesset et al., 1990] and [Richart et al., 1970] respectively propose:

- $V_S = (1{,}135 - 0{,}182\nu)V_R$ for $\nu \geq 0{,}1$

with ν the Poisson's ratio of the material.

- V_R/V_S is solution of the following equation :

$$K^6 - 8 \cdot K^4 + (24 - 16 \cdot \alpha^2) \cdot K^2 - 16 \cdot (\alpha^2 - 1) = 0$$

With $\alpha = \frac{V_S}{V_P} = \sqrt{\frac{1-2\nu}{2-2\nu}}$ **(0-4)**

V_P being the P-waves velocity,

and $V_S = \sqrt{G/\rho} = \sqrt{E/(2\rho(1+\nu))}$,
ρ, E and G being respectively the material mass density, and the Young's and shear elastic moduli.

Let then suppose that V_S can be calculated in this manner for a f sampling of frequencies in a given λ range. Two means are possible. Either harmonic vibrations or impulse loadings are used.

In the first case, experiment shall be reiterated for all expected λ values.

In the second case, like with the Spectral Analysis of Surface Waves (SASW) method [Roesset, 1990], the stress signal has to be transferred into the frequency domain. It is thus possible to obtain the dispersion curve defined as the velocity profile as a function of depth. This is made possible since the penetration depth (d) of the wave increases with its wavelength (d≈λ). For instance for a wave whose wavelength is less than the first layer thickness, its velocity will be representative of the layer stiffness. For higher wavelengths, wave propagation is influenced by the stiffness of the different layers. Then it is possible using surface waves over a wide range of wavelengths to assess material properties over a broad range of depths.

A theoretical determination of the Young's moduli value based on the wave equations resolution is provided in [Yuan and Nazarian, 1993]. Some empirical relationships between d and λ are also available in the literature, allowing lighter inverse analyses.

A Young's modulus profile is backcalculated (Fig. 0-10, right), so that the theoretical dispersion curve fits the experimental one (Fig. 0-10, left).

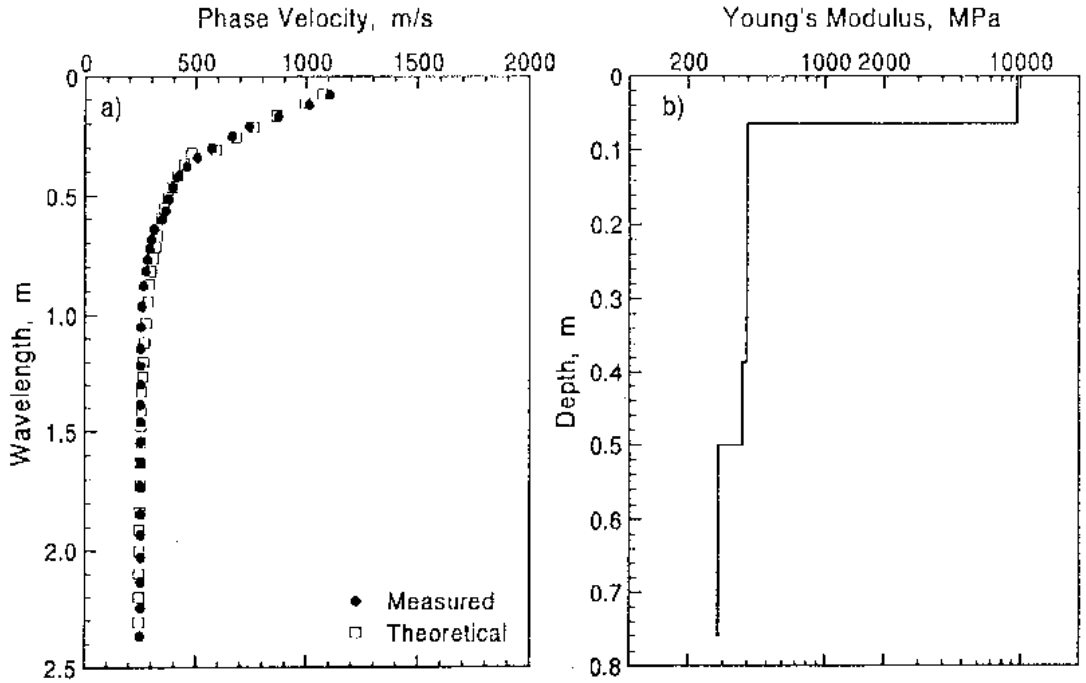

Fig. 0-10 Typical dispersion curve and corresponding modulus profile, after [Yuan et al., 1998]

1.2.2 Main Devices

a - Goodman Vibratory

The first pavement testing device based on wave propagation techniques is the Goodman Vibratory [BL, 1968] developed in1961 by the Laboratoire des Ponts et Chaussées. This device was applying harmonic vibratory stresses over the pavement. A receiver was placed at the surface of the pavement near the source so that excitation and response were initially in phase. The receiver was then shift until the signals were again in phase. That meant that the receiver had been shift of one wave length. The same operation had to be performed with different frequencies.
Interpretation consisted in manually comparing the experimental dispersion curves to the theoretical data set. The time-consuming tests and the empirical manner to analyse results prevented the development of the method. Nowadays this device is not used any more.

b - Seismic Pavement Analyzer

[Nazarian et al., 1993] propose the so-called "seismic pavement analyser" (SPA) device. This device is trailermounted and enables to monitor the conditions associated to pavement deterioration using several measurements methods. Actually, amongst other assessment techniques as the impact echo method [Simonin, 2005], ultrasonic-surface-wave-velocity or ultrasonic-body-wave-velocity analysis, the SPA also enables performing the Spectral Analysis of Surface Waves (SASW) of pavements.

1.2.3 Advantages/Shortcomings

This method is recommended in [Hildebrand, 2002] as a potential supplement to the FWD method (see infra) for its ability to provide information on the stiffness of the asphalt surface layers, and layer thicknesses.

Nevertheless, the seismically determined moduli are moduli at small strain amplitudes and at high frequency with regard to the strains imparted to the pavement by an aircraft rolling wheel [Roesset et al., 1990].
It raises a double problem. First material behaviour (especially the untreated materials) may be affected by this large deviation (10^3 ratio) in the imparted strains. Fig. 0-11 after [Puech et al., 2004] shows the typical dependence of the normalized shear modulus Gs / Go with shear strain γ. Gs is the shear stress modulus and G_0 is the dynamic shear modulus, obtained by the seismic method. Note that design strain in untreated materials of an airfield structure is of the order of 10^{-3}, what corresponds to a Gs / Go of about 0,45 for the considered material.
Secondly, asphalt material behaviour depends on the stress frequency. Therefore the backcalculated moduli values should be adjusted to be representative of the behaviour under real loadings.

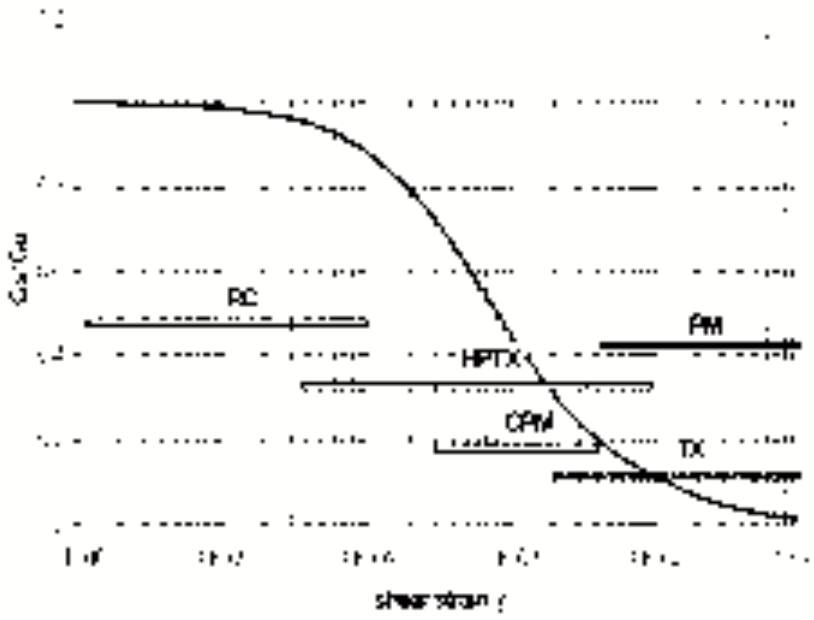

Fig. 0-11 Typical variation of normalized shear modulus as a function of shear strain (blue curve), after [Puech et al., 2004]

Several methods have been proposed to correct the untreated material modulus with respect to the strain level. [Puech et al., 2004] propose the general following stress-strain relationship:

$$G_S / G_0 = 1/\left(1 + a \cdot \gamma \cdot \left(1 + 10^{-b\gamma}\right)\right) \quad \textbf{(0-5)}$$

where the coefficients *a* and *b* are soil type dependent.

In the absence of an empirical relation between G_S and G_0 [Kurtulus, 2006] proposes (Fig. 0-12), to find G_S, to use the laboratory trend.

$$G_{S,field} = \left(G_{S,lab} / G_{0,lab}\right) \times G_{0,field} \quad \textbf{(0-6)}$$

where $G_{S,field}$ is the shear modulus at γ strain, $G_{0,field}$ the seismically determined moduli, and $\left(G_{S,lab} / G_{0,lab}\right)$ the laboratory normalized shear modulus.

(0-6) is eventually corrected to take into account the uncertainty in the trend of the shear modulus reduction curve. The reference shear strain (shear strain at which G_S/G_0 is 0.5) is thus adjusted using:

$$\gamma_{r,field} = \left(V_{S,field} / V_{S,lab}\right) \times \gamma_{r,lab} \quad \textbf{(0-7)}$$

Laboratory values are obtained from Resonant Column tests (see appendix 1.1) for strains under 10^{-4}, and using classical triaxial testings above this threshold. Laboratory results are necessarily affected by sample disturbance [Puech et al., 2004].

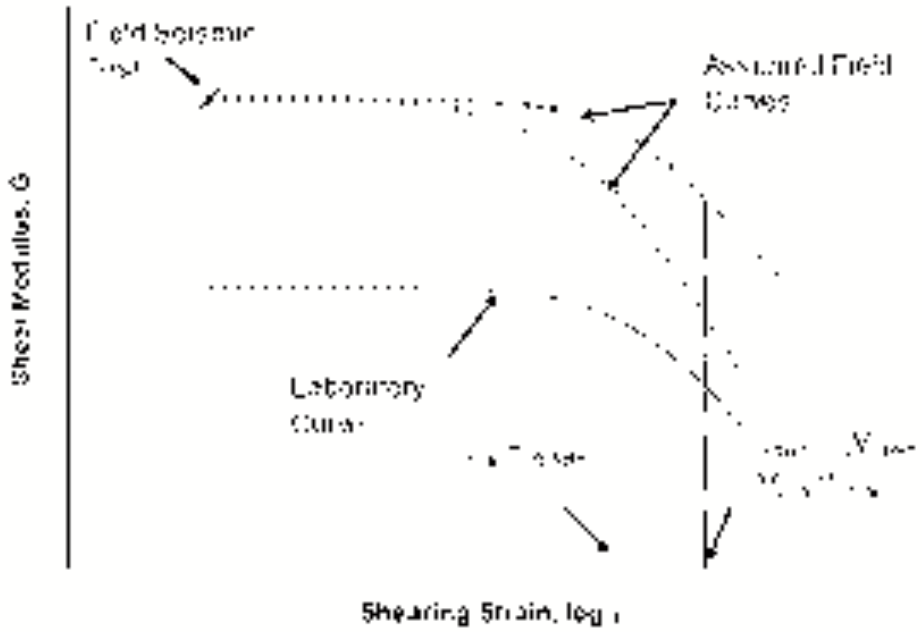

Fig. 0-12 Extrapolation of the field shear modulus from seismic determined shear modulus, after [Kustulus, 2006]

It can be observed in Fig. 0-12 that the laboratory G moduli are less than the in-situ values. [Puech et al., 2004] note that laboratory tests can underestimate the dynamic shear modulus by a ratio of 2 to 3.

As a conclusion, the strain level produced during the SASW tests is problematical. Corrections are possible, but they necessitate information on the material and scientific know-how.

Besides, note that the method provides discrete measurements of the structural conditions.

1.3 Deflection-based methods

Four subcategories can be distinguished for these methods, according to the nature of the applied load. This one can be a static or quasi-static (slow moving) load, steady-state vibratory load, impulsive transient load, or traffic speed rolling wheel methods.

1.3.1 Static or slow moving loads devices

a - Measuring principle

These tests consist in measuring the deformation of the pavement surface under a static loading or during the pass of a test vehicle at low speed. Measurement can be manual or automated.

b - Main devices

– Manual measurements

Deflections are measured by 1- placing manually a Benkelman Beam (BB) [Kruse, 1968] at the pavement surface. This measurement device was invented in 1953 by A. C. Benkelman of the U.S. Bureau of Public Roads for use at the AASHO Road Test and is still a classical evaluation tool, or 2- using other measurement systems, before applying a static or slow moving load.

STAC has developed its own slow moving method for airfield pavement testing, based on an inclinometer system (Fig. 0-13 and Fig. 0-14). An array of inclinometers is placed at the surface of the pavement before the pass of a test vehicle towing an A340 two-wheel landing gear, loaded at 25 tons (250 kN) per wheel. The inclinometer system allows measuring the slopes at the surface of the pavement at the pass of the reference 25 tons rolling wheel. Double integrating allows reconstituting the deflection basin. The test vehicle travels at speeds of up to 3 km/h (creep speed).

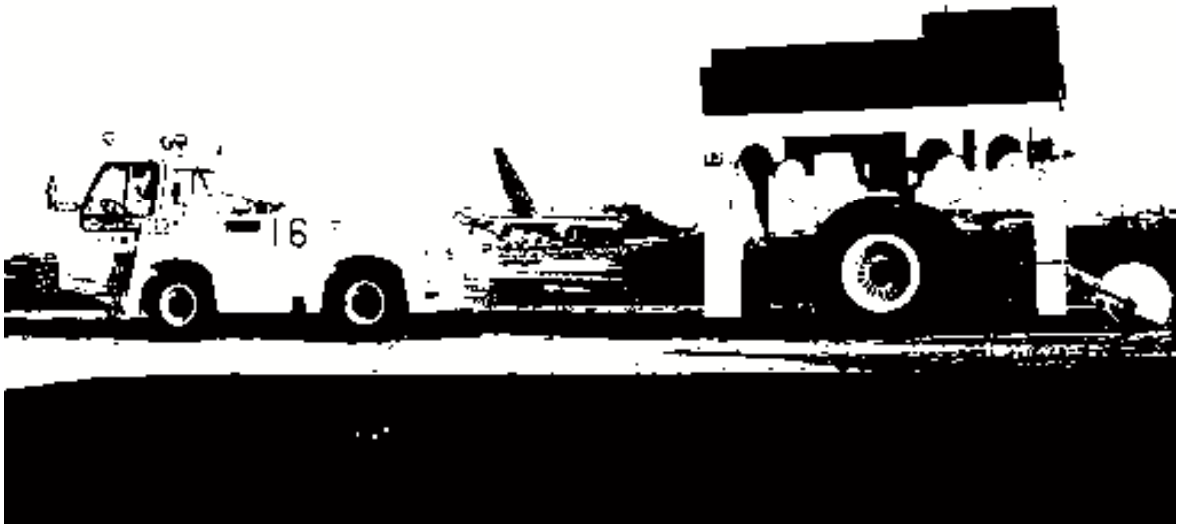

Fig. 0-13 STAC's A_{340} two-wheel landing gear loaded at 25 tons (250 kN) per wheel here trailed by the Airbus truck on the HTPT test facility (Photograph by D. Guédon, Toulouse LRPC)

Fig. 0-14 STAC's inclinometer system, zoom view (Photograph by D. Guédon, Toulouse LRPC)

- Automated slow moving loads measurements

Testing devices including automatic recording of deflections during slow rolling of a truck have been developed. Interpretation relies on the analysis of the general deflections basins and/or on the pavement curvature C (x) = d''(x)/V^2 where *d"(x)* is the second derivative of displacement with respect to distance and *V* the vehicle forward velocity.

- Lacroix deflectograph

Fig. 0-15 The Lacroix Deflectograph (source: LCPC's database)

The technology of the deflection beam was automated in 1957 by Lacroix who developed the French so-called Lacroix Deflectograph ([Lacroix, 1963], Fig. 0-15). This apparatus is widely used in Europe and other parts of the world for road testing. It inspired the British deflectograph and the Traveling Deflectometer developed by the California Division of Highways [Zube and Forsyth, 1966]. Several versions of this device have been constructed [de Boissoudy et al., 1984] until the actual one: the "Flash" version [Vialletel and Simonin,1997].

The measurement relies on automated Benkelman Beam tests under both rear dual wheels. A measurement cycle is divided into 3 steps. First, each beam is placed on the pavement surface. Second the slopes variations under pass of the corresponding dual rear wheels are measured and third the beam is taken away and repositioned front to its initial position for the next measurement cycle. Vertical displacements are deduced from measured slopes, so that the influence line of the vertical displacement is obtained.

With the assumption that the pavement is longitudinally homogeneous and at constant vehicle speed, the deflection basin is easily deduced.

The load applied is usually 80 kN and the vehicle forward velocity is limited to 5 km/h (8 with the Flash version) (walk speed). The interval between 2 consecutive measurements is 5 m. The respective velocities of the British deflectograph and travelling deflectometer are 2,5 and 0,8 km/h, standard rear axle loading are respectively 6 to 10 tons and 15 000 lbs (= 68 kN) and the interval between 2 consecutive measures are 4 m and 3,8 m.

The main drawbacks of these apparatus are:

- the load moves at walk speed
- the measurements are not continuous but discrete
- the limited length of the measuring beam whose main consequence is the lack of a fixed reference for the deflection readings (the supposed reference being in reality in the influence area of the loaded wheels), and which also prevents the full deflection basin from being recorded. This problem is increased when testing thick pavements. Geometrical modifications are regularly brought to improve the device.
- it is generally dedicated to road testing as the weight is too light for airfield pavements assessment, and heavier weights would imply an even larger influence radius.

- Curviameter

The curviameter (Fig. 0-16) is classified here even if its speed (18 km/h ; running speed) is intermediate between the creep and walking speed and the traffic speed. This apparatus used in France and Belgium is presented in detail in [Paquet,1977] and [Lepert et al., 1997]. It was invented by the French Centre Experimental de Recherches et d'Etudes du Bâtiment et des Travaux Public (CEBTP). The measuring principle is comparable to the Lacroix Deflectograph, except that the Benkelman Beam is replaced by a measurement geophone fixed on a continuous 15 m chain. Contrarily to the Lacroix Deflectograph, only one rear dual wheel (the right one) is instrumented. The chain lays on the pavement surface from 2,5 m in front of the dual wheels and until 1,5 meters behind, passing between the two wheels. In reality 3 geophones are fixed on the chain. The system is studied so that at each measurement time only one geophone lies on the pavement surface. The considered geophone remains at the same position on the pavement as the dual rear wheels roll over it, deforming the pavement. This process allows the measurement of an asymmetric (2,5m + 1,5m) 4 m deflection basin. One basin is measured each 15/3 = 5 meters.

The main shortcomings of the Curviameter are:

- its low driving speed (even much better than Lacroix Deflectograph)
- the measurements are not continuous
- it is generally dedicated to road testing as the weight is too light for airfield pavements assessment.

It is also evoked in [Hildebrand, 2002]:

- its in-ability to drive in curves
- a limited deflection data sampling frequency.

Fig. 0-16 Curviameter

c - Advantages/shortcomings of the method

The main shortcoming of these methods is that the vehicle displaces over the pavement at creep velocities (except for curviameter for which velocity is intermediate). This raises the problem of the representativity of the test, asphalt layers being highly dependent of the stress frequency.

Note that these apparatus provide only discrete structural information on the pavement.

1.3.2 Steady-state vibratory loading devices

The devices presented here impart steady-state vibratory loading at the surface of the pavement, supposed to well simulate the effect of a wheel pass. Another apparatus has been classified in this category, even if tests are not stationary but performed at creep speed: the RDD.

Background

First researches on these pavement testing methods were conducted by the U. S. Army Corps of Engineers (USACE) at the Waterways Experiment Station (WES), in cooperation with Shell researchers in the mid-1950's. By the mid-1970's, these methods have become the standard methods to assess pavement strength in the US, with the massive 16-kip (70 kN) vibrator (Fig. 0-17) becoming the reference testing device.

a - Measuring principle

The principle of these apparatus is to reproduce the load induced by the pass of a rolling wheel without driving a vehicle. Thanks to a dynamic force generator, a sinusoidal force is produced, superimposed on a static preload weight. The magnitude and shape of the induced deflection basin are analysed to assess the pavement subsurface structure.
Two manners of generating the force are possible:

1) using counter-rotating eccentric weights
2) using electrohydraulic systems

In the first case, the vibrator can apply only one force amplitude at any given frequency. On the contrary for electrohydraulic systems the amplitude of the loading is independent of the driving frequency. Thus any given load can be generated at different frequencies.

In order to simulate the pass of a vehicle, the force signal should start from zero, rise to peak, and return back to zero i.e. the sinusoid amplitude and the preload weight should be similar. According to [Barksdale, 1971] a 25 Hz frequency is necessary to simulate a vehicle passing at 45 mph (75 km/h) over the pavement. Thus the generated response is low-frequency oscillatory with regards to the SASW method.

Interpretation of the results is detailed in [Weiss, 1975]. This study gives a method for determining the shear modulus and thickness of each pavement layer directly from the measured dynamic load-deflection curves. An expression of the dynamic stiffness of the pavement is given. The study shows the dependence of the dynamic stiffness values on the dynamic load, static load and baseplate radius used during the measurements.
Recommendations of Weiss are that the vibrator must be capable of:

- applying a series of static loads
- generating a series of dynamic loads over a range of constant frequencies
- operating in a frequency range that includes the critical frequency introduced in the study
- applying a series of baseplate sizes to the pavement

b - Main devices

Several devices were designed over the world, the main devices being the different WES vibrators (The 9 and 16 kips and the 50 WES kips), the NDPT (non destructive pavement test) van developed by the Civil Engineering Research Facility (CERF), the Federal Highway Administration's NDT Thumper and the Dynaflect and the Road Rater (existing in various models). The two last devices, are still available commercially. All the quoted devices are described in details by [Green and Hall, 1975]. In this paper a comparative study of the main existing vibrator devices was carried out, by choosing as the reference apparatus the WES 16-kips vibrator. The dynamic stiffness given by the different apparatus were found to be significantly different. [Green and Hall, 1975] recommended further studies to establish correlations between the different apparatus. Let us interest here to the WES-16kips, the Dynaflect and the Road Rater.

- The WES-16kips

This device, not in use any more, presented an electrohydraulic system embanked in a semitrailer, which allowed applying a static preload of 16 000 lbs (70 kN) on the studied pavement surface, and then producing a vibratory load up to 30 000 lbs peak-to-peak over a frequency range from 5 to 100 Hz. These loads were transferred to the pavement surface through a 45 cm diameter steel plate, approximating the surface area covered by a Boeing 747 tire. Three load cells monitored the vibratory load while velocity transducers on the load plate and at radial points on the pavement measured the deflection. Embanked electronic system allowed immediate determination of dynamic stiffness. This device was in the 70's and 80's extensively used on airfield pavements and was considered as the reference testing device. Nevertheless the heavy vehicle was not practical to use and necessitated four persons for tests. Hence the development of light devices like Dynaflect and Road Rater was privileged.

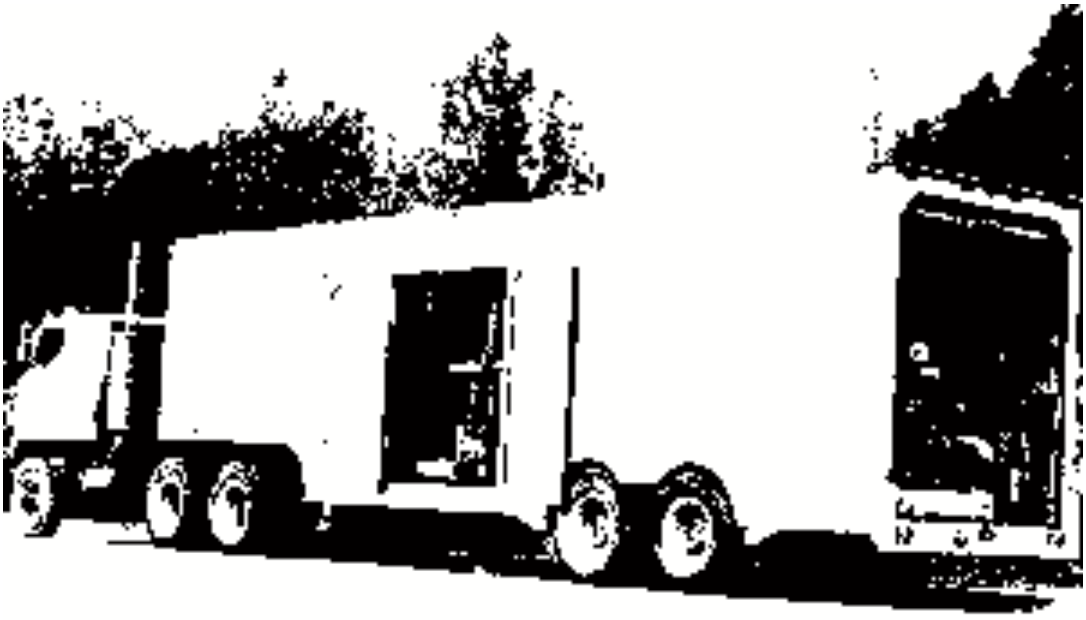

Fig.0-17 The WES 16-kip Vibrator; sources: US army website (http://gsl.erdc.usace.army.mil/gl-history/Chap7.html)

- The Dynaflect

The Dynaflect is a trailer mounted device presenting counter-rotating eccentric weights generating a peak-to-peak load of 1 000 lbs (= 4,5 kN) superimposed to a 1 800 lbs (8 kN) at a (fixed) frequency of 8 Hz. Force is applied on two steel load wheels placed 0.5 meters apart. The peak-to-peak deflections are measured with five geophones, the first one being placed directly between the wheels, and the others on the central symmetry line.

The Dynaflect is fast and simple to operate. The total time required for performing a test is about 2 minutes which includes the time required for the lowering and raising of the force generator and deflection sensors.

Nevertheless, the 4,5 kN maximum peak-to-peak force generated by the Dynaflect may not be enough to simulate the field deflection expected due to heavy loadings. Furthermore, the Dynaflect can measure deflection basins up to a 1 m radius. This is not large enough for thick pavement like airfields pavement.

- The Road Rater

The Road Rater is another trailer mounted device. It includes a hydraulic vibrator capable of varying both the load magnitude and the frequency. Ranges depend on the considered model. For intermediate models for instance, the dynamic force can vary between 500 and 5500 lbs (2 to 24 kN), the most expensive models of the Road Rater being able to generate peak to peak forces as high as 8000 lbs (35 kN), while the frequency ranges from 6 to 60Hz. The loads are transferred to the pavement surface through a 45 cm diameter steel plate. The deflection basin is measured with a set of four geophones, one of them being located at the centre of the load and the others being located radially with 300mm spacing. As for the Dynaflect, maximal width of the measured deflection basin is about 1 m, what is not enough for airfield pavements.

- Rolling Dynamic Deflectometer (RDD)

The rolling dynamic deflectometer (RDD) [Bay and Stokoe, 1998], developed at the University of Texas at Austin is another truck-mounted device which applies large sinusoidal dynamic forces to the pavement through specially designed loading rollers. The resulting deflections are simultaneously measured by rolling sensors. Forces applied to the pavement and resulting dynamic displacements are recorded. The peak-to-peak load is up to 45 kN superimposed to a 22,5 kN static load.

Unlike the previously described devices, the RDD allows performing continuous measurements.
Furthermore, the principle of moving the load over the pavement allows limiting the creep phenomena encountered in steady-state devices due to static constant load. However displacement speed of the test vehicle is only 2,4 km/h (creep speed).

c - Advantages/shortcomings of the method

The steady-state vibratory methods allow approaching the load effect of a rolling wheel.

Nevertheless the historical device (the WES-16kips) presented an operational weakness: it was of too heavy functioning and has been discarded. Furthermore light commercial devices are limited, especially for airport use. Actually the Dynaflect has a fixed magnitude and frequency of loading, while the Road Rater applies too low loads with basic versions. For both apparatus the length of the measured deflection basin is too short to allow a good assessment of the deep layers properties.

The RDD principle is interesting as it allows continuous measurements over the pavement. However the applied load is too light to be representative of airfield traffic.

1.3.3 Transient impulsive loads devices

By the mid-1980's the transient impulsive load devices moved gradually from a research to an operational phase. They had the advantages of being much lighter, easier to operate, and less expensive than the vibratory devices, so that they began gradually to replace them.

a - Principle

The principle of these devices consists in 1- delivering a transient impulsive load to the pavement surface which simulates the loading history associated with the pass of an aircraft rolling wheel and 2- analyzing the ensuing pavement response.

b - Main devices

The only commercially available impulse device is the Falling Weight Deflectometer for roads and the Heavy Weight Deflectometer (Fig. 0-18) its heavy version for airport pavements. They are evolved from the so-called French "déflectomètre à boulet" [Bretonnière, 1963] developed by the LCPC.

As the name of the apparatus indicates it, the transient impulsive load is generated onto the surface of the pavement by a mass dropped on a load plate and transmitted to the pavement through a buffer system (Fig. 0-18 b). The induced pulse time ranges from 30 to 40 ms, which corresponds to a 30 to 45 MPH (50 to 70 km/h) velocity range [Barksdale, 1971]. The pulse shape is approximately sinusoidal, and representative of the shape of the surface stress induced by a rolling wheel [Barksdale, 1971]. The maximal impact load applied by the falling mass may be set up to 300 kN. This value is close to the maximal load ever reached with a single-wheel tire (297 kN for the Airbus A340-600), while larger aircraft (A380-800 and B777- 300 ER) are characterized by loads on single-wheel tire ranging from 260 to 270 kN. The induced surface deflections are continuously measured during the HWD test by means of velocity transducers (geophones) placed directly beneath the plate and at several radial offsets from the plate centre (Fig. 0-18 c).

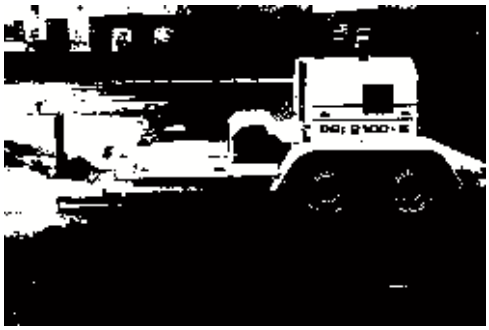

(a)

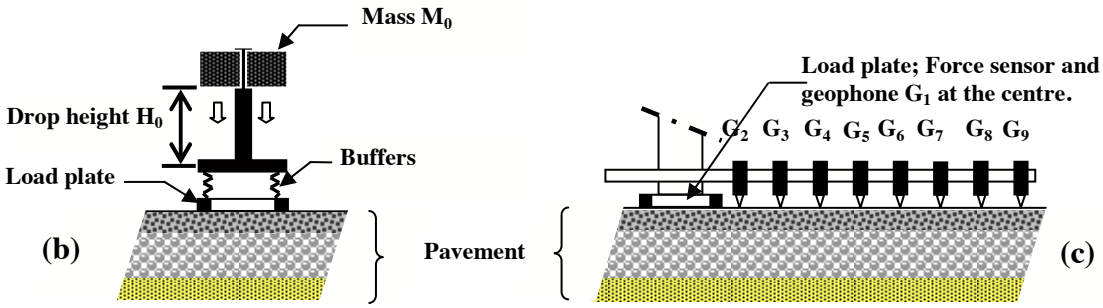

Fig. 0-18 a- The HWD of the STAC, b- The falling weight system, c- Recording of the deflection basin, after [Broutin, 2009b]

HWD measurement has been proven efficient by numerous studies and has become a standard for airfield pavement testing. Presentation of the apparatus is here intentionally synthetic. Further pieces of information are available in [COST, 1999]. This guide enumerates the European recommendations for its use. In the appendix 1.3, STAC's protocol for operational operating and routine data analysis is presented. The second part of this literature overview is dedicated to usual methods for data analysis.

c - Advantages/shortcomings

The HWD recreates closely the load effect of an aircraft rolling wheel over the pavement. Its main shortcoming is that it only allows performing single point bearing capacity tests. The resulting discrete structural mapping of the tested area, is associated to several risks highlighted *supra*.

1.3.4 Automated high speed rolling wheel loading devices

F/HWD perform single-point bearing capacity tests. The apparatus is successively positioned over each test point and remains stationary during the test. It has a double shortcoming.

The first one, already discussed, is linked to the measurement discreteness. The second one raises the problems of safety (particularly for FWD on highways), traffic disturbance, and cost. Therefore research efforts have been made within the last years in several countries, amongst which US, Sweden and Denmark, to produce a high speed monitoring device for the follow-up of network pavement bearing capacity. An advanced technology, based on structured light analysis, is also in research phase in France.

a - Measuring principle

The measuring principle varies according to the considered devices. Nevertheless the general principle is the same for all devices. It consists in measuring with embanked non-contact systems the pavement deformation at the pass of a loaded rolling wheel and in comparing the profile in loading conditions with a reference (i.e. unloaded) profile.

Note that the objective is not necessarily to assess the bearing capacity of pavement along the whole profile, even if this information would be the ideal one to obtain. First objective is to allow 1-determining bearing capacity levels, in order to define homogeneous areas and better target FWD tests 2- obtaining reliable relative measurements, in order to follow the evolution of the bearing capacity with time.

b - Devices

The American devices are the (Airfield) Rolling Weight Deflectometer ((A)RWD) [Briggs et al., 1999], and the Rolling Wheel Deflectometer (RWD) [Herr and Johnson, 1995], respectively developed by Dynatest Consulting and Quest Integrating and Applied Research Associates. The Swedish device developed by VTI (the national Swedish research institute for roads and transports) is called the Road Deflection Tester (RDT) [Andren and Lenngren, 2000]. Finally the Danish device jointly developed by DRI (the Danish Institute for Roads) and the Greenwood SAS Engineering enterprise was initially called High Speed Deflectograph (HSD) and then renamed as TSD (Traffic Speed Deflectometer).

All of these apparatus (except airfield RWD) allow performing measurements at normal traffic speed (up to 80 km/h). All characteristics (maximal velocity speed, maximal load) are summarized in the Table 0-1. Note that since these apparatus correspond to road network management stakes, load levels have been designed accordingly. The airfield rolling weight deflectometer, dedicated to airfield pavements, is the exception. Its original version allowed performing measurements at a maximum speed of 10 km/h with load up to 222 kN but it has then been modified to measure deflection at an increased speed of 32 km/h under a 40 kN wheel load.

In the forthcoming section, the measurement principle is briefly presented and the device advantages and shortcomings discussed.

- **Laser distance-measurement methods**

Road Deflection Tester, Rolling Wheel Deflectometer, (Airfield) Rolling Weight Deflectometer all use laser sensors to measure distances to pavement surface. General measurement principle consists in measuring twice the same profile of the pavement. In the case of RDT the transverse profile is studied whereas in the case of both other devices the longitudinal profile is considered. In a first step the profile is taken outside the influence area of the loaded wheel and in a second step it is measured inside. The deflection imparted to the pavement by the loading wheel is then calculated as the difference between the loaded and unloaded profiles of the pavement. This relies on the assumption that the initial deflection at extreme points of the profile is negligible.

RDT has been evaluated in the frame of the European FORMAT (Fully Optimized Road MainTenance) project [FORMAT, 2005], based on field testing performed in UK and in France, and regarding to the two following reference apparatus. Independent reports by the UK Highway agency and the LCPC draw similar conclusions: 1- the definition of homogeneous area from RDT does not correspond to the one obtained from FWD tests, 2- a pretty good accordance exists between FWD and Lacroix deflectograph, no correlation is found between RDT and these apparatus, 3- RDT is not capable of determining significant deflections levels, 4- RDT measurements are not repeatable between two consecutive runs on the same site both in terms of deflection levels and deflection variability.

These observations can have several explanations: 1- the principle implies that the laser sensors must cover two times the exact same point on the pavement surface ; this is not obvious, especially in curves and the effects of macrotexture or rutting can distort the results. 2- deflections are so small that the resolution of distance laser sensors may not be sufficient, but above all 3- the reference point (where deflection is supposed null) is only 1,20 meter in the principle (0,50 meter in practice) from the wheel.

A similar comparative field study performed in Texas in 2003 demonstrated the usefulness of the Rolling Wheel Deflectometer as a network structural evaluation tool.

- **Doppler-laser systems**

The Traffic Speed Deflectograph ([Hildebrand et al., 2000] or [Rasmussen et al., 2002]), (Fig. 0-19), uses a more complicated measuring principle than the previous devices and is though to overcome the previous problems. Four laser Doppler sensors mounted on a rigid beam in front of the loading wheel measure the vertical velocity of the deflection of the pavement surface due to a 10 tons (100 kN) axle load with a velocity speed of up to 80 km/h. Three of the sensors are inside the deflection basin and one outside for reference.
The deflection slope is calculated by dividing the deflection velocity by the driving velocity. A simple 2–parameter model (considering that the pavement behaves like an elastic beam on a foundation of linear springs) is then used to evaluate the full basin. The model parameters are identified using the slopes measured by the 3 sensors. Their knowledge allows the determination of the Structural Curvature Index 300, (SCI_{300}), defined as the central

deflection minus deflection at 300 mm offset ($SCI_{300} = d_0 - d_{300}$) and the centre deflection (d_0), which will be used to assess the bearing capacity of the pavement.

LCPC evaluated the TSD in the frame of the FORMAT project (2005). Detailed results are available in [Lièvre, 2004]. Main conclusions are 1- the data provided by the TSD, present a good repeatability, with regards to the one of Lacroix Deflectograph and FWD, 2- TSD can detect significant differences of deflections and 3- deflections variations present the same trends as those obtained by the FWD.
Furthermore [Simonin, 2006] demonstrated using the Alizé software [Alize] that a relation allows deducing the maximal deflection measured by the traditional apparatus (FWD, Flash deflectographs) from the slope deduced from TSD tests. Repeatability of the measurements was studied with regard to the one of Lacroix Deflectograph and FWD. Conclusion is that TSD can detect significant differences of deflections so as to provide a reliable mapping in terms of homogeneous areas.
[Rasmussen et al., 2008] studied the comparison between measurements on tests sections repeated at a one-year interval. The results show a good repeatability of SCI_{300} and d_0 and that TSD is capable of detecting changes in bearing capacity, repair work and differences caused by road condition or maintenance actions.

Fig. 0-19 Traffic Speed Deflectometer (TSD) on the LCPC's Nantes site in 2003, after J.M. Simonin, French "Assessment of the Road Deflection Tester in France" report, [FORMAT, 2005]

- **Structured light (SL) system**

This advanced method for non-contact measurement of pavement deformation under moving load consists in projecting a structured light on the road pavement and studying its reflection. The principle of mathematical analysis will not be detailed here. Is is presented in [Muzet et al., 2009] or [Simonin et al., 2009]. General idea is the following: A fringe is projected on the pavement with an alpha angle with the horizontal plane (Fig. 0-20). The reflected image reflected is studied using a video camera placed at the vertical of the test point. The resulting distortion of the projected pattern depends on pavement surface shape.
Letting p_p be the period of fringes projected on a planar surface and p_a the one the reflected fringes, and α the angle between the incidence of light and the observation direction, the height increment Δh is expressed by:

$$\Delta h = p_p - p_a / \tan \alpha \qquad \textbf{(0-8)}$$

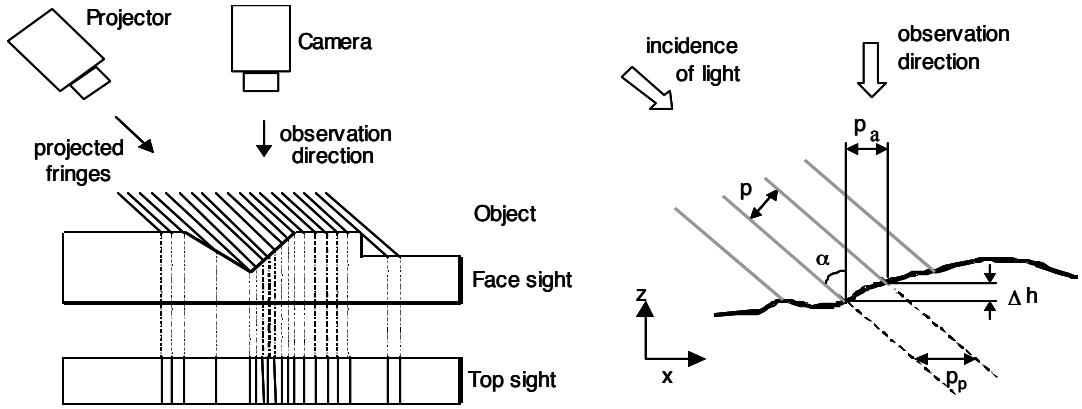

Fig. 0-20 Principle of the fringe projection method, after [Simonin et al., 2009]

The determination of the deformation under a loaded wheel is based on the difference between the under-load image and a reference image corresponding to a non loaded state.

First feasibility tests have been performed on structures of the LCPC's "fatigue carrousel"at slow speed; velocity of the carrousel arm was 4,3 km/h.
Fig.0-21 shows the successive images in grey levels corresponding to the pass of a wheel (at the right of the image).

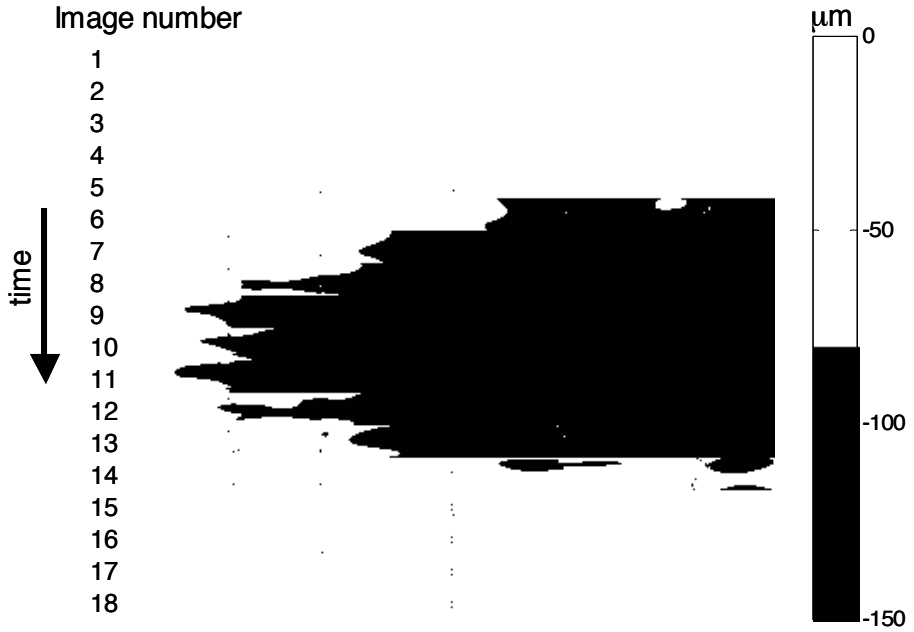

Fig. 0-21 Successive images of displacements taken at 10Hz during the pass of the carrousel arm. The load is on the right side

c - Advantages/shortcomings

None of the traffic speed rolling wheel devices is yet operational for routine testing. However it can be expected that this type of equipment will play a main role in pavement structural assessment in the coming years.

General conclusion of NDT methods overview

Table 0-1 summarizes the main characteristics of the aforementioned devices. Positive points are highlighted in green, drawbacks in red, and intermediate cases in orange.

	Continue /Discrete	Max. speed [m.s^{-1}]	Max. load [kN/wheel or dual wheel]	Possible improvements
STBA Trailer	D		400	Operational weakness (Heavy + Time consuming tests)
Goodman	D			This device has been given up
SPA	D			Representativity of SASW tests?
STAC's Inclinometers	D	3-4	250	Speed to be increased because of creep phenomena.
Lacroix Deflectograph	D	8	65	Load to be adapted for airfield pavement. Speed to be increased because of creep phenomena.
Curviameter	D	18	65	Load to be adapted for airfield pavement
WES 16-kip	D		Static: 70 Dynamic: 70	This device has been given up (Operational weakness)
Road Rater	D		Static: 35 Dynamic: 35	Load and measurement system to be adapted to airfield pavements
Dynaflect	D		Static: 8 Dynamic: 4,5	Load and measurement system to be adapted to airfield pavements
F/HWD	D		300	
RDD	C	2,4	Static: 45 Dynamic: 22,5	Load to be adapted to airfield pavements. Speed to be increased because of creep phenomena.
RWD	C	105	80	Laser maybe not adapted to problem Problem of the reference to be solved.
ARWD v0	C	10	222	
ARWD v1	C	32	40	
RDT	C	97	70	
HSD/TSD	C	80	49	Load to be adapted for airfield pavement
SL	C			In early test phase

Table 0-1 General overview of existing pavement structural assessment devices

As a conclusion, HWD seems to be the ideal device to assess airfield pavements, in the sense that applied load is the most representative of real traffic amongst existing routine test devices. Indeed, nature of the imparted action (sinusoidal dynamic force), force magnitude and pulse time duration are close to real traffic load effect. Tests are operationally efficient. Its main shortcoming is that it only provides discrete data on the pavement structural conditions.
Some devices are being developed which study the response of the pavement under a loaded wheel at traffic speed. For the moment these devices do not allow measuring deflections, but other structural index giving valuable information about homogeneous area and local weak zones. Let imagine in a near future a method to assess airfield pavements which would combine both types of devices, the traffic speed devices allowing determining a relevant distribution of the HWD tests over the pavement for further analysis.

2 - HWD tests modellings

As aforementioned, general HWD principle consists in identifying parameters of a predefined pavement model, and using obtained information for the determination of the pavement remaining structural conditions in a so-called “forward calculation” phase. Thus, in this part, an overview of existing mechanical modellings is first given. Then backcalculation procedures are discussed. Finally the “forward calculation” is presented.

2.1 Modelling

A model is defined by 1- a geometry with associated boundary conditions and external actions, 2- cinematic laws (reduced to equilibrium in static modelling) governing allowable internal displacements, 3- constitutive local bulk behaviour laws linking strains to applied (imparted) stresses and 4- surface behaviour laws modelling interface conditions when studying stratified media.

The flexible pavement is generally modelled as a multilayered domain. The underlying subgrade can either be of infinite extent, or lie on bedrock. The pavement lateral extent is generally supposed to be infinite and the material behaviour to be isotropic (no effect of the loading distribution on the material properties) so that the model can be considered as axisymmetric.

Usual F/HWD data analysis methods propose static modelling, but some dynamic modellings are available.

The behaviour laws are usually elastic laws. Nevertheless, nonlinear or viscoelastic behaviours can be introduced to improve respectively the unbound and asphalt materials modelling.

Interfaces are generally assumed to be fully bonded under heavy dynamic load. The most usual pavement models rely on this hypothesis. Nevertheless, [Romanoschi and Metcalf, 2002] show that this hypothesis is not so obviously justified and can lead to significant errors.

2.1.1 Behaviour laws

a - Bulk constitutive behaviour laws

- Linear elastic isotropic behaviours

The behaviour of these materials obeys Hooke's law, written as follows in tensorial form:

$\underline{\underline{\varepsilon}} = \frac{-\nu}{E} Trace\left(\underline{\underline{\sigma}}\right)\underline{\underline{\delta}} + \frac{1+\nu}{E}\underline{\underline{\sigma}}$, with $\underline{\underline{\varepsilon}}$ and $\underline{\underline{\sigma}}$ respectively the strains and stresses tensors, and E and ν the Young's modulus and Poisson's ratio of the considered material

Physical meaning of these parameters is the following:
When applying axial compressive or tensile strength to a sample of linear elastic isotropic material, the ratio between axial stress and strain is E, and ν is the ratio between transverse and axial strain.

- Non linear isotropic behaviours

Unbound material (gravels, subgrade) constitutive of the pavement may present non linear behaviours, which means that the elastic modulus depends on the stress state.

Several models are available, presented in details in [Samaris, 2006] and [Absammad, 2006]. The most usual ones are the deviator stress model, the bulk stress model or so-called "K-θ model" the Uzan model, and the Boyce model.

Let $\sigma_1 > \sigma_2 > \sigma_3$ be in 3-D the principal stresses, p be the mean normal stress,

$$p = \frac{1}{3}\left(\sigma_1 + \sigma_2 + \sigma_3\right) \quad \textbf{(0-9)}$$

and q be the deviatoric stress,

$$q = \sigma_1 - \sigma_3 \quad \textbf{(0-10)}$$

Let E be the material secant modulus. According to the chosen modelling, it is linked to stresses by the following relationships:

<u>- the deviator stress model</u>

$$E = k_1 \cdot q^{k_2} \quad \textbf{(0-11)}$$

Where k_1 and k_2 are constant (k_1>0).

<u>- the bulk stress, or "K-θ"model</u>

$$E = k_1 \cdot \left(3p\right)^{k_2} \quad \textbf{(0-12)}$$

For both previous models, if k_2 is positive material is qualified as stress-hardening. On the contrary, with k_2 negative, the material is stress-softening.

- Uzan model

The two previous models are combined in Uzan model, according to which:

$$E = k_1 \cdot p^{k_2} q^{k_3} \quad \textbf{(0-13)}$$

Where k_1, k_2 and k_3 are constant (k_1>0).

- Boyce model

A more complex relationship is proposed by Boyce:

Let K be the bulk compression modulus, and G the bulk shear stress modulus.

According to the Boyce model, these parameters can be expressed as:

$$K = \frac{\left(\frac{p}{p_a}\right)^{1-n}}{\frac{1}{K_a} - \frac{\beta}{K_a}\left(\frac{q}{p}\right)^2} \quad \textbf{(0-14)}$$

And

$$G = \frac{\left(\frac{p}{p_a}\right)^{1-n}}{\left(\frac{1}{G_a}\right)} \quad \textbf{(0-15)}$$

With K_a, G_a and n the parameters of the model, p_a the atmospheric pressure,

and $\beta = (1-n)\frac{K_a}{6G_a}$ **(0-16)**

The secant modulus is:

$$E = \frac{9G_a\left(\frac{p}{p_a}\right)^{1-n}}{3 + \frac{G_a}{K_a}\left(1 - \beta\left(\frac{q}{p}\right)^2\right)} \quad \textbf{(0-17)}$$

- Viscoelastic behaviour

In the previous modellings, the material behaviour is independent of time. In schematic representation, elastic (linear or non linear, regarding the secant modulus) behaviours are

represented with a spring. The relationship between stress and stain is $\sigma = k\varepsilon$ with k the spring constant.

On the contrary, asphalt materials present time-dependent behaviours, so that their modelling in the same schematic representation includes dashpots. At the dashpot, $\sigma = \eta \frac{\partial \varepsilon}{\partial t}$ with η the viscosity.

Fig. 0-22 presents several rheological models [Semblat, 1998]. The Q^{-1} parameter represented by Semblat is the quality factor

$$Q^{-1} \approx 2\xi \qquad \textbf{(0-18)}$$

ξ being the damping ratio in material

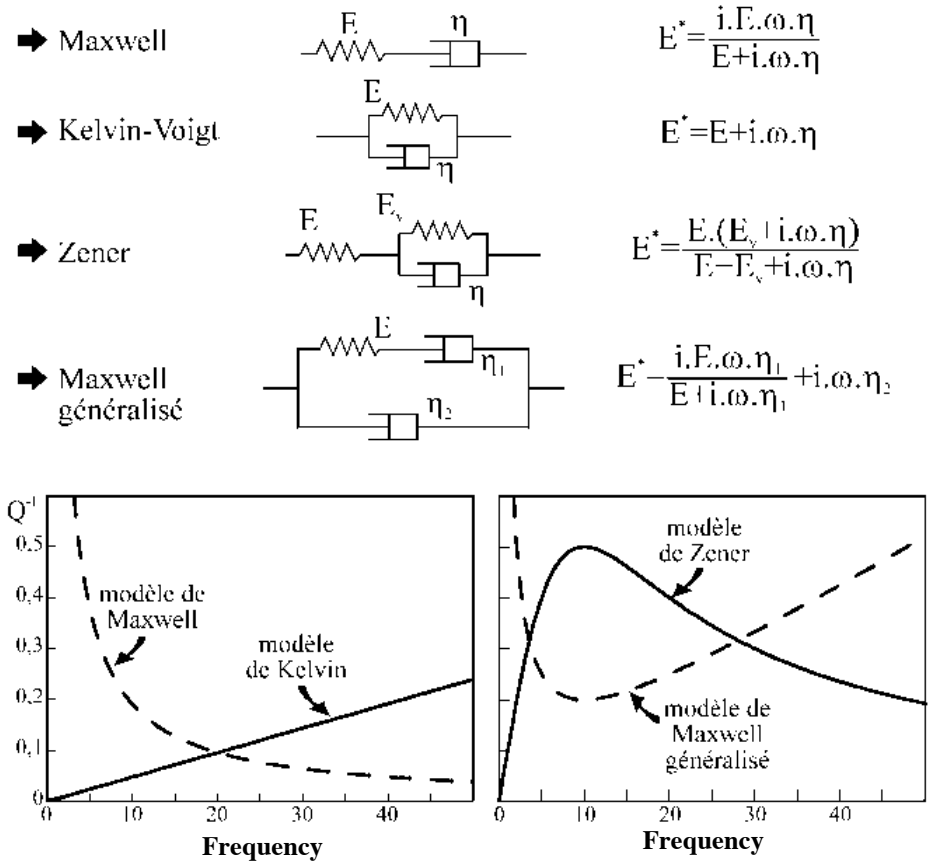

Fig. 0-22 Examples of rheological models and associated attenuation curve, after [Semblat, 1998]

The usual model used in France to model asphalt material behaviour is a little more complex that the previous models. It is the Huet and Sayegh model [Heck et al., 1998]. The rheological model is made of two branches. The first one is composed of a spring and corresponds to the static and long-term behaviours of the material. The second branch presents a spring and two parabolic (i.e. whose viscosity is frequency-dependent) dashpots.

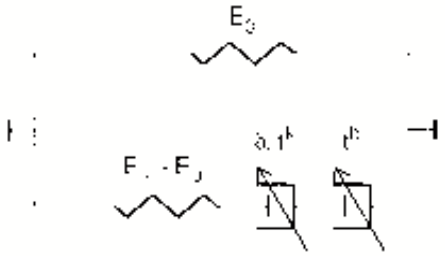

Fig. 0-23 The Huet and Sayegh model, after [Fabre et al., 2005]

According to this model, the complex modulus for a ω angular frequency and a θ temperature is given by:

$$E^*(\omega,\theta) = E_0 + \frac{E_\infty - E_0}{1 + \delta(-j\omega\tau(\theta))^{-k} + (-j\omega\tau(\theta))^{-h}} \quad \textbf{(0-19)}$$

Where E_∞ is the instantaneous elastic modulus, E_0 the static elastic modulus, k and h the parabolic dashpot coefficients (1>h>k>0) and δ a non-dimensional coefficient. Finally τ has the dimension of a time, and can be viewed as a delay time. Its expression depends on temperature according to:

$$\tau(\theta) = \exp(A_0 + A_1\theta + A_2\theta^2) \quad \textbf{(0-20)}$$

With A_0, A_1 and A_2 three scalar numbers.

The Huet and Sayegh model is thus a seven-parameter rheological model.

b - Interface modelling

The two basic modellings of interface conditions consider fully bonded interfaces or fully frictionless interfaces.

In all usual HWD modellings, pavement layers are assumed to be fully bonded under heavy load.

However as highlighted by [Romanoschi and Metcalf, 2002], from experimental observations, even if all usual backcalculation programms retain this hypothesis, it does not take place in the most situations. According to him, the simplistic modelling can lead to significant errors on moduli backcalculated with F/HWD, as shown by numerical studies.

The finite element method (see infra) has allowed the development of more precise interface modelling, than the aforementioned binary choice. Improved modellings can for instance involve:

- a Mohr Coulomb interface law can be introduced, with or without dilatancy, available in the main FEM codes.

- a Goodman model, proposed by [Romanoschi and Metcalf, 2002] in the context of HWD tests modelling. In this model, the shear stress at interface is proportional to the difference in the horizontal displacements of the 2 considered layers.

2.1.2 Pavement models

Different pavement models exist, according to the problem geometry, the nature of the load, or the behaviour laws. Main models are briefly described here, and their respective advantages and shortcomings are discussed.

a - The Boussinesq model

Boussinesq developed in 1885 a calculation method to determined stresses and strains due to a point load applied on the surface of an infinite homogeneous isotropic linear-elastic half-space (Fig. 0-24). Integration of his results allows determining stresses and strains for surface loads.

For the case of a q uniform pressure applied onto a circular load plate of « a » radius, the Boussinesq model gives the following vertical σ_z and ε_z stress and strain at the z depth:

$$\sigma_z = q \times \left(1 - \frac{z^3}{\left(a^2 + z^2\right)^{3/2}} \right) \quad \textbf{(0-21)}$$

$$\text{and } \varepsilon_z = \frac{(1+\nu)q}{E} \times \left((1-2\nu) + \frac{2\nu z}{\left(a^2 + z^2\right)^{1/2}} - \frac{z^3}{\left(a^2 + z^2\right)^{3/2}} \right) \quad \textbf{(0-22)}$$

Central surface deflection $d_z(0)$ is calculated using:

$$d_z(0) = \frac{2\left(1-\nu^2\right)a\,q}{E} \quad \textbf{(0-23)}$$

with E and ν the Young's modulus and Poisson's ratio of the constitutive material

Several calculation methods were developed from Boussinesq equations to determine surface deflection at a *r* radial distance from plate centre. General expression is:

$$d_z(r) = \frac{2\left(1-\nu^2\right)a\,q}{E} \times f\left(\frac{a}{r}\right) \quad \textbf{(0-24)}$$

where f is a function which is worth 1 for r = 0.

A standard choice [Ullidtz, 1987] is $f\left(\frac{a}{r}\right) = \frac{a}{r}$.

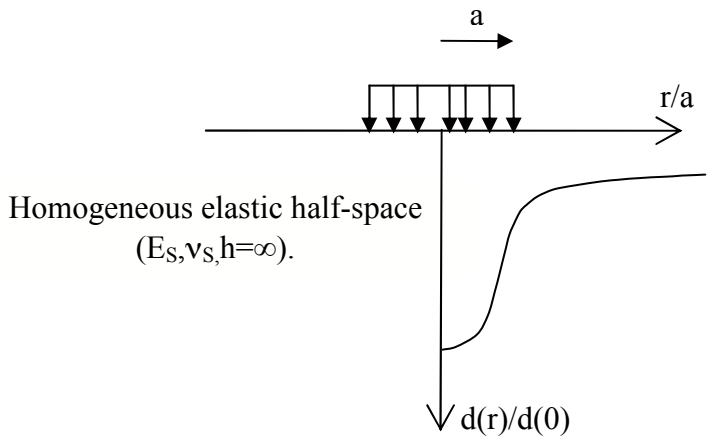

Fig. 0-24 The Boussinesq half-space model

- Model advantages/limitations

This model is well adapted to infinite subgrade. It proposes a very simple closed-form solution. However, it is not adapted for the whole pavement modelling, due to high stiffnesses of surface layers with regard to subgrade.

b - Burmister multilayered elastic static model

[Burmister, 1943] proposed a multilayer (at origin a two-layer) elastic model (Fig. 0-25). Layer interfaces are in this model either fully-bonded, either fully-frictionless. [Dejong et al., 1973] improved the interface modelling by allowing a continuum of bonding conditions between these two limits. [Van Cauwelaert et al., 1988] refined again the model by considering a Coulomb's law.

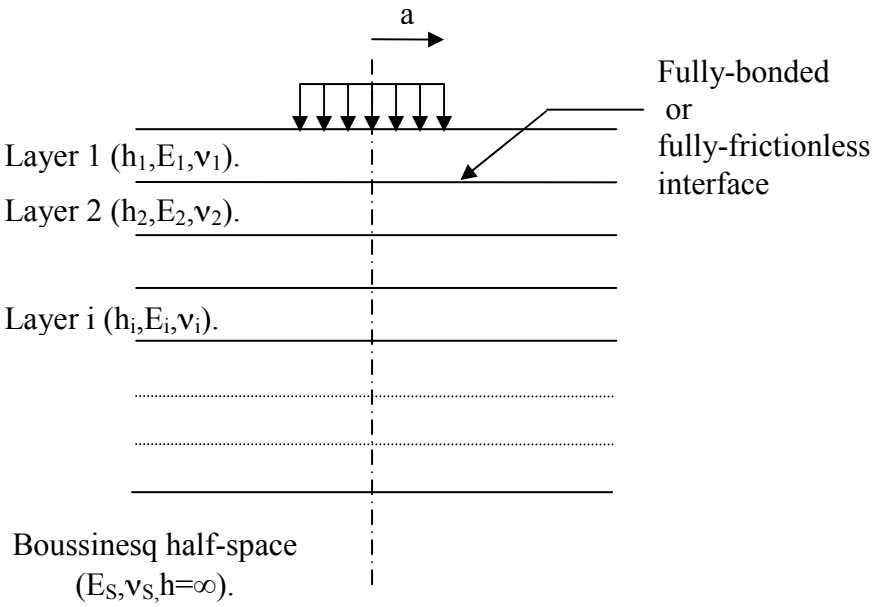

Fig. 0-25 The Burmister elastic multi-layered pavement model

Calculation of the stresses and strains imparted to the pavement relies on 3 assumptions:
- equilibrium,
- compatibility between normal and shear strains,
- stresses and strains are related according to Hooke's law.

Resolution method is not detailed here. It is available in appendix 3.2.

- Model advantages/limitations

The model provides efficient calculation of deformations, stresses and strains in multilayered elastic media. Bonding conditions can be chosen fully-bonded, fully-frictionless, or using a Coulomb's law.
However the model is static, so that no inertia and no viscoelasticity can be included for F/HWD data analysis. Neither can nonlinear behaviours be taken into account. Moreover the contact pressure is considered as constant, and the load plate cannot be modelled as rigid.

c - Method of Equivalent Thickness (MET)

The MET is an approximate calculation method of a multi-layered elastic pavement response.

It was invented in 1949 by Odemark and is presented in details in [Ullidtz, 1987]. It relies on the assumption that stresses and strains below a layer depend only on the stiffness of that layer. The multi-layered system is transformed in an equivalent half-space in which the Boussinesq equations are valid. Transformation is performed by equalling the inertias, i.e.:

$$I = \frac{\frac{1}{12} \cdot l \cdot h^3 \cdot E}{1-\nu^2} = Cste \qquad \textbf{(0-25)}$$

with E and ν the Young's modulus and Poisson's ratio of the constitutive material, h the layer thickness, and l an arbitrary length.

Let us interest to the transformation of a two-layer system into a Boussinesq half-space (Fig. 0-26) When considering pavement response in the upper layer (left), calculation is independent of the lower layer modulus E_2, arbitrarily chosen as equal to the upper modulus E_1. When considering pavement response in the lower layer (right), the two layers are replaced by an equivalent layer of h_e thickness. h_e is determined by writing:

$$\frac{\frac{1}{12} \cdot l \cdot {h_1}^3 \cdot E_1}{1-{\nu_1}^2} = \frac{\frac{1}{12} \cdot l \cdot {h_e}^3 \cdot E_2}{1-{\nu_2}^2}, \qquad \textbf{(0-26)}$$

Hence, if ν is the same for both layers

$$h_e = h_1 \cdot \sqrt[3]{\frac{E_1}{E_2}} \cdot \qquad \textbf{(0-27)}$$

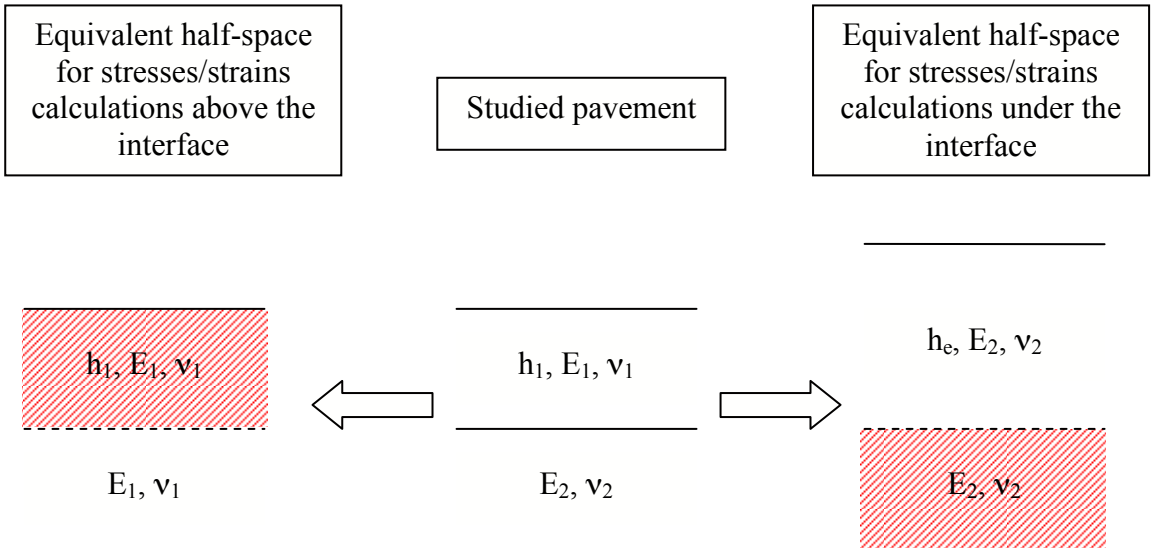

Fig. 0-26 Method of Equivalent Thickness ; transformation of the two-layer pavement into an equivalent Boussinesq half-space ; after [Ullidtz, 1987]

This calculation can be generalized to a n-layer system. The equivalent thickness is in this case:

$$h_e = f_{i-1} \cdot \sum_{i=1}^{n-1} h_i \cdot \sqrt[3]{\frac{E_i}{E_n}} \cdot \qquad \textbf{(0-28)}$$

Where f_{i-1} are coefficients introduced by Ullidtz for a better agreement with the Burmister model. They are worth 0,9 or 1 for the upper layer in the respective cases of two-layered and multi-layered systems, and 0,8 for other layers.

- Model advantages/limitations

This model allows simplifying the pavement behaviour to a simple Boussinesq model. It improves backcalculations efficiency.
Limitations include the Burmister ones, but also that: - Moduli must decrease with depth (a 2-ratio is recommended), - Layer thicknesses should at least be equal to the radius of loading plate and - Interfaces are implicitly assumed to be fully-bonded.

d - The finite element method (FEM)

The finite element method is a powerful numerical technique allowing finding approximate solutions of mechanical complex problems.

- FEM models advantages/limitations

It allows both static and dynamic calculations, or choice of non-linear and viscoelastic behaviours and advanced interface modellings.
Nevertheless, on the contrary of previously described closed-form based problems, this numerical method is very time-consuming.

2.2 Backcalculation

2.2.1 Parameters

The backcalculation using F/HWD may allow determining several kinds of parameters, provided the equations system is overdetermined enough – hence the interest for dynamic calculations as explained in the following- and the backcalculation procedure is robust enough. Thus the test could theoretically be used to determine material properties (stiffnesses, Poisson's ratio, mass densities or damping ratios in the case of dynamical analysis), bonding conditions and layer thicknesses.

In the practice, Poisson's ratios are assumed to be known, layers are supposed to be fully-bonded, and layer thicknesses to be known. The latter are determined thanks to pavement historic, and Ground Penetrating Radar calibrated on corings. Moreover the underlying subgrade may be of non infinite extent. In this case, depth-to-bedrock is to be determined. Methods are hereafter presented.

a - Ground penetrating radar for thickness determination

Ground Penetrating Radar (GPR) allows a non destructive vehicle-speed assessment of the pavement layer thicknesses [Dérobert et al., 2001]. A very good precision can be obtained, using multi-antennas models. Several measurement lanes are generally performed, inside and outside the wheelpath. It should be noticed that the GPR needs to be calibrated using results of corings.

b - Depth to bedrock determination

- Importance of bedrock modelling

Traditional pavement models (MET, Burmister) assume that the subgrade layer is an infinite half-space. Nevertheless, as emphasized in [Irwin, 2002], if the subgrade layer is in reality only a few meters deep, this assumption leads to significant errors in the backcalculated upper layers moduli. It is shown in [Mera, 1995] that deflections imparted to the pavement by the F/HWD loading are especially sensitive to the depth to bedrock parameter in the case of the static modelling. He also demonstrates that shallow bedrock has an influence on deflections until the 20 ft (about 7 m) depth value. Beyond this value, the bedrock is shown to have no influence and the behaviour is similar to that of an infinite half-space. These two authors developed their own method for determining depth to bedrock, which is presented hereafter.

- Bedrock physical meaning

Bedrock can correspond to an effective stiff substratum. Nevertheless as highlighted in [Liu et al., 2001], a shallow water table can have the same effect. As Liu explains it, because of the incompressible nature of water, a portion of the applied dynamic load is carried by water as excess pore pressure, and this leads to an apparent stiffness increase of the saturated subgrade material. This explanation is confirmed by the material permeability, examined by Liu in the same study. Material permeability is shown to have no influence on the deflection peak. Differences between signals appear in the latter times of the acquisition, which confirms that the F/HWD dynamic loading is short enough for significant flow to develop.

Liu studies influence of pulse duration on results. For soft materials (25 MPa), higher pulse time leads to lower modulus. This effect is negligible for stiff subgrades (100 MPa). He established that soft subgrades were more sensitive to water table level. He showed using numerical simulations of a standard flexible pavement that a 5 MPa saturated subgrade can lead to the same deflections than a 15 MPa dry subgrade. Some studies referred to by Liu show that a 5 % error in subgrade stiffness can lead to 25 % error in pavement residual life prediction. Neglecting the influence of the shallow water table can render the maintenance scheme irrelevant, what confirms importance of depth to bedrock determination.

- Depth to bedrock determination methods

- **Use of the SASW method coupled with F/HWD measurements**

It is proposed in [Aouad et al, 2000] to combine F/HWD measurements with SASW measurements. The dispersion curve obtained with the latter allows determining the depth to bedrock.

The two next methods allow determining this parameter assuming that only F/HWD measurements are available.

- **Pseudo-static method**

A method is proposed in [Irwin 2002] to determine the depth to bedrock based on the deflections peak values measured by outer geophones. As Irwin notices, for a half-space the deflection is expected to be zero when the radius is infinite, and when plotting deflections as a function of a/r (a being the plate radius, and r the distance to load centre) the interpolated curve should intercept the origin. On the contrary, with shallow bedrock, this curve should intercept the abscissas axis in a point with strictly positive abscissa. By considering that depth to bedrock corresponds to the distance to load centre where no displacement is measured at the pavement surface, abscissa of the intercept is a/b_d with b_d the depth to bedrock.

Fig. 0-27 illustrates the method. In the example, obtained a/b_d value equals 0,02 and a = 0,45, so that b_d = 11 m.

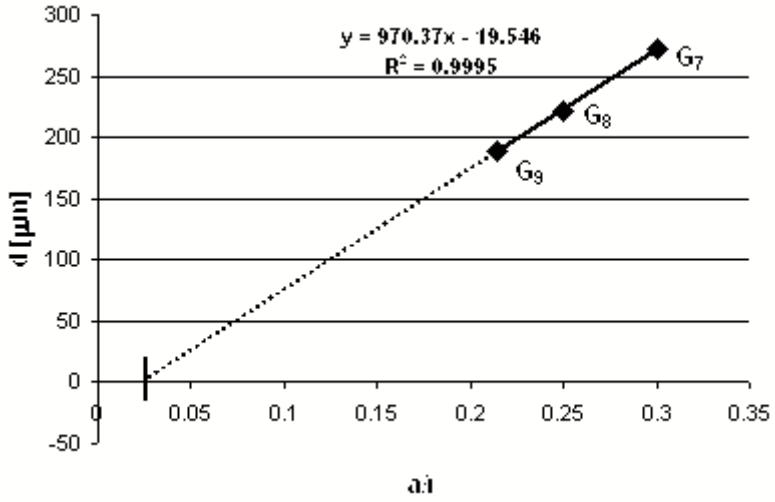

Fig. 0-27 Pseudo-static method for depth-to-bedrock determination, according to [Irwin, 2002] methodology

Method will be assessed on practice cases in part 3. Nevertheless, one can already suspect that it turns out to be very inaccurate, even if reliability can be improved when considering mean values on a great number of points of the homogeneous section (when available). Actually it depends on the number of considered geophones used for interpolation (the 2 outer ones? the 3 outer ones?), and on their position. Furthermore, it relies on the assumptions that a static modelling is convenient for F/HWD modelling and implicitly that a stresses cone whose angle is 45° is imparted to the pavement (to ensure that depth to bedrock corresponds and the distance to load centre where displacement is null are equal). The legitimacy of the first assumption is discussed in the following. The second one is a debatable approximation.

- **Resonant frequency-based dynamic method**

A dynamical modelling for F/HWD backcalculation is proposed in [Mera 1995]. When studying the displacement/force frequency response function (FRF) on the surface of a pavement at different radial offsets from centre, he establishes that this transfer function presents a peak reached at a given frequency and that this frequency is related to the depth to bedrock. By studying the ratio between dynamic and static numerical deflections (called "dynamic amplification factor") for a given data set, he proves that this ratio increases with distance to the load. Noting that the surface deflection imparted to the pavement far from the load depends mostly on the subgrade properties, Mera suggests a procedure to assess the depth to bedrock using the FRF calculated at the outer geophone, regardless of the upper layers.

Letting f_r be the resonant frequency related to the outer geophone, Mera shows that, in the absence of material damping, it satisfies the following approximate relationships:

$$\frac{f_r}{f_S} = \begin{cases} \dfrac{V_P}{V_S} = \sqrt{\dfrac{2(1-\nu)}{(1-2\nu)}} & 0 \le \nu \le 0.2 \\ 1.63 + 1.9(\nu - 0.20) & 0.2 < \nu \le 0.3 \\ 1.82 + 1.06(\nu - 0.30) & 0.3 < \nu \le 0.47 \\ 2.0 + 5.0(\nu - 0.47) & 0.47 < \nu \le 0.5 \end{cases} \qquad \textbf{(0-29)}$$

where V_S and V_P are respectively the S and P wave velocities within the subgrade, ν is the Poisson's ratio, and f_S is the shear wave fundamental frequency.

Let H be the depth to bedrock. f_S and H are linked by the following relationship:

$$f_S = V_S / 4H \qquad \textbf{(0-30)}$$

with

$$V_S = \sqrt{G/\rho} = \sqrt{E/(2\rho(1+\nu))} \qquad \textbf{(0-31)}$$

ρ, G and E respectively being the subgrade density, shear elastic modulus and Young's modulus.

Hence, by combining (0-30) and (0-31) expressions, H can be expressed as:

$$H = \frac{\left(f_r / f_S\right)}{4 f_r} \sqrt{\frac{E}{2\rho(1+\nu)}} \qquad \textbf{(0-32)}$$

In this expression, $\left(f_r / f_S\right)$ is deduced from (0-29) and f_r from experimental data, and ρ and ν are assumed to be known. Nevertheless, E is generally unknown since the main purpose of the F/HWD is precisely to determine the pavement layers moduli. [Mera, 1995] proposes a minimization procedure, which consists in an iterative procedure. E is first initialized to the E_0 value by performing a static backcalculation for a subgrade of infinite extent, with regard to the outer geophone peak deflection. A corresponding H_0 value is determined using (0-32). A new backcalculation is performed with the new structure considering bedrock at the H_0 depth. Procedure allows successive adjustments of E and H, until stabilization. It is experimentally tested in the body of the thesis (part 3).

2.2.2 Analysis methods

a - Semi-empirical analyses

This part deals with direct analyses which can be conducted without performing a full backcalculation procedure, and provide direct information about general pavement behaviour. A backcalculation is generally performed in any case in a second time. First, structural indexes give, according to some authors, information about relative material stiffnesses. However, their interpretation requires however experience and know-how. The analysis of surface moduli is also a classical tool to obtain information about layer stiffnesses, especially for subgrade. Other parameters can be studied, as for instance the study of hysteretic loops giving information about damping.

- Structural indexes

The R×D product [Autret, 1969], with R the radius of curvature and D the maximal deflection, is a classical parameter used in pavement testing to determine subgrade modulus. However in the case of the HWD load is applied through a wide (45 cm diameter) and rigid plate, so that this parameter is not relevant.

Other structural index can be defined. [Horak and Emery, 2009] propose a full semi-empirical analysis where FWD deflections are used in a relative benchmarking methodology. Five structural indexes are retained and thresholds are defined to assess pavement conditions. Table 0-2 summarizes the results. In this table, D_0 is the maximum deflection, R_0C the Radius of Curvature, BLI the "Base Layer Index" also referred to in other documents as the SCI "Surface Curvature Index" (BLI =D_0-D_{300}), MLI the "Middle Layer Index" (MLI =D_{300}-D_{600}) and LLI the Lower Layer Index (LLI =D_{900}-D_{600}), with D_X is the deflection at the X distance [mm] from plate centre. According to these authors, this table can replace backcalculation.

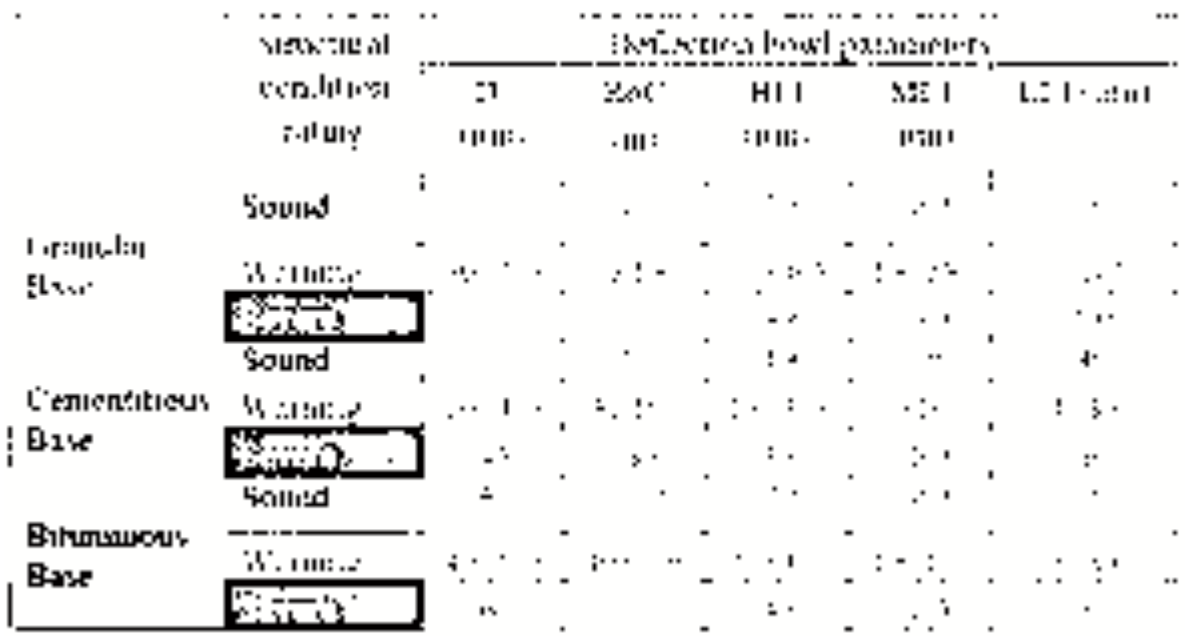

Table 0-2 Structural index thresholds for various pavement types, after [Horak and Emery, 2009]

- Surface moduli analysis

Surface moduli are defined as the equivalent modulus of the whole pavement structure at a radial r distance from the load. They are calculated using the reciprocal formulation of the Boussinesq equation. Their expression [Ullidtz, 1987] is provided by the following (0-33) and (0-34) expressions, respectively related to central and other geophones.

$$E_1 = \frac{f \times \left(1 - \nu^2\right) \times a \times p}{d_1} \qquad \textbf{(0-33)}$$

$$E_i = \frac{\left(1 - \nu^2\right) \times a \times p}{d_i} \times \frac{a}{r} = \frac{\left(1 - \nu^2\right) \times a^2 \times p}{d_i \times r} \qquad \textbf{(0-34)}$$

with d_i the measured deflection on i^{th} geophone, r_i its radial offset from load centre, ν the material Poisson's ratio, a the load plate radius, and f a weighting coefficient related to the pressure distribution beneath the load plate (Table 0-3).

Pressure distribution	f
Uniform pressure	2
Rigid plate	$\pi/2$

Table 0-3 Weighting coefficient for surface moduli calculation according to the pressure distribution, after [Ullidtz 1987]

Notion of surface modulus is interesting when assuming that surface modulus at a distance r is representative of the mean modulus in the pavement between the H = r depth and infinity,

so that the surface moduli calculated at outer geophones are representative of the subgrade modulus. Furthermore it is suggested in [Ullidtz, 1987] to study the general trend of the curve representing surface modulus evolution with regard to radial offset in order to detect possible nonlinear behaviour of the subgrade material. Two trends can be encountered: 1- The curve presents a horizontal asymptote or 2- Surface modulus increases with distance to depth (Fig. 0-28).

According to [Ullidtz, 1987], first case is symptomatic of a linear subgrade, whereas in the second case it presents nonlinear behaviour.

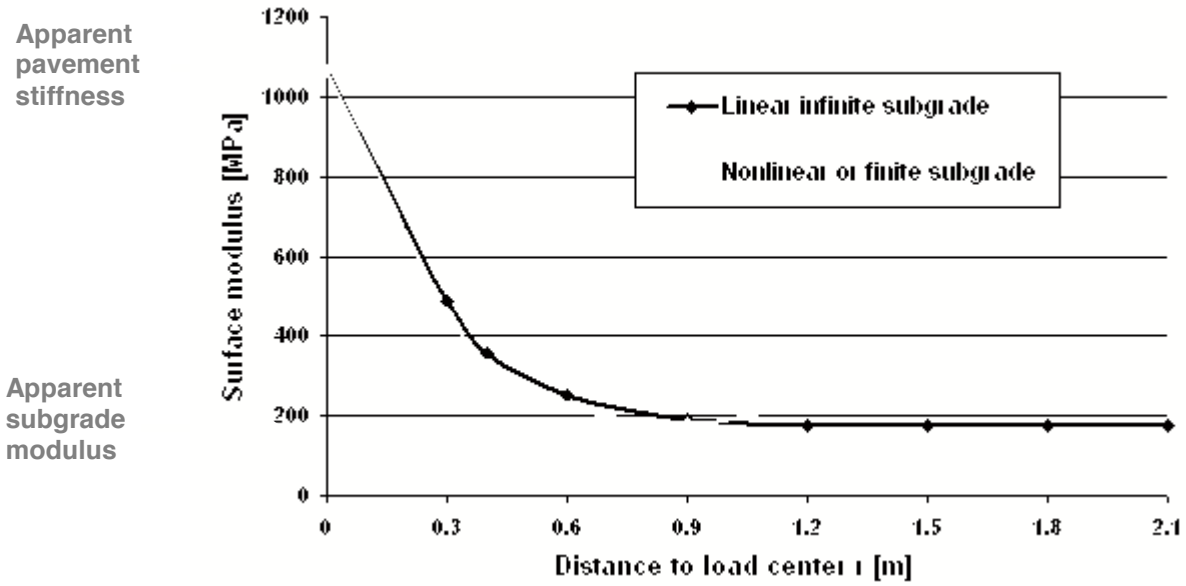

Fig. 0-28 Apparent surface moduli of the pavement; shallow bedrock and subgrade of infinite extent

The author point of view is the analysis of surface modulus evolution shall in some cases be combined with information about deflections linearity with load. Two cases are possible: if the curve presents an horizontal asymptote, the subgrade can actually be considered as linear and of infinite extent. However, if surface modulus increases, it seems to be difficult to assert that it reflects a material nonlinearity. Actually the occurrence of a shallow subgrade would have the same effect. Thus the author suggests to systematically perform on some test points some extra HWD test sequences with a significantly different load (a 2-ratio is targeted). This data allow deciding if observed modulus increase is due to nonlinearity of material, or to shallow bedrock.

As a conclusion, surface moduli analysis provides interesting information about the relative stiffnesses of layers, and especially about the underlying subgrade. Nevertheless, information is only approximate and cannot replace the backcalculation. Actually the hidden hypothesis is, as in the Irwin method for determining the depth-to-bedrock, that a 45° stress cone is imparted to the pavement, what is debatable.

b - Backcalculation procedures

Three main types of approach can be distinguished. The pseudo-static, and the time- and frequency- domain dynamic ones. The first ones are the usual HWD data analysis methods, whereas a recent interest has grown for the dynamic methods.

- Pseudo-static backcalculations

In usual methods, backcalculation phase is performed by fitting a static theoretical deflection basin on the artificial pseudo-static basin generated from experimental peak values as shown in Fig. 0-29, even if the latter do not occur at the same times.

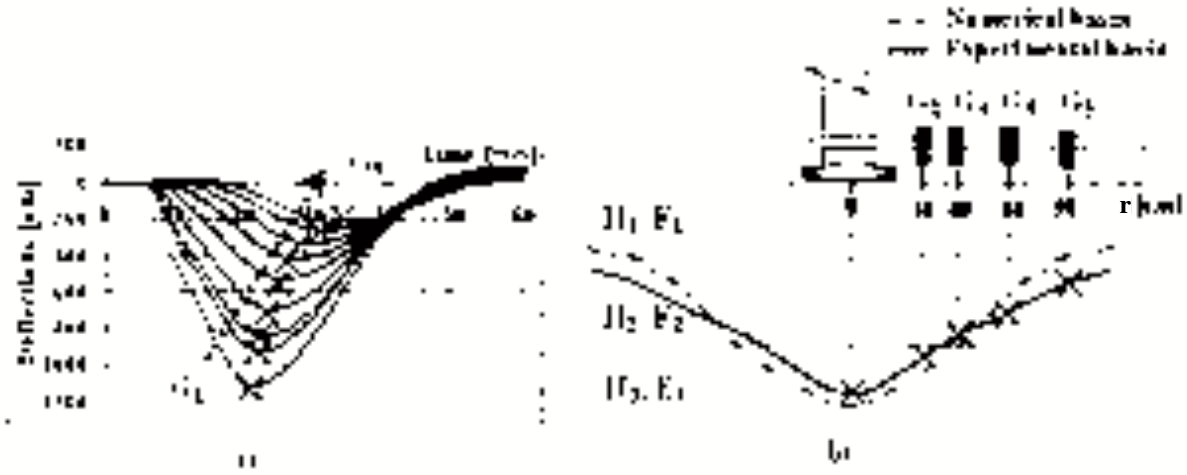

Fig. 0-29 Principle of the pseudo-static HWD data analysis method, a- Deflections measured on the 9 geophones, b- Fitting of deflection basin, after [Broutin, 2009b]

Method advantages/limitations

Advantage of these methods is they involve a simple modelling (in general the aforementioned Burmister or MET models) so that calculation times are reasonable.

Nevertheless, the use of this static approach is questionable because the model is quite far from the observed physical phenomenon. Moreover it is made use of only part of available information.

- Dynamic time-domain backcalculations

In these representations the dynamic load is modelled and applied over the pavement and the whole imparted time-related deflection signals are computed based on dynamical FEM calculations.

Method advantages/limitations

Modelling is close to the physical observed phenomenon and it allows calculating the whole time-related deflection signals.
Main shortcoming is the computations are time-consuming.

- Dynamic frequency-domain backcalculations

This method called Spectral Element Method (SEM) combines the contributions of FEM theory and spectral method. The initial physical time-domain problem is transferred to the frequency-domain using a Fourier transform. A spatial decomposition is also performed to model the circular load over the pavement. Elementary stiffness matrices are obtained for each ω_n frequency and each k_m wave number, and assembled to obtain the system stiffness matrix. An inverse Fourier transform is then necessary to obtain the time-related displacements.

Mathematical resolution is detailed in the triptych [Al Khoury et al., 2001], [Al Khoury et al., 2001b] and [Al Khoury et al., 2002]. It is shown that, for an axisymmetric layer, general frequency-domain relationships between displacements and force can be expressed by:

$$\begin{Bmatrix} \hat{w}(r,z,\omega_n) \\ \hat{u}(r,z,\omega_n) \end{Bmatrix} = \sum_m \hat{P}_{mn} \hat{G}(k_m,\omega_n,z) \begin{Bmatrix} J_0(k_m r) \\ J_1(k_m r) \end{Bmatrix} \quad \textbf{(0-35)}$$

with $\hat{w}(r,z,\omega_n)$ and $\hat{u}(r,z,\omega_n)$ respectively the vertical and horizontal displacements, $\hat{P}_{mn}$ the force pulse, $\hat{G}(k_m,\omega_n,z)$ the transfer function of the layer, J_0 and J_1 the Bessel functions of the first kind of order zero and one, and k_m and ω_n respectively the wave numbers and angular frequencies.

For a multi-layered system, force and displacement are related by

$$\hat{K}(k_m,\omega_n)\left\{\hat{D}(r,z,\omega_n)\right\} = \left\{\hat{P}(k_m,\omega_n)\right\} \quad \textbf{(0-36)}$$

with $\hat{K}(k_m,\omega_n)$ the stiffness matrix of the system, $\left\{\hat{D}(r,z,\omega_n)\right\}$ the nodal displacements vector, and $\left\{\hat{P}(k_m,\omega_n)\right\}$ the external force vector.

This equation is solved in the particular case of the HWD test where a single load is applied at the surface.

Method advantages/limitations

Advantage of these methods with regard to time-domain modellings is they are computationally much more efficient than the time-domain ones.
Nevertheless, as [Chatti, 2004] highlights it, significant errors can be made when Fast Fourier Transform (FFT) calculations are inaccurate, or if a too short time range is considered. Let us highlight that accuracy of the method highly depends on the quality of measured signals.

2.2.3 Identification numerical methods

a - Database methods

In these methods, a database of calculated basins is first generated, by parametrically varying the pavement layer moduli within specified ranges. Once the database is obtained, an

algorithm allows identifying the numerical deflections that best match the experimental data, and the best moduli set can be calculated by interpolation.

Method advantages/limitations

The main shortcoming of these methods is they are time-consuming, with regard to iterative methods which are described just after.
Nevertheless, they present the great interest of calculating the whole available solutions in a "physically acceptable" moduli range, defined by an experienced pavement engineer. As the backcalculation solution is not unique, the moduli set determined by an automated method may not be the most physically satisfactory. With the database method, all "numerically acceptable" solutions can be examined and the most "physically reasonable" retained.

b - Iterative methods

The second type of methods gathers whole iterative algorithm based procedures. The general principle consists in:
- defining an objective function which reflects the quality of fitting between numerical and experimental data, and an associated target error,
- choosing a seed moduli set,
- updating at each step the moduli set, until target error is obtained or limit iterations number is reached.

Iterative methods are generally classified into 3 categories: the methods of orders zero, one and two. A specific method called the "self-adjoint states method" is also presented in the following.

- Methods of zero order

These methods do not require calculation of the objective function gradient. [Forestier, 2004] distinguishes two main methods: the Nealder Mead Simplex method and the genetic algorithms.

The simplex method consists in defining a "simplex" which is a n+1 vertex polygon, n being the number of parameters to be calculated. It aims at constructing a sequence of simplexes in $\Re^n$ tending to a local minimum. Algorithm is detailed in [Forestier, 2004]. The procedure starts with an arbitrary simplex. At each step, the point of the simplex where the objective function is maximal is removed and replaced by its reflection regarding the isobarycentre of the n other points if this point is better. Otherwise, this means that points are in a valley and simplex is reduced by performing a similitude centred on the point where objective function is minimal.

The genetic algorithms are inspired from the theory of evolution and genetics. Principle consist in generating new generation of solutions from an existing parent pool, and select the best-fit solution to form the next parent pool. The procedure is repeated until the worst individual solution in the considered generation presents an objective function lower than a given threshold. [Fwa et al., 1997] demonstrates the possibility of using this type of algorithm for HWD analysis.

- First order methods

In these methods, the gradient is calculated to define a descending strategy. The most used first order method is the method of steepest descent, or Gradient descent method.

The first order methods present the property of converging very rapidly in a first time, when far from the solution, but of becoming very slow when in its neighborhood. Furthermore they only allow reaching a local minimum, so that in the case of the HWD backcalculation, the choice of the seed moduli may influence the final result.

- Second order methods

These methods use the Hessian matrix of the objective function. The terms of the matrix are generally calculated using finite differences, so that at each calculation step, n+1 calculations are necessary, n being the number of parameters to be backcalculated. Its principle is not detailed here, but resolution of the problem with the Gauss Newton algorithm, belonging to these methods is presented in appendix 3.1.

- The self-adjoints states method

This method is an advanced numerical method for gradient calculations. Its principle is not detailed here, but is available in appendix 3.3.

Interest of the method is that only 2 direct calculations are necessary at each algorithm step, against n+1 for Gauss Newton.

c - Artificial neural networks (ANN) methods

Former studies about ANN were conducted in order to better understand the workings of the human brain. They revealed the mathematical and computational interest of these systems.

- Principle

As biological neural networks, ANN are build up with numerous neurons, connected together, each one being capable of very simple elementary actions. Nevertheless many researches have proven that it is possible to model very complex behaviours from this sum of elementary actions. Another property of the ANN is similar to their biological counterparts: they are capable of learning a functional mapping, through repeated exposure to that mapping. In the case of the F/HWD backcalculation an ANN can be taught to map deflection basins onto their corresponding pavement properties by repeatedly showing it examples of the correct mapping.

As [Meier, 1995] highlights it interest of ANN is allowing real-time F/HWD backcalculations, the ANN method being almost instantaneous. This interest is strengthened when modelling complex and time-consuming process. This is the case for dynamical modellings.

- The ANN network

As reminded in [Meier, 1995] a biological neuron consists of:
- a soma (or cell body),
- dendrites that receive signal to other neurons,
- a single axon sending signals to other neurons,
- synapses, where communication between neurons takes place.

A neuron is continually receiving inputs from other neurons via chemical transmitters sent through the synapses and modifying (increasing or decreasing) the electrical potential in its soma. When this potential reaches a given threshold value the cell "fires" and sends a signal through its axon to other neurons.

General organization of the network corresponds to Fig. 0-30. It is at least composed of an input layer and an output layer, with eventually intermediate layers called "hidden layers", each neuron of the network sending information to neurons of the down layers.

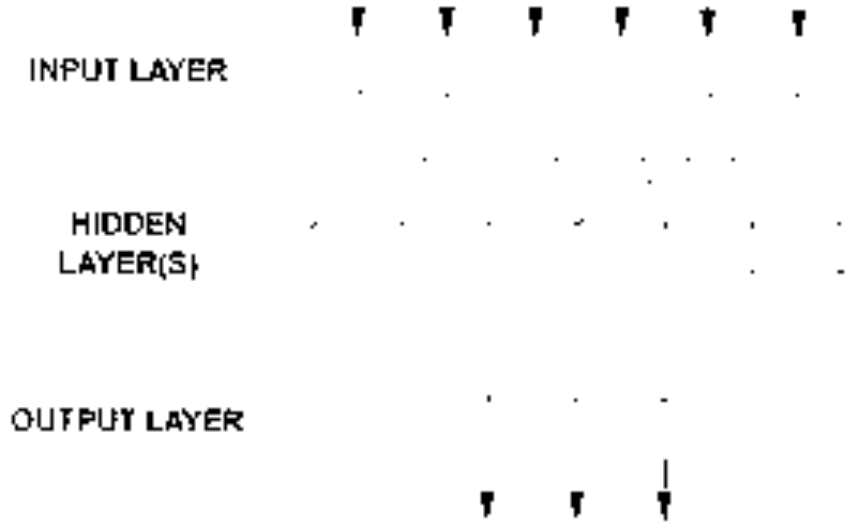

Fig. 0-30 Schematic drawing of a typical multi-layered artificial neural network, after [Meier, 1995]

Historically numerous modellings of the single neuron have followed each other. In former modelling (McCulloch and Pitts, 1943), neurons were binary logical entities (either they fired or they didn't), a minimal number of synapses had to be excited to fire the neuron, an active inhibitory synapse prevented completely the neuron of firing regardless of the number of excitatory synapses. Rosenblatt (1958) improved the modelling by introducing weighting coefficient to each connection ("synaptic weights"). Its neuron called "perceptron" acquired in this manner the capability to "learn", i.e. to encode information, by modifying its weighting coefficients / synapses weights. The neuron fired when the weighted sum reached a given threshold. Hopfield introduced in 1984 the nonlinear neuron. Its principle is the same than for the perceptron except the Heavyside function is replaced by a nonlinear continuously-differentiable function.

Let x_i be the inputs received from the i^{th} neuron of the upper layer, and y_j the output of neuron j, and w_{ij} the synapse weight corresponding to the connection between the i^{th} and j^{th} neurons, and β_j the "firing threshold" of the synapse.
Let us define s_j as:

$$s_j = \sum_i w_{ij} x_i - \beta_j \qquad \textbf{(0-37)}$$

By definition $y_j = g(s_j)$

The nonlinear continuously-differentiable function g is generally $g(x) = \frac{1}{1+e^{-x}}$

Number of layers is at minimum 1 output layer. Many studies have shown that a 3 layers network (1 output layer plus two hidden layers) is the best architecture for $\Re^n$ (the n-dimensional real Euclidean vector space) to $\Re^p$ problems.

Let now choose the number of neurons constituting each layer. For the input and output layers, they are imposed: they respectively correspond to the numbers of input parameters and of unknown in the backcalculation procedure. Nevertheless as [Meier, 1995] highlights it, there is no established rule for choosing the number of neurons in each of the hidden layers. A compromise is to be found between insufficient and excessive knowledge capacity. In the first case the network would be incapable of accurate result. In the second one, schematically, it would have memorized all training examples and would be incapable of generalizing. Optimization is generally performed by trial-and-error procedures.

- The training

Principle consists in exposing the ANN to deflection basins and to "teach" it to recognize the corresponding moduli. In practice w_{ij} synapses weights have to be adjusted.
The ideal case would consist in training the neural network on in-situ measured HWD deflection basins. Nevertheless, thicknesses may not be accurately known, just as target material properties, since laboratory testing are expensive, time-consuming and not undoubtedly representative of in-situ material due to sampling extraction. This is the reason why training is in practice generally performed on synthetic simulated data set (Fig. 0-31).

It must be emphasized that efficiency of the final procedure relies on a shrewd choice of a training data set. The latter must be representative of real values. It means that realistic boundaries have to be chosen for test parameters, and that the test sample must span the whole range of values, with statistically representative weights. Training data set must be used in a random order.

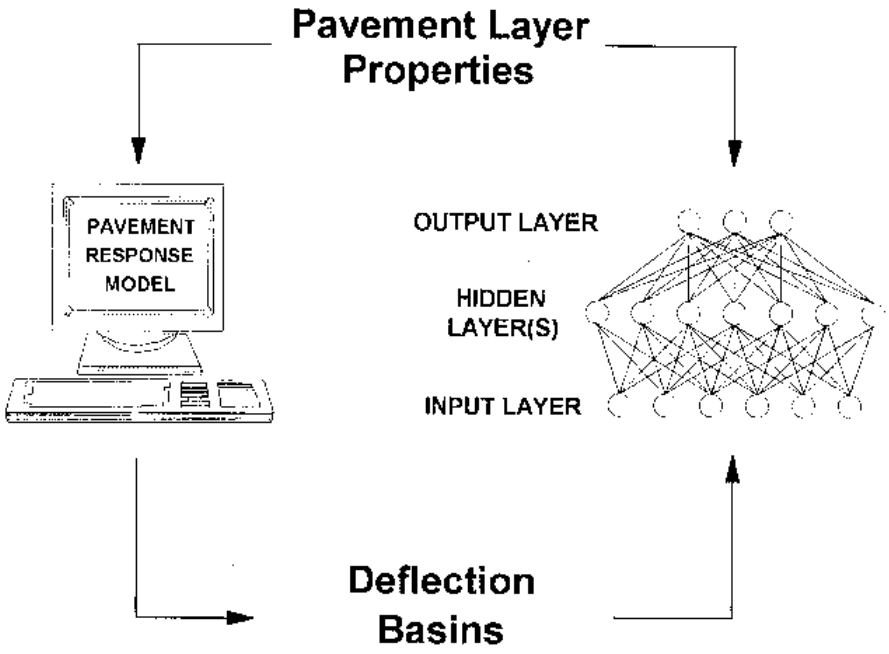

Fig. 0-31 Basic neural network training procedure, after [Meier, 1995]

The most usually used method for multi-layered network training is the "backpropagation" method (Rumelhart, Hinton and Williams, 1986). Its principle consists in applying a given error on the outputs and propagating the error backward through the network.
Noting k the number of the training set and E the error, the w_{ij} synaptic weight is adjusted using a gradient descent method:

$$\Delta w_{ij} = -\eta \frac{\partial E}{\partial w_{ij}} = \sum_k -\eta \frac{\partial E^k}{\partial w_{ij}} \qquad \textbf{(0-38)}$$

η being a constant called « learning rate ».

Noting $y_j^{\,k}$ and $t_j^{\,k}$ the realized and target output on the j^{th} neuron,

$$E^k = \frac{1}{2}\sum_j \left(t_j^{\,k} - y_j^{\,k}\right)^2 = \frac{1}{2}\sum_j \left(t_j^{\,k} - g\left(s_j^{\,k}\right)\right)^2 \qquad \textbf{(0-39)}$$

$\frac{\partial E^k}{\partial w_{ij}}$ is decomposed as the product of three partial derivatives :

$$\frac{\partial E^k}{\partial w_{ij}} = \frac{\partial E^k}{\partial y_j^{\,k}} \frac{\partial y_j^{\,k}}{\partial s_j^{\,k}} \frac{\partial s_j^{\,k}}{\partial w_{ij}} \qquad \textbf{(0-40)}$$

As $\frac{\partial s_j^{\,k}}{\partial w_{ij}} = x_i^{\,k}$,

and defining δ_j^k as:

$$\delta_j^k = -\frac{\partial E^k}{\partial y_j^k}\frac{\partial y_j^k}{\partial s_j^k} \quad \textbf{(0-41)}$$

The weight update rule is rewritten:

$$\Delta w_{ij} = \eta \sum_k \delta_j^k x_i^k \quad \textbf{(0-42)}$$

For the output layer

$$\frac{\partial E^k}{\partial y_j^k} = -\left(t_j^k - y_j^k\right) \quad \textbf{(0-43)}$$

$$\delta_j^k = g'\left(s_j^k\right)\left(t_j^k - y_j^k\right) \quad \textbf{(0-44)}$$

For the hidden layers, denoting m the neurons of the underlying layer

$$\frac{\partial E^k}{\partial y_j^k} = \sum_m \frac{\partial E^k}{\partial s_m^k}\frac{\partial s_m^k}{\partial y_j^k} \quad \textbf{(0-45)}$$

$$\frac{\partial E^k}{\partial y_j^k} = \sum_m \delta_m^k w_{jm} \quad \textbf{(0-46)}$$

$$\text{Thus } \delta_j^k = g'\left(s_j^k\right)\sum_m \delta_m^k w_{jm} \quad \textbf{(0-47)}$$

(0-47) defines a relationship allowing computation of the deltas in any layer from the deltas in the layer under it. As the deltas of the output layer are known, it is possible to calculate the delta in the whole network.

Some methods introduce a “momentum”, working as a damper that prevents the search from oscillating endlessly about a global minimum.

$$\Delta w_{ij} = \eta \sum_k \delta_j^k x_i^k + \beta \Delta w_{ij}^{old} \quad \textbf{(0-48)}$$

Δw_{ij}^{old} is the Δw_{ij} value at previous step; β is called “momentum factor”.

- Examples of F/HWD using ANN

[Meier, 1995] used the method on both a static and an elastodynamic pavement model.
The training data set was constituted of 100 000 three-layers (AC/UGA/Subgrade) pavement profiles.
The inputs were the deflections on the 7 first geophones plus the AC and UGA thicknesses, the outputs the AC, UGA and Subgrade moduli, and thus the network architecture: 9-11-8-3
Meier showed that accuracy was as good as or better than for the traditional backcalculation method using the same mechanical model than the training. The dynamical method does not require more time than the static one. The calculation time is 3 orders of magnitude faster for the ANN method.

[Gopalakrishnan, 2007] studies a three-layer (AC/UGA/Subgrade) pavement using a non-linear finite element modelling. A first ANN is here used to determine the AC the input set being constituted of the deflections on the 5 first geophones (D_0 to D_5) and the first output set the E_{AC} modulus. Network architecture is 6-40-40-1. A second ANN, whose architecture is 8-40-40-1, allowed determination of the subgrade modulus from the deflections on the 5 first geophones (D_0 to D_5) plus the Base Curvature Index BCI = D_2-D_3 + Area Index AI_4=(D_2+D_4)/2D_0. Results are once more satisfactory.

Method advantages/limitations

As a conclusion, the ANN method seems to be a good way to improve computation times of computationally inefficient backcalculation methods. Nevertheless it necessitates a substantial upstream work for each new study. It is well adapted for repeated works, for instance for regular network survey where it allows obtaining real-time information about the studied structure.

2.3 Pavement evaluation

This part deals with the further analyses performed on the basis of the HWD backcalculation results to assess the pavement bearing capacity and a residual life. This analysis phase is in the following called “Forward analysis”. It relies on 1- a direct calculation of the strains at critical levels of the pavement, taking into account the parameters backcalculated at previous step, and 2- a damage calculation involving material performances. Damage calculation involves determination of the elementary damages, introduced in a cumulative damage model.

2.3.1 Cumulative fatigue damage model

The Miner’s linear law is widely retained to describe the cumulative damage on road materials. According to it, damage at a particular point in time is the sum of the elementary damages imparted to the material by the various loads. Decomposing the traffic mix into N imparted stress or strains cases (in a large sense, as illustrated in paragraph 3.1 of part 3), the damage due to the N load groups can be written as:

$$S = \sum_{i=1}^{N} S_i \qquad \textbf{(0-49)}$$

Where S_i is the elementary damage ratio due to ith group. It corresponds to the ratio of the N_i actual and the $N_{all,i}$ allowable number of load repetition of the ith load group:

$$S_i = \frac{N_i}{N_{all,i}} \qquad \textbf{(0-50)}$$

The pavement fails when S reaches the 1 value.

2.3.2 Elementary damages

Calculation of each elementary damage ratio requires knowing $N_{all,i}$ values. It necessitates for each critical strain the knowledge of the performances of the corresponding material. The latter can be obtained from laboratory tests and tests performed on Accelerated Loading Facilities (ALF).

- Critical strains

It is commonly admitted that three failure modes affect the pavement**:**

- fatigue in the asphalt layer under repeated loads,
- permanent deformation in unbound materials,
- rutting in asphalt materials due to their visco-thermoplastic behaviour.

Current modellings do not conveniently predict the last phenomenon, which yet constitute a main pavement failure mode, especially when considering airport pavements. Design related to this parameter is generally performed on purely empirical basis.

Conversely, the failure by fatigue in the asphalt layer and the permanent deformations in unbound materials are well predicted. Critical strains to be considered are respectively the tensile strain at the base of the asphalt layer, and the compressive strain at the top of unbound materials, since strains are the highest at these levels.

- Elementary damages relative to each critical strain

Constitutive material performance laws are required. They can either be obtained from laboratory tests (French rational design method), or directly derived from tests performed on full-scale pavements (American rational design method). In the first case, adjustment coefficients have to be introduced, which are determined from feedback from real network, or from empirical tests performed on ALF. Both approachs are described and discussed in [Caron et al., 2010].

One of the most famous ALF for road design is the French LCPC's "fatigue carrousel" [LCPC's Accelerated Load Test Facility]. The main ALF dedicated to airfield pavements are the American NAPTF facility for airports and the Airbus test facility. Three main experiments relative to the latter facility can be mentioned. The flexible and rigid Pavement Experimental Programs [Fabre et al., 2005] which provided valuable information about the fatigue and permanent deformations observed in airfield pavements, and a specific study in progress about the influence of tire pressure on rutting.

Laboratory material testing consists in subjecting material specimens to repetitive either stress-controlled, or strain-controlled, actions.

In France fatigue resistance of asphalt material is tested using strain-controlled sinusoidal loadings applied at the head of trapezoidal specimens restraint at their base. Material is assumed to be fully damaged when initial stiffness has been divided by two.

General form of the fatigue law relative to asphalt materials used for road design [LCPC - SETRA, 1997] is:

$$\varepsilon_{XX,all} = \varepsilon_6(\theta) \cdot \left(Ne/10^6\right)^b \cdot k_C \cdot k_d \cdot k_r \cdot k_S \quad \textbf{(0-51)}$$

Where:

- ε_6 is the strain at which the tensile failure is obtained after 10^6 load cycles,
- Ne is the number of load repetitions (equivalent standard truck axle loads in road design),
- b is the fatigue slope of the material in a bi-logarithmic representation (for usual materials b=-0,20),
- k_d is a coefficient relative to discontinuities in structures ($k_d = 1$ for flexible structures),
- k_S is a safety factor taking into account local variations in the bearing capacity of the underlying unbound materials,
- k_C is a calibration coefficient (calculated on the basis of ALF experiments),
- k_r is a coefficient adjusting the allowable deformation to consider a given design risk,
- θ is the reference temperature.

Note that in France, for airfield pavements, road fatigue laws calculated for 10^6 cycles are generally extrapolate to 10^4 cycles. It is recommended in [Merbouh et al., 2007] to adapt for airfield pavements strains magnitude and signal frequency, to be more representative of real strains levels (4 or 5 higher in airport than in road design) and aircraft velocities, and to perform tests made up 10^4 to 10^5 cycles.

Permanent deformations in unbound materials and subgrade are tested using repeated triaxial tests.
The general form of the expression predicting permanent deformation in unbound materials is:

$$\varepsilon_{Z,all} = A \cdot (Ne)^{b'} \quad \textbf{(0-52)}$$

For heavy traffics A is chosen equal to 16 000 (when giving ε_Z in microstrains) and b' to -0,222.

2.3.3 Damage calculation

- Usual modellings

Classical modellings (for instance in [Ullidtz, 1987] or [Park and Kim, 2003] calculate damages by decomposing the traffic in groups and the year in "seasons". Indeed, in-situ moduli are affected by seasonal variations, as asphalt materials stiffnesses for instance are closely related to temperature. Several laws providing correction of moduli with temperature are available in the literature. [LTPP, 2000] proposes linear correction in the semi-logarithmic space [T°C, log(E)]. Slopes for current material are assumed to vary between -0,0195 and -0,021. Retained temperature is the mid-depth asphalt layer temperature.

Subgrade stiffness may also be affected by seasonal variations. Moisture is this time involved.

Let N_P and N_T respectively be the number of design aircraft and considered seasons, and assume that traffic is known during the whole design period of the pavement. Damage can be expressed by:

$$S = \sum_{j=1}^{N_T} \sum_{i=1}^{N_P} \frac{P_{i,j}}{N_{all,i,j}} \times Y \qquad \textbf{(0-53)}$$

Where:

- Y is the design period in year,
- $P_{i,j}$ is the number of passages of the i^{th} aircraft during the j^{th} season,
- $N_{all,i,j}$ is the number of allowable passages of the i^{th} aircraft during the j^{th} season.

The $P_{i,j}$ traffics can be weighted by lateral distributions. As demonstrated in [HoSang, 1975], normal laws represent well lateral distribution either on runways or taxiways.

- Limitations

These models assume that evolution of the moduli during their life expectancy can be neglected and moduli only vary with seasonal variations.

Nevertheless, as [Collop, 1996] or [Ullidtz, 2005] highlight it, in reality moduli vary during the pavement life, due to ageing and deterioration.

- Taking stiffness reduction into account

Laboratory tests

Letting E be the instantaneous modulus and E_0 the initial one, the typical evolution of E/E_0 during laboratory fatigue tests is the following (Fig. 0-32):

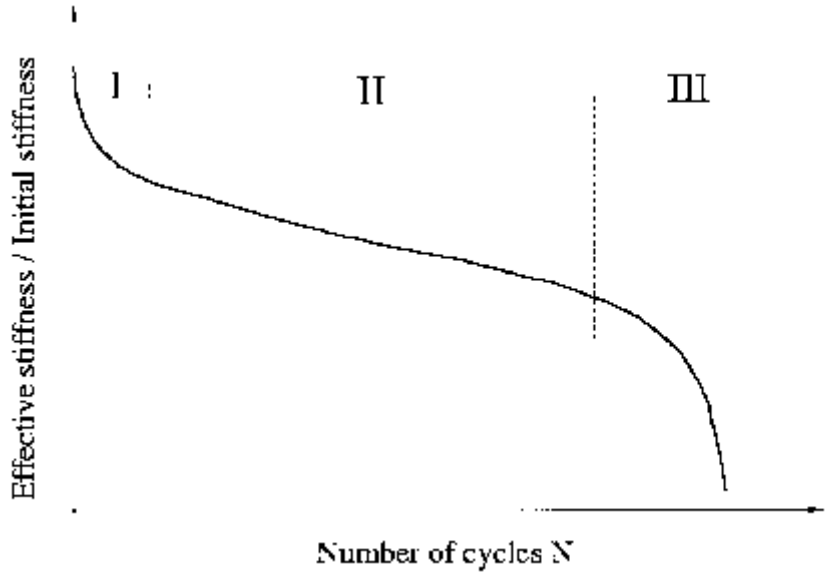

Fig. 0-32 Typical asphalt material stiffness evolution during a laboratory fatigue test. After [Bodin, 2004]

Evolution presents three phases. First a rapid decrease of initial modulus. Second an almost linear evolution. In the third phase, damage growth accelerates until failure. As [Lefeuvre, 2001] explains it, in phases I and II damage in the specimen consists in a diffuse microfissuration. Then localized damage occurs in the most damaged area, leading to macrofissuration and a fast decrease of the stiffness during phase III.

[Bodin et al, 2004] propose a continuum model to describe the curve of the Fig. 0-32, including initial stiffness loss in phase I. Nevertheless laboratory results are not easy to transfer to field analysis. [Bodin, 2002] refers to phenomena of material overheating and thixothropy during the laboratory test.

[de La Roche, 1996] also mentions a self-repairing (some kind of a "healing") property of asphalt materials. Actually when applying rest times to specimens (what makes loadings closer to the reality), these one find their initial stiffness back. However, stiffness decrease is much faster.

Another limitation of the current fatigue test method is it does not take into account multi-peak actions systematically encountered in airfield pavements due to multi-wheel landing gear. A wide-scale experiment about this issue is in progress in France ([Merbouh et al., 2007]). It aims to better understand the influence of multi-wheel landing gear configuration on material fatigue. Principle consists in applying at the head of the sample complex deformations (Fig. 0-33) instead of the usual sinusoidal ones. The λ parameter describing the non return to zero (function of the landing gear configuration, and its velocity over the pavement surface) varies from 0 to 1. Provisional conclusion of the study is that the pass of a two-wheel boggie has the same effect as 3 single-axle passes.

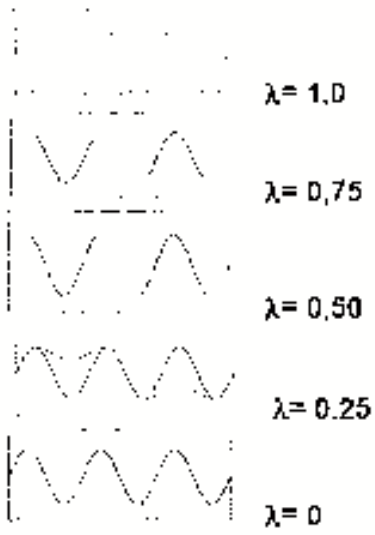

Fig. 0-33 Complex deformations signals applied to the sample; multi-peak experiment, after [Merbouh 2007]

Empirical rules from field surveys

It strengthens interest of ALF.

[Collop, 1996] examines stiffness reduction from ALF tests by studying the evolution of backcalculated moduli during the (accelerated) pavement life. He shows that a semi-log regression model fit the results better than linear regression model. The proposed relationship is:

$$E/E_0 = e^{C_1 S} \quad \textbf{(0-54)}$$

Where C_1 is a constant.

Based on Heavy Vehicle Simulator tests, which is a commercial device allowing accelerated fatigue of pavements, [Ullidtz et al., 2008] also exhibits a semi-log regression linking damage and modulus. The general expression is:

$$\log(E) = \delta + \frac{\alpha \times (1 - S)}{1 + \exp(\beta + \gamma \log(tr))} \quad \textbf{(0-55)}$$

Where:

- *tr* is the reduced time, which is a coefficient allowing normalizing test to a reference material viscosity,
- $\alpha, \beta, \gamma, \delta$ are constants.

Ullidtz suggests therefore an incremental calculation of damage taking into account the decrease in modulus.

However the application of the method is tricky. It implies that either the constants of the Ullidtz or Collop models are transferable to all pavements, or several HWD surveys have been performed at regular times during the pavement life, with the assumption that temperature corrections are reliable and precise enough, so that the phenomenon of stiffness reduction can easily be isolated.

Moreover, in France, no consensus has been found to admit that the measurement of apparent stiffness can actually be used as a state variable of the structural conditions of the pavement. The main reason is that this reduction has never been properly observed, even on ALF. On the contrary in most cases moduli increase due to two phenomena in competition with material damage: ageing, but especially post-compaction. The latter phenomenon has been studied in [Fabre et al., 2005].

The French rational pavement design model considers an initial modulus and does not consider the decrease in modulus during the pavement life

From the French point of view, damage of the pavement can be seen as the damage in a material sample, at a higher scale. As above mentioned, diffuse damage is first observed in the sample, corresponding to microfissuration, before a damage localisation and a rapid failure in third phase of the curve in Fig. 0-32. The same phenomenon occurs for the pavement: first a diffuse fissuration and then damage localization with severe bottom-up cracking (Fig. 0-34). In the apparent sound zone, stiffness reduction due to damage is negligible.

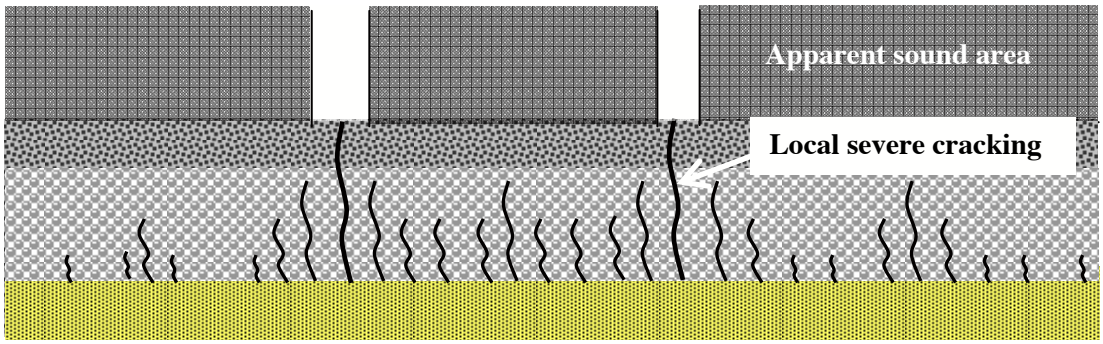

Fig. 0-34 Schematic damage appearance in a pavement

This strengthens the importance of coupling bearing capacity measurement with visual inspections. A long-term experiment is planed, which includes regular HWD surveys and superficial observations on a given plate-form.

Conclusions to literature review

This literature review has first presented the main existing pavement testing devices. It appears that the HWD test is among the routine devices the most representative of the pass of aircraft wheels, in terms of dynamic effects, loading amplitude and duration.

Then main usual and advanced modellings related to the data analysis have been presented. It appears that usual modellings used for the backcalculation phase are not satisfactory, so that interest for dynamic modellings has been growing for a few years. It also appears that no consensus has been found so far for the forward calculation phase, which consists in determining pavement bearing capacity and residual life from the backcalculation results. French rational design model relies on a static Burmister model, involvong a constant material stiffness during the whole pavement life.

Part 1 – Preliminary studies

Introduction to Part 1

This first part describes preliminary studies considered as essential to develop a refined HWD backcalculation. First a typical HWD test is examined. Then the reliability of HWD data for dynamical analysis is studied. This study is based on: 1- an experimental repeatability study, conducted on a well-known pavement, 2- a specific experiment which has required the assembly of an external instrumentation and 3- crossed tests with other HWD on known test facilities. Finally, an empirical analysis of pavement response has been carried out. The latter was attended to study 1- the relative linearity of the deformations with applied loading, from tests conducted on various flexible pavements, and 2- the presence of viscoelastic phenomena in the pavement from gauge readings.

Introduction de la partie 1

Cette première partie décrit les études préliminaires qui s'avèrent nécessaires au développement de la méthode avancée de calcul inverse proposée. Tout d'abord un essai HWD type est examiné. Ensuite, la fiabilité des résultats, en vue d'analyses dynamiques, est étudiée, par l'intermédiaire 1- d'une étude expérimentale de répétabilité, menée sur une chaussée bien connue, 2- d'une étude spécifique nécessitant la mise en place d'une instrumentation externe, et 3- d'essais croisés avec d'autres HWD sur des planches d'essais. Enfin une analyse empirique de la réponse de la chaussée est conduite, dont le but est d'étudier 1- la linéarité des déformations engendrées en fonction de l'effort appliqué, et 2- la présence de phénomènes visqueux dans la structure, à partir de la réponse des jauges d'une chaussée instrumentée.

1 - Study of a typical HWD test

1.1 Device configuration

As mentioned in the dedicated part of the literature review, the HWD principle consists (Fig. 1-1) in 1- dropping a mass over the pavement through a load plate and a buffer system, in order to generate an impulse sinusoidal transient stress simulating the load effect of an aircraft wheel pass and 2- measuring and analyzing the resulting surface deflections.

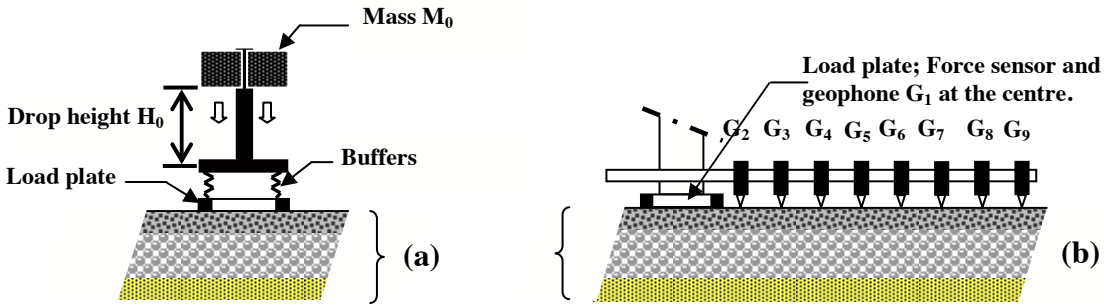

Fig. 1-1 HWD measuring principle: a- Creation of an impulse load; b- Recording of the surface deflections

The STAC's device provides the possibility to use two load plates respectively 30 and 45 cm diameter. Quick calculations show that the larger plate must be used in order to ensure that the pressure is in a consistent range with the 15 bar (1,5 MPa) standard pressure for airfield load levels.

The buffer system is composed (Fig. 1-2 a) of 2 lanes of 4 rubber buffers. Several sets of buffers are available, defined by their SHORE hardness. A specific study on these elements has been led and is presented hereafter.

The HWD device also includes 9 geophones for deflection determination. These velocity transducers are placed on a support beam (Fig. 1-2 b). During a test, their displacement is perfectly coeval and coincident with the displacement of the pavement surface, thanks to a metal tip and a spring system.

Table 1-1 indicates the radial offsets of geophones from the plate centre as chosen by STAC.

Geophone	G_1	G_2	G_3	G_4	G_5	G_6	G_7	G_8	G_9
Radial offset r [cm]	0	30	40	60	90	120	150	180	210

Table 1-1 Geophones configuration

These offsets respect the recommendations of the [COST, 1999] except for the G_3 geophone, for which a 40 cm offset has been retained by the STAC instead of the recommended 45 cm, in order to better take into account the plate effect. This geophone configuration is kept for all the experiments presented in the thesis.

(a) (b)

Fig. 1-2 a- The HWD buffer system, b- The geophones

The applied force is measured by a force sensor integrated to the HWD foot. The provided acquisition system allows a 4 kHz acquisition rate either on the measured force or on the deflections.

1.2 Typical test

1.2.1 Time-related applied force and resulting surface deflections

Fig. 1-3 depicts a typical HWD test. Test was performed on the S_1 reference structure (i.e. with standard asphalt materials). Temperature in the surface course was about 5 °C.

Deflection magnitudes decrease with distance to the load centre. Peak deflections at each geophone are reached at distinct time increments and reflect propagation delays.

A δt time delay is also noticed between the appearance of the force and the central deflection signals. [Kim, 1997] interprets this delay as due to the viscous behaviour of asphalt materials. Nevertheless, as detailed infra, this delay is mostly independent on the pavement temperature, which is contrary to predictions, viscosity increasing with temperature, so that a specific thorough study has been necessary (see 2.2.2) to assess if observed delay comes from real viscous effects or from a bias in measurement (or a combination of these two elements).

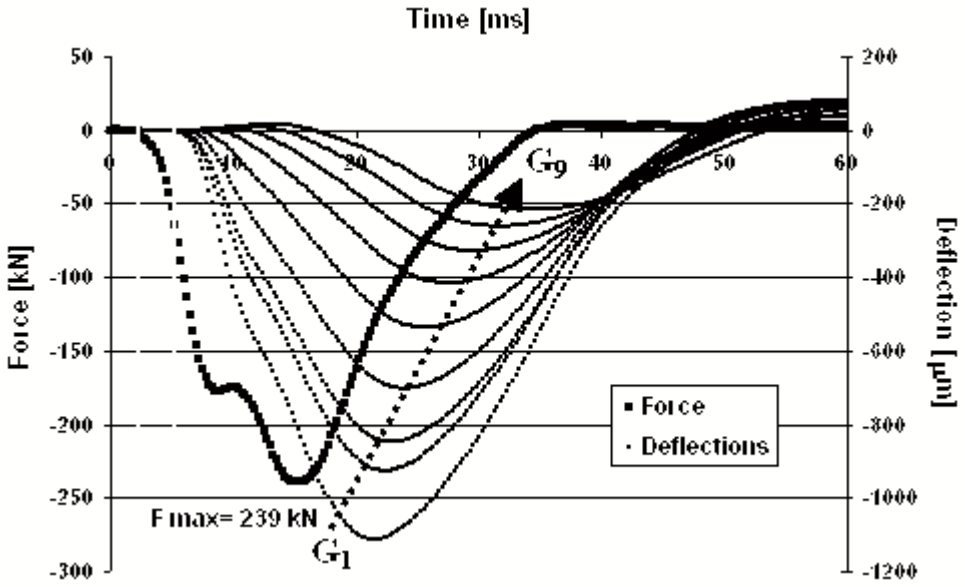

Fig. 1-3 Typical HWD test; Time-related applied force and resulting surface deflections

In addition, the force signal is characterized by a double peak. This phenomenon is quoted in most of the HWD tests presented in literature. No explanation has been found yet. An attempt to elucidate this typical trend will be provided in the following 1.3 section.

1.2.2 Frequency spectrum

Fig. 1-4 provides the results a frequency analysis (FFT) performed on force and deflections signals for the HWD test evolved in the previous paragraph. It appears that the frequency spectrum is in the 0-80 Hz range.

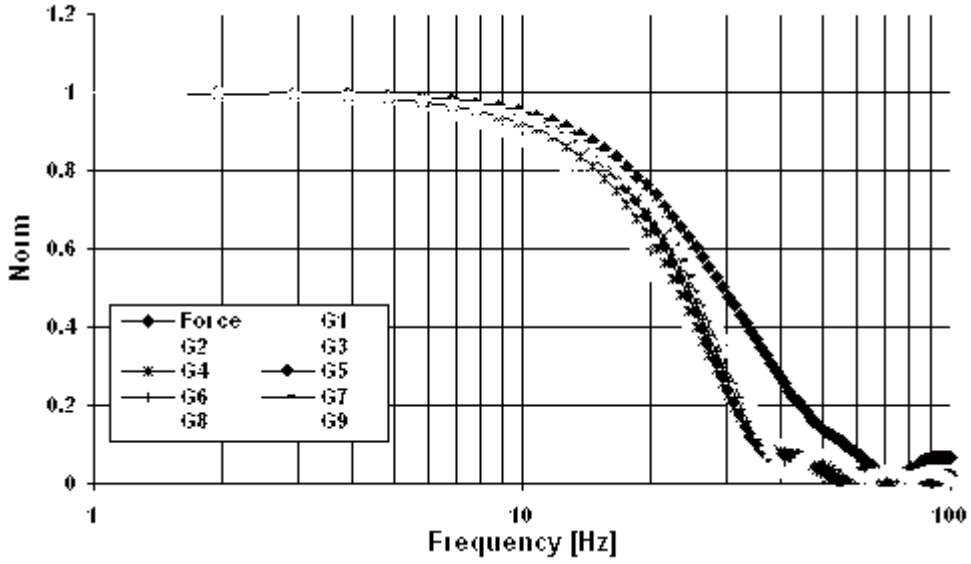

Fig. 1-4 Frequency spectra of force and deflection signals from a typical HWD test

1.2.3 Construction of deflection basins

As explained in the literature survey, usual methods (referred in this work to as “pseudo-static methods”) use a so-called “deflection basin”.

In these methods the backcalculation phase is performed by fitting a static theoretical deflection basin on a reconstructed pseudo-static basin. The latter is generated by the experimental peak values as shown in Fig. 1-3, even though the maxima do not occur at the same times.

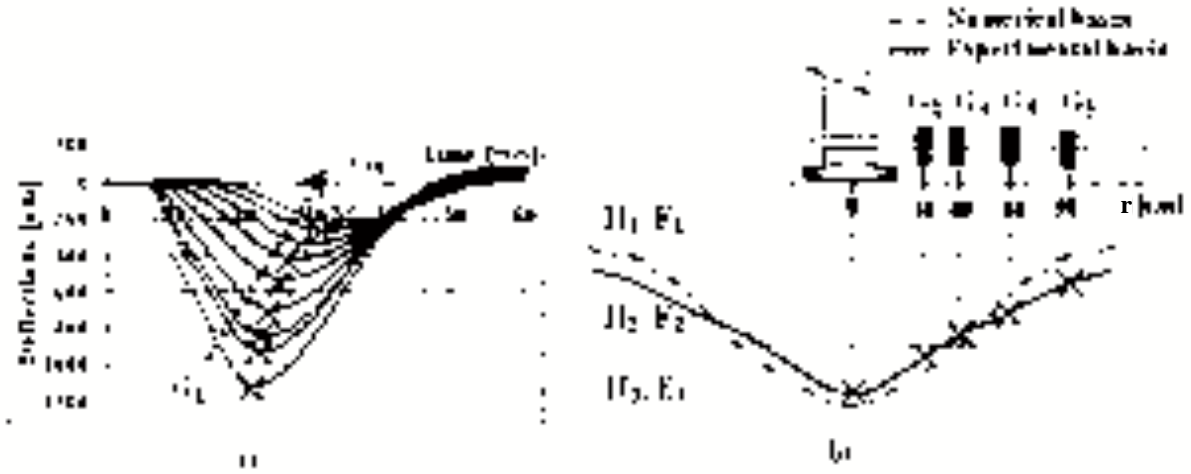

Fig. 1-5 Reconstruction of a pseudo-static deflection basin and fitting (Pseudo-static methods), after [Broutin, 2009b]

1.3 Theoretical considerations

A basic semi-empirical analysis of the HWD force signal shape is presented here. This work presents a double aim. The first one is to better understand the macroscopic phenomena occurring during a test. The second application is operational. It is important during a field survey to be able to find rapidly a convenient test configuration to reach a target load. The objective is to determine and validate relationships between test parameters (fall height, mass, and buffer set) and resulting applied load, defined in terms of F_{max} maximal strength and Δt pulse time values.

1.3.1 Study of the buffer system

First, a specific study of the buffer system has been performed. The purpose is to 1- examine the homogeneity of the buffer system with the intent to interpret the aforementioned double peak, and 2- assess the buffer behaviour and especially stiffness for specific modellings (initial speed modelling in part 2). Two experiments were conducted. The first one was made

in static conditions (M Broutin/JC Deffieux collaboration). It was made twice (January and March 2006), since initially provided hard buffer set was highly heterogeneous. It has been replaced by a new one. Only the second experiment (with the new hard buffer set) is presented here. As the behaviour of the buffer material may be different under static and dynamic (HWD) load, the experiment has been reiterated under dynamic conditions, using external instrumentation on the HWD. Feasibility studies (M Broutin/JC Deffieux collaboration) were performed in February 2008 and June 2008, and the final experiment in March 2009.

a - Static buffer analysis experiment

Details on the experiment are in (2006 internal publication)

Three buffer sets have been considered, which consist of height (8) hard buffers ("HB" in the following; SHORE 75), four (4) intermediate buffers ("IB" in the following; SHORE 55), and four (4) soft buffers ("SB" in the following; SHORE 45). Each buffer was placed between two metal plates (Fig. 1-6) and tested using a static press, by progressively increasing the applied load at constant low speed. Precision on the applied force was 1 kg. Precision on the buffer deformation, measured by three comparators placed at 120°, was better that 0,01 mm. The whole experiment was performed with a constant temperature of 15 °C.

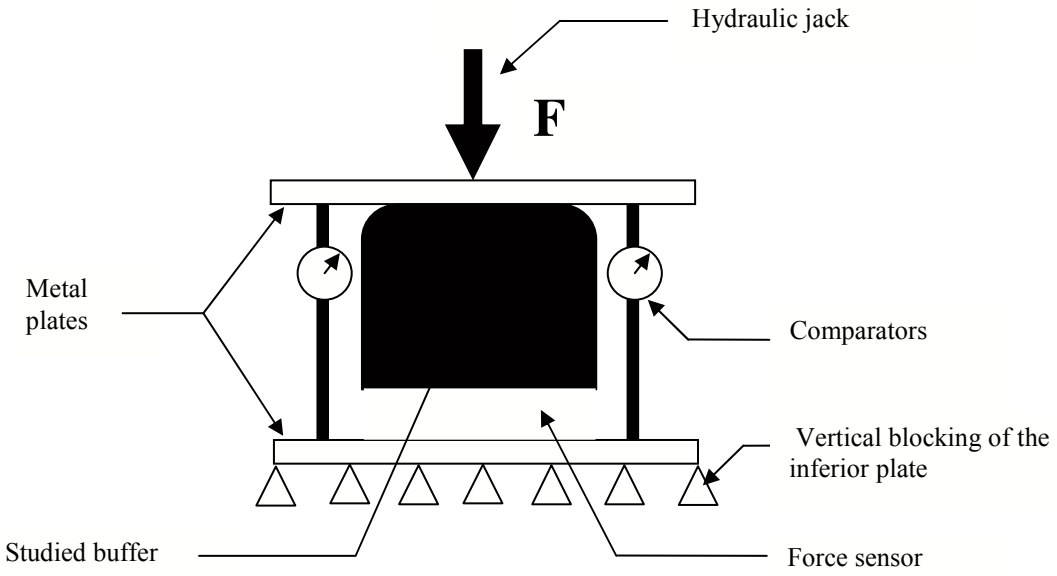

Fig. 1-6 Test setup of the static buffer experiment

The three following parameters have successively been assessed:

1- Test repeatability
2- Influence of repositioning on test repeatability
3- Homogeneity of each buffer set

- Test repeatability

The repeatability of the test has been assessed by repeating the measurement three times for each buffer, with a one (1) minute rest time between successive tests.
Fig. 1-7 displays the result for the first hard buffer (SHORE 75). Similar repeatability is observed for all buffers. Note that a perfect linearity is observed. Once more, this behaviour is common to all buffers.
Mean variance between the three measurements, calculated on all buffers and at all force levels, is 0,87 %.

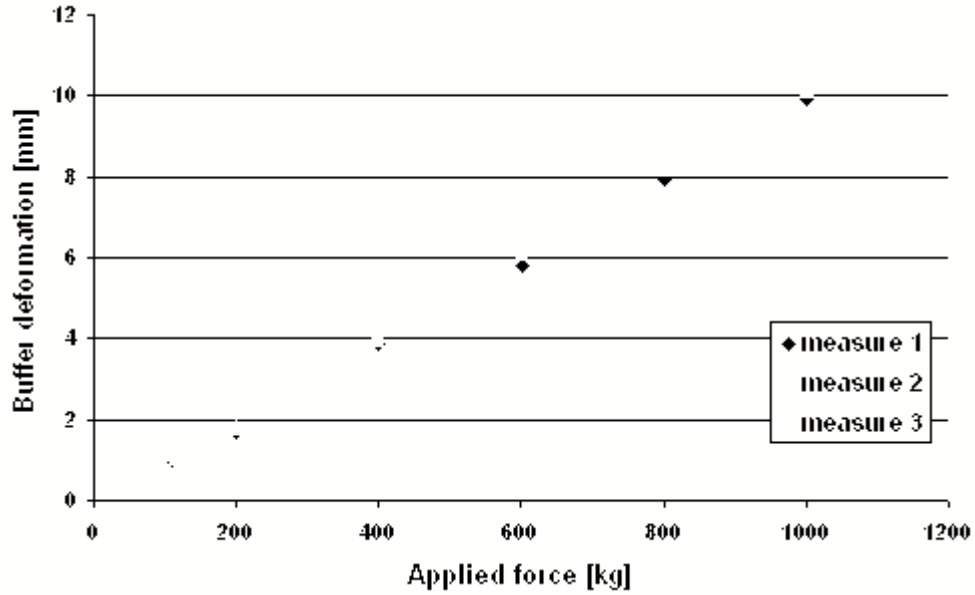

Fig. 1-7 Repeatability between 3 consecutives measurements on a given buffer (first HB buffer on example)

- Influence of buffer repositioning

The same experiment has been led, but by removing and by repositioning the buffer between each of the three measurements. Mean variance between the three measurements is this time 0,91 %. It may be concluded that repositioning has no influence on the results.

- Homogeneity of each buffer set

Once it has been demonstrated that repositioning do not affect the results, homogeneity of each buffer set can be assessed (Fig. 1-8).

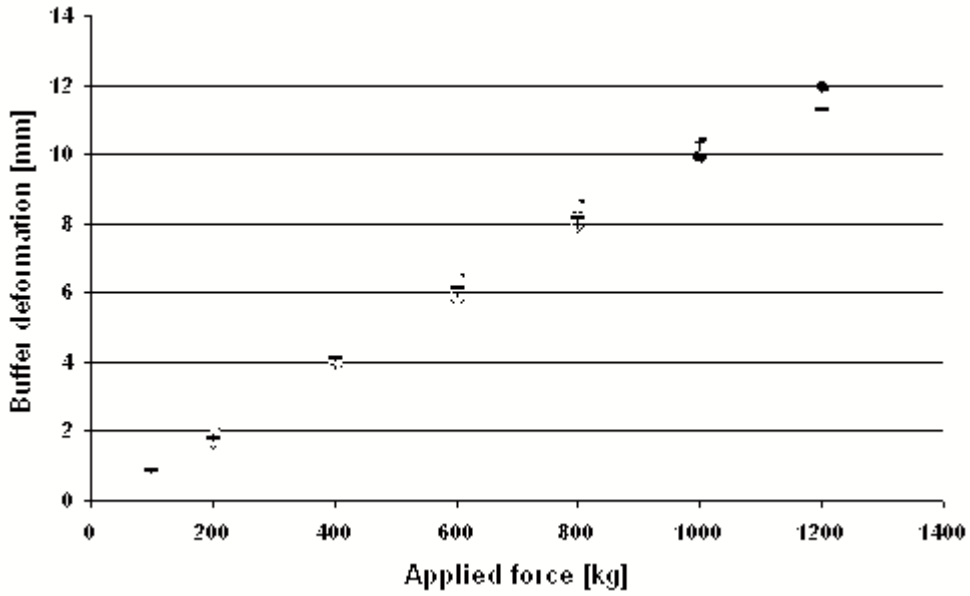

Fig. 1-8 Stiffness homogeneity of a buffer set (HB buffer on example)

Table 1-2 presents corresponding variances. Note that a $1/\sqrt{8}$ ratio for HB and $1/\sqrt{4}$ ratio for IB and SB have been applied to theoretical results, as studied values correspond to a mean value on respectively 8, 4 and 4 buffers, considering for each buffer the mean value on the three measurements.

Actually, let us consider N measurement results (m_i) of common U uncertainty, and name m their mean value. $m = \frac{1}{N}\sum_{i=1}^{N} m_i$, so that sensitivity coefficients of m_i are $\lambda_i = \partial m/\partial m_i = 1/N$ for each i[th] measurement and $U_m = \sqrt{\sum_{i=1}^{3} \lambda_i^2 U^2} = \frac{U}{\sqrt{N}}$.

	HB	IB	SB
Standard deviation [mm]	**0,0004**	**0,00035**	**0,0007**
Variance	**3,9%**	**1,5%**	**2,2%**

Table 1-2 Stiffness homogeneity of the buffer sets

Scatter of results is 1,5 to 3 times higher than for a single buffer, what implies that test precision is sufficient to judge homogeneity of the buffer sets. Precision seems very good. A translation in terms of precision on elastic moduli is given in the following.

- **Interpretation in terms of elastic moduli**

An approximate calculation of elastic modulus of buffers consists in applying the (1-1) relationship:

$$E = \frac{F}{S\,\varepsilon} = \frac{F\,H}{S\,v} \qquad \textbf{(1-1)}$$

Where H is the buffer height, S its section, and v the axial deformation imparted by the axial F applied load. According to Fig. 1-9, apparent moduli calculated by this method are 10,2; 4,1 and 2,8 MPa for the hard, intermediate, and soft buffers respectively.

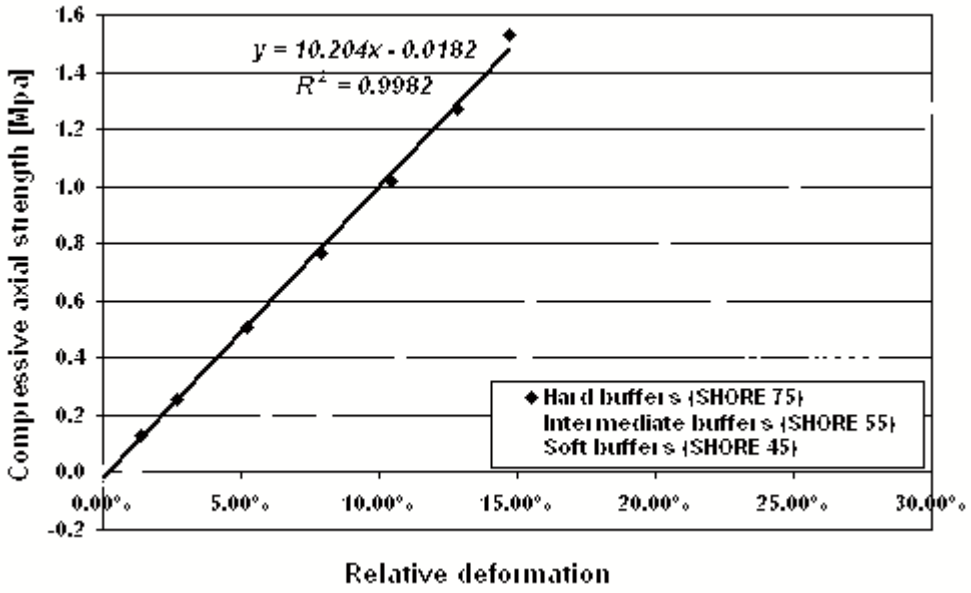

Fig. 1-9 Apparent stiffnesses of the different buffer sets

Precision on moduli is calculated in the following manner:

Let U_X and λ_X be respectively the uncertainty on parameter X and sensitivity coefficients relative to E. Parameters to be considered are the measured force, and the relative deformation (whose uncertainty is due to the scatter of buffer diameters and uncertainty on buffer deformation measurement). Thus:

$U_E = \sqrt{\lambda_F^2 U_F^2 + \lambda_S^2 U_S^2 + \lambda_\varepsilon^2 U_\varepsilon^2}$ with λ_i the sensitivity coefficient relative to the i parameter:

$\lambda_i = \frac{\partial E}{\partial i}$

with $\lambda_F = \frac{\partial E}{\partial F} = \frac{1}{S\varepsilon}, \lambda_S = \frac{\partial E}{\partial S} = -\frac{1}{S^2}\frac{F}{\varepsilon}, \lambda_\varepsilon = \frac{\partial E}{\partial \varepsilon} = -\frac{1}{\varepsilon^2}\frac{F}{S},$

and:

$$U_\varepsilon = \sqrt{\lambda_v^2 U_v^2 + \lambda_H^2 U_H^2} \;;\; \lambda_H = -\frac{v}{H^2} \;;\; \lambda_v = \frac{1}{H}$$

$U_S = \lambda_S U_S = \frac{\pi}{2} D \times U_D$, with U_D the uncertainty on diameter.

Table 1-3 collects all results. Uncertainties on D and H have been obtained from Vernier caliper measurements.

	U_F (MN)	U_D (m)	U_S (m^2)	U_H (m)	U_v (m)	U_ε (s.u)
HB	10^{-5}	$2{,}2.10^{-4}$	$3{,}45.10^{-5}$	$1{,}9.10^{-4}$	10^{-5}	$3{,}7.10^{-4}$
IB	10^{-5}	$1{,}4.10^{-4}$	$2{,}20.10^{-5}$	4.10^{-4}	10^{-5}	$1{,}5.10^{-3}$
SB	10^{-5}	$4{,}8.10^{-4}$	$7{,}54.10^{-5}$	$6{,}4.10^{-4}$	10^{-5}	$2{,}2.10^{-3}$

Table 1-3 Elementary uncertainties relative to the buffer moduli calculation

Sensitivity coefficients (Table 1-4) have been calculated using:

- D = 100 mm = 0,1 m,
- H = 80 mm = 0,08 m,
- F_{HB} = 1 200 kg = 0,012 MN, F_{IB} = 0,010 MN and F_{SB} = 0,006 MN,
- and the corresponding ε: ε_{HB} = 14,7 %, ε_{IB} = 29,9 % and ε_{SB} = 27,0 %.

	λ_F	λ_S	λ_ε
HB	867	1325	71
IB	426	543	14
SB	472	361	10

Table 1-4 Sensitivity coefficients relative to the parameters of the problem

Table 1-5 provides final precisions on moduli values.

	$\lambda_F U_F$ (MPa)	$\lambda_S U_S$ (MPa)	$\lambda_\varepsilon U_\varepsilon$ (MPa)	U_E (MPa)
HB	9.10^{-3}	$4{,}6.10^{-2}$	$2{,}6.10^{-2}$	0,0534
IB	4.10^{-3}	$1{,}2.10^{-2}$	$2{,}1.10^{-2}$	0,0248
SB	5.10^{-3}	$2{,}7.10^{-2}$	$2{,}3.10^{-2}$	0,0357

Table 1-5 Final precisions on moduli values

The previous approximate determination of elastic modulus does not take into account buffer radial deformation. An improved method is thus proposed using an identification procedure performed in CESAR-LCPC software [Humbert et al., 2005].

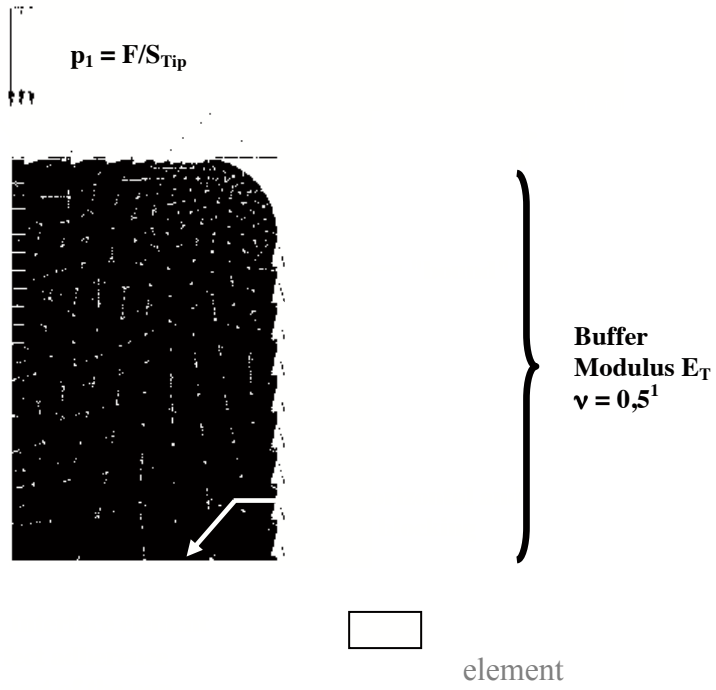

Fig. 1-10 Finite Elements modelling of the buffer behaviour under axial loading

Fig. 1-11 presents an example of buffer deformation under load.

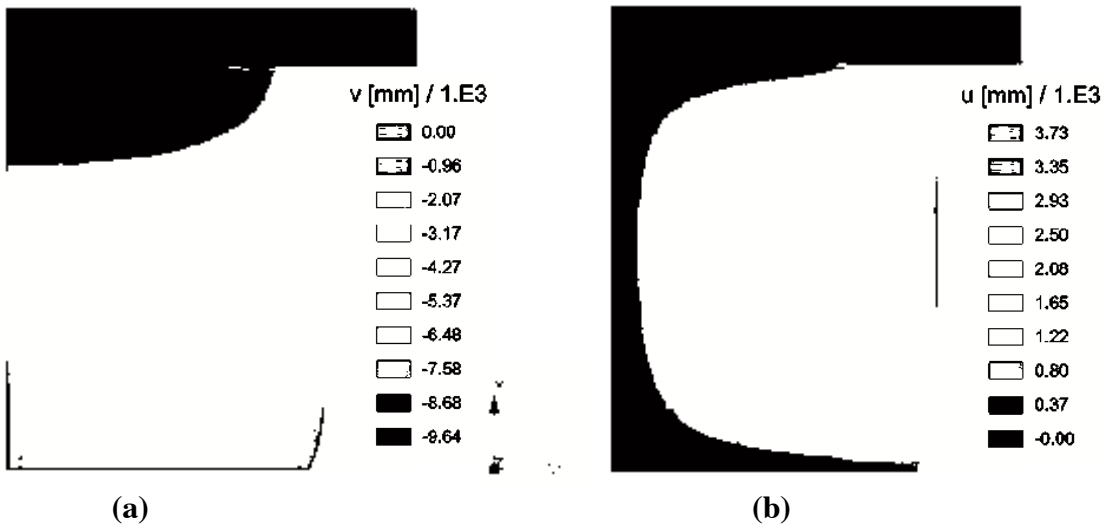

Fig. 1-11 a - Vertical deformation of the buffer under axial load, b - Radial deformation of the buffer under axial load

[1] In practice 0,499, as in CESAR the ν=0,5 is forbidden due to presence of « 1-2ν » in the denominator.

Table 1-6 presents the results of the identification procedure for the three buffer sets. The values are slightly lower than the apparent moduli. This identification has been performed using axial deformation (1 equation and 1 unknown). The last two columns compare the radial numerical deformation corresponding to the identified modulus with the experimentally-determined radial deformation. FEM calculated values are slightly lower than experimentally determined deformations, so that the model is considered to be consistent.

	CESAR identified modulus ($E_{fitting}$)	FEM calculated radial relative deformation (ε_r)	Experimental radial relative deformation (ε_r)
HB	8,5 MPa	8,65%	10%
IB	3,4 MPa	17,5%	20%
SB	2,2 MPa	15,9%	18%

Table 1-6 Buffer moduli, identified from FEM calculation

Partial conclusions

This experiment has allowed demonstrating that all buffers present, at least under static action, an elastic linear behaviour, homogeneous for each buffer set.
An identification using a FEM model has allowed determining a static modulus value, which is in good agreement with the experimentally-determined apparent modulus. Note although that temperature may have a significant influence on rubber stiffnesses.

b - Dynamic analysis

The following results are taken from a more general experiment involving an accelerometer-based external instrumentation. The last part of this experiment will be presented in section 3.2.2.
The presented testing consists in positioning accelerometers on the falling mass and on the tray to which buffer bases are fixed. The experiment has been performed on the S_3 structure. Temperatures during the tests are provided in appendix 1.2. The buffer set used is composed of the 8 hard buffers.

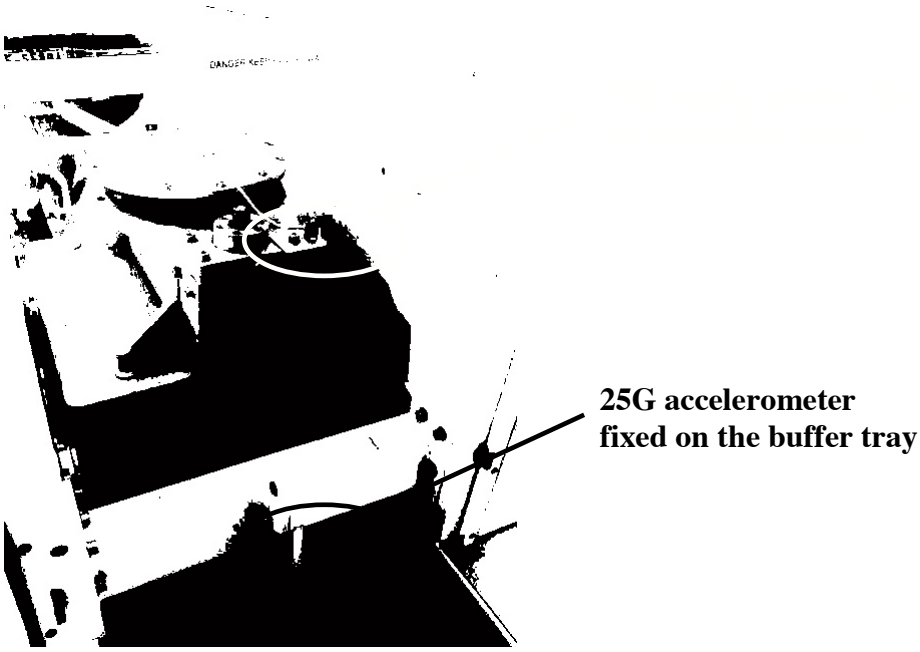

Fig. 1-12 Test setup related to the accelerometer-based mass motion study

An approximate calculation is needed to determine *a priori* the necessary measurement ranges. Assuming a free fall, the initial mass velocity at the impact point at buffer top is respectively $V_0 = 2{,}8$ m.s^{-1} or 1,4 m.s^{-1} at $H_0 = 400$ mm and $H_0 = 100$ mm,. Velocity varies from V_0 to zero between occurrence of the signal and peak value (occurring 15 ms later), so that the mean acceleration on this time frame is about 19 G and 9,5 G for the two H_0 values. In the case of a sinusoidal $F(t)$ force signal (and consequently the $\gamma(t)$ vertical acceleration signal as the fundamental principle applied to falling mass implies $\gamma(t) = F(t) / M_0$), relation between maximal value and mean value presents a ratio of 2, so that the expected maximal acceleration values of the falling mass is about 38 G for $H_0 = 400$ mm (19 G for H = 100). A 50 G accelerometer is thus chosen for following the falling mass motion.
The same reasoning is conducted for the second accelerometer, when supposing that displacement corresponds to the plate displacement, so that displacement varies from zero to maximal deflection in a half pulse time. Maximal expected acceleration is in this case about 9 G for $H_0 = 400$ and the half for $H_0 = 100$ mm. A 25 G accelerometer is used, what gives a good security margin.

As seen before, the frequency spectrum of the HWD force-signal and ensuing deflections occupies the 0 – 80 Hz range. Accelerometer transfer function is of low-pass type, with a cut-off frequency around 250 Hz (see 50 G accelerometer response in Fig. 1-13 for instance), so that no undesirable filtering is applied to the signal.

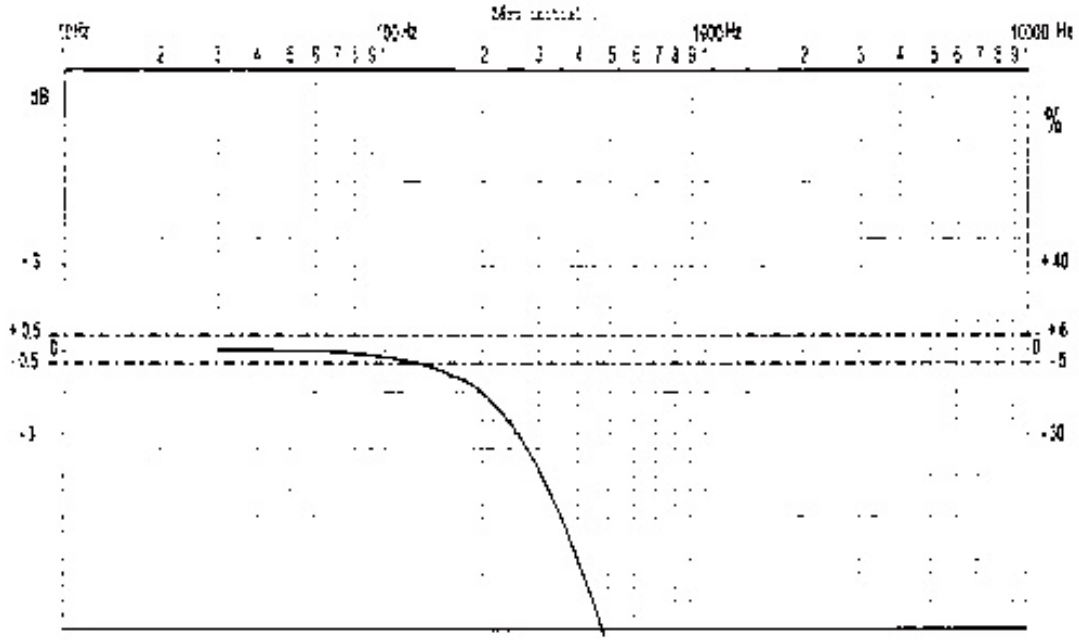

Fig. 1-13 Transfer function of the accelerometer fixed on the falling mass

Collection of the accelerometer responses is performed using a spider acquisition unit ( ). Acquisition rate is 3 200 Hz. Raw data have been filtered with a 300 Hz Bessel filter what does not affect the results.

Fig. 1-14 and Fig. 1-15 display the recorded raw acceleration signals for a 100 mm fall height. Acceleration is taken positive when directed downwards. Zero base is made before dropping of the mass. Then the free fall is characterized by a 1 G constant acceleration. A negative acceleration (upwards sense) is then observed corresponding to the first impact. Note that maximal measured mass acceleration is about 15 G (against 19 G in the approximated calculation). Several free fall and rebounds succeed then. The elapsed time between principal impact and first rebound is about 200 ms. Note that this value depends on the fall height (see for instance Fig. 1-44 in 2.2.2. hereafter, corresponding to a 400 mm fall height).

The second accelerometer presents accelerations higher than predicted, what may be due to rapid vibrations of the thin metal tray under impact. As acceleration has an important magnitude but short pulse time, corresponding displacement, obtained by double integration, is less than 1 mm. It will be neglected in the following.

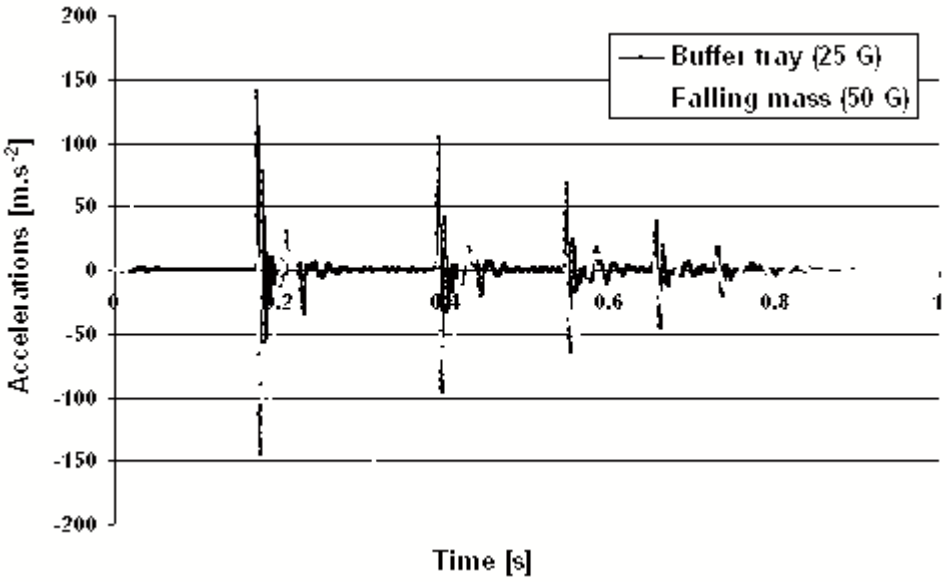

Fig. 1-14 Accelerations measured on the falling mass and buffer tray during a HWD test (1/2)

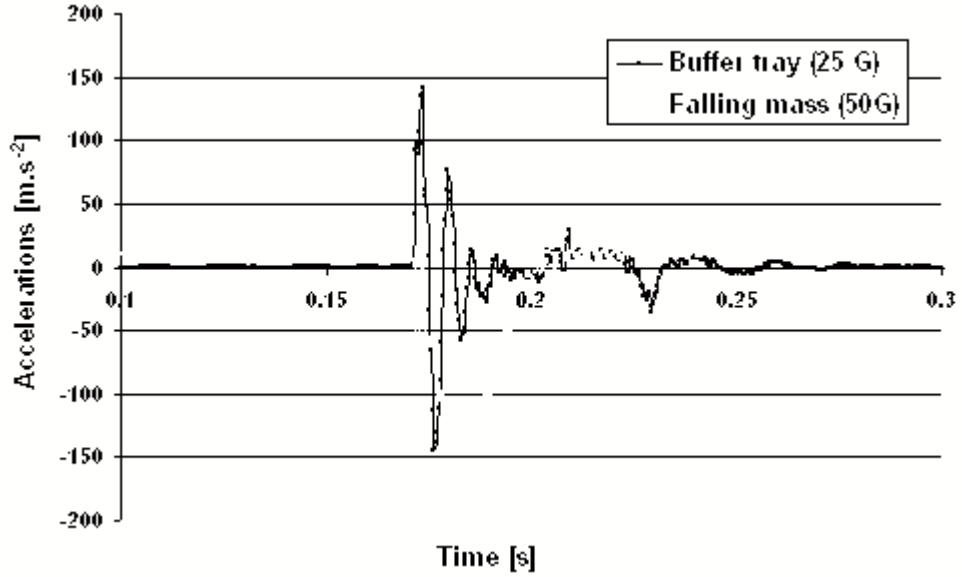

Fig. 1-15 Accelerations measured on the falling mass and buffer tray during a HWD test (2/2)

Fig. 1-16 presents the displacement of the falling mass obtained from a double integration of the 50 G accelerometer signal. As displacement of the base of the buffers is neglected, negative parts of the curve reflect deformation of the buffer under the successive rebounds until stabilization around the final position. It appears that final deformation under static weight (6,8 kN) is negligible in comparison with the one under the dynamic load (120 kN).

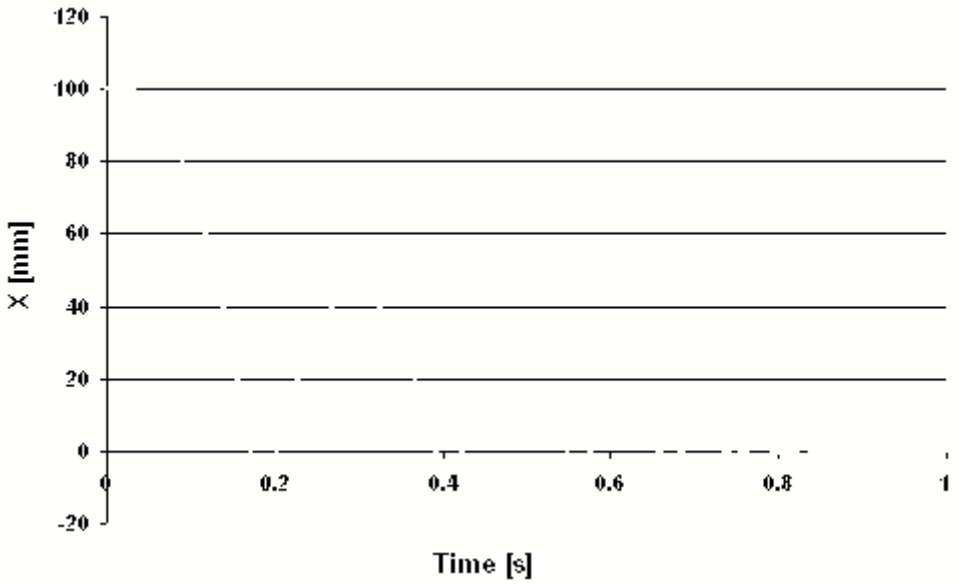

Fig. 1-16 Buffer axial deformation during a HWD test, from double integration of acceleration measurements

Buffer modulus is obtained by studying the relationship between force and deformation, considering an equivalent buffer (of same height and modulus as the 8 buffers, but a $\sqrt{8}D_0$ diameter, with D_0 the diameter of each buffer). Deformation under the 120 kN applied force is around 12 mm. This corresponds to a 10,5 MPa modulus, when performing the same identification procedure as previously.

Partial conclusions

This paragraph has shown that all buffers of a given set present, at least under static conditions, an identical behaviour. As their geometry is also identical, the force signal double peak can not be explained by buffers heterogeneity.
Static and dynamic moduli have been calculated.

1.3.2 Theoretical prediction of maximal force and pulse time

The experimental study presented in § 1.3.1 has shown that the rubber buffers have a linear-elastic behaviour and present similar stiffness values. The 8 buffers system may be modelled as a unique equivalent spring of k spring value.

Under this assumption, the applied strength over the pavement surface can be expressed as:

$$F(t) = -k\,x(t). \qquad \textbf{(1-2)}$$

With *x(t)* the buffer axial deformation.

Note that this expression is valid as long as the mass is in contact with the spring, that is to say between 0 and Δt.

A simplified calculation where the pavement deformation is neglected is first proposed. This approach is refined in a second step.

a - Simplified calculation neglecting pavement deformation (1 mass-spring system)

- Time-related applied force

The fundamental principle of mechanics applied to the falling mass gives:

$$M_0 \ddot{x} = -k x + M_0 g \qquad \textbf{(1-3)}$$

When defining $\omega^2 = \frac{k}{M_0}$, (1-3) becomes

$\ddot{x} + \omega^2 x = g$,

The general expression of this differential equation is:

$$x(t) = A\sin(\omega t) + B\cos(\omega t) + \frac{g}{\omega^2}$$

with A and B scalar numbers.

When considering the limit conditions $x(0) = 0$ et $\dot{x}(0) = \sqrt{2gH_0}$

one can find : $A = \frac{\sqrt{2gH_0}}{\omega}$ et $B = -\frac{g}{\omega^2}$

so that $x(t)$ can be expressed as :

$$\boxed{x(t) = \sqrt{\frac{2gH_0}{\omega^2} + \frac{g^2}{\omega^4}}\sin(\omega t + \varphi) + \frac{g}{\omega^2}}, \qquad \textbf{(1-4)}$$

with $\tan(\varphi) = \frac{B}{A} = -\frac{1}{\omega}\sqrt{\frac{g}{2H_0}}$

Thus it is proven that in the case of rigorously identical buffers with purely elastic behaviour, and in the absence of friction during the free fall phase, the external action applied to the pavement is of sinusoidal shape.

- F_{max} maximal force calculation

F_{max} is directly calculated as:

$$F_{max} = k \cdot x_{max} = \sqrt{2kgM_0H_0 + M^2g^2} + M_0 g \qquad \textbf{(1-5)}$$

Two extreme cases can be encountered:

- $H_0 = 0$ (mass placed without initial velocity at the top of the buffer system)

$F_{max} = 2 \times M_0 g$

In this case applied force is double the static force at equilibrium.

- H_0 is great ($H_0 >> \frac{M_0 g}{2k}$)

In this case the applied force is:

$$F_{max} = k.x_{max} = \sqrt{2k.M_0.g.H_0} \quad \textbf{(1-6)}$$

In this case the static part is negligible. The dynamic effort is found, which could have been calculated with an energy-based reasoning, when supposing negligible the friction during free fall phase. The principle of energy conservation implies:

$E_P = E_C = E_D$ **(1-7)**

where $E_P = M_0 g H_0$ is the potential energy of the mass at initial time, E_C the kinetic energy at the instant of the impact, and E_D the deformation energy of the buffer. The (1-7) equality means that the buffer warps until the whole kinetic energy has been converted.

The buffer deformation energy is expressed as:

$$E_D = \int_{x=0}^{x\,max} F\delta W = \int_{\varepsilon=0}^{\varepsilon\,max} k.x.\delta x = \frac{1}{2} k.x_{max}^2$$

x_{max} is determined by equalling E_P and E_D , which leads to:

$$x_{max} = \sqrt{2\,\frac{M_0.g.H_0}{k}}$$

Hence the value of maximal applied force is:

$$F_{max} = k.x_{max} = \sqrt{2k.M_0.g.H_0}$$

– Δt pulse time calculation

Δt is the first non null root of x(t), so that :

$$x(\Delta t) = \sqrt{\frac{2gH_0}{\omega^2} + \frac{g^2}{\omega^4}}\left(\sin(\omega\Delta t + \varphi) - \sin(\varphi)\right) = 0$$

$$\Rightarrow \omega\Delta t + \varphi = \pi - \varphi$$

$$\Rightarrow \Delta t = \frac{\pi - 2\varphi}{\omega} = \pi\sqrt{\frac{M_0}{k}} - 2 \times \varphi\sqrt{\frac{M_0}{k}}$$

In our case, $\varphi << 1$, so that $\varphi \approx \tan(\varphi) = -\sqrt{\frac{M_0 g}{2kH_0}}$

Hence $\Delta t \approx \pi\sqrt{\frac{M_0}{k}} + \frac{M_0}{k}\sqrt{\frac{2g}{H_0}}$ **(1-8)**

This expression implies the following variations:

- Δt increases with increasing static mass M_0,
- Δt increases when buffer system stiffness decreases,
- Δt increases when fall height H_0 decreases.

These trends have been confirmed from field observations.

- Numerical application and comparison with experimental data

- **k spring-constant value**

HB are here considered and their related dynamic stiffness.

When calling St the section of the equivalent buffer (same height, same apparent stiffness E), and x its deformation, the applied force is:
$F = k.x = k.H.\varepsilon = E.S_t.\varepsilon$
so that

$$k_{eq} = \frac{E.S_t}{H}$$

Section radius of each of the eight buffers is 5 cm.
Thus $S_t = 8 \times \pi \times 0{,}05^2 = 6{,}3.10^{-2}\ m^2$.
Their height is 0,08 m.
The experimentally determined apparent value under dynamic load is for the hard buffers set: EHB_{dyn} = 13 MPa what corresponds to kHB_{dyn} = 10 200 kN/m.

- **F_{max} and Δt values**

If M_0 = 680 kg, H_0 = 400 mm and k = 10 200 kN/m, then $\omega = 125\ s^{-1}$ and $\sqrt{2gH_0} = 2{,}8\ m.s^{-1}$.
Table 1-7 provides the numerical and experimental values, obtained from tests (performed on the Bonneuil-sur-Marne test facility; structure S_3 of appendix 1.1) used to determine EHB_{dyn}, for respective fall heights of 400, 300, 200 and 100 mm.

M_0 [kg]	**680**	**680**	**680**	**680**
k [kN/m]	**10210**	**10210**	**10210**	**10210**
H_0 [mm]	**400**	**300**	**200**	**100**
F_{max} Calc [kN]	240	209	172	124
F_{max} Exp [kN]	235	212	168	122
Δt Calc [ms]	26.1	26.2	26.3	26.6
Δt Exp [ms]	25.4	29.5	29.7	31.7

Table 1-7 Comparison between theoretical and field maximal force and pulse time values; pavement deformation neglected

Approximation is pretty good for F_{max}. However, for Δt, the influence of H_0 variation seems to be underestimated by the calculation.

- **Comparison between theoretical and experimental force signal**

Fig. 1.17 displays the theoretical versus experimental force signals corresponding to the "M_0=640kg / H_0 = 400 mm / Hard buffers set" material configuration.

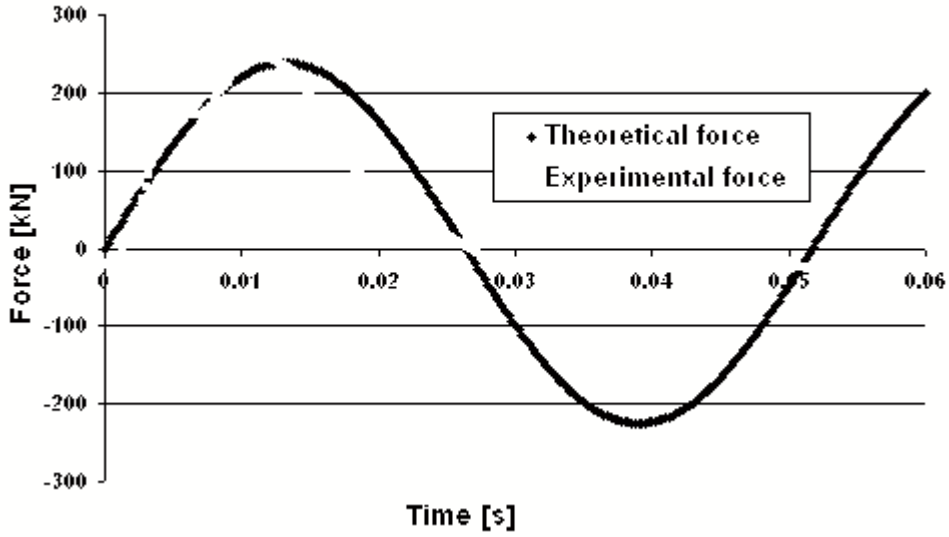

Fig. 1-17 Comparison between theoretical and field force history

The force signal, theoretically sinusoidal, presents in reality a double peak. This behaviour is widely reported in the literature. Nevertheless no explanation has been found. A refined calculation involving two mass-spring systems (one for the falling mass and buffers, and one for the pavement) is proposed in b-, since it seems that the observed trend may be obtained by the superposition of two sinusoids.

- ***A posteriori*** **verification of the hypothesis of incompressible pavement**

According to x(t) expression, maximal deformation of the spring is x_{max} = 23 mm. Since the mean range of deformation measured by the G_1 geophone is 0,5 mm, deformation of the pavement is well negligible with regard to the buffers one, so that the previous calculation seems to be good approximation. Nevertheless an improved calculation is conducted hereafter, in order to assess the difference.

In this calculation, an equivalent spring including the buffers and the pavement is considered.

Pavement is modelled as a multi-layered elastic media, with bedrock lying at the H depth. In the present case, H = 10 m. Nevertheless the whole subgrade volume is not affected during the HWD test.

When approximating the vertical propagation velocity using the shear waves velocity in subgrade (see literature review; $V_S = \sqrt{E_S/(2\rho_S(1+\nu))} \approx 100\ m.s^{-1}$ when $E_S = 75$ MPa and $\rho_S = 1\ 800$ kg.m^{-3}), neglecting the propagation times in surface materials (same calculation of V_S with E_S included between 5 000 and 20 000 MPa and ρ_S worthing about 2 300 kg.m^{-3} providing significantly higher velocities in asphalt materials, and thickness of these materials being significantly thinner), and considering a 30 ms time frame (corresponding to the pulse time), the subgrade layer to be considered in the calculation is about 3 m.

The sections S are approximated considering that a 45° stress cone is imparted to the pavement (Fig. 1-18).

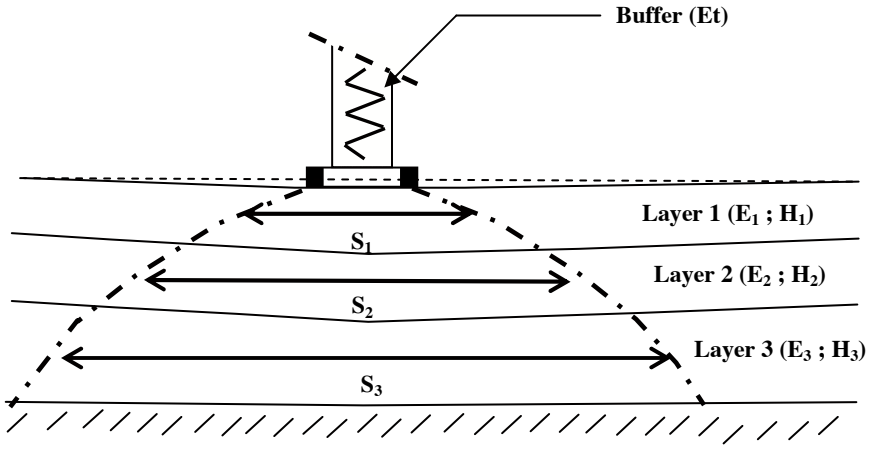

Fig. 1-18 Pavement cone model

A system of springs in series is thus studied, for which the inverse of spring constants have to be summed. Elementary stiffnesses are expressed as:

$$k_i = \frac{S_i.E_i}{H_i} \qquad \textbf{(1-9)}$$

The equivalent spring presents a spring constant of k_{eq} = 10 040 kN/m. Its calculation is detailed in Table 1-8. This value is very close to the equivalent buffer spring constant, so that the force signal is mainly governed by the buffer.

	H_i [m]	Mean depth [m]	R_i [m]	S_i [m]	E_i [MPa]	k_i [kN/m]	$1/k_i$ [N/m]
Buffer						1.02E04	9.8E-08
AC_1+AC_2	0.3	0.15	0.375	0.44	7 500	1.1E07	9.1E-11
UGA	0.5	0.55	0.775	1.89	420	1.6E06	6.3E-10
Gravel	0.7	1.15	1.375	5.94	270	2.3E06	4.4E-10
Subgrade	3	3	3.225	32.6	150	1.6E06	6.1E-10
						1/keq=Σ(1/ki)	1.0E-07
						keq (N/m)	1.0E+07

Table 1-8 Calculation of the pavement equivalent spring constant

Corresponding maximal force and pulse time are provided in Table 1-9.

M_0 [kg]	680	680	680	680
k [kN/m]	10040	10040	10040	10040
H_0 [mm]	400	300	200	100
Fmax Calc [kN]	238	207	170	123
Fmax Exp [kN]	235	212	168	122
Δt Calc [ms]	26.3	26.4	26.5	26.8
Δt Exp [ms]	25.4	29.5	29.7	31.7

Table 1-9 Comparison between theoretical and field maximal force and pulse time values; pavement modelled using a cone model

These numerical values confirm that the differences between simplified case considering that the pavement deformation is negligible with regard to the buffer one and the case where it is taken into account (through a cone model) are negligible.

b - Refined calculation (2 mass-spring systems connected in series modelling)

The previous simplified calculation provides a satisfactory approximation of the F_{max} and Δt values. Nevertheless, it does not explain the double peak.

A modelling involving 2 mass-spring systems connected in series is here proposed.

Let us call M and K the mass and spring constant corresponding to the falling mass and buffer system, and m and k the corresponding values for the pavement.

After contact between the falling mass and the top of buffers (time origin), the fundamental principle of mechanics applied to each of the mass implies:

$$\begin{cases} m\ddot{z} + (k+K)z - KZ = 0 \\ M\ddot{Z} + KZ - Kz = 0 \end{cases}$$

With z(t) and Z(t) respectively the vertical displacements of the pavement surface and the falling mass

Initial conditions are :

$$Z(0) = z(0) = \frac{Mg}{k}(1 - \cos\omega T)$$

$$\dot{z}(0) = \frac{Mg}{k}\omega \sin\omega T$$

$$\dot{Z}(0) = -V_0 = -\sqrt{2 \cdot g \cdot H_0}$$

Harmonic solutions of the form $\alpha\cos\omega t + \beta\sin\omega t + \gamma\cos\Omega t + \delta\sin\Omega t$ are searched

The angular frequencies ω and Ω are thus solutions of the system:

$$\begin{pmatrix} k+K-m\omega^2 & -K \\ -K & K-M\omega^2 \end{pmatrix}\begin{pmatrix} z \\ Z \end{pmatrix}=\begin{pmatrix} 0 \\ 0 \end{pmatrix}$$

and thus the solutions of:

$$mM\omega^4-(MK+Mk+mK)\omega^2+Kk=0$$

According to initial conditions, $\alpha=\gamma=0$, $\beta=\frac{1}{\omega}\frac{V}{K}\frac{K-M\Omega^2}{M\left(\Omega^2-\omega^2\right)}$ and

$$\delta=-\frac{1}{\Omega}\frac{V}{K}\frac{K-M\omega^2}{M\left(\Omega^2-\omega^2\right)}$$

$$z(t)=\beta(K-M\omega^2)\sin\omega t+\delta(K-M\Omega^2)\sin\Omega t$$
$$Z(t)=\beta K\sin\omega t+\delta K\sin\Omega t$$

$$z=\frac{1}{\omega}\frac{V}{K}\frac{\left(K-M\Omega^2\right)\left(K-M\omega^2\right)}{M\left(\Omega^2-\omega^2\right)}\sin\omega t-\frac{1}{\Omega}\frac{V}{K}\frac{\left(K-M\Omega^2\right)\left(K-M\omega^2\right)}{M\left(\Omega^2-\omega^2\right)}\sin\Omega t$$

$$Z=\frac{V}{\omega}\frac{K-M\Omega^2}{M\left(\Omega^2-\omega^2\right)}\sin\omega t-\frac{V}{\Omega}\frac{K-M\omega^2}{M\left(\Omega^2-\omega^2\right)}\sin\Omega t$$

Finally resulting force is provided by:
$F(t)=K\left(z(t)-Z(t)\right)=M\ddot{Z}(t)$

what gives:

$$F(t)=\frac{V}{\Omega^2-\omega^2}\left((M\Omega^2-K)\omega\sin\omega t+(K-M\omega^2)\Omega\sin\Omega t\right)$$

It appears that a 10-ratio between the deformations of buffer and pavement surface, and a 4-ratio between angular frequencies are required for this theoretical expression to match the field force signal from Fig. 1-3 i.e.:

$$(K-M\omega^2)\Omega=\frac{(M\Omega^2-K)\omega}{10}$$

and $\Omega=4\omega$

With the considered test, pavement deformation is about 1,2 mm against 23 mm for the buffers, i.e. deformations are in a 20-ratio, which is acceptable.
Nevertheless, condition on angular frequencies is not fulfilled. Actually, according to the previous relation, typical rebound frequency is about 16 Hz. A 50 Hz frequency is thus required. In practice characteristic frequency of the pavement response is lower than 16 Hz,

what allows ascertaining that the pavement deformation is not the right cause of the observed double peak in the force signal.

One can imagine, to explain the observed phenomenon, that a part of the HWD foot would vibrate at a 50 Hz frequency with a 1 mm amplitude after the shock. Another explanation would be that the buffers behaviour, apparently linear and homogeneous for the whole buffer set under static action, is more complex in dynamic mode.

As a conclusion, simplified modelling with a double spring-mass system fails to interpret the observed double peak on force signal. A FEM calculation considering initial falling mass velocity is proposed in part 2 to confirm this result.

2 - Reliability of HWD tests

2.1 Repeatability study

2.1.1 Presentation of the experiment

- **Purpose**

The presented experiment is aimed at:

- studying repeatability of measurements on given test points, and understanding the involved phenomena,
- assessing influence of the relative heterogeneity of the pavement (supposed to be rather homogeneous, as being a test facility structure) and of the HWD repositioning. Tests have been performed using the STAC's HWD protocol on flexible structures presented in Appendix B-I. According to this protocol, test points are previously marked and a video camera helps the driver to precisely position the loading plate; a few centimetres precision is possible in the repositioning,
- evaluating the influence of temperature on results. This work is in progress: it is expected that the experiment presented here will be performed again in the future for other pavement temperatures.

Repeatability data will be used in the main second part, coupled with the results of a theoretical sensitivity study, in order to assess expected precisions of the dynamical backcalculation procedure and choose a consistent target mean squared error value. Note that the latter study will use time-related deflections. Nevertheless, for readability of the results, only the deflection basins will be displayed.

Linearity of the pavement response has been also studied in the frame of this experiment. Results are not presented in this paragraph but the dedicated part of the document (§ 3.3.1).

- **The studied structure**

The experiment has been performed on the STAC's test facility, presented in details in appendix 1.1 (structure S_3). The construction of this pavement was initiated on 2005 (M. Broutin / J.C Deffieux collaboration).

The structure is:

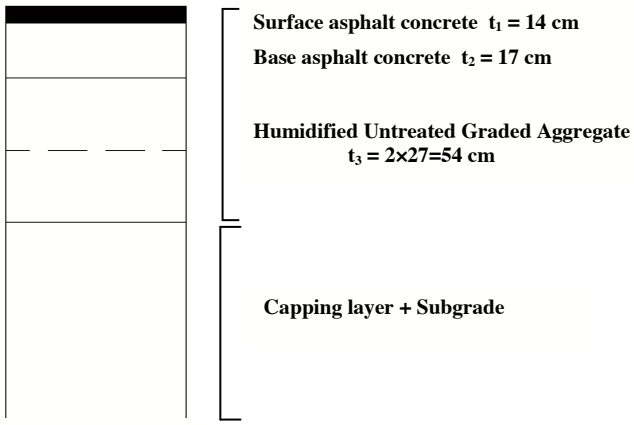

Fig. 1-19 Studied S_3 structure

Homogeneity of the structure is assumed to be representative of an usual airfield pavement, even if imposed construction specifications have been more rigorous than for real pavements.

- **Organization of a general test cycle**

Eleven (11) test points have been chosen (Fig. 1-20) with a regular offset of 1,50 m, settled in the centre area of the facility in order to avoid any boundary effects (maximal distance to facility edge of 10 m).

Four test cycles have been performed, each one composed of three phases:

- Phase 1: Successive testing of the points 1 to 11. Each test is made of 2 test sequences. The first one presents four (4) HWD falls from the 400 mm drop height (about 252 kN) and the second one four (4) falls from the 100 mm (about 116 kN) drop height.
- Phase 2: HWD is positioned again on the first measurement point. The two same sequences (four falls from the 400 mm fall height and four falls from the100 mm fall height) are performed consecutively ten times.
- Phase 3: again on the first point, the two same sequences (four falls from the 400 mm drop height and four falls from the 100 mm drop height) are again performed consecutively ten times, but inserting a one (1) minute rest time between the ten (10) series.

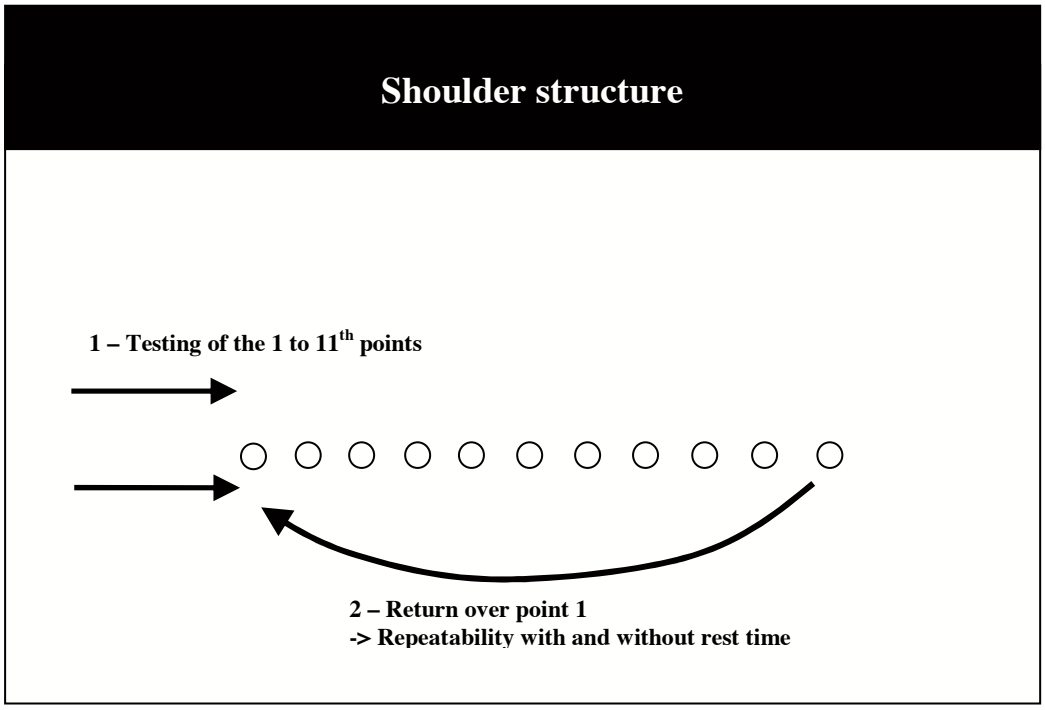

Fig. 1-20 Organization of a test cycle

This testing protocol provides valuable information about:

- the scatter of test results on 10 test points (points 2 to 11, the first point being left) of a theoretically homogeneous area,
- repeatability on a same test point, with or without rest time,
- influence of the device repositioning, when comparing results of cycles 1 to 4,
- possible occurrence of material consolidation (point 1).

Test time is about 70 minutes for each test cycle.

Note that this work relies on the analysis of raw data, considering that fall height is rigorously constant between the falls. The uncertainty on this parameter is unknown, i.e. no normalization process has been performed. Actually, normalization of the results is not obvious, since a variation in the fall height implies a variation, not only in the maximal force but in the whole signal, as seen above. This point will be discussed hereafter.

- **Temperature evolution**

The experiment has been performed in the early morning in order to prevent large temperature variations. According to the STAC's HWD experimental protocol (see appendix 1.3), temperature probes have been set in the asphalt layer, the first one at the top of the layer, the second one at mid-depth, and the last at the bottom, in order to monitor the evolution of this parameter during the experiment (Fig. 1-21). It can be estimated that temperature has remained constant during the whole experiment, a minor variation of 0,4 °C being noticed on mean temperature. Uniformization of temperature in the pavement is observed. Its consequence is a minor increase in surface stiffness and on the contrary a decrease in stiffness under, the mean stiffness being preserved.

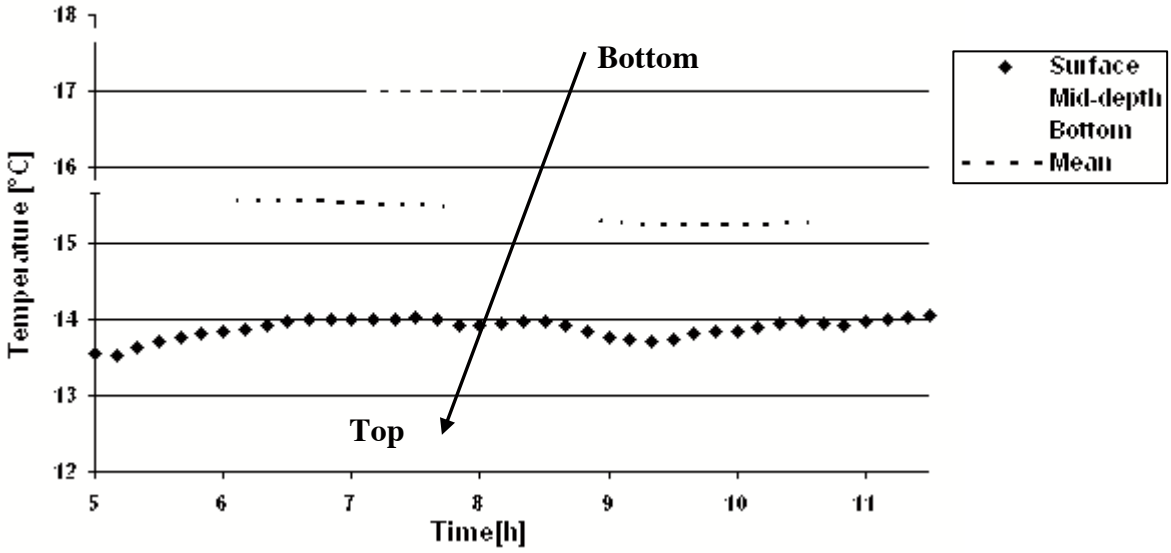

Fig. 1-21Temperature evolution in asphalt layer during the whole experiment

2.1.2 Repeatability inside a test sequence

Usual practice ([COST 1999] or protocol proposed in appendix 1.3) consists in applying for each HWD test sequence, three identical (i.e. of same fall height) repeated tests, preceded by a "setting fall". This setting fall is not recorded. No consensus has been found to decide whether the mean value over the three falls or only the last fall results have to be considered for backcalculation. The second hypothesis is the most widely admitted and is retained in the STAC's protocol, under the assumption that good repeatability nevertheless exists between the three falls (no aberrant value). The following results will determine whether this choice has an importance.

In this experiment, the setting fall has been made ineffective and four-falls tests sequences have been performed.

An example of results is presented and compared to theoretical geophones uncertainties provided by the manufacturer. Then, slight evolution of results is examined by studying for all tests normalized deflections with regard to first fall.

- **Example of results**

Fig. 1-22 displays the deflection basins for the four 400 mm falls of the first series of the first test cycle.

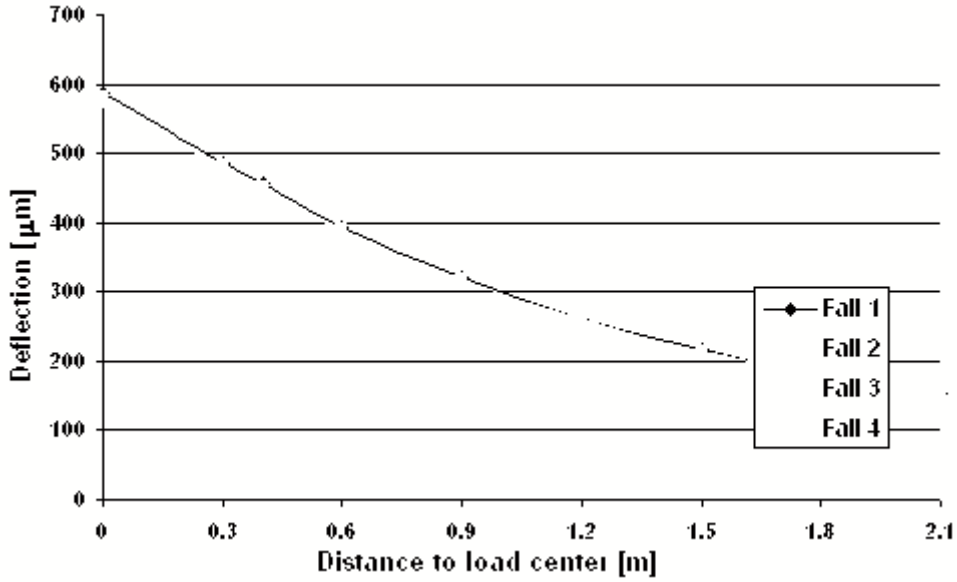

Fig. 1-22 Example of deflection basins

Repeatability of results seems *a priori* pretty good, as curves are almost superposed. Nevertheless, a general decreasing trend near the load and an increasing one for outer geophones is observed. Note that pavement temperature is not involved since each test only lasts a couple of seconds.

- **General study**

These results are confirmed by all tests.
Table 1-10 collects mean peak values calculated for each geophone on all tests performed on points 2 to 11 (point 1 being a particular point, subjected to more tests than the others) for cycles 1 to 4, corresponding to the first sequence of each test (H= 400 mm).

	d_1	d_2	d_3	d_4	d_5	d_6	d_7	d_8	d_9
Fall 1	597,8	502,4	472,7	411,5	336,7	274,5	226,7	188,5	159,4
Fall 2	590,6	496,9	467,5	407,5	334,4	273,4	226,5	188,8	160,1
Fall 3	588,4	495,1	466,0	406,5	334,0	273,2	226,5	189,0	160,2
Fall 4	587,4	494,7	465,8	406,5	334,1	273,4	226,7	189,3	160,5

Table 1-10 Evolution of deflections (in [µm]) with regard to considered fall for the 9 geophones

Repeatability between consecutive falls is good. For instance the mean difference between the second and fourth fall on central geophone is about 3 µm for a 600 µm value so that the choice of considering the mean value of these 3 falls or the last fall seems to be *a priori* insignificant.

- **Slight evolution**

The aforementioned trend is observed on each result, so that it is statistically not due to a coincidence. It is well emphasized on Fig. 1-23 which displays normalized deflection basins with regard to first fall, still corresponding to mean value for all tests.

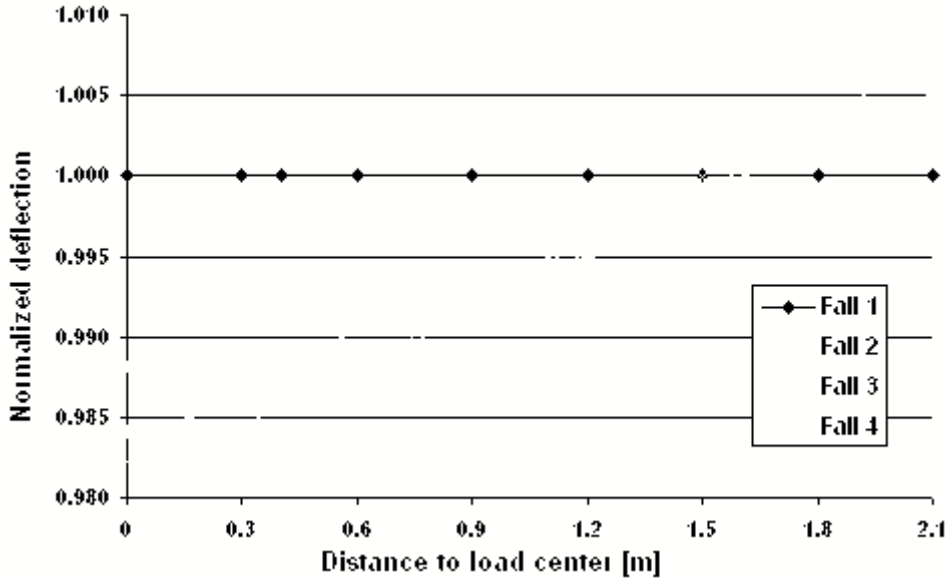

Fig. 1-23 Evolution of deflection between the four consecutive falls of a test sequence

Besides, comparison with theoretical geophones uncertainties provided by the manufacturer confirms that the geophones uncertainty does not explain the observed differences.

The latter is ± 2 % or better and resolution is 1 μm. The relative $U_{2\%\ st}$ and $U_{1\mu m\ st}$ standard uncertainties are thus respectively 2 % × d_i and 0,5 μm, d_i being the maximal deflection measured on the i^{th} geophone. The global standard uncertainty $U_{tot\ st}$ is given by:

$$U_{tot\ st} = \sqrt{U_{2\%\ st}^2 + U_{1\mu m\ st}^2}$$

A $1/\sqrt{44}$ ratio has been applied to theoretical results, as studied values correspond to a mean value on 11×4 = 44 tests (11 test points and 4 cycles).

Table 1-11 collects results for all geophones.

Geophone	Deflection [μm]	$U_{2\%}$	$U_{1\mu m}$	U_{tot}
G_1	588,8	1,78 (0,30%)	0,08 (0,01%)	1,78 (0,30%)
G_2	497,1	1,50 (0,30%)	0,08 (0,02%)	1,50 (0,30%)
G_3	468,0	1,41 (0,30%)	0,08 (0,02%)	1,41 (0,30%)
G_4	408,6	1,23 (0,30%)	0,08 (0,02%)	1,23 (0,30%)
G_5	335,8	1,01 (0,30%)	0,08 (0,02%)	1,02 (0,30%)
G_6	274,8	0,83 (0,30%)	0,08 (0,03%)	0,83 (0,30%)
G_7	227,8	0,69 (0,30%)	0,08 (0,03%)	0,69 (0,30%)
G_8	190,1	0,57 (0,30%)	0,08 (0,04%)	0,58 (0,30%)
G_9	161,1	0,49 (0,30%)	0,08 (0,05%)	0,49 (0,30%)

Table 1-11 Theoretical uncertainties measured on geophones (manufacturer data)

- **Stabilization**

A stabilization of the phenomena is observed. Fig. 1-24 compares deflection standard deviations between falls 1 to 3 and between falls 2 to 4.

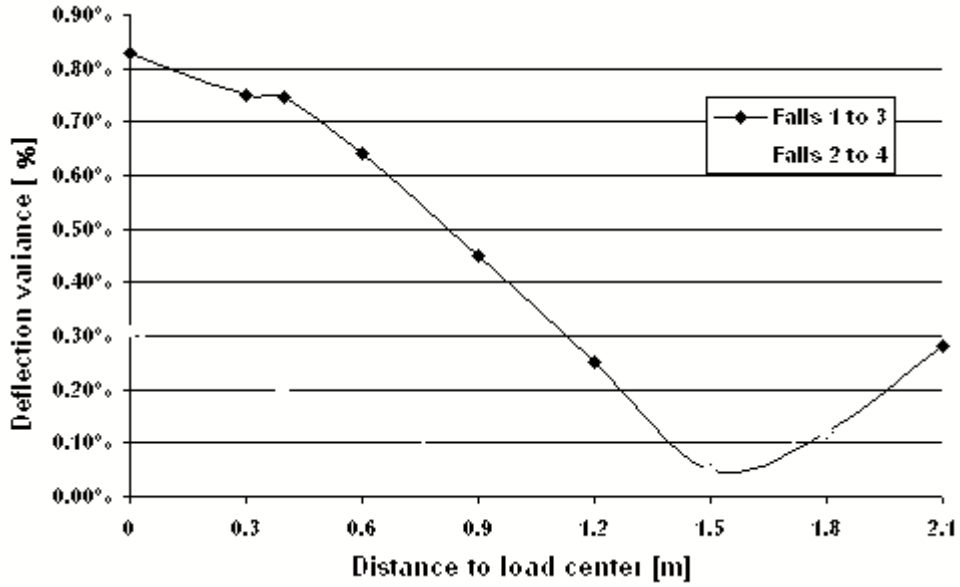

Fig. 1-24 Standard deviation calculated on 3 falls

As a conclusion, HWD test sequence presents a good repeatability. Nevertheless the general observed trend denotes an evolution of the pavement under repeated loads. Many interpretations can be imagined. One of them could be a consolidation of the pavement under the load, what would be consistent with the stabilization aspect.

2.1.3 Repeatability of tests

In this paragraph only, the mean values on the falls number 2 to 4 is considered. It has been seen that this choice is of no importance.

- **Influence of repositioning**

Fig. 1-25 and 1-26 present the evolution of the d_1 and d_5 deflections with regard to the cycle number. Repeatability is very good with regard to the scatter of results between the different test points. Operationally, it means that the repositioning of the device has no influence on the pavement testing, when respecting the STAC's experimental protocol (see appendix 1.3).

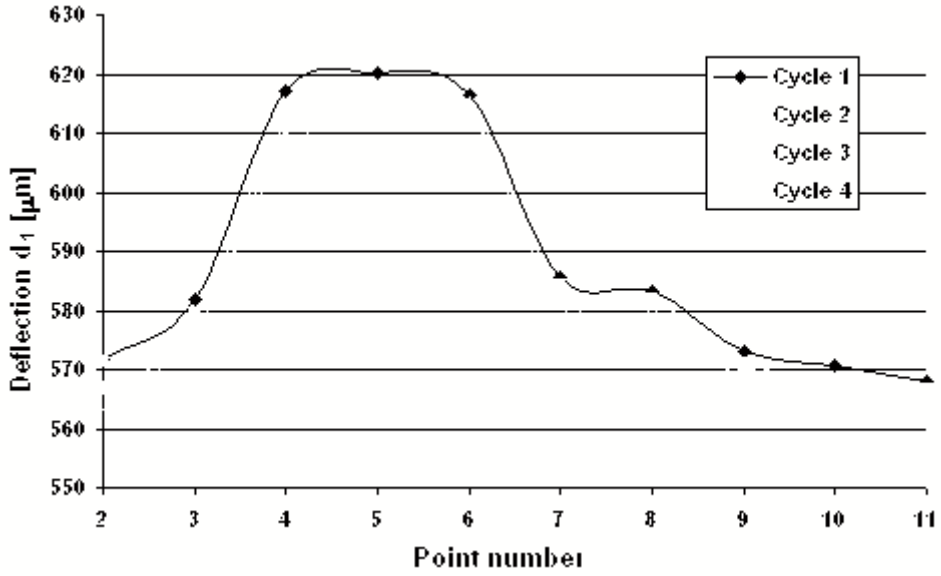

Fig. 1-25 Evolution of the deflections between the four measurement cycles (Geophone 1)

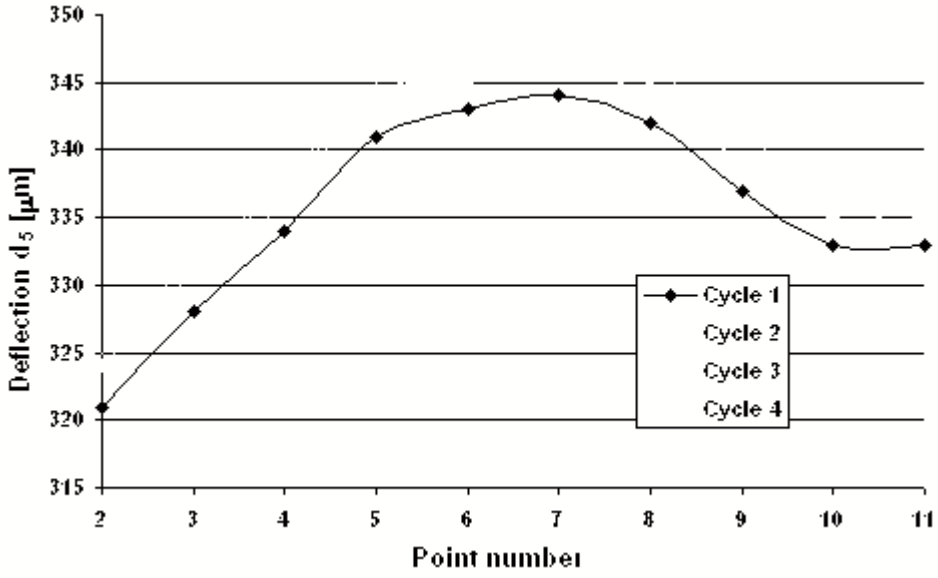

Fig. 1-26 Evolution of the deflections between the four measurement cycles (Geophone 5)

Besides, a general trend is also observed, so that it can again be assumed that differences are representative of an evolution of the pavement. Curves corresponding to others geophones are not presented here. General trend is that deflection decreases (i.e. apparent stiffness increases) near the load plate (geophones 1 to 3), and increases far from it (geophones 5 to 9).
On the contrary to comparison between the different falls of a same sequence, temperature effect can not be dismissed here, even if its variation is limited.

- **Repeatability of test vs spatial scatter**

Fig. 1-27 and 1-28 compare the scatter of results on the ten (10) measurement points (points 2 to 11) with the scatter resulting from ten (10) sequences performed on a same point, with and without rest time.
It appears that scatter of results relative to different points is much higher, especially when comparing to the repeatability on a same point with rest times. It implies that the HWD is well adapted to assess pavement behaviour homogeneity.

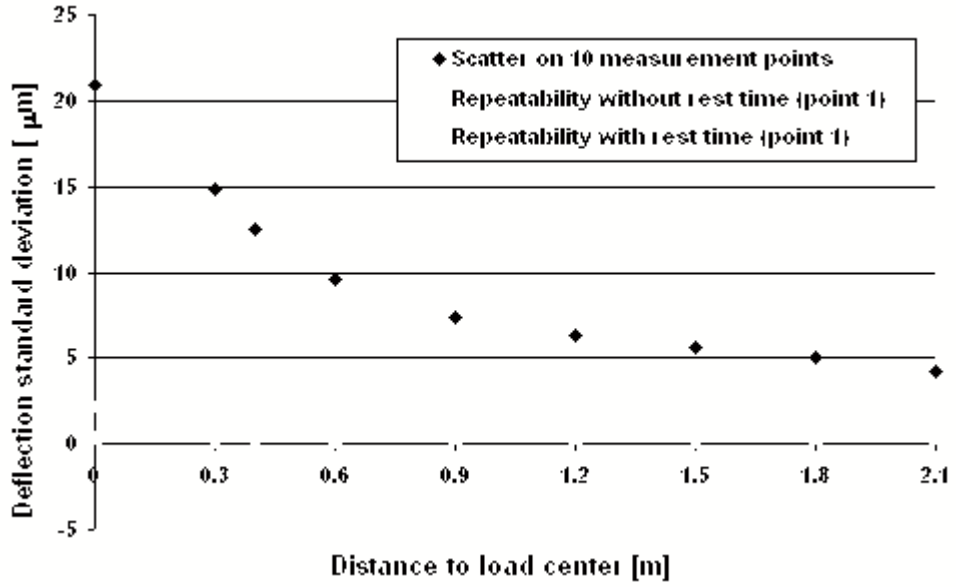

Fig. 1-27 Comparison between scatter on 10 measurement points and repeatability on a given test point, with and without rest time between HWD tests

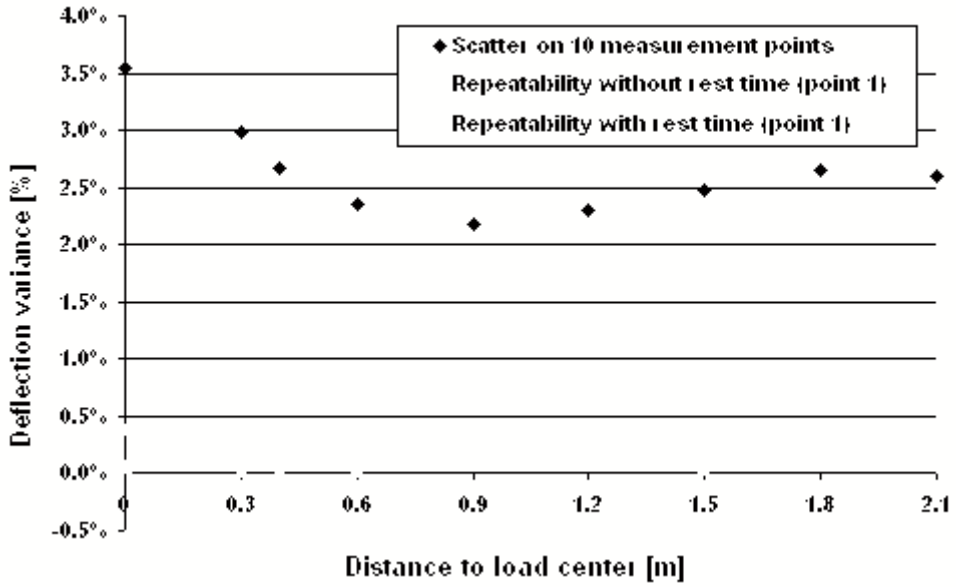

Fig. 1-28 Comparison between scatter on 10 measurement points and repeatability on a given test point, with and without rest time between HWD tests; normalized values

- **Detections of weak zones**

Geophones close to the load plate provide information about the whole structure bearing capacity, whereas outer geophones are representative of the deeper layers behaviour.
Now, the analysis of Fig. 1-25 and 1-26 demonstrates that weak zones are observed respectively between points 4 to 6 and 5 to 8. It indicates a local weakness of deep layers between points 5 to 8, and a relatively better surface layer on points 7 and 8, and worse on point 4. As the tested pavement has been recently built, it should present no distresses. Therefore, the most reasonable hypothesis is interpreting deflection variations in terms of layer thicknesses.

This hypothesis has been confirmed, since two corings have been performed on the test facility, after the experiment: one on the P_2 point, and one on the P_5 (see appendix 1.1 for further details). Thickness of the UGA layer is actually 11 cm thinner on point P_5, whereas the asphalt layers have equivalent thicknesses (1 cm higher on P_5).

- **Rest time**

As displayed in Fig. 1-27 and 1-28, repeatability is improved when rest time are inserted between test sequences.
Fig. 1-29 compares the variation of the deflection under the plate on a same test point with and without rest times. Deflection decreases in both cases but in a much slower manner when the material is allowed to rest.

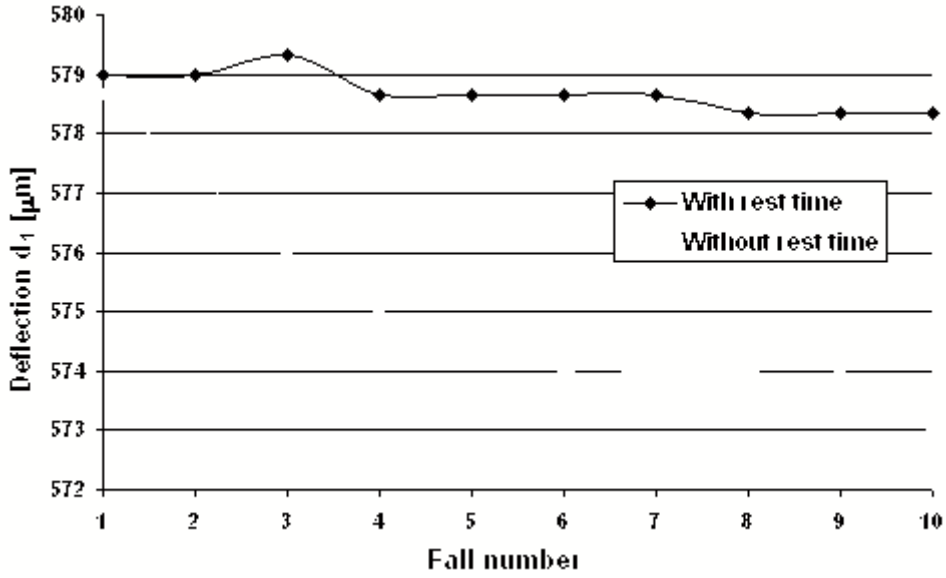

Fig. 1-29 Influence of rest time on HWD tests repeatability

It must be emphasized that the observed differences are in the range of few microns, so that even without any rest time, repeatability remains pretty good. Nevertheless a general decreasing trend is well observed.

It would be interesting to perform a parametric study where the Dt rest time would vary.

This behaviour could be interpreted by a reversible rearrangement of asphalt materials under repeated loads, rather than consolidation in granular layers, what would explain that after a rest time, pavement finds back its initial state. One can imagine a material reorganization under heavy load, leading to a decrease in void ratio, and consequently to a stiffness increase. Deflection under load would accordingly decrease. In a second phase, material would then relax.

The differences noticed inside a sequence could also originate from this phenomenon. Table 1-12 shows that Point 1 does not present a higher deflection decrease than the others when considering only the first sequence, what confirms that consolidation is negligible.

Point →	1	2	3	4	5	6	7	8	9	10	11
Cycle 1	576.0	571.7	582.0	617.0	620.3	616.3	585.7	583.3	573.0	570.7	568.0
Cycle 2	578.7	571.3	579.3	611.3	615.3	613.0	584.3	582.0	570.7	566.7	566.7
Cycle 3	574.7	567.0	576.0	609.7	614.3	615.0	583.0	576.3	571.0	567.3	562.3
Cycle 4	575.3	563.3	576.3	606.7	613.3	612.7	581.0	579.0	568.3	564.0	561.3
Mean value M	576.17	568.33	578.42	611.17	615.83	614.25	583.50	580.17	570.75	567.17	564.58
St. deviation σ	1.75	3.95	2.82	4.34	3.11	1.73	1.99	3.13	1.91	2.74	3.25
Variance σ /M	0.30%	0.70%	0.49%	0.71%	0.50%	0.28%	0.34%	0.54%	0.34%	0.48%	0.58%

Table 1-12 Evolution of deflections between the different test cycles; points 1 to 11

Nevertheless, this phenomenon does not explain the slight evolution observed between the consecutive test cycles. One can assume that the latter is due to a slight evolution in temperature values.

- **Influence of applied force**

Fig. 1-30 presents the influence of force on results for the two considered fall heights.

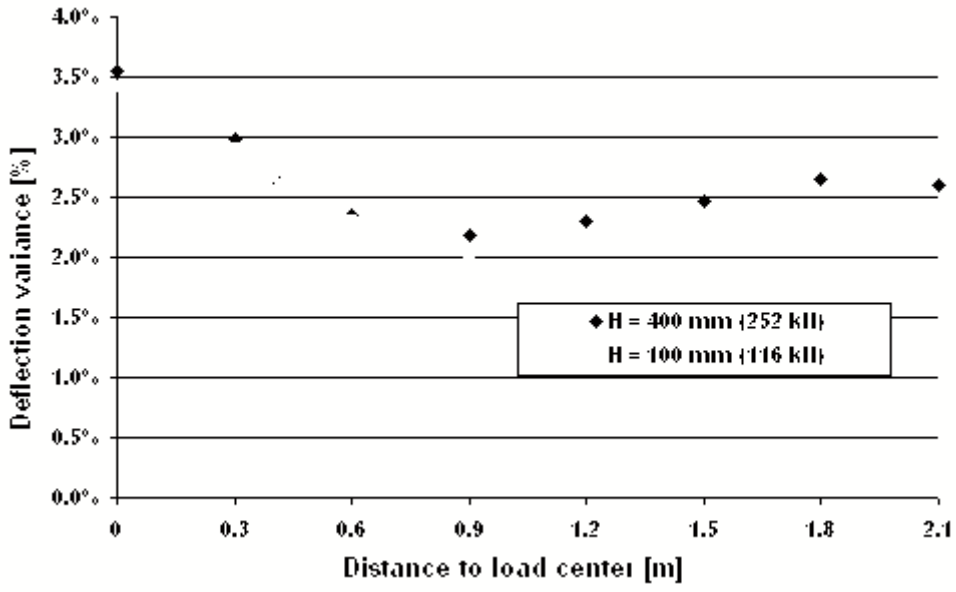

Fig. 1-30 Influence of applied force on HWD tests repeatability

Force level has a limited influence on the results scatter, so that it can be considered that the obtained variance ranges can be extended to all HWD tests, at least when performed on similar pavement structures.

2.1.4 Normalization attempts

Normalizations with regard to the maximal F_{max} force have been tested. Scatter of results is higher than without normalization. Thus it appears that the Δt evolution is not negligible. Other types of normalizations attempts have failed. They considered:

- the dissipated energy (area under the d_1 signal),
- $F_{max} \times \Delta t$.

Thus a specific experiment has been performed in order to analyze evolution of maximal force and pulse time with fall height and to assess the influence of the second parameter.

It appears that F_{max}/d_1 decreases with fall height, what is contradictory to the assumed linear behaviour of pavement. Moreover, relative influence of pulse time is higher than the one of maximal force.

The experiment has consisted in applying repeated loads, at different fall heights. It has been performed on the 5^{th}, 6^{th} and 7^{th} points of the repeatability experiment. Mid-depth temperature in the asphalt layer was 20°C. In practice, fall height has been set from $H_0 = 400$ mm to 100 mm with a constant 10 mm step. Corresponding maximal force has decreased from 240 to 110 kN and the central deflection from about 600 to 300 μm, whereas the Δt pulse time has increased from 29,5 to 34 ms. These trends are in accordance with previous theoretical results: deflection decreases and pulse time increases when fall height decreases, even if these calculations assumed a rigorously elastic behaviour of pavement ($F_{max}/d_1 = Cste$).

Fig. 1-31 displays the relationship between F/d_1 and Δt for point 5. It is almost linear. When considering a mean deflection of 450 μm it seems that a 1 ms (about 3 %) variation in Δt corresponds to a 20 kN variation in F_{max} (about 15 %).

It implies that the Δt parameter is preponderant and confirms that a normalization only considering maximal force value is not correct.

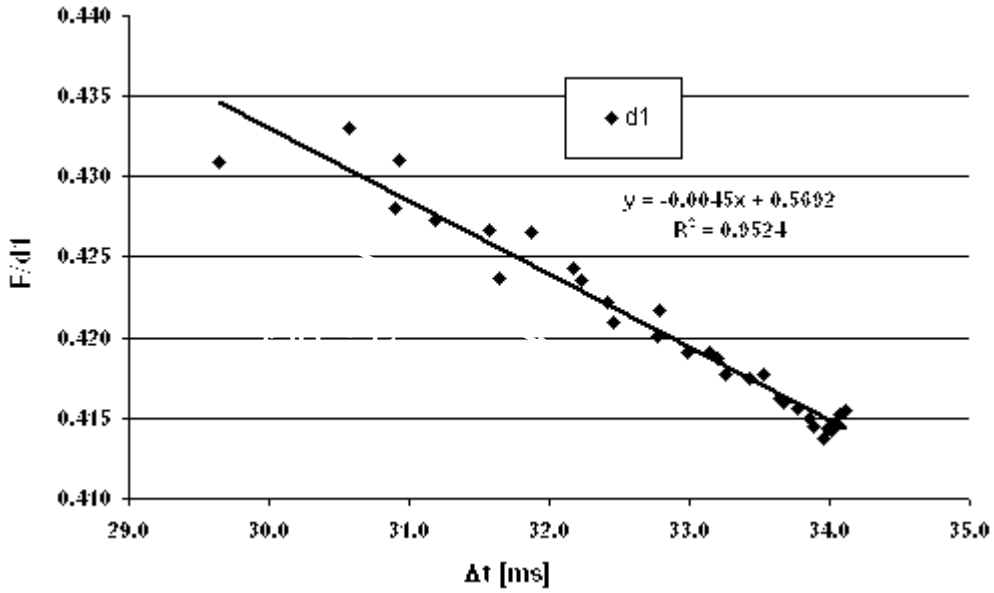

Fig. 1-31 Evolution of apparent pavement modulus with pulse time; central geophone

Decrease in F_{max}/d_1 may be explained by viscous phenomena in asphalt pavement. Actually, the response of these materials is frequency-dependent. Their modulus decreases when load application time increases, hence a reduced pavement apparent modulus (proportional to F_{max}/d_1) is obtained.

Fig. 1-32 displays normalized values for central and outer geophones. It appears that variation in apparent modulus is reduced when distance to load centre increases.

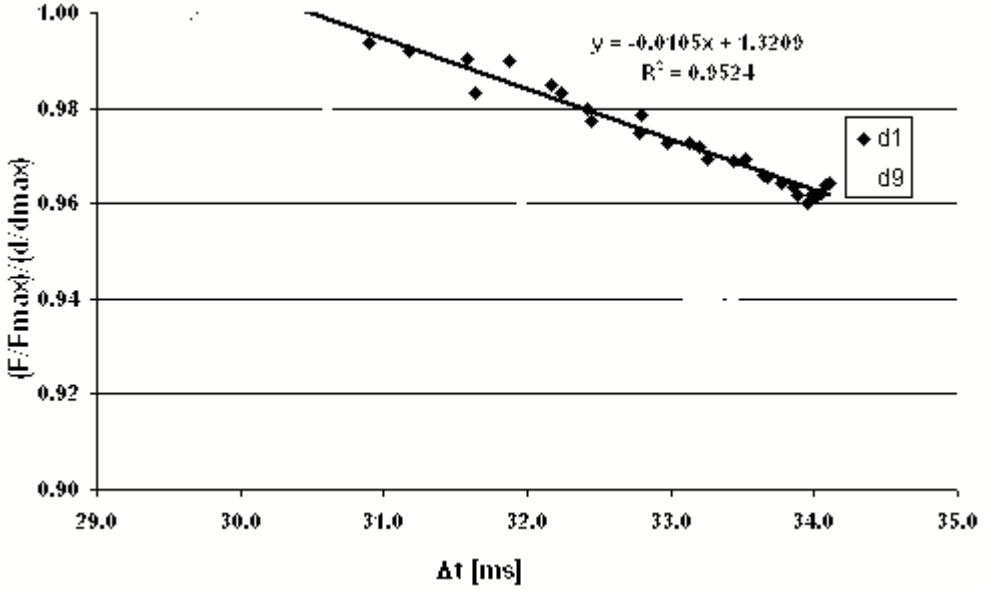

Fig. 1-32 Comparison between apparent modulus of pavement with regard to central and outer geophones; normalized values

As the impact of the surface layers in the deflection results decreases with distance to the load centre, it confirms that asphalt materials are involved in the observed phenomenon. This could suggest that difficulties encountered to normalize HWD tests could come from the viscoelastic behaviour, specific to asphalt materials. This assumption is reasonable since the

modulus of asphalt materials decreases when the application time of strength increases due to viscoelastic effects. That could explain the decrease in F_{max}/d_1.

Note that deviations between theoretical and experimental pulse time values previously observed for low fall heights (§ 1.3.1), could partly be explained by these viscoelastic effects. Actually the proposed numerical resolution is based on a purely elastic modelling.

Equivalent results are found on points 6 and 7.

A normalization of the repeatability study using d_1 dependence with F_{max} and Δt was tried but without any success. An explanation could be that it is not possible to generalize the previous results to all pavements, since it may depend on temperature in the asphalt layer, and on type of asphalt materials.

Question needs to be deepened.

In the following of the work, no normalization has been performed.

Partial conclusion

This paragraph has allowed determining available precisions on HWD raw data, and deflections scatter to be expected between test points of a theoretically homogeneous pavement. It also highlighted that the device positioning has a limited influence on HWD results, in the case of flexible pavements.
A slight and reversible evolution in the pavement behaviour under repeated loadings has also been evidenced.
Finally, the influence of the force pulse time on pavement apparent stiffness has been emphasized, which could be attributed to creep phenomena in the asphalt materials. This dependency renders the results normalization complex.

2.2 Reliability of measurements

2.2.1 HWD deflection measurements vs deep anchor information

A wide-scale HWD survey has been performed on the LCPC's fatigue carrousel between April 2008 and July 2009 on pavements dedicated to a multiwheel effect study [Homsi et al., 2010] consisting in studying influence of axle configuration on different road pavement structures.

Several studies have been carried out using HWD, as
- a deflection study on the several structures of the annulus,
- a specific study of the water table influence (not presented in this work) ,
- HWD measurements over embedded gauge profiles. This work will be detailed in part 3. It has been performed on the S_2 structure described in appendix A, which is the thicker pavement of the annulus and thus the closer to airport structures.
- a comparison between deflections given by HWD and a deep anchor.

Let us interest here to the latter experiment. It has been performed July 2009. The deep anchor is composed of a LVDT (Linear Variable Differential Transformer sensor) measuring the surface displacement with regard to a deep reference (here a 3 m deep concrete blocking).

Measurements have consisted in (manually, due to sought precision) placing, for geophones 2 to 9 successively, the HWD so that the considered geophone metal tip is placed over the deep anchor head, and performing a HWD test in this configuration, when recording in parallel the LVDT response.

Fig. 1-33 displays the comparison between HWD and deep anchor time-related deflections measurements for the second geophone. Note that time was manually adjusted as HWD and external recording systems are independent. Applied peak force was about 75 kN. Tests have been performed in the early morning to minimize temperature variations and gradient. This gradient is all the same 7 °C. Temperature ranges from 24°C (surface) to 31°C (see appendix 1.2). A slight non return to zero at the end of signal is observed. As this phenomenon is not observed in Fig. 1-3, at low temperatures, this may reflect some viscous behaviour of asphalt materials.

Correlation between the two signals is of same quality for the 3 falls and the 8 considered geophones, so that it can be assumed that deep anchors measurements are reliable for HWD dynamic assessment. Geophone 1 has not been tested because positioning was too complicated.

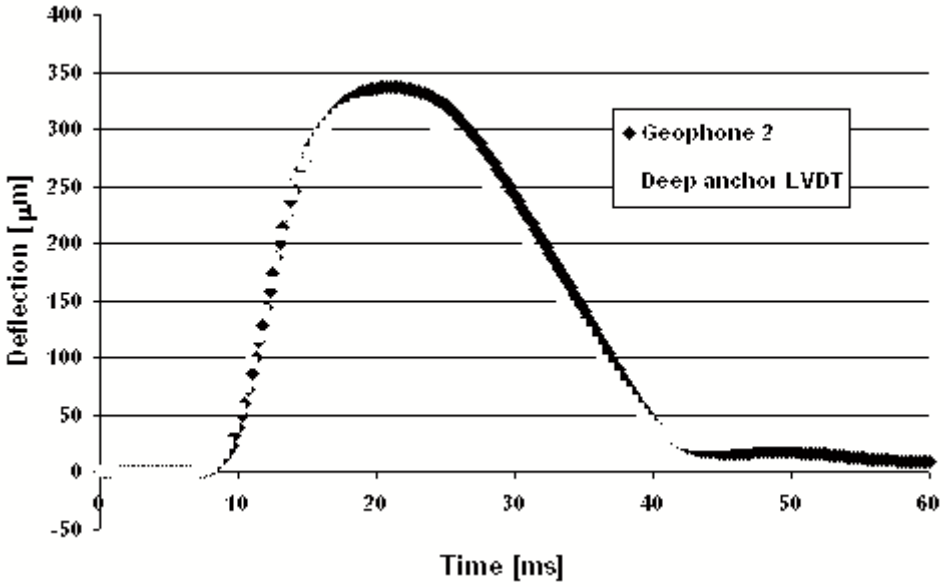

Fig. 1-33 Correlation between HWD and deep anchor surface deflection measurement; geophone 2

This experiment opens interesting new prospects. Whereas HWD record is limited to a 120 ms time frame, the external instrumentation presents the advantage of allowing deflection measurement on time frames as large as requested. It allows:

- following the response of the pavement under static setting of the HWD foot,
- observing successive occurring rebounds,
- studying long-time pavement response.

Fig. 1-34 displays results for all geophones. Force and geophone 1 response are provided by HWD. Time origin has been fitted using HWD geophone 1 response. Fig. 1-35 shows the good repeatability of applied load for all tests.

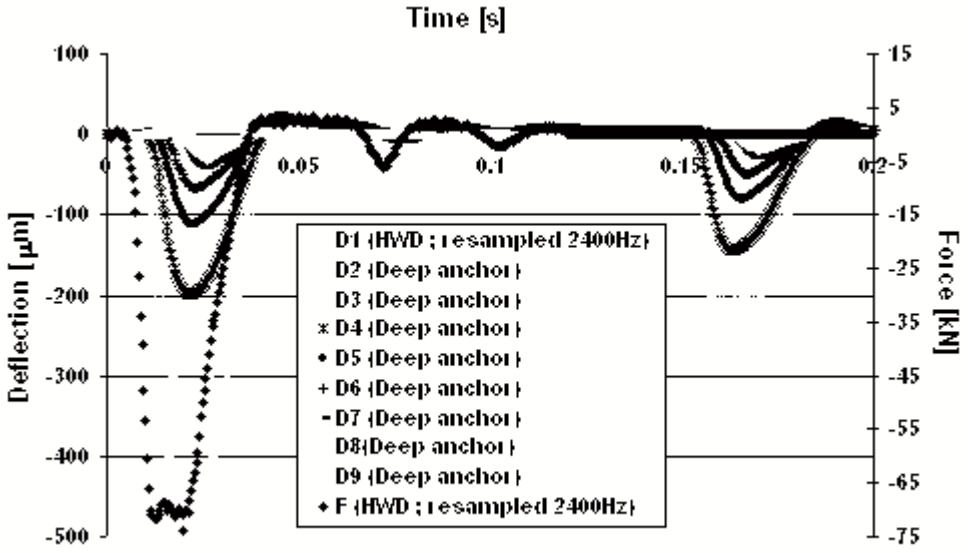

Fig. 1-34 Long-time time-related deflections provided by a deep anchor

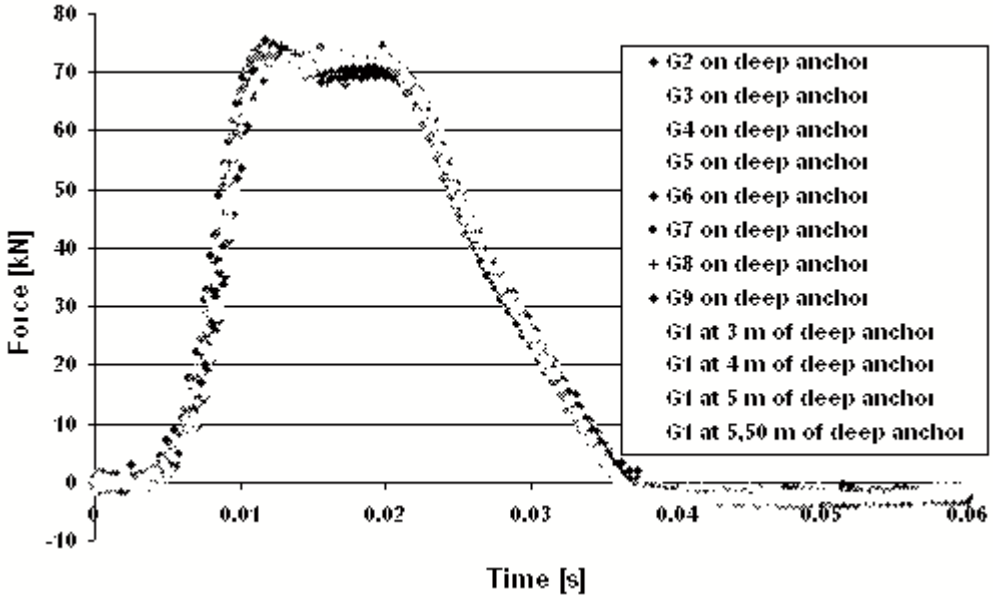

Fig. 1-35 Repeatability of applied force between tests

Partial conclusion

The deep anchor of LCPC's fatigue carrousel has allowed checking deflections values provided by HWD. Thus it appears that this type of external instrumentation is an interesting tool to assess HWD deflections reliability. Two deep anchors have been set on the STAC's Bonneuil test facility in this purpose.
Second interest of deep anchors is allowing measurements on extended time frames. It will be taken advantage of these findings in the following (see § 3.2).

2.2.2 Comparison with external instrumentation data

The study presented here is the second part of the accelerometer-based external instrumentation experiment. The main purpose is here to check the value of time delay observed in Fig. 1-3. Direct measurements of force sensor and central geophone raw signals are used, as it is practically too complicated to measure central deflection with an accelerometer. Besides acceleration measurements are used to assess the applied force and deflections. These values are compared with data from HWD data measuring chain.

Once more a spider has been used. Unfortunately, because of limited memory of the apparatus, when desiring recording at least principal impact and first rebounds with a 3 200 Hz acquisition rate, only two channels can simultaneously been followed. Nevertheless repeatability of results is good enough so that tests can be multiplied.

- **Preliminary studies**

- influence of external parallel connection

Before testing, it was necessary to check that parallel connection on the spider has no influence on the HWD results. This study has been performed by repeating tests with and without external connection. It appears that the latter has no effect. Results are not presented here.

- integration of geophone raw signals

Fig. 1-36 presents results of integration of the geophones raw signals, compared with signals provided by HWD measuring chain, for geophones 1, 2, 5 and 9. No transfer function has been applied as the latter is unknown. A “k” gain has been applied, which seems to be common to all geophones.
A very good match is found, when only considering the increasing part of signal. It demonstrates that geophones raw signals can be used in the frame of this study.

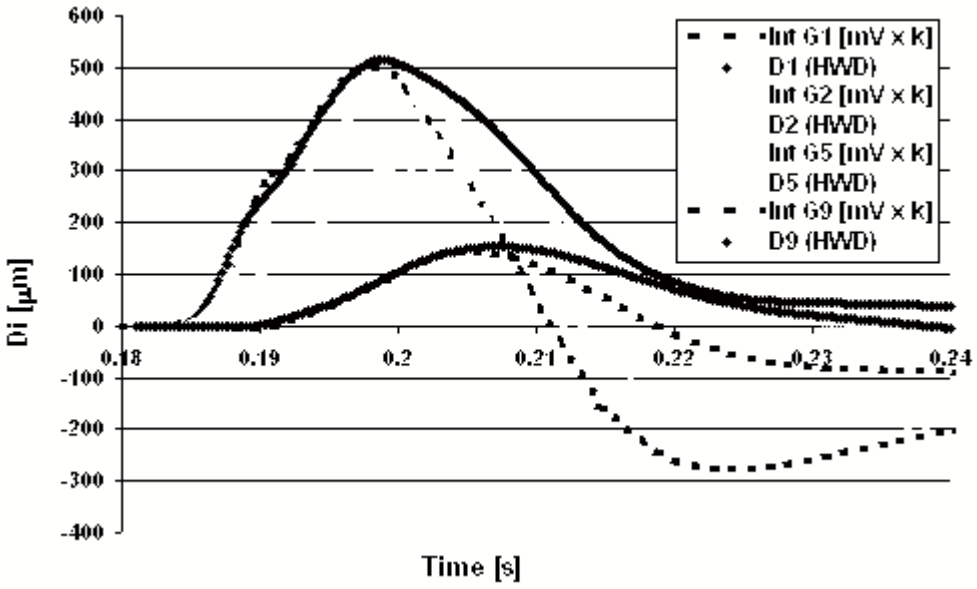

Fig. 1-36 Comparison between direct integration and treated geophones signals

- **Time delay study**

Two sets of data are compared. On the one hand the force and central geophone signals given by HWD, and on the other hand the same signals acquired by spider. When the time origin is manually fitted to superpose both force signals (Fig. 1-37; note that a gain has been applied to electrical force signal), a 3,5 ms gap is observed between the peak values of central geophone (Fig. 1-38).

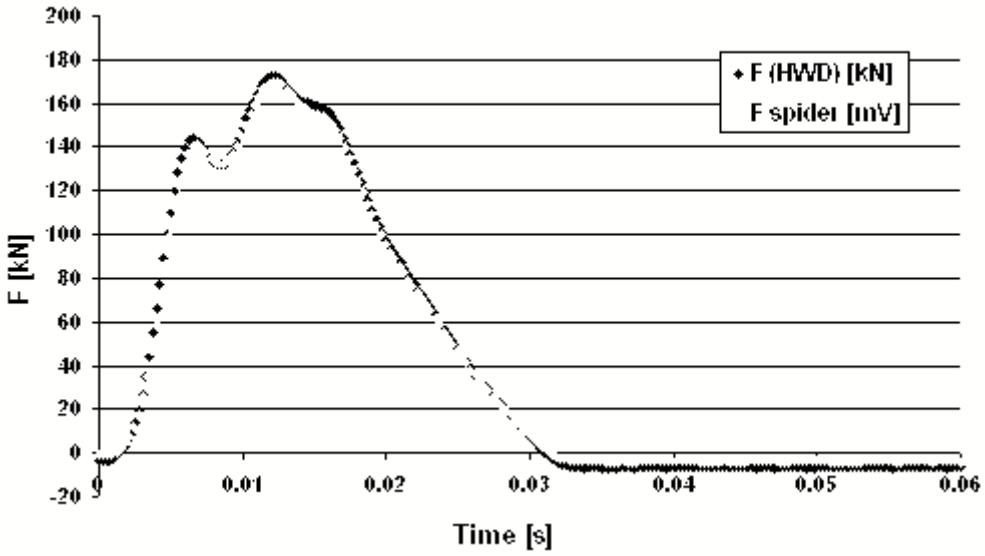

Fig. 1-37 Time fitting performed on force signals

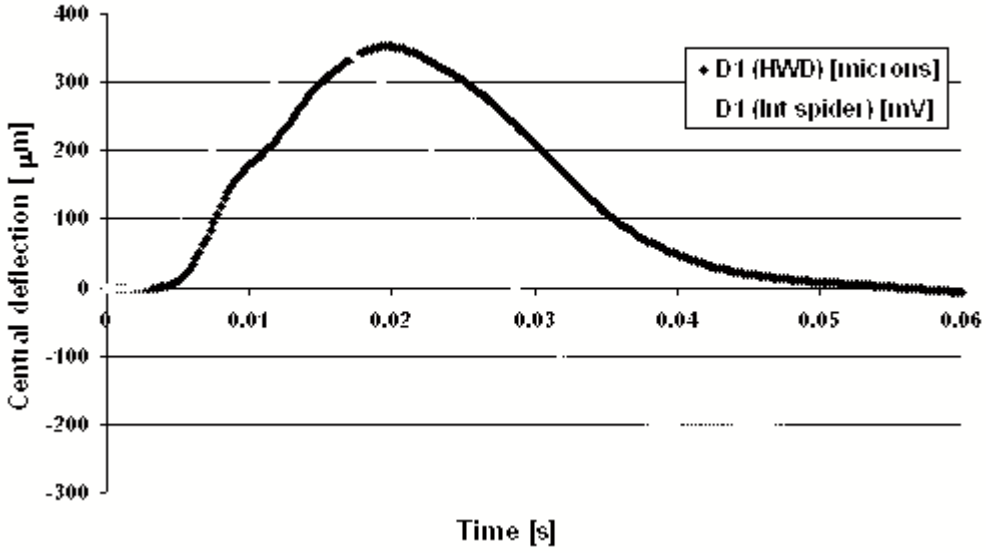

Fig. 1-38 Time gap between HWD and spider-measured central deflection signal

Results of the two test surveys (winter and summer) performed on the S_1 structure have been used to study evolution of time delay with the different parameters (buffers type, plate, fall height, temperature).
Temperature has only a limited influence, what is a first argument confirming that such an important time delay is not attributable to viscous effects.
The most important parameter is the fall height.
Respective mean time delays for the 400, 300, 200 and 100 mm fall heights are 3,39/3,35/3,41/3,59 ms for the winter experiment (mean pavement temperature: 6°C) and 3,56/3,61/3,67/3,90 ms for the summer experiment (mean pavement temperature: 30°C)

No answer about the observed bias has been found from the manufacturer. It may be due to a buffering in the HWD acquisition chain which would start the deflections measurements only when a threshold signal is observed on the force value. This issue is to be deepened.

- **Force vs acceleration of the falling mass**

Fig. 1-39 compares applied force recorded by the HWD measuring chain and the one deduced from acceleration measurement for a 100 mm fall height. Both signals match relatively well. Nevertheless rapid oscillations are observed on the mass acceleration. They are of constant period so that they can traduce the natural frequency of a piece of the HWD foot.

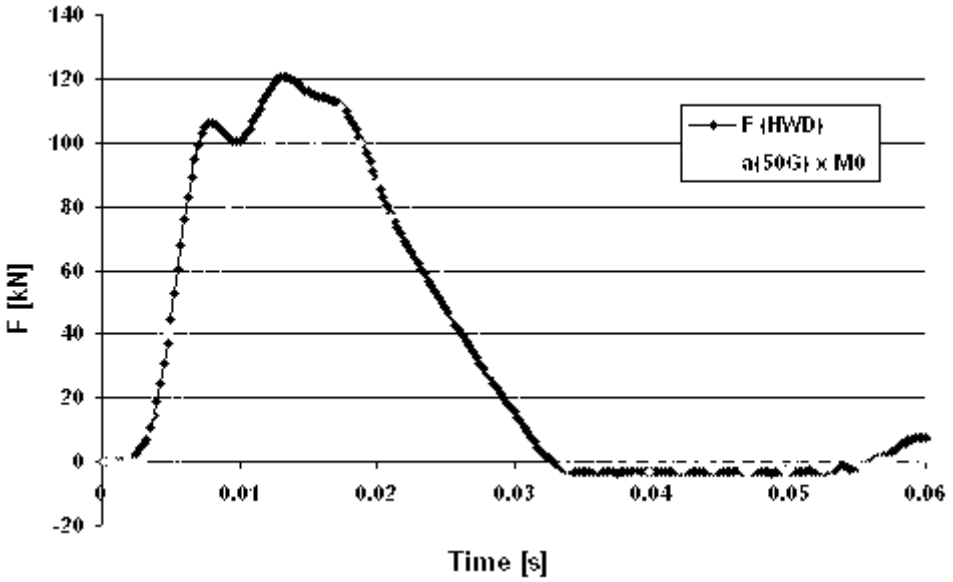

Fig. 1-39 Comparison between directly measured and acceleration-deducted applied force signal

- **Deflection signals; geophones vs accelerometers**

The relationship between HWD measured deflections and accelerometers is studied here. As a limited range of accelerations is required, 5 G accelerometers are used to provide better precisions. They are made interdependent with geophones thanks to a metal plate fixed on the geophones metal boxes (Fig. 1-40).

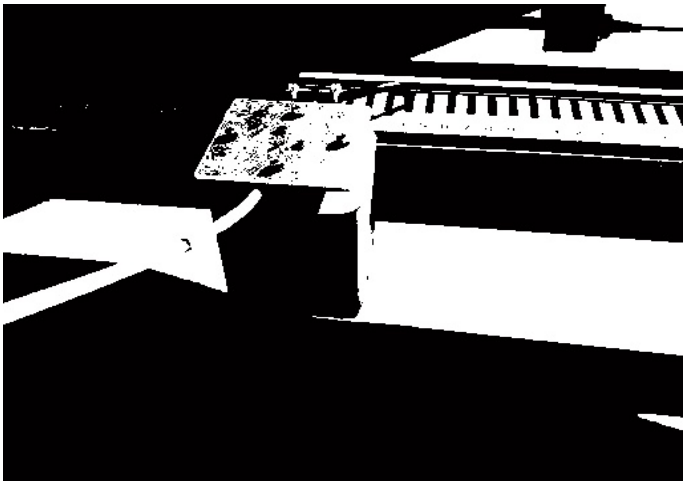

Fig. 1-40 Fixing of accelerometers on the geophones boxes

Fig. 1-41 and 1-42 display the comparison between deflections provided by HWD and a double integration on accelerometer signals, respectively for geophones 5 and 9. Note that acceleration and velocity signals are not at scale, but have been adjusted for readability. Matching is excellent for both geophones.

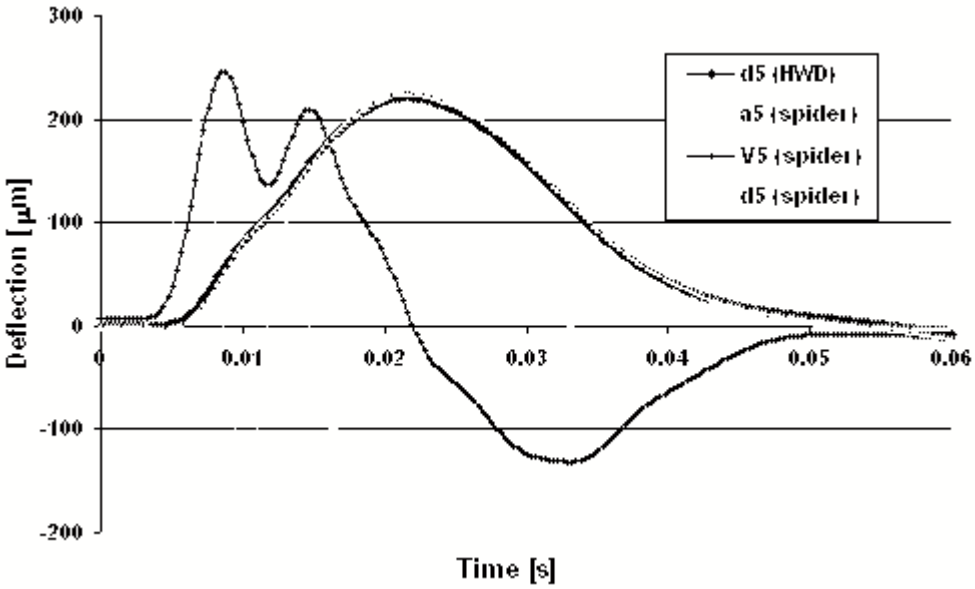

Fig. 1-41 Comparison between HWD and accelerometer deduced time-related deflection on geophone 5

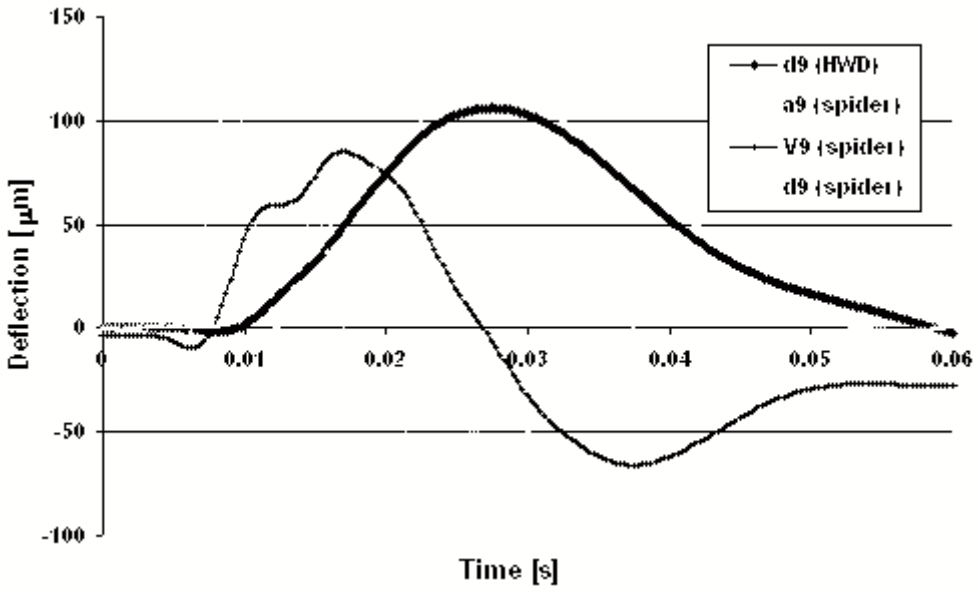

Fig. 1-42 Comparison between HWD and accelerometer deduced time-related deflection on geophone 9

- **Possibility of measuring wider deflections basins, during longer times**

A feasibility study to measure time-related deflections on a longer time and at higher distances is proposed here. Let us here interest to geophone signals, recorded by the spider. The protocol involves a long external heighten beam on which geophone boxes are fixed (Fig. 1-43) for high distances. First, it has been demonstrated that the external beam choice has no influence on the results. In that goal raw geophones data measured at 90 cm and 210 cm respectively mounted on the HWD and on this external beam have been compared. Conclusion is geophone measurements using external beam are valuable.
Then 6 distances have been chosen: geophones 1, 2, 5 and 9 in standard configuration, and geophones at 3 m and at 6 m on the external beam.
In order to have significant signals at 6 m from load centre, the H_0 = 400 mm is retained.

Fig. 1-43 Test setup to measure long radial distances deflections

As previously explained, only two signals can simultaneously be recorded. The chosen protocol consists thus in performing 5 successive tests, the central geophone being common to all tests, and performing a time fitting on it.
Fig. 1-44 shows the electrical signals of central geophone after time fitting for the different tests. Curves match very well, what demonstrates the repeatability of the test. Elapsed time between principal impact and first rebound is this time about 450 ms.

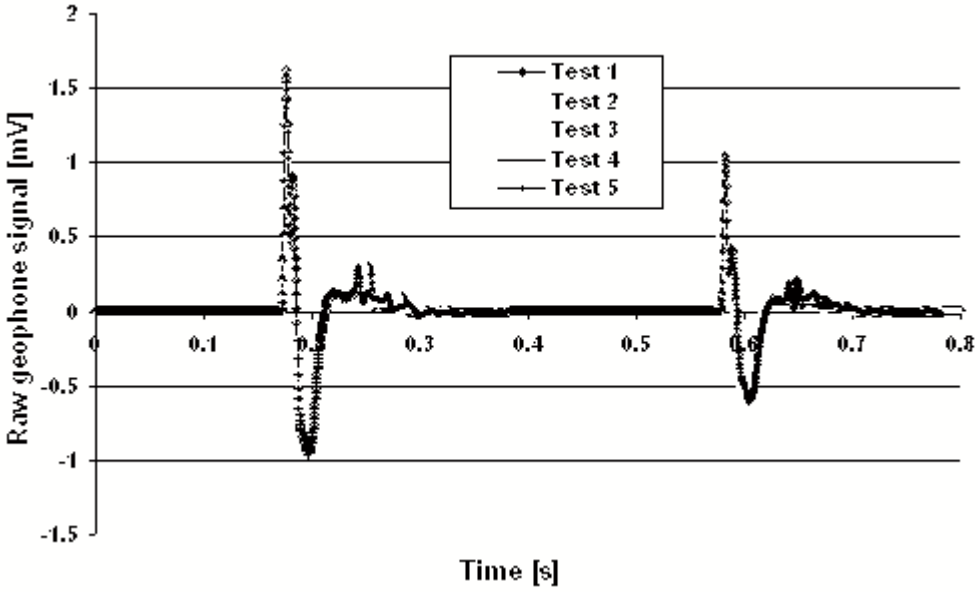

Fig. 1-44 Electrical signals related to the different tests (central geophone)

Integrated time-related signals corresponding to the 6 geophones are displayed in Fig. 1-45 and Fig. 1-46.

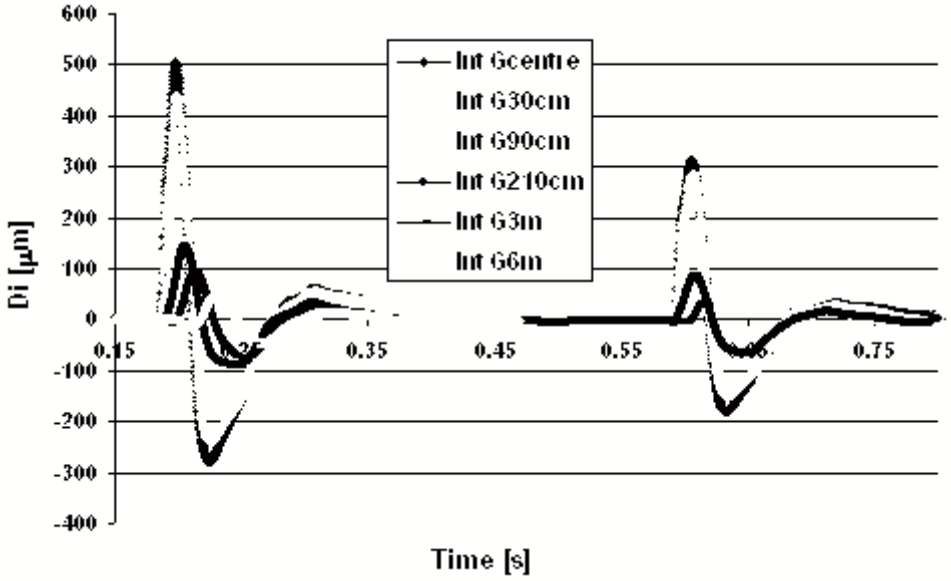

Fig. 1-45 Surface displacements at several distances from load centre; integration from geophone electrical signals (1/2)

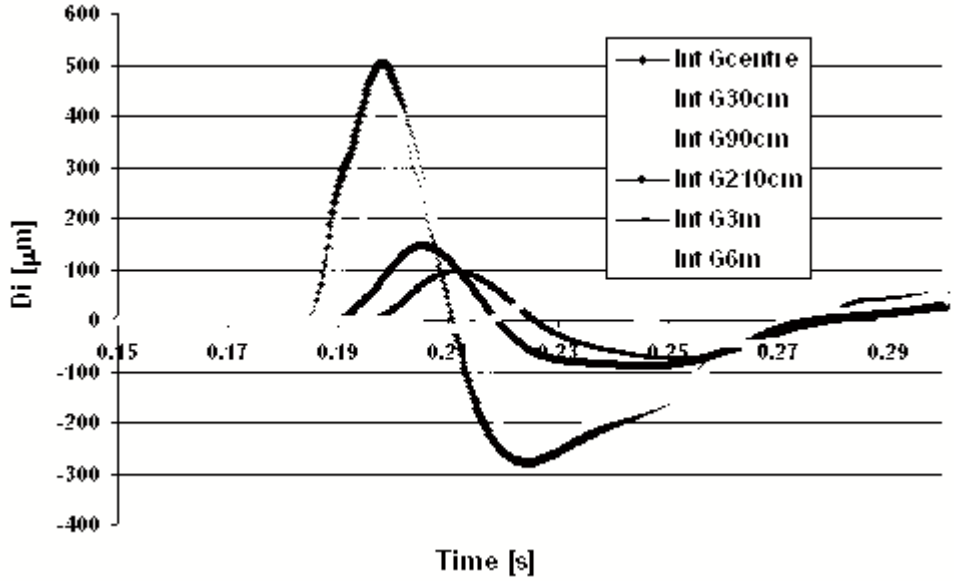

Fig. 1-46 Surface displacements at several distances from load centre; integration from geophone electrical signals (2/2)

These curves are of valuable help when interesting to waves propagation or to deflection basins. Nevertheless, it was initially expected that geophones raw data could be used, but in reality decreasing part of signals is unfortunately incorrect, so that they can not be used for dynamical analysis. It is expected that the experiment is performed again with accelerometers.

Partial conclusion

This paragraph has shown that the observed time delay between occurrence of force and central deflection signals is at least partially attributable to a measurement bias and not viscous phenomena. It will be emphasized in part 3 that this bias can have significant influence on dynamical backcalculation results, so that the issue needs to be deepened.
It has also been shown that fixing an accelerometer on the falling mass is not the appropriate method to evaluate force applied to the pavement due to mechanical vibrations in the HWD foot. A dedicated calibration bank is in preparation on the STAC's test site.
Feasibility of measuring wide deflection basins on long times has been demonstrated. The last mentioned experiment is to be performed again with accelerometers. STAC has acquired rapid acquisition system unit allowing 10 kHz acquisition rates on 24 measuring tracks.

2.2.3 Crossed tests with other F/HWD

Crossed tests with the FWD of road ministry have been performed in the frame of the LCPC fatigue carrousel experiment. 22 test points have been tested in July 2009 (pavement temperature in the 24-31°C range; see appendix 1.2). Same load level and same loading plate have been used. Results are very good in terms of maximal deflections. Results are not presented in this document.

Nevertheless time delays between force and central deflection signals are different, what confirms the sensed aforementioned bias. Fig. 1-47 summarizes results.

Mean gap between the two apparatus values is about 2 ms i.e. about 50 % of the HWD value.

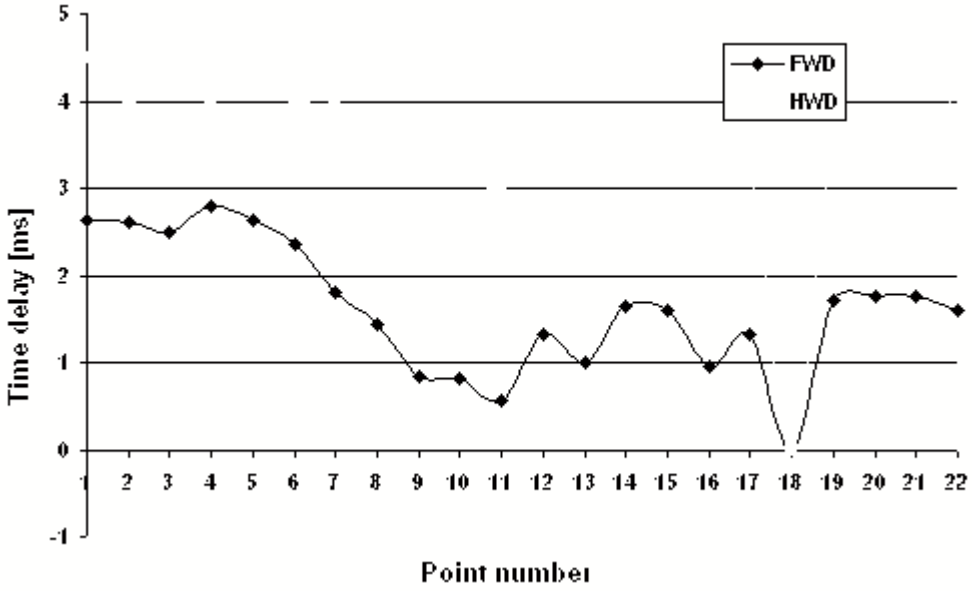

Fig. 1-47 Differences between STAC's HWD and French road ministry's FWD occurrence of the central deflection

3 - Empirical analysis of the pavement response

3.1 Linearity of results

Two fall height levels were used in the frame of the repeatability study (§ 2.1). Comparison between results obtained for the two load levels (respectively 252 kN and 110 kN on average for H_0 = 400 and H_0 = 100 mm fall heights) allows evaluating linearity of the subgrade behaviour.

A simple indicator is the $\delta=F_{max}/d_1$. Respective values calculated for H_0 = 400 and H_0 = 100 mm are δ_{400} = 2,33 μm/kN et δ_{100} = 2,37 μm/kN for the test series considered, what indicates that subgrade behaviour can approximately be considered as linear ; the slight decrease in δ versus force denotes a slight stress-softening behaviour.

Apparent modulus calculated using the Boussinesq formulation (see dedicated part in the literature survey part) confirms that. The curves corresponding to the two load levels are almost superposed, and horizontal when d≥90cm. These two pieces of information imply a linear behaviour and the absence of shallow bedrock what has been confirmed by a geotechnical survey (see appendix 1.1).

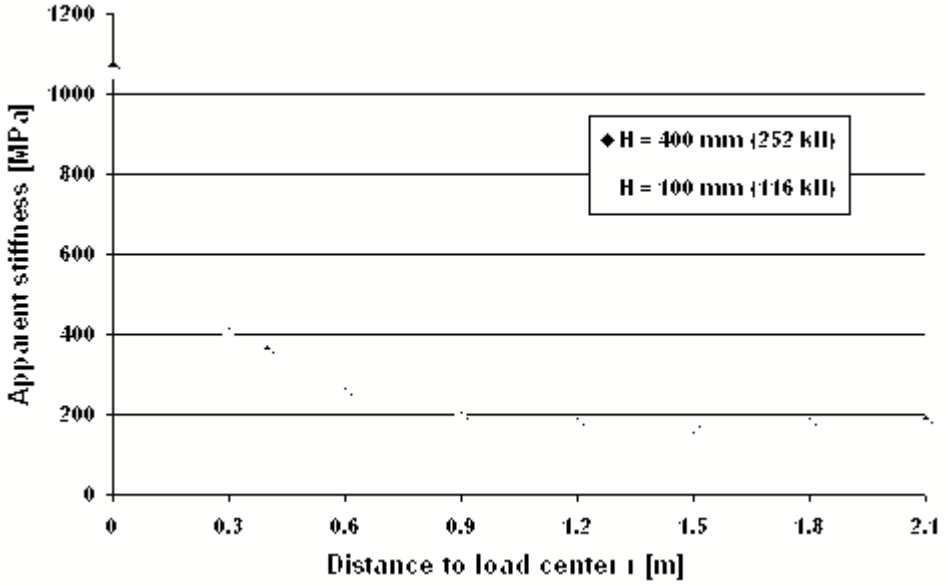

Fig. 1-48 Apparent moduli vs applied load

3.2 Emphasis of damping phenomena

Non return at zero at the end of HWD tests in most cases, or influence of rest time on measurements repeatability enable to assume that creep phenomena occur in the pavement during HWD tests. Damping is here evidenced in two manners. First observation of pavement behaviour on larger time frames is possible using the fatigue carrousel deep anchor measurements. Study of hysteretic loops is a second solution. Nevertheless in the latter case, bias in time delay (see 2.1) can distort results, so that a precise knowledge of real occurrence times of signals has to be known.

- **Deep anchor experiment**

Fig. 1-49 and Fig. 1-50 present pavement surface deformation under a typical three falls HWD test when geophone 2 is positioned over the deep anchor head. It appears (Fig. 1-49) that two different responses are superposed: a slow creep occurring when HWD foot plate is statically positioned, and a rapid dynamic response under HWD test. HWD only records the dynamic phenomenon, a blank being made just before each fall. A good repeatability between the 3 falls (peak to peak values) is observed, even if a slight decrease is noticed, corresponding to the decrease observed between consecutive measurements of a same test in the repeatability study. Fig. 1-50 focuses on the first fall. 5 rebounds are observed after the main impact. It can be taken advantage of the decrease of their peak values in energy-based reasonings. This work is not proposed here.

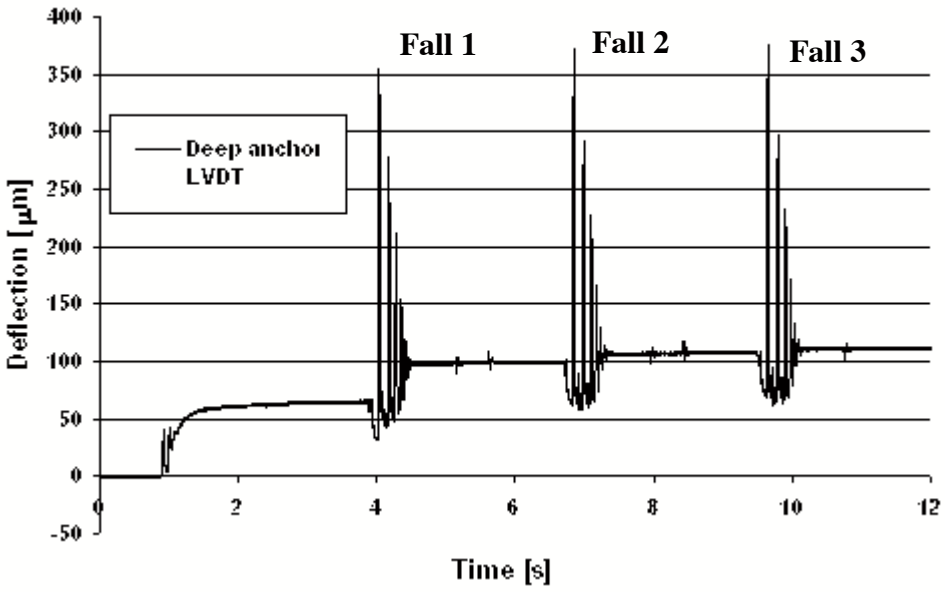

Fig. 1-49 Pavement surface deflections under HWD test sequence; from deep anchor measurement (1/2)

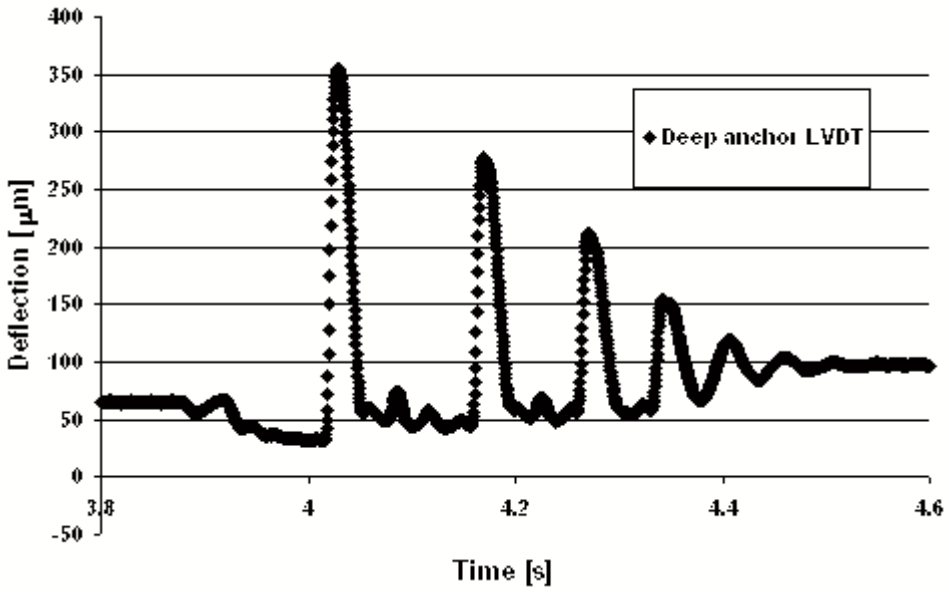

Fig. 1-50 Pavement surface deflections under HWD test sequence; from deep anchor measurement (2/2)

Fig. 1-51 focuses on the resilient creeping part (between 1 and 4 s). Deflection curve presents a sharp increase until a Y value. Then a slight linear increase is observed.

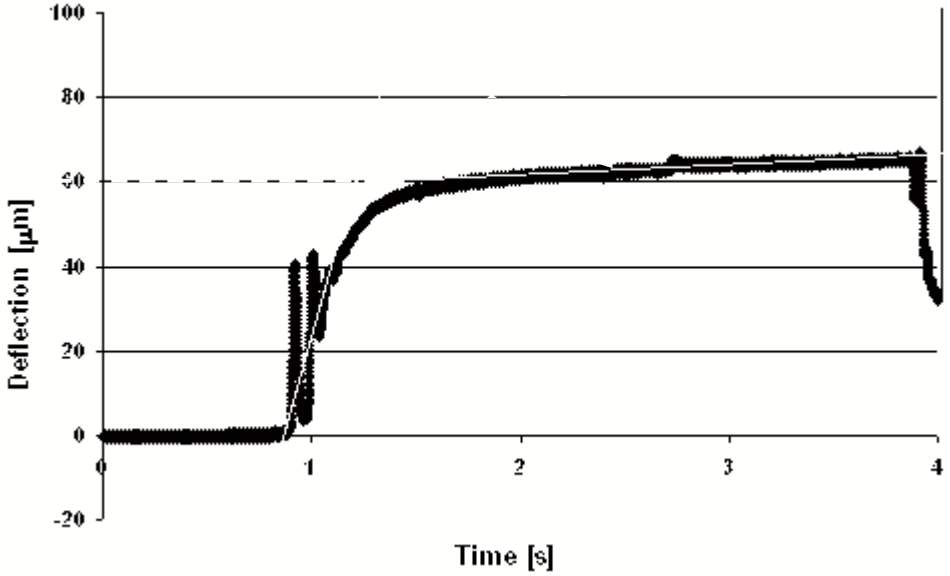

Fig. 1-51 Pavement creep under static positioning of the HWD foot; from deep anchor measurement

The same general curve is observed for other geophones.

It appears that modelling the asphalt layer using a viscoelastic Maxwell model leads to the same trend.

According to this model, evolution of the vertical strain under a constant σ_0 surface stress is provided by:

$$\varepsilon_{AC} = \frac{\sigma_0}{\eta_{AC}}(t - t_0) + \frac{\sigma_0}{E_{AC}} \quad \textbf{(1-10)}$$

with E_{AC} the (instantaneous) elastic modulus and η_{AC} the material viscous constant of the AC layer.

Unfortunately, the deflection signal corresponding to central geophone has not been measured for practical reasons. A protocol is to be imagined to obtain it. This data could enable to assess the asphalt elastic behaviour and viscosity, by fitting a Maxwell model on experimental curve (Fig. 1-52).

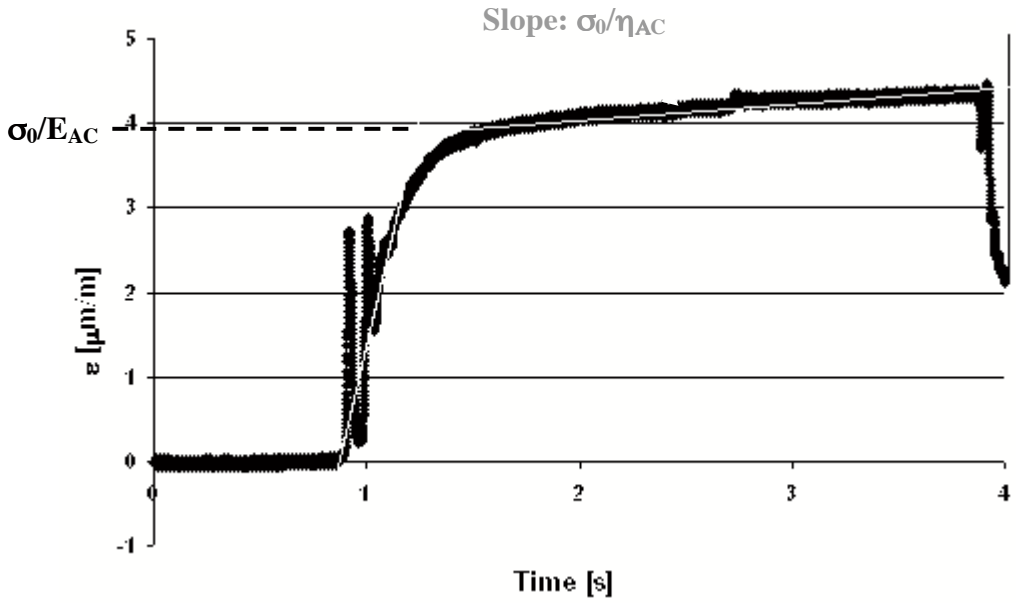

Fig. 1-52 Fitting of a Maxwell model on experimental results

Problem presents four unknown parameters: the three layer moduli (AC layer, UGA and subgrade) and η_{AC}.

Four equations are thus required to solve the problem. In practice it is for instance possible to use the Y value, the s_1 slope, and vertical strains at the top of UGA and subgrade.

For numerical applications the unity “Falling mass plus HWD Foot” has been weighted. Its exact mass is 975 kg for a 680 kg falling mass.

- **Load-deflection relationship**

When considering load-deflection relationship, a hysteretic behaviour is observed. When supposing stress is almost sinusoidal, [Kim, 1997] shows that an ellipse is expected in the

(ε,σ) representation and that interception with the abscissas axes is $\varepsilon_0.\sin\delta$ with δ the phase angle of viscoelastic asphalt material and ε_0 the maximal strain (Fig. 1-53).

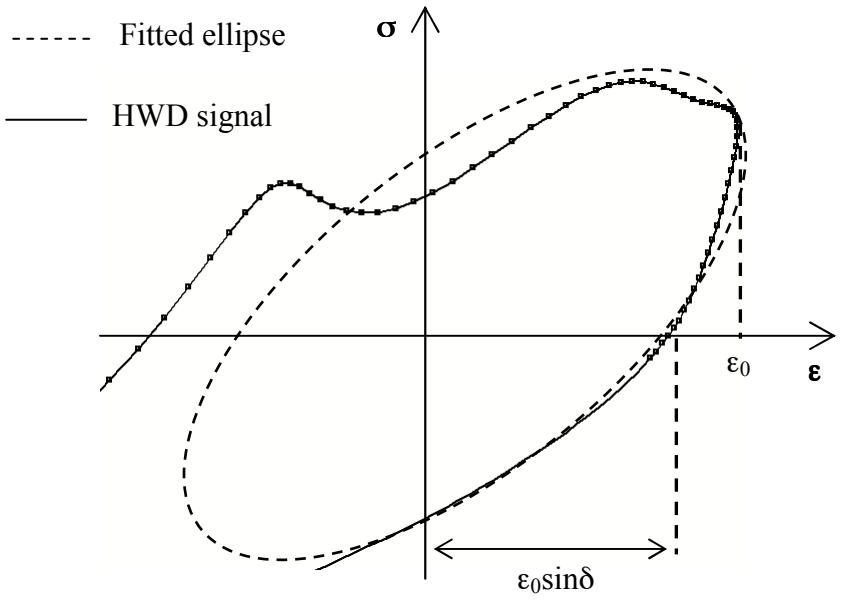

Fig. 1-53 Hysteretic behaviour related to HWD tests

Let here try to empirically determine the damping ratio in asphalt materials using this technique.

Damping ratio is defined as:

$$\xi = Q^{-1} = \frac{1}{2} \times \frac{E_2}{E_1} = \frac{1}{2} \times \tan(\delta) \qquad \textbf{(1-11)}$$

with E_1 and E_2 respectively the material complex modulus real and imaginary parts.

In reality signal is not an ellipse due to double force peak, as observed in Fig. 1-53. Blue curve corresponds to a real HWD test on the S_2 structure. It is here chosen to use the decreasing part of signal. Procedure to determine ξ is automated in the PREDIWARE STAC's software, which will be presented in part 2.

ξ value for the S_2 structure without manually adjusting time delay is 85 % what is not realistic. When a 3,5 ms readjustment is applied, a more relevant value of 10 % is obtained. It confirms again that it is important to have at disposal reliable experimental data, especially concerning times. Otherwise, biased results, such as unrealistic damping ratio values in materials could be obtained.

Conclusion to Part 1

A specific experimental study of the buffer system has first been conducted in this part, to better understand the HWD functioning. It has made possible the theoretical characterisation of the force signal, which is rather satisfactory. An attempt has been also made to explain the observed double peak when considering a double mass-spring system modelling deformations of buffers and pavement in series. It seems that this phenomenon is not attributable to the pavement deformation.

Then, it has been demonstrated, from field measurements performed on a test facility, that repeatability of HWD measurements on a given test point is very good. The comparison with scatter between results obtained on different test points has shown that the HWD enables to detect structural differences between several points. The experiment has also emphasized that variance values are not affected by the load level, so that it is assumed that the results can be enlarged. Experimental uncertainties obtained will be used in the following part, in the frame of precision calculations on identified parameters and choice of a consistent target error for automated backcalculation procedure.

A slight and reversible evolution of the pavement response has nevertheless been observed, maybe due to a rearrangement of the asphalt materials under heavy load.

Relative linearity of pavement response with applied load has also been demonstrated in the frame of this experiment.

Importance of the force pulse time on pavement response has also been highlighted. It implies difficulties to normalize HWD results. This effect can be attributable to the viscoelastic behaviour of asphalt materials.

Then, reliability of deflection signals has been checked, from several experiments involving external instrumentation (accelerometer system and deep anchor). Nevertheless, an error in time origins provided by the HWD has been highlighted, whose misinterpretation could lead to significantly biased results when performing dynamic backcalculations on time-related signals. It is envisaged to duplicate the HWD acquisition chain with an external one, more reliable.

External instrumentation has also provided valuable extra data, such as 1- deflection measurements at long distances from load centre, which can be used to obtain more precise information about the subgrade, and propagation velocity measurements, or 2- large acquisition time frames, what has allowed confirming the occurrence of viscoelastic behaviours.

Conclusions de la partie 1

Une étude expérimentale spécifique du système de tampons a d'abord été menée dans cette partie, afin de mieux appréhender le fonctionnement du HWD. Elle a permis de montrer que le niveau d'effort appliqué sur la plaque de chargement est essentiellement gouverné par la déformation des tampons, et d'établir une expression théorique approchant de façon plutôt satisfaisante le signal d'effort temporel expérimental. Il a aussi été tenté d'expliquer la présence du double pic constaté sur ce dernier à l'aide de deux systèmes masse-ressort en série, représentant pour le premier la masse tombante et les tampons, et pour le deuxième la chaussée. Il en ressort que le double pic n'est pas imputable à la déformation de cette dernière.

Ensuite, il a été démontré, à partir de mesures réalisées sur une planche expérimentale, que la répétabilité des essais HWD sur un même point est très bonne. La comparaison avec les résultats de dispersion sur plusieurs points d'essais montre que le HWD permet de détecter des différences structurelles entre différents points d'une planche supposée être homogène. L'expérience a aussi souligné que les valeurs de variance obtenues ne sont pas affectées par le niveau de chargement, si bien qu'il est admis que les résultats trouvés peuvent être généralisés. Les incertitudes expérimentales obtenues seront utilisées dans la partie suivante, pour le calcul des précisions sur les paramètres identifiés et le choix d'une erreur cible cohérente pour la procédure automatisée de calcul inverse.

Une subtile et réversible évolution de la réponse de la chaussée a néanmoins été observée, peut-être due à un réarrangement des matériaux bitumineux sous chargement lourd.

La relative linéarité de la réponse de la chaussée par rapport à la charge appliquée a aussi été démontrée dans le cadre de cette expérience.

L'importance de la durée de chargement sur la réponse de la chaussée a aussi été mise en valeur. Cet effet peut être attribué à la présence d'effets viscoélastiques dans les matériaux bitumineux. Elle complexifie le processus de normalisation des résultats HWD.

Ensuite, la fiabilité des signaux de déflexion a été vérifiée, à partir de plusieurs expérimentations ayant nécessité la mise en place d'une instrumentation externe (système d'accéléromètres et ancrage profond). Néanmoins une erreur systématique sur l'origine temporelle des historiques de déflexion a été mise en évidence. Une mauvaise interprétation de cette dernière peut conduire à des résultats significativement biaisés, lors d'analyses dynamiques. Il est envisagé de doubler le système d'acquisition du HWD à l'aide d'une acquisition externe, plus fiable.

Il a aussi été montré que l'instrumentation externe permet d'obtenir des données complémentaires précieuses comme 1- la mesure de déflexions à des distances éloignées du point de chargement, qui peuvent être utilisées pour obtenir des information plus précises sur le sol support, et autorisent des mesures de vitesses de propagation plus précises, ou 2- des mesures sur des temps d'acquisition élargis, qui ont notamment permis de confirmer la présence de comportements visqueux.

Part 2 – Modelling, backcalculation and forward analysis procedures

Introduction to part 2

The method for HWD data analysis is presented here. It rests on the two classically used steps:

- First a backcalculation phase consisting in determining the pavement characteristics.
- Secondly a forward analysis consisting in calculating the critical strains in the structure and the entailed residual performances of the pavement, with regard to the fatigue behaviour of constitutive materials.

Identification of the parameters (« backcalculation »)

Determining the bearing capacity of a pavement requires the knowledge of its characteristics.

However, these ones are not directly measurable; in any case not using non destructive tests. The general objective of backcalculation methods is determining quantities which are measurable with difficulty, from easily observable quantities. HWD pavement testing method pertains to this frame. Its principle consists in determining pavement characteristics from surface deflections, measured by means of geophones.

Dynamical mechanical models developed in the frame of this study allow calculating, for a given characteristics set, theoretical surface time-related deflections. Thus, the backcalculation problem amounts to find a set of pavement characteristics resulting in a satisfactory fitting between theoretical and experimental signals. A thorough study is necessary to assess if a characteristics set is satisfactory or not. It relies on the choice of an objective function and a linked target error. A sensitivity study is conducted in this work to choose the latter consistently. An automated algorithm is used for numerical resolution.

Evaluation of structure performances (« forward calculation»)

When knowing pavement characteristics, forward calculations can be performed using the same mechanical model and the previously backcalculated parameters. Thanks to the knowledge of the mechanical performances of the materials (obtained from laboratory tests or from experience) it is then possible to evaluate:

- the bearing capacity of the pavement,
- the residual life of the pavement for a given traffic mix, and if necessary an overlay design.

Outline of Part 2

The dynamical mechanical model developed in the frame of this study is presented first.

Then, a backcalculation procedure is proposed. An objective function is first chosen to describe the identification problem. An automated convergence method is then retained. Finally, a sensitivity study is led with regard to the defined objective function in order to

choose a target error with the best consistency with experimental and modelling uncertainties. This study also allows determining which precision is attainable on backcalculated parameters.

Next subsection is dedicated to the description of later forward analyses.

Finally, the numerical tool developed in the frame of the thesis, and used for all previous developments is presented: the so-called PREDIWARE software. It is used for both backcalculations and direct calculations. A detailed description is provided in appendix 2. A brief overview of PREDIWARE is provided here, as well as a numerical validation of both forward calculation and backcalculation procedures.

Introduction de la partie 2

Cette partie présente la méthode d'exploitation des essais HWD. Elle repose sur les deux étapes classiques de l'interprétation des résultats de cet appareil :

- Premièrement une phase de calcul inverse dont le but est de déterminer les caractéristiques de la chaussée,
- Deuxièmement une phase d'analyse directe qui consiste à calculer les contraintes dans la structure et, en intégrant des lois de fatigue des matériaux constitutifs, les performances résiduelles de la chaussée.

Identification des paramètres (« calcul inverse »)

La détermination de la capacité portante d'une chaussée nécessite la connaissance de ses caractéristiques.

Cependant, ces dernières ne sont pas directement mesurables, tout du moins pas à l'aide d'essais non destructifs. Le principe général des méthodes de calcul inverse est de déterminer des grandeurs difficilement mesurables, par le biais de paramètres facilement enregistrables. La méthode d'auscultation d'une chaussée au HWD entre dans ce cadre. Elle consiste à déterminer les caractéristiques de la structure étudiée à partir des déflexions surfaciques, mesurées à l'aide de géophones.

Le modèle mécanique développé dans le cadre de cette thèse, et présenté ci-dessous, permet de calculer, pour un jeu de données fixé, les signaux temporels correspondant aux déflexions de surface. Le problème de calcul inverse revient alors à déterminer un jeu de paramètres induisant un calage satisfaisant entre signaux théoriques et expérimentaux. Une étude minutieuse est menée en amont afin de pouvoir facilement évaluer si un jeu de données est correct ou non. Elle repose sur le choix d'une fonction objective et d'une erreur cible correspondante. Une étude de sensibilité est réalisée afin de choisir cette dernière de façon cohérente. Un algorithme automatisé est utilisé pour la résolution numérique.

Evaluation des performances de la structure («analyse directe»)

Les caractéristiques de la chaussée étant connues, des calculs directs peuvent être menés, en utilisant le même modèle mécanique et les paramètres identifiés à l'étape précédente. En s'appuyant sur les performances mécaniques des matériaux (obtenues à partir d'essais de laboratoire, ou par expérience), il est alors possible d'évaluer entre autres :

- la capacité portante de la chaussée,
- sa durée de vie pour un trafic donné, et si nécessaire l'épaisseur de rechargement requise.

Organisation de la partie 2

Le modèle dynamique développé est présenté en premier lieu.

Une procédure de calcul inverse associée est ensuite proposée. A cette fin, une fonction objective est choisie pour décrire le problème d'identification. Un algorithme de convergence est ensuite retenu. Enfin, une étude de sensibilité est menée dans le but de choisir, pour la fonction objective définie, une erreur cible aussi cohérente que possible avec les incertitudes expérimentales et relatives à la modélisation. Cette étude permet aussi de déterminer quelle précision peut être espérée sur les paramètres identifiés.

La section suivante est dédiée à la description des analyses directes ultérieures.

En dernier lieu, l'outil numérique développé dans le cadre de la thèse, et utilisé pour tous les développements précédemment cités, est présenté. Il s'agit du logiciel PREDIWARE. Ce dernier peut être utilisé aussi bien pour les phases de calcul inverse ou direct. Une description détaillée est fournie dans l'annexe 2. Une présentation sommaire est proposée dans cette partie, ainsi qu'une validation numérique des phases de calcul inverse et direct.

1 - Dynamical modelling

A time-domain modelling has been developed for HWD data analysis. The model considers the applied dynamical load. Three alternative versions of the model have been studied, which distinguish themselves by the applied dynamical load modelling. First model takes into account the time-related load imparted to the pavement surface through the plate. In the second model, rubber buffers are included in the mesh and velocity of the dropped mass at impact is imposed at their top. Third model is based on the shock theory [Frémond, 2007]. Let us call for readability M_1 to M_3 the respective alternative versions.

This model, implemented in the finite element software CESAR-LCPC (DYNI modulus) [Humbert et al., 2005], is likely to better take into account the dynamic nature of the load and also the damping phenomenon occurring in pavement materials, not considered in the pseudo-static method.

The model relies on a 2D axis-symmetric layered mesh made up of quadratic elements. A typical mesh for a standard flexible aeronautical pavement is presented in Fig. 2-1. It includes the load plate.

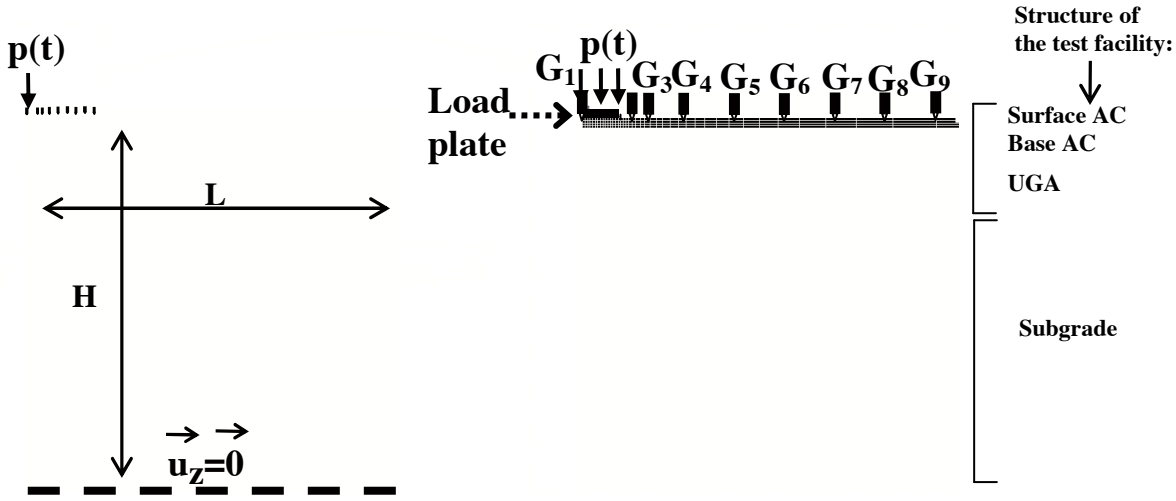

(Respective radial distances of G_1 to G_9 to the plate centre: 0, 30, 40, 60, 90, 120, 150, 180 and 210 cm).

Fig. 2-1 The mesh

1.1 Geometrical considerations and boundary conditions

General geometry is here described. Conclusions of an upstream mesh optimization, performed on the M_1 alternative model, are provided.

1.1.1 Mesh dimensions

Dimensions on the mesh have been optimized thanks to a numerical study on the S_1 structure with usual material moduli.

The "L" width of the mesh has been optimized to avoid reflections on the lateral boundary due to imposed boundary conditions, as no energy absorbing boundaries are available in the CESAR version used. The method has been numerical, by performing calculations for different L values meter by meter considering a timeframe of 60 ms. Parameter used was the computed vertical displacement at the outer geophone position. This parametric study on L has established that L must be at least L_{min} = 7 meters. Actually displacement is above this value not affected by any width variation, with regard to a 1 μm precision. The value L = 10 meters has been chosen in order to have a security margin so as to generalize this mesh geometry for all pavements.

The "H" height of the mesh corresponds to the depth to bedrock. A theoretical sensitivity study led upstream (see part 3) has shown that the presence of bedrock deeper than 6 meters has no influence on the results and the subgrade can be considered as infinite. Foinquinos Mera [Mera, 1995] already observed this phenomenon and retained the very close value of 20 ft. To save once more a security margin the height "H" has thus been limited to H = 10 m. The depth to bedrock can be determined from HWD tests (see the dedicated section of the literature review).

1.1.2 Layer thicknesses

Thicknesses of constitutive material layers are adjustable. As explained in the following, this thesis limits to known thickness pavements analysis. Upper layer thicknesses are usually known thanks to construction records, cores or GPR results. A preliminary determination of the depth to bedrock may be required (see part 3).

1.1.3 Spatial discretization

Eight-nodes 2D elements have been used. For calculation time reasons the fineness of the mesh has been chosen in accordance with a preliminary optimization study. In the latter the optimization has been made numerically by successive refinements until stabilization of the theoretical deflections, given the expected precision (1 μm). Final discretization led to a constant 3 cm step (Δx_1) under the plate and a constant 50 cm step (Δx_2) far from it (d >3 m) with a geometric progression between these 2 areas to avoid introduction of any artificial stiffness in the system which could induce undesirable reflections. Results of this numerical

optimization are in general accordance with literature-proposed empirical rules, for instance [Simonin, 2005]'s ones: $\Delta x \leq \frac{\lambda}{20}$ in the stressed portions of the mesh, and $\Delta x \leq \frac{\lambda}{10}$ in the rest.

1.1.4 Boundary conditions

Boundary conditions are depicted in Fig. 2.1: the radial displacement is null on the axis for symmetry considerations and on the external boundary, as well as the vertical one at the bottom of the mesh.

1.2 External action modelling

1.2.1 Applied force modelling (M_1)

The external action is here the real stress applied at each time step on the load plate during the HWD test, which is recorded. Pressure p(t) applied on the loading plate is considered as uniform. Simulation has shown that this hypothesis has no incidence on the pressure under the plate, this one being stiff enough.

Time discretization has been optimized. It has been based on a previous optimization study which has established that it is possible to keep only 1 time increment over 3 without any incidence on results. Once more results of this numerical analysis are in accordance with [Simonin, 2005] who recommends $\Delta t \leq 0{,}8\frac{\min(\Delta x)}{V}$ with V the wave propagation velocity.

1.2.2 Initial velocity modelling (M_2)

The complex "Falling mass plus Buffers plus load plate plus pavement" is this time included in the mesh. Note the thin rubber mat under the plate is also included in the mesh; the latter seems to have little influence on numerical results. Also note that the plate mass density has been modified to take into account the HWD foot static load (975 kg minus 640 kg).

According to the preliminary studies (see part 1), buffers are assumed to present an elastic behaviour. They are modelled using an equivalent buffer in the axisymmetric mesh, of same height of each single buffer and same total area (i.e. but presenting a $\sqrt{8}D_0$ diameter, with D_0 the diameter of each single buffer). The dynamic modulus found in part 1 (§1.3.1.) is retained, when supposing that temperature has a limited effect on its value.

The mass presents an initial $V_0 = \sqrt{2gH_0}$ velocity.

No external force is applied.

The rest of the modelling is unchanged in comparison with M_1 alternative version.

1.2.3 Shock theory (M_3)

The shock theory is a specific theory developed by Michel Frémond in which problem is solved by considering two steps. The first one consists in calculating the velocity field in the pavement following the impact, and the second one in determining the evolution of the pavement from this initial condition, using usual methods. Assuming that the shock is instantaneous in the modelling, the initial displacement field is null.

This approach states that:
- the shock is instantaneous,
- it induces an instantaneous discontinuity of the velocity field in the deformable bodies system,
- load effects applied during the shock are percussions.

Shock equations are obtained:
- by determining equations of motion from the virtual work principle,
- by introducing behaviour laws linking deformation velocities and internal percussions.

The velocity field is assumed to adapt instantaneously to the collision. The velocities inconsistency implies that deformation velocities before and after the shock are different. Let the velocities at each point x, respectively before and after the shock occurring at time t_0, be:
$\overrightarrow{U^-}(x,t_0) = Lim_{\Delta t->0} \frac{\vec{x}(t_0) - \vec{x}(t_0 - \Delta t)}{\Delta t}$ and $\overrightarrow{U^+}(x,t_0) = Lim_{\Delta t->0} \frac{\vec{x}(t_0 + \Delta t) - \vec{x}(t_0)}{\Delta t}$
and $\left[\vec{U}\right] = \overrightarrow{U^+} - \overrightarrow{U^-}$ the velocity discontinuity.
This velocity discontinuity at time t_0 is associated with great surface strengths and great internal stresses within each deformable body. These actions are assumed to be instantaneous. They will be referred to as “percussions”.
In this matter, by applying the virtual works principle, it is shown in [Dimnet, 2002] that a field of surface internal percussion vectors $\overrightarrow{P^{int}}$ and a field of volume percussion tensor $\underline{\underline{\Sigma}}^{int}$ need to be introduced in the modelling. By duality (in the sense of the internal strengths works) these fields are associated with $\frac{1}{2}\left(\overrightarrow{V^+} + \overrightarrow{V^-}\right)$ where $\overrightarrow{V^-}$ and $\overrightarrow{V^+}$ are virtual velocities before and after the collision respectively (in the same way as internal forces $\overrightarrow{T^{int}}$ and stress tensor $\underline{\underline{\sigma}}^{int}$ are associated with virtual velocity $\vec{V}$ in the case of a regular evolution).
An external percussion $\overrightarrow{P^{ext}}$ may also be applied to the system (for instance to take into account a hammer blow on the system). Unlike $\overrightarrow{P^{int}}$ which depends on the deformation velocity of the system, $\overrightarrow{P^{ext}}$ is known. In our case, a $\overrightarrow{P^{ext}} = \frac{m_0 \vec{V_0}}{S_0} = -\frac{m_0 \sqrt{2gH_0}}{S_0}\vec{N}$ is applied at the surface of the buffers (see Fig. 2-2), with S_0 the equivalent buffer section, H_0 the fall height and m_0 the static dropped mass.

The pavement is modelled (Fig. 2-2) using the same mesh than in M_1 and M_2.

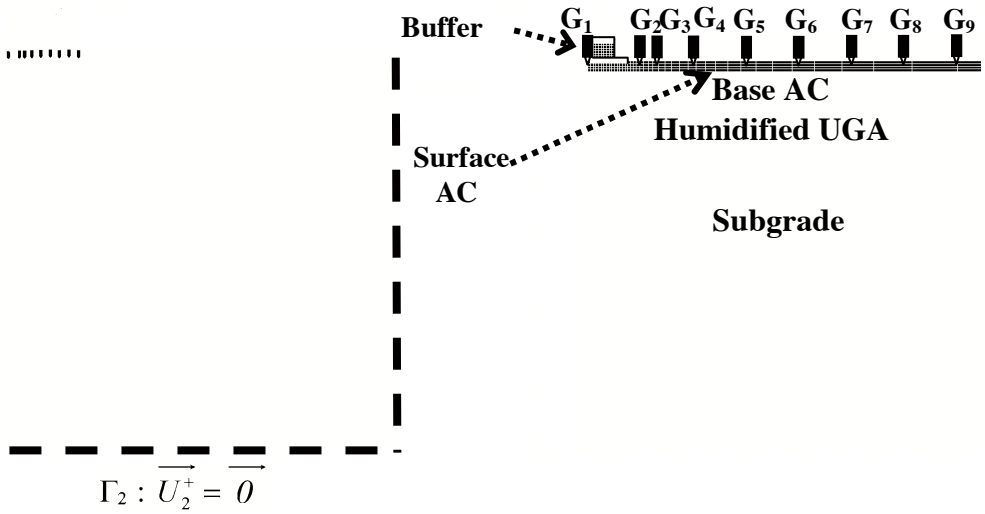

Fig. 2-2 Mesh discretization; shock model

1.3 Mathematical resolution

1.3.1 Applied force modelling (M_1)

- **Local equations**

According to the conclusion of preliminary studies (see part 1), all materials are considered to have an isotropic linear elastic behaviour and damping is introduced in the model.

In the absence of damping, the evolution is governed by equations of the regular dynamic:

$$\overrightarrow{div}\,\underline{\underline{\sigma}} + \vec{f} = \rho\vec{\gamma} \text{ in } \Omega \qquad \textbf{(2-1)}$$

The finite element discretization of problem described by equation (2–1) leads to the classical expression:

$$M\,\ddot{u}(t) + K\,u(t) = P(t) \qquad \textbf{(2-2)}$$

with M and K respectively the mass and stiffness matrices, and $u(t)$ the displacement vector at t time, and $P(t)$ the vectors containing external strengths.

The $M_{i,j}$ generic (i, j) entry of M is a function of the ρ_i densities of materials and the $K_{i,j}$ generic (i, j) entry of K is a function of the E_i Young's moduli of materials and the ν_i Poisson's ratios.

Only a global Rayleigh damping is available so far in the CESAR-LCPC software. Its introduction amounts to add a $C\,\dot{u}(t)$ term in the previous local equations of motions with C a matrix which is proportional to mass and stiffness ones. Local equations can thus been expressed as:

$$M\,\ddot{u}(t) + C\,\dot{u}(t) + K\,u(t) = P(t) \qquad \textbf{(2-3)}$$

C is related to K and M thanks to the (2-4) relationship:

$$C = \alpha M + \beta K \qquad \textbf{(2-4)}$$

with α and β scalar, constant for the whole structure. These parameters are called Rayleigh coefficients. They are linked for each ω_i pulsation to the ξ_i damping ratio by the relation:

$$\xi_i = \frac{1}{2}\left(\frac{\alpha}{\omega_i} + \beta \cdot \omega_i\right) \qquad \textbf{(2-5)}$$

As illustrated in Fig. 2-3, the provisional method adopted to determine α and β consists in optimizing these two parameters to obtain an assigned value of ξ % for mean damping ratio on the considered frequency range (0 to 80 Hz for HWD pulse times according to FFT of part 1; in practice the lower boundary is chosen non null to avoid infinite values; 5 Hz is here arbitrary chosen). It can be noticed that damping is not uniform with frequency, but is higher for low and high frequencies. Typical frequency dependence, displayed in Fig. 2-3, is indicative of the generalized Maxwell evolution trend. [Semblat, 1997] besides provides a rheological interpretation of Rayleigh damping by finding an equivalent generalized Maxwell model with well chosen coefficients.

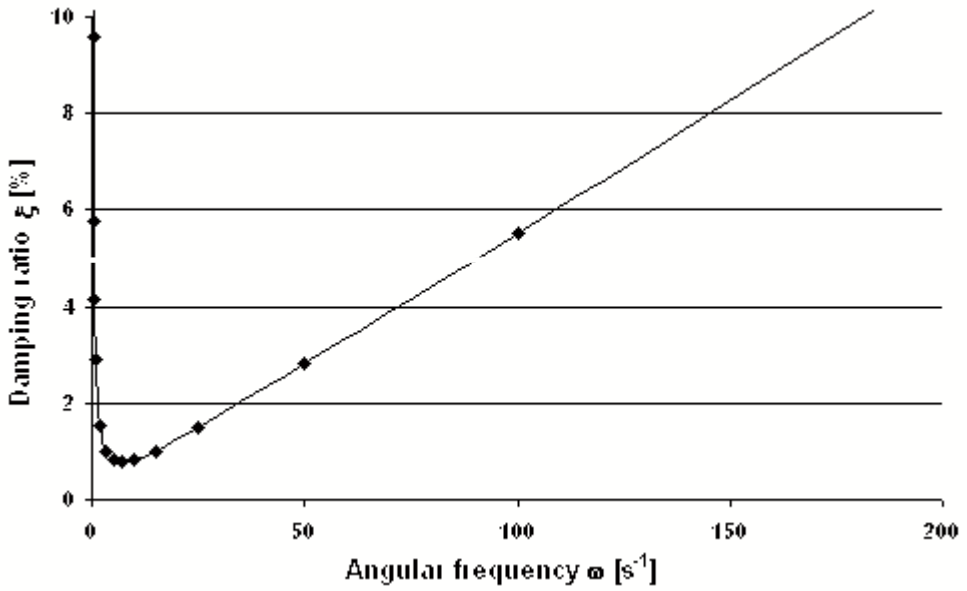

Fig. 2-3 Relationship between Rayleigh coefficients and damping ratio ξ

- **Interface conditions**

Modelling allows considering both fully bonded and fully frictionless interfaces. Layers are assumed to be bonded by default as in usual modellings.

1.3.2 Initial velocity modelling (M_2)

The local motion equations are the same as for the applied-force modelling. Only the initial condition is different: no external force is applied, the mass presents an initial velocity.

1.3.3 Shock theory (M_3)

The two steps of calculation are hereafter detailed. First shock calculation. Then, the regular evolution of the system.

a - Shock calculation

The equations are settled in three steps:

- Settling of the local equations of motion and of the behaviour laws,
- Conversion of these equations into their variational equivalent,
- Discretization.

- **Settling the local equations of motion and the behaviour laws**

The simplified problem of an infinitely rigid body falling on a deformable pavement is studied hereafter. For this purpose, one considers an Ω pavement volume with a $\partial\Omega$ boundary (Fig. 2-4). This volume is a deformable body undergoing a collision at time t_0. An external percussion $\overrightarrow{P^{ext}} = \frac{m_0 \overrightarrow{V_0}}{S_0} = -\frac{m_0 \sqrt{2gH_0}}{S_0}\vec{N}$ is applied on a Γ_1 part of $\partial\Omega$, S_0 being the buffer section. Let Γ_2 be a part of $\partial\Omega$ on which displacements (and therefore deformation velocities) are imposed as null. Trying to impose speed on Γ_2 results in a reaction which is a percussion referred to as $\overrightarrow{P^{ind}}$.

The simplifying hypothesis consisting in considering the system as one solid allows discarding of any internal percussion $\overrightarrow{P^{\text{int}}}$.

The virtual works principle is then applied:

$$\underbrace{\int_\Omega \rho\left[\overrightarrow{U}\right]\cdot\vec{\alpha}\, d\Omega}_{W^{acc}} = \underbrace{-\int_\Omega \underline{\underline{\Sigma}}^{\text{int}} : \underline{\underline{D}}\left(\vec{\alpha}\right) d\Omega}_{W^{\text{int}}} + \underbrace{\int_{\Gamma_1} \overrightarrow{P^{ext}}\cdot\vec{\alpha}\, d\Gamma + \int_{\Gamma_2} \overrightarrow{P^{ind}}\cdot\vec{\alpha}\, d\Gamma}_{W^{ext}} \quad \text{where } \vec{\alpha} = \frac{1}{2}\left(\overrightarrow{V^+} + \overrightarrow{V^-}\right) \qquad \textbf{(2-6)}$$

This equation can be re-written by transforming the expression of the internal work W^{int} thanks to an integration by parts:

$$\boxed{\int_\Omega \rho\left[\overrightarrow{U}\right]\cdot\vec{\alpha}\,d\Omega = \int_\Omega \overrightarrow{div}\underline{\underline{\Sigma}}^{int}\cdot\vec{\alpha}\,d\Omega - \int_{\partial\Omega}\underline{\underline{\Sigma}}^{int}\vec{N}\cdot\vec{\alpha}\,d\Gamma + \int_{\Gamma_2}\overrightarrow{P^{ext}}\cdot\vec{\alpha}\,d\Gamma + \int_{\Gamma_3}\overrightarrow{P^{ind}}\cdot\vec{\alpha}\,d\Gamma} \quad \textbf{(2-7)}$$

Equation **(3)** is valid for any virtual velocities. This allows proceeding to a term by term identification resulting in the following local equations of motion:

$$\begin{cases} \rho\left[\overrightarrow{U}\right] = \overrightarrow{div}\underline{\underline{\Sigma}}^{int} \text{ in } \Omega & \textbf{(2-8)} \\ \underline{\underline{\Sigma}}^{int}\vec{N} = \overrightarrow{P^{ext}} \text{ on } \Gamma_1 & \textbf{(2-9)} \\ \overrightarrow{U^+} = \overrightarrow{U_2^+} \text{ on } \Gamma_2 & \textbf{(2-10)} \\ \underline{\underline{\Sigma}}^{int}\vec{N} = \vec{0} \text{ on } \Gamma_L = \partial\Omega \setminus (\Gamma_1 \cup \Gamma_2) & \textbf{(2-11)} \end{cases}$$

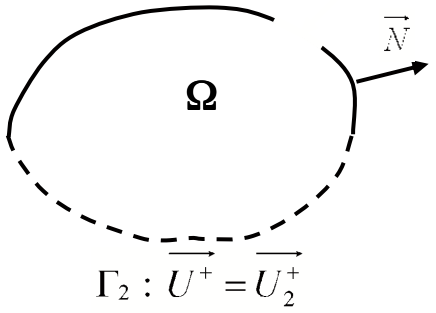

Fig. 2-4 – Settling equations of the shock ; the boundary value problem.

This boundary value problem where $\overrightarrow{U^+}$ is the unknown field is referred to as **(P)**.

The behaviour laws are then required to solve the problem. Only the $\underline{\underline{\Sigma}}^{int}$ related law is required in our case. $\underline{\underline{\Sigma}}^{int}$ is supposed to derive from a pseudo-potential of volume dissipation (ϕ_v), as defined by [Moreau, 1966]: a convex function, positive, null at origin, and infra semi continuous.

$$\underline{\underline{\Sigma}}^{int} \in \partial\phi_v\left(\underline{\underline{D}}\left(\frac{\overrightarrow{U^+}+\overrightarrow{U^-}}{2}\right)\right) \quad \textbf{(2-12)}$$

A linear law is chosen (volume percussion proportional to speed deformation)

$\phi_v = E_V\left(\underline{\underline{D}}\left(\frac{\overrightarrow{U^+}+\overrightarrow{U^-}}{2}\right)\right)^2$ where E_V is a n×n matrix whose coefficients are experimentally determined, n being the dimension of the problem.

In this case $\underline{\underline{\Sigma}}^{int} = \frac{\partial\phi_v}{\partial\left(\underline{\underline{D}}\left(\frac{\overrightarrow{U^+}+\overrightarrow{U^-}}{2}\right)\right)} = E_V\,\underline{\underline{D}}\left(\overrightarrow{U^+}+\overrightarrow{U^-}\right)$ **(2-13)**

It can be noticed that the « ϕ_v is a pseudo potential » condition proves that the laws of thermodynamics are respected. In the linear case, Det $E_V \geq 0$, and so $\underline{\underline{\Sigma}} : \underline{\underline{D}} \geq 0$ (Clausius Duhem inequality): the shock is dissipative.

An elastic linear isotropic law is chosen to describe $\underline{\underline{\Sigma}}^{int}$. It means, in regards to our geometry (Problem in dimension 2 with axisymmetry) that the general expression for E_V is:

$$E_V = \begin{pmatrix} \lambda + 2\mu & 2\mu \\ 2\mu & \lambda + 2\mu \end{pmatrix}$$

With λ and μ scalar numbers.

It can be noticed that Det $E_V \geq 0$.

Internal percussion is $\underline{\underline{\Sigma}}^{int} = \lambda tr\underline{\underline{D}}\left(\overrightarrow{U^+} + \overrightarrow{U^-}\right)\underline{\underline{\delta}} + 2\mu\,\underline{\underline{D}}\left(\overrightarrow{U^+} + \overrightarrow{U^-}\right)$. The associated pseudopotential is $\phi_v = \frac{\lambda}{2} tr\underline{\underline{D}}\left(\overrightarrow{U^+} + \overrightarrow{U^-}\right)^2 \underline{\underline{\delta}} + \mu\,\underline{\underline{D}}\left(\overrightarrow{U^+} + \overrightarrow{U^-}\right)^2$

Numerical values of λ and μ are empirically determined.
Considering $E = \frac{3\lambda + 2\mu}{\lambda + \mu}\mu$ and $\nu = \frac{\lambda}{2(\lambda + \mu)}$ the following expression is obtained:

$$\underline{\underline{\Sigma}}^{int} = \frac{E\nu}{(1+\nu)\cdot(1-2\nu)} tr\underline{\underline{D}}\left(\overrightarrow{U^+} + \overrightarrow{U^-}\right)\underline{\underline{\delta}} + \frac{E}{1+\nu}\underline{\underline{D}}\left(\overrightarrow{U^+} + \overrightarrow{U^-}\right) \qquad \textbf{(2-14)}$$

- **Conversion into the variational equivalent problem**

As at t=0$^-$, before the shock, the field of speed vectors $\overrightarrow{U^-}$ is uniformly nil. Let $\overrightarrow{X} = \left[\overrightarrow{U}\right] = \overrightarrow{U^+} - \overrightarrow{U^-} = \overrightarrow{U^+}$ be the unknown of the problem.
The variational problem **(Pv)** equivalent to **(P)** is obtained by multiplying each member of **(2–8)** by the vector $\left(\vec{Y} - \vec{X}\right)$ and by integrating on Ω. It can be written:

$$\boxed{Find\ \overrightarrow{X} \in H_0^1(\Omega) / \forall \vec{Y} \in H_0^1(\Omega) \quad \int_\Omega \rho\left[\overrightarrow{U}\right]\cdot\left(\vec{Y} - \vec{X}\right)d\Omega = \int_\Omega \overrightarrow{div}\,\underline{\underline{\Sigma}}^{int}\cdot\left(\vec{Y} - \vec{X}\right)d\Omega}$$

where $H^1(\Omega)$ is the space containing all integrable functions of Ω in the sense of the norm 1, and $H_0^1(\Omega)$ is the vector space defined by $H_0^1(\Omega) = \left\{\vec{X} \in H^1(\Omega) / \vec{X}_{\Gamma 2} = \vec{0}\right\}$.

This choice for boundary conditions relies on the hypothesis that the volume V is wide enough so that no velocity gap occurs on Γ_2 at the time of the shock.
As $\vec{Y}(P) = \vec{0}\ \forall P \in \Gamma_2$, $\int_{\Gamma_2} \overrightarrow{P^{ind}}\left(\vec{X}\right)\cdot\vec{Y}d\Gamma = 0$, problem **(Pv)** becomes:

$$\boxed{\begin{array}{ll} & \text{« Find } \overrightarrow{X} \in H_0^1(\Omega) / \forall \vec{Y} \in H_0^1(\Omega)\ ,\ a\left(\overrightarrow{X}, \vec{Y}\right) = L\left(\vec{Y}\right) \\ \text{with} & a\left(\overrightarrow{X}, \vec{Y}\right) = \int_\Omega \underline{\underline{\Sigma}}^{int}\left(\vec{X}\right) : \underline{\underline{D}}\left(\vec{Y}\right)d\Omega + 2\int_\Omega \rho\overrightarrow{X}\cdot\vec{Y} \\ \text{and} & L\left(\vec{Y}\right) = \int_{\Gamma_2} \overrightarrow{P^{ext}}\cdot\vec{Y}d\Gamma \text{ »} \end{array}} \qquad \textbf{(Pv)}$$

- **Discretization**

The solution of the problem **(Pv)** belongs to $H_0^1(\Omega)$ which is an infinite-dimensional vector space.
A calculation method to approximate this solution consists in projecting it on a finite-dimensional subspace H_N of $H_0^1(\Omega)$.
The finite element method is chosen. It consists in :

- choosing N particular scalar functions (v_i) in Ω.
- considering, in the case of our two-dimensional problem, $\vec{v_i} = v_i \vec{e_x}$ and $\overrightarrow{v_{i+N}} = v_i \vec{e_y}$ $\forall i \in \{1..N\}$.

v_i functions are N functions linearly independent from $H_0^1(\Omega)$ to $\Re$
The new work space H_N is therefore defined by H_N = Vect($\vec{v_i}$) =

$$\left\{ \vec{X} \in H_0^1(\Omega) / \vec{X} = \sum_{i=1}^{2N} x_i \vec{v_i}, x_i \in \Re \right\}$$

Let **(P_N)** be the approximate problem associated to problem **(Pv)** and v_i functions.
It can be written as:

« Find $\widetilde{X} \in H_N / \forall \widetilde{Y} \in H_N$, $a(\widetilde{X}, \widetilde{Y}) = L(\widetilde{Y})$ » **(P_N)**

$\widetilde{X}$ and $\widetilde{Y}$ are decomposed on (v_i) : $\widetilde{X} = \sum_{i=1}^{2N} x_i \vec{v_i}$ and $\widetilde{Y} = \sum_{i=1}^{2N} y_i \vec{v_i}$

so that $a(\widetilde{X}, \widetilde{Y})$ and $L(\widetilde{Y})$ can respectively be transformed to:

$$a(\widetilde{X}, \widetilde{Y}) = \sum_{i,j=1}^{2N} x_i y_j \int_\Omega \left(\underline{\underline{\Sigma}}^{\text{int}}(\vec{v_i}) : \underline{\underline{D}}(\vec{v_j}) + 2\rho \vec{v_i} \cdot \vec{v_j} \right) d\Omega$$

and $L(\widetilde{Y}) = \sum_{j=1}^{2N} y_j \int_{\Gamma_2} \overrightarrow{P^{ext}} \cdot \vec{v_j} d\Gamma$

Replacing internal percussion by its expression leads to:

$$a(\widetilde{X}, \widetilde{Y}) = \sum_{i,j=1}^{2N} x_i y_j \int_\Omega \left(\frac{E\nu}{(1+\nu)\cdot(1-2\nu)} tr\, \underline{\underline{D}}(\vec{v_i}) \underline{\underline{\delta}} : \underline{\underline{D}}(\vec{v_j}) + \frac{E}{1+\nu} \underline{\underline{D}}(\vec{v_i}) : \underline{\underline{D}}(\vec{v_j}) + 2\rho \vec{v_i} \cdot \vec{v_j} \right) d\Omega$$

Let A_{ij} , b_j , x, y and b be:

$$A_{ij} = \int_\Omega \left(\frac{E\nu}{(1+\nu)\cdot(1-2\nu)} tr\, \underline{\underline{D}}(\vec{v_i}) \underline{\underline{\delta}} : \underline{\underline{D}}(\vec{v_j}) + \frac{E}{1+\nu} \underline{\underline{D}}(\vec{v_i}) : \underline{\underline{D}}(\vec{v_j}) + 2\rho \vec{v_i} \cdot \vec{v_j} \right) d\Omega$$

$$b_j = \int_{\Gamma_2} \overrightarrow{P^{ext}} \cdot \vec{v_j} d\Gamma$$

and $x = (x_1, x_2, \ldots x_{2N})$, $y = (y_1, y_2, \ldots y_{2N})$, $b = (b_1, b_2, \ldots b_{2N})$,

Equation $a(\widetilde{X}, \widetilde{Y}) = L(\widetilde{Y})$ $\forall \widetilde{Y} \in H_N$ reduces to ${}^t yAx = {}^t yb$ $\forall y / \sum_{i=1}^{2N} y_i \vec{v_i} \in H_N$

Existence and uniqueness of the solution come from strong convexity of $a(\vec{X}, \vec{X})$ which is equivalent [Frémond, 1983] to A_{ij}=a(v_i,v_j) being a positive-definite matrix.

Let $x_N = (x_{N1}, x_{N2}, \ldots x_{N2N})$ be this solution and $\widetilde{X}_N = \sum_{i=1}^{2N} x_{Ni} \overrightarrow{v_i}$ the unique solution of the problem **(P_N).**

Second member coefficients $b_j = \int_{\Gamma_2} \overrightarrow{P^{ext}} \cdot \overrightarrow{v_j} d\Gamma$ and A components are calculated by a finite elements software. The latter allows calculating separately each term $\int_\Omega \frac{E\nu}{(1+\nu)\cdot(1-2\nu)} tr\, \underline{\underline{D}}(\overrightarrow{v_i}) \underline{\underline{\delta}} : \underline{\underline{D}}(\overrightarrow{v_j}) d\Omega$, $\int_\Omega \frac{E}{1+\nu} \underline{\underline{D}}(\overrightarrow{v_i}) : \underline{\underline{D}}(\overrightarrow{v_j}) d\Omega$, and $\int_\Omega 2\rho \overrightarrow{v_i} \cdot \overrightarrow{v_j} d\Omega$ constituting A_{ij}.. These terms are then summed.

– Shock calculation

v_i functions used for the calculation are quadratic elements and rely on the 2D aforementioned axisymmetric mesh created with CESAR-LCPC software. The coarseness of the mesh has been optimized. The boundary condition $\overrightarrow{U_2^+} = \vec{0}$ imposed on Γ_2 warrants that $\int_{\Gamma_2} \overrightarrow{P^{ind}} \cdot \overrightarrow{U_2^+} d\Gamma = 0$.

Load plate and buffers (replaced in our modelling by an unique equivalent buffer) have also been discretized. The surface Γ_1 on which percussion $\overrightarrow{P^{ext}}$ is applied is the upper surface of this buffer.

The pavement volume studied is the S_1 structure of appendix 1.1..

b - Regular evolution

When knowing the $\overrightarrow{U^+}$ velocity field after the impact, i.e. at time $t = 0^+$ of the simulation, the second phase of the calculation consists in the study of the system evolution after the shock.

With $\vec{u}$ and $\vec{v}$ being respectively the displacements and speeds, boundary conditions (BC) are:

$$(BC)\begin{cases} \vec{u} = \vec{0} \text{ on } \Gamma_2 & \textbf{(2-15)} \\ \underline{\underline{\sigma}}\overrightarrow{N} = \vec{0} \text{ on } \Gamma_L' = \partial\Omega \setminus \Gamma_2 & \textbf{(2-16)} \end{cases}$$

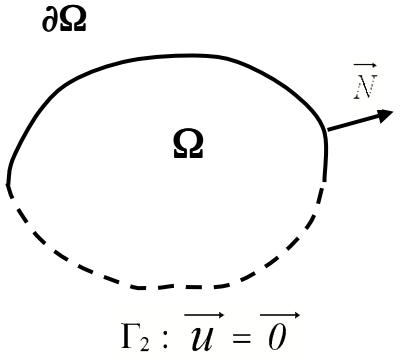

Figure 2-5 – Regular evolution of the system; Boundary values problem.

and the initial conditions (IC):

$$\text{(IC)} \begin{cases} \vec{u}(P,t=0^+) = \vec{0} \ \forall P \in \Omega \quad \textbf{(2-17)} \\ \vec{v}(P,t=0^+) = \overrightarrow{U^+} \text{ (resulting from the shock calculation) } \forall P \in \Omega \quad \textbf{(2-18)} \end{cases}$$

As above a Rayleigh structural damping can be introduced in the model, so that local equations of motions are unchanged with regard to (1-3). The mesh used is identical to the shock calculation step one.

2 - Backcalculation procedure

Principle consists in fitting the parameters of the model in order to line up numerical data with experimental ones, what amounts in practice to solve a minimization problem. The objective function to minimize is presented first. The mathematical convergence retained is described in a second step. Minimization error to be reached is finally discussed.

2.1 Objective function

2.1.1 Parameters

This part focuses on the M_1 modelling. The backcalculation on M_3 modelling is specific as the parameters of the shock law have to be also determined. Work on this M_3 model will be detailed in 2.2.1.

The dynamical backcalculation developed in this work consists in finding numerical time-related deflections close enough to experimental ones.
Let $w_{k,t}$ be the numerical deflection at time t measured by the k^{th} geophone.

Parameters influencing $w_{k,t}$ can be sorted into two types, letting m be the number of geophones and n the number of layers: mechanical and geometrical parameters.

- mechanical parameters

- the ρ_i, E_i, ν_i, density Young's modulus and Poisson's ratio of each of the i^{th} layer for i ranging from 1 to n, and the global ξ damping ratio,
- the IC_i interface conditions between the i^{th} and $(i+1)^{th}$ layer for i ranging from 1 to n-1.

- geometrical ones

- the e_i layer thicknesses for each of the i^{th} layer for i ranging from 1 to n-1, and p the depth to bedrock,
- x_k the position of the k^{th} geophone for k ranging from 1 to m.

The tricky next step consists in defining main parameters governing the $w_{k,t}$, the others being arbitrary imposed. An *a posteriori* sensitivity study will be performed to demonstrate that the precision in the *a priori* determination of these parameters is sufficient so that their influence on the objective function can be neglected.

It is here assumed that:

- the interface conditions are in every case fully bonded. This hypothesis is commonly admitted as highlighted by [Romanoschi and Metcalf, 2002] in the case of pavements stressed by heavy weight.
- variations in ρ_i and ν_i have a limited influence on the numerical surface deflections,
- the layer thicknesses and depth to bedrock are quite precisely known. Regarding the layers, as emphasized in appendix 1.3, general organization of an airfield assessment campaign systematically includes a Ground Penetrating Radar (GPR) survey coupled with corings that allows getting an accurate mapping of the tested area. Concerning the depth to bedrock, the method proposed by [Mera, 1995] has been used in the frame of this work. It is assumed to be accurate enough.
- Error on the calculated deflections implied by uncertainties on the geophone placements is negligible.

All these hypotheses will be *a posteriori* checked in the sensitivity study carried out hereafter

As a conclusion the only parameters to be backcalculated from HWD data (applied load and resulting surface deflections) are the Young's modulus of each material and the damping ratio in the structure.

2.1.2 Mathematical expression

The considered problem is highly overdetermined. The number of unknowns is actually *n+1*, *n* layer moduli plus one damping ratio (so 5 or 6 unknowns at maximum), whereas the number of equations is equal to the number of geophones (9) multiplied by the number of time steps considered (up to 480).

The least squares method is suitable to approximate solutions of overdetermined systems. Thus the following objective function is to be minimized:

$$f_t(\vec{E}) = \sum_{k=1}^{m} q_k \int_{t=t\,\min}^{t\,\max} \left(w_k\left(\vec{E}, t\right) - d_k(t)\right)^2 dt \approx \sum_{st=st\,\min}^{st\,\max} \sum_{k=1}^{m} q_k \left(w_k\left(\vec{E}, st\right) - d_k(st)\right)^2 \qquad \textbf{(2-19)}$$

where d_k is the deflection measured at time t by the k^{th} of the m geophones, w_k is the corresponding theoretical deflection and q_k are weighting coefficients, E is a (n+1)-sized column vector containing elastic modulus (E_i) of each of the n layers of the structure and the damping ratio ξ in the volume. st_{min} and st_{max} are time steps relative to lower and upper boundaries considered in the minimization. (The double sum in (2-19) should be multiplied by the length of the time step. This factor is intentionally left out).

Problem to be solved is thus:

« Find $\min_{\vec{E}\in\Re_+^{n+1}} f_t(\vec{E}) = \sum_{st=st\min}^{st\max}\sum_{k=1}^{m} q_k\left(w_k\left(\vec{E}, st\right) - d_k\left(st\right)\right)^2$ » **(P)**

2.2 Resolution method

Two steps have succeeded. At the beginning of the study, no automated calculation was available, so that a semi-manual method was used. In a second time an automated calculation by continual approach has been developed. The two methods are described below.

2.2.1 Early semi-manual method

In the absence of an automated resolution method, a semi-manual technique was developed which is some kind of an improved data base method. A complete numerical sensitivity study has been led, which consisted in choosing for a given structure (S_1 from appendix 1.1) a reference data set, and studying the influence of each parameter, the others being kept constant, by comparing deflections computed for the reference configuration and the modified one.

Sensitivity coefficients relative to each modulus are given by slopes of the regression straight line (Fig. 2-6). This work is made for each modulus and damping ratio. Reference data set was respectively 4700MPa / 7500MPa / 320MPa / 260MPa / 85MPa / 5% for surface AC, base AC, upper and lower UGA layers, subgrade, and damping ratio.

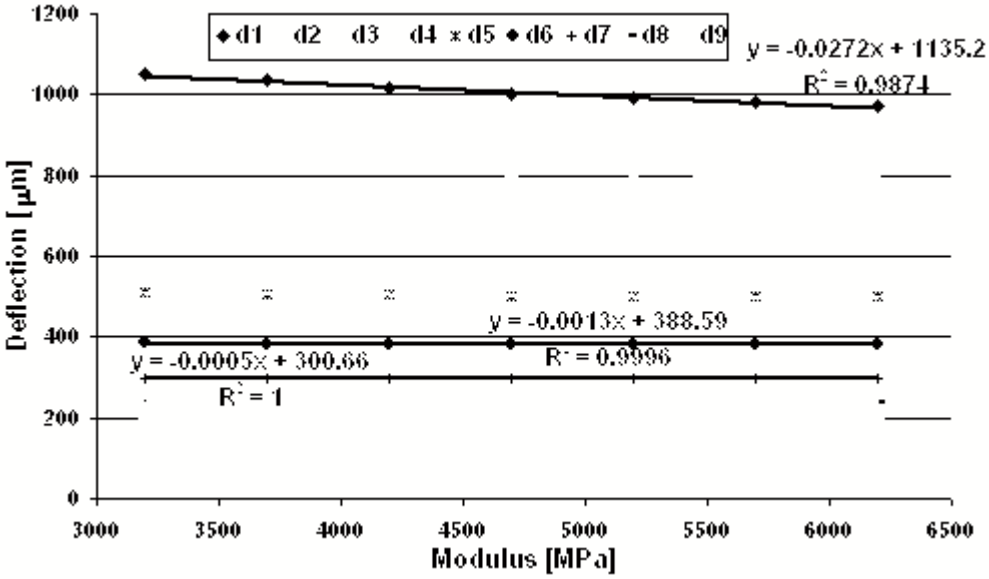

Fig. 2-6 Calculation of sensitivity coefficients relative to the different deflections, for surface AC modulus

Fig. 2-7 presents the moduli sensitivity coefficients relative to deflections with regard to distance to load centre. As expected, it appears that surface layers have a limited influence on outer deflections, which are almost entirely governed by subgrade modulus. The latter is the preponderant parameter. Actually, when observing the respective sensitivity coefficients, it comes that its influence on central deflection is about 150 times higher than for asphalt concrete. When considering the mean value on whole geophones, this value becomes 350. It means that (on this structure and considering only peak values) a 1 MPa error on subgrade (1 %) has the same effect than a 350 MPa error on surface AC moduli (5 %), what already highlights that expected precision on backcalculated moduli is higher for subgrade than for other layers. This sensitivity study has been continued on whole model parameters (mass densities, Poisson's ratio, depth to bedrock, etc..). Results are presented in the following. They take advantage of the time-related signals.

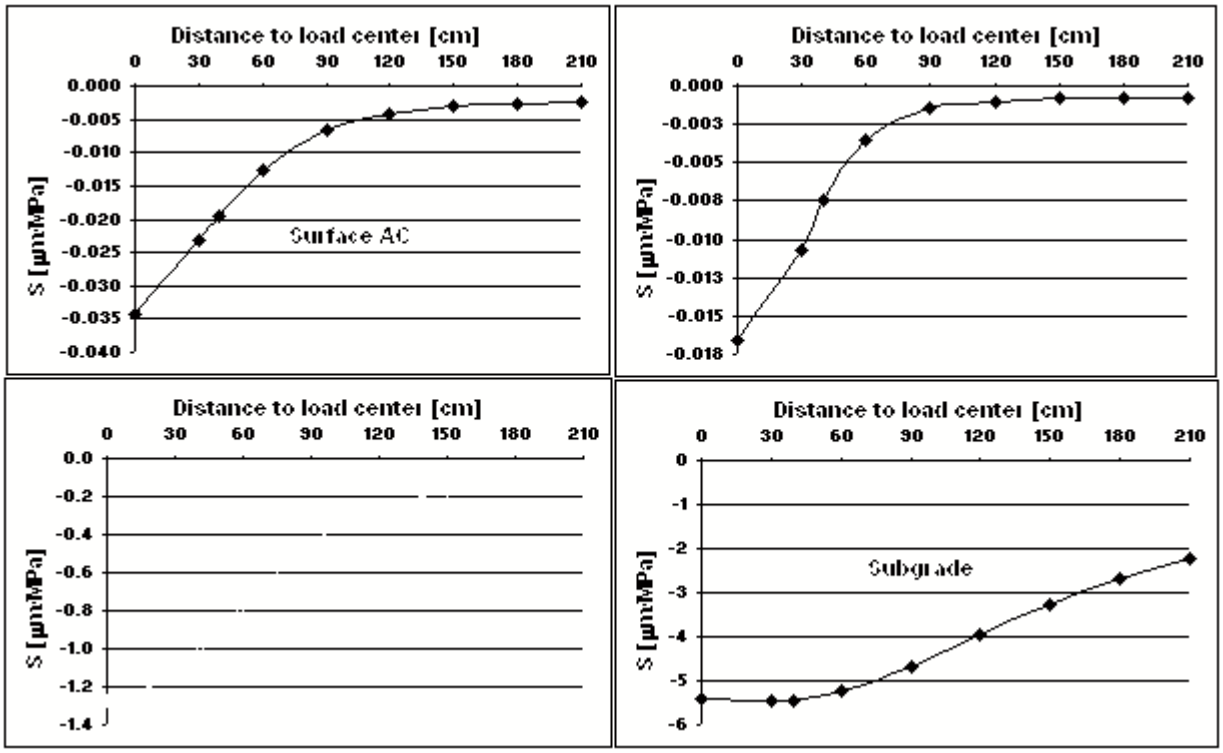

Fig. 2-7 Moduli sensitivity coefficients relative to deflections with regard to distance to load centre

The same work has been performed with propagation times (measured on peaks).

These data allow an efficient semi-manual backcalculation procedure, when starting from subgrade and then going up in the structure. A second pass is required to adjust values. With this method, good fittings are obtained in ten to fifteen calculations.

A similar procedure has been adopted for shock modelling. The only difference is that real time abscissas are replaced by adjusted values corresponding to the elapsed time from impact, since the shock is assumed to be instantaneous. The time origin is thus chosen when maximum is reached on central geophone.

As a conclusion, a semi-manual method has been proposed. It has highlighted respective influence of modulus. Nevertheless this method is laborious. Moreover it implicitly implies

that results of the sensitivity study performed on a particular pavement can be transposed to all pavements. Therefore it appears necessary to develop an automated procedure.

2.2.2 Development of an automated method

a - Choice of an algorithm

Several methods belonging to 0^{th} to 2^{nd} order method classes have been tested in the frame of three training courses ([Nguyen 2008],[Point 2009] and Minghini) supervised jointly by STAC (M Broutin) and ENPC (P Argoul) :

- 0^{th} order methods: Simplex method,
- 1^{st} order methods : Method of steepest descent,
- 2^{nd} order methods. Gauss Newton, BFVG Quasi Newton and Levenberg Marquardt.

These methods have been tested on a simulated data set, that is to say a direct calculation has been performed and the raised issue has consisted in finding initial parameters back. These works have led to the conclusion that the method of steepest descent is not suitable to the problem. [Nguyen 2008] explained it by the presence of a big valley when plotting in 3D the deflections as a function of $E_{subgrade}$ and E_{UGA}. The speeds to reach convergence for the Simplex and the Gauss Newton methods have been compared. The first one is too slow to be efficient. Gauss Newton has appeared to be the quickest algorithm among the second order methods. This algorithm has been retained.

b - Retained algorithm

The retained Gauss Newton algorithm is here briefly presented. Mathematical details are provided in appendix 3.1.

Finding the f_t minimum is equivalent to make its gradient null, i.e.:

$$\forall\ j \in [1; n+1]\ \ f_t j(\vec{E}) = \sum_{st=st\,\min}^{st\,\max} \sum_{k=1}^{m} q_k \left(w_k(\vec{E}, st) - d_k(st) \right) \times \frac{\partial w_k}{\partial E_j} = 0 \qquad \text{(Ej)}$$

The (S1) system constituted of the n+1 (Ej) equations is solved using the Gauss Newton method.

This method consists of an iterative process consisting in 1- choosing a seed moduli data set 2-updating this data set by a given process and 3- stopping the process when a given criteria is reached.

- **Initialization**

An initial data set $\vec{E}^0$ is arbitrary chosen. The most realistic values as possible have to be taken. Their choice leans on preliminary experimental tests or failing that on knowledge of current values for considered materials in the test conditions.

- **Resolution at Nth step**

Let $\vec{E}^{N-1}$ be the parameters set at beginning of Nth step. Let call it "reference parameters set at step N".

Each (Ej) equation is solved using the Newton method. It necessitates solving at each step of the iterative process the following (S2) system:

$$S^N \cdot d\vec{E}^N = \vec{R}^N \qquad \text{(S2)}$$

where S^N is the (n+1)×(n+1) real-valued matrix whose generic (i, j) entry is:

$$S_{ij}^N = \sum_{st=st\min}^{st\max} \sum_{k=1}^{m} q_k \frac{\partial w_k}{\partial E_i} \frac{\partial w_k}{\partial E_j} \qquad \textbf{(2-20)}$$

and $\vec{R}^N$ and $d\vec{E}^N$ the (n+1)-sized real-valued column vectors whose j entries are respectively

$$\vec{R}_j^N = -\sum_{st=st\min}^{st\max} \sum_{k=1}^{m} q_k \left(w_k\left(\vec{E}^N, t\right) - d_k(t)\right) \times \frac{\partial w_k}{\partial E_j} \qquad \textbf{(2-21)}$$

And

$$d\vec{E}_j = dE_j \qquad \textbf{(2-22)}$$

S^N is called sensitivity matrix (or Hessian matrix). $\vec{R}^N$ is called remainder vector.

The equivalency between the (S1) and (S2) systems has been demonstrated in details in this work; all relative developments are available in appendix 3.1.

In practice derivatives are approximated by the forward finite differences method (2-23).

$$\forall\ j \in [1; n+1],$$

$$\frac{\partial w_k}{\partial E_j} \approx \frac{w_k\left(E_1^{N-1}, \ldots\ldots, E_j^{N-1} + \Delta E_j^N, \ldots\ldots, E_{n+1}^{N-1}\right) - w_k\left(E_1^{N-1}, \ldots\ldots, E_j^{N-1}, \ldots\ldots, E_{n+1}^{N-1}\right)}{\Delta E_j^N} \qquad \textbf{(2-23)}$$

$w_k\left(E_1^{N-1}, \ldots\ldots, E_j^{N-1}, \ldots\ldots, E_{n+1}^{N-1}\right)$ is the kth deflection calculated using the reference parameters set, whereas $w_k\left(E_1^{N-1}, \ldots\ldots, E_j^{N-1} + \Delta E_j^N, \ldots\ldots, E_{n+1}^{N-1}\right)$ is the kth deflection calculated with a perturbation ΔE_j^N on the jth parameter.

This implies n+2 (or n+1 without damping) direct calculations at each step of the algorithm.

Resolution of the S2 system is presented in details in appendix 3.1. It is based on a singular value decomposition [Dong 2001; Lang 2002] of the real symmetric S matrix combined with a regularization method [Hansen 2008] to avoid any instability in the convergence algorithm.

- Updating parameters

At the end of Nth step, the reference parameters set is updated by adding $d\vec{E}^N$ to it:

$$\vec{E}^N = \vec{E}^{N-1} + d\vec{E}^N \qquad \textbf{(2-24)}$$

- **Stopping of the process**

The process is carry on until one of the 2 following conditions is fulfilled:

- The target Mean Square Error (MSE) is obtained.

Choice of this target error is discussed hereafter. It relies on repeatability data and sensitivity studies

- maximal number of iterations is reached

2.3 Target error

A thorough study has been performed, with regard to the f_t objective function, in order to:
- investigate the relative influence of the different parameters on the deflection time-histories
- to discuss *a posteriori* the relevance of arbitrarily setting of some parameters (in 2.1.1)
- to assess expected precisions on backcalculated parameters.
- to establish a criterion to assess if the resulting set of backcalculated parameters is appropriate or not i.e. practically to recommend a Mean Squared Error (MSE) value

Uncertainties on $f_t(\vec{E})$ are first listed and evaluated. Then, a related MSE value is defined and expected precisions on backcalculation due to aforementioned uncertainties are discussed.

2.3.1 Uncertainty on $f_t(\vec{E})$

Sources of uncertainties on $f_t(\vec{E})$ come on the one hand from uncertainties on experimental deflections values $d_{i,st}$, and on the other hand from uncertainties on the numerical w_i , due to uncertainties on imposed parameters. $d_{i,st}$ and $w_{i,st}$ being independent, one can write, with U as the uncertainties:

$$U^2(f_t) = \sum_{k=1}^{m}\left(\sum_{st=st\,\min}^{st\,\max}\lambda_{k,st}^2 U^2(d_{k,st})\right) + \sum_{k=1}^{m}\left(\sum_{st=st\,\min}^{st\,\max}\lambda'^2_{k,st} U^2(w_{k,st})\right) \text{ with } \lambda_{k,st} = \frac{\partial f_t}{\partial d_{k,st}} \text{ and}$$

$\lambda'_{k,st} = \dfrac{\partial f_t}{\partial w_{k,st}}$ the sensitivity coefficients of $f_t(\vec{E})$ relative to parameters $d_{k,st}$ et $w_{k,st}$.

Assuming that for each k, $w_k \approx d_k$,

$$U^2(f_t) = \sum_{k=1}^{m}\sum_{st=st\,\min}^{st\,\max} 4 q_{k,st}^2 d_{k,st}^2 \left(U^2(d_{k,st}) + U^2(w_{k,st})\right) \qquad \textbf{(2-25)}$$

Determination of the uncertainties on $w_{i,st}$ for each parameter relies on calculation of sensitivity coefficients.

The uncertainties on $w_{i,st}$ generated by different parameters are calculated by multiplying the uncertainty on the considered parameters by their sensitivity coefficients. The latter are calculated in the same manner than previously (variation on parameter and use of the slope of regression straight line).

- Uncertainty on f_t due to experimental imprecisions

It is deduced from the repeatability study presented in part 1. Standard deviations between the 10 measurement points have been considered for each time step to assess $U\left(d_{k,st}\right)$.

Corresponding global uncertainty on $f_t(\vec{E})$ is:

$$U_{\exp}\left(f_t\right)=\sum_{k=1}^{m}\sum_{st=st\min}^{st\max}4\,q_{k,st}^2\,d_{k,st}^2\,U^2\left(d_{k,st}\right)=9{,}6.10^4\ \mu\text{m}^2.$$

Note that experimental uncertainties retained have to be normalized with regard to applied load. Actually it has been shown in part 1 (Fig.1-48) that they are proportional to applied load.

- Uncertainty on f_t due to numerical imprecisions

Assuming that parameters are independent, one can write for the kth geophone:

$$U^2\left(w_k\right)=\sum_{i=1}^{n}\sum_{st=st\min}^{st\max}S_{i,k,st}^2U^2\left(\rho_i\right)+\sum_{i=1}^{n}\sum_{st=st\min}^{st\max}S'^2_{i,k,st}\,U^2\left(\nu_i\right)+\sum_{i=1}^{n}\sum_{st=st\min}^{st\max}S''^2_{i,k,st}\,U^2\left(t_i\right)+\sum_{st=st\min}^{st\max}S'''^2_{k,st}\,U^2\left(bd\right)+\sum_{st=st\min}^{st\max}S''''^2_{k,st}\,U^2\left(x_k\right)$$

with $U\left(\rho_i\right)$, $U\left(\nu_i\right),U\left(t_i\right),U\left(bd\right),U\left(x_k\right)$ the uncertainties respectively on the material densities and Poisson's ratio, layer thicknesses, depth-to-bedrock and geophone position and $S^2_{i,k,st}$, $S'^2_{i,k,st}$, $S''^2_{i,k,st}$, $S'''^2_{i,k,st}$ and $S''''^2_{i,k,st}$ the associated sensitivity coefficients relative to $f(\vec{E})$.

Observe that as the experimental uncertainties, theoretical uncertainties are also proportional to applied load. Actually, $U\left(\rho_i\right)$, $U\left(\nu_i\right),U\left(t_i\right),U\left(bd\right),U\left(x_k\right)$ are all independent of load, and sensitivity coefficients are proportional to it, since the chosen mechanical model is linear. As a consequence, all following results are thus valid whatever the applied load.

The sensitivity coefficients are determined numerically as previously explained.

A special care is here given to depth to bedrock, as the influence of this parameter is particular. As observed in Fig. 2-8 which displays surface deflections normalized with regard to the infinite extent case, it appears that this parameter presents a negligible influence above a 5 m depth, whereas its effect becomes preponderant for shallow bedrocks, especially for outer deflections. This is the reason why several cases are considered in the final summary table.

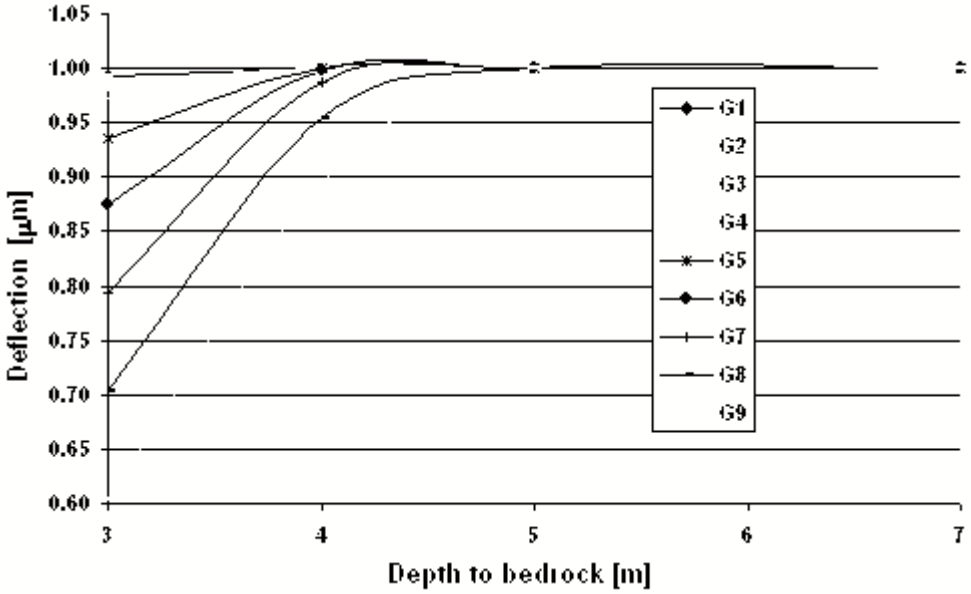

Fig. 2-8 Influence of depth to bedrock on deflections

It is assumed that accuracy on mass density is 100 kg/m^3 or better, and the one on ν is 0,05 or better.

Precision on geophones positioning on the support beam is assumed to be 3 mm or better for all geophones, except for the central one whose position is supposed to be exact.

Finally, concerning the thicknesses, the 0,5 cm and 3 cm precisions are respectively admitted for asphalt and unbounded material thicknesses. They correspond to standard tolerances imposed in French contract specifications.

The determination of uncertainty on depth to bedrock (d_b) is more complex. Let us interest for that to the method proposed by [Mera 1995] and used in part 3 for practical cases. It consists in determining depth to bedrock using resonant frequency of the structure. Depth to bedrock is determined by performing a FRF between the force signal and the deflection measured on the outer geophone. It is linked to resonant frequency and subgrade modulus. The iterative process proposed (see dedicated literature review part) allows determining depth to bedrock and an approximation of subgrade modulus by successive backcalculations on the last geophone.

Upper layers are assumed to have a limited influence on the backcalculation results. The incidence of their stiffness on the bedrock depth determination has nevertheless been studied. Another parameter to be taken into account is the deflection on the outer geophone used in the backcalculation process.

Precision on depth to bedrock can thus be expressed as:

$$U(d_b) = \sqrt{\sum_{i=1}^{n} \lambda_{E_i}{}^2 U(E_i)^2 + \lambda_{f_R}{}^2 U(f_R)^2 + \lambda_{d_9}{}^2 U(d_9)^2}$$

Where the $U(E_i)$, $U(f_R)$ and $U(d_9)$ are respectively the precisions on the upper layers moduli (i.e. all layers except subgrade), the resonant frequency of the structure and deflection on the outer geophone, and λ_{E_i}, λ_{f_R} and λ_{d_9} the corresponding sensitivity coefficients.

Precision on f is assumed to be 1 Hz, according to repeatability tests on 10 HWD test points from the fatigue carrousel experiment.

This leads to U(d_b) = 0,40 m.

Main results are presented in Table 2-1 hereafter.

	b_d>4m	b_d>3m	b_d<3m
$U_{Exp}(f_t) = \sqrt{\sum_{k=1}^{m} \sum_{st=st\min}^{st\max} 4q_{k,st}^2 d_{k,st}^2 U^2(d_{k,st})}$	9.6.E+04	9.6.E+04	9.6.E+04
$U_{\rho}(f_t) = \sqrt{\sum_{k=1}^{m} \sum_{st=st\min}^{st\max} 4q_{k,st}^2 d_{k,st}^2 \left(\sum_{i=1}^{n} S_{i,k,st}^2 U^2(\rho_i) \right)}$	4.9.E+04	4.9E+04	4.9.E+04
$U_{\nu}(f_t) = \sqrt{\sum_{k=1}^{m} \sum_{st=st\min}^{st\max} 4q_{k,st}^2 d_{k,st}^2 \left(\sum_{i=1}^{n} S'^2_{i,k,st} U^2(\nu_i) \right)}$	9.6.E+04	9.6E+04	9.6E+04
$U_{t}(f_t) = \sqrt{\sum_{k=1}^{m} \sum_{st=st\min}^{st\max} 4q_{k,st}^2 d_{k,st}^2 \left(\sum_{i=1}^{n} S''^2_{i,k,st} U^2(t_i) \right)}$	2.2.E+05	2.2E+05	2.2.E+05
$U_{db}(f_t) = \sqrt{\sum_{k=1}^{m} \sum_{st=st\min}^{st\max} 4q_{k,st}^2 d_{k,st}^2 S'''^2_{k,st} U^2(bd)}$	**2.3.E+04**	**1.7.E+05**	**5.1.E+05**
$U_{x}(f_t) = \sqrt{\sum_{k=1}^{m} \sum_{st=st\min}^{st\max} 4q_{k,st}^2 d_{k,st}^2 S''''^2_{k,st} U^2(x_k)}$	9.1.E+03	9.1E+03	9.1.E+03
$U(f_t)$	2.5E+05	3.1E+05	5.7E+05

Table 2-1 Summary of uncertainties on f relative to the different parameters

The d_b > 4m U_{db} value has been calculated between the 4 and 5 m configurations, the d_b > 3m value between 3 and 4 m, and the d_b < 3m value between 2 and 3 m.

These data emphasizes that the main source of error comes from imprecision on layer thicknesses, except for very shallow bedrocks, where the depth to bedrock is preponderant. In the following, let us interest to the intermediate condition with regard to this parameter (d_b > 3m).

2.3.2 Final choice and related precisions on backcalculated moduli

The aim of the previous calculations is to choose a consistent Mean Squared Error with uncertainties. They also allow determining precisions obtained on moduli.

a - Mean Squared Error (MSE)

As it is assumed that bedrock is deeper than 3 m, then $U(f_t) = 3{,}1.10^5\ \mu m^2$. An arbitrary choice is to be made on MSE. The latter must be of the same order of magnitude as $U(f_t)$. In practice, the normalized MSE is considered i.e. the MSE divided by the number of geophones multiplied by time steps. The number of time steps considered in the previous calculation is 240, and the number of geophones 9, so that the target normalized mean squared error retained in the following is 150 μm^2.

b - Expected precisions on backcalculated moduli

The second column of Table 2-2 provides the $\lambda^2(Ei)$ squared sensitivity coefficient with respect to each material modulus.
When considering the worst case where the whole $3{,}1.10^5$ error is attributable to the E_i modulus, it comes that precision on E_i is better than the upper limit $U(E_i) = U(f_t)/\sqrt{\lambda(E_i)}$

b_d>3m

ith parameter :	$\sum_{k=1}^{m}\left(\sum_{st=st\,\min}^{st\,\max} 4 q_{k,st}^2 d_{k,st}^2 S_{i,k,st}^2\right)$	$U(E_i)$	E_i	$\frac{U(E_i)}{E_i}$	$\frac{U(E_i)}{U(E_{Subgrade})}$
Surface AC stiffness	2.19E+04	**2098**	4700	45%	379
Base AC stiffness	5.89E+03	**4048**	7500	54%	731
UGA stiffness	4.25E+07	**48**	260	18%	9
Subgrade stiffness	3.15E+09	**5.5**	85	7%	1
ξ	2.5E+09	**6.2**	10	62%	

Table 2-2 Expected precisions on moduli (MPa) due to parameters and experimental uncertainties

Last column values indicates that an error of 1 MPa on the subgrade modulus has the same incidence on the RMS error as an error of respectively 10 MPa, 750 and 400 on the UGA, base and surface asphalt concrete moduli.

Thus the test allows reaching very accurate backcalculated values for subgrade and UGA, and less precise for upper layers, even though values of Table 2-2 are maximal values.

The influence of the backcalculated moduli uncertainty is not the decision-making criterion. The latter is rather the uncertainty on critical strains derived from the direct calculation performed using these moduli. The corresponding value is estimated in the following. Nevertheless significant imprecisions on surface moduli mainly due to error on thicknesses highlight the need to:
- conduct systematically a GPR survey before each HWD campaign
- perform on each homogeneous area statistical significant samples of HWD tests, in order to limit the uncertainty on layer thicknesses.

3 - Forward calculations

A personal forward calculation procedure is here proposed as an illustration of the possible practical use of the previous backcalculation results. It is linked to the choice of the model used for the calculation of material damage. Constant moduli through time and classical behaviour laws are here considered, as it is considered that the command of stiffness reductions during pavement life, multi-peak influence, or repair phenomena (see the literature review corresponding part) is not so far satisfactory.

Forward calculations allow evaluating:
- the bearing capacity of the pavement,
- or, for a given traffic mix, the residual life of the pavement, and if necessary an overlay design.

The procedure relies on the computation of critical strains in the pavement. The cumulative damages in the different layers are evaluated according to material performances.

3.1 Determination of critical strains

Critical strains to be determined are:
- the tensile strains at the bottom of the asphalt base layer: $\varepsilon_T = \max(\varepsilon_{rr}, \varepsilon_{\theta\theta})$,
- the ε_{ZZ} vertical strain at the top of the untreated materials.

Stresses applied to the pavement by external considered actions are computed thanks to a forward calculation using the same mechanical model as the one used in the backcalculation phase. Parameters are *a priori* different from the backcalculated Young's moduli, due to temperature and frequency to be applied (see infra). Damping ratio taken into account is the backcalculated one.

Associated strains are then deduced. Noting X_{rr} $X_{\theta\theta}$ X_{ZZ} the components of the X quantity in the radial orthoradial and vertical directions, and E and ν respectively the Young's modulus and Poisson's ratio of the considered material, the ε strains are linked in axis-symmetric systems to the σ stresses by the following equations:

$$\varepsilon_{rr} = \frac{1}{E}\sigma_{rr} - \frac{\nu}{E}\sigma_{\theta\theta} - \frac{\nu}{E}\sigma_{ZZ}$$

$$\varepsilon_{\theta\theta} = -\frac{\nu}{E}\sigma_{rr} + \frac{1}{E}\sigma_{\theta\theta} - \frac{\nu}{E}\sigma_{ZZ}$$

$$\varepsilon_{ZZ} = -\frac{\nu}{E}\sigma_{rr} - \frac{\nu}{E}\sigma_{\theta\theta} + \frac{1}{E}\sigma_{ZZ}$$

3.2 Cumulative damages

Knowledge of these calculated strains allows evaluating the cumulative damages induced by traffic, either real or theoretical.

This determination requires complementary data about:

- the mechanical material performances: laboratory tests are used to establish the allowable strains versus the number of coverages. When this information is not available, a mean behaviour is assumed,
- the traffic,
- the climate, for temperature corrections to be applied: the year is cut into "seasons" each one presenting a constant temperature. "Seasons" can be the 4 seasons of the year but they can also be periods of a day. The considered temperature is the asphalt layer mid-depth temperature.

The general calculation principle proposed consists in:

- correcting backcalculated asphalt materials stiffnesses as a function of the θ_i reference temperatures and the stress frequency (aircraft speed variations depending on the considered traffic area affects the latter), using master curves when available, or by default empirical laws, such as the LTPP one relative to temperature (see literature review, § 2.3.3)
- performing for each reference temperature a direct calculation, taking into account the corrected moduli for surface layers. This leads to temperature-related critical strains $\varepsilon(\theta i)$
- calculating for each critical strain, damages in the considered material, generated by the traffic at temperature θ_i. This calculation is based on (0-51) for asphalt materials, and on (0-52) for unbound materials and subgrade.
- deducing cumulative damage using the Miner's law. The latter can take into account lateral distribution. This approach is innovative with regard to traditional procedures applying an inclusive pass-to-coverage ratio to traffic data.

The thickness design is based on the assumption that failure occurs when the cumulative damage equals to 1 with the risk of failure chosen for the design (through the k_r coefficient).

3.3 Bearing capacity, residual life and overlay design

3.3.1 Calculation of pavement bearing capacity

In this case, the unknown parameter is the allowable load (on a theoretical single wheel) for which the pavement failure is obtained after N load applications. The most discriminating imparted strain amongst the critical strains is to be considered. A practical example will be presented in part 3.

3.3.2 Calculation of structural remaining life

In this case traffic data are imposed. Multi-wheel landing gear configurations can easily be studied, since the problem is linear. The strains calculations rely on a direct superimposition principle of the results from elementary calculation considering isolated wheels.

The problem consists in determining the fraction of the structural fatigue life used (cumulative damage less than 1) and the related remaining life. A practical example will also be presented in part 3.

3.3.3 Calculation of pavement overlay

When bearing capacity of the pavement is too low, a flexible overlay can be designed. The principle consists in calculating the necessary thickness that will reduce the strains in the pavement to obtain allowable levels with respect to the traffic data.

3.3.4 Associated precisions

a - Uncertainties on strains

Uncertainties on the critical strains are calculated by comparing “extreme” data set moduli according to the uncertainty on moduli. The “extreme” term does not refer to the data set where all moduli are maximal and minimal, but is related to the induced strains, what is not equivalent as shown hereafter.

Note that strain calculation from backcalculated moduli is performed using the static model, even if a dynamical calculation is available in PREDIWARE. Actually the current French design method relies on this type of models.

Suppose that at least N_{test} = 15 HWD tests are available per homogeneous area. The uncertainties from Table 2-2 are thus to be divided by $\sqrt{N_{test}}$, what results in an approximate uncertainty of 500 MPa on AC_1 modulus, 1 000 MPa on AC_2 one, and 2 MPa on subgrade one.

To simplify the problem only the σ_{XX} tensile strain at the bottom of the asphalt layer and the σ_{ZZ} vertical strain at the top of subgrade are considered, and uncertainty on UGA is not considered. Let us consider for each modulus the value range comprised between the reference value and an upper value corresponding to the reference value increased of one uncertainty value.

Table 2-3 collects moduli, stresses and strains for four characteristic data sets in this moduli range. “Ref” is the reference data set, with the lowest data values for all layers and “LH+” is the upper value data set i.e. involving the highest data values for all layers. “H+” is a mix data set data set presenting the highest value for surface materials and a reference value for subgrade, whereas the inverse configuration is encountered in “L+”. By convention compressions are denoted by positive values. The combination of moduli for which strains are maximal is not the one including the lowest moduli values for all layers. The data set resulting in a minimal tensile strain at the bottom of AC layer is L+ and the one resulting in a minimal vertical strain at the top of subgrade is H+. Some kind of balance occurs: when surface modulus decreases, the subgrade undergoes larger stresses and strains. On the contrary, with a low bearing subgrade, the stresses to be spread by the surface layer increase.

	E_{AC1} [MPa]	E_{AC2} [MPa]	E_{UGA} [MPa]	U_S [MPa]	σ_{XX} (bottom AC_2) [MPa]	σ_{ZZ} (bottom AC_2) [MPa]	ε_{XX} (Top of S) [μm/m]	ε_{ZZ} (Top of S) [μm/m]
Ref	4700	7500	260/320	85	-2,77	0,093	-267,1	1131
H+	5200	8500	260/320	85	-2,77	0,087	-267,2	1061
L+	4700	7500	260/320	87	-2,60	0,091	-252	1113
LH+	5200	8500	260/320	87	-2,76	0,088	-266,7	1074

Table 2-3 Stress and strains for characteristic data sets in the uncertainty range

According to Table 2-3, uncertainties on ε_{XX} (base of AC layer) and ε_{ZZ} (top of the subgrade) are $\varepsilon_{XX} = \frac{267-252}{267} = 5{,}6\%$ and $\varepsilon_{ZZ} = \frac{1131-1061}{1131} = 6{,}2\%$

b - Uncertainty on the remaining pavement life

Let us consider the usual relationship between the number of load applications and the allowable strain (See literature survey):

$$Ne/10^4 = \left(\varepsilon_{XX} / \left(\varepsilon_4 \cdot k_C \cdot k_r \cdot k_S\right)\right)^{\frac{1}{b}}$$

According to this relationship, if $\varepsilon_{XX}1/\varepsilon_{XX}2 = 1{,}06$, then $Ne1/Ne2 = 1{,}06^{\frac{1}{b}}$
Practical application gives $Ne1/Ne2 = 0{,}75$

This means that an uncertainty of 6% on ε_{XX} results in a 25 % uncertainty on number of allowable coverages.

The same calculation performed on permanent deformation observed at the top of subgrade, according to (equation 0-48 from literature review) provides a 23 % uncertainty on number of allowable coverages.

4 - Calculation tool: PREDIWARE Software

The aim is here to provide a brief presentation of the possibilities of the PREDIWARE (**P**avement **R**ational **E**valuation using **D**eflections **I**nduced by falling **W**eights, for **A**irfield and **R**oad **E**ngineers) software. A more detailed presentation is given in appendix 2.

4.1 Brief overview

The PREDIWARE software provides the following possibilities:

4.1.1 Automating the creation of a mesh and the associated CESAR data file

The mesh creation respects the optimization rules described in 1.1. The user has only to provide layer thicknesses and material properties. The choice of the latter are optional, as they can be let as default values and modified, after creation, directly in the data file, or even on screen before launching the calculation. Default plate geometry refers to the large radius one (22,5 cm) but this value can be modified by the user.

4.1.2 Performing direct calculations for a given structure

Computation options are the following:
- static or dynamic calculations,
- computation of either surface deflections, stresses and strains at critical levels in the structure, or all of them. Default geophone number and positions correspond to the distances provided in part 1 but can be modified by the user.

4.1.3 Performing backcalculations

Computation options are the following:

- backcalculation on real HWD data, or simulated data

The latter option is not used in the frame of operational assessment, but can be very useful for the numerical testing of new convergence algorithms.

- static or dynamic calculations

In the static case, the only backcalculated parameters are elastic moduli.
In the dynamic case, damping can be fixed (at a null or undefined value) or backcalculated.

- computation using surface deflections, gage measurements, or the combined information with related q_k weighting coefficients to be chosen by the user (set to 1 by default).

When using surface deflections, data can directly been imported from HWD raw data files. The user has only to provide the test point(s), sequence(s) and fall(s) of interest.
When using gage measurements, the latter experimental data must be stored in an Excel sheet with a standard organization.

The parameter evolution is followed during the procedure, so as the MSE error. This evolution is plotted at each epoch of the iterative process. Quality of the fitting is also viewed. The possibility is provided to save these pictures, or even to directly extract a movie file displaying the evolution of the fitting (deflection or strain basins, or corresponding time-related values).

All parameters are stored in a .txt file well formatted for a direct opening with Excel.

Flow calculation is available, which is appreciable in the case of long dynamic calculations.

Frame time used, as well as the time sampling (consider 1 time step on N), and automated time adjustment taking into account bias evoked in part 1 are chosen by the user. Default value for the latter parameter is 3,5 ms.

Other secondary options are available:

- the automated plot of basin deflections or time-related deflections from a HWD raw data file,
- the creation of a "mean" raw data file, which would take into account pre-defined points of an homogeneous area, options being 1- use of mean values on whole parameters (force and deflections) 2- use of mean value plus one standard deviation on deflections, or 3- use of mean value plus one standard deviation on deflections and mean value minus standard deviation on force,
- plot of the hysteretic loops in the frame of damping studies.

4.2 Validation

The PREDIWARE tool has been validated in two manners.

First, the accuracy of the direct calculation phase has been assessed by comparing the computed deflections and strains with a reference calculation software: the LCPC's Alize software [Alize]. In the Alizé software, computed mechanical values are based on a layered elastic analysis (Burmister model). Values at critical levels of the designed structure (ε_T at the bottom of asphalt layers and ε_{ZZ} at top of subgrade) are in accordance with field data (measurement of strains from embedded gauges, [Fabre et al. 2005]) and with the values derived from other rational softwares [Balay, et al. 2008] when similar structural and loading conditions are selected.

Secondly, the backcalculation phase has been tested using a simulated data set.

4.2.1 Validation of the direct calculation

The comparison with Alizé-LCPC software mechanical computation has been studied on the S_2 structure (see appendix 1.1). Moduli taken into account are respectively 6 000, 10 000, 200, and 120 MPa for surface (AC_1) and base (AC_2) asphalt concrete layers, humidified Unbound Graded Aggregate (UGA) and Subgrade (S). These values are *a priori* predicted values at the 20°C test temperature, in the absence of material data or backcalculation analysis performed on the structure.

Since the Burmister model, which constitutes the calculation core of the Alizé-LCPC software, does not take into account the loading plate existence, it was necessary to modify the automated mesh generation routine, in order to provide a special mesh without the latter.

Surface deflections, critical stresses and strains in the pavement calculated using this modified mesh and a static load are first be compared to the Alize-computed ones.
In a second time, influence of the plate and the dynamic nature of the load are examined.

Tables 2-4 to 2-6 summarize all the results.

Geophone	G1	G2	G3	G4	G5	G6	G7	G8	G9
Alizé LCPC	258	220	203		122	86	58	38	24
PREDIWARE Static without plate	258	220	203		122	86	58	38	24
PREDIWARE Static with plate	241	212	197	166	122	86	59	39	24
PREDIWARE Dynamic with plate	296	262	246	213	169	133	105	82	64

Table 2-4 Comparison between PREDIWARE direct calculation results and Alize ones; deflections [μm]; S_2 structure

Considered stress	σ_{xx} AC bottom	σ_{zz} AC bottom	σ_{xx} UGA Top	σ_{zz} UGA Top	σ_{xx} S Top	σ_{zz} S Top
Alizé LCPC	-1,166	0,05	0,003	0,05	0,001	0,028
PREDIWARE Static without plate	-1,159	0,048	0,0033	0,050	0,0014	0,0281
PREDIWARE Static with plate	-1,180	0,046	0,0069	0,048	0,0039	0,0281
PREDIWARE Dynamic with plate	-0,854	0,035	0,0070	0,036	0,0040	0,0253

Table 2-5 Comparison between PREDIWARE direct calculation results and Alize ones; stresses [MPa]; S_2 structure

Considered strain	ε_{xx} AC bottom	ε_{zz} UGA Top	ε_{zz} S Top
Alizé LCPC	-77,6	240,4	226,9
PREDIWARE Static without plate	-77,0	239,5	226,4
PREDIWARE Static with plate	-78,2	232,6	227,9
PREDIWARE Dynamic with plate	-73,9	250,5	171,5

Table 2-6 Comparison between PREDIWARE direct calculation results and Alize ones; strains [μm/m]; S_2 structure

It appears that surface deflections, stresses and strains provided by Alize and PREDIWARE calculation in static mode and without the loading plate are rigorously the same (1 μm difference only for G_4). Precision on geophones is of the micron range whereas precisions on stresses and strains are respectively better than 0,01 MPa and 1 μm/m.

Adding a loading plate is of no effect on outer deflections. Nevertheless some discrepancies are observed in the plate area with regard to the no-plate configuration. The influence on stresses is negligible, except for tangent compression in both unbound materials. Effect on strains is limited.

Comparison between static and dynamic modellings shows that deflections are higher in the dynamic case. This implies that the static modelling overestimates backcalculated moduli with regards to the dynamic one. Let us remind that the tested structure presents shallow bedrock (3 m).

Let us also consider the half-space case.

The latter is dealt with on structure S_3 (point Pl_1; see appendix 1.1). Moduli of the reference set are usual moduli. The respective values of 4 700, 9 000, 200, 150 and 120 MPa have been chosen for surface (AC_1) and base (AC_2) asphalt concrete layers, humidified Unbound Graded Aggregate (UGA), untreated gravel (G) and Subgrade (S).

Geophone	G1	G2	G3	G4	G5	G6	G7	G8	G9
PREDIWARE Static with plate	415	334	316	276	229	189	160	135	117
PREDIWARE Dynamic with plate	213	168	159	138	114	92	78	67	59

Table 2-7 Comparison between static and dynamic calculations; S_3 structure

This time, the inverse observation is made i.e. static modelling underestimates backcalculated moduli with regard to a dynamic one.

This supports [Mera, 1995] observations (see literature review) on numerical signals, who shows that the static modellings tends to overestimate stiffnesses for shallow bedrocks and underestimate them on half-spaces.

4.2.2 Validation of the backcalculation phase

The main principle consists in choosing for a pavement structure a reference moduli data set and determining, using the previously validated PREDIWARE direct calculation option, the related simulated deflection data set.
Then accuracy and robustness of algorithm is tested by performing backcalculations with several seed moduli set, when considering that the previously simulated deflections are the experimental data to be matched. Dispersion on backcalculated moduli is studied.

This work is performed on static and M_1 dynamic (both with and without damping) modellings, using a common seed moduli set. The S_3 structure (point Pl_1) of appendix 1.1 has been retained for this study. First, static and dynamic without damping results are compared. Then, the influence of damping is studied.

Note that due to very time-consuming calculations in dynamic mode, the work is performed using a ten (10) seed moduli sets sample (called Reference set (Ref) and SMS 2 to 9 in the following). It could be interesting to reiterate it on larger data set (100 seed moduli data sets for instance.)

Reference moduli set is, as above 4700, 9000, 200, 150 and 120 MPa from highest to lowest layer. Other seed moduli sets have been arbitrary defined using the Random Excel function, when imposing a realistic variation range. Mean, standard deviation (Std. Dev.) and variance (Var.) are collected in Table 2-8 and Table 2-9 (blue part)

The latter collect results of the respective pseudo-static and dynamic without damping methods (modulus values are given in MPa). Number of iterations has been fixed at 20 for all

calculations. Note that the quality of fitting, expressed in terms of normalized mean squared error (Norm. MSE) is in all cases excellent.

The comparison of resulting backcalculated mean values with reference values demonstrates that a good accuracy on backcalculated moduli can be reached with only twenty (20) iterations. The study of variances of results (yellow boxes), compared to initial scatter (blue boxes) shows that robustness is much better in the dynamic case. Such a result can be explained by the high overdetermination of the problem when the whole time-histories are considered instead of the peak values only.

	Seed moduli sets					Backcalculated moduli sets					Norm. MSE
	AC1	AC2	UGA	G	S	AC1	AC2	UGA	G	S	
Ref	4700	9000	200	150	120	4700	9000	200	150	120	0
SMS2	4476	10957	241	342	138	4657	9211	192	157	119	6.91E-03
SMS3	6572	13368	275	260	108	4677	9115	196	154	119	2.27E-03
SMS4	5054	10458	281	234	74	4654	9229	191	158	119	8.67E-03
SMS5	2741	6691	255	205	38	4640	9292	189	160	118	1.36E-02
SMS6	2645	3635	199	211	49	4837	8467	216	138	123	4.26E-02
SMS7	2014	8236	280	192	79	4681	9080	197	152	120	9.27E-04
SMS8	4848	4366	338	204	146	5154	7446	250	116	129	4.17E-01
SMS9	3443	7908	256	237	82	4682	9083	197	153	120	1.05E-03
SMS10	6332	8377	160	182	41	4672	9148	194	156	119	4.37E-03
Mean	4055	8291	258	226	93	4742	8880	203	149	121	
Std Dev	1450	3120	43	53	38	165	589	19	14	3	
Var	35.8%	37.6%	16.7%	23.6%	40.8%	3.5%	6.7%	9.5%	9.3%	2.9%	

Table 2-8 Robustness of the pseudo-static backcalculation procedure; S_3 structure

	Seed moduli sets					Backcalculated moduli sets					Norm. MSE
	AC1	AC2	UGA	G	S	AC1	AC2	UGA	G	S	
Ref	4700	9000	200	150	120	4700	9000	200	150	120	0
SMS2	4476	10957	241	342	138	4665	9088	200.04	150.04	120.02	2.7E-03
SMS3	6572	13368	275	260	108	4938	8464	199.31	149.81	119.82	9.9E-02
SMS4	5054	10458	281	234	74	4747	8889	199.90	149.95	119.96	4.8E-03
SMS5	2741	6691	255	205	38	4755	8871	199.87	149.94	119.96	6.2E-03
SMS6	2645	3635	199	211	49	4762	8843	200.01	149.93	119.95	8.5E-03
SMS7	2014	8236	280	192	79	4545	9383	200.43	150.18	120.11	4.2E-02
SMS8	4848	4366	338	204	146	4844	8621	200.23	149.85	119.86	4.5E-02
SMS9	3443	7908	256	237	82	4688	9033	199.99	150.02	120.01	6.4E-04
SMS10	6332	8377	160	182	41	4723	8944	199.97	149.97	119.98	1.5E-03
Mean	4055	8291	258	226	93	4736	8914	200	150	120	
Std Dev	1450	3120	43	53	38	105	251	0	0	0	
Var	35.8%	37.6%	16.7%	23.6%	40.8%	2.2%	2.8%	0.1%	0.1%	0.1%	

Table 2-9 Robustness of the dynamic without damping backcalculation procedure; S_3 structure

Note that in the dynamic case, precision found on backcalculated moduli is excellent for deepest layers (subgrade, untreated gravel, and UGA), and slightly less satisfactory for surface layers, which is consistent with the previous sensitivity study conclusions.

Associated results obtained when introducing damping are not presented here. The corresponding precision on backcalculated moduli is once more excellent.

4.2.3 Computation times

Static direct calculations are virtually instantaneous (less than 1 s calculation time) Nevertheless, computation times for the dynamic direct calculations relative to the S_3 structure (1 time step out of 3, i.e. 80 time increments) was 30 s per calculation, with a ratio CPU time / machine residence time of 0,96.

The structure presents 4 layers, so that each step of the iterative process using the Gauss Newton algorithm requires respectively 6 and 5 direct calculations with and without damping. Considering a mean value of 15 iterations to converge, mean computation time for the whole backcalculation procedure is about 25 to 45 min.

Material configuration was:
- Intel Core 2 Quad CPU Q6600; 4 × 2,4 GHz
- 2Go RAM
- OS: Windows XP

A calculation accelerator (option MUL in CESAR) allows significant computation gains (ratio in the range of 2 to 5 according to tested meshs). It is for the moment only available in the development version, also owned by STAC, in a LINUX environment. PREDIWARE works at present only in a Windows environment. It is planned to adapt PREDIWARE to LINUX but this has not been done at the time of working.

Partial conclusion

It has been shown that the accuracy of the direct calculation using PREDIWARE is sufficiently good, so that the mesh discretization has no discernable influence on the global HWD moduli determination.

Accuracy and robustness of the dynamic numerical backcalculation procedure has also been demonstrated for both pseudo-static and dynamic methods. Normalized mean squared errors are negligible compared with errors generated by imposed parameters (especially layer thicknesses), so that the errors on backcalculated moduli inherent to numerical backcalculation can be neglected.

Comparison between static and dynamic without damping corresponding results asserts that the dynamic backcalculation method provides more robust convergence than the pseudo-static one. Influence of damping has also been studied. It appears that this parameter can be integrated in the backcalculation process.

Nevertheless, dynamic calculations present an operational weakness due to their computational time. It strengthens interest for the self-adjoints theory (see appendix 3.3), whose implementation in PREDIWARE is in progress.

Conclusions to part 2

A dynamical FEM time-domain modelling has been developed which allows calculation of the time-related surface deflections and strains in the pavement induced by an external load, with regard to a known pavement characteristics.

An associated numerical backcalculation method has been developed, which consists in an iterative procedure using repeated links to the previous direct calculation. A related target mean squared error has been defined, in accordance with the coupled results of a numerical sensitivity study and the experimental repeatability study described in part 1.

A general interpretation method of HWD data in terms of bearing capacity and remaining life of pavement has also been proposed. This method will be applied in practical cases in part 3, just as an indication, since no accelerated loading facility is available for in-situ validation. Further experiments are expected in the coming months on the subject.

The direct- and back- calculations have been automated in the so-called PREDIWARE tool. Accuracy and robustness of this numerical tool have been studied, and the proposed method seems to be well adapted to solve the problem. Nevertheless the only way to assert that the model is representative of the pavement behaviour relies on full-scale experiments. Part 3 will be dedicated to such validation.

Conclusions de la partie 2

Une modélisation dynamique aux éléments finis dans le domaine temporel a été développée. Elle permet de calculer, pour une chaussée de caractéristiques connues, les signaux temporels de déflexion surfacique et de déformations relatives dans la structure, induits par un chargement.

Une méthode numérique de calcul inverse associée a été développée, qui consiste en un processus itératif basé sur des appels répétés à la phase de calcul direct précédente. Une erreur cible associée a été définie, en cohérence avec les résultats couplés d'une étude de sensibilité théorique et de l'étude de répétabilité expérimentale présentée en partie 1.

Une méthode générale d'interprétation des données HWD, en termes de capacité portante et de durée de vie résiduelle de la chaussée, est aussi proposée. Cette méthode sera appliquée sur des cas pratiques dans la partie 3, juste à titre indicatif, puisqu'aucune donnée expérimentale de dégradation à long terme n'est disponible. Des expériences en ce sens sont prévues dans les prochains mois sur le sujet.

Les phases de calcul inverse et direct ont été automatisées dans un outil appelé PREDIWARE. La précision de la phase de calcul direct et la robustesse de la phase de calcul inverse ont été étudiées numériquement. Il semble que la méthode proposée soit bien adaptée à la résolution du problème posé. Cependant, le seul moyen d'affirmer que le modèle est représentatif du comportement de la chaussée repose sur des essais de validation expérimentale à pleine échelle. La partie 3 est dédiée à ce travail.

Part 3 – Case studies and field validation

Introduction to part 3

This part deals with the experimental validation of the modelling presented in the second part. The successive validation surveys performed during the thesis have been conducted on three main structures, which are “well-known” pavements, with regard to layer thicknesses and material properties.

First, the method to determine the depth to bedrock is assessed in the cases of half-space and shallow bedrock, since both configurations are encountered within the three structures.

Then, the results from dynamic backcalculations performed using surface deflections are presented and compared to pseudo-static corresponding ones. The quality of fitting and robustness of the procedure are assessed. Backcalculated values are then discussed. Depending on the considered structure, this work is based on: 1- the comparison between backcalculated and expected values, which can be either usual values for considered materials, or values obtained from geotechnical surveys and laboratory testing, and/or 2- information from pavement instrumentation, when available. In this second case embedded sensors provide information about strains at critical levels of the structure. The strains computed from the modelling involving backcalculated moduli are compared to field measurements.

Finally, the bearing capacities and remaining lives of two structures are deduced. This work step is just an illustration of the method, since no long-term information is available so far to validate the calculated values.

Introduction de la partie 3

Cette partie s'intéresse à la validation expérimentale du modèle présenté dans la partie précédente. Les campagnes de validation successives menées au cours de la thèse ont été réalisées sur trois structures de chaussée, « bien connues » en termes d'épaisseurs et de propriétés des matériaux.

D'abord la méthode de détermination de la profondeur de substratum est évaluée dans les cas d'un semi-espace infini et d'un substratum peu profond, les deux configurations étant représentées parmi les trois structures retenues.

Ensuite les résultats des calculs inverses dynamiques menés à partir des déflexions surfaciques sont présentés et comparés aux résultats pseudo-statiques correspondants. La qualité du calage et la robustesse de l'algorithme sont évaluées. Les valeurs des paramètres identifiés sont ensuite discutées. Selon la structure considérée, ce travail s'appuie 1- sur la comparaison entre les valeurs rétrocalculées et les valeurs attendues, qui peuvent être soit des valeurs usuelles pour les matériaux considérés, soit issues d'études géotechniques ou d'essais de laboratoire, et/ou 2- sur des données provenant de l'instrumentation de chaussées, si disponibles. Dans ce second cas, des capteurs enregistrent les déformations relatives aux niveaux critiques de la structure. Les déformations calculées en tenant compte des paramètres identifiés sont comparées aux valeurs expérimentales.

Finalement, les capacité portante et durée de vie résiduelle de deux des structures sont déduites, à titre d'illustration de la méthode, aucune information sur le comportement à long terme des chaussées étudiées n'étant disponible.

1 - Experimental data

1.1 Structures under study

Amongst the three structures used in this validation phase, two structures are STAC's test facilities. Both structures are typical airfield structures. The first one was constructed in 1995 to assess in-situ characteristics of new high moduli asphalt materials. It has since been destroyed. Construction of the second one was initiated within the time frame of the PhD, for HWD developed models validation and in the more general frame of new interest for rational pavement design methods. Construction was achieved in November 2007. It presents the interest to be instrumented. No tests on sensors are here proposed, as instrumentation is still in a validation phase. The last structure is a typical road structure from the multiple axle loading effect experiment [Homsi et al., 2010] performed between March 2008 and June 2009 on the LCPC's fatigue carrousel. Structure is the P_1 structure of this experiment. This structure was instrumented. One gage profile has been tested under HWD loading.

Let us call, to keep up the chronological order of first tests on the considered structure, S_1 the 1995 STAC's test facility, S_2 the fatigue carrousel tested structure, and S_3 the instrumented STAC's test facility.

Note that the Bonneuil site (STAC) presents a 12 m depth to bedrock (obtained from geotechnical survey) whereas the Nantes fatigue carrousel (LCPC) presents a 3 m deep concrete blocking, so that both shallow bedrock and half-space configuration are represented.

In all cases layer thicknesses are well-known, with more or less accuracy depending on the determination type: 1-contract specifications and controls during construction, or 2 - *a posteriori* corings and GPR survey.

Geotechnical surveys and laboratory tests on materials have also been conducted.

Table 3-1 describes available information for each structure.

Considered structure	S1	S2	S3
Knowledge of layer thicknesses	From contract specifications and control during construction	1) From contract specifications and control during construction 2) From *a posteriori* corings	1) From contract specifications and control during construction 2) From *a posteriori* corings and GPR survey
Depth to bedrock	>10m	3m	>10m
Laboratory stiffness determination tests available	- Asphalt materials - Subgrade	- Asphalt materials	- Asphalt materials - Subgrade
Fatigue tests available	Yes	No	No
Presence of instrumentation	No	Yes	To be laid out

Table 3-1 Summary of available information relative to each tested experimental pavement structure

The corresponding structures and material data are gathered in the appendix 1.1.

1.2 Field deflections

Table 3-2 provides maximal force and deflections experimental values for the three structures.

Structure	F	d_1	d_2	d_3	d_4	d_5	d_6	d_7	d_8	d_9
S_1	237	1123	929	850	699	531	408	320	253	209
S_2	75	391	297	259	189	116	69	45	32	26
S_3	187	415	334	316	276	229	189	160	135	117

Table 3-2 Maximal force and deflections experimental values; structures S_1 to S_3 (F in kN and d_i in [µm])

These values are in accordance with expectations. Actually the apparent stiffness (assessed by F/d_1) shows than S_2 (road structure) is the weakest structure. S_3 is stiffer than S_1 what is in accordance with relative thicknesses (see appendix 1.1).

1.3 Material laboratory testing

Laboratory tests were performed on materials to validate backcalculated moduli and damping ratio if necessary. All results are available in appendix 1.1.

- Asphalt materials

Concerning asphalt materials, complex moduli $E^* = E_1+iE_2$ have been determined for different combinations of temperatures and frequencies in the usual ranges where the HWD tests are performed. These tests were performed in the LCPC.
The norms of the complex moduli are used for comparison with backcalculated moduli. Their expression is:

$$|E^*| = \sqrt{E_1^{\,2} + E_2^{\,2}} \qquad \textbf{(3-1)}$$

Damping ratios are estimated thanks to the relation:

$$\xi = Q^{-1} = \frac{1}{2} \times \frac{E_2}{E_1}. \qquad \textbf{(3-2)}$$

- Unbound materials

Concerning unbound materials and subgrade, resonant column tests [ASTM] have been performed. These tests allow obtaining a modulus range for these materials, but also damping ratios.

1.4 Specific data from instrumented test facility

The LCPC's fatigue carrousel is a ring-shaped test facility, 10 m wide and 19 m mean radius. The studied structure is the S_2 structure (Fig. 3-1). This tested structure presents the interest of been instrumented. The instrumentation allows recording longitudinal (ε_{XX}) and transverse (ε_{YY}) tensile strains at bottom of the asphalt layer, as well as vertical strains at the top of UGA and Subgrade. One gage profile has been tested under HWD loading.

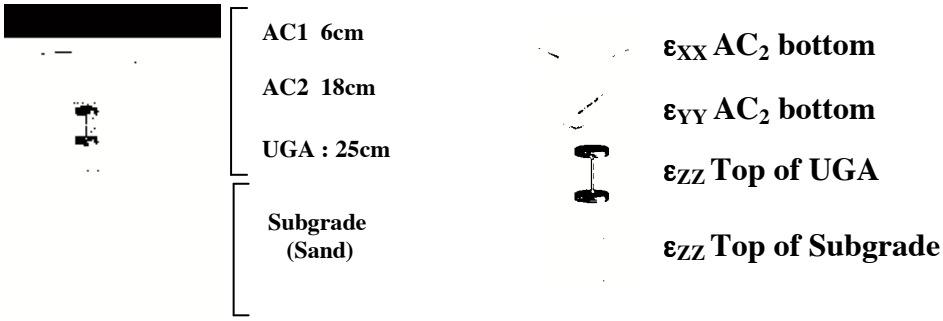

Fig. 3-1 Studied S_2 structure and corresponding instrumentation

The experiment requires the development of a specific protocol. The experiment is then divided into two phases. First step, named "preliminary studies" in the following aims to demonstrate the relevance of this protocol, and to pre-locate gages. Second step is the final experiment, which provides time-related strains in the pavement under HWD loading for the considered the gages profile.

Fig. 3-2 HWD test on the LCPC's fatigue carrousel test facility (photograph by M Broutin)

1.4.1 Preliminary studies

a - Experimental protocol

An experimental protocol has been defined in the frame of the experiment.

A particular care is taken to provide repeatable force signals. The main idea of the experiment is to transform influence lines into basins, i.e., “strain basins” and time-related strain signals at different distances from load centre are reconstituted with a unique gage profile, by varying position of the HWD tests. This idea rests on two assumptions: 1- the structure is longitudinally homogeneous and 2- the external applied force is constant.

The second main point, related to the former one, is the pavement temperature. Actually, as explained previously, asphalt material behaviour is highly dependent on pavement temperature.

A specific positioning system has been introduced for this experiment, which provides high precision placement with regard to routine tests.

Finally it has been checked that chosen acquisition rate is relevant.

- Test configuration

The common test configuration for all tests is “M_0 = 680 kg, H_0 = 40 mm, hard buffers set”. It provides a 75 kN load on the large HWD diameter plate (45 cm). This load corresponds to a compromise between a significant signal on gages and a reasonable level, not to damage the structure (designed for trucks loaded at 65 kN per wheel).

It is *a posteriori* checked that the time-related load can be considered as constant on the whole experiment. Repeatability is of same quality as in Fig. 1-34. Mean maximal value, calculated on the final experiment for 111 falls is 75,0 kN with a 1,15 kN standard deviation, what corresponds to a 1,5 % variance.

For each test, three consecutive falls are applied. Note that the 111 falls considered in the previous mean value and standard deviation calculation include all falls. It will nevertheless been noticed in the following that a general subtle evolution is observed between the 3 falls of each test, in accordance with first observations (part 1).

- Precise positioning

Contrary to routine HWD surveys of flexible pavements where precise positioning of the plate is not necessary (the pavement being supposed homogeneous), accuracy of plate positioning and HWD bringing into alignment are here of the highest importance. Actually a precise positioning of the HWD plate against the gages is required. As strain deteriorates quickly away from the load, more rapidly than deflection, accuracy of 1 cm or less in the HWD positioning over the gages is targeted. With regard to this requirement, the HWD is unhitched and moved manually. A system of two vertical fixed metal bars (one in front of the

plate, the other symmetrically behind, as observed in Fig. 3-3) allows a precise positioning and alignment. Error on positioning with the previous system is evaluated at less than 5 mm.

Fig. 3-3 Assisted positioning system over gages profiles (photographs by M. Broutin)

- Acquisition rate

Mean pulse time of the HWD force signal is 32 ms, which corresponds to an apparent frequency of 31,5 Hz. Let *a priori* assume that the corresponding values for gage signals are in the same range. Considering that at least 10 measures are required to properly study the signal, the minimal acquisition rate is 315 Hz. A 3 200 Hz acquisition rate is here taken, what gives a significant security margin and allows a thorough following of time-related strain signals.

- Work at constant temperature

Main difficulty of the experiment is that temperature has a significant effect on asphalt material stiffnesses and thus on gage response. It has imposed 1- to take a maximum care in order to reduce these variations. Thus tests have been performed in the early morning, and surface has been kept wet by a continuous spraying (Fig. 3-4) and 2- to find a compromise between fineness of the test points mesh, and a limited experiment time in order to work at constant temperature.

It leads to a two-steps work: 1- rough scanning using HWD tests in order to locate with a 5 cm precision the underlying gages, and 2- final experiment for which scanning is denser close to the gages.

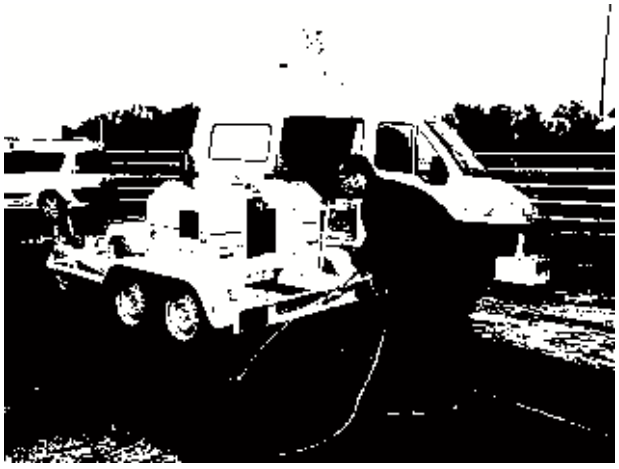

Fig. 3-4 Continuous spraying of the surface pavement during the whole tests series duration (Photograph by M. Broutin)

b - Typical result

Fig. 3-5 presents a typical result. (ε is here displayed positively in the case of traction).

Transverse tensile strain gage at bottom of AC layer unfortunately broke down during the experiment.

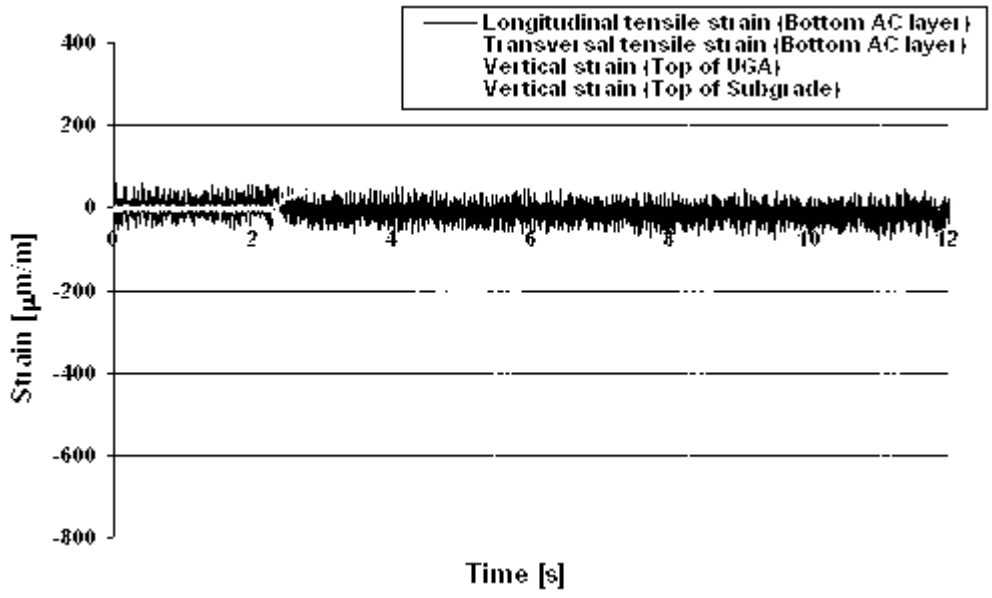

Fig. 3-5 A typical gage record during a HWD test

For a better readability, Fig. 3-6 displays the signal only of the transverse tensile strain gage at the bottom of AC layer. It allows highlighting two phenomena, also observed on other gages, and in accordance with deep anchor experiment and accelerometer measurements presented in part 1:

- a multi-rebounds phenomenon for each fall,
- a resilient creeping phenomenon, occurring as soon as the foot plate (975 kg) is positioned over the pavement.

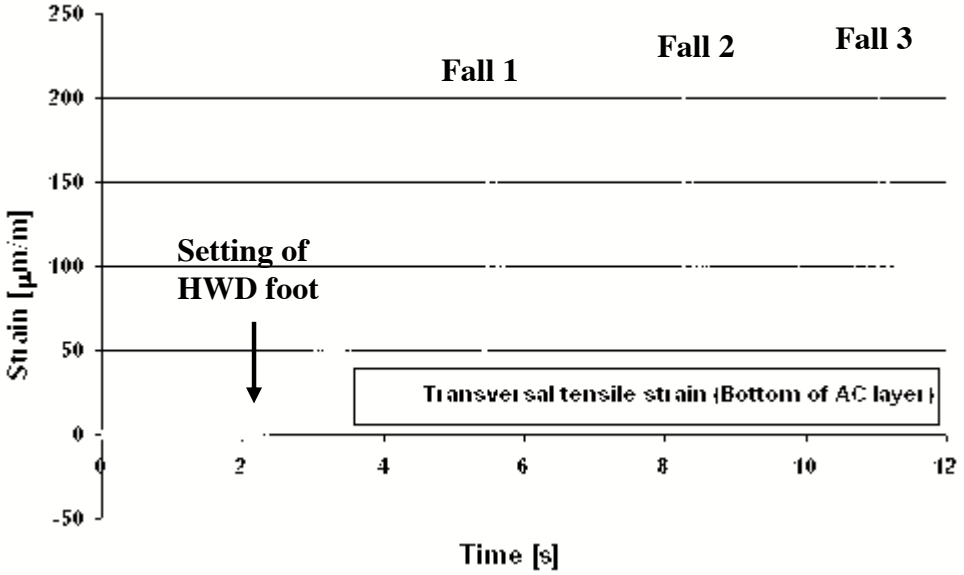

Fig. 3-6 A typical gage record during a HWD test. Longitudinal tensile strain isolated

c - Gage pre-localization

Sensors are precisely placed over the 19 m carrousel mean radius (with an accuracy better than 1 cm), which was checked thanks to a HWD transverse sweeping. On the contrary, position of the different gages on this axis is approximate. For technical reasons, all gages are not on a same vertical profile. First job was thus to pre-locate them for the aforementioned need to limit test points number.

A first rough sweeping has thus first been performed. A regular step of 10 cm was retained so that a 5 cm precision on the gages location is obtained, when limiting number of test points: a total of 19 test points have been performed, what corresponds to less than one hour tests. Temperature probes show that the latter has remained constant during the whole experiment.

Fig. 3-7 presents the evolution of the surface deflections implied by the HWD impact (i.e. only the quick dynamic deformations are considered, the low creep part of signals being left) as a function of the curvilinear abscissa.

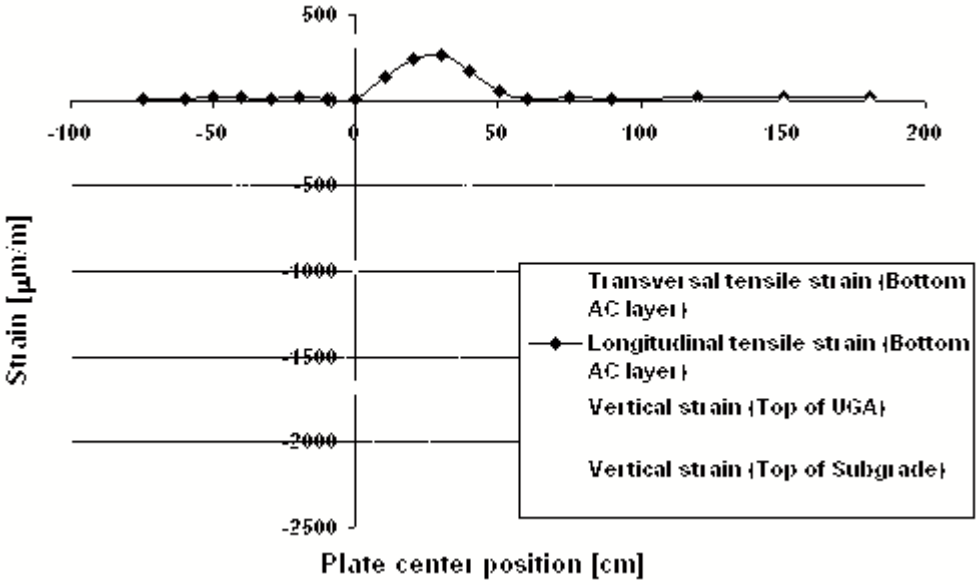

Fig. 3-7 Influence line of the HWD plate positioning on the different gages. Rough test point mesh

This first sweeping allows approximately locating each embedded gage since maximal strain is obtained when HWD plate is positioned over it. Observed basins are symmetrical about the maximal values. Table 3-3 collects the corresponding abscissas where the latter are obtained. For readability of Table 3-3, respective longitudinal and transverse tensile strains at bottom of AC layer are denoted ε_LAC and ε_TAC, and vertical strains at top of UGA and subgrade ε_Z UGA and ε_Z S. The zero value was a priori arbitrarily stated, so as to correspond to the subgrade gage position.

Gage	ε_L AC	ε_T AC	ε_Z UGA	ε_Z S
Abscissa [cm]	28	-8	-17	0

Table 3-3 Approximate position of gages

1.4.2 Final experiment

a - Refined gage pre-localization

- Final optimized mesh

It has been taken advantage of the previous preliminary study to elaborate an optimal mesh for tests. Offset between test points is of:

- 2 cm around each tensile strain gage,
- 5 cm for the vertical strains which are deeper, and consecutively less sensitive to placement,
- 10 cm in the close vicinity (< 1 m) of the test area,
- 30 cm beyond 1 m.

It has been decided, not to duplicate test points, as the signal symmetry has been evidenced in the previous study (Fig. 3-7).

The mesh contains a total of 37 points. The whole experiment lasted 1h05, between 6.30 a.m. and 7.35 a.m. Fig. 3-8 shows that temperature can be considered as constant during this time period.

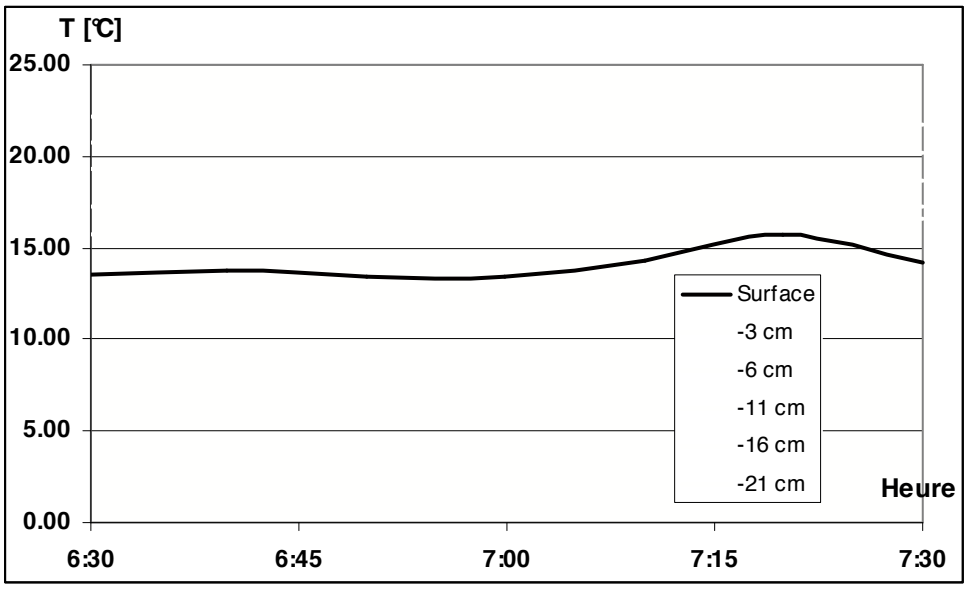

Fig. 3-8 Temperature in asphalt layers during the final experiment

- Raw results

Fig. 3-9 presents results obtained, for each test point, when calculating a mean value on the 3 test falls. For convenience, all signals have been counted as positive. Curvilinear abscissas have been adjusted.

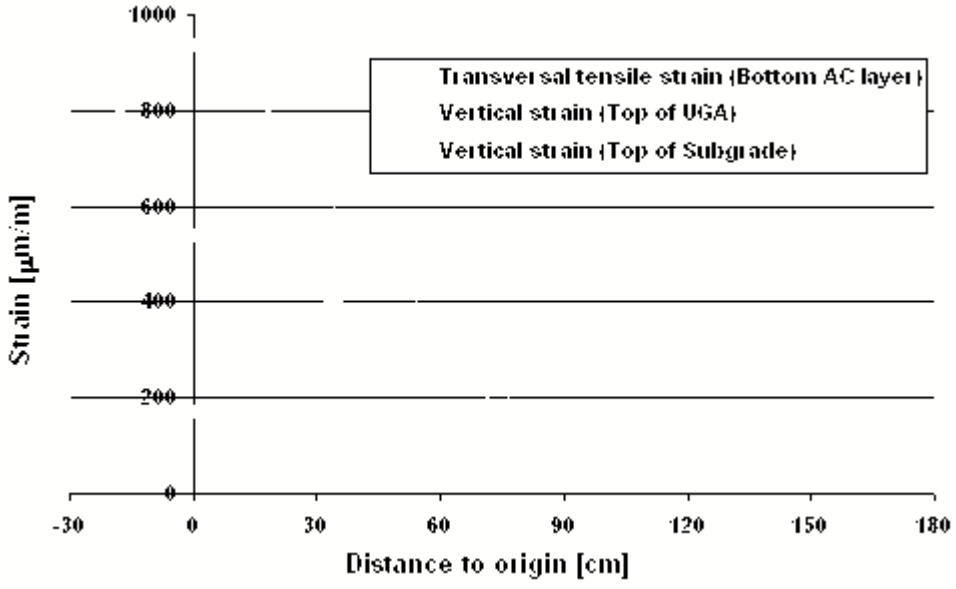

Fig. 3-9 Influence line of the load point on the different gages; fine mesh

b - Repeatability of tests

Standard deviation between the three falls is 2,2 % for transverse tensile strain (Bottom of AC layer), 2 % for vertical strain at top of UGA, and 1 % for vertical strain at top of subgrade. The aforementioned systematic slight evolution is highlighted by considering normalized strains with regard to the three falls.

$\frac{\varepsilon_i}{\sum_{i=1}^{3}\varepsilon_i}$ where ε_i is strain measured on the i^{th} fall.

Mean values on the 37 tests are considered. Results are provided in Table 3-4.

	Fall 1	Fall 2	Fall 3
Transverse tensile strain (Bottom of AC layer)	1,02	1	0,98
Vertical strain (Top of UGA)	1,03	1	0,97
Vertical strain (Top of Subgrade)	1,01	1	0,99

Table 3-4 Evolution of ε with regard to the considered fall

c - Time-related strains

Fig. 3-10 presents time-related strains recorded by each gage when the HWD plate is placed over it, i.e. time-related signals presenting, amongst all HWD plate locations, the maximal amplitude, have been extracted for each gage, and superimposed. Time has been adjusted manually as signals come from different HWD tests.

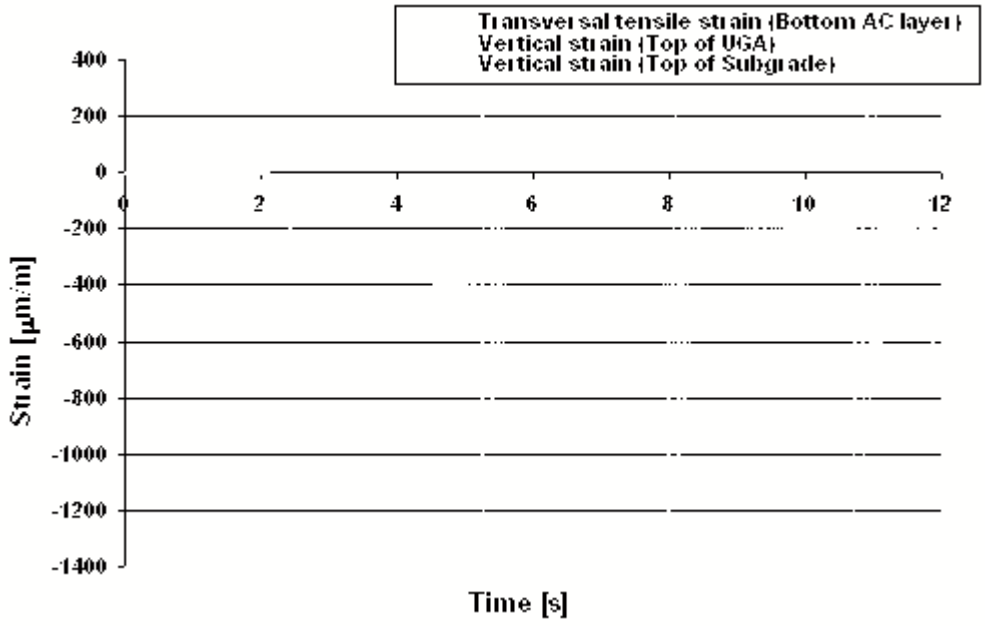

Fig. 3-10 Field time-related strains in the pavement during a HWD test sequence (1/3)

Fig. 3-11 presents the same results, when focusing on the first HWD fall.

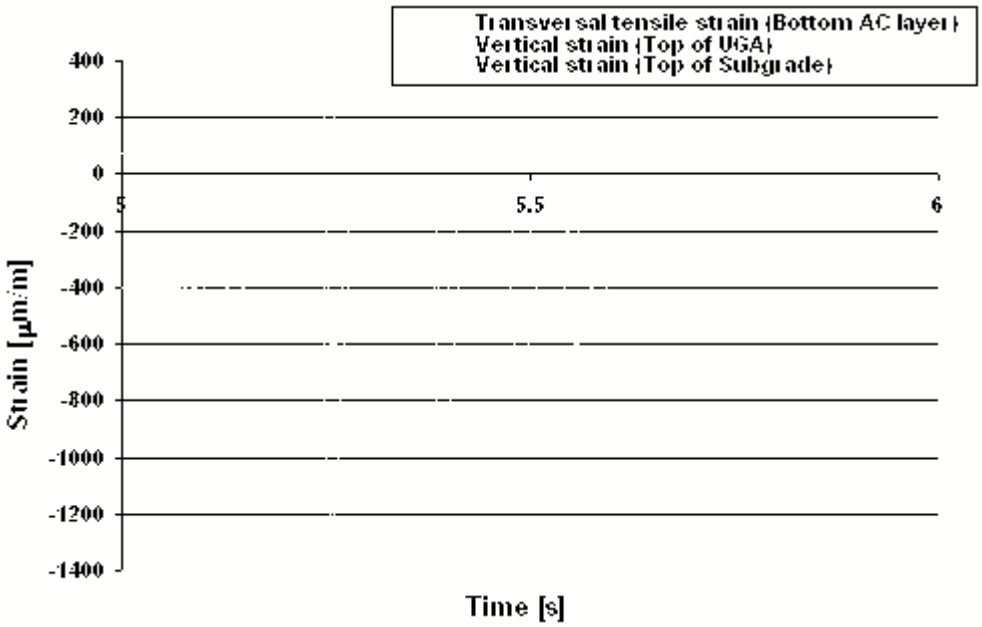

Fig. 3-11 Field time-related strains in the pavement during a HWD test sequence (2/3)

By considering only the short-term elastic response, i.e. adjusting the beginning of signals to the zero value, and focusing on the 0-60 ms time frame, Fig 3-12 is obtained.

Note that time has been manually adjusted, since the HWD acquisition system (providing the force signal) and spider (recording gage signals) are not synchronised, and gage measurements are in any case extracted from different tests.

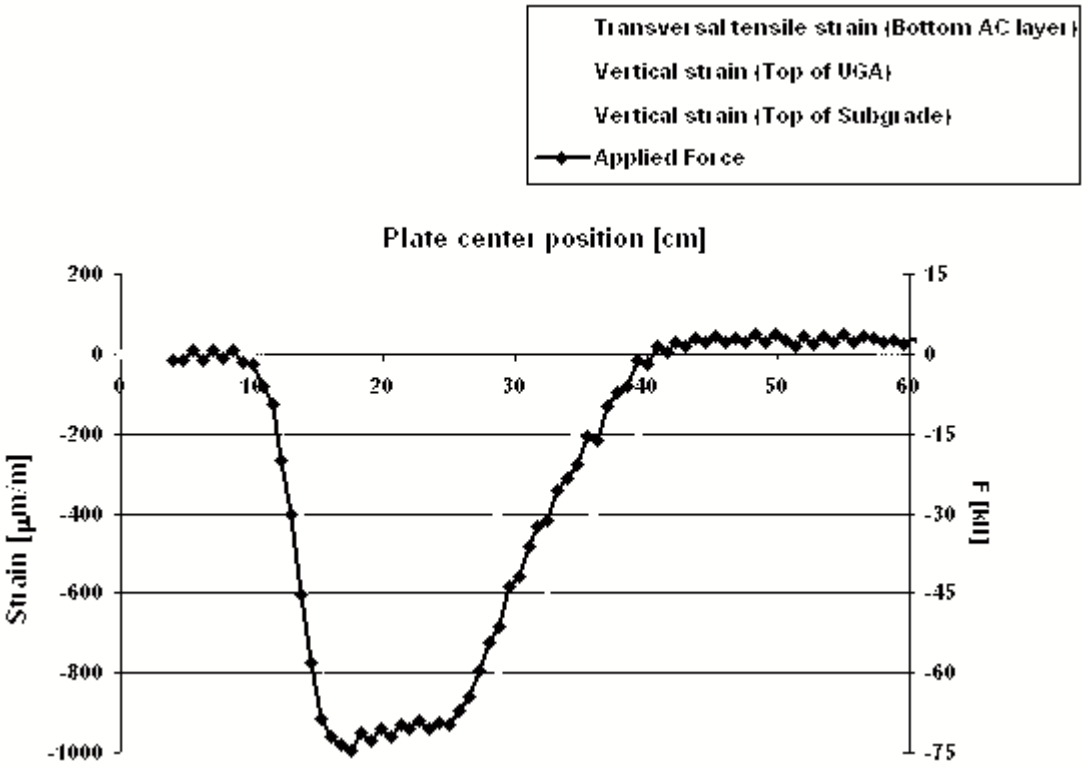

Fig. 3-12 Field time-related strains in the pavement during a HWD test sequence (3/3)

These time-related strain values will be used in the following section, in the context of the validation of dynamic backcalculation results.

2 - Validation of the pavement assessment method

First the depth to bedrock determination methods have been tested. Then, the backcalculation procedure has been assessed.

2.1 Assessment of the depth to bedrock determination methods

This paragraph is dedicated to depth to bedrock assessment. Both cases of infinite subgrade and shallow bedrock are studied, using respectively the S_3 and S_2 structures. Deflection values retained are respectively for S_2 the deflections of the final study of gauges profiles presented hereafter, and for S_3 the mean deflections from the repeatability study.
First, surface moduli are analysed. Actually the latter are intended to provide a valuable qualitative indication about occurrence of bedrock. Then the pseudo-static Irwin method and the Mera's dynamical one (both presented in the literature review dedicated part) are tested.

2.1.1 Surface (apparent) moduli

a - Half-space

Fig. 3-13 presents the apparent modulus vs distance to load centre. An horizontal asymptote is observed, which well reflects the response of a pavement lying on an infinite subgrade.

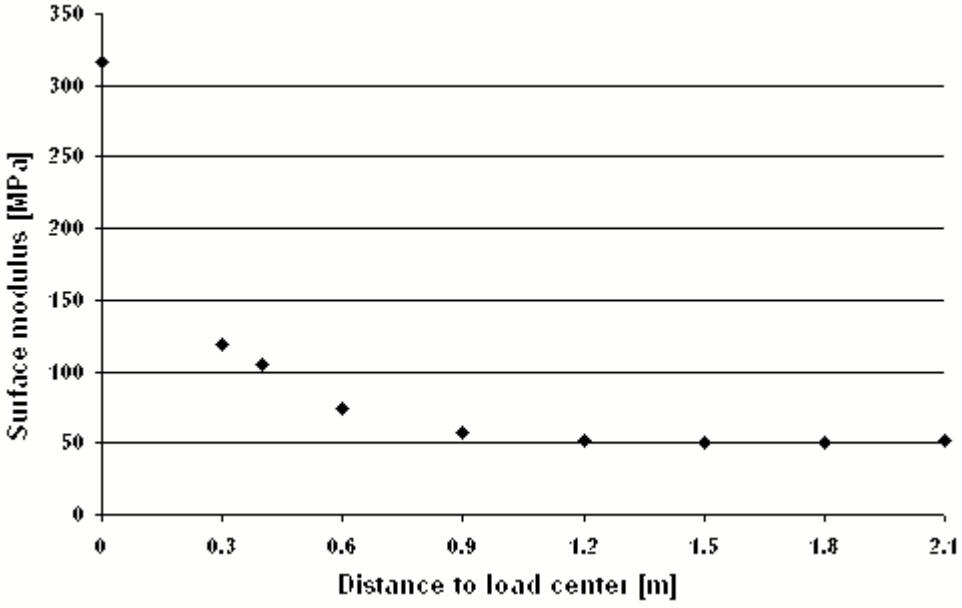

Fig. 3-13 Apparent moduli; S_3 structure

b - Shallow bedrock

In this case, apparent modulus reaches a minimum before increasing with distance to load centre for outer geophones. Once more, this response is in accordance with theoretical expectations.

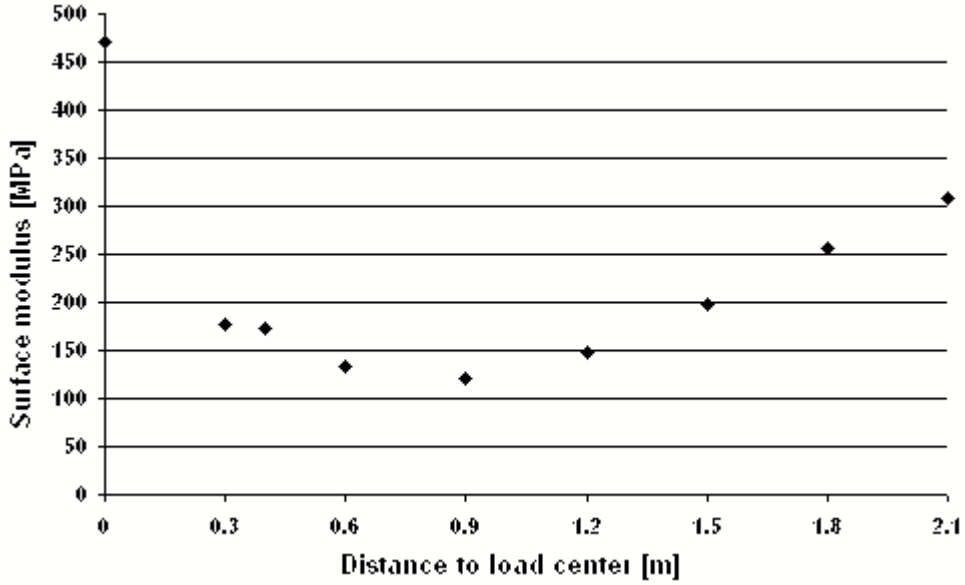

Fig. 3-14 Apparent moduli; S_2 structure

2.1.2 Pseudo-static method

a - Half-space

Fig. 3-15 displays deflection vs a/r where a is the plate radius and r the distance to load centre. According to the Irwin method the regression line obtained from outer geophones values intersects the abscissa's axis at the a/d_b value, where d_b is the depth to bedrock.
Here two cases are compared: the regression considering geophones G_6 to G_8 and G_7 to G_9. In the first case intersection is negative and in the second one the obtained d_b value is 36 m. Both cases are consistent with an infinite subgrade.

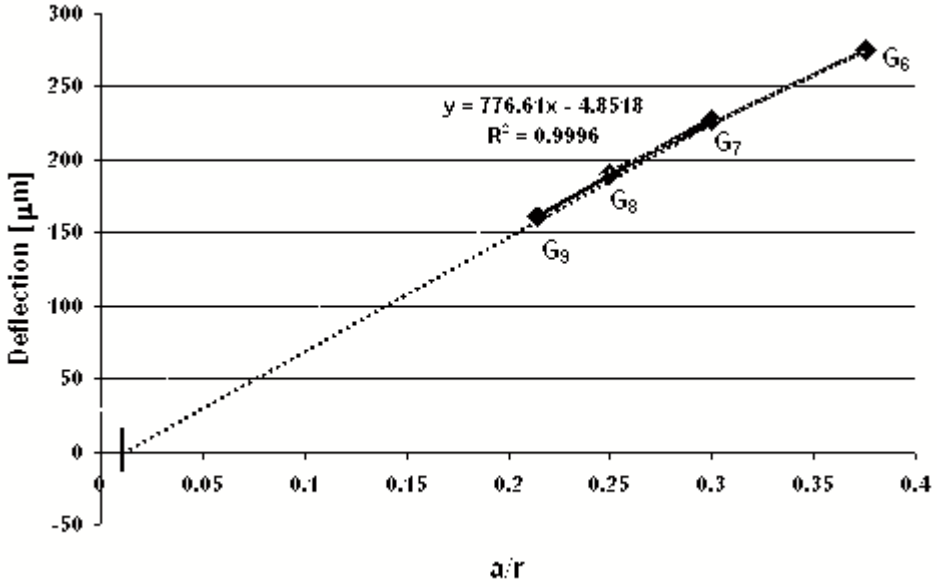

Fig. 3-15 Irwin pseudo-static depth to bedrock determination; S_3 structure

b - Shallow bedrock

The same work is performed on the S_2 structure. Geophones 6 to 8 are considered, as geophone 9 seems to be anomalous. This time d_b = 1,5 m, against 3 m in reality.

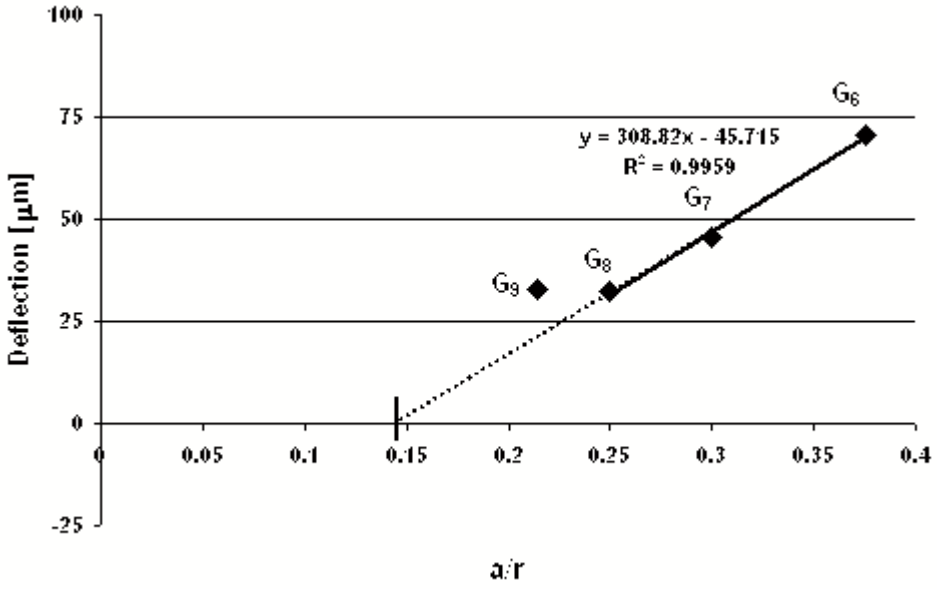

Fig. 3-16 Irwin pseudo-static depth to bedrock determination; S_2 structure

2.1.3 Dynamic resonant frequency-based method

Mera's dynamical method to determine depth to bedrock using structure resonant frequency (see literature review) is here tested. It is split in two phases. First, the resonant frequency of the pavement is determined. Then, an algorithm allows determining both depth to bedrock, and subgrade modulus.

a - Shallow bedrock

- **Determination of the resonant frequency of pavement**

Fig. 3-17 presents a FRF (frequency response function) performed on the outer geophone. Signal presents a main peak at 22 Hz which is the resonant frequency. A second peak appears around 40 Hz, maybe due to the double peak on HWD force signal.

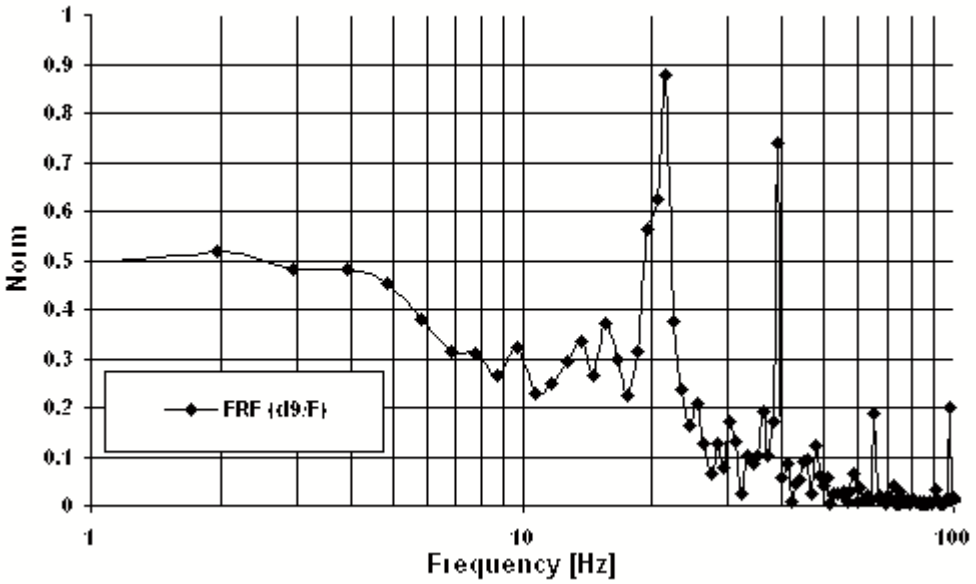

Fig. 3-17 Determination of the resonant frequency of pavement; S_2 structure

- **Test of the algorithm**

Initial subgrade modulus (from static backcalculation in infinite space) is 350 MPa, when considering for surface layer moduli E_{AC1} = 4 700 MPa, E_{AC2} = 9 500 MPa and E_{UGA} = 500 MPa. This manner of imposing surface moduli has little influence on the results, as demonstrated in part 2.

According to Fig. 3-17 resonant frequency taken into account is 22 Hz.

Procedure described by Mera is then performed on geophone 9. It appears (see Fig. 3-18) that the algorithm converges very fast (from 6th iteration).

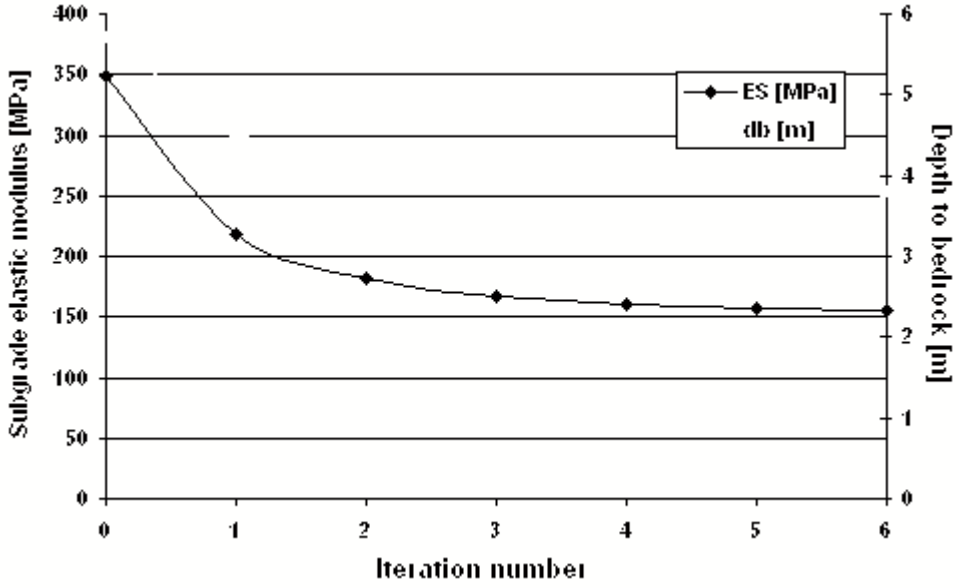

Fig. 3-18 Evolution of depth to bedrock (d_b) and subgrade modulus (E_S) during the Mera's algorithm of depth to bedrock determination

Final values are d_b = 3,80 m and $E_{Subgrade}$ = 154 MPa

Calculation provided in part 2 assessed a 0,40 m uncertainty value on the result. The error made on the d_b value is here 0,80 m (3,80 m instead of 3 m). Uncertainty on f, chosen as 1 Hz with regard to results scatter, is maybe underestimated, due to measurements imprecision and, above all, time frame (120 ms) maybe too short to expect frequency-domain analyses to give sufficient accuracy.

Note that the obtained value is nevertheless much better than the one calculated using the Irwin pseudo-static method (1,5 m).

b - Half-space

The same procedure is performed on the S_3 structure. Obtained FRF is displayed in Fig. 3-19. Resonant frequency is 4,5 Hz. Algorithm provides the respective values of 11 m and 62 MPa for d and $E_{subgrade}$ which is good assessment of both parameters, according to performed geotechnical survey conclusions (see appendix 1.1).

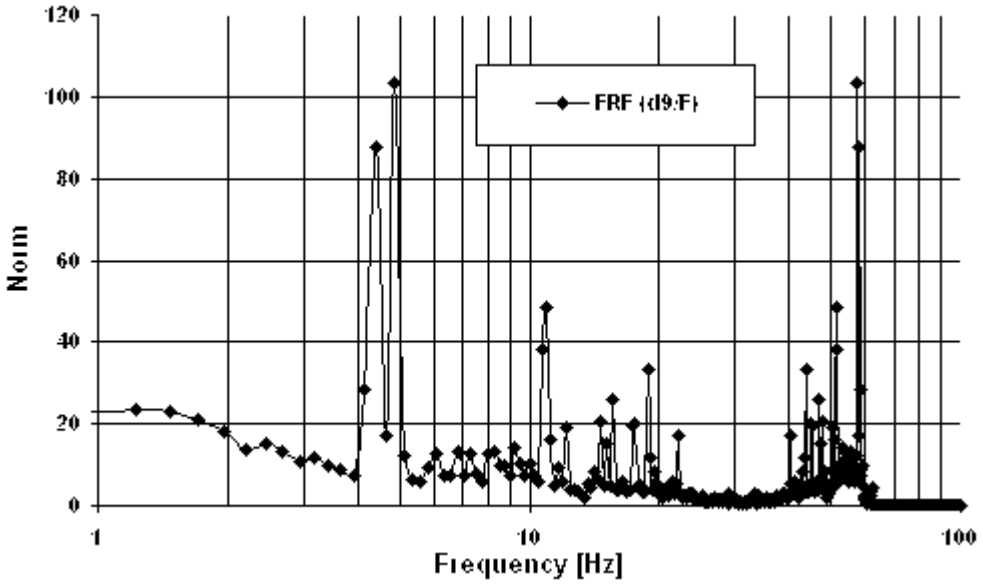

Fig. 3-19 Determination of the resonant frequency of pavement; S_3 structure

Partial conclusion

This paragraph has allowed highlighting that surface moduli are a valuable indicator of shallow bedrock presence. Then, the Irwin's pseudo-static and the Mera's dynamic methods have been assessed. As suspected, the first one is rather inaccurate. The second one provides an approximate value of depth to bedrock.

2.2 Validation of the backcalculation procedure

2.2.1 Backcalculation results

- S1 structure

Thus, four modellings are here tested: the pseudo-static method, the dynamical M_1 model, the dynamical M_2 model, and the shock theory-based M_3 model.

The pseudo-static and M_1 dynamic fitting have been performed using the semi-empirical method presented in part 2, based on sensitivity results, since no automated tool existed at that time when analysis was performed.

Before performing any backcalculation using the M_2 model, the consistency of the latter is to be assessed, when checking that the force signal obtained with the modelling corresponds to the experimental one.

In the case of the shock theory, a second set of moduli is to be backcalculated: the shock law moduli. In practice, elastic moduli found in the frame of the M_1 model are retained for the second step of calculation. The shock moduli are taken equal for all materials.

In both M_1 and M_3 dynamical cases, a 5% damping is assumed.

a - M_1 model

Fig. 3-20 and Fig. 3-21 display fitting results for the M_1 model. For sake of readability, Fig. 3-20 displays signals related to only 3 geophones: geophone 1 (located at the centre of the load plate), geophone 5 (at 90 cm offset) and geophone 9 (at 210 cm offset). The excellent quality of the fitting here observed is comparable for the other geophones. Fig. 3-21 represents theoretical versus experimental deflection for geophone 1. Only the rising part of the signal in the neighbourhood of the maximum (blue stippled frame in Fig. 3-20) has been taken into account. In the case of a perfect correlation, correlation coefficient R^2 and slope a of the regression straight line should be both equal to 1. The values found for geophone 1 are respectively 0,9994 and 1,0068. The curves corresponding to the other eight geophones are comparable. Mean values calculated on the 9 geophones are respectively 1,011 and 0,996 for a and R^2.

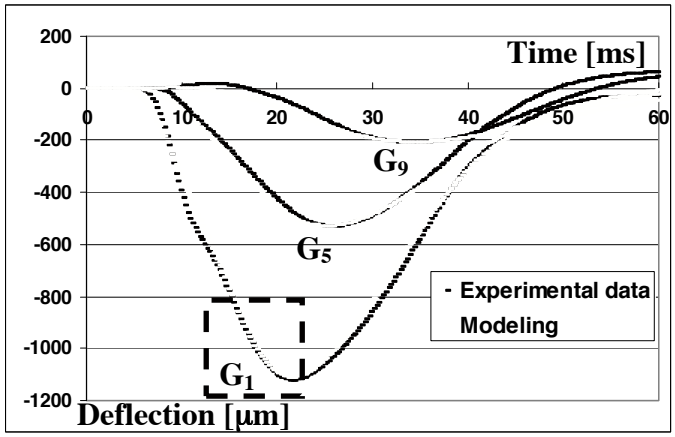

Fig. 3-20 Comparison between experimental and numerical values (M_1 dynamic modelling)

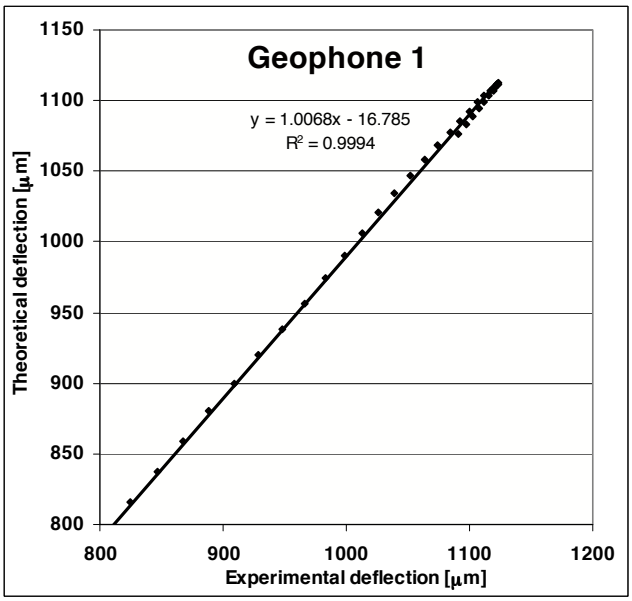

Fig. 3-21 Correlation between theoretical and experimental deflections on the first geophone (M_1 modelling)

b - M_2 model

H_0 = 400 mm. This correspond to a 2,8 $m.s^{-1}$ initial mass velocity. Fig. 3-22 displays the force signal induced by this external action, in both cases of a rigid and deformable pavement. The modulus selected for the deformable pavement correspond to the previously backcalculated ones from M_1 modelling. No damping is considered, since only damping is available so far (what would introduce significant damping in the buffer and falling mass). It appears that the two signals are similar. This confirms the conclusions of the approximate calculations of part 1 (§ 1.3.2) i.e. the pavement deformation has little influence on the force level, and it does not allow explaining the double peak. On the contrary, the force signal is mainly governed by the buffer system (force signal at the first order proportional to the buffer modulus).

It also appears that the pulse time is in a narrow range of the experimental one (23 ms against 25,5).

Fig. 3-23 shows the corresponding deflections. They are higher than the experimental ones. This can be due to the absence of damping with regard to the M_1 modelling.

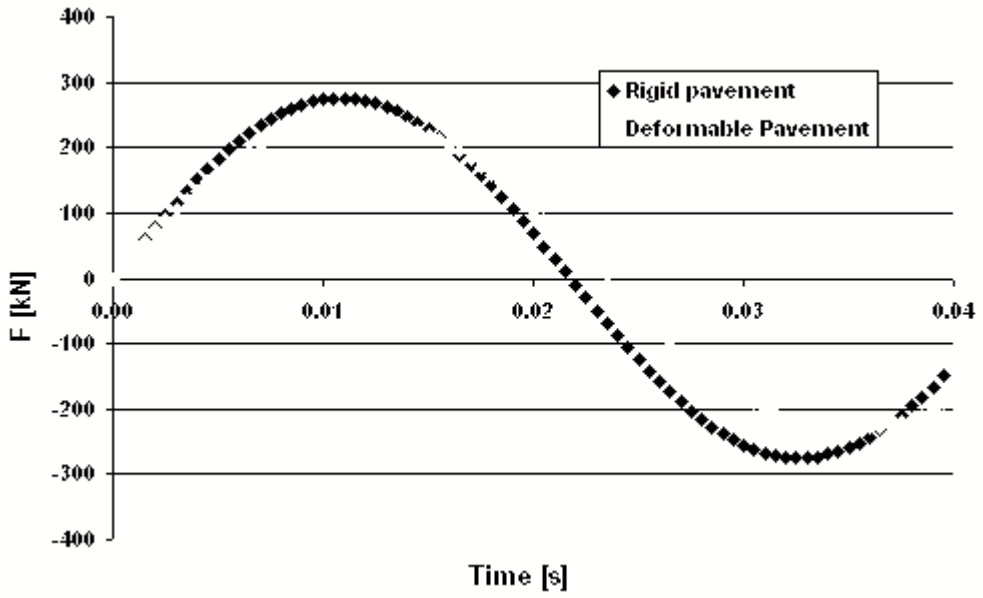

Fig. 3-22 Theoretical force signals; M_2 modelling; S_1 structure

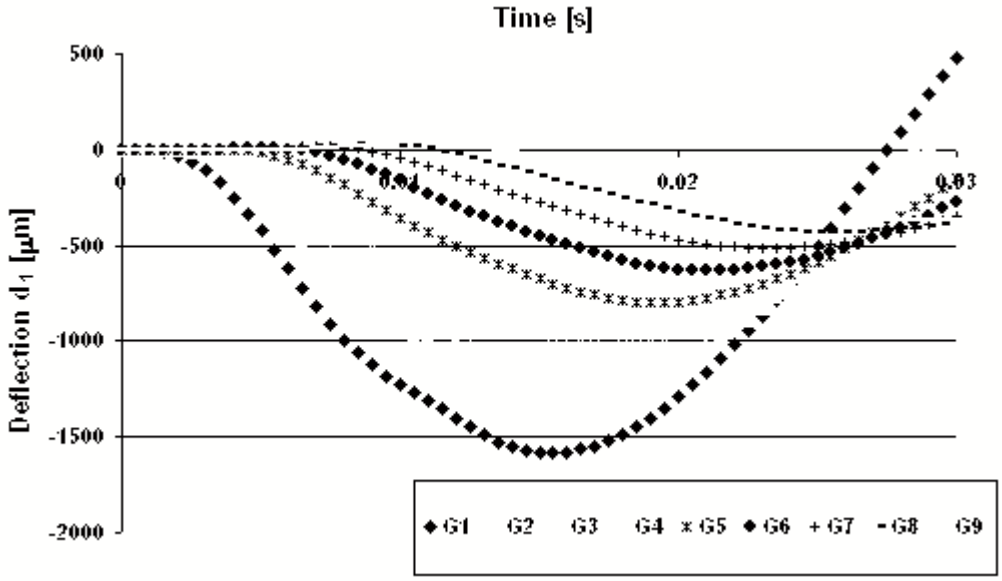

Fig. 3-23 Theoretical deflections; M_2 model; S_1 structure

The M_2 alternative version of the dynamic model was not made operational in time to perform any backcalculation. Nevertheless the double peak (which is an epiphenomenon) is not observed when calculating the force signal. It implies that the HWD foot is more complex to model that planned.

c – M_3 modelling

Fig. 3-24 to 3-27 refer to the backcalculation performed using M_3 model.

Fig. 3-24 exhibits the velocity field in the pavement obtained from the first step of the calculation i.e. velocity field after the shock.

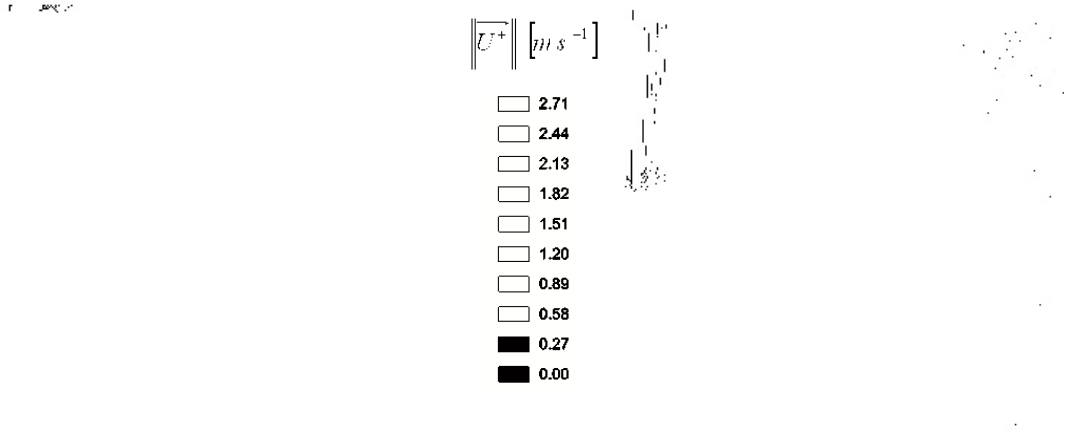

Fig. 3-24 Velocity field $\overrightarrow{U^+}$ obtained after the shock

Fig. 3-25 provides deflections obtained when this initial velocity field is applied to the pavement. Time increment is 0,25 ms.

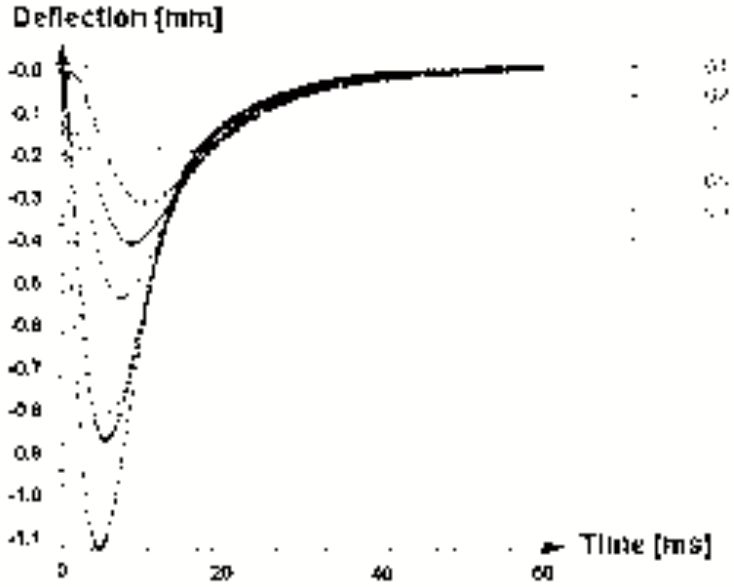

Fig. 3-25 Time-related deflections from M_1 modelling

Fig. 3-26 and Fig. 3-27 represent the quality of the fitting, in terms of deflection peak value and propagation time. Note that, as the shock is assumed to be instantaneous, time origin is taken when force signal is maximal.

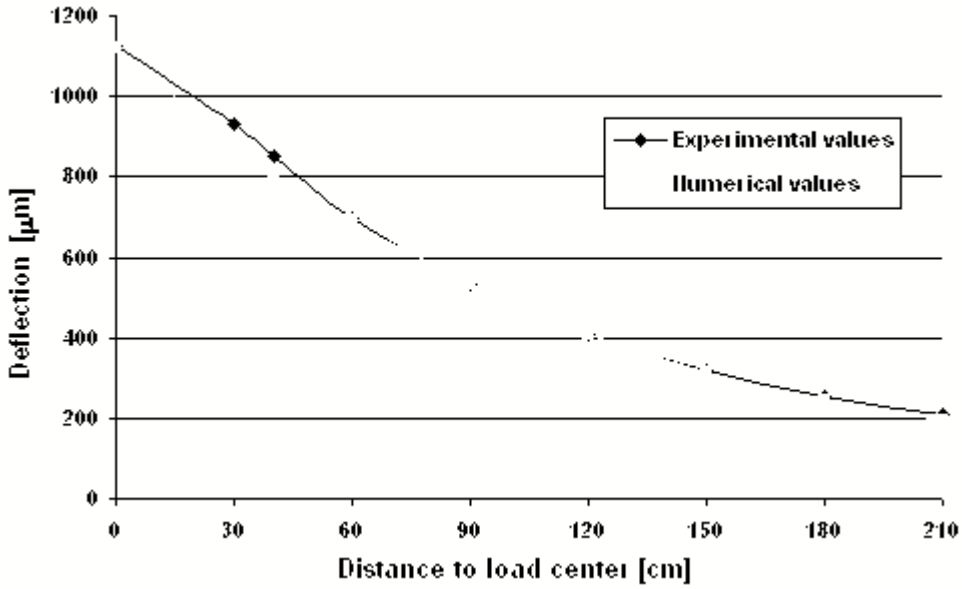

Fig. 3-26 Peak deflection matching; shock theory modelling; S_1 structure

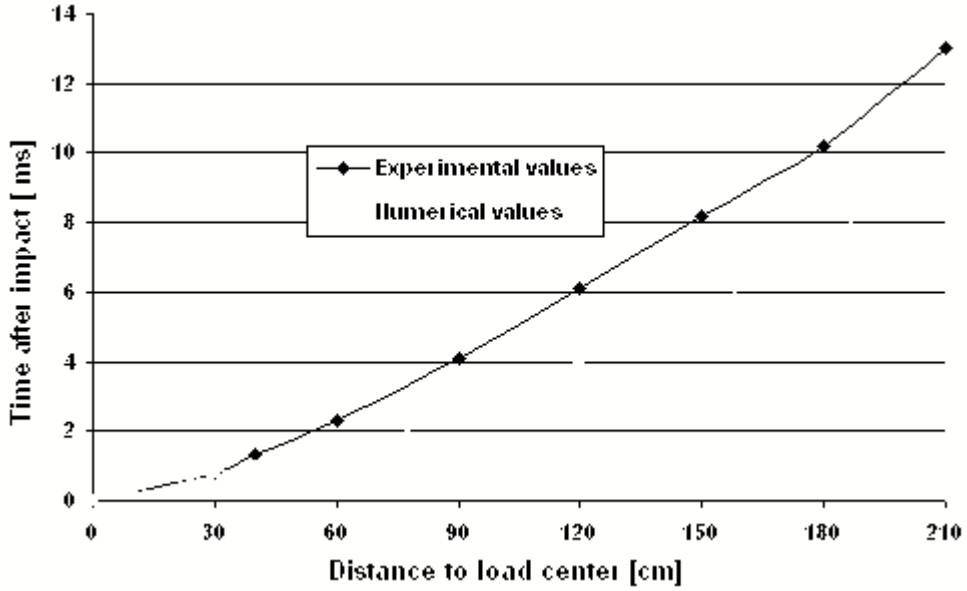

Fig. 3-27 Peak deflections temporal abscissas matching; shock theory modelling; S_1 structure

Maximal deflections match very well. Fitting is poorer for temporal abscissas. The observed differences could be explained by an underestimation of the damping ratio.

Table 3-5 summarizes all field and numerical deflections relative to the S_1 structure.

	d_1	d_2	d_3	d_4	d_5	d_6	d_7	d_8	d_9
Field data	1123	929	850	699	531	408	320	253	209
Pseudo-static method	1017	902	833	697	531	409	320	255	207
M_1 dynamic modelling	1013	908	840	703	534	412	325	263	218
M_3 dynamic modelling	1122	870	807	690	532	406	312	243	194

Table 3-5 Field and numerical deflections; S_1 structure

Table 3-6 collects the corresponding elastic moduli backcalculated using the three considered methods, as well as the common backcalculated value of the shock parameters.

	AC_1	AC_2	UGA_1	UGA_2	S	Buffer
Pseudo-static method elastic moduli [MPa]	4700	9000	580	290	120	
M_1 and M_3 dynamic methods elastic moduli [MPa]	4000	7500	510	240	77	
Shock law parameters [$kg.m^{-1}$]	2.10^{18}	2.10^{18}	2.10^{18}	2.10^{18}	2.10^{18}	2.10^{18}

Table 3-6 Backcalculated parameters; pseudo-static, and M_1 and M_3 dynamic methods

- S_2 structure

A test is arbitrary chosen from the "final experiment" on the tested gage profile (see supra), a very good repeatability being observed between all test points.

Three backcalculations are performed: a pseudo-static one, and two dynamic ones (M_1 model), respectively without and with damping. The PREDIWARE software is used.

The seed moduli are 4 700, 9 000, 200 and 150 MPa respectively for AC_1, AC_2, UGA and S, and the damping ratio 5% in the third backcalculation.

For dynamic backcalculations, the time frame retained for the fitting is 7 ms - 35 ms.

The 6 following figures (Fig. 3-28 to 3-33) display the obtained fittings, as well as the evolution of moduli (E(N) being the modulus of the considered layer at N^{th} step) and MSE error during the during the iterative process.

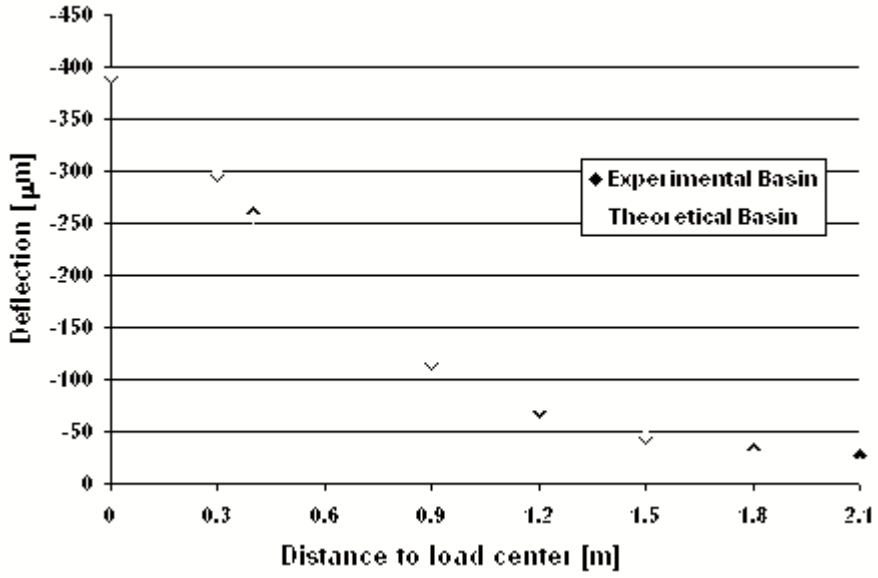

Fig. 3-28 Pseudo-static fitting, S_2 structure

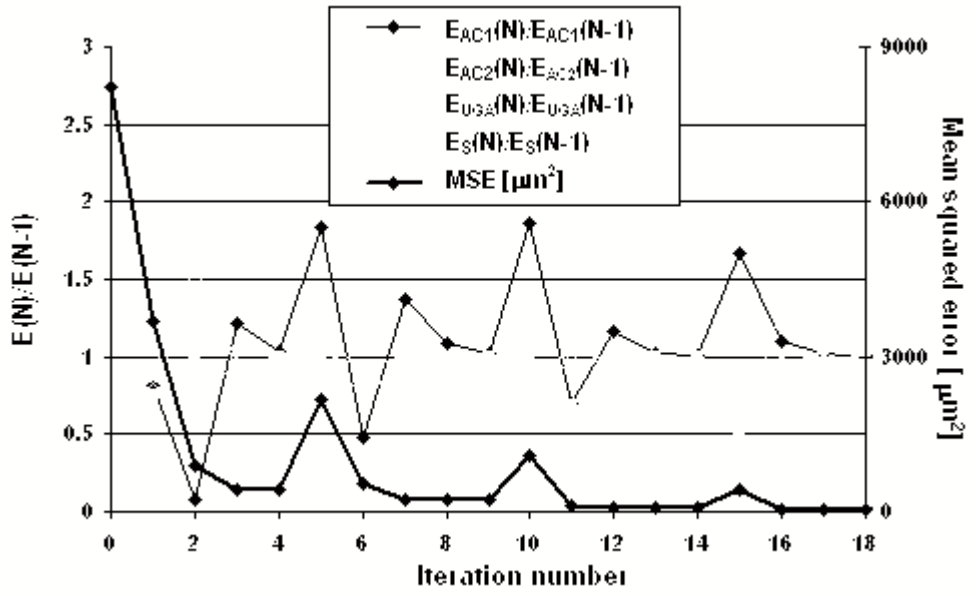

Fig. 3-29 Convergence in the pseudo-static case, S_2 structure

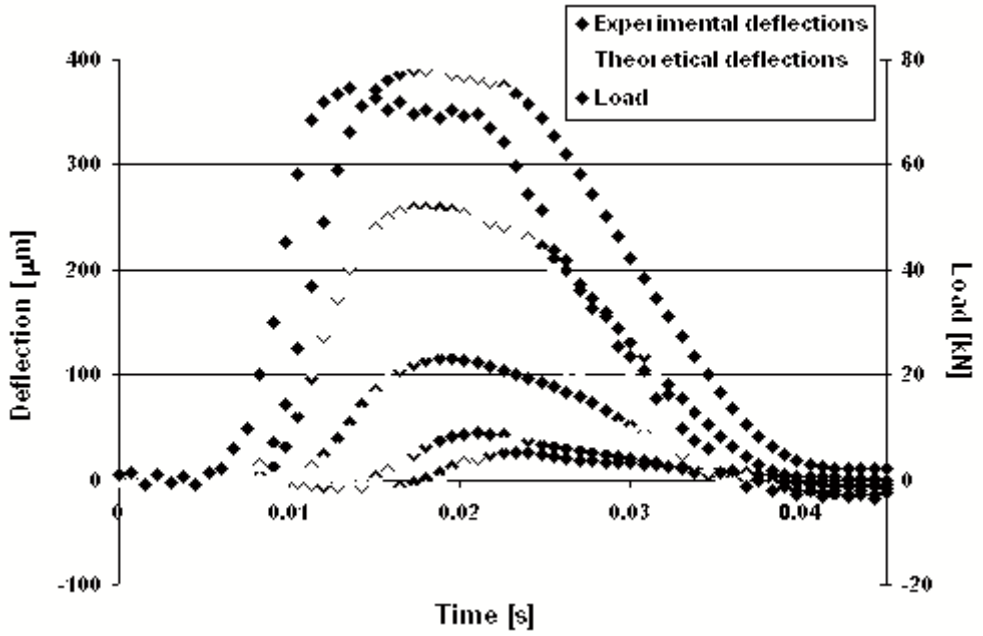

Fig. 3-30 Dynamic fitting without damping, S_2 structure

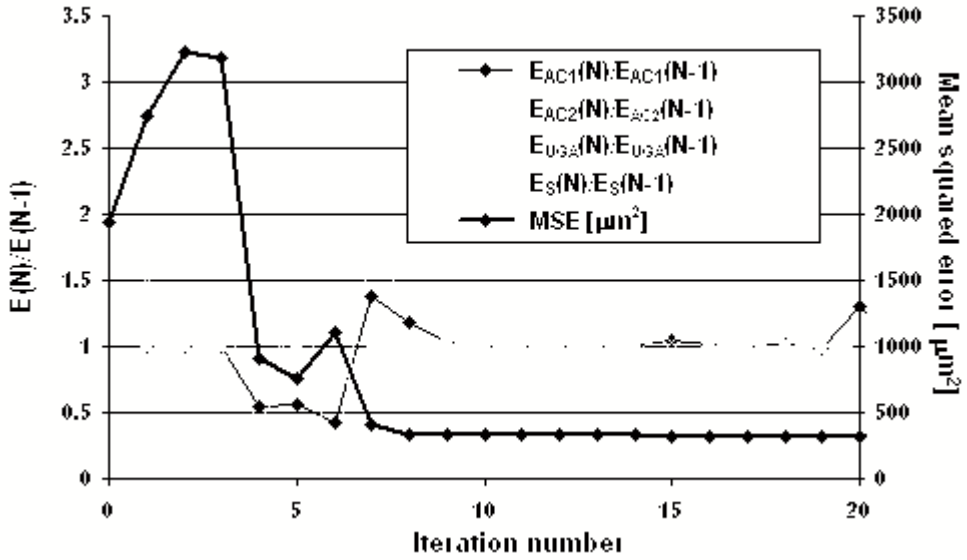

Fig. 3-31 Convergence in the dynamic case without damping, S_2 structure

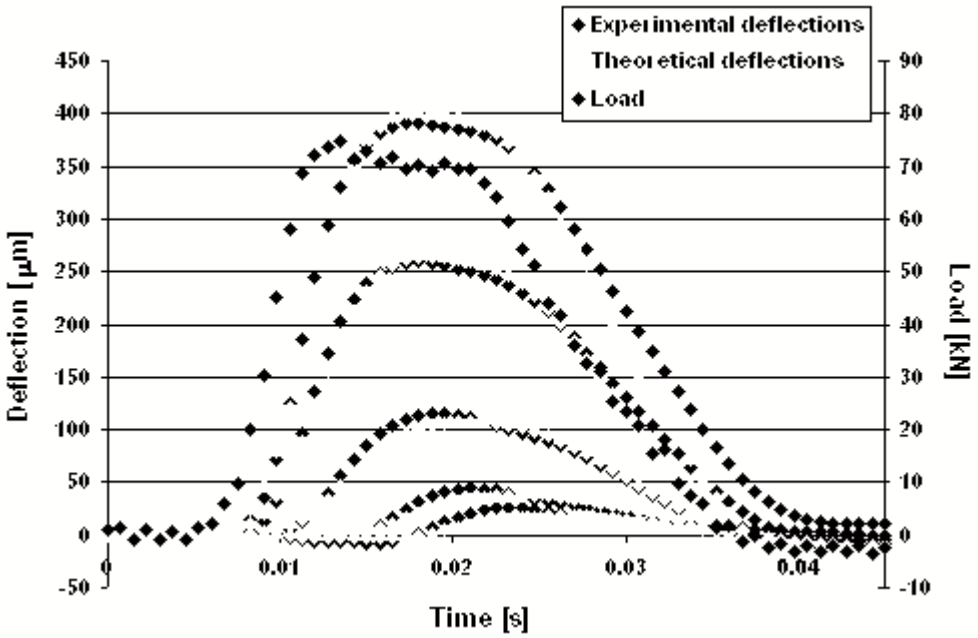

Fig. 3-32 Dynamic fitting with damping, S_2 structure

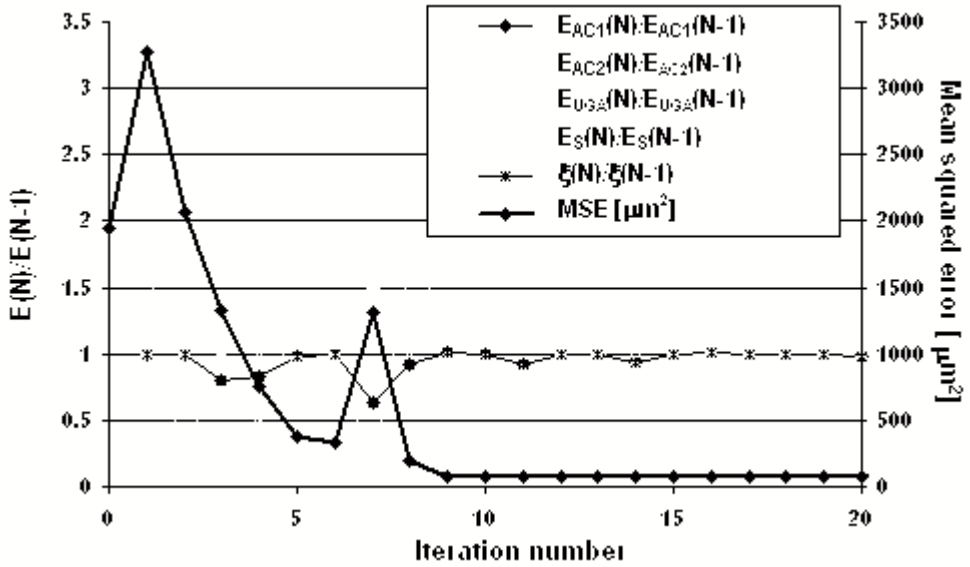

Fig. 3-33 Convergence in the dynamic case with damping, S_2 structure

Obtained fittings are very good in all cases. It also appears that MSE error seems to be stabilized at the end of the process.

Table 3-7 provides the backcalculated elastic moduli for the three backcalculations, as well as the backcalculated ξ damping ratio in the case of the last backcalculation.

	AC_1	AC_2	UGA	S	ξ
Pseudo-static method	1784	1735	161	145	
M_1 dynamic modelling without damping	1230	1709	170	191	
M_1 dynamic modelling with damping	1227	2562	55	276	24.7 %

Table 3-7 Pseudo-static, and dynamic with and without damping backcalculated elastic moduli and damping ratio, S_2 structure

- S3 structure test facility

The Pl_1 test point (see appendix 1.1 for corresponding layer thicknesses) is chosen. Once more, the PREDIWARE software is used to perform a pseudo-static one, and M1 with and without damping dynamic backcalculations.

The seed moduli are 4 700, 9 000, 200, 150 and 120 MPa respectively for AC_1, AC_2, UGA, G and S, and the damping ratio 5 % in the third backcalculation.

Time frame is still 7 ms - 35 ms for dynamic fittings.

Fig. 3-34 to 3-39 display results relative to the three methods.

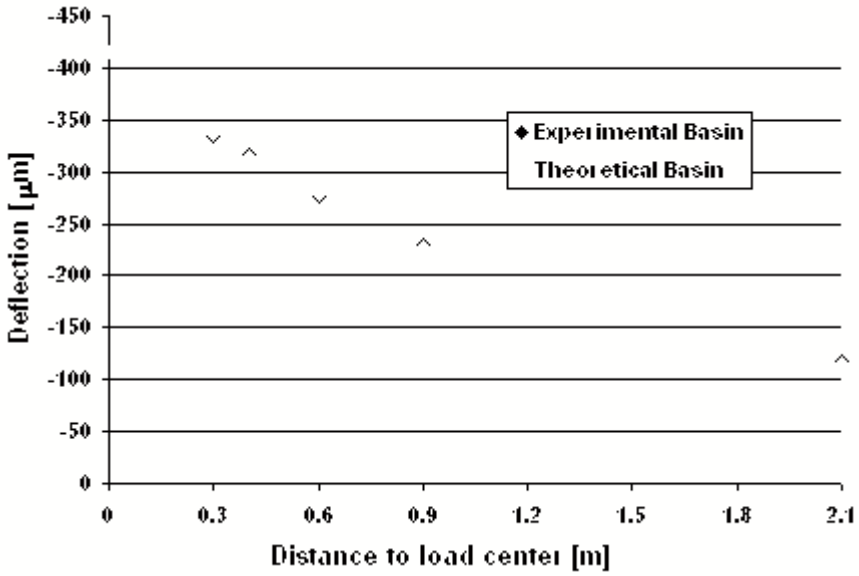

Fig. 3-34 Pseudo-static fitting, S_3 structure, Pl_1 test point

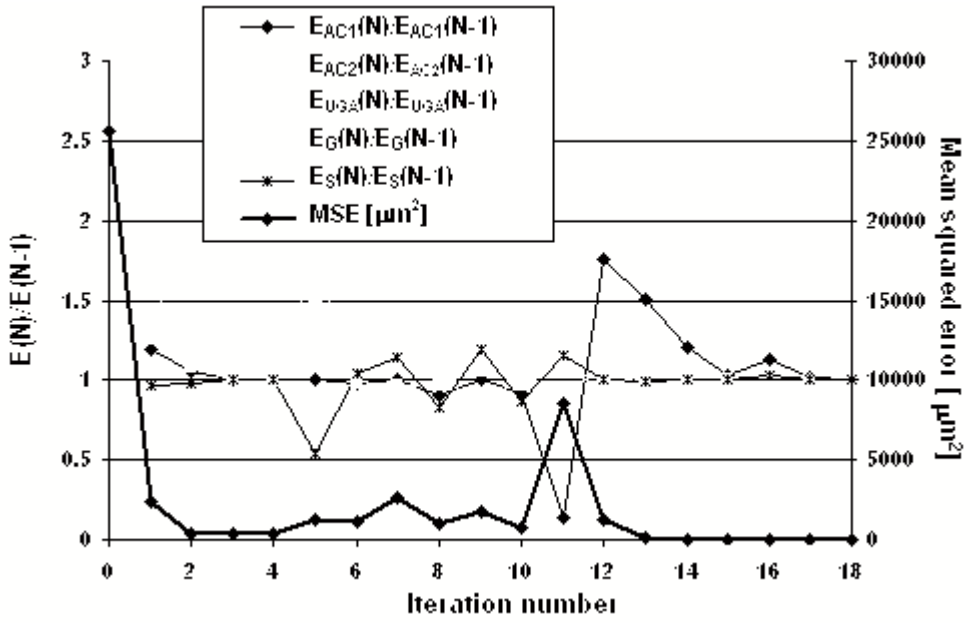

Fig. 3-35 Convergence in the pseudo-static case, S_3 structure, Pl_1 test point

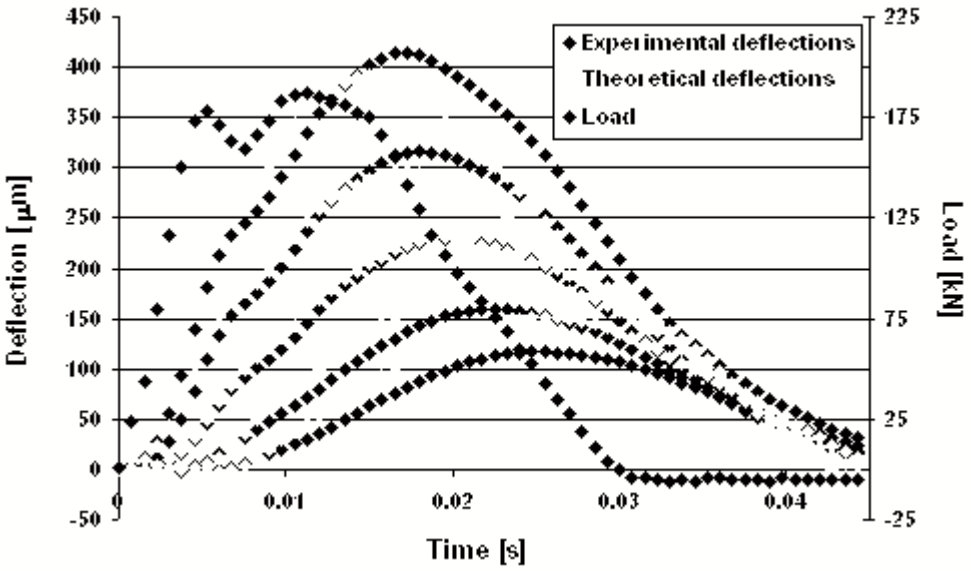

Fig. 3-36 Dynamic fitting without damping, S_3 structure, Pl_1 test point

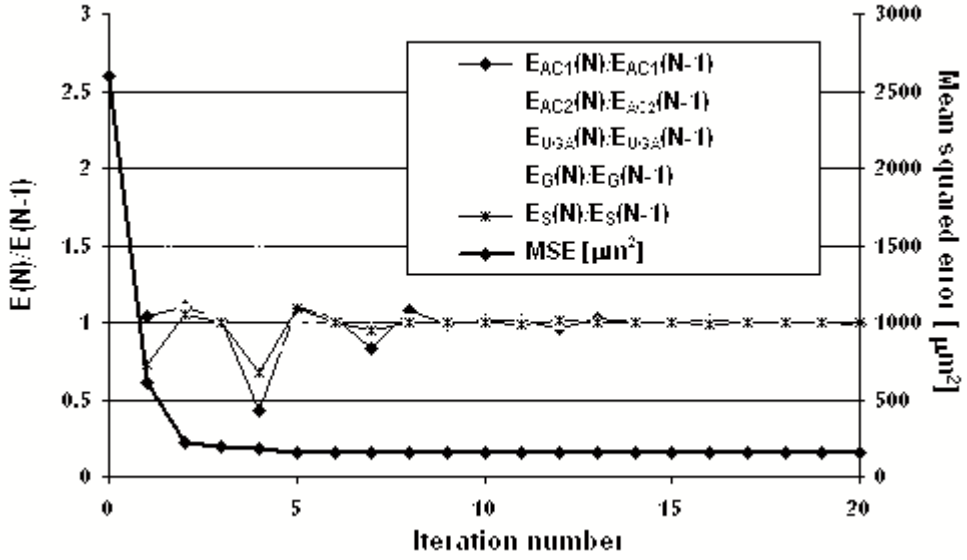

Fig. 3-37 Convergence in the dynamic case without damping, S_3 structure, Pl_1 test point

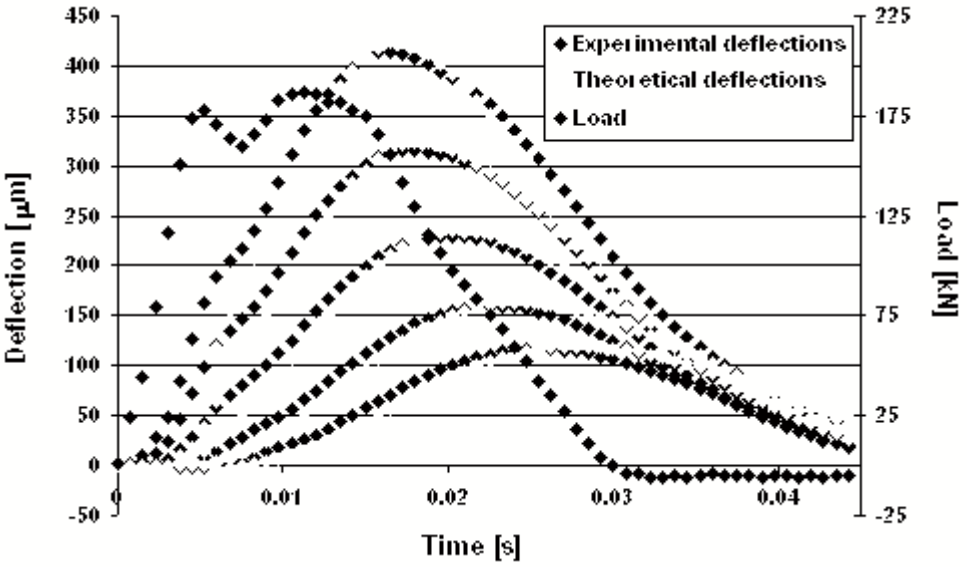

Fig. 3-38 Dynamic fitting with damping, S_3 structure, Pl_1 test point

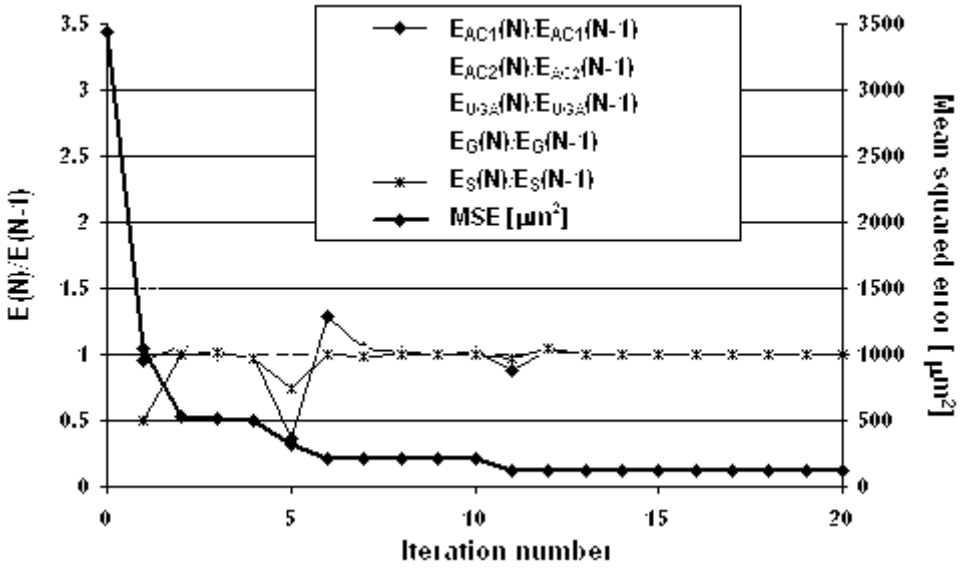

Fig. 3-39 Convergence in the dynamic case with damping, S_3 structure, Pl_1 test point

Once more, fittings are very good.

Table 3-8 summarizes backcalculation results.

	AC_1	AC_2	UG_A	G	S	ξ
Pseudo-static method	2691	15447	507	538	76	
Dynamic without damping	2471	9337	704	560	66	
Dynamic with damping	2902	15626	444	516	71	38,5 %

Table 3-8 Pseudo-static, and dynamic with and without damping backcalculated elastic moduli and damping ratio, S3 structure, Pl_1 test point

2.2.2 Reliability of results

a - Quality of the fitting and robustness

- S_1 structure

Robustness has not been tested on S_1 as the calculation has relied on the pseudo-empirical method described *supra*.

- S_2 structure

Influence of the seed moduli set has been assessed for the three backcalculations. Robustness of the process is tested by repeating experience with different seed moduli sets: a reference seed moduli set (Ref) and the nine (9) SMS'$_2$ to SMS'$_9$ ones.

Tables 3-9 to 3-11 collect all results.

	Seed moduli sets				Backcalculated moduli sets				Norm.
	AC1	AC2	UGA	S	AC1	AC2	UGA	S	MSE
Ref	4700	9000	200	150	1784	1735	161	145	28
SMS'2	4476	10957	241	342	1785	1734	161	145	28
SMS'3	6572	13368	275	260	1782	1736	161	145	28
SMS'4	5054	10458	281	234	1789	1731	161	145	28
SMS'5	2741	6691	255	205	1791	1730	161	145	28
SMS'6	2645	3635	199	211	1799	1725	161	145	28
SMS'7	2014	8236	280	192	1780	1737	161	145	28
SMS'8	4848	4366	338	204	1802	1723	161	145	28
SMS'9	3443	7908	256	237	1787	1733	161	145	28
SMS'10	6332	8377	160	182	1794	1728	161	145	28
Mean	4055	8291	258	226	1789.4	1731.3	160.5	144.7	
Std Dev	1450	3120	43	53	7	5	0	0	
Var	35.8%	37.6%	16.7%	23.6%	0.42%	0.27%	0.01%	0.01%	

Table 3-9 Backcalculated moduli from field deflections and procedure robustness; S_2 structure; Pseudo-static modelling

	Seed moduli sets				Backcalculated moduli sets				Norm. MSE
	AC1	AC2	UGA	S	AC1	AC2	UGA	S	
Ref	4700	9000	200	120	1230	1709	170	191	324
SMS'2	4476	10957	241	138	1335	1634	168	191	324
SMS'3	6572	13368	275	108	1195	1686	176	190	324
SMS'4	5054	10458	281	74	1182	1711	174	190	324
SMS'5	2741	6691	255	38	1173	1767	170	191	324
SMS'6	2645	3635	199	49	1183	1749	171	191	324
SMS'7	2014	8236	280	79	1139	1847	168	191	324
SMS'8	4848	4366	338	146	1139	1828	169	191	324
SMS'9	3443	7908	256	82	1193	1686	169	191	324
SMS'10	6332	8377	160	41	1189	1716	173	190	324
Mean	4055	8291	258	93	1199	1746	170	191	
Std Dev	1450	3120	43	38	68	76	3	0	
Var	35.75%	37.63%	16.72%	40.75%	5.7%	4.4%	1.6%	0.2%	

Table 3-10 Backcalculated moduli from field deflections and procedure robustness; S_2 structure; Dynamic modelling without damping

	Seed moduli sets					Backcalculated moduli sets					Norm. MSE
	AC1	AC2	UGA	S	ξ	AC1	AC2	UGA	S	ξ	
Ref	4700	9000	200	120	5	1227	2562	55	276	24.7	69.9
SMS'2	4476	10957	241	138	5.4	1049	2867	55	276	24.6	69.5
SMS'3	6572	13368	275	108	7.1	1871	1903	56	275	24.8	69.8
SMS'4	5054	10458	281	74	4.7	1526	2173	57	272	24.4	70.2
SMS'5	2741	6691	255	38	3.2	1403	2301	57	272	24.3	70.1
SMS'6	2645	3635	199	49	5.5	1946	1844	58	269	24.3	70.6
SMS'7	2014	8236	280	79	7.0	844	3498	52	284	25.1	69.2
SMS'8	4848	4366	338	146	5.5	991	2970	56	275	24.4	69.2
SMS'9	3443	7908	256	82	5.5	1737	2012	56	274	24.6	70.0
SMS'10	6332	8377	160	41	3.7	991	2970	56	275	24.4	70.3
Mean	4055	8291	258	93	5	1399	2459	56	275	24.6	
Std Dev	1450	3120	43	38	1	400	560	2	4	0	
Var	35.8%	37.6%	16.7%	40.8%	21.7%	28.6%	22.8%	3.1%	1.5%	1.1%	

Table 3-11 Backcalculated moduli from field deflections and procedure robustness; S_2 structure; Dynamic modelling with damping

It appears that, on the studied example and in the considered variation range, the choice of the seed moduli has no influence on backcalculation results (i.e. on parameters values and normalized MSE).

Actually, in all cases method converges with regard to recommended error values of part 2. Besides, when considering the evolution of error it appears that this parameter is well

stabilized (what is also confirmed by the excellent homogeneity of reached errors between different seed moduli sets).

Nevertheless, errors reached remain largely higher than the results of the theoretical robustness study provided in part 2. This is an indication that the model is not perfect.

Also note that introduction of damping improves fitting quality (compare normalized MSE).

- S_3 structure

The same experiment as for the carrousel tested structure has been performed on the Bonneuil test facility for the pseudo-static and the dynamic without damping backcalculations (Tables 3-12 and 3-13). It confirms previous results. Note an aberrant point in the static calculation (in red) which has been removed from the analysis.

	Seed moduli sets					Backcalculated moduli sets					Norm.
	AC1	AC2	UGA	G	S	AC1	AC2	UGA	G	S	MSE
Ref	4700	9000	200	150	120	2613	17465	445	614	74	3.3
SMS2	4476	10957	241	342	138	2608	17632	439	624	74	3.3
SMS3	6572	13368	275	260	108	2612	17485	444	616	74	3.3
SMS4	5054	10458	281	234	74	2638	16365	488	550	76	3.4
SMS5	2741	6691	255	205	38	2728	14401	540	494	77	3.8
SMS6	2645	3635	199	211	49	2794	13336	556	485	77	4.0
SMS7	2014	8236	280	192	79	2729	14238	552	481	78	3.9
SMS8	4848	4366	338	204	146	2801	13055	577	463	78	4.2
SMS9	3443	7908	256	237	82	2700	15042	520	515	77	3.6
SMS10	6332	8377	160	182	41						
Mean	4055	8291	258	226	93	2691	15447	507	538	76	
Std Dev	1450	3120	43	53	38	77	1828	54	65	2	
Var	35.8%	37.6%	16.7%	23.6%	40.8%	2.9%	11.8%	10.7%	12.0%	2.3%	

Table 3-12 Backcalculated moduli from field deflections and procedure robustness ; S_3 structure, Pl_1 test point; Pseudo-static modelling

	Seed moduli sets					Backcalculated moduli sets					Norm.
	AC1	AC2	UGA	G	S	AC1	AC2	UGA	G	S	MSE
Ref	4700	9000	200	150	120	2351	9525	693	569	65	151
SMS2	4476	10957	241	342	138	2285	11039	657	604	62	151
SMS3	6572	13368	275	260	108	2280	13255	622	602	63	151
SMS4	5054	10458	281	234	74	2254	11486	696	554	66	151
SMS5	2741	6691	255	205	38	2928	5702	755	524	69	151
SMS6	2645	3635	199	211	49	2462	8557	695	582	63	151
SMS7	2014	8236	280	192	79	2381	8170	812	468	73	151
SMS8	4848	4366	338	204	146	2933	5331	811	485	71	151
SMS9	3443	7908	256	237	82	2283	11192	650	609	61	151
SMS10	6332	8377	160	182	41	2558	9109	646	601	63	151
Mean	4055	8291	258	226	93	2471	9337	704	560	66	
Std Dev	1450	3120	43	53	38	260	2530	68	52	4	
Var	35.8%	37.6%	16.7%	23.6%	40.8%	10.5%	27.1%	9.6%	9.2%	6.1%	

Table 3-13 Backcalculated moduli from field deflections and procedure robustness ; S_3 structure, Pl_1 test point; Dynamic modelling without damping

This experiment has also allowed (Table 3-14) comparing mean value of backcalculated moduli on different tests points of a homogeneous structure, with results from an unique backcalculation considering the mean pavement structure and the mean measured deflections (last line). This experiment has been performed on points Pl_1 to Pl_{10} (see appendix 1.1). Result is convincing i.e. moduli are very close. It can present the operational interest, especially in the case of time-consuming dynamic backcalculations, to perform only one backcalculation per homogeneous area.

	Seed moduli sets					Backcalculated moduli sets					Norm.
	AC1	AC2	UGA	G	S	AC1	AC2	UGA	G	S	MSE
Pl1	4700	9000	200	150	120	2613	17465	445	614	74	3.3
Pl2	4700	9000	200	150	120	3016	12568	485	599	75	7.0
Pl3	4700	9000	200	150	120	3276	13212	524	541	70	4.3
Pl4	4700	9000	200	150	120	2902	18210	428	692	68	6.1
Pl5	4700	9000	200	150	120	3090	14360	463	590	71	4.2
Pl6	4700	9000	200	150	120	3093	8174	401	404	57	5.6
Pl7	4700	9000	200	150	120	2541	12866	359	491	68	9.0
Pl8	4700	9000	200	150	120	2915	12171	404	429	73	8.7
Pl9	4700	9000	200	150	120	2631	24677	513	373	81	3.8
Pl10	4700	9000	200	150	120	2943	22559	412	427	76	7.8
Mean						2902	15626	444	516	71	
Std Dev						239	5076	53	107	6	
Var						8.2%	32.5%	11.9%	20.7%	9.1%	
Mean Back	4700	9000	200	150	120	2865	15287	420	527	70	5.3

Table 3-14 Backcalculated moduli from field deflections; S_3 structure, test points Pl_1 to Pl_{10}; Dynamic modelling without damping

b - Comparison with expected values

- S_1 structure

- Elastic moduli

For asphalt materials, backcalculated moduli are compared to complex moduli laboratory tests (see appendix 1.1). Test temperature was 10 °C. Usual retained frequency is the f_{app} pseudo-frequency expressed as:

$$f_{app} = \frac{1}{\Delta t}$$

with Δt the force signal pulse-time. Here Δt=35 ms, so that f_{app} = 30 Hz.

According to appendix 1.1, expected values for AC_1 and AC_2 are both 20 000 MPa.

No information about UGA layers is available.

For subgrade, a geotechnical survey (see appendix 1.1) predicts a modulus weaker than 50 MPa. This value is confirmed by resonant column tests (see appendix 1.1) which assess a 40 MPa modulus.

Results are collected in Table 3-15.

	AC_1	**AC_2**	**UGA_1**	**UGA_2**	**S**
Expected values	20 000	20 000	?	?	40
Pseudo-static method	4700	9000	580	290	120
M_1 and M_3 dynamic methods	4000	7500	510	240	77

Table 3-15 Comparison between backcalculated and field moduli; S_1 structure

It appears that the dynamic methods provide much better results than the pseudo-static one for the subgrade.

Nevertheless, whatever the method used, the backcalculated values for asphalt layer are significantly underestimated, at least when considering the pseudo-frequency of signal for laboratory values. It will be shown in the following that this choice is debatable.

- Damping ratio

For asphalt materials, complex moduli provide, when using the relationship provided by equation (3-2), respective damping values of 7,5 and 9,2 %.

A 2 to 3 % value is assessed in the subgrade, from resonant column tests.

The intermediate 5 % mean value is thus consistent.

- S_2 structure

According to the measured profile (Fig. 3-8), a 17 °C temperature is retained in the AC_1 layer, and 20 °C in the AC_2 one.

- Elastic moduli

	AC_1	AC_2	UGA	S
Expected values	14 000	12 000	80 to 100	150 to 200
Pseudo-static method	1784	1735	161	145
M_1 dynamic modelling without damping	1230	1709	170	191
M_1 dynamic modelling with damping	1227	2562	55	276

Table 3-16 Comparison between backcalculated and field moduli; S_2 structure

Once more, values provided by the dynamic methods for deep layers are more consistent than in the pseudo-static case. Nevertheless, surface moduli are unrealistic. It will be attempted in the following to find an explanation to this inconsistency.

- Damping ratio

Damping ratios in AC_1 and AC_2 are respectively 14 % and 13 %.

No information about damping in unbound materials is available, but usual values are in the 2-5% range.

Backcalculated damping ratio (24,5 %) is thus largely overestimated.

- S_3 structure

A rather homogeneous temperature is observed (Figure 17, Appendix 1.2) during the test survey.
Temperatures retained are 17 °C in the AC_1 layer, and 18 °C in the AC_2 one.
Besides, impulsion time was very repeatable around the 30 ms mean value. It corresponds to a 33 Hz mean pseudo-frequency.

Elastic modulus and damping ratio of the AC_2 material at (18 °C, 33 Hz) can be determined using a linear interpolation between (15 °C, 30 Hz), (20 °C, 30 Hz), (15 °C, 40 Hz) and (20 °C, 40 Hz) values. Values found are $|E^*|_{AC2}$ = 17 000 MPa. The value of test laboratory for elastic modulus and damping ratio of the AC1 are $|E^*|_{AC1}$ = 11 000 MPa for test conditions (17 °C, 33 Hz).

Subgrade is the same as for the S_1 structure.

	AC_1	AC_2	UGA	G	S
Expected values	11 000	17 000	?	?	40
Pseudo-static method	2 700	15 400	500	540	76
M_1 dynamic modelling without damping	2 500	9 300	700	560	66
M_1 dynamic modelling with damping	2 900	15 600	450	520	71

Table 3-17 Comparison between backcalculated and field moduli; S_3 structure

Backcalculated values for AC_2 are consistent with experimental data. Nevertheless obtained values for AC_1 are very low. Note that precision on the latter value is limited by the thinness of the layer. It is also largely affected by the plate effect, whose modelling is maybe not completely true. It would be interesting to impose a variation range for the ratio E_{AC1}/E_{AC2}. This option is not available so far in PREDIWARE.

Subgrade modulus is overevaluated whatever the considered method, as in the S_1 case. An explanation could be a shallow water table. As suggested in the literature review (§ 2.2.1) the latter could lead to an apparent stiffness increase of the saturated subgrade material. It has been attempted to study this phenomenon in the frame of the thesis, by performing HWD tests with different time table levels on the LCPC's fatigue carrousel where the latter can be adjusted. The experiment was unfortunately aborted due to a problem on the pump. It is planed to repeat it.

- Damping ratio

Respective damping values for AC_1 and AC_2 are 19 % and 12 %. A 2 to 3 % value is assessed in the subgrade, from resonant column tests. Once more the 38,5 % value is largely overestimated.

c - Validation against gage measurements

Direct strain calculations are performed, using the previously backcalculated parameters related to S_3 structure.

Table 3-18 provides experimental and numerical maximum strains related to each gages.

	Tensile strain; Bottom of AC [µm/m]	**Vertical strain; Top of UGA [µm/m]**	**Vertical strain; Top of Subgrade [µm/m]**
Experimental values	-170	936	538
Pseudo-static	-166	514	337
Dynamic without damping	-181	568	345
Dynamic with damping	-171	910	161

Table 3-18 Field and numerical strains from direct calculation ; S_3 structure

Matching related to the dynamic modelling including damping is displayed in Fig. 3-40. Tensile strain at the bottom of AC layer is in blue, vertical compressive strain at the top of UGA in green, and vertical compressive strain at the top of subgrade in red.

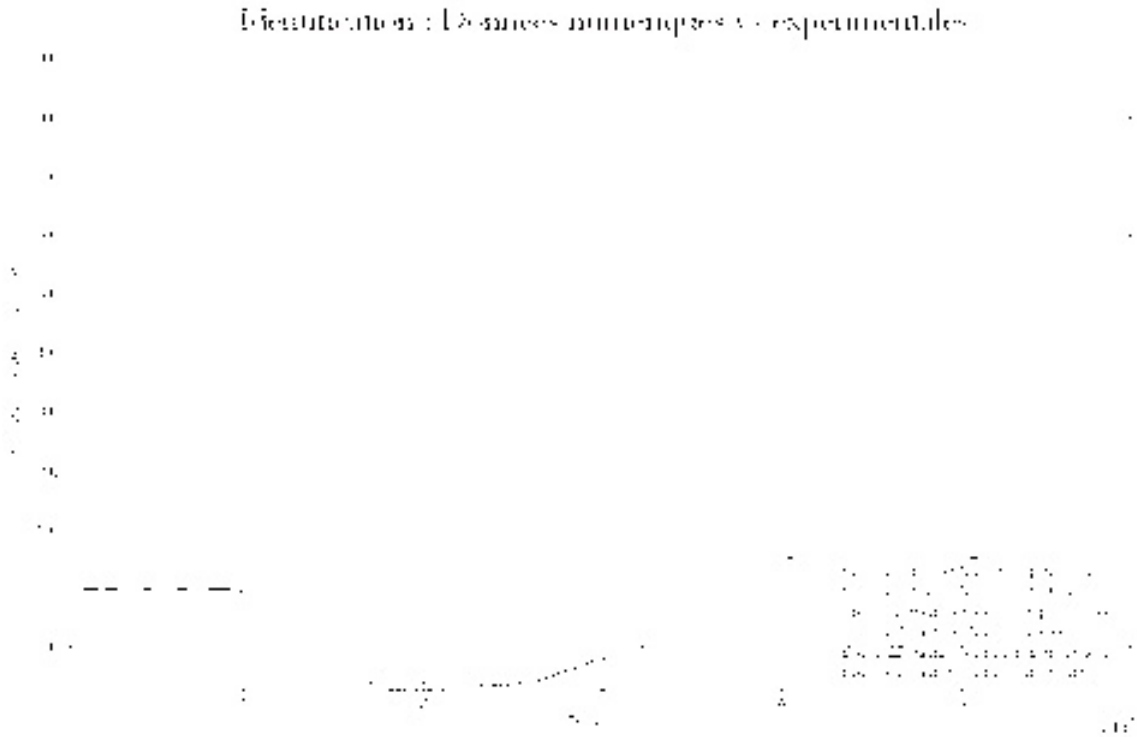

Fig. 3-40 Fitting of numerical deflections on field data; from PREDIWARE dynamic calculation with damping

It seems hard to decide which model is the best, since no one consistently gives better results:
- pseudo-static and dynamic without damping modelling seem to provide similar theoretical gage measurements, but this is apparently a hazard: both backcalculated AC_2 moduli are similar whereas either AC_1 or subgrade moduli are significantly different.
- introduction of damping in the modelling improves significantly the UGA strain modelling. Nevertheless the contrary is observed on the subgrade gage.
- this analysis is complicated by the poor repeatability of measurements in the unbound materials. Unfortunately only one gage profile has here been tested.

Partial conclusion

Dynamic backcalculations provide globally better results than the pseudo-static method. Nevertheless, deviations from expected values are observed, especially:

- an overestimation of subgrade on the Bonneuil site (structures S_1 and S_3),
- a general underestimation of the asphalt materials moduli, especially for the S_2 structure,
- unrealistic values of damping, when introduced in the dynamic backcalculation.

The following section intends to find potential origins to these differences.

2.2.3 Possible sources of the observed deviations

a - Approximate damping modelling

Results from laboratory tests show that the damping modelling is far from reality. First it is limited to a global damping at the structure scale. Then, Rayleigh modelling itself seems not to be faithful to real material behaviours.

- Global damping

The (3-2) relation, applied to the complex moduli results from S_3 structure, allows determining evolution of damping ratio with temperature and frequency. Fig. 3-41 displays the results related to AC_2 material.

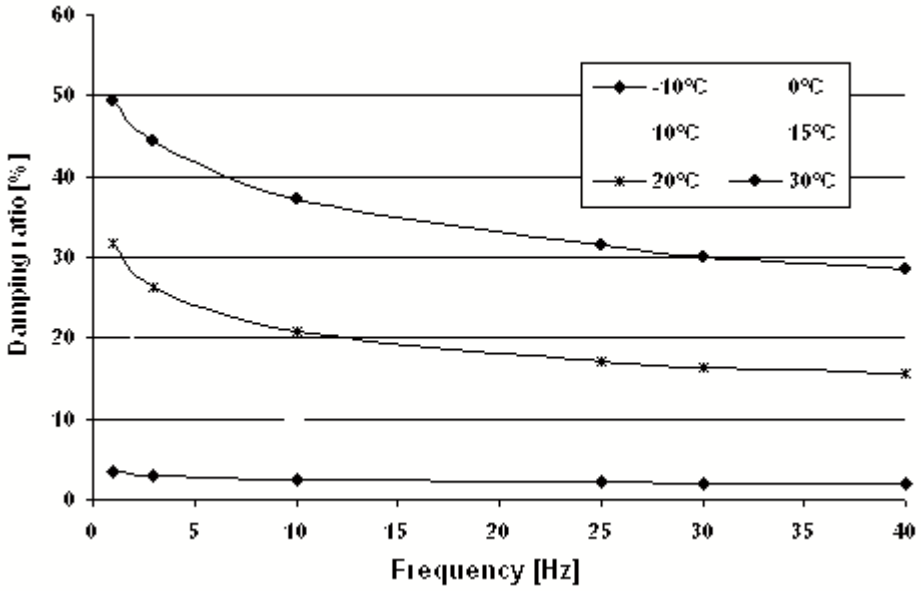

Fig. 3-41 Temperature and frequency dependency of damping ratio in asphalt AC_2 material

At 17 °C (temperature during the tests performed on Pl_1 to Pl_{10} points), it appears that the damping ratio never passes under the 10 % threshold.

On the contrary resonant column tests predict a damping ratio of about 2-3 % for subgrade (see appendix 1.1).

- Rayleigh damping

The Rayleigh modelling imposes the frequency transfer response shape (see Fig. 2-3). It is of generalized Maxwell type. This shape is:

- neither adapted to unbound materials whose behaviour is independent on frequency,

- nor adapted to asphalt material (see in Fig 3-42 the best obtained adjustment concerning the AC_2 material related to S_3 structure).

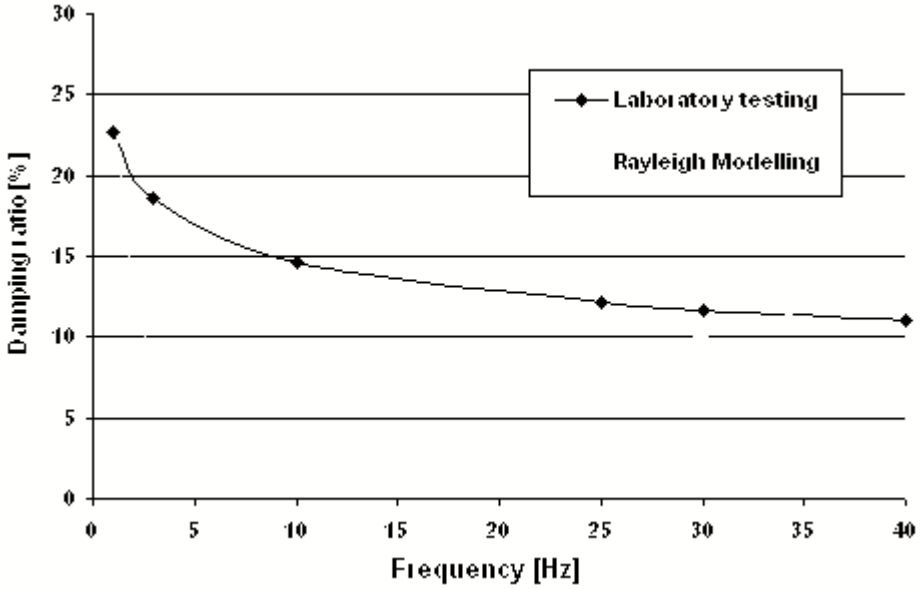

Fig. 3-42 Damping ratio in asphalt AC_2 material; Numerical fitting attempt with Rayleigh modelling

b - Asphalt material visco-elastic behaviour

The Viscoanalyse software developed by LCPC [Chailleux, 2007] makes possible to calculate viscoelastic deformation of an asphalt material subjected to an external time-related force signal, based on the Huet and Sayegh's modelling.

Fig. 3-43 shows the theoretical response (in green) of the AC_2 material of S_2 pavement, subjected to a 30 ms pulse time sinusoidal load (in blue) supposed to reflect the HWD loading. Parameters of the Huet and Sayegh model have been obtained from laboratory complex moduli tests.

Note that both signals occur consecutively. Nevertheless a time delay is observed between maxima of the two curves.

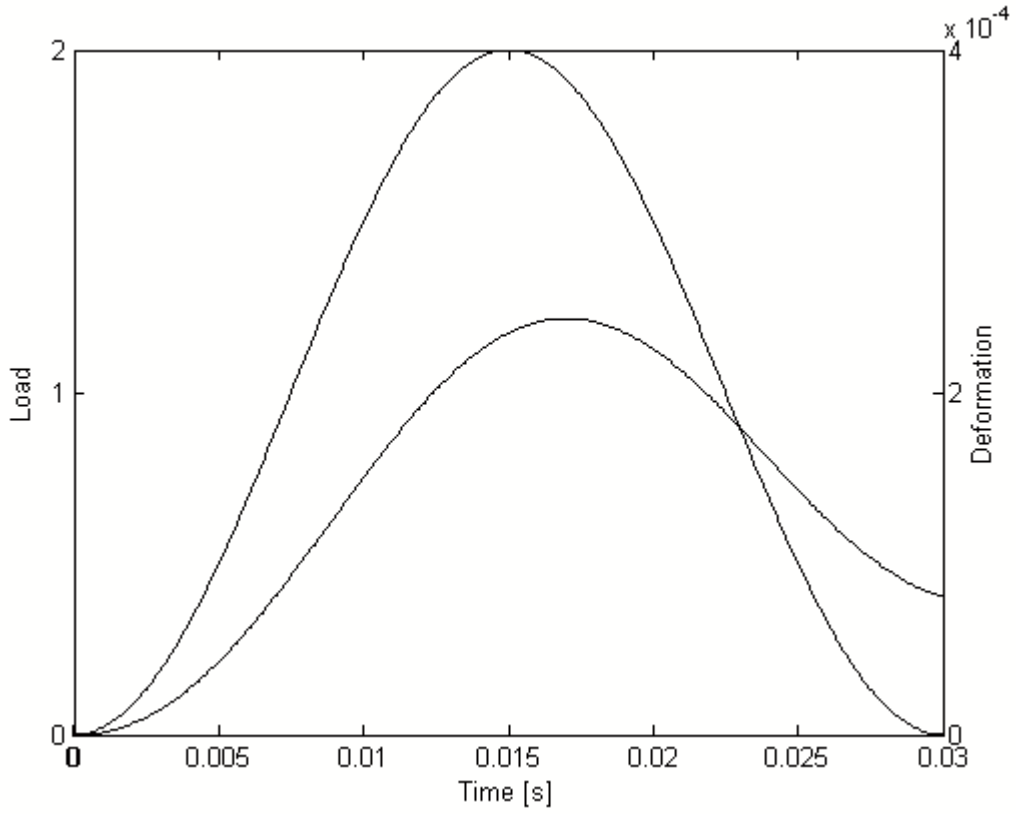

Fig. 3-43 Viscoelastic response under sinusoidal load of S_2 AC_2 material; After Viscoanalyse

Fig. 3-44 displays the evolution of secant moduli during the previous theoretical HWD load (solid line). The other curve provides a pretty good approximation of this modulus, at least for earliest times, using the relation:

$$E(t) = \left|E^*\left(f = 1/2\pi t\right)\right| \qquad \textbf{(3-3)}$$

where *E(t)* is the secant modulus at t time, and *E*(f)* the complex modulus at f frequency.

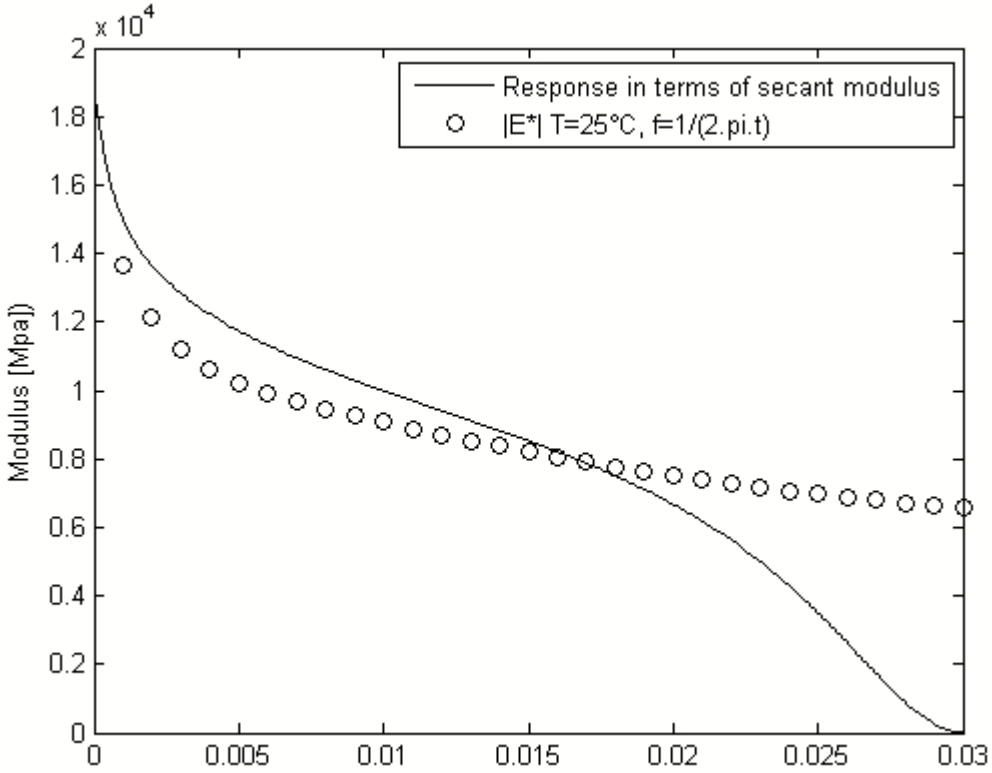

Fig. 3-44 Secant modulus of S_2 AC_2 material under sinusoidal load; after Viscoanalyse

It implies in both cases that apparent modulus decreases during the HWD test so that the modulus estimated by the backcalculation, assumed to be constant with regard to time in our modelling, is a global mean modulus over the whole considered frame time. The Backcalculated modulus which is a mean modulus estimated over the considered 0-30 ms time frame should thus not be compared to the 11 000 MPa (30 Hz; 24 °C) value, but to a mean value comprised between 0 and 18 000 MPa, apparently about 7 000 MPa

Note that this renders the asphalt materials backcalculated moduli more reasonable, except in the S_2 case, where values are much too weak.

In the future, and when assuming that Gauss Newton is a robust enough algorithm for such identifications, more advanced modellings of asphalt layer materials with more than only one parameter, as generalized Maxwell model, or Huet and Sayegh's one may be tested.

c - Interface conditions

Backcalculated moduli for the S_2 structure asphalt materials are abnormally weak. Interfaces have been assumed fully bonded by default. Let us here test the opposite case: unbonded interfaces.

Let assume that the AC_1 and AC_2 layers, as well as the AC_2 and UGA layers are unbonded. The AC_2 had been settled in two phases. It is subdivised, and both layers are also assumed unbonded.

Both pseudo-static method and dynamic M_1 modelling without damping are here considered.

First, results of two direct calculations (one with fully bonded layers and one with fully unbonded) are compared in each case. The retained moduli are the previous backcalculated moduli related to the fully bonded configuration.

Then, results backcalculations with unbonded layers are presented

- Comparison between direct calculation results

Fig. 3-45 and Fig. 3-46 display the results respectively related to the static and dynamic calculations.

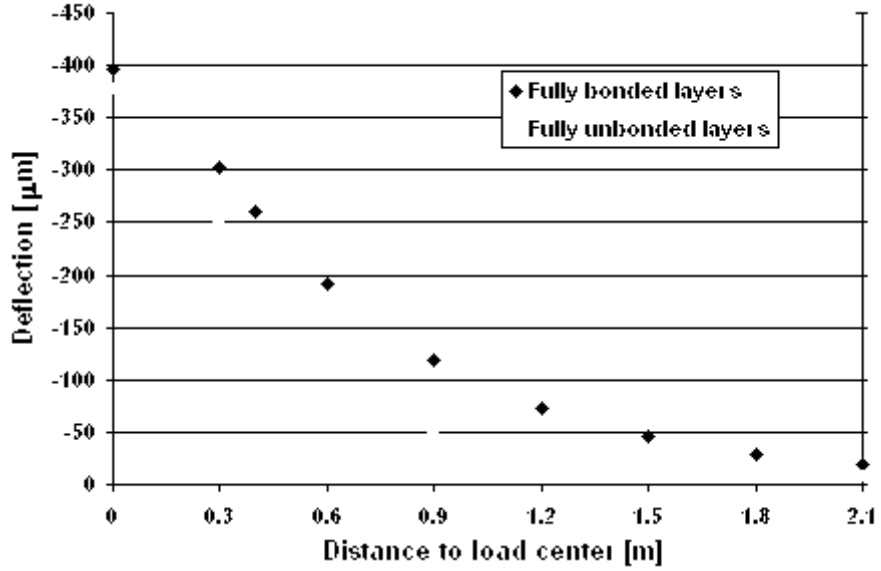

Fig. 3-45 Comparison between bonded and unbonded configurations, pseudo-static method

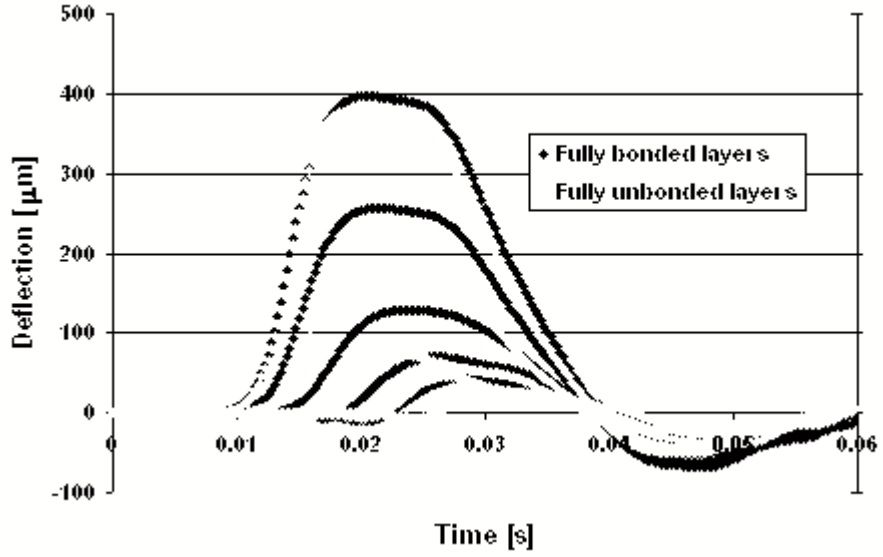

Fig. 3-46 Comparison between bonded and unbonded configurations, dynamic method

In both cases, it appears that deflections are double in the fully unbonded case.

- Backcalculation with fully unbonded layers

Fig. 3-47 and Fig. 3-48 display matching in the pseudo-static and dynamic cases. Time frame in dynamic case is still 7-35 ms.

Both fittings are very good.

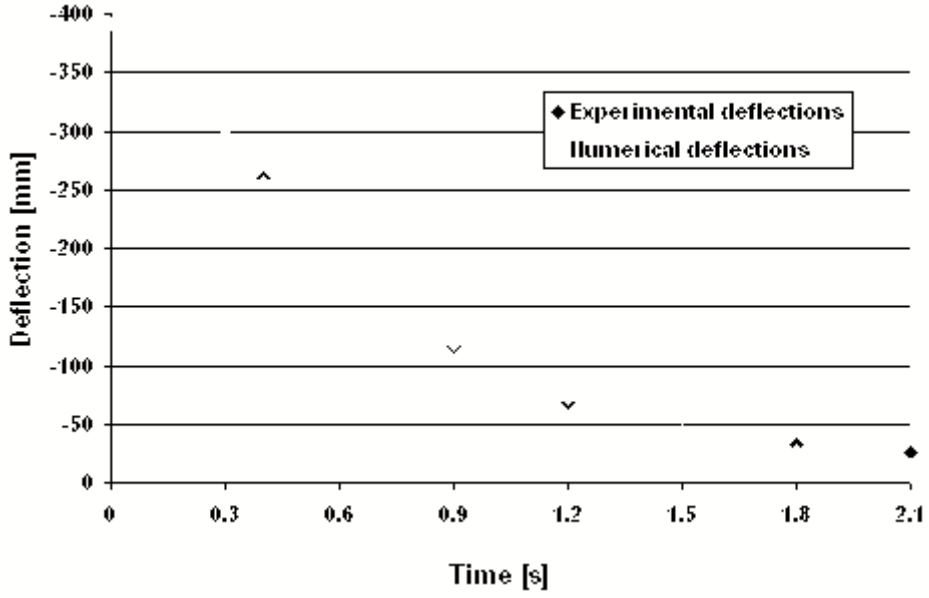

Fig. 3-47 Backcalculation result; pseudo-static modelling

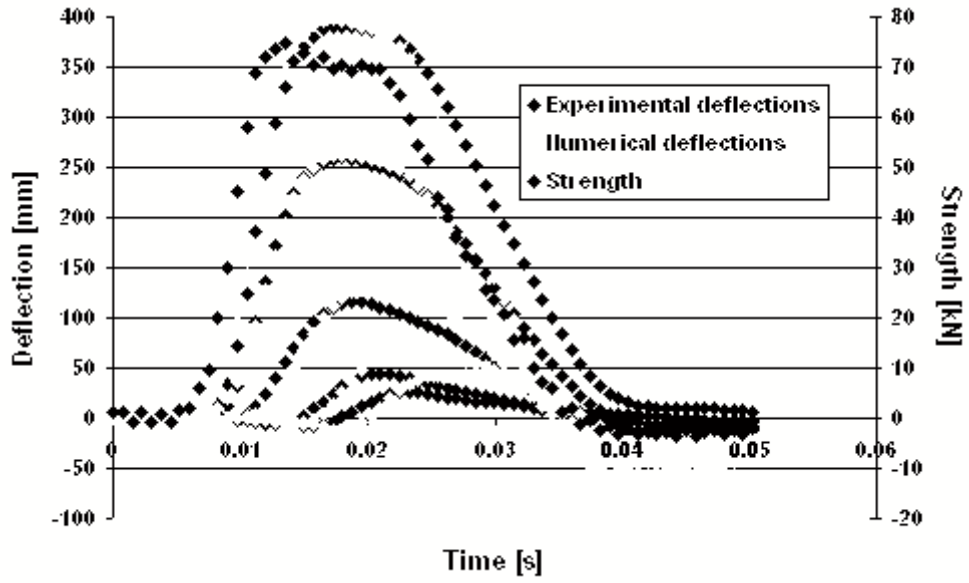

Fig. 3-48 Backcalculation result; dynamic modelling

Table 3-19 provides backcalculated moduli values. Upper and lower AC2 layers are respectively referred to as $AC_2(1)$ and $AC_2(2)$. Note that both values should be similar. It is unfortunately not available so far in PREDIWARE to link parameters together.

	AC_1	$AC_2(1)$	$AC_2(2)$	UGA	S
Pseudo-static method	3 200	8 000	4 300	1 870	143
M_1 dynamic modelling without damping	5 200	3 100	8 500	890	196

Table 3-19 Comparison between backcalculated and field moduli; S_3 structure

AC_2 modulus is more consistent (6 000 MPa mean value between the two layers). Nevertheless, results for unbound materials are unrealistic.

It could be interesting to test intermediate cases between the fully bonded and fully unbonded configurations. Unfortunately, no advanced interface modelling is so far available in CESAR for dynamic calculations.

Partial conclusion

Three potential sources of errors have been here considered:
- a too approximate damping modelling,
- the absence of visco-elastic modelling for asphalt materials description,
- interfaces not systematically fully-bonded.

With regard to unrealistic backcalculated damping ratio, and observations from Viscoanalyse analyses, the first two improvements have priority.

If they fail to explain the weak moduli obtained in the S_2 structure case, a precise study about layer interfaces could be interesting.

These three improvements all imply developments in the CESAR-LCPC code.

A specific study about the water table shall also be reiterated.

3 - Example of remaining life and bearing capacity calculation

The objective of a HWD test survey is the assessment of the bearing capacity and/or residual life of the tested pavement. The results of this evaluation eventually lead to the decision to plan an overlay.

Unfortunately, the data obtained in the frame of the thesis do not provide the opportunity to compare the assessment of a residual life from HWD results, with the one obtained from observation of damage under traffic effect.

Furthermore, whereas some standards exist for the backcalculation procedure, no consensus exists for this residual life. The following methodology is thus to be considered as a “personal” proposition. The aim is here to illustrate it, not to validate it.

A long-term experiment is planed in the latter purpose, which will include regular HWD surveys and superficial observations on a given plate-form.

3.1 General expression of damage

Example of remaining life calculation is proposed here, based on the elements of in 2.3.
According to the French rational design method, the assumption is made that material stiffness remains constant during the whole pavement life.
Let us consider in the absence of any temperature data, a simplified case in which the year is dissected into 4 seasons:
- a winter with a 10 °C asphalt layer mid-depth temperature,
- a spring and fall with a 20 °C,
- a summer with 30 °C.

On the S_2 structure, tests have been performed with a 17 °C surface temperature and 24 °C at bottom of the asphalt layer, so that it is roughly considered that tests have been performed at a 20 °C mean temperature.

According to Miner's law, damage *d* is expressed as:

$$d = \sum_{j=1}^{NLoad} \sum_{i=1}^{Ntemp} \frac{p_{ij} N}{N_{All}(\theta i)} \qquad \textbf{(3-4)}$$

With p_{ij} the fraction of j^{th} load traffic accepted by the pavement at θ_i temperature, and N_{All} the allowable coverage number.
Let us assume here that traffic is equally distributed over the 4 seasons.

3.2 Elementary damages calculation

3.2.1 Number of allowable coverages regarding the fatigue of AC layer

In the case of AC materials, the considered damaging parameter is fatigue at bottom of the AC layer due to the repetition of tensile strains.
According to the literature review (§ 2.3.2), and when assuming that the fatigue law adjusted for road traffics ranging from one to several millions passes is extendable to airport traffics in of 10^4 passes order of magnitudes, allowable traffic N_{All} can be expressed as:

$$N_{All}(\theta i) = 10^4 \cdot \left(\frac{\varepsilon_T(\theta i)}{\varepsilon_4(\theta i) \cdot k_C \cdot k_r \cdot k_S} \right)^{\frac{1}{b}} \qquad \textbf{(3-5)}$$

Where ε_T is the tensile strain at the base of the AC layer, and ε_4 the allowable strain for 10^4 applications of the considered loading case.

$k_C \cdot k_r \cdot k_S$ are defined in the literature review
Usual value for b is:
b = -0,2.

a - Number of allowable coverages regarding the permanent deformation of the unbound materials

$$N_{All}(\theta i) = \left(\frac{\varepsilon_Z(\theta i)}{A} \right)^{\frac{1}{b'}} \qquad \textbf{(3-6)}$$

Where ε_Z is the vertical strain at the top of the considered layer.

Considering road pavement designed for heavy vehicles, the usual parameters values are:
b' = -0,222,
A = 16 000.
Let us assume that these coefficients are still valid for airfield pavements.

3.2.2 Strain calculations

$\varepsilon_T(\theta i)$ and $\varepsilon_Z(\theta i)$ are calculated by computing direct calculation using the backcalculated moduli, using the same model as for the backcalculation phase. These moduli are corrected with regard to temperature for AC layers, and letting the modulus of other materials unchanged. Frequency-related correction could also be applied in refined calculations, to take into account the type of the studied area (runway, taxiway, …), but is neglected here.

Material data are used for temperature correction, when available.

When it is not the case, it is recommended in [LTPP, 2000] (see literature review) a linear correction in semi-log [T°C, log(E)] scale is applied to $E(\theta_i)$. Advocated slopes range between -0,0195 and -0,021.

Fig. 3-49 and Fig. 3-50, constructed from LCPC raw complex moduli obtained on the S_2 structure, confirm this variation range.

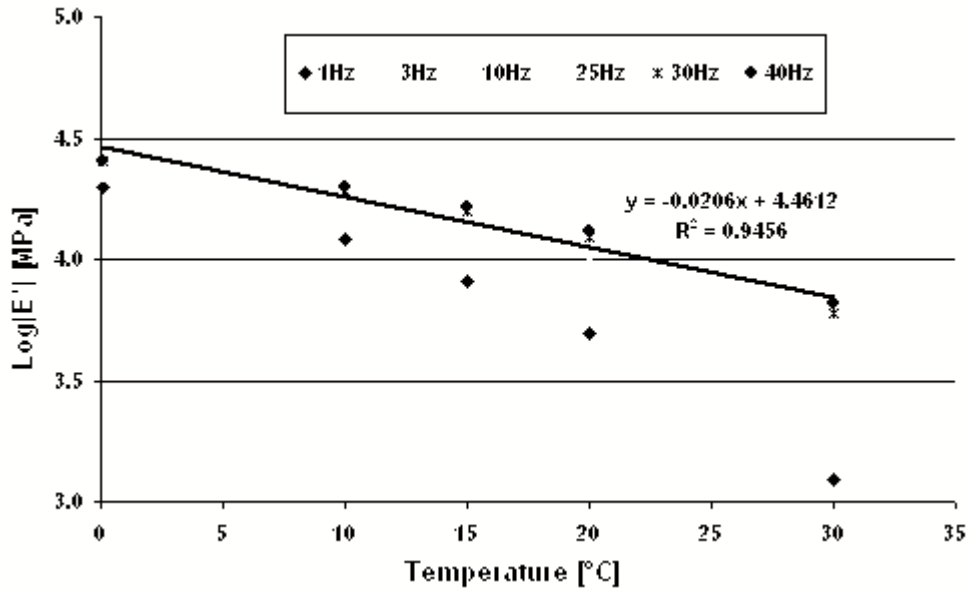

Fig. 3-49 Laboratory-determined temperature corrections to be applied to AC_1 material modulus (S_2 structure)

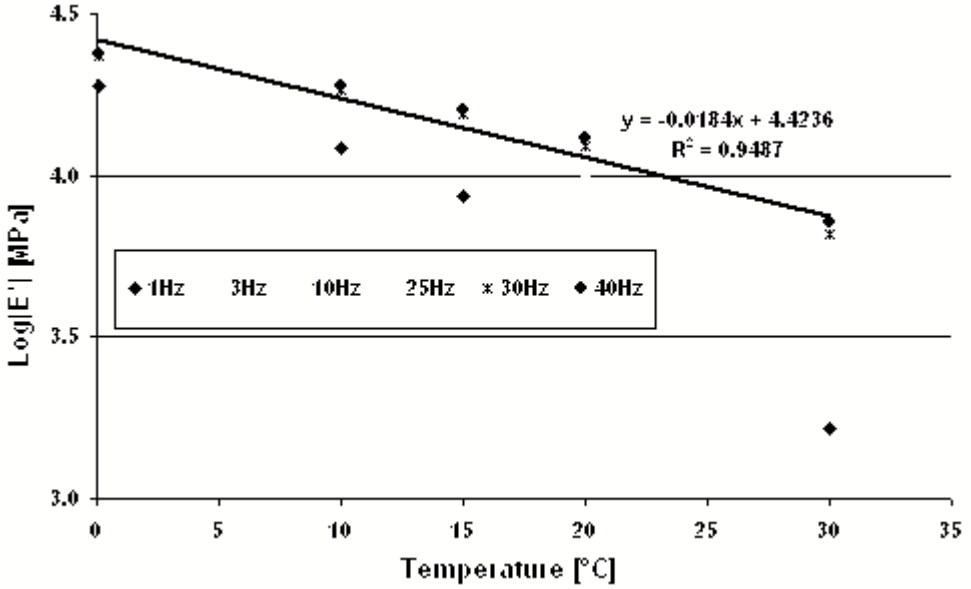

Fig. 3-50 Laboratory-determined temperature corrections to be applied to AC_2 material modulus (S_2 structure)

$\varepsilon_4(\theta i)$ is also corrected. The following empirical relation is considered:

$$\varepsilon_4(\theta i)\sqrt{E(\theta i)} = Cste \qquad \textbf{(3-7)}$$

3.3 Determination of the bearing capacity and the potential remaining life

3.3.1 Bearing capacity

Let us consider the maximal standardized single wheel, which is defined here as the HWD 45 cm diameter load plate.

The purpose is to determine the maximal load to be applied 10 000 times on the pavement until failure.
It corresponds to the loading configuration that induces the highest damage (cumulated damage equal to 1).
In practice, the chosen method consists in determining the strains imparted by a F_0 load, and the corresponding d_0i damages for each i^{th} critical strain. Let us call $d_0 = \max(d_0i)$. As the problem is linear, and considering the elementary damage expression, the maximal F_{All} force whose repeated application results in a damage equal to 1 is expressed as:

$$F_{All} = F_0 \times \left(\frac{1}{d_0} \right)^{-b} \qquad \textbf{(3-8)}$$

3.3.2 Remaining life

The problem is more direct. In this case the traffic mix is well known. Actual damage is calculated from traffic previously supported by the pavement. Remaining life corresponds to the time until damage reaches the 1 value.

3.3.3 Numerical study

a - Bearing capacity

- S_2 structure

Surface backcalculated moduli are abnormally weak (see infra), so that for this numerical case, theoretical usual values are preferred to the former values. Let us take the 30 Hz material modulus even if these values seems to be overevaluated according to § 2.2.3-b.

First step consists in calculating the strains in the structure for each temperature, i.e. using corrected moduli (see *supra*). As the tested structure is a road structure, designed for F_0 = 65 kN, this load is retained for the following direct calculations (Note that this choice has no influence on results, as problem is linear). Table 3-20 gathers results.

	HWD Test temperature	θ_1=10°C	θ_2=20°C	θ_3=30°C
AC_1	**15000**	24 100	15 000	9 350
AC_2	**12500**	19 100	12 500	8 200
UGA	**170**	170	170	170
S	**190**	190	190	190
Fmax [kN]	**65.0**	65.0	65.0	65.0
$\varepsilon_T(\theta_i)_{AC2}$ [μm/m]	**37.2**	27.4	37.2	51.4
$\varepsilon_Z(\theta_i)_{UGA}$ [μm/m]	**138.4**	106.1	138.4	180.0
$\varepsilon_Z(\theta_i)_S$ [μm/m]	**104.1**	82.6	104.1	130.9

Table 3-20 Results from direct calculations for the θ_i temperatures, S_3 structure

Damage calculation details for AC_2 layer are provided in Table 3-21. It relies on (0-51). Total damage ($\theta_1+2\times\theta_2+\theta_3$) is 0,061, what corresponds according to (3-8) to a F_{All} = 166 kN allowable load on single wheel.

	HWD Test temperature	θ_1=10°C	θ_2=20°C	θ_3=30°C
AC_1	**15000**	24104	15000	9335
AC_2	**12500**	19095	12500	8183
UGA	**170**	170	170	170
S	**190**	190	190	190
Fmax [kN]	**65.0**	65.0	65.0	65.0
$\varepsilon_T(\theta_i)_{AC2}$ [μm/m]	**37.2**	27.4	37.2	51.4
$\varepsilon 6(AC_2)$	**111**	90	111	137
p_i		0.25	0.50	0.25
$p_i\times(\varepsilon/\varepsilon 6)^{-1/b}$		0.00066	0.0021	0.0018
$d_i= p_i\times(\varepsilon/\varepsilon 6)^{-1/b}\times 10^4/10^4$		0.00066	0.0021	0.0018
$d_0=\Sigma d_i$	**0.0092**			
$F_{all} =(1/d_0)^{-b}$ [kN]	**166**			

Table 3-21 Bearing capacity calculation. AC detailed calculation.

As expected, it appears that the damage is the highest with high temperatures.

	θ_1=10°C (pi=0,25)	θ_2=20°C (pi=0,25)	θ_3=30°C (pi=0,25)
d_i	0.00066	0.00105	0.018

Table 3-22 Proportion of damages applied according to season (for a same traffic)

The same reasoning is made for both others layers, based on (0-52). Allowable loads are respectively 279 kN and 377 kN for UGA and subgrade. It thus appears that the critical layer is the AC layer, and that admissible load for the pavement is thus 166 kN.

This value is reasonable. Actually, this 166 kN allowable value for 10^4 passes corresponds to a 66 kN value for 1 million passes, and 41 kN for 10 millions. The pavement has been designed for 5 millions passes of a 65 kN half-axle.

Remark: The previous equivalences follow from the problem linearity. Actually, when calling F_{All1}, ε_1, and N_1 respectively the bearing allowable load, strain and number of coverage of the load case number 1, and F_{All2}, ε_2, and N_2 the corresponding parameters for relative to the load case number 2, one can write:

$$F_1/F_2 = \varepsilon_1/\varepsilon_2 = (\varepsilon_1/\varepsilon_2)^b$$

- S_3 structure

Results relative to the three backcalculations methods are in this practice case compared. The simplifying assumption is here made that temperature is constant during the whole pavement life and corresponds the test temperature (17 °C in AC_1 and 18°C in AC_2).

Table 3-23 provides the strains obtained when performing a direct calculation using the considered method, and the corresponding backcalculated parameters.

	Tensile strain; Bottom of AC_2	Vertical strain; Top of UGA	Vertical strain; Top of G	Vertical strain; Top of S
Pseudo-static	-89	320	110	145
Dynamic without damping	-94	300	127	160
Dynamic with damping	-85	325	131	190

Table 3-23 Field and numerical strains [μm/m] from direct calculation; S_3 structure; Pl_1 test point

Table 3-24 provides the final results for each strain, and the resulting pavement bearing capacity.

	Pseudo-static method	Dynamic without damping	Dynamic with damping
Tensile strain; Bottom of AC_2	219	207	229
Vertical strain; Top of UGA	1200	1300	1200
Vertical strain; Top of G	3500	3050	2950
Vertical strain; Top of S	2700	2400	2000
Pavement bearing capacity	**219**	**207**	**229**

Table 3-24 Pavement bearing capacity obtained from strain values; S_3 structure, Pl_1 point

It appears that the pavement will fail by excessive strain at bottom of the AC_2 layer. Global pavement bearing capacity ranges from 207 to 229 kN according to the considered method.

The three methods provide a similar final result. This is a coincidence. Actually, the design criterion is here the tensile strain at the bottom of AC_2 and the corresponding values for all methods are very close, with regard to vertical strain at subgrade for instance.

The pavement was designed for 10 000 single wheel 300 kN loads. The 210 to 230 value is reasonable according to the simplifying assumptions on temperature.

Note that obtained strains for unbound materials are very far from failure criterion.

Remark: the ICAO prescribes to express the bearing capacity using the concept of Pavement Classification Number (PCN). The PCN of the pavement corresponds to double of the load it can accept 10 000 times. In practice, the calculation relies on empirical formulas, from the CBR method, whose limitations have been demonstrated when considering modern pavement materials and new complex landing gears. A method for PCN calculation, based on rational methods could bring valuable improvements.

b - Residual life

Previous example from S_3 structure is studied, with now the assumption that a new aircraft is accepted, whose single wheel maximal load is 270 kN (wheels interaction is here neglected, as well as the lateral distribution). Unknown of the problem is the number of allowable passes of this aircraft, when assuming it is the design aircraft for the structure, i.e. effect of other aircraft is neglected.

Elementary damages are expressed as:

$$d_i = \frac{N_i}{N_{All}}$$

so that, with only one aircraft, the damage is:

$$d = \frac{N}{N_{All}}$$

Problems amounts to determine N_i so as to have $d_i=1$

$$N_{All} = 1 \times 10^4 \left(\frac{\varepsilon}{\varepsilon_4} \right)^{\frac{1}{b}}$$

Problem being linear, ε =129 μm/m.

Numerical application provides N= 3 500 passes.

Conclusions to part 3

This part has been dedicated to the experimental validation of the proposed numerical method. Three well-known pavements have been tested, one of them being instrumented. The validation has relied on the comparison between backcalculated and laboratory-determined material properties, and on the comparison between theoretically expected strains and gage measurements, when available.

First, the resonant-frequency dynamic method has been assessed in both shallow bedrock and infinite subgrade cases. Satisfactory results have been obtained in both cases.

Then, dynamical backcalculations performed for all test surveys have shown that good fittings are achieved, corresponding to low values of the objective function, with regard to the conclusions of the repeatability and sensitivity studies. However, the obtained errors remain higher than those reached with simulated data. This means that the model is not completely reliable for describing the physical test and can be improved. The experiment relative to the instrumented pavement has given a satisfactory correlation between calculated strains and gage measurements. Unfortunately, only one gage profile has been tested, so that this result needs to be confirmed by other experiments.

Comparison between backcalculated and laboratory-determined material properties has emphasized that the dynamical backcalculation provides better results than the pseudo-static one for deep layer moduli determination. Backcalculated values in the dynamical method are close to expected values. Netherveless, numerical moduli obtained for surface asphalt layers are significantly different from laboratory results, in both dynamic and pseudo-static methods. Additionally damping modelling is not a good approximation of the reality.

Finally, the use of HWD backcalculation results for pavement bearing capacity and residual life assessment has been thought about. No experimental validation is provided as no long term information was available in the frame of this work. Nevertheless the obtained results are reasonable according to the value range expected from initial design of pavements.

At this phase of the study, potential sources of errors envisaged for the backcalculation phase are:
- a too approximate damping modelling,
- the absence of visco-elastic modelling to describe the asphalt materials behaviour,
- the deviation of interfaces type from the fully-bonded case.

Future works will focus on these possible improvements. Further validation phase of the mechanical model is also to be continued, especially on instrumented pavements. A wide-scale validation will start in the near future, using the STAC's instrumented test facility.

Conclusions de la partie 3

Cette partie est dédiée à la validation expérimentale de la méthode numérique proposée. Trois chaussées connues ont été testées, dont l'une est instrumentée. La validation s'est appuyée sur la comparaison entre propriétés des matériaux identifiées par le biais du calcul inverse, et déterminées en laboratoire, ainsi que sur la comparaison des déformations relatives aux niveaux critiques de la chaussée prédites par le modèle, et mesurées par des jauges de déformation, dans le cas de la chaussée instrumentée.

D'abord, la méthode dynamique de détermination de la profondeur de substratum basée sur l'analyse de la fréquence de résonnance de la structure a été évaluée, dans les deux configurations extrêmes correspondant aux cas d'un substratum peu profond et d'un sol assimilable à un semi-espace infini. Les résultats sont satisfaisants dans les deux cas.

Ensuite, des calculs inverses dynamiques ont été menés pour chaque structure. Ils ont tous permis d'atteindre de très bons calages, c'est-à-dire de faibles valeurs de la fonction objective, selon le critère établi dans la partie précédente à partir des conclusions des études de répétabilité et sensibilité. Néanmoins, les erreurs finales restent supérieures à celles obtenues dans le cas de données simulées, ce qui signifie que le modèle ne reproduit pas tout à fait fidèlement le phénomène physique observé, et peut donc encore être amélioré. L'étude menée sur la chaussée instrumentée a permis d'élaborer un protocole expérimental précis, permettant l'analyse de la réponse d'un profile de jauges sous chargement HWD. L'expérience finale a montré des corrélations plutôt satisfaisantes entre valeurs théoriques et mesures sur jauges. Cependant, un seul profil de jauges a été étudié, et il convient de rééditer l'expérience sur d'autres chaussées instrumentées avant de pouvoir généraliser ces premiers résultats.

La comparaison entre propriétés des matériaux rétrocalculées et issues d'essais en laboratoire a montré que la méthode dynamique proposée présente de meilleurs résultats que la méthode pseudo-statique pour les couches profondes, les valeurs identifiées étant assez proches des valeurs attendues. Cependant, les valeurs de modules élastiques obtenues pour les couches de matériaux bitumineux sont significativement différentes des résultats en laboratoire, et ce aussi bien pour les méthodes pseudo-statique et dynamique, et il semble par ailleurs que la modélisation de l'amortissement doive être améliorée.

Finalement, une réflexion a été menée sur l'utilisation des résultats de calcul inverse du HWD pour déterminer la capacité portante de la chaussée ainsi que sa durée de vie résiduelle. Ce point n'a pas été validé expérimentalement, aucune donnée sur le comportement à long terme des chaussées étudiées n'étant disponible dans le cadre de la thèse. Néanmoins, les résultats obtenus sont raisonnables au vu des gammes de valeurs préconisées par le dimensionnement initial des chaussées.

Les sources d'erreur suivantes peuvent être soupçonnées à ce stade de l'étude, pour expliquer les écarts constatés, à l'issue de la phase de calcul inverse, avec les valeurs attendues :
- une modélisation trop approximative de l'amortissement,
- l'absence de modélisation viscoélastique pour la description du comportement des matériaux bitumineux,

- l'hypothèse systématiquement retenue d'interfaces parfaitement collées, peut-être pas toujours adaptée.

Les améliorations prioritaires du modèle correspondent donc aux précédents points. Elles s'appuieront sur la poursuite de la validation expérimentale, qui sera réalisée principalement sur chaussées instrumentées. Une expérimentation à grande échelle doit débuter dans les prochains mois, sur la planche instrumentée du STAC (située à Bonneuil, près de Paris).

General conclusion and planned improvements

This PhD work has been motivated by the acknowledgement that usual pseudo-static methods for HWD data analysis were unsatisfactory. Thus, the purpose of the thesis was to develop a dynamical data analysis method, sensed to be more appropriate to describe the observed physical phenomenon.

It was first necessary to take in hand the device, acquired by the STAC at the beginning of the PhD, and establish a related pavement evaluation procedure.

The thesis has focused on the development of a dynamical mechanical modelling and an associated backcalculation procedure. Nevertheless, lines of thought have also been provided for the later use of the backcalculation results in forward analyses, resulting in bearing capacity of the studied pavement and/or residual life calculation. No consensus exists for this second phase of HWD data analysis. A personal method has been proposed, to be assessed using a wide-scale field study including a steady test survey of selected trafficked airfield pavements coupled with visual inspections.

A first part has been dedicated to preliminary field data, which appeared to be necessary to assess the feasibility of dynamic methods developments, and to choose a consistent pavement modelling.

It has been demonstrated, from field measurements performed on a test facility, that repeatability of HWD measurements on a selected test point is very good. The comparison with scatter between results obtained on different test points has shown that the HWD enables to detect structural differences between several points. The experiment has also emphasized that variance values are not affected by the load level, so that it is assumed that the repeatability results can be enlarged. Experimental uncertainties obtained can be used, in the frame of calculation of precisions on identified parameters and choice of a consistent target error for automated backcalculation procedure.

Relative linearity of pavement response with applied load has also been demonstrated in the frame of this experiment.

Reliability of deflection signals has also been checked, from several experiments involving external instrumentation. Nevertheless, an error in time origins provided by the HWD has been highlighted. A misinterpretation of the observed time gap could lead to significantly biased results when performing dynamic backcalculations on time-related signals. It is envisaged in the light to these observations to duplicate the HWD acquisition chain with an external one, more reliable.

External instrumentation has also provided valuable extra data, such as 1- deflection measurements at long distances from load centre, which can be used to obtain more precise information about the subgrade, and propagation velocity measurements, or 2- large acquisition time frames, what has allowed confirming the occurrence of viscoelastic behaviours.

The second part has been dedicated to the mechanical modelling.

A dynamical time-domain modelling has been developed. It relies on a 2D axisymmetric finite element dynamical model implemented in the Cesar-LCPC FEM software. Using the knowledge gained from preliminary field studies, a multilayered isotropic elastic model with damping has been chosen. Load plate modelling is included in the mesh. The model takes into account the dynamical nature of the external stress. Three alternative versions of the model have been studied, which differ by the applied dynamical stress modelling. The first model considers the time-related load imparted to the pavement surface through the plate. In the second model, rubber buffers and the falling mass are included in the mesh. The velocity of the dropped mass at the time of impact is imposed. Third alternative version is based on shock theory.

An associated numerical backcalculation method has been developed, which consists in an iterative procedure using repeated links to the previous direct calculation. A related target mean squared error has been defined, in accordance with the coupled results of a numerical sensitivity study and the aforementioned experimental repeatability study. This sensitivity study has highlighted the importance of precision on data for input parameters such as layers depths, including depth to bedrock. The latter is determined from HWD results analysis, using a resonant frequency-based method, found in the literature.

A computer tool, called PREDIWARE, which allows automating both backcalculation and forward calculation phases for the force model has also been developed. It relies on the computer program Cesar, and on a regularized Gauss Newton algorithm. The robustness of the backcalculation using this algorithm has been demonstrated. It is much better than for the pseudo-static method. The only drawback of the dynamic method is the time-consuming calculation.

The last part has been dedicated to the field validation of the proposed numerical method. To this end, three well-known test facilities have been tested, one of them being instrumented.

Firstly, the resonant-frequency dynamic method has been assessed in both shallow bedrock and infinite subgrade cases. Satisfactory results have been obtained in both configurations.

Secondly, the backcalculation phase has been assessed.

It is first observed that the dynamical backcalculations performed for all test surveys show good fit to data, corresponding to low values of the objective function, with regard to the conclusions of the repeatability and sensitivity studies. However, the obtained errors remain higher than those reached with simulated data. This means that the model is not completely reliable for describing the physical test.

Then, the validation phase of the backcalculated values has been described. It relies on the comparison between backcalculated and laboratory-determined material properties, and on the comparison between theoretically expected strains and gage measurements, when available. This second comparison required the establishment of a specific experimental protocol for gage profiles assessment under HWD load. This protocol can be extended to the study of all instrumented test facilities.

The single experiment performed on the instrumented pavement gave a satisfactory correlation between calculated strains and gage measurements. Unfortunately, only one gage profile has been tested, so this result needs to be confirmed by other experiments.

The initial velocity model is not so far suitable for backcalculations.

Comparison between backcalculated and laboratory-determined material properties has emphasized that the both force model and shock theory-based one have shown interesting capabilities and provide better results than the usual pseudo-static method for deep layer moduli determination, backcalculated values in the dynamical method being close to expected values. Netherveless, numerical moduli obtained for surface asphalt layers are significantly different from laboratory results, in both dynamic and pseudo-static methods. Additionally, damping modelling is not a good approximation of the reality.

Thus, even though better than the pseudo-static method, the dynamic one fails as it is to represent faithfully the HWD test. The first thoughts to explain discrepancies observed between backcalculated and expected parameters have led to envisage the following improvements: 1- implementation of advanced behaviour laws for asphalt materials considering a time-dependent modulus. LCPC advanced research, based on the use of the Huet and Sayegh model, is in progress. The latter allows determining the evolution of the secant elastic moduli according to the applied stress path; 2- improvement in the damping modelling, 3 – a better modelling of interfaces, if required. A more thorough examination of the influence of their bonding on HWD results will be performed to address this question.

The validation of the next developments will rely on the STAC's instrumented test facility (located in Bonneuil-sur-Marne, near Paris, France). Test campaigns are expected in spring 2010.

In parallel, the reduction of execution times for the backcalculation phase will be pursued. Development of a method relying on the self-adjoints theory is in progress, which would allow performing at each calculation step only 2 direct calculations instead of $n+1$. Note that the value of this method will be strengthened further with the increase in the number of model parameters due to the introduction of viscoelastic modelling or layered damping.

Conclusion générale et perspectives

Ce travail de thèse a été motivé par le constat que les méthodes usuelles (pseudo-statiques) d'exploitation des essais HWD ne sont pas satisfaisantes. Le but du travail était donc de développer une méthode d'analyse dynamique, à même de mieux décrire le phénomène physique observé.

Un premier travail amont a consisté à prendre en main l'appareil, acquis par le STAC en début de thèse, et d'établir une procédure d'auscultation des chaussées.

La thèse s'est concentrée sur le développement d'un modèle mécanique dynamique, et d'une procédure de calcul inverse associée. Néanmoins, des réflexions ont aussi été menées sur l'exploitation ultérieure des données de calcul inverse, aboutissant à la détermination d'une durée de vie résiduelle de la chaussée et/ou à une durée de vie résiduelle. Il n'existe aujourd'hui pas de consensus pour cette seconde phase d'analyse. Une méthode personnelle est proposée, qui devra être évaluée dans le cadre d'un suivi régulier de pistes trafiquées sélectionnées, couplé avec des relevés de dégradation.

La première partie a été dédiée aux études préliminaires, nécessaires pour évaluer la faisabilité du développement d'une méthode dynamique, et pour choisir de manière cohérente le modèle mécanique.

Il a été démontré, à l'aide d'essais réalisés sur une planche expérimentale, que la répétabilité des essais sur un même point est très bonne. La comparaison avec les résultats de dispersion sur plusieurs points d'essais a montré que le HWD permet de détecter des différences structurelles sur une même structure. Il ressort de l'expérience que les variances obtenues ne sont pas affectées par le niveau de chargement, si bien que l'on peut supposer que les données de répétabilité observées peuvent être généralisées. Les incertitudes expérimentales obtenues peuvent être utilisées pour le calcul des précisions atteignables sur les paramètres identifiés, et pour le choix d'une erreur cible cohérente dans la procédure de calcul inverse.

La relative linéarité de la réponse de la chaussée en fonction du niveau de chargement a aussi été démontrée dans le cadre de cette expérimentation.

La fiabilité des signaux de déflexion fournis par le HWD a aussi été vérifiée, à l'aide de plusieurs expériences ayant nécessité la mise en place d'une instrumentation externe. Néanmoins, une erreur dans l'origine des temps fournis par le HWD a été mise en évidence. Une mauvaise interprétation du décalage observé pourrait conduire à des résultats significativement biaisés lorsque des calages dynamiques des signaux temporels sont réalisés. Il est donc envisagé, à la lumière de ces observations, de doubler le système d'acquisition du HWD par une chaîne d'acquisition externe, plus fiable.

L'instrumentation externe a aussi fourni des données intéressantes telles que 1 - des mesures de déflexion à des distances plus éloignées du centre de chargement que les emplacements classiques, qui fournissent des informations plus précises sur le sol support, et les vitesses de

propagation des signaux, ou 2 - des temps d'acquisition plus larges, qui ont permis de confirmer l'existence de comportements viscoélastiques.

La seconde partie a porté sur le modèle mécanique.

Une modélisation dynamique dans le domaine temporel a été développée. Elle repose sur un modèle aux éléments finis 2D axisymétrique faisant appel au code Cesar-LCPC. Conformément aux enseignements des études préliminaires, un modèle multicouche linéaire élastique a été choisi. La plaque de chargement est incluse dans le maillage. Le modèle prend en compte la nature dynamique de la sollicitation appliquée. Trois versions du modèle ont été étudiées, qui se distinguent par la modélisation de la sollicitation. Le premier modèle permet d'appliquer l'effort temporel réel sur le plaque de chargement. Dans le second modèle, les tampons amortisseurs et la masse tombante sont intégrés au maillage ; la sollicitation extérieure est la vitesse initiale de la masse. La troisième version est basée sur la théorie des chocs.

Une méthode associée de calcul inverse a été développée, qui consiste en une procédure itérative impliquant des appels répétés à la phase de calcul direct précédente. Une erreur cible des moindres carrés a été définie, en liaison avec les résultats d'une étude de sensibilité théorique et les répétabilités expérimentales mentionnées plus haut. Cette étude de sensibilité a souligné l'importance de la précision sur des paramètres d'entrée tels que les épaisseurs des couches ou la profondeur de substratum. Cette dernière est déterminée à l'aide d'une analyse dynamique des résultats HWD proposée dans la littérature, faisant appel à la fréquence de résonnance de la structure.

Un outil informatique permettant d'automatiser aussi bien les phases de calcul inverse que direct a été développé. Il repose sur Cesar et un algorithme de Gauss Newton régularisé. La robustesse de la procédure de calcul inverse a été démontrée. Elle est bien meilleure que pour la méthode pseudo-statique. Le seul défaut de la méthode dynamique réside dans les temps de calculs élevés.

La dernière partie s'intéresse à la validation expérimentale de la méthode numérique proposée. Trois chaussées expérimentales ont été utilisées, dont l'une est instrumentée.

Dans un premier temps, la méthode dynamique d'évaluation de la profondeur de substratum a été testée dans les cas d'un substratum peu profond et d'un sol d'étendue infinie. Les résultats sont satisfaisants dans les deux cas.

Dans un second temps la cohérence des résultats de la phase de calcul inverse a été testée.

Il est apparu que les calculs inverses dynamiques réalisés sur chacune des structures étudiées conduisent à de très bons calages, correspondants à des valeurs faibles de la fonction objective finale, au regard des conclusions des études de repétabilité expérimentale et de sensibilité théorique. Cependant les valeurs restent plus élevées que dans le cas de calculs inverses réalisés sur données simulées, ce qui signifie que le modèle mécanique n'est pas tout à fait fidèle à la réalité physique de l'essai.

La phase de validation des valeurs rétrocalculées a ensuite été décrite. Elle s'est appuyée d'une part sur la comparaison entre valeurs rétrocalculées et issues d'essais en laboratoires, et d'autre part sur celle entre contraintes théoriquement attendues et résultats de jauges

extensométriques, lorsque la chaussée est instrumentée. Cette dernière comparaison a nécessité la mise en place d'un protocole expérimental spécifique à l'étude des profils de jauge sous chargement HWD qui peut être étendu à l'étude de toute chaussée instrumentée.

L'expérience menée sur la chaussée instrumentée a montré une correlation plutôt satisfaisante entre déformations relatives calculées et mesurées par les jauges. Malheureusement, un seul profil a été testé, si bien que les résultats doivent être confirmés par d'autres expériences.

La modélisation avec vitesse initiale n'est pas opérationnelle pour le moment pour la phase de calcul inverse.

La comparaison entre paramètres rétrocalculés et identifiés à l'aide d'essais en laboratoire a montré que le modèle mécanique dynamique (aussi bien dans la version comportant comme paramètre d'entrée l'effort appliqué que dans celle faisant appel à la théorie des chocs) offre des perspectives intéressantes et procure des résultats meilleurs que la méthode pseudo-statique pour les modules des couches profondes. Néanmoins, les modules rétrocalculés pour les couches de surface sont significativement différent des résultats en laboratoire, et ce aussi bien pour les méthodes dynamiques que pour la méthode pseudo-statique. De plus la modélisation de l'amortissement semble être à améliorer.

Ainsi, bien que meilleure que la méthode pseudo-statique, la méthode dynamique ne représente pas fidèlement en l'état l'essai HWD. Les premières pistes d'explications pour expliquer les différences observées entre paramètres attendus et rétrocalculés ont conduit à envisager les améliorations suivantes : 1- introduction de lois de comportement avancées pour les matériaux bitumineux, permettant de prendre en compte un module dépendant du temps. Des recherches sont en cours au LCPC, basées sur l'utilisation d'un modèle de Huet et Sayegh, qui permettent de déterminer l'évolution du module élastique sécant en fonction du chemin de contrainte appliqué ; 2- une amélioration de la prise en compte de l'amortissement ; 3- une meilleure modélisation des interfaces, si cela apparaît nécessaire. Une étude plus précise de l'influence du collage sous essai HWD sera réalisée pour répondre à cette question.

La validation de ces prochains développements reposera sur les résultats expérimentaux issus de la planche d'essais du STAC (située à Bonneuil-sur-Marne, près de Paris, France). Le début de la campagne d'essais est prévu au printemps 2010.

En parallèle, la méthode des états auto-adjoints, en cours de développement, sera introduite dans la procédure de calcul inverse afin de réduire significativement les temps de calculs (passage de *2* à *n+1* calculs directs par itération). Cette méthode apparaît d'autant plus intéressante que le nombre de paramètres actuels du modèle est amené à augmenter avec l'introduction de modèles viscoélastiques, ou bien d'amortissement par couche.

References

[Abraham et al., 1997] ABRAHAM O., BLANCHARD D. and HEVIN G. "Exemples d'utilisation des ondes de surface pour la reconnaissance d'objets du génie civil" *Proc., Colloque GEOFCAN, Bondy, France, sept 1997*.

[Alize] Alize LCPC's pavement rational design software;

.

[Al Khoury et al., 2001] AL KHOURY R., SCARPAS A., KASTERGEN C., and BLAAUWENDRAAD J., "Spectral element technique for efficient parameter identification of layered media. I.Forward calculation", *International Journal of Solids and Structures 38*, 2001, pp.1605-1623.

[Al Khoury et al., 2001b] AL KHOURY R., SCARPAS A., KASTERGEN C., and BLAAUWENDRAAD J., "Spectral element technique for efficient parameter identification of layered media. Part II.Inverse calculation", *International Journal of Solids and Structures 38*, 2001, pp.8753-8772.

[Al Khoury et al., 2002] AL KHOURY R., SCARPAS A., KASTERGEN C., and BLAAUWENDRAAD J., "Spectral element technique for efficient parameter identification of layered media. Part III.viscoelastic aspects", *International Journal of Solids and Structures 39*, 2002, pp.2189-2201.

[Al Khoury et al.,, 2002b] AL KHOURY R., SCARPAS A., KASTERGEN C., and BLAAUWENDRAAD J., "Dynamic Interpretation of Falling Weight Deflectometer Test Results, Spectral Elements Method", *Transportation Research Record 1869*, 2002, pp. 49-54.

[Andren and Lenngren, 2000] ANDREN P. and LENNGREN C.A. "Evaluating pavement layer properties with a high-speed rolling deflectometer", *Nondestructive evaluation of aging aircraft, airports, and aerospace hardware. Conference n°4, Newport Beach CA, USA, SPIE proceedings series*, 2000, pp. 192-200.

[Aouad et al., 2000] Aouad M.F., Stokoe II K.H. and Joh S.H. "Estimating subgrade stiffness and bedrock depth. Combined Falling Weight Deflectometer and Simplified Spectral Analysis of Surface Waves Measurements", *Transportation Research Record 1716*, 2000.

[ASTM] ASTM, "Standard Test Methods for Modulus and Damping of Soils by Resonant-Column" ASTM standard D 4015-07.

[Autret, 1969] AUTRET P. "Utilisation du produit Rd pour l'auscultation des chaussées à couche de base traitée", *Bulletin de liaison des laboratoires des Ponts et Chaussées*, n°42, décembre 1969.

[Balay et al., 2008] BALAY J.M., CARON C., and LERAT P., "A rational design method for airfield pavements: the French Alizé-Airfield pavement software", *European Road Review n°13,* Fall 2008, pp. 4-15.

[Barksdale, 1971] BARKSDALE R.D. "Compressive stress pulse time in flexible pavement for use in dynamic testing", Highway Research Record n°345, 1971.

[Bay and Stokoe, 1998] BAY J.A. and STOKOE K.H. "Development of a rolling dynamic deflectometer for continuous deflection testing of pavements", project summary report 1422-3F, Center for Transportation Research, Bureau of engineering research; the university of Texas at Austin, May 1998.

[Benoist and Schaeffner, 1982] BENOIST J. and SCHAEFFNER M. (1982) "La Dynaplaque" - *Bulletin de liaison des laboratoires des Ponts et Chaussées n°122, nov.-déc. 1982.*

[BL, 1968] Bulletin de liaison des laboratoires routiers - spécial J, juillet 1968. "*Utilisation du vibreur Goodman en auscultation des chaussées*". LCPC - 58, bd Lefèbvre, 75015 Paris (France), 187 pp.

[Boddapati and Nazarian, 1994] BODDAPATI K.M., and NAZARIAN S., "Effects of Pavement-Falling Weight Deflectometer Interaction on Measured Pavement Response", *Nondestructive Testing of Pavements and Backcalculation of Moduli, Second Volume, ASTM SPT 1198, Harold L. Von Quintus, Albert J.Bush, III, and Gilbert Y. Baladi, Eds., American Society for Testing and Materials, Philadelphie,* 1994, pp. 326-340.

[Bodin, 2002] BODIN D. "Modèle d'endommagement cyclique : Application à la fatigue des enrobés bitumineux" PhD thesis, Ecole centrale Nante, France, 2002.

[Bodin et al., 2004] BODIN D., PIJAUDIER-CABOT G , DE LA ROCHE C. , PIAU J.M. and CHABOT A. "Continuum dapage approach to asphalt concrete fatigue modeling", *Journal of engineering mechanics*, june 2004.

[Bretonnière, 1963] BRETONNIERE S. " Etude d'un déflectomètre à boulet" - *Bulletin de liaison des laboratoires des Ponts et Chaussées n°2, 1963.*

[Briggs et al., 1999] BRIGGS R.C, JOHNSON R.F., STUBSTAD R.N. and PIERCE L. "A comparison of the Rolling Weight Deflectometer with the Falling Weight Deflectometer" *Nondestructive Testing of Pavement and Backcalculation of moduli: third volume, ASTM STP 1375, S.D. Tayabji and E.O.Lukanen, Eds, American Society for Testing and Materials, West Conshohocken, PA*, 1999.

[Broutin et al., 2008] BROUTIN M., CARON C., and DEFFIEUX J.C., "Dynamic versus static testing of airfield pavements: a full-scale experiment in France", *European Road Review n°13,* Fall 2008, pp. 17-25.

[Broutin and Dimnet, 2009] BROUTIN M. and DIMNET E. "A new dynamic analysis of HWD results using collision theory" *Proc., 88th annual meeting of Transportation Research Board, Washington D. C., January 2009.*

[Broutin, 2009b] BROUTIN M. "Towards dynamical methods for HWD data analysis; a FEM model proposal" *Proc., 2nd European Airport Pavement Workshop, Amsterdam, May 2009*.

[Broutin, 2010] BROUTIN M. "Heavy Weight Deflectometer for airport pavement testing" *Comptes rendus de l'Académie des Sciences,* submitted.

[Broutin and Theillout, 2010b] BROUTIN M. and THEILLOUT J.N. "Towards a dynamical back-calculation procedure for HWD; A full-scale validation experiment" *Proc., FAA Technology Transfer Conference, Atlantic City, April 2010.*

[Broutin, 2010c] BROUTIN M. "A new dynamic analysis of HWD results using collision theory", *Annals of Solid and Structural Mechanics*, submitted.

[Broutin et al., 2010d] BROUTIN M., CARON C. and LERAT P., "Behaviour of flexible structures under heavy dynamic loads", *International Journal of Road Materials and Pavement Design,* submitted.

[Burmister, 1943] BURMISTER D.M "The theory of stresses and displacements in layered systems and applications to the design of airport runways" *Proc., Highway Research Board, Vol.23, 1943*.

[Caron et al., 2010] CARON C., THEILLOUT J.N. and BRILL D., "Comparison of US and French rational procedures for the design of flexible airfield pavements", *Proc., FAA Technology Transfer Conference, Atlantic City, April 2010.*

[Chailleux, 2007] CHAILLEUX E., "Directions for use of the visco-analyse software" Laboratoire Central des Ponts et Chaussées, 2007. (Software and directions for use available at).

[Chassaing et al., 1995] CHASSAING P., CORTE J.F., FROUMENTIN M. and SCHAEFFNER M. (1995) "La Dynaplaque 2. Etude d'un nouveau matériel" - *Bulletin de liaison des laboratoires des Ponts et Chaussées*, n°195, jan.-fév. 1995.

[Chatti et al., 2004] CHATTI K., JI Y., and HARICHANDRAN R.S., "Dynamic Time Domain Backcalculation of Layer Moduli, Damping and Thicknesses in Flexible Pavements", *Transportation Research Record 1869*, 2004, pp. 106-116.

[Chatti et al., 2006] CHATTI K., JI Y., and HARICHANDRAN R.S., "Dynamic backcalculation of pavement layer parameters using frequency and time domain methods" *Proc., 10th International Conference on Asphalt Pavements, Québec City, Canada, August 2006*.

[Chen et al., 2008] CHEN D.H., NAM B. H. and STOKOE II K.H., "Application of the rolling dynamic deflectometer to forensic studies and pavement rehabilitation projects" *Proc., 87th annual meeting of Transportation Research Board, Washington D. C. , January 2008*.

[Collop and Cebon, 1996] COLLOP A.C and CEBON D. "Stiffness reductions of flexible pavements due to cumulative fatigue damage", *Journal of transportation engineering* 1996, vol. 122, n°2, pp. 131-139.

[COST, 1999] COST 336, "Falling Weight Deflectometer", *Final report of the 1996 COST Action 336,* 1999.

[de Boissoudy et al., 1984] DE BOISSOUDY A., GRAMSAMMER J.C., KERYELL P. and PAILLARD M. "Le déflectographe 04", *Bulletin de liaison des laboratoires des Ponts et Chaussées,* n°129, jan.-fév. 1984, pp. 81-98.

[de Jong et al., 1973] DE JONG D. L., PEUTZ M.G.F and KORSWAGEN A.R. "Computer program BISAR", *External Report, Koninklijkel/Shell laboratorium, Amsterdam, Netherlands*, 1973.

[de la Roche, 1996] DE LA ROCHE C. "Module de rigidité et comportement en fatigue des enrobés bitumineux, expérimentations et nouvelles perspectives d'analyse" PhD thesis, Ecole Centrale Paris, France, 1996.

[Dérobert et al., 2001] DEROBERT X., FAUCHARD C., COTE P. and GUILLANTON E. "Performances de radars d'auscultation des chaussées sur des sites tests", *Bulletin de liaison des laboratoires des Ponts et Chaussées n°230, jan.-fév. 2001*.

[Dimnet, 2002] DIMNET E. "Mouvements et collisions de solides rigides ou déformables" PhD thesis, Ecole Nationale des Ponts et Chaussées, France, 2002.

[Domec, 2005] DOMEC V. "Endommagement par fatigue des enrobes bitumineux en condition de traffic simulé et de temperature" PhD thesis, Université Bordeaux I, France, 2005.

[Dong et al., 2002] DONG Q.X., HACHIYA Y., TAKAHASHI O., TSUBOKAWA Y. and MATSUI K. "An efficient backcalculation algorithm of time domain for large-scale pavement structures using Ritz vectors" *Finite Elements in Analysis and Design,* n°38, 2002, pp. 1131–1150.

[El Abd, 2006] EL ABD A. "Développement d'une méthode de prédiction des déformations de surface des chaussées à assises non traitées" PhD thesis, Université de Bordeaux 1, 2006.

[Fabre et al., 2005] FABRE C., BALAY J.-M., MAZARS A. and GUEDON D. "Chaussées pour avions gros porteurs. Les programmes expérimentaux sur piste Airbus A380" ; *Revue Générale des Routes et Aérodromes*, n°840, juin 2005.

[Florence, 2005] FLORENCE C. "Etude expérimentale de la fissuration réflective et modélisation de la résistance des structures cellulaires" PhD thesis, Ecole Nationale des Ponts et Chaussées, France, 2005.

[Foinquinos Mera, 1995] FOINQUINOS MERA R., "Dynamic Nondestructive Testing of Pavements", Geotechnical Engineering Report GR95-4, Geotechnical Engineering Center, University of Texas at Austin, Austin, Texas, 1995.

[Forestier, 2004] FORESTIER R. "Développement d'une méthode d'identification de paramètres par analyse inverse couplée ave un modèle éléments finis 3D" PhD thesis, Ecole Nationale Supérieure des Mines de Paris, France, 2004.

[FORMAT, 2005] FORMAT, final technical report, March 2005, WP6:

- French report: SIMONIN J.M. "Assessment of the Road Deflection Tester in France", Technical report, Laboratoire Central des Ponts et Chaussées,

- English report: JORDAN P. and FEVRE P. "Evaluation of high-speed deflection measurements by the Swedish Road Deflection Tester (RDT)", TRL.

[Frémond, 1983] FREMOND M. "Méthodes variationnelles en calcul des structures" - *Course given at the Ecole Nationale des Ponts et Chaussées (France), 1983*.

[Frémond, 2007] FRÉMOND M. "Collisions"; Edizioni del Dipartimento di Ingegneria Civile dell'Università di Roma Tor Vergata, ISBN 978-88-6296-000-7, 2007.

[Fwa et al., 1997] FWA T. F., TAN C. Y. and CHAN W. T., "Backcalculation analysis of pavement-layer moduli using genetic algorithms", *Transportation Research Record n°1570*, 1997, pp.134-142.

[Gopalakrishnan et al., 2007] GOPALAKRISHNAN K., YHOMPSON M.R. and MANIK A. "Rapid Finite-Element Based Airport Pavement Moduli Solutions using Neural Networks", *International Journal of computational Intelligence*, Vol. 3 Number 1 , 2007.

[Green and Hall, 1975] GREEN J.L. and HALL J.W. "Nondestructive vibratory testing of airport pavements", Vol.1 -*Evaluation Methodology and Experimental Test Results*, Sept 1975, Final Report.

[Grenier, 2007] GRENIER, S. "Analyse dynamique du déflectomètre à masse tombante" PhD thesis, 2007, Université Laval, Québec.

[Heck et al., 1998] HECK J.V., PIAU J.M., GRAMSAMMER J.C., KERZREHO J.P. and ODEON H. "Thermo-visco-elastic modelling of pavements behaviour and comparison with experimental data from LCPC test track" *Proc., 5th BCRA, Trondheim, Norway, 6–8 July 1998*.

[Herr et al., 1995] HERR W.J., HALL J.W JR, WHITE T.D and JOHNSON W. "Continuous Deflection Basin Measurement and Backcalculation Under a Rolling Wheel Load Using Scanning Laser Technology" *Proc., Transportation Congress, San Diego, California, October 22-26, 1995*.

[Hildebrand, 2002] HILDEBRAND G., "Verification of Flexible Pavement Response from a Field Test", *Danish Road Institute,* report n° 121, 2002.

[Hildebrand and Rasmussen, 2002b] HILDEBRAND G. and RASMUSSEN S. "Development of a High Speed Deflectograph", Danish Road Institute, Report 117, Road Directorate, Ministry of Transport, Danemark, 2002.

[Homsi et al., 2010] HOMSI F., BODIN D., BALAY J.M., YOTTE S. and BREYSSE D., "Multiple axle loading effect on fatigue damage of asphalt mixes: a statistical analysis of field and laboratory data", *Proc., International Conference on Accelerated Life Testing, Reliability-based Analysis and Design, Clermont-Ferrand, France, 19-21 May 2010*.

[Horak and Emery, 2009] HORAK E. and EMERY S. "Evaluation of airport pavements with FWD deflection bowl parameter benchmarking methodology", *Proc., 2nd European Airport Pavement Workshop, Amsterdam, May 2009*.

[HoSang, 1975] HOSANG V.A. "Field survey and analysis of aircraft distribution on airport pavements", U.S. Department of Transportation, Federal Aviation Administration, Report n° FAA-RD-74-36, February 1975.

[Humbert et al., 2005] HUMBERT P., FEZANS G., DUBOUCHET A.and REMAUD D. (2005). "CESAR-LCPC : A computation software package dedicated to civil engineering uses", *Bulletin des Laboratoires des Ponts et Chaussées*, n°256-257, 2005, pp. 7-37.

[Inoue and Matsui, 1990] INOUE T., and MATSUI K., "Structural analysis of asphalt pavement by FWD and backcalculation of elastic layered model" *Proc., 3rd International Conference on Bearing Capacity of Roads and Airfields, Vol.1, Trondheim, 1990.*

[Irwin, 2002] IRWIN L.H. "Backcalculation: An Overview and Perspective", *Proc., FWD User's Group Meeting , 2002*.

[ITAC, 1999] I.T.A.C (Instruction Technique sur les Aérodromes Civils), Chapitre 7 : Suivi et auscultation des chaussées aéronautiques – DGAC/STBA, 1999.

[Kim, 1997] KIM J.R."Dynamic Analysis of Falling Weight Deflectometer (FWD) tests on airfield pavements", *Proc., Airfield Pavement Conference, Seattle, August 1997*.

[Kim and Munb, 2008] KIM J.M. and MUNB S., "Fast spectral analysis of an axisymmetric layered structure", *Mechanics Research Communications* n°35, 2008, pp.222–228.

[Kruse and Skok, 1968] KRUSE C.G. and SKOK E.L. "Flexible pavement evaluation with Benkelman beam", technical report , Department of Highways, State of Minnesota, 1968.

[Kurtulus, 2006] KURTULUS A. "Field measurements of the linear and nonlinear shear moduli of soils using drilled shafts as dynamic cylindrical sources", PhD thesis, The University of Texas at Austin, 2006.

[Lacroix, 1963] LACROIX J. "Déflectographe pour l'auscultation rapide des chaussées", *Bulletin de liaison des laboratoires des Ponts et Chaussées,* n°3, septembre-octobre 1963.

[Lepert et al., 1997] Lepert P. Aussedat G. and Simonin J.M. "Evaluation du curviamètre MT15"; Laboratoire Central des Ponts et Chaussées; *Bulletin de liaison des laboratoires des Ponts et Chaussées,* n°209, mai-juin 1997.

[LCPC – SETRA, 1997] French design manual for pavement structures, Technical Guide, LCPC – SETRA Edition, May 1997.

[LCPC's Accelerated Load Testing Facility]

[Lefeuvre, 2001] LEFEUVRE Y. "Contribution à l'étude du comportement en fatigue des enrobés bitumineux. Etude de l'allongement des éprouvettes comme manifestation de l'endommagement diffus. Expérimentation – modélisation", PhD thesis, Ecole Nationale des Ponts et Chaussées, France, 2001.

[Liu et al., 2001] LIU X., SCARPAS A. and BLAAUWENDRAAD J. "Finite Element Investigation of Saturated Subgrade on FWD Testing", *Proc., 80th annual meeting of Transportation Research Board, Washington D. C., 2001*.

[LTPP, 2000] LUKANEN E.O., STUBSTAD R. and BRIGGS R. "Temperature predictions and adjustment factors for asphalt pavement", US Department of Transportation, Federal Highway Administration, Long Term Pavement Performance program, june 2000.

[Matlab] Matlab optimization toolbox, by Hansen P.C.

[Meier, 1995] MEIER R.W. "Backcalculation of flexible pavement moduli from Falling Weight Deflectometer data using Artificial Neural Network", US Army Corps of Engineers, Waterways Experiment Station, Technical Report GL-95-3 April 1995.

[Merbouh et al., 2007] MERBOUH M., BREYSSE D., MORICEAU L. and LARADI N. "comportement en fatigue des enrobés de chaussées aéronautiques sous actions de grande intensité", *Proc., 25e rencontres de l'AUGC, 23-25 mai 2007, Bordeaux*.

[Moreau, 1966] MOREAU J.J. "Fonctionnelles convexes" , *Seminar on partial differential equations – Collège de France, Paris, 1966*.

[Muzet et al., 2009] MUZET V., HEINKELE C., GUILLARD Y. and SIMONIN J.M., "Surface deflection measurement using structured light", *Proc., Non-destructive Testing in Civil Engineering 2009 meeting, Nantes, France, July 2009*.

[Nazarian et al., 1993] NAZARIAN S. BAKER M. R. and CRAIN K. "Development and Testing of a Seismic Pavement Analyzer", Strategic Highway Research Program SHRP-H-375 National Research Council, Washington, DC 1993.

[Nguyen, 2008] NGUYEN H.T. "Auscultation des chaussées aéronautiques au déflectomètre à masse tombante. Mise au point d'une méthode d'identification des caractéristiques mécaniques des différentes couches de chaussée" Master's degree final report, june 2008.

[Paquet, 1977] PAQUET J. "Un nouvel appareil d'auscultation des chaussées: le Curviamètre", *Revue Générale des Routes et Aérodromes*, n°530, avril 1977.

[Park and Kim, 2003] PARK H.M and KIM Y.R. "Prediction of remaining life of asphalt pavement using FWD multiload level deflections", *Proc., 82th annual meeting of Transportation Research Board, Washington D. C., 2003*.

[Piau, 1989] PIAU J.M. "Thermomechanical modelling of the behaviour of bituminous mixes", *Bulletin de Liaison du Laboratoire Central des Ponts et Chaussées*, vol.163, septembre-octobre1989, pp. 41-55.

[Point, 2009] POINT N. "Méthode d'optimisation pour l'identification des caractéristiques de chaussées aéronautiques à partir d'essais au déflectomètre à masse tombante" Master's degree final report, february 2009.

[Puech et al., 2004] PUECH A., RIVOALLAN X. and CHEREL L. "The use of surface waves in the characterization of seabed sediments: development of a MASW system for offshore applications", *Seatech week, Brest "Caractérisation in situ des fonds marins" symposium, 2004*.

[Rasmussen et al., 2002] RASMUSSEN S., KRARUP J. and HILDEBRAND G. "Non-contact Deflection Measurement at High Speed", in Bearing Capacity of Roads, Railways and Airfields, Correia & Branco (eds), 2002.

[Rasmussen et al., 2008] RASMUSSEN S. AAGAARD L. BALTZER S. and KRARUP J. "A comparison of two years of network level measurements with the Traffic Speed Deflectometer", *Proc., Transport Research Arena Europe, Ljubljana, 2008*.

[Richart et al., 1970] RICHART, F.E., HALL, J.R. and WOODS, R.D. (1970) "Vibrations of Soils and Foundations", Englewood Cliffs, New Jersey, Prentice Hall, 414 pp.

[Roesset et al., 1990] ROESSET J.M., CHANG D.W, STOKOE II K.H. and AOUAD M. "Modulus and Thickness of the Pavement Surface Layer from SASW Tests", *Transportation Research Record 1260*.,1990.

[Romanoschi and Metcalf, 2002] ROMANOSCHI S.A. and METCALF J.B. "Errors in pavement layer moduli backcalculation due to improper modeling of the layer interface condition" *Proc., 82th annual meeting of Transportation Research Board, Washington D. C., 2003*.

[Samaris, 2006] Sustainable and Advanced Materials for Road Infrastructure - *5th European Framework Research Programme, initiated by the Forum of Europe's National Road Research Centres*, December 2002 to March 2006. Web site .

[Semblat, 1998] SEMBLAT J.F. "Amortissement et dispersion des ondes : points de vue physique et numérique", *Revue Française de Génie Civil*, Vol 2, n°1/1998, pp. 91-111.

[Semblat, 1997] SEMBLAT J.F."Rheological interpretation of Rayleigh damping", *Journal of Sound and Vibration*, 206(5), 1997, pp. 741-744.

[Semblat, 2009] SEMBLAT J.F. and Pecker A. Waves and Vibrations in Soils: Earthquakes, Traffic, Shocks, Construction works, IUSS Press, 500 pp. ISBN: 88-6198-030-3 2009.

[Simonin, 2005] SIMONIN J.M. "Contribution à l'étude de l'auscultation des chaussées par méthode d'impact mécanique pour la détection et la caractérisation des défauts d'interface", PhD thesis, 2005. Insa de Rennes, France.

[Simonin et al., 2006] SIMONIN J.M., HILDEBRAND G., and LELIEVRE D. "Evaluation d'un prototype Danois du déflectographe à grande vitesse (HSD) ", *Bulletin de liaison des laboratoires des Ponts et Chaussées*, n°260, janvier- février-mars 2006, pp. 3-11.

[Simonin et al., 2009] SIMONIN J.M., COTTINEAU L.M., MUZET V., HEINKELE C. and GUILLARD Y. "Deflection measurement : the need of a continuous and full view approach", *Proc., Bearing Capacity of Roads, Railways and Airfields 2009 meeting, Chaimpaign Illinois, USA, June 2009*.

[Stokoe et al., 2004] STOKOE, K.H., JOH, S.H.and WOODS, R.D. (2004) "The contribution of in situ geophysical measurements to solving geotechnical engineering problems", *Proc., 2nd International Conference on Site Characterization, ISC'2 , Porto, 19-22 September 2004*.

[Ullidtz, 1987] ULLIDTZ P., *Pavement analysis*, Amsterdam, Elsevier, 1987.

[Ullidtz, 1999] ULLIDTZ P., "Deterioration models for managing flexible pavements", *Transportation Research Record,* n°1655, 1999, pp. 31-34.

[Ullidtz, 2005] ULLIDTZ P., "Simple model for pavement damage", *Transportation Research Record,* n°1905, 2005, pp.128-137.

[Ullidtz et al., 2008] ULLIDTZ P., HARVEY J., GHUZLAN K, TSAI B.W. STEVEN B. and MONISMITH C. "Calibration of mechanistic-empirical models for cracking and rutting of new pavements using Heavy Vehicle Simulator tests", *Journal, Association of Asphalt Paving Technology*, 2008, Vol 77, pp. 591-630.

[Van Cauwelaert and White, 1988] VAN CAUWELAERT A. and WHITE B. "Multilayer elastic program for Backcalculating Layer Moduli in Pavement Evaluation", *Nondestructive Testing of Pavements and Backcalculation Moduli. Bush III and Baladi Editors. STP 1026. ASTM, Philadelphia, PA*.

[Vialletel and Simonin, 1997] VIALLETEL H. and SIMONIN J.M. "Le Déflectographe Flash", *Bulletin de liaison des laboratoires des Ponts et Chaussées n°208,mars.-avr. 1997*.

[Weiss, 1975] WEISS R.A. "Nondestructive vibratory testing of airport pavements", Volume 2 – *Theoretical Study of the Dynamic Stiffness and Its Application to the Vibratory Nondestructive Method of Testing Pavements* , April 1975, Final Report.

[Yang and Bin, 2009] YANG Z. and BIN T. "New Analytical Method for Response of Flexible Pavement", Road materials and pavement design, Vol.10 n°2, pp387-397, 2009.

[Yuan and Nazarian, 1993] YUAN D. and NAZARIAN S. "Automated surface wave method: Inversion technique" *Journal of geotechnical engineering*, vol. 119, pp. 1112-1126, 1993.

[Yuan et al., 1998] YUAN D. NAZARIAN S. CHEN D.H. and HUGO F. "Use of seismic pavement analyzer to monitor degradation of flexible pavements under Texas mobile load simulator", *Transportation Research Record,* n° 1615, 1998.

[Zube and Forsyth, 1966] ZUBE, E. and FORSYTH, R. (1966), "Flexible Pavement Maintenance Requirements as Determined by Deflection Measurement" *Transportation Research Record* n° 129, 1966, pp. 60-75.

Appendices

Appendix 1

Experimental data and HWD protocol

Appendix 1.1
Characteristics of the studied structures

1.1.1 S_1 structure: STAC's Bonneuil 1995 test facility

This structure was constructed in1995 to assess the in-situ properties of new asphalt materials. It has been destructed since then.

- Structure (« CCTP profile » i.e. according to the specifications of the Construction Contract)

The studied structure is a conventional airport structure made up of surface Asphalt Concrete (AC_1), base Asphalt Concrete (AC_2), humidified Untreated Graded Aggregate (UGA)[2], and subgrade (S).
AC_1 and AC_2 were either usual aeronautical asphalt materials or high stiffness materials, so that the combination of these 4 materials led to a facility subdivided into 4 sections.
The UGA has been laid down in two layers. The depth to bedrock, experimentally measured (see infra) is greater than 10 m.
The layer thicknesses are assumed to conform to the requirements of the construction contract (Figure 1). Each test section is supposed to be homogeneous in terms of layer thickness and material properties.

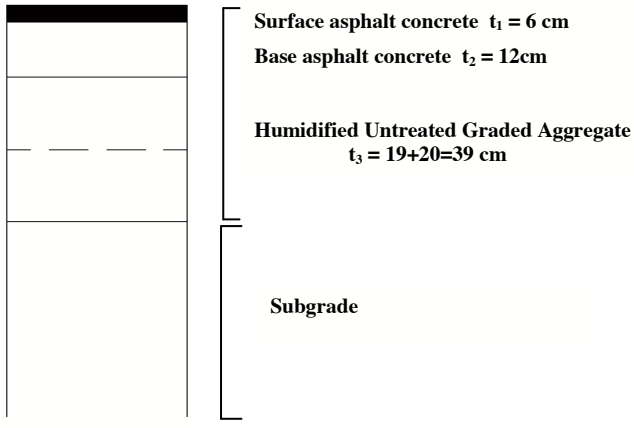

Figure 1- STAC's Bonneuil 1995 test facility structure

[2] French untreated material, obtained by confining several separate granular fractions in defined proportions, which are mixed and humidified in a mixing plant

- Material data

- **information about subgrade**

a- Geotechnical survey

A full geotechnical survey has been conducted on the experimental site Fifty five (55) static cone penetrometer tests have been regularly positioned on the test facility as well as five (5) deep auger holes. Material analyses (in particularly proctor tests) have been performed, and five (5) piezometers have been set in order to monitor the ground water level.
The contents of the geotechnical report will not be detailed hereafter. The main conclusions are:
- The natural basement (composed of silt) is homogeneous on the whole area.
- Its bearing capacity is very low (lower than 50MPa) on the whole depth (10 meters).

Figure 2 displays the results of a static cone penetrometer test. High mechanical resistances are found in the first meter (corresponding to the pavement thickness) whereas much weaker homogeneous resistances (corresponding to a bulk modulus lower than 50MPa) characterise the underlying clayey-silty material.
- Bedrock is found about 11 or 12 meters deep under this material.

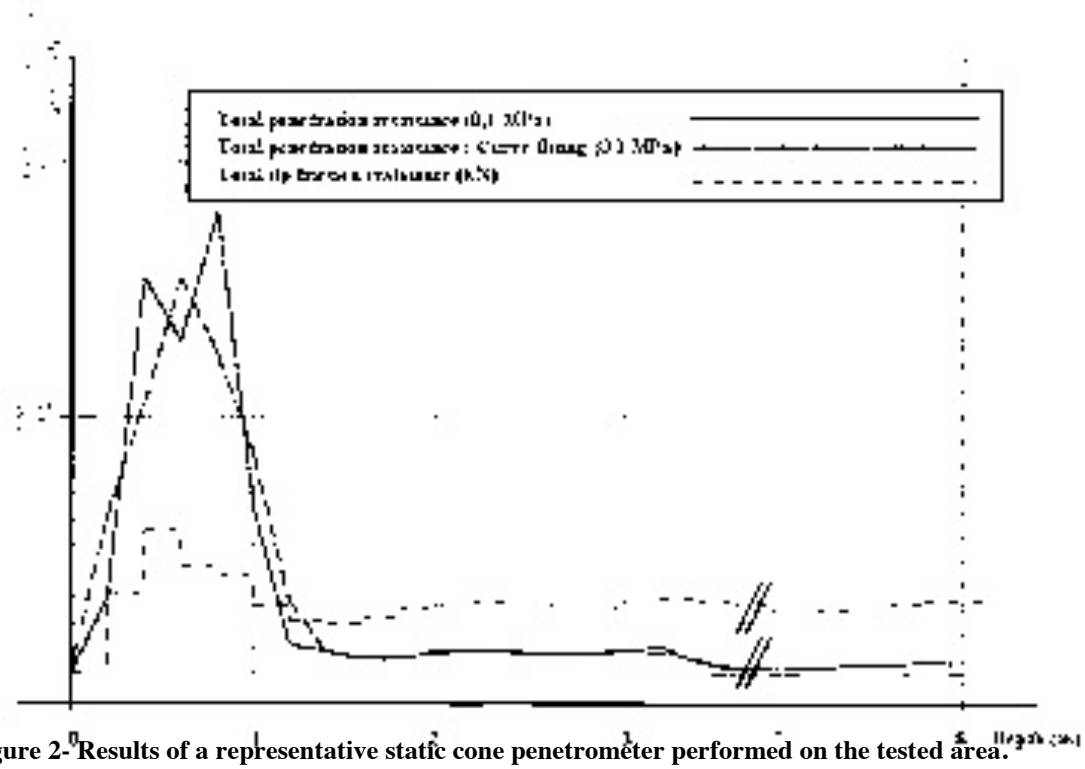

Figure 2- Results of a representative static cone penetrometer performed on the tested area.

b- Resonant column tests

The low subgrade modulus value has been confirmed by Resonant Column Tests [ASTM] performed in the LCPC. The tests allow determining the shear modulus of this material, and in this way its elastic modulus E, linked to shear modulus G by the relation:

$$G = \frac{E}{2 \times (1 + \nu)} \qquad (1)$$

where ν is the Poisson's ratio (taken equal to 0,35).

The results are presented in Figure 12 , taken from LCPC's « Essais à la colonne résonnante sur GRH et terrains naturels » report for STAC, dated 22 December 2009, written by P. Reiffsteck, S. Fanelli and J-L.Tacita.

As the shear modulus depends on the γ distortion and the *p* confining pressure range, these parameters need to be approximated. In this work, evaluation of the γ distortion has been based on strain calculations in the pavement using backcalculated modulus and on the hypothesis that $\gamma \approx \varepsilon_{ZZ}$. The evaluation of the p confining pressure has implied the use of a cone model for calculation (not presented here, Broutin, personal publication, 2009).

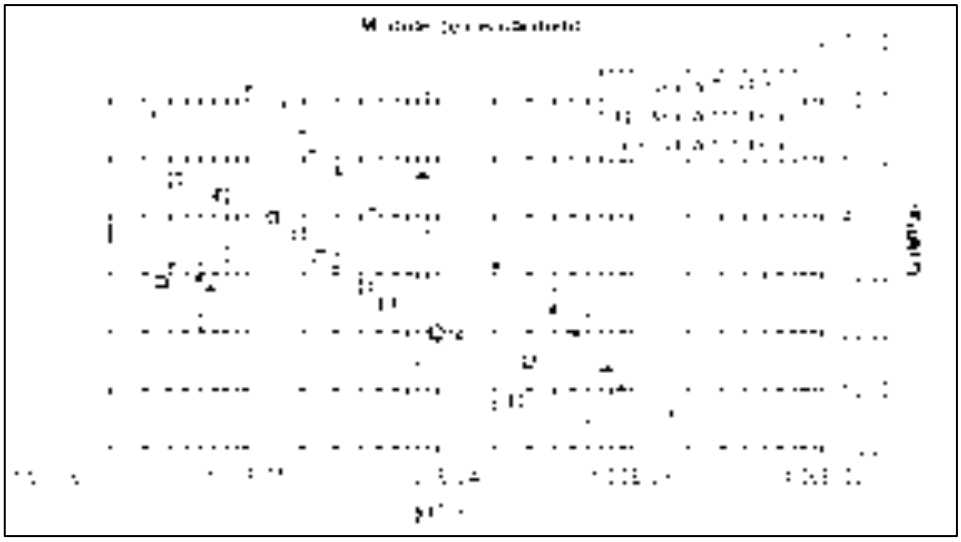

Figure 3 Evolution of subgrade shear modulus with distortion and confining pressure; after Reiffsteck et al.

.

Strain range is 1 to 2.10^{-4} and the cone model predicts a 65 kPa value for confining pressure. These parameters allow calculating the shear and elastic modulus in the subgrade.

Resonant column test also allow determining the damping ratio in the subgrade. The evolution of this parameter is displayed in Figure 4.

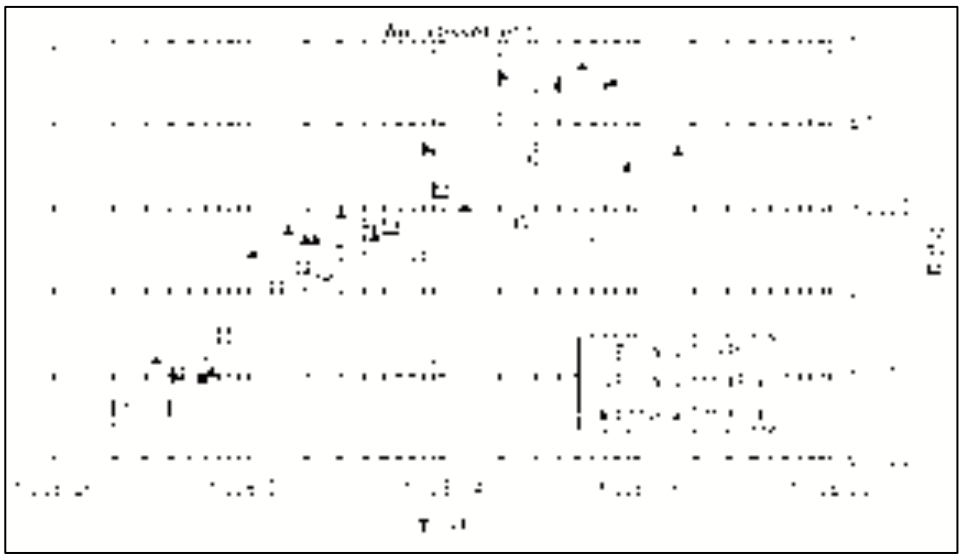

Figure 4 - Evolution of damping ratio in subgrade with distortion and confining pressure

Results are collected in Table 1.

ε_{ZZ}	ξ [%]	G [MPa]	E [MPa]
$1{,}65.10^{-4}$	3	15	40

Table 1 Elastic modulus and damping ratio of the subgrade

Note that these laboratory moduli must be considered with caution because they are derived from laboratory tests on samples of re-confined material. They only provide an approximate range value.

- **information about UGA**

No information is available about UGA.

- **information about asphalt materials**

The validation of the layer backcalculated moduli in the frame of the thesis has requested complex moduli tests, and the determination of the remaining life through fatigue tests. These tests have been performed by the LCPC.

Complex moduli tests have been performed on asphalt materials. For each material, tables 2 to 5 indicate the storage E_1 and loss modulus E_2 and the $|E^*|$ and ϕ corresponding norm and phase difference for different combinations of temperatures and frequencies. The $|E^*|$ is usually used as the data input value of Young modulus in linear elastic models.

a- complex moduli

Temperature (°C)	Frequency (Hz)	E1 (MPa)	E2 (MPa)	|E*| (MPa)	ϕ (°)
-10	40	31983	1478	32018	2.7
	30	31733	1515	31769	2.7
	25	31556	1554	31594	2.8
	10	30580	1709	30628	3.2
	3	29229	1933	29293	3.8
	1	27800	2104	27879	4.3
0	40	27190	2267	27284	4.8
	30	26813	2298	26911	4.9
	25	26550	2365	26656	5.1
	10	25087	2512	25212	5.7
	3	23117	2704	23275	6.7
	1	21192	2811	21378	7.6
10	40	20878	3054	21101	8.3
	30	20308	3050	20536	8.5
	25	19937	3096	20177	8.9
	10	18128	3191	18407	10.0
	3	15656	3248	15990	11.8
	1	13395	3179	13768	13.4
15	40	17422	3319	17736	10.8
	30	16827	3303	17149	11.1
	25	16446	3350	16785	11.6
	10	14471	3349	14855	13.0
	3	11940	3283	12384	15.4
	1	9713	3075	10189	17.6
20	40	14007	3452	14427	13.9
	30	13391	3405	13819	14.3
	25	12960	3429	13407	14.9
	10	10998	3334	11493	16.9
	3	8541	3095	9086	20.0
	1	6515	2728	7065	22.8
30	40	7895	3209	8524	22.2
	30	7324	3089	7951	22.9
	25	6962	3057	7605	23.8
	10	5299	2685	5941	27.0
	3	3512	2125	4106	31.3
	1	2300	1582	2792	34.7
40	40	3365	2235	4041	33.7
	30	3014	2075	3660	34.7
	25	2783	1984	3419	35.6
	10	1857	1502	2390	39.1
	3	1051	965	1427	42.8
	1	619	597	860	44.1

Table 2 - Laboratory-determined complex moduli (LCPC data) of the surface asphalt concrete from the 1995 STAC's facility

Temperature (°C)	Frequency (Hz)	E1 (MPa)	E2 (MPa)	|E*| (MPa)	ϕ (°)
-10	40	32624	1466	32657	2.6
-10	30	32516	1435	32548	2.5
-10	25	32180	1558	32218	2.8
-10	10	31416	1700	31463	3.1
-10	3	30122	1940	30184	3.7
-10	1	28701	2136	28781	4.3
0	40	28162	2357	28261	4.8
0	30	27722	2372	27823	4.9
0	25	27455	2463	27566	5.1
0	10	25977	2666	26114	5.9
0	3	23839	2987	24026	7.2
0	1	21686	3177	21918	8.4
10	40	20892	3554	21192	9.7
10	30	20237	3572	20551	10.0
10	25	19814	3658	20149	10.5
10	10	17616	3848	18031	12.3
10	3	14603	4013	15146	15.4
10	1	11781	3942	12424	18.5
15	40	16858	4046	17337	13.5
15	30	15943	4024	16444	14.2
15	25	15607	4148	16149	14.9
15	10	13107	4219	13771	17.9
15	3	9896	4051	10694	22.3
15	1	7222	3612	8077	26.7
20	40	12509	4288	13225	19.0
20	30	11710	4229	12451	19.9
20	25	11158	4269	11947	21.0
20	10	8687	4054	9588	25.1
20	3	5847	3475	6804	30.8
20	1	3779	2712	4653	35.8
30	40	5572	3603	6636	33.0
30	30	4937	3371	5979	34.4
30	25	4529	3255	5578	35.8
30	10	2929	2540	3878	41.0
30	3	1502	1623	2212	47.3
30	1	837	986	1294	49.8
40	40	1613	1843	2449	48.9
40	30	1318	1597	2071	50.5
40	25	1164	1464	1870	51.6
40	10	653	921	1129	54.7
40	3	325	470	572	55.4
40	1	193	246	313	52.0

Table 3 - Laboratory-determined complex moduli (LCPC data) of the base asphalt concrete from the 1995 STAC's facility

Temperature (°C)	Frequency (Hz)	E1 (MPa)	E2 (MPa)	|E*| (MPa)	ϕ (°)
-10	40	32032	1437	32064	2.6
-10	30	31778	1483	31812	2.7
-10	25	31671	1541	31708	2.8
-10	10	30692	1693	30739	3.2
-10	3	29317	1964	29383	3.9
-10	1	27845	2167	27930	4.5
0	40	26910	2389	27016	5.1
0	30	26492	2407	26601	5.2
0	25	26240	2489	26358	5.4
0	10	24682	2690	24829	6.2
0	3	22558	2936	22749	7.5
0	1	20435	3065	20664	8.5
10	40	19871	3338	20150	9.6
10	30	19247	3330	19533	9.9
10	25	18870	3389	19172	10.2
10	10	16828	3481	17185	11.7
10	3	14153	3516	14583	14.0
10	1	11717	3387	12197	16.2
15	40	16015	3602	16415	12.7
15	30	15375	3577	15786	13.2
15	25	14948	3626	15382	13.7
15	10	12823	3585	13315	15.7
15	3	10133	3417	10694	18.7
15	1	7852	3075	8433	21.4
20	40	12470	3672	13000	16.5
20	30	11815	3611	12355	17.0
20	25	11377	3619	11939	17.7
20	10	9300	3423	9910	20.3
20	3	6837	3025	7476	23.9
20	1	4931	2506	5531	27.0
30	40	5940	3023	6666	27.0
30	30	5421	2858	6129	27.8
30	25	5073	2777	5784	28.7
30	10	3656	2285	4312	32.1
30	3	2265	1639	2796	35.9
30	1	1407	1112	1793	38.3
40	40	1744	1455	2271	39.8
40	30	1542	1305	2020	40.2
40	25	1411	1230	1872	41.1
40	10	921	858	1259	43.0
40	3	517	508	725	44.5
40	1	301	294	421	44.4

Table 4 - Laboratory-determined complex moduli (LCPC data) of the high modulus surface asphalt concrete from the 1995 STAC's facility

Temperature (°C)	Frequency (Hz)	E1 (MPa)	E2 (MPa)	|E*| (MPa)	ϕ (°)
-10	40	32069	1060	32087	1.9
	30	31869	1078	31887	2.0
	25	31767	1079	31785	2.0
	10	31084	1223	31109	2.3
	3	30123	1391	30155	2.6
	1	29121	1535	29162	3.0
0	40	28300	1712	28352	3.5
	30	27985	1732	28039	3.5
	25	27815	1783	27872	3.7
	10	26753	1929	26822	4.1
	3	25217	2128	25307	4.8
	1	23695	2268	23804	5.5
10	40	23477	2431	23602	5.9
	30	23051	2450	23181	6.1
	25	22761	2479	22895	6.2
	10	21258	2633	21421	7.1
	3	19227	2801	19430	8.3
	1	17250	2871	17488	9.5
15	40	20691	2762	20874	7.6
	30	20210	2771	20400	7.8
	25	19879	2815	20078	8.1
	10	18215	2932	18449	9.2
	3	15952	3044	16240	10.8
	1	13819	3037	14149	12.4
20	40	17770	3038	18028	9.7
	30	17214	3041	17481	10.1
	25	16867	3087	17147	10.4
	10	15050	3138	15374	11.8
	3	12649	3149	13036	14.0
	1	10465	3026	10894	16.1
30	40	11696	3292	12151	15.7
	30	11113	3246	11578	16.3
	25	10720	3252	11203	16.9
	10	8852	3104	9381	19.4
	3	6588	2791	7155	23.0
	1	4797	2362	5348	26.2
40	40	6286	2922	6932	24.9
	30	5775	2790	6414	25.8
	25	5440	2739	6091	26.8
	10	3988	2326	4616	30.3
	3	2492	1739	3039	34.9
	1	1548	1221	1972	38.3

Table 5 - Laboratory-determined complex moduli (LCPC data) of the high modulus base asphalt concrete from the 1995 STAC's facility

b- fatigue test

Only the base AC fatigue test is displayed here since it is the only one to have been used in this work.

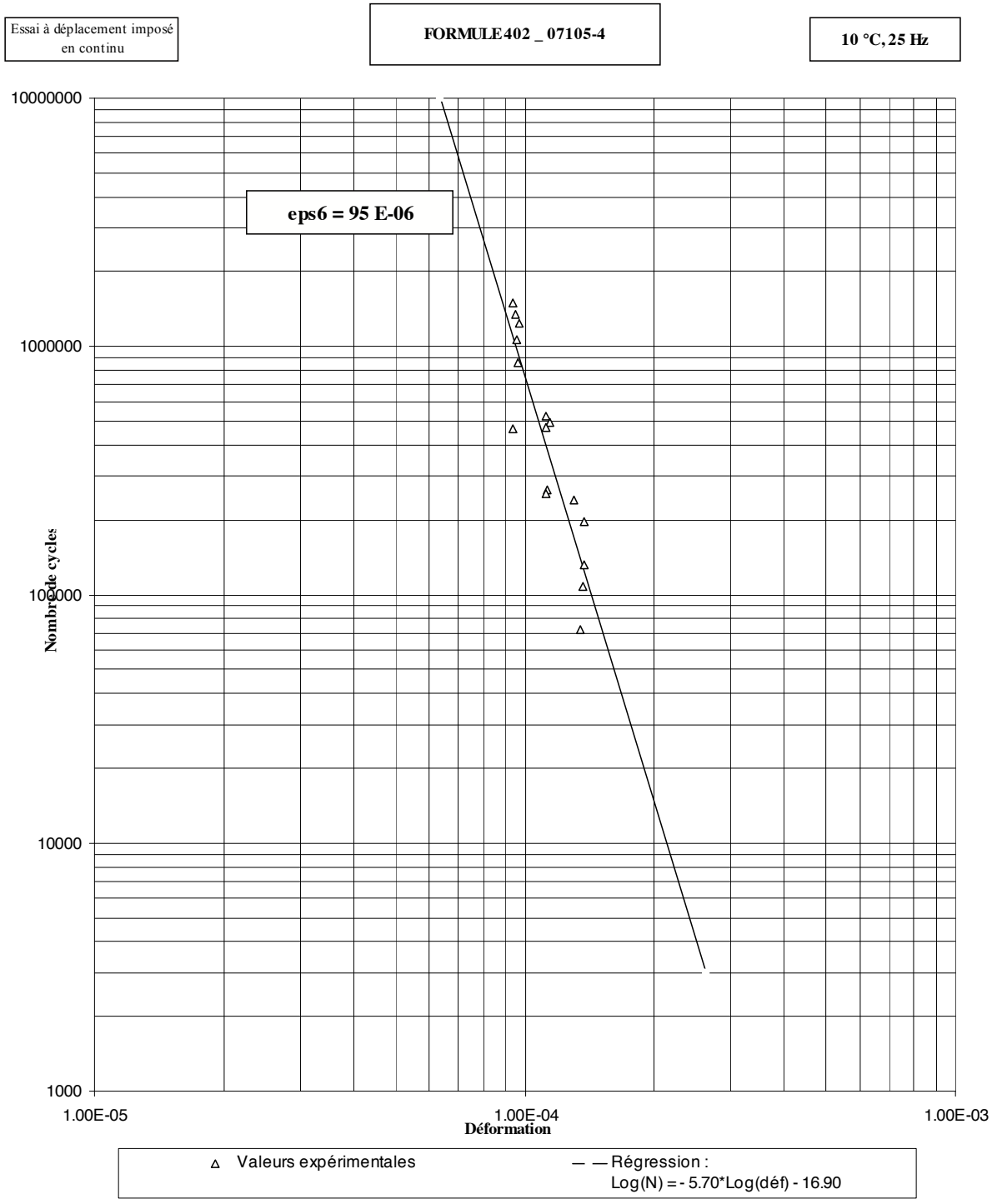

Figure 5 - Laboratory fatigue test results (LCPC internal report) obtained on the base asphalt concrete from the 1995 STAC's facility

1.1.2 S_2 structure

It corresponds to the P_1 structure from the multiple axle loading effect experiment [Homsi et al., 2010] performed on the LCPC's fatigue carousel.

- Structure (studied profile)

The studied structure is a conventional road structure made up of surface Asphalt Concrete (AC_1), base Asphalt Concrete (AC_2), humidified Untreated Graded Aggregate (UGA) and subgrade (S). The depth to bedrock, corresponding to a hydraulic concrete-made blocking, is 3 m.

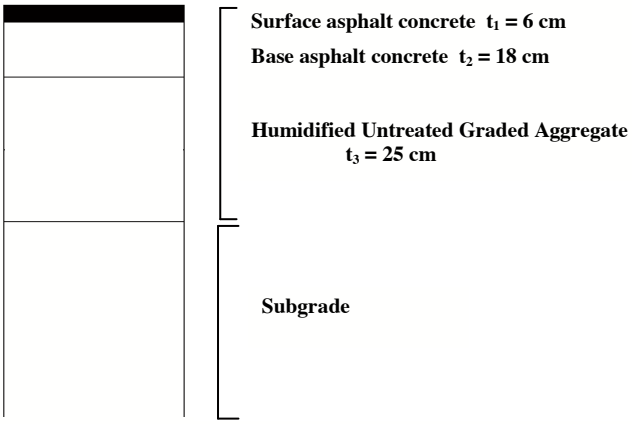

Figure 6 - LCPC's fatigue Carousel P1 structure (caption not to scale)

- Material data

- **information about the subgrade**

Expected value for subgrade modulus ranges from 150 to 200 MPa.

- **information about UGA**

Expected value for subgrade modulus ranges from 80 to 120 MPa.

- **information about asphalt materials**

Temperature (°C)	Frequency (Hz)	E1 (MPa)	E2 (MPa)	|E*| (MPa)	ϕ (°)
-10	40	29712	1200	29736	2.3
-10	30	29492	1233	29518	2.375
-10	25	29359	1269	29386	2.5
-10	10	28582	1449	28619	2.9
-10	3	27403	1708	27456	3.575
-10	1	26142	1923	26213	4.225
0	40	25469	2093	25555	4.7
0	30	25113	2131	25203	4.825
0	25	24867	2202	24965	5.05
0	10	23493	2423	23617	5.9
0	3	21582	2722	21753	7.2
0	1	19618	2932	19836	8.5
10	40	19538	3112	19785	9.025
10	30	18979	3150	19239	9.4
10	25	18601	3212	18876	9.775
10	10	16698	3412	17044	11.525
10	3	13990	3583	14441	14.35
10	1	11439	3568	11983	17.325
15	40	16009	3551	16399	12.525
15	30	15371	3568	15779	13.05
15	25	14946	3624	15380	13.625
15	10	12736	3708	13265	16.225
15	3	9889	3683	10552	20.425
15	1	7350	3388	8094	24.75
20	40	12479	3815	13049	17
20	30	11785	3786	12378	17.825
20	25	11315	3824	11943	18.675
20	10	9071	3726	9807	22.325
20	3	6288	3351	7126	28.05
20	1	4140	2739	4964	33.5
30	40	5690	3417	6637	31
30	30	5083	3233	6024	32.475
30	25	4680	3145	5639	33.9
30	10	3033	2518	3942	39.7
30	3	1536	1648	2253	47.025
30	1	774	975	1244	51.55
40	40	1543	1791	2364	49.225
40	30	1282	1566	2024	50.7
40	25	1120	1438	1823	52.075
40	10	590	888	1066	56.4
40	3	260	428	501	58.7
40	1	139	205	248	55.875

Table 6 - Laboratory-determined complex moduli of the AC_1 from the LCPC's fatigue carousel (LCPC data)

Temperature (°C)	Frequency (Hz)	E1 (MPa)	E2 (MPa)	|E*| (MPa)	ϕ (°)
-10	40	27514	1066	27534	2.225
-10	30	27302	1081	27324	2.275
-10	25	27211	1154	27235	2.45
-10	10	26546	1276	26577	2.775
-10	3	25496	1488	25539	3.35
-10	1	24406	1669	24463	3.9
0	40	23768	1812	23837	4.375
0	30	23472	1858	23546	4.525
0	25	23257	1903	23334	4.7
0	10	22111	2086	22209	5.4
0	3	20445	2328	20577	6.5
0	1	18776	2500	18941	7.575
10	40	18662	2667	18852	8.15
10	30	18206	2703	18406	8.45
10	25	17885	2762	18097	8.775
10	10	16251	2929	16513	10.225
10	3	13934	3102	14275	12.575
10	1	11747	3140	12160	14.975
15	40	15647	3062	15944	11.05
15	30	15105	3087	15417	11.55
15	25	14724	3137	15055	12.025
15	10	12889	3254	13293	14.175
15	3	10345	3294	10857	17.675
15	1	8058	3143	8649	21.3
20	40	12555	3349	12994	14.95
20	30	11956	3343	12414	15.65
20	25	11530	3384	12016	16.35
20	10	9551	3371	10129	19.425
20	3	7005	3170	7689	24.35
20	1	4916	2740	5628	29.125
30	40	6361	3268	7152	27.175
30	30	5781	3141	6579	28.525
30	25	5380	3085	6201	29.85
30	10	3718	2603	4539	35.025
30	3	2080	1856	2787	41.75
30	1	1145	1196	1655	46.25
40	40	2038	1991	2849	44.325
40	30	1736	1778	2485	45.7
40	25	1546	1658	2267	47
40	10	877	1097	1405	51.4
40	3	414	578	712	54.375
40	1	228	299	376	52.7

Table 7 - Laboratory-determined complex moduli of the AC_2 from the LCPC's fatigue carousel (LCPC data)

- Instrumentation

The tested pavement of the LCPC's fatigue carousel is instrumented. It includes various sensors monitoring:
- longitudinal and transverse strains at the bottom of the base course.
- vertical strain in the untreated materials i.e. at top of the UGA and at top of the subgrade.

Deep anchors have also been set, which allow measuring absolute surface displacements.

1.1.3 S_3 structure: STAC's instrumented test facility

The project was initiated in the frame of this thesis (Broutin, Deffieux) in order to validate the developed models for HWD data analysis. It takes place in the more general frame of the development of a rational airport design method. It includes a flexible and a rigid pavement (Figure 7). In this thesis, HWD data analysis has been restricted to the flexible case.

The flexible pavement has been designed (internal note, M. Broutin and J.C. Deffieux) using the French rational design method with the Alizé software [Alize] developed by the LCPC, and using the analytical Burmister model. The structure was designed to support 10 HWD loads per day, during a 10 years lifetime, considering a 300 kN load on a 45 cm diameter. This configuration corresponds to a tire pressure of about 1.5 MPa, which is the value currently in use for conventional aircraft.

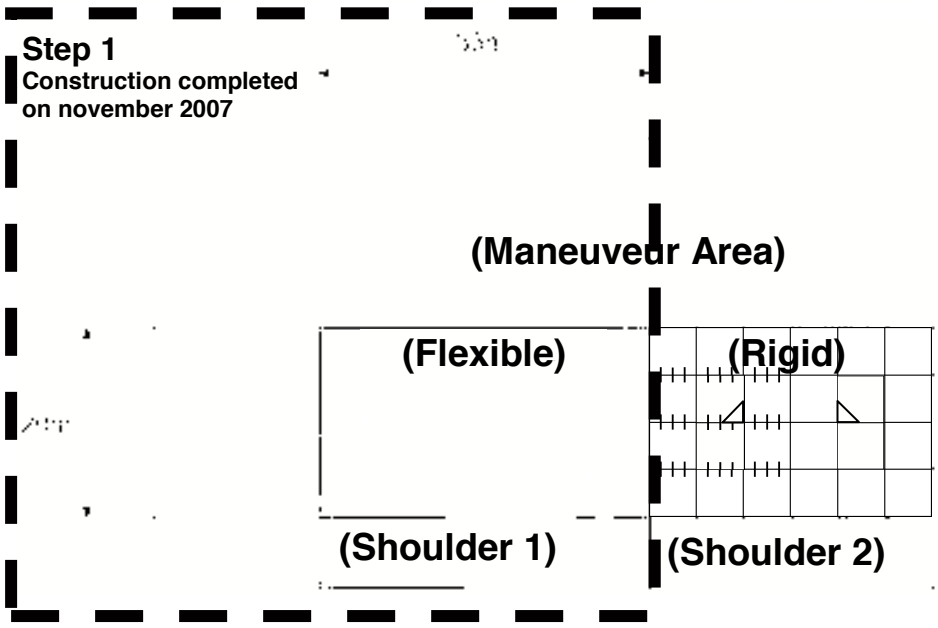

Figure 7 - General view of the facility

The flexible pavement was built on November 2007 in Bonneuil-sur-Marne, 20 km south-east from Paris. The picture of figure 10 was taken during the setting of the Untreated graded aggregate.

Figure 8 – The flexible pavement during construction (Photograph by M. Broutin)

- Structure (Mean profile)

The designed structure is a conventional airfield structure made up of surface aeronautical Asphalt Concrete (AC_1), base Asphalt Concrete (AC_2), humidified Untreated Graded Aggregate (UGA) and subgrade (S). The 54 cm –thick UGA has been placed in two layers. It has been built on the area of the 1995 facility (S_1 structure removed). The depth to bedrock is greater than 10 m. The Figure 9 gives a representative profile of the structure. Due to the poor quality of subgrade, a 70 cm-thick capping layer (CL) made of untreated graded aggregate has been superimposed to the subgrade.

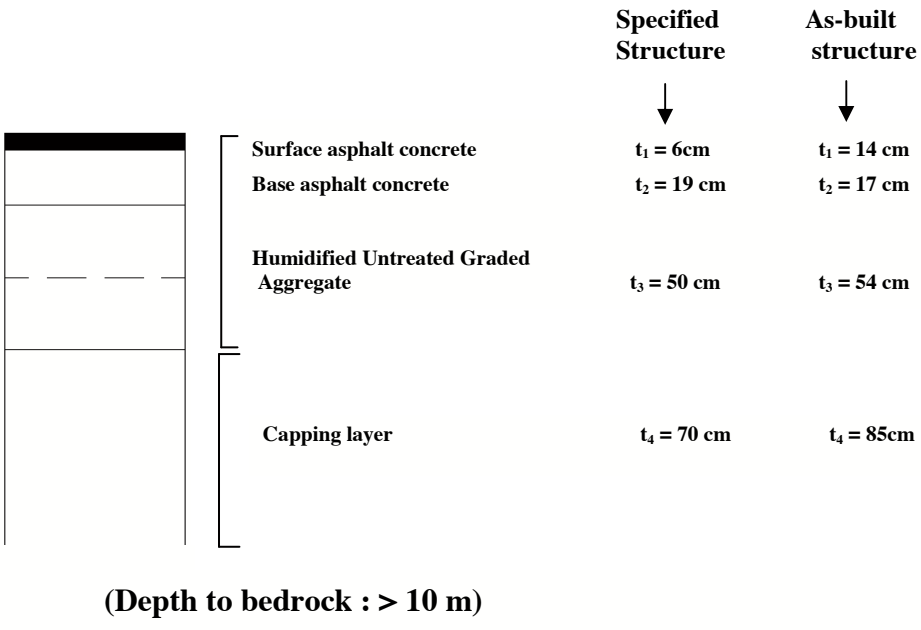

Figure 9 - STAC's Bonneuil instrumented test facility structure

Post-construction corings and Ground Penetrating Radar (GPR) surveys have been performed in order to characterize the layer geometry and interface quality on the whole test facility.

These studies revealed a deviation from the specified thicknesses:

Layer Test point	AC_1	AC_2	UGA	CL	Method of determination
P_1	14	15	61	90	Coring
P_5	12	18	50	70	Coring
Pl_1 to Pl_6	14.6	17.8	53.7	81.9	GPR
Pl_7	13.1	17.7	55.5	79.9	GPR
Pl_8	12.2	18.3	49.7	90.7	GPR
Pl_9	12	16	52	100	GPR
Pl_{10}	14	15	61	90	Coring (P_1)
Mean (Pl_1 to Pl_{10})	13.9	17.4	54.0	85.0	
Standard deviation	1.1	1.4	4.8	9.7	

Table 8 - Relative layer thicknesses ([cm]) on the HWD tested points

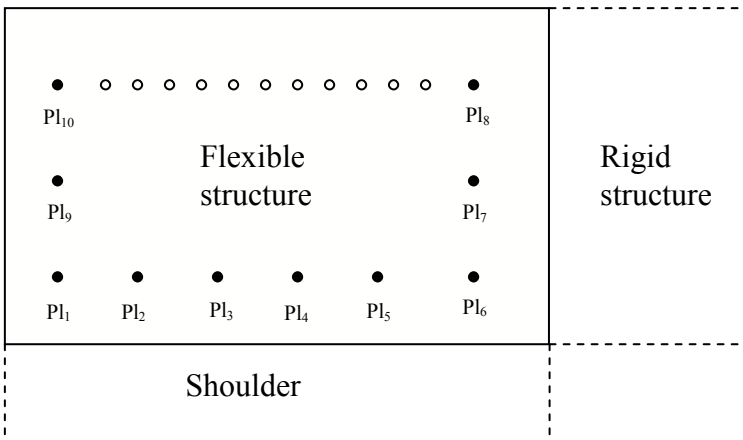

Figure 10 - Location of the test points on the S_3 test facility (Not to scale)

Surface asphalt concrete thickness deviation comes from the partial removal and reinforcement of the surface course due to the detection of unbonded layer interfaces in asphalt materials (GPR data). Apart from this deviation and from the thickness of the capping layer (probably due to a lack of topographic), the as-built structure globally conforms to the specified structure. However, thickness non-homogeneities were identified, maily oriented transversally to the construction lanes. Even so, results from corings and GPR surveys were precise enough to build a 3D mapping of the test facility, allowing performing a refined HWD backcalculation procedure based on single-point measurements. The test facility was scanned in detail by operating the GPR equipment along 14 longitudinal and 18 transverse alignments with a 2 m spacing. The GPR equipment used during the 2008 and 2009 investigation phases was composed of a GSSI air-launched horn antenna (2,5 GHz) and a GSSI contact antenna operating at 900 MHz connected with a SRI 3000 data acquisition unit.

- Material data

- **information about the subgrade**

Subgrade is the same than in the S_1 structure.

- **information about UGA**

No laboratory tests are for the while available on these materials. Triaxial tests in progress will provide information about the UGA moduli.

Nevertheless, Dynaplaque tests ([Benoist and Schaeffner, 1982], [Chassaing et al., 1995]) have been performed at each level (top of subgrade, top of CL, top of each UGA layer) during the construction phase.
Dynaplaque principle is the same that the HWD but for platform testing.
The modulus at top of subgrade could not be determined with the Dynaplaque apparatus (too weak; E< 20 MPa) Mean dynaplaque values at the top of the CL was 75 MPa, and 90 MPa at the top of the UGA.
Note that this modulus is an apparent bulk modulus of the underlying structure (i.e. at the top of UGA for instance, measured modulus is representative of the complex
Subgrade / CL / UGA).

- **information about asphalt materials**

Complex moduli tests have been performed on asphalt materials.

Température (°C)	Fréquence (Hz)	E1 (MPa)	E2 (MPa)	|E*| (MPa)	ϕ (°)
-10	40	29709	1417	29743	2.7
-10	30	29469	1453	29505	2.8
-10	25	29296	1497	29334	2.9
-10	10	28394	1707	28445	3.4
-10	3	26962	1997	27036	4.2
-10	1	25479	2246	25577	5.0
0	40	24824	2404	24940	5.6
0	30	24394	2436	24515	5.7
0	25	24102	2509	24233	5.9
0	10	22585	2776	22755	7.0
0	3	20331	3082	20563	8.6
0	1	18083	3270	18376	10.3
10	40	17392	3532	17747	11.5
10	30	16747	3553	17120	12.0
10	25	16312	3619	16709	12.5
10	10	14081	3722	14565	14.8
10	3	11225	3762	11839	18.6
10	1	8605	3549	9308	22.4
15	40	13252	3861	13803	16.3
15	30	12561	3842	13136	17.0
15	25	12089	3878	12696	17.8
15	10	9793	3798	10503	21.2
15	3	6936	3476	7758	26.6
15	1	4654	2913	5491	32.1
20	40	9420	3879	10188	22.4
20	30	8703	3789	9492	23.5
20	25	8229	3772	9052	24.6
20	10	6064	3407	6956	29.3
20	3	3696	2717	4588	36.4
20	1	2118	1932	2867	42.4
30	40	3565	2817	4543	38.3
30	30	3081	2588	4024	40.0
30	25	2781	2464	3715	41.6
30	10	1619	1763	2394	47.4
30	3	736	998	1240	53.6
30	1	360	528	639	55.7
40	40	773	1127	1366	55.5
40	30	628	957	1145	56.7
40	25	546	862	1020	57.7
40	10	283	489	565	59.9
40	3	141	220	261	57.3
40	1	88	105	137	50.0

Table 9 - Laboratory-determined complex moduli (LCPC data) of the surface asphalt concrete from the 2007 STAC's instrumented facility

Température (°C)	Fréquence (Hz)	E1 (MPa)	E2 (MPa)	|E*| (MPa)	ϕ (°)
-10	40	31974	1123	31993	2.0
-10	30	31795	1157	31816	2.1
-10	25	31680	1215	31703	2.2
-10	10	30911	1327	30939	2.4
-10	3	29864	1558	29904	3.0
-10	1	28722	1750	28775	3.5
0	40	28186	1904	28250	3.9
0	30	27847	1960	27916	4.0
0	25	27598	1997	27670	4.1
0	10	26396	2227	26490	4.8
0	3	24598	2529	24728	5.9
0	1	22776	2760	22942	6.9
10	40	22222	3045	22430	7.8
10	30	21645	3105	21866	8.2
10	25	21259	3167	21494	8.5
10	10	19297	3408	19596	10.0
10	3	16636	3707	17044	12.6
10	1	13988	3828	14502	15.3
15	40	18458	3616	18809	11.1
15	30	17803	3657	18174	11.6
15	25	17346	3747	17746	12.2
15	10	15094	3929	15597	14.6
15	3	12022	4037	12682	18.5
15	1	9221	3853	9994	22.7
20	40	14587	4052	15140	15.5
20	30	13841	4070	14427	16.4
20	25	13317	4126	13941	17.2
20	10	10875	4125	11631	20.8
20	3	7764	3848	8666	26.4
20	1	5264	3261	6192	31.8
30	40	7311	3969	8319	28.5
30	30	6570	3796	7588	30.0
30	25	6092	3727	7142	31.4
30	10	4106	3106	5148	37.1
30	3	2203	2159	3085	44.4
30	1	1167	1358	1791	49.3
40	40	2287	2343	3274	45.7
40	30	1930	2085	2841	47.2
40	25	1712	1943	2589	48.6
40	10	943	1265	1578	53.3
40	3	439	655	789	56.1
40	1	247	335	416	53.6
50	40	529	869	1018	58.7
50	30	433	728	847	59.2
50	25	385	643	749	59.1
50	10	224	365	429	58.4
50	3	136	171	219	51.6
50	1	101	88	134	41.0

Table 10 - Laboratory-determined complex moduli (LCPC data) of the base asphalt concrete from the 2007 STAC's instrumented facility

- Instrumentation

Sensors types and organization

More than one hundred sensors have been installed within the flexible pavement in order to monitor:

- longitudinal and transverse strains at the bottom of the base course. The sensors (Figure 11 a-) used consist of two aluminium anchor bars fixed on a proof body made of a hollow aluminium cylinder with a full-bridge instrumentation.
- vertical strains in the unbound materials namely at each layer of the humidified untreated graded aggregate and at top of the subgrade. Sensors (Figure 11 b-) consist of a proof body in epoxy material equipped with a longitudinal strain gauge, and two aluminium dishes (quarter-bridge instrumentation).
- temperature profiles in asphalt materials: three locations have been chosen with gauges spaced apart vertically from each other by 3 cm.
- moisture content in the subgrade : four vertical profiles reconstituted from three sensors monitor this parameter in the top 70 cm.
- water pressure in the subgrade : three vertical profiles are available derived from three sensors placed in the top 70 cm.

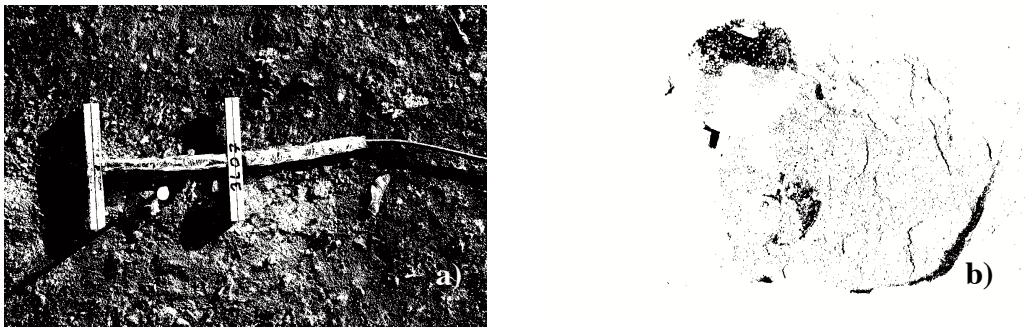

Figure 11 - a) Horizontal X and Y strain sensors (base of the asphalt layer), b) Vertical strain sensor (untreated materials), after [Broutin et al., 2008]

The flexible instrumented pavement includes 3 instrumentation strips (called S_1 to S_3 in Figure 7) with a common mesh configuration. The latter has been studied (M.Broutin, J.C.Deffieux) so as to find a compromise between:

- the density of sensors, in order to benefit from a mesh of strain measurements as fine as possible for each layer,
- the offset between sensors which has to be large enough to avoid any disturbance of the structure material.

The resulting mesh is presented in Figures 12 and 13. It consists of a four-lanes mesh with a 45 cm offset. For each instrumentation level the distance of the sensor the farthest to the axis has been chosen long enough to monitor strains on the whole influence area. Four HWD tests performed on the position P_1 to P_4 (see infra) on the axis will enable to reconstruct fine strain measurement meshes (1 sensor every 30 cm) for each strain. This will allow measuring not only strains values, but also the propagation velocity of the signal in the structure.

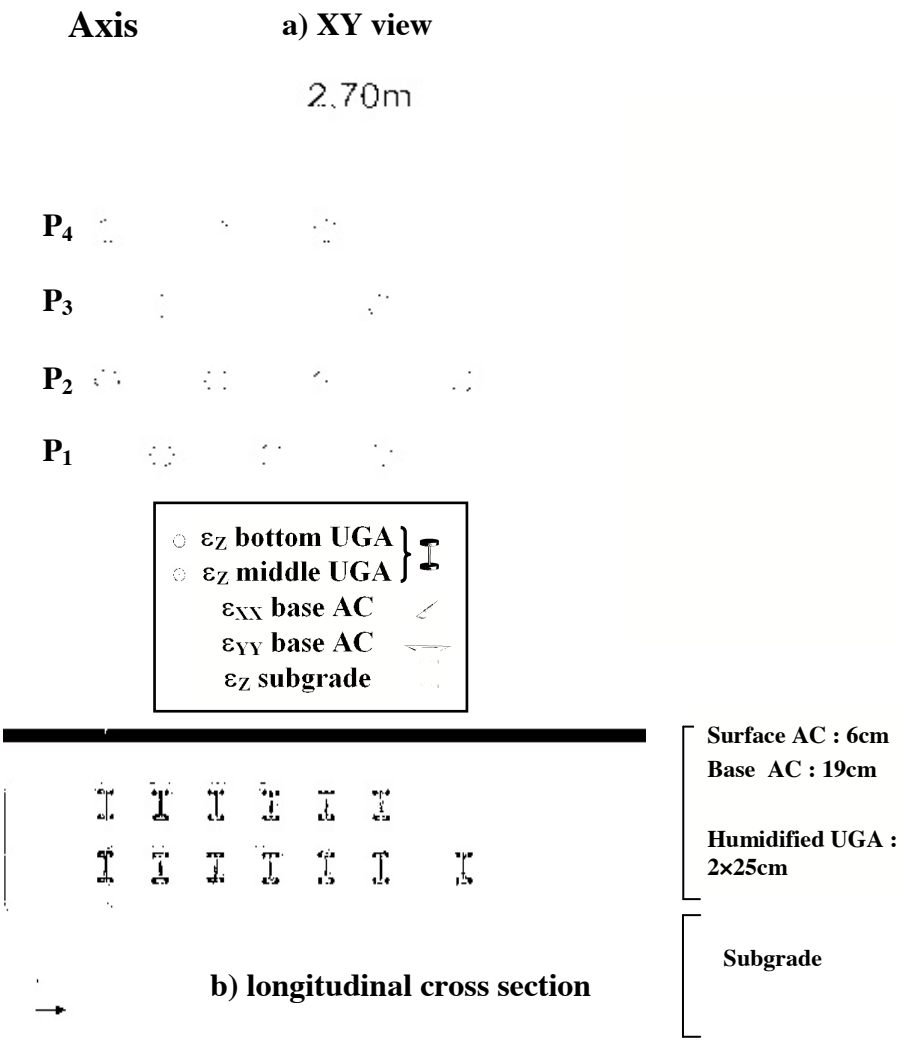

Figure 12 - Flexible structure and embedded instrumentation, after [Broutin et al., 2008]

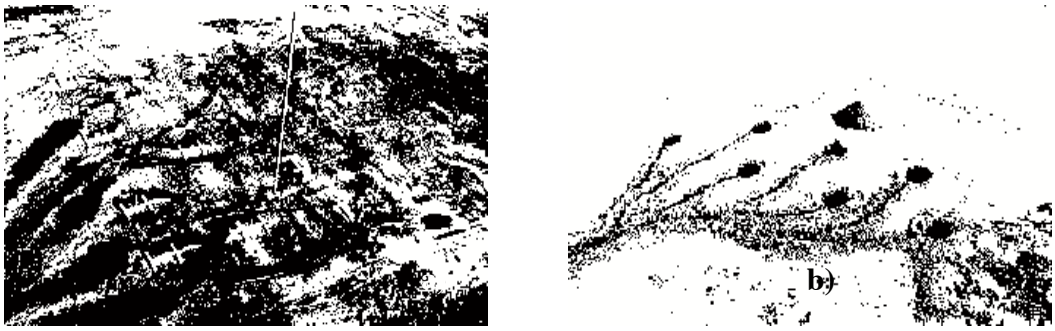

Figure 13 a - Mesh of horizontal X and Y strain sensors (base of the asphalt layer), b - Mesh of vertical strain sensors (untreated materials), after [Broutin et al., 2008]

Two deep anchors have also been set.

Sensor installation

Much care has been taken during the gauge installation and construction phases of the project to ensure maximum gauge survival and reliable data. Each gauge had cable running from it to the roadside instrumentation cabinet. For all sensors embedded in unbound materials, the cables were run through flexible conduits in trenches cut into the sub-base course. The conduits were used to help prevent coarse fragments of granular aggregates from punctuning the cable. The trenches were then covered first with fine sand and then with the material excavated from the trenches and earlier sieved to an appropriate gradation. The trenches were compacted with a vibrating plate compactor.
Just prior to paving the base asphalt concrete bottom layer, the X and Y strain sensors were fixed into their respective surveyed locations on the bituminous tack coat. To protect the sensors from the paver screed, the gauges were covered with hot mix asphalt taken from the discharge hopper of the bituminous paver. Once the asphalt material was placed, it was compacted carefully by hand using a steel plate.

Sensor data acquisition

The sensor data obtained on structure S_3 have not been available for this study but will be supplied and analyzed in the frame of further publications. The main reason for this non-availability is that the test facility was subjected to rehabilitation works consisting in removing the superficial part of the pavement by cold micro milling and applying a new surface course. The specified depth to be removed was 10 cm, due to the poor quality of interfaces at the transition between surface and base asphalt concrete layers, as detected by the GPR equipment in 2008 (unbound interfaces for 20 % of the total scanned length). This rehabilitation phase caused a great delay in the project (delay in material sampling for laboratory tests, delay in connecting sensors..).

Appendix 1.2 - Temperature data

1.2.1 S_3; repeatability study

Temperature probes have been positioned in the asphalt layer, according to the STAC's HWD survey protocol i.e. the first one at the top of the layer, the second one in the middle, and the last at bottom in order to monitor evolution of this parameter during the experiment. Figure 14 depicts evolution. It can be estimated that temperature has remained constant during the whole experiment, a 0,4 °C variation being noticed when considering mean temperature. Only a uniformization of temperature in the pavement is observed. Its consequence is a minor increase in surface stiffness and at the inverse a decrease in stiffness under, the mean stiffness being preserved.

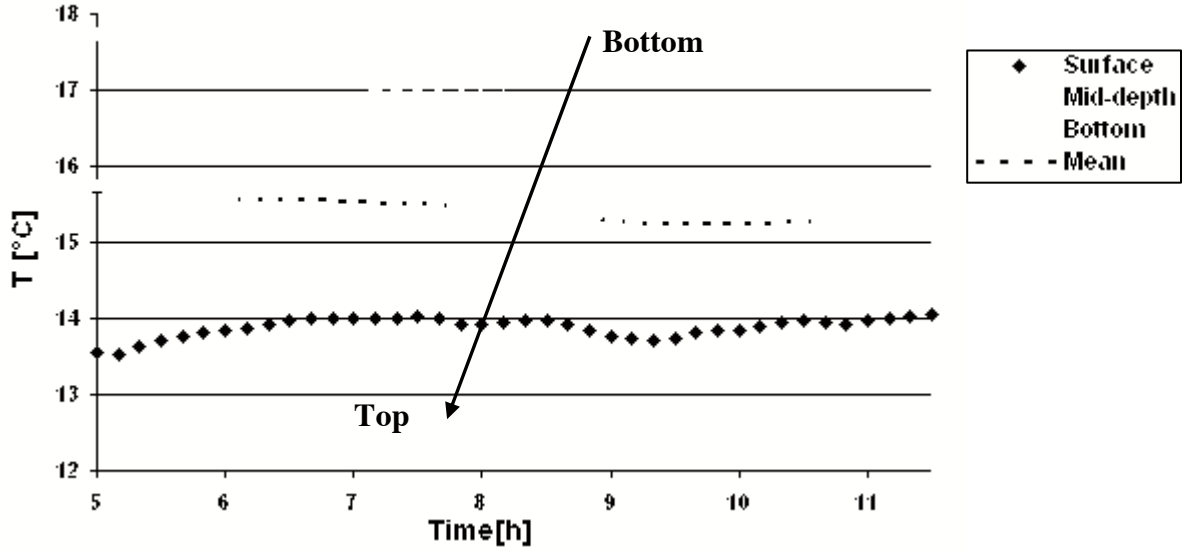

Figure 14 - Temperature evolution in asphalt layer during the whole experiment

1.2.2 S2 structure

- **Usual test points ; April 17th 2008**

Temperature probes have been positioned in the asphalt layer.

Structures	Point number	Mean d_1 value [μm]	T [℃] Depths: 10cm/20cm/30cm
P1	100	227	13,03/12,5/13,21
	200	243	13,03/12,5/13,21
	300	213	12,7/12,44/13,23
	400	223	12,7/12,44/13,23
P2	500	381	12,7/12,44/13,23
	600	379	12,7/12,44/13,23
	700	420	12,7/12,44/13,23
P3a	800	1915.5	12,7/12,44/13,23
	900	1396	12,37/12,38/13,24
	1000	1436	12,37/12,38/13,24
	1100	1282	12,37/12,38/13,24
	1200	977	12,37/12,38/13,24
P3b	1300	964	12,07/12,34/13,26
	1400	755	12,07/12,34/13,26
	1500	904	12,07/12,34/13,26
	1600	945	12,07/12,34/13,26
	1700	795	12,07/12,34/13,26
P3c	1800	1197	12,07/12,34/13,26
	1900	884	12,07/12,34/13,26
	2000	1121	12,07/12,34/13,26
	2100	923	12,07/12,34/13,26
	2200	1015	12,07/12,34/13,26

Table 11 – Temperature in he S_3 structure; usual test points; April 2008

- **Gage measurements; June 6th 2008**

The following temperatures have been recorded by embedded temperature probes of the P_1 structure.

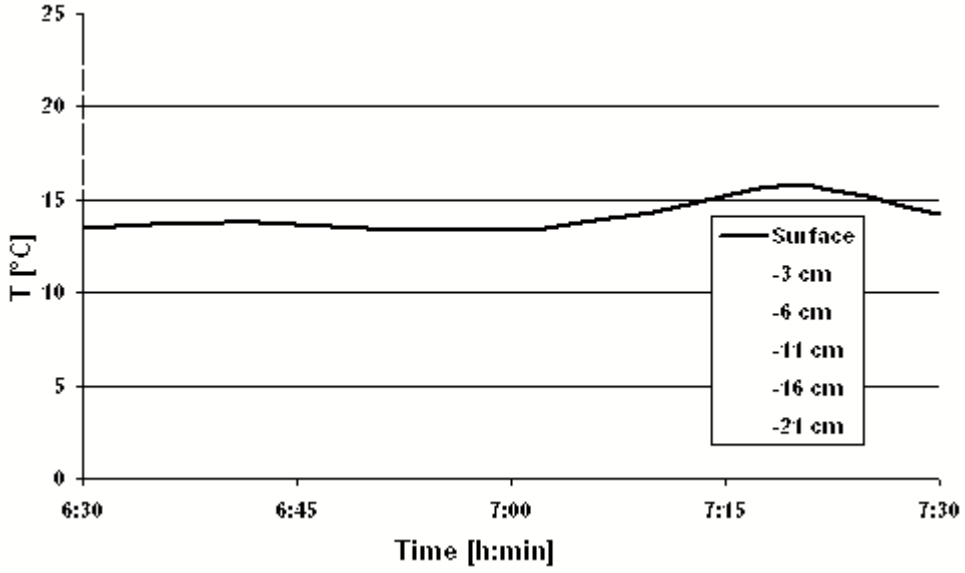

Figure 15 - Temperature in the asphalt layer during June 6th gage experiment

- **Deep anchor ; July 2nd 2009**

So do the following.

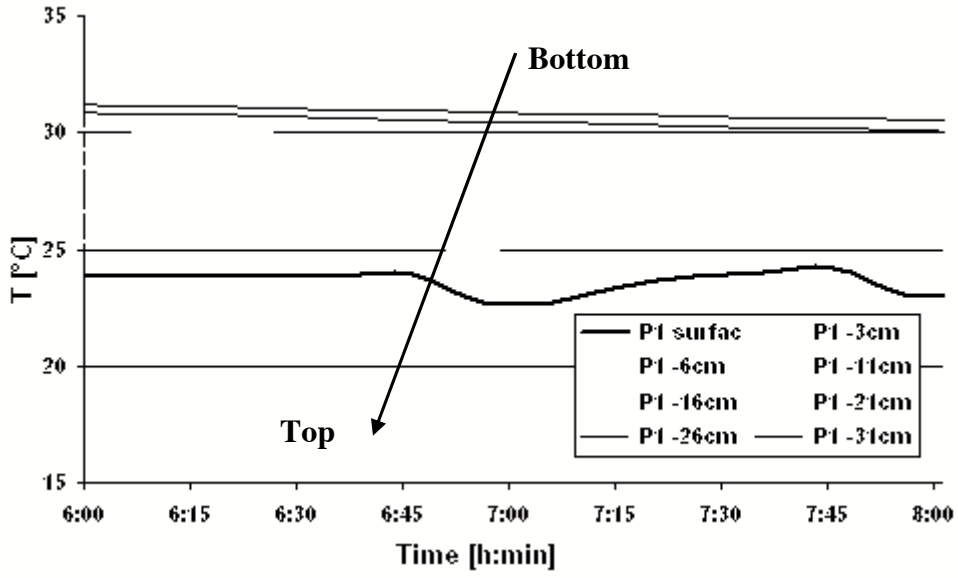

Figure 16 - Temperature in the asphalt layer during July 2th deep anchor experiment

1.2.3 S_3 structure – Crossed tests against the STBA trailer

Tests have been performed in the early morning, in order to limit the temperature variations during the experiment and to have a low gradient of temperature in the bituminous materials. The temperatures at different depths, measured using a portable data acquisition device, are summed up in Figure 17. These temperatures are almost constant during the whole measurement series. A minor gradient is observed, the bottom of the layer being a little warmer due to inertia of the pavement, but mean temperature in the bituminous layer is constant, and that way its mean stiffness too. The influence of mean temperature and gradient is not treated in this paper.

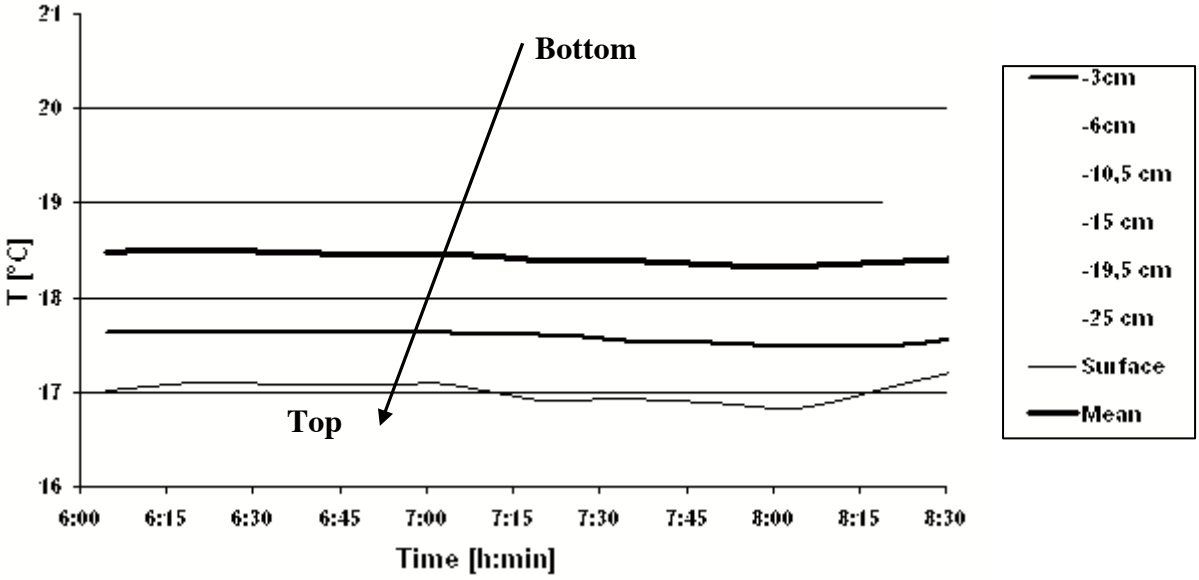

Figure 17 Temperature evolution in asphalt layer during the experiment

Temperatures retained are 18 °C in the AC_2 layer and 17 °C in the AC_1.
Besides, impulsion time was very repeatable around the 30 ms mean value. That corresponds to a 33 Hz mean frequency.

Appendix 1.3
Pavement evaluation procedure using HWD equipment

This section is extracted from a more general document written by M. Broutin and V.Souque (STAC) which constitutes the provisional "STAC's HWD technical guide" (internal document so far). It includes a test protocol, the usual maintenance and calibration procedures of the apparatus, and specific handlings procedures.

This technical guide deals with both flexible and rigid pavements testing. It describes the current procedure used by the STAC to assess a platform with HWD. It has been established from:
- the learnings from first platform testings,
- what is practised in the world.

STAC's operators conform to this guide for routine surveys

The present section is restricted to flexible pavements. The first subsection deals with the fundaments which have governed the technical choices. The measurement principle is reminded as well as the complementary data required for the data analysis. The second subsection describes the operational procedure to be followed. The last subsection proposes a provisional method for data analysis. It has relied so far on an usual pseudo-static analysis. This part will be replaced short-term by the dynamic method proposed in the thesis main body.

1.3.1 Fundaments

a - Test principle

The Heavy Weight Deflectometer (HWD) is a Non Destructive Testing (NDT) device for airfield structures which applies a transient impulsive load simulating the weight effect of an aircraft rolling wheel, onto a stationary load plate placed over the pavement, through a buffer system, and records the vertical displacements of the pavement surface (deflections) induced by this dynamic loading by means of geophones placed under the plate and at predetermined locations at the pavement surface.

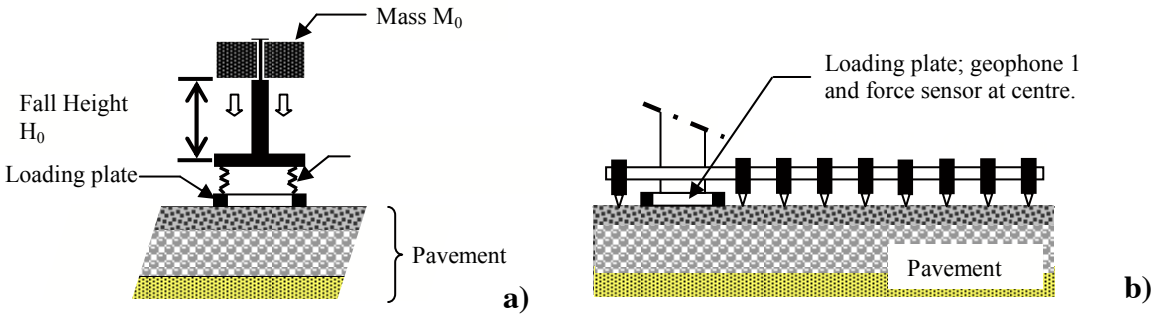

Figure 18 – HWD measuring principle

HWD is today viewed worldwide as the most appropriate device to assess the bearing capacity of airport pavements. It enables the testing of both main types of airport structures (flexible and rigid). The geophones are positioned, in the case of flexible pavements on a main beam placed ahead of the apparatus, whereas three geophones are placed on an extension beam for the study of rigid pavements.

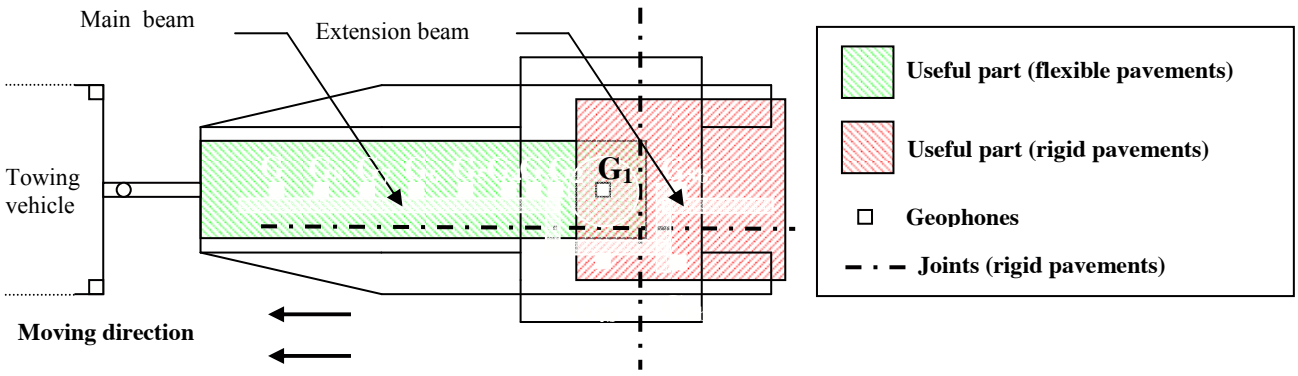

Figure 19 - Device configuration

This difference in geophones positioning is due to the distinct testing methods for the two pavement types.

Geophones G_1 to G_9 are used in the frame of the flexible structures analysis.

The analysis includes two steps. The first one called “backcalculation” consists in a parameters identification. A mechanical model is chosen to describe the pavement behaviour under load, and its parameters are identified (or “backcalculated”) using field data. The second step called “forward analysis” consists in estimating the pavement residual life using the previously defined model with the parameters backcalculated at first step.

Backcalculation

The HWD data analysis relies on the so-called backcalculation method which consists in:
- choosing a mechanical model for the pavement,
- identifying the parameters of the model for which theoretical computed deflections fit the experimental data set.

Usual processing methods are based on static Burmister model [Burmister, 1943]. This model describes the deformation of a multilayered linear elastic pavement under static plate load. The unknown parameters to be backcalculated are the stiffnesses (Young’s moduli) of the different layers. The backcalculation is performed from the pseudo-static deflection basin. These basins are reconstituted from the deflection peak values measured by each geophone (maxima measured on the blue curves of Figure 20).

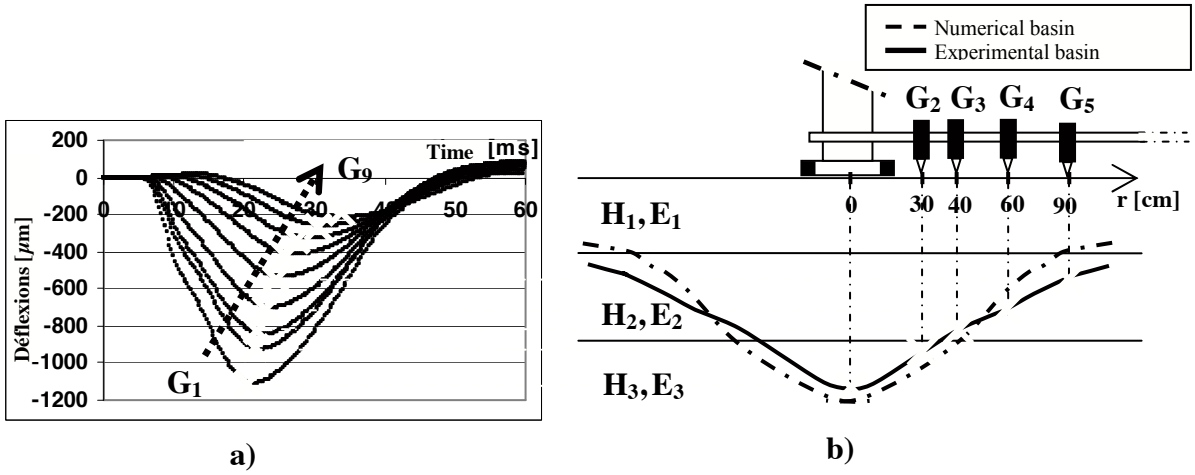

Figure 20 - a- Deflections measured on the 9 geophones, b- Fitting of deflection basin

The problem amounts to minimize the following f objective function:

$$f(\vec{E}) = \sum_{k=1}^{m} q_k \left(w_k \left(\vec{E}, \vec{H}, \vec{\nu}, \overrightarrow{IC}, r_k, p, a \right) - d_k \right)^2 \qquad [E_1]$$

with:

- d_k the maximal deflection measured by the kth of the m geophones,
- w_k the corresponding maximal theoretical deflection,
- q_k weighting coefficients,
- $\vec{E}$, $\vec{H}$ et $\vec{\nu}$ n-sized column vectors containing respectively the elastic moduli (E_i), the thicknesses (H_i) and the Poisson's ratios (ν_i) of each of the n layers of the structure,
- $\overrightarrow{IC}$ the (n-1)-sized column vectors containing the IC_i interface conditions between layers i and i +1,
- r_k the distance of the kth geophone to load centre,
- p the pressure applied on the plate,
- a the load plate radius.

In practice, the r_k, as well as p and a parameters are known, the ν_i are fixed for each reference material. It is assumed that the H_i are well-known, and the interfaces are arbitrarily considered as fully bonded in the case of a heavy load such as the one applied during a HWD test.

Consequently the only parameters to backcalculate are the Young's moduli of the materials.

✣ Direct analysis

Moduli obtained at the close of the backcalculation phase are used to compute, still using the Burmister model, the critical strains in the pavement.

The knowledge of the latter allows determining, on the basis of material performance laws:
- the bearing capacity of the pavement,
- or, for a given traffic mix, the residual life of the pavement, and if necessary an overlay design.

b - Input parameters of the test

A - Characteristics of the applied force signal

The determination of the bearing capacity of a pavement relies on the analysis of the deflection basin induced by an impulse load (Figure 21).
The response of the pavement depends on the force signal shape. Two main parameters allow describing the force signal: its peak value (F_{max}) and its pulse time (Δt).
The p_{max} maximal pressure applied depends on F_{max} and on the load plate diameter.

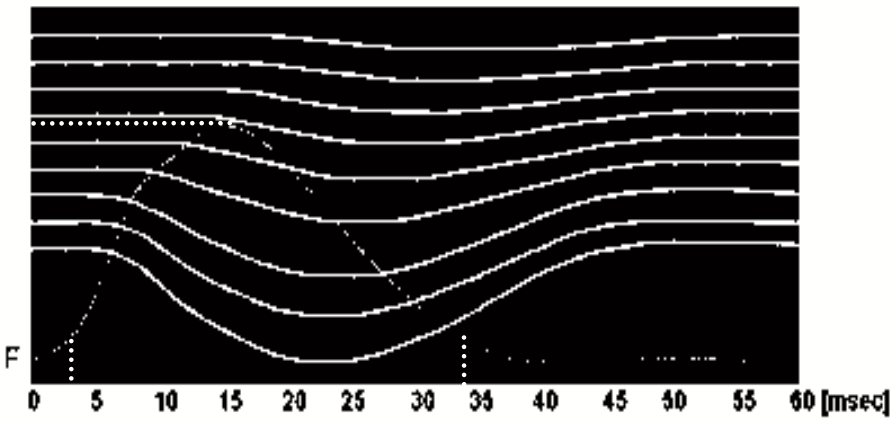

Figure 21 – Recording of the applied force and deflections

B - Target values

The target values for F_{max}, Δt and p_{max} are the following:

F_{max}

- Isolated single wheel of the design aircraft

Ideally, the peak value should be as close as possible to the equivalent single wheel of the design aircraft. This equivalent single wheel is a conceptual load applied on a circular plate which has the same effect on the pavement as the studied landing gear. For deep layers, it differs from the isolated single wheel due to the interaction between the different wheels.

Nevertheless, the determination of the equivalent single wheel requires an *a priori* knowledge of the pavement properties, so that in practice, the isolated single wheel is retained as first approximation.

The determination of the latter requires the knowledge of:

- The traffic, and especially the design aircraft.

- Study of the nonlinearity

The pavement behaviour is supposed to be linear. This hypothesis is checked by performing tests with different load levels.

Δt

Pulse time affects the pavement response. Actually, the moduli of the bituminous materials depend on the applied stress frequency.
Even though material master curves are supposed to be systematically asked for by STAC, (availability of temperature and frequency corrections), it is advocated to target a Δt value in the 30ms ± 5ms range.

p_{max}

The plate diameter is to be chosen so that the field pressure is as close as possible to the 15 bars standard pressure.

C - Parameters to be adjusted

The force signal characteristics depend on four elements:

1) the dropped mass,
2) the fall height,
3) the buffer system,
4) the pavement.

The last element is imposed. The first three are parameters linked to the test. Their relative influence can be summed up as follows:

- an increase in the dropped mass induces an increase in the peak value and in the pulse time,
- an increase in the fall height induces an increase in the peak value and a decrease in the pulse time,
- an increase in the buffer system stiffness induces an increase in the peak value and a decrease in the pulse time.

In practice, replacing the buffers and the dropped mass is tedious, so that it is chosen to use a default configuration for these two parameters, and to adapt the fall height.

This configuration is:
- M_0 = 720 kg,
- Hard buffer system (SHORE 75 hardness).

The fall height is adjusted in order to reach the appropriate (see § B supra) load level. From experience, pulse time falls automatically in the suitable range.

Two load plates are available: a 30 cm diameter one and a 45 cm diameter. In the case of heavy loads ($F_{max} \geq 200$ kN), the use of the 45 cm diameter plate is advocated. Actually, this plate allows reaching pressure levels in a suitable range i.e. close to 15 bars (see Table 12).

F_{max} [kN]	p_{max} (30cm) [bars]	p_{max} (45cm) [bars]
200	28.3	12.6
250	35.4	15.7
300	42.4	18.9

Table 12 - Pressure ranges according to the load plate

c – Data required for the platform testing and the data analysis

The following data are required for the testing phase and/or for the subsequent data analysis.

A - Airport layout plan

It is necessary:

- For the testing phase, in order to evaluate the testing duration, and to define the test points.

B - Knowledge of the structures

It is necessary:

- For the testing phase, in order to know the cutting up into homogeneous areas. It affects directly the test points distribution.
- For the analysis phase, in order to determine the bearing capacity and/or residual life of the tested pavements. Actually, backcalculation and forward analysis phases both require the knowledge of the nature and thicknesses of each constitutive layer.

It relies on:

- A background history,
- A preliminary GPR test survey.

Actually, the background histories are usually incomplete, so that the second item is systematically imposed by STAC, before each HWD test survey. It consists in a Ground Penetrating Radar (GPR) survey combined with corings (which are used as reference to adjust precisely the level depths measured by the GPR). This preliminary study results in such kind

of a very precise “structural mapping” providing the cutting up into homogeneous areas, and for each of the latter the precise layer thicknesses.

C - Traffic data

The latter are necessary:

- For the testing phase, in order to define consistently the load level to be applied over the structure.
- For the analysis phase, in order to predict accordingly a residual life for the pavement.

D - Material database

The latter is necessary:

- For the analysis phase, 1- for the validation of the backcalculation phase (i.e. consistency of results?), and 2- for the determination of the pavement structural performances.

The required data are:

- Information about the subgrade and the unbound materials: obtained with Dynaplaque tests [Benoist and Schaeffner, 1982]

- Information about the asphalt materials:

  - Complex moduli tests, in order to estimate 1- the moduli values in the test conditions (temperature and frequency) for the validation of the backcalculation phase, and 2- their dependence with temperature and frequency, for the adjustments required during the forward analysis phase.
  - Fatigue tests, in order to assess the bearing capacity and/or residual life of the pavement.

E - Report of the last IS (optional)

The latter provides valuable information about the superficial and structural condition of the structure. If steadily performed, it allows examining the evolution of the pavement condition with time. Areas with abnormally poor condition or where a rapid increase in distresses level is noticed are pinpointed. The decision can be made to condense HWD test points in these weak areas.

1.3.2 Platform testing

A - Manœuvre areas under concern

The flexible sections are usually encountered over:
- the running part of runways,
- most taxiways.

B - Preparation

Settling of the temperature recording

First step consists in boring, at least 6 hours before the beginning of tests, 3 holes at the runway side, at depths corresponding to:
- the middle of the surface asphalt layer,
- the top of the base asphalt layer,
- the bottom of the base asphalt layer.

The purpose is to know the temperature profile in the asphalt materials for the adjustments in the forward analyses.

The first 3 cm of each hole are then to be filled with a water-glycerine mix (1 glycerine volume for 2 water ones) and the holes are restoppered with an isolating paste.

Temperature gages are settled at the beginning of the tests. A temperature acquisition unit is used, whose functioning is detailed in the dedicated STAC's internal procedure.

Warming up of the material

Preliminary tests are required to warm up the material. The procedure is detailed in the "STAC's test protocol" associated document.

Checking of the Distance Measurement Instrument

The precision of the Distance Measurement Instrument (DMI) is to be checked before the beginning of the test survey, using a known distance (length of the runway for instance) as a comparison. In the case of significant deviation, a calibration is to be performed, according to the dedicated STAC's internal procedure.

C - Selection and pinpointing of the test points

✣ Spacing between test points

A 50 m default spacing between test points is retained on an homogeneous section. This distance is measured using the DMI.
However, this value may be adapted depending on the heterogeneity of the tested area, or on the conclusions of the last IS report, which may recommend condensing points in selected areas.

Remark: The testing of a 3 000 m runway requires 120 test points with the 50 m default spacing. With a 3 to 5 min test time (depending on the selected number of sequences and drops), this leads to a 6 to 10 hours test survey.

✣ Distance to axis

The distance to the runway or taxiway centreline shall correspond to half the distance of axis of the design aircraft, as this area is the most stressed. The default value is 3,50 m.

✣ Numbering

In the case of an homogeneous runway, the first point (chaining 0) is conventionally placed at the extremity of the runway corresponding to the lowest threshold, right of the centreline. The following points are placed with a 50 m spacing (Figure 22). When arriving at the end of the runway, the device is driven across the axis and placed, in the opposite direction, at the same abscissa as the last point of the first measurement lane. The chaining of the last performed point is entered, and the option “opposite displacement sense” is ticked for the DMI. The device is moved 25 m ahead. The first test of the new measurement lane is performed at this location. Other tests are performed each 50 m. This procedure allows arranging test points in a quincunx, and pinpointing their locations from the lowest threshold.

The same reasoning is followed for taxiways, even though the notion of threshold does not exist, so that an edge is to be arbitrarily chosen for numbering.

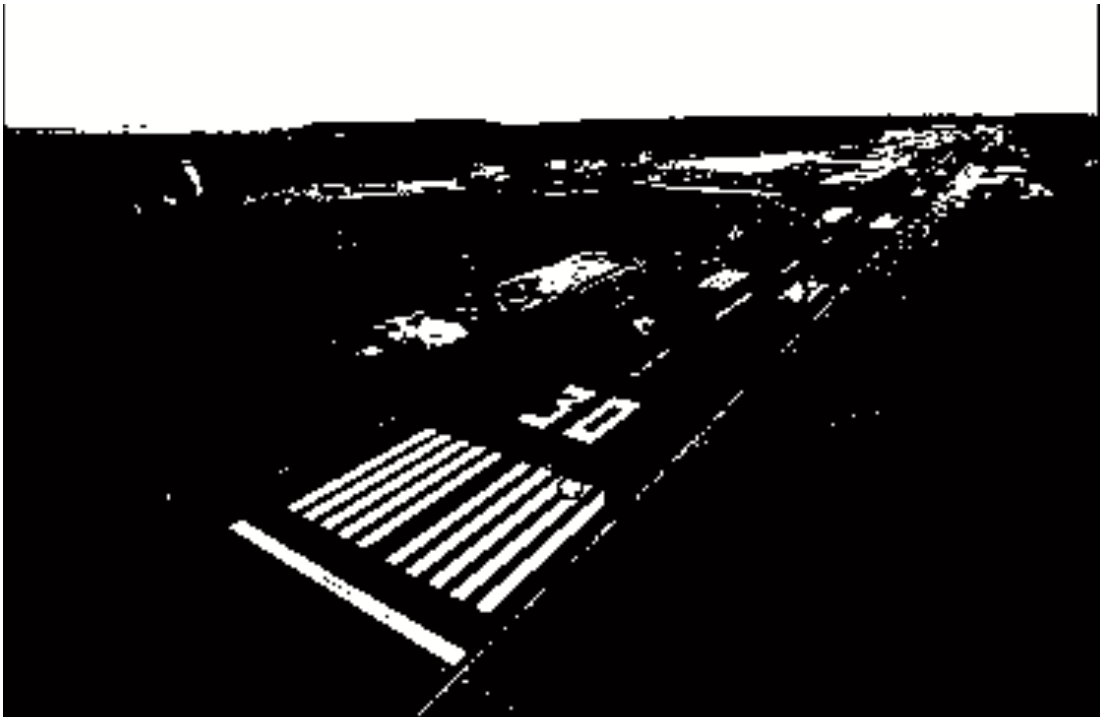

Figure 22 - Positioning of the test points on a runway (flexible structures)

✣ Pinpointing

The test points are to be spotted and numbered using a spraycan, and gradually pinpointed on the supplied map.

D - Selection of a drop sequence

✣ Load peak value

Ideally

As explained supra, if the traffic is well-known, the peak value is chosen as corresponding to the Isolated Single Wheel of the design aircraft.

By default

In the absence of any traffic data, a target deflection under the load plate is defined. The target value is 700 μm.

This value allows:
- remaining in the geophone measurement range (0 to 2 mm), and in the allowable strains values range for an usual airfield pavement.
- applying an external action strong enough, so as to produce a significant deformation at outer geophones.

✣ Pulse time value

As explained above, the Δt pulse time value shall be in the 30ms ± 5ms range.

E - Selection of a measurement sequence

When a correct configuration is obtained (in terms of force peak value and pulse time), drop sequences with different fall heights may be defined, to evidence potential nonlinearity of the unbound materials and subgrade.

A drop sequence is made up of several test series composed of n_i drops from the H_i fall height. n_i shall not be equal to 1, in order to check repeatability of the test and to squeeze any aberrant value when happening.

Thus, a typical test sequence is composed of a setting fall (systematically applied) and the following drop sequence: $n_1 \times H_1 + n_2 \times H_2 + n_3 \times H_3 + \ldots$

✣ Adjustment of the reference fall height

The reference H_1 fall height is to be adjusted so that the applied force corresponds to the Isolated Single Wheel of the design aircraft, or by default, to reach a 700 μm central deflection.

✣ Number of drops

By default, the number of falls is 3 for each fall height ($n_i = 3, \forall\, i$).

✣ Study of potential nonlinearity

By default, two load levels are retained. First fall height corresponds to the H_1 value; the second one to $H_1/4$.
Accordingly, a typical test sequence is composed of a setting fall followed by three falls from the H_1 height, and three falls from the $H_1/4$ height.

F - Testing

✣ Test protocol

The retained test points are performed with respect to the aforedefined test sequences, and according to the STAC's test protocol.

✣ Filling in of the « test follow-up » file

The follow-up file must be filled after each test.

✣ Listing of the tests

The variable fields « name of the file », « structure reference », « date » and « operator » shall systematically be filled in the corresponding Window.
The name of file shall have the following structure: « Airfield_Areaxx_f_ddmmyy », where «Airfield» is the name of the tested platform, «Area» the type of manoeuvre area (runway, taxiway, parking), «xx» the number of the area, «f» the type of structure («f» for flexible, «r» for rigid, ..) and «ddmmyy» the date.

1.3.3 Data analysis

A - Preliminary analyses

✣ Determination of the homogeneous areas

- **criterion**

The criterion retained is the central deflection (geophone G_1) for the H_1 fall height.

The obtained values are compared, without any normalization process according to the real applied force, for the reasons evoked in the main body of the thesis.

- **deflections retained for the analysis phase**

For each k^{th} homogeneous area, a unique backcalculation is performed. The deflection considered for each i^{th} geophone is:

$$d_{i,k} = m_{i,k} + 2 \times \sigma_{i,k}$$

with $m_{i,k}$ the mean deflection recorded by the i^{th} geophone over the N_k test points performed on the k^{th} area, and $\sigma_{i,k}$ the corresponding standard deviation, i.e., when naming $d_{i,k,n}$ the deflection recorded at the n^{th} point by the i^{th} geophone:

$$m_{i,k} = \frac{1}{N_k} \sum_{n=1}^{N_k} d_{i,k,n}$$

$$\sigma_{i,k} = \sqrt{\frac{1}{N_k} \sum_{n=1}^{N_k} \left(d_{i,k,n} - m_{i,k} \right)^2}$$

Remark: The sample shall be representative enough i.e. $N_k \geq 10$.

✣ Pavement stiffness

The $\frac{d_0 - d_{300}}{d_0}$ coefficient is calculated as a rough guide, where d_0 is the central deflection (geophone G_1) and d_{300} the deflection at 300 mm from centre (geophone G_2). This parameter provides an indication of the stiffness contrast between the uppermost layers and subgrade.

✣ Surface moduli calculation

- **General principle**

Surface moduli are defined as the equivalent modulus of the whole pavement structure at a radial *r* distance from the load. They are calculated using the reciprocal formulation of the Boussinesq equation.

The observation of the surface moduli with regard to the considered geophone (as depicted in Figure 23) provides valuable information about:

- the global stiffness of the structure,
- the stiffness contrasts between the different layers,
- the occurrence of shallow depth to bedrock and/or nonlinearity of materials.

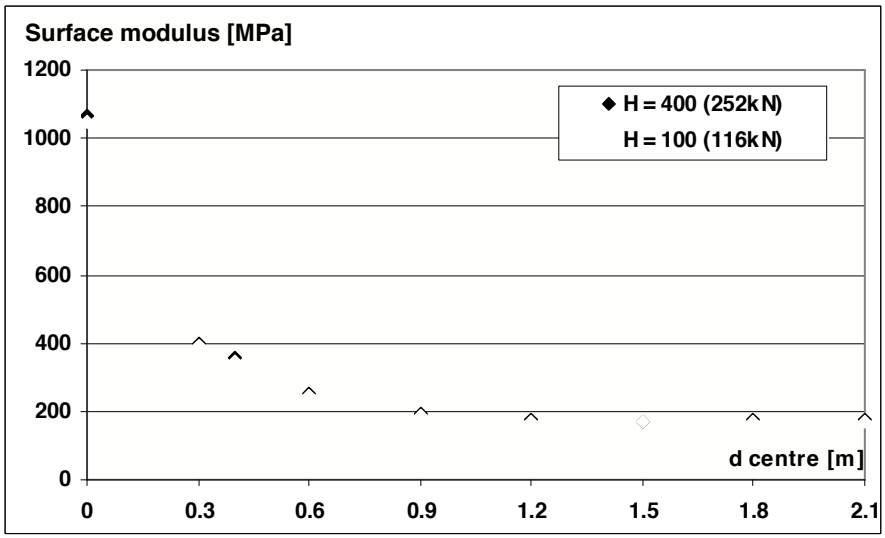

Figure 23 – Example of surface moduli results; Bonneuil instrumented test facility; February 2009

- **Expression**

Their expression [Ullidtz, 1987] is provided by the following [E_2] and [E_3] equations.

The surface modulus for the central geophone is expressed as:

$$E_1 = \frac{f \times (1-\nu^2) \times a \times p}{d_1} \qquad \textbf{[E2]}$$

The surface moduli for other geophones are expressed as:

$$E_i = \frac{(1-\nu^2) \times a \times p}{d_i} \times \frac{a}{r} = \frac{(1-\nu^2) \times a^2 \times p}{d_i \times r} \qquad \textbf{[E3]}$$

with d_i the measured deflection on i^{th} geophone, r_i its radial offset from load centre, ν the material Poisson's ratio, a the load plate radius, and f a weighting coefficient related to the pressure distribution beneath the load plate (Table 13). The hypothesis of uniform pressure is retained by the STAC.

Pressure distribution	f
Uniform pressure	2
Rigid plate	$\pi/2$

Table 13 - Weighting coefficient for surface moduli calculation according to the pressure distribution, after [Ullidtz 1987]

- **Interpretation of results**

As previously mentioned, the moduli evolution allows comparing the behaviour of the structure under load with a theoretical Boussinesq half-space.
The expected results in the case of an half space would be an horizontal lane (see Figure 24).

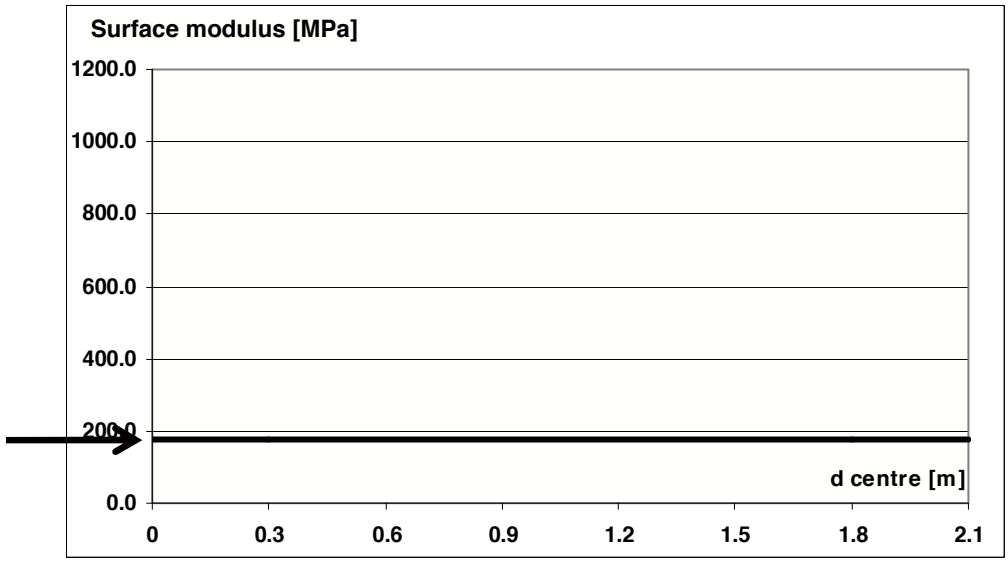

Figure 24 - Surface modulus (HWD test performed over a Boussinesq half-space)

Typical results obtained in the case of a structure lying over a Boussinesq half-space is depicted in Figure 25. The curve presents an horizontal asymptote. Surface modulus on the central geophone is representative of the Pavement-Subgrade complex, whereas the outer geophones provide an approximate value of the subgrade modulus.

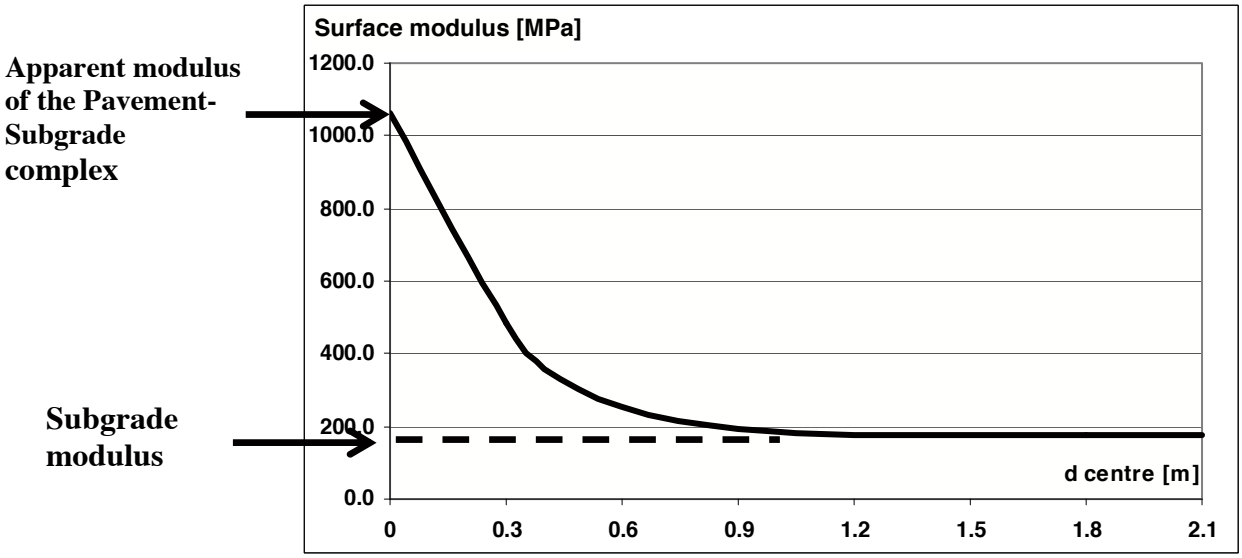

Figure 25 - Surface modulus (HWD test performed over a pavement lying over a Boussinesq half-space)

Conversely, deviation from the horizontal asymptote (see Figure 26) highlights a nonlinear behaviour, or the occurrence of shallow bedrock ($d_b \leq 6m$)

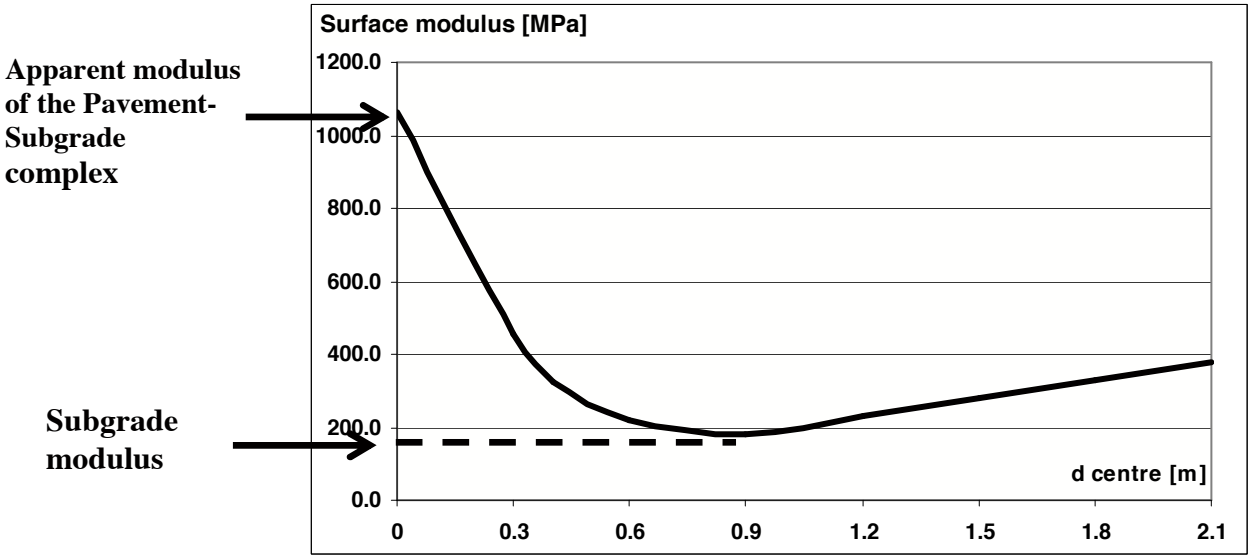

Figure 26 - Surface modulus (HWD test performed over a pavement with nonlinear or non infinite subgrade)

✣ Nonlinearity study

This step is squeezed when the surface moduli evolution is similar to Figure 25.

The linearity is tested when comparing (such as in Figure 16), the surface moduli calculated for two fall heights.
The subgrade presents a linear behaviour if the curves are superimposed.
In that case, the deviation from the horizontal asymptote is due to shallow bedrock.

✣ Calculation of the depth to bedrock

This step is squeezed when the surface moduli evolution is similar to Figure 25.

The Irwin method is used [Irwin, 2002]. It consists in displaying (see Figure 20) a/r_i versus d_i with a the load plate radius, and r_i and d_i the distance from load centre and measured deflection relative to the i^{th} geophone. The intercept point is a/H, with H the depth to bedrock.

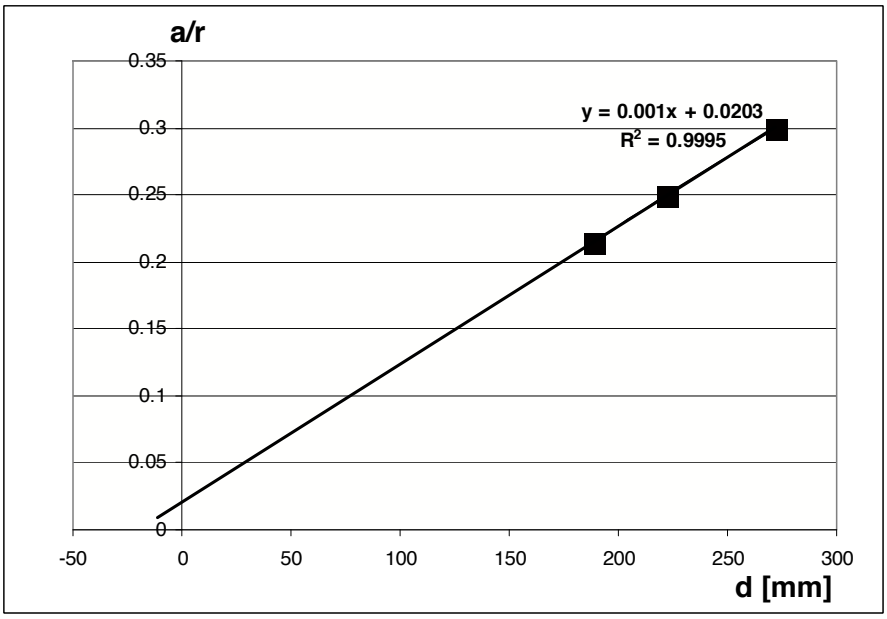

Figure 27 - Depth to bedrock determination, according to Irwin

Remark: In practice the method is rather inaccurate, so that a mean value on a significant number of test points is required.

B - Backcalculation

✣ Calculation hypothesis

The model used is the Burmister model [Burmister, 1943], which is a multilayered linear elastic model allowing the calculation of a pavement deformation under static circular load plate. As detailed in the part I of this appendix section, the load considered in the modelling corresponds to the maximal load recorded by the force sensor integrated to the HWD foot, and the considered deflections are the peak values measured by the geophones.

The backcalculated parameters are the only Young's moduli of the different layers, i.e. the thickness (including the depth to bedrock previously calculated) are known, as well as the Poisson's ratio (imposed) and the interface conditions (layers are assumed to be fully bonded).

Remark: Nonlinear models are too complex for operational use. Hence it is necessary to choose shrewdly the field load according to the traffic. If the comparison between the results from different fall heights reveals significant nonlinearity, two backcalculations are perfomed and backcalculated moduli for unbound and subgrade are straightlined.

✣ Analysis tools

The STAC uses the Alizé – LCPC software [Alize] to perform inverse calculation. This software is based on the Burmister model. A structure is first defined (Figure 28), as well as a load case (in our case a « HWD load » corresponding to an uniform static load on a circular plate).

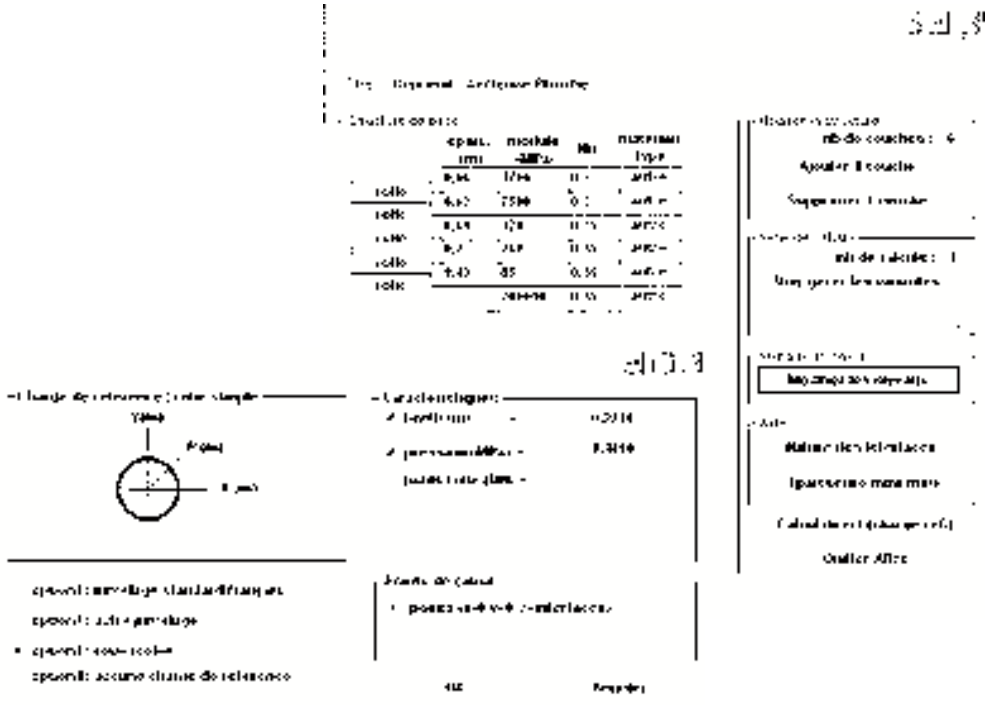

Figure 28 - Preparation of a Alize calculation: a- Selection of a structure, b-Selection of a load case

The backcalculation module (Figure 29) proposes two options:

- a grid algorithm (or « database method »),
- an optimized calculation involving a Newton Raphson convergence algorithm.

The second option is advocated.

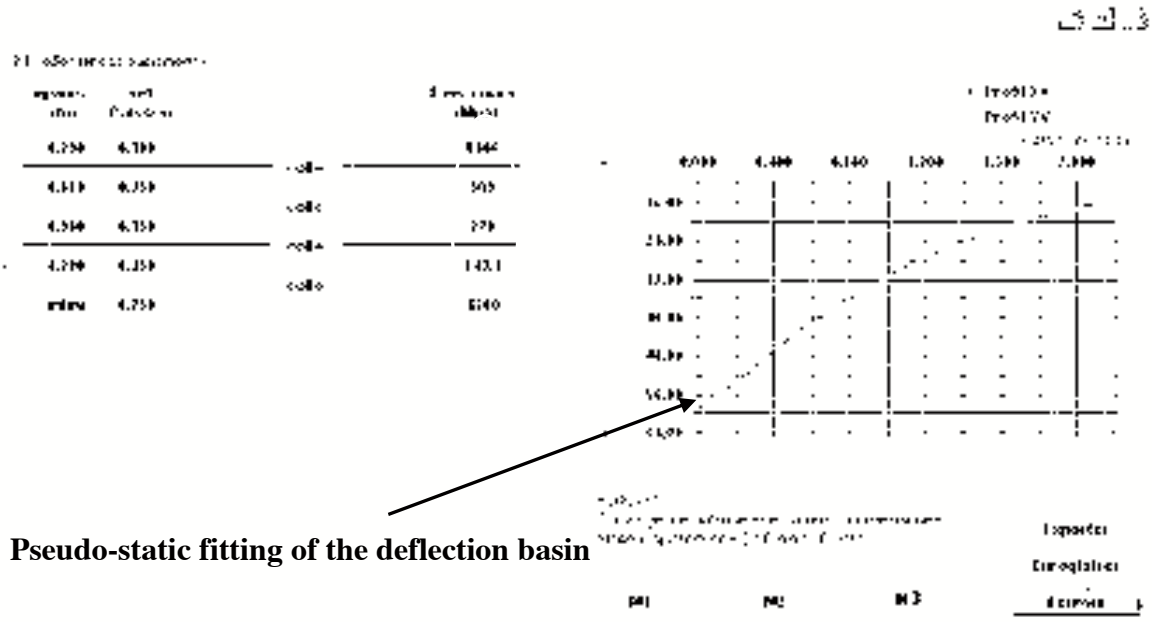

Figure 29 - Example of backcalculation performed using the Alize-LCPC software

Contrary to most backcalculation softwares, Alize presents the double advantage to allow:

- imposing boudaries for backcalculated moduli,
- imposing links between moduli of the different layers.

✣ Verification of the results consistency

The study leader shall keep a critical eye over the backcalculation results. The backcalculated moduli shall be consistent with:

- the usual moduli range, in the test condition (temperature and frequency). These values are available in the Alize database, or in the STAC's "Guide to the application of standards".
- the results from laboratory testing (complex moduli are resonant column tests).

Let also remind that the moduli shall normally decrease with depth.

C - Determination of the pavement structural performances

✣ Parameters to be determined

Two parameters can be assessed:

- **The bearing capacity of the pavement**

The bearing capacity of the pavement is the isolated single wheel allowable load which can be applied 10 000 times over the pavement during its life.

- **The residual life of the pavement**

The residual life of the pavement is calculated from the allowable number of passes of the design(s) aircraft(s) during its life. This calculation takes into account the real traffic, and the main landing gear configuration. Each wheel is modelled as a circular plate with a uniform pressure. The calculation considers the superposition of the stresses and strains imparted by each wheel, the Burmister model being linear. Lateral distribution data can also be integrated.

If the residual life is lower than the manager expectations, a flexible overlay is to be designed, in order to bring the strains back at allowable levels.

✣ General approach

Whatever the value to be determined (bearing capacity or residual life) the general approach is composed of two main steps:

- **Adjustment of the backcalculated moduli**

The previously backcaculated moduli are intrinsic moduli determine at the temperature and frequency of the test.
The direct calculation is made at $T_{reference}$ depending on meteorological data, and with a frequency linked to the aircraft velocity on the considered area. Thus, the moduli of the asphalt material have to be adjusted according to temperature and frequency, using master curves obtained from complex moduli laboratory tests.

- **Determination of the critical strains**

This step consists in performing a direct calculation with Alize, using the same structure than previously, but taking into account the adjusted moduli.

The critical strains are usually the tensile strain (ε_{XX}) at the bottom of the base asphalt layer, and the vertical one (ε_{ZZ}) at the top of the unbound material and subgrade.

Depending on the parameter to determine (bearing capacity or residual life), the theoretical load is either a unique load plate or a complex landing gear.

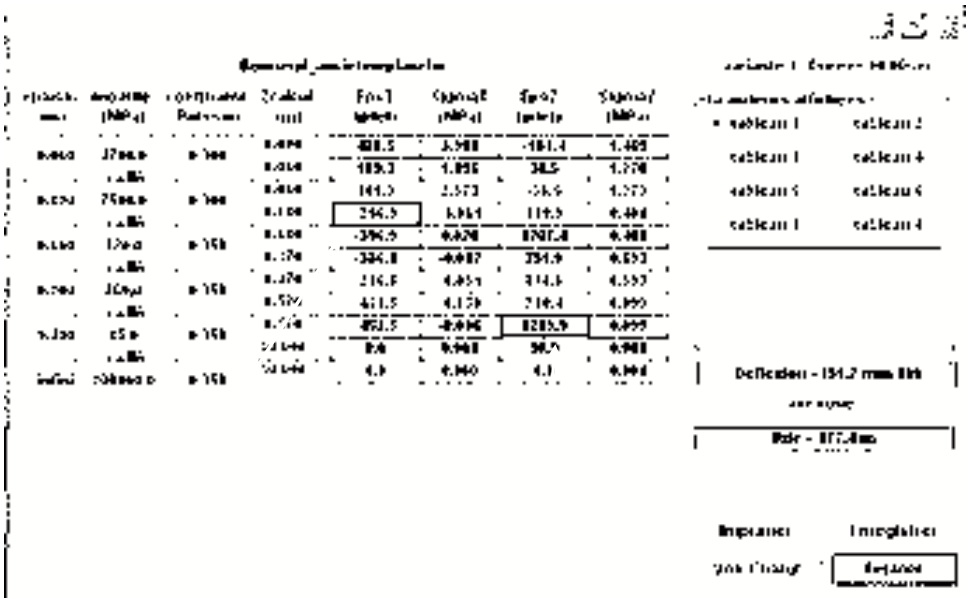

Figure 30 - Calculation of the critical strains using the Alize-LCPC software

- **Introduction of fatigue laws**

The results from fatigue tests allow obtaining the bearing capacity or residual life. Figure 31 provides an example of law. The allowable strain is plotted versus the number of load cycles.

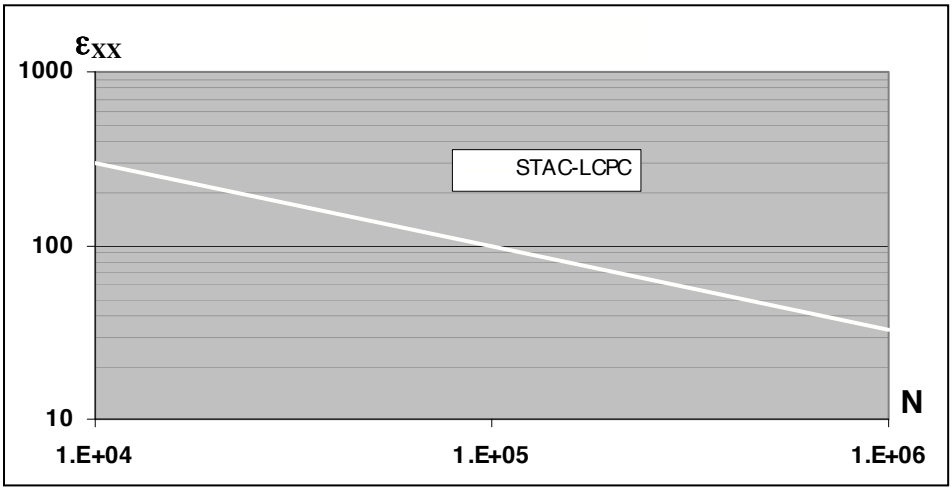

Figure 31 - Example of fatigue law (usual asphalt materials)

Appendix 2

PREDIWARE user's manual

This appendix presents the 3 main possibilities provided by PREDIWARE: mesh creation, direct calculation, and backcalculation. Other options are available, such as automated displaying of HWD raw data results, flow calculations, creation of a "mean raw file" involving representative values over an homogeneous area, or finally calculation about hysteretical loops. These options are not presented here.

Appendix 2.0
General organization of the work directory

PREDIWARE is so far a Matlab tool, using links to the CESAR FEM software. The main work directory can be placed anywhere. Nevertheless, its internal organization is fixed (even though links can be changed by the mature users). It is the following:

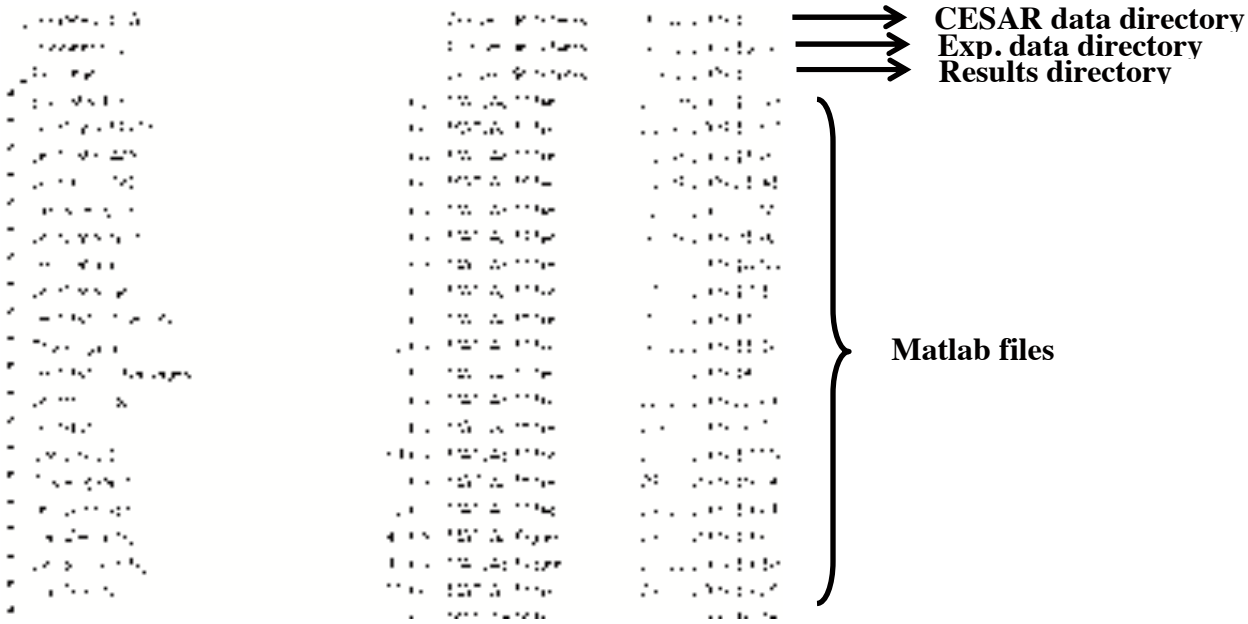

The CESAR data directory contains the CESAR FEM meshes and the corresponding data files.

The experimental data one contains the FWD raw results consisting, for each test survey, of:
- a **.fwd** file gathering, for each chaining and corresponding sequences and falls, the force and deflection peak values,
- an history (**.his**) file gathering the corresponding time-related values.

The results are stored in the last directory. They consist of
- pictures (and movie files in the backcalculation case)
- PREDIWARE results files, which are .ascii files, formatted for a direct displaying with Excel.

Organization of the FWD result files

The precise format of the .fwd and .his file depends on the manufacturer. Main organization consists in sorting the tests by chainings (i.e. test locations). Inside a selected chaining, different test sequences can be performed. Each sequence can contain several falls.

Organization of the strain result files

The strain experimental results shall conform to the following standardization.
For the dynamic analysis, the file shall consist of a unique sheet. The First column contains time; the other columns the strain measurements.

	A	B	C	D
1		1	2	3
2		EpsilonYY	EpsilonZZ	EpsilonZZ
3	Temps [ms]	Bas_GB	Sommet_GRI	Sommet_Sol
4	0	0	0	0
5	0.25	0.22	0.72	0.29
6	0.5	0.43	1.44	0.58
7	0.75	0.65	2.16	0.86
8	1	1.01	1.44	0.91
9	1.25	1.44	0.00	0.84
10	1.5	1.87	-1.44	0.77
11	1.75	2.02	-1.97	0.86
12	2	1.58	-0.67	1.30
13	2.25	1.15	0.62	1.73
14	2.5	0.72	1.92	2.16
15	2.75	0.86	1.49	1.94
16	3	1.01	1.06	1.73
17	3.25	1.15	0.62	1.51
18	3.5	0.96	-0.77	1.10
19	3.75	0.60	-2.64	0.60
20	4	0.24	-4.51	0.10
21	4.25	-0.07	-5.21	0.17
22	4.5	-0.29	-3.55	1.39
23	4.75	-0.50	-1.90	2.62
24	5	-0.72	-0.24	3.84
25	5.25	-0.50	0.41	4.13
26	5.5	-0.29	1.06	4.42
27	5.75	-0.07	1.70	4.70
28	6	-0.05	0.38	4.27
29	6.25	-0.12	-1.92	3.48
30	6.5	-0.19	-4.22	2.69
31	6.75	-0.19	-5.23	2.40
32	7	-0.05	-3.65	3.12
33	7.25	0.10	-2.06	3.84
34	7.5	0.24	-0.48	4.56
35	7.75	0.38	0.96	3.84

Jaugesmaneg

Gage number

Strain

Location

Figure 1 Standard experimental file relative to gage values; dynamic method

For pseudo-static analysis, the “strain basins” are considered. One sheet is required by gage. Name of the sheet shall be the gage name. First raw contain the distances to centre; the second one the corresponding strains values.

	A	B	C	D	E	F	G
1	0	5	10	14	16	18	20
2	-538.88	-527.76	-518.16	-501.44	-493.2	-487.28	-475.52
3							

EpsilonZZ(Sommet_Sol) EpsilonZZ(Sommet_GRH) EpsilonYY(Bas_GB) 1 2 3 Jaug

Figure 2 Standard experimental file relative to gage values; pseudo-static method

Appendix 2.1
Automated creation of CESAR mesh and associated data file

The creation of the mesh and associated data file is illustrated using the S_2 structure (see appendix 1.1. for later dynamic analysis (the option "static file is also available). Questions to be asked at screen are the following:

```
Nom du maillage à créer ? S2
Nombre de couches de la structure (y compris sol support ;
 en revanche substratum non comptabilisé le cas échéant...)?
 4
Présence d'un substratum peu profond (p<6m...) ?
 Non(1)
 Oui(2)
2
----------Entrée des noms des matériaux------------
Nom de la couche1? (pas d'espace svp...)
AC1
Nom de la couche2? (pas d'espace svp...)
AC2
Nom de la couche3? (pas d'espace svp...)
UGA
Nom de la couche4? (pas d'espace svp...)
Subgrade
----------Entrée des propriétés matériaux------------
Propriétés de l'acier constitutif de la plaque de chargement :
 Valeurs par défaut (Ro=7600kg.m-3, E=210000MPa, nu=0.25? (1)
 Entrée manuelle ?(2)
1

Propriétés de la couche "AC1"
Masse volumique de la couche "AC1" [kg.m-3] ?
2300
Module d'Young de la couche "AC1" [MPa] ?
7000
Coefficient de Poisson de la couche "AC1" ?
0.3

Propriétés de la couche "AC2"
Masse volumique de la couche "AC2" [kg.m-3] ?
2300
Module d'Young de la couche "AC2" [MPa] ?
9000
Coefficient de Poisson de la couche "AC2" ?
0.3

Propriétés de la couche "UGA"
Masse volumique de la couche "UGA" [kg.m-3] ?
2100
Module d'Young de la couche "UGA" [MPa] ?
150
Coefficient de Poisson de la couche "UGA" ?
0.35

Propriétés de la couche "Subgrade"
Masse volumique de la couche "Subgrade" [kg.m-3] ?
1800
Module d'Young de la couche "Subgrade" [MPa] ?
85
Coefficient de Poisson de la couche "Subgrade" ?
0.35
```

→ **Mesh name**

→ **Number of layers**

→ **Occurrence of bedrock**

→ **Layer names**

→ **Steel characteristics**

→ **AC_1 layer characteristics (mass density, stiffness, Poisson's ratio)**

```
----------Entrée des épaisseurs------------
Epaisseur de la couche "AC1" [cm] ?
6
Epaisseur de la couche "AC2" [cm] ?
18
Epaisseur de la couche "UGA" [cm] ?
25
Profondeur du substratum" [m] ?
3
----------Propriétés géométriques de la plaque de chargement : ------------
Valeurs par défaut ? (Grande plaque : diamètre D=45cm ; Epaisseur e=1,5cm) (1)
 Entrée manuelle ?(2)
1
donnees de chargement :
 Entrée à la main (1)
 Lecture dans fichier expérimental (2)
2
Nom du fichier .his ?  (entrée pour afficher la liste des fichiers existants)
```

→ **Layer thicknesses**

→ **Depth to bedrock (only if existing; see *supra*)**

→ **Load plate geometry (45 cm diameter by default)**

→ **Load (manual input or reading in experimental file)**

The option "reading in an experimental file" is here chosen: (in dynamic, history (.his) files; in static the .fwd files would have been considered)

```
Temp.his                  nantes6juin08.his          nantes6juin08decoup_3.his

Nom du fichier .his ?
nantes6juin08
fichier d'etude : nantes6juin08.his
Chaînage du point ? (entrée pour afficher la liste des chaînages disponibles)

Liste des chaînages disponibles :
8000   8000  10000  12000   4000  14000   2000  16000      1  18000      5  19500
Chaînage du point ?
1
Chaînage du point étudié : 1
numéro de séquence ?  (nombre de séquences disponibles :1)
1
numéro de chute ?  (nombre de chutes disponibles :3)
3
```

→ **List**

→ **Name of experimental file**

→ **Considered chaining**

→ **Considered sequence**

→ **Considered fall**

The resulting mesh and data file are by default created in the CESAR data directory (see 2.0). The resulting CESAR data file is:

```
EXEC
COOR
1 1
ELEM
1 1
Gr1 Acier
1 2 6700 210000e+006 0.25
Gr2 AC1
1 2 2300 7000e+006 0.3
Gr3 AC2
1 2 2300 9000e+006 0.3
Gr4 UGA
1 2 2100 150e+006 0.35
Gr5 Subgrade
1 2 1800 85e+006 0.35
Gr6 Substratum
1 2 6700 210000e+006 0.25
COND
  0
NUL
 2
  228
      1      3      7      9     19     21     37     39     61     63
     91     93    127    129    169    171    217    219    271    273
    331    333    397    399    469    471    547    549    631    633
    721    723    817    819    919    921   1027   1029   1141   1143
   1261   1263   1387   1389   1519   1521   1657   1659   1801   1803
   1951   1953   2107   2109   2269   2271   2437   2439   2611   2613
   2791   2793   2977   2979   3169   3171   3367   3369   3571   3573
   3781   3783   3997   3999   4219   4221   4447   4449   4681   4683
   4921   4923   5167   5169   5419   5421   5677   5679   5941   5943
   6211   6213   6487   6489   6769   6771   7057   7059   7351   7353
   7651   7653   7957   7959   8269   8271   8587   8589   8911   8913
   9241   9243   9660   9663   9664  13650  13652  13655  13657  13660
  13662  13665  13667  13670  13672  13675  13677  13680  13682  13685
  13687  13690  13692  13695  13697  13700  13702  13705  13707  13710
  13712  13715  13717  13720  13722  13725  13727  13730  13732  13735
  13737  13740  13742  13745  13747  13750  13752  13755  13757  13760
  13762  13765  13767  13770  13772  13775  13777  13780  13782  13785
  13787  13790  13792  13795  13797  13800  13802  13805  13807  13810
  13812  13815  13817  13820  13822  13825  13827  13830  13832  13835
  13837  13840  13842  13845  13847  13850  13852  13855  13857  13860
  13862  13865  13867  13870  13872  13875  13877  13880  13882  13885
  13887  13890  13892  13895  13897  13900  13902  13905  13907  13910
  13912  13915  13917  13920  13922  13925  13929  13930
 1 0 0
 0
NUL
 2
  163
      1      2      4      5     13     14     28     29     49     50
     76     77    109    110    148    149    193    194    244    245
    301    302    364    365    433    434    508    509    589    590
    676    677    769    770    868    869    973    974   1084   1085
   1201   1202   1324   1325   1453   1454   1588   1589   1729   1730
   1876   1877   2029   2030   2188   2189   2353   2354   2524   2525
   2701   2702   2884   2885   3073   3074   3268   3269   3469   3470
   3676   3677   3889   3890   4108   4109   4333   4334   4564   4565
```

Layer characteristics (ρ [kg.m-3], E [MPa], ν)

Boundary conditions

```
   4801   4802   5044   5045   5293   5294   5548   5549   5809   5810
   6076   6077   6349   6350   6628   6629   6913   6914   7204   7205
   7501   7502   7804   7805   8113   8114   8428   8429   8749   8750
   9076   9077   9490   9491   9738   9739   9908   9909  10078  10079
  10248  10249  10418  10419  10588  10589  10758  10759  10928  10929
  11098  11099  11268  11269  11438  11439  11608  11609  11778  11779
  11948  11949  12118  12119  12288  12289  12458  12459  12628  12629
  12798  12799  12968  12969  13138  13139  13308  13309  13478  13479
  13648  13649  13652
 0 1 0
 0
CHAR
  2
PUR       1
  15   3
  9664  9669  9662     9669  9674  9667
  9674  9679  9672     9679  9684  9677
  9684  9689  9682     9689  9694  9687
  9694  9699  9692     9699  9704  9697
  9704  9709  9702     9709  9714  9707
  9714  9719  9712     9719  9724  9717
  9724  9729  9722     9729  9736  9727
  9736  9737  9733
  469228.125000
GEFI
1 1
DYNI
1 2
240
0 0.00025
AMO
0 0
CFT
0
0.015152
-0.024767
0.014569
-0.012238
0.013112
-0.0075758
0.009324
-0.0061189
0.0058275
-0.0072844
0
-0.00058274
-0.006993
0.02331
-0.013112
0.019814
-0.033508
0.017191
-0.013986
0.013695
-0.010198
0.011946
-0.021562
0.015152
-0.0075758
0.014277
-0.009324
```

Load data

Maximal pressure

Number of time steps

Time origin / Time step

Damping (β, α) ; by default (0,0)

Normalized force history

0.014569
-0.01049
0.0084499
-0.0061189
0.011655
-0.011655
0.011946
-0.01486
0.019522
0.0037879
0.035839
0.026515
0.064103
0.046911
0.082168
0.069639
0.12354
0.12879
0.18939
0.1926
0.26981
0.28904
0.37413
0.40385
0.49038
0.52273
0.60606
0.66841
0.75058
0.77826
0.84324
0.86538
0.92016
0.92745
0.96212
0.96591
0.98893
0.97552
0.98601
0.9729
0.97552
1
0.96154
0.97727
0.95396
0.98572
0.94289
0.9764
0.93852
0.97436
0.94493
0.95309
0.94464
0.96358
0.93561
0.95396
0.93298
0.9458
0.92745
0.94289
0.92075

0.94027
0.92512
0.93765
0.92949
0.9458
0.9324
0.9426
0.93007
0.9359
0.92657
0.93298
0.91463
0.91521
0.89685
0.89481
0.87383
0.86131
0.83916
0.82721
0.80012
0.77972
0.78089
0.72902
0.7398
0.68531
0.68881
0.63724
0.64073
0.58858
0.60519
0.54604
0.55915
0.51661
0.51748
0.48368
0.47552
0.44551
0.4359
0.4391
0.40035
0.41754
0.36072
0.38054
0.34237
0.3549
0.31469
0.31381
0.29021
0.27593
0.28089
0.23485
0.26369
0.20979
0.23456
0.19464
0.21649
0.16317
0.14802
0.13287
0.13287
0.11218

0.098776
0.11713
0.072844
0.082168
0.042832
0.058275
0.017483
0.045455
0.013403
0.025058
-0.006993
0.011655
-0.017191
0.0081585
-0.020979
-0.0032051
-0.027389
-0.0075758
-0.02972
-0.010198
-0.035839
-0.019522
-0.041084
-0.020688
-0.04021
-0.022436
-0.046911
-0.029429
-0.048077
-0.02535
-0.04458
-0.025641
-0.048077
-0.028846
-0.045455
-0.022436
-0.040793
-0.020979
-0.043415
-0.027098
-0.047786
-0.028846
-0.047494
-0.027389
-0.043998
-0.030886
-0.046911
-0.034965
-0.048077
-0.037005
-0.045163
-0.036131
-0.040793
-0.038753
-0.018065
-0.045746
-0.028555
-0.045455
-0.025641
-0.050408
-0.023019

```
-0.043706
-0.02331
-0.044289
-0.027098
-0.047786
-0.028555
-0.046037
-0.030886
-0.047494
-0.033508
-0.043415
-0.031177
-0.042832
-0.036422
-0.042832
-0.038753
-0.045746
-0.039918
-0.019522
-0.038462
-0.028263
-0.042249
-0.027389
-0.034674
-0.017191
-0.036713
-0.022145
-0.036422
-0.024476
-0.037296
SRE
240*1
1
```

The resulting mesh (here displayed using the Cleo commercial interface of CESAR) is the following:

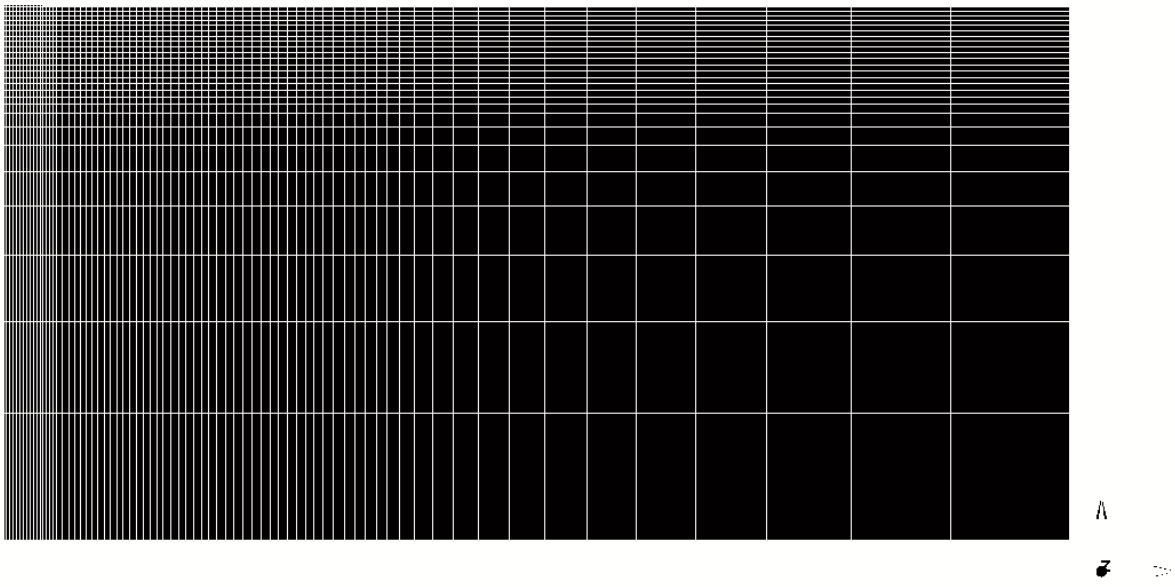

Figure 3 S_2 mesh

Appendix 2.2
Direct calculations

Direct calculations can now be performed using the previously established mesh, and the corresponding data file. The data file related to the static case has also been created. Surface deflections and critical strains are dealt with.
The parameters input related to the surface deflections and critical strains are first described in the dynamic case. Then the results corresponding to the 4 cases (static or dynamic case; surface deflections or strains) are displayed.

Input parameters (surface deflections; dynamic method)

```
Nom du fichier .data CESAR utilisé ?
S2
Type de sollicitation prise en compte dans la modélisation:
 (1) dynamique(option par défaut)
 (2) statique
1
Trace:
 (1) des valeurs théoriques et expérimentales(option par défaut)
 (2) théoriques uniquement
 (3) expérimentales uniquement
1
Choix des paramètres de départ:
 (1) Entrée des données des modules et amortissement de départ
 (2) Entrée uniquement de l'amortissement
 (3) Lecture dans fichier (option par défaut)
 1
Fréquence de résonnance de la structure ? (Utilisée pour l'établissement
 de la relation entre les coefficients de Rayleigh alpha et beta d'une
 part, et le taux d'amortissement xi d'autre part ; Valeur par défaut : 6,5Hz)

Optimization terminated: first-order optimality less than OPTIONS.TolFun,
 and no negative/zero curvature detected in trust region model.
Valeur du taux d amortissement Xi (%)?
5
EGr2 (AC1) ,MPa ?6000
EGr3 (AC2) ,MPa ?7500
EGr4 (UGA) ,MPa ?200
EGr5 (Subgrade) ,MPa ?120

Grandeurs calculées :
 (1) Déflexions du HWD uniquement (option par défaut)
 (2) Signaux mesurés sur jauges uniquement
 (3) Déflexions du HWD et signaux mesurés sur jauges
1
Nombre de géophones ? (Valeur par défaut : 9)

Option par défaut: 9 géophones
Emplacement des géophones:
 (1) Valeurs par défaut (Distances au centre par défaut [cm] : 0, 30, 40, 60, 90, 120, 150, 180, 210 )
 (2) Lecture dans le fichier expérimental (uniquement cas du calage sur données réelles)
 (3) Entrée à la main

Nom du fichier expérimental (déflexions HWD) ?  (entrée pour afficher la liste des fichiers existants)
nantes6juin08
fichier d'etude : nantes6juin08.his
Chaînage du point ? (entrée pour afficher la liste des chaînages disponibles)
1
Chaînage du point étudié : 1
numéro de séquence ?  (nombre de séquences disponibles :1)
1
numéro de chute ?  (nombre de chutes disponibles :3)
3
```

Considered calculation

Considered method (pseudo-static or dynamic)

Input parameters (default from data file, or new input)

Damping ratio

Input of new stiffnesses

Output (surface deflections and / or critical strains)

Number of geophones

Locations (here default ones)

Input parameters (critical strains; dynamic method)

```
Nom du fichier .data CESAR utilisé ?
S2
Type de sollicitation prise en compte dans la modélisation:
 (1) dynamique(option par défaut)
 (2) statique
1
Trace:
 (1) des valeurs théoriques et expérimentales(option par défaut)
 (2) théoriques uniquement
 (3) expérimentales uniquement
1
Choix des paramètres de départ:
 (1) Entrée des données des modules et amortissement de départ
 (2) Entrée uniquement de l'amortissement
 (3) Lecture dans fichier (option par défaut)
 3
Grandeurs calculées :
 (1) Déflexions du HWD uniquement (option par défaut)
 (2) Signaux mesurés sur jauges uniquement
 (3) Déflexions du HWD et signaux mesurés sur jauges
2
 Nom du fichier expérimental (déflexions HWD) ?  (entrée pour afficher la liste des fichiers existants)
 nantes6juin08
 fichier d'etude : nantes6juin08.his
 Chaînage du point ? (entrée pour afficher la liste des chaînages disponibles)
 1
 Chaînage du point étudié : 1
 numéro de séquence ?  (nombre de séquences disponibles :1)
 1
 numéro de chute ?  (nombre de chutes disponibles :3)
 3
 nom du fichier expérimental (données extensométriques) ? (A défaut, "JaugesStructureétudiée.xls")Jaugesmaneg
 nombre de jauges utilisées pour le calage ; valeur par défaut :3
 3
 Utilisation de l'ensemble des jauges, ie jauges 1 à 3 : EpsilonYY(Bas_GB),EpsilonZZ(Sommet_GRH),EpsilonZZ(Sommet_Sol)
```

In the studied case all available gage signals provided in the .xls file are taken into account, i.e. transverse tensile strain at the bottom of AC_2 layer, and vertical ones at the top of the UGA and subgrade layers.

Results (surface deflections; pseudo-static method)

The following pictures are provided by PREDIWARE at the close of the direct calculation phase. According to the selected option, the numerical values only, or superimposed with the experimental ones as a comparison are displayed.

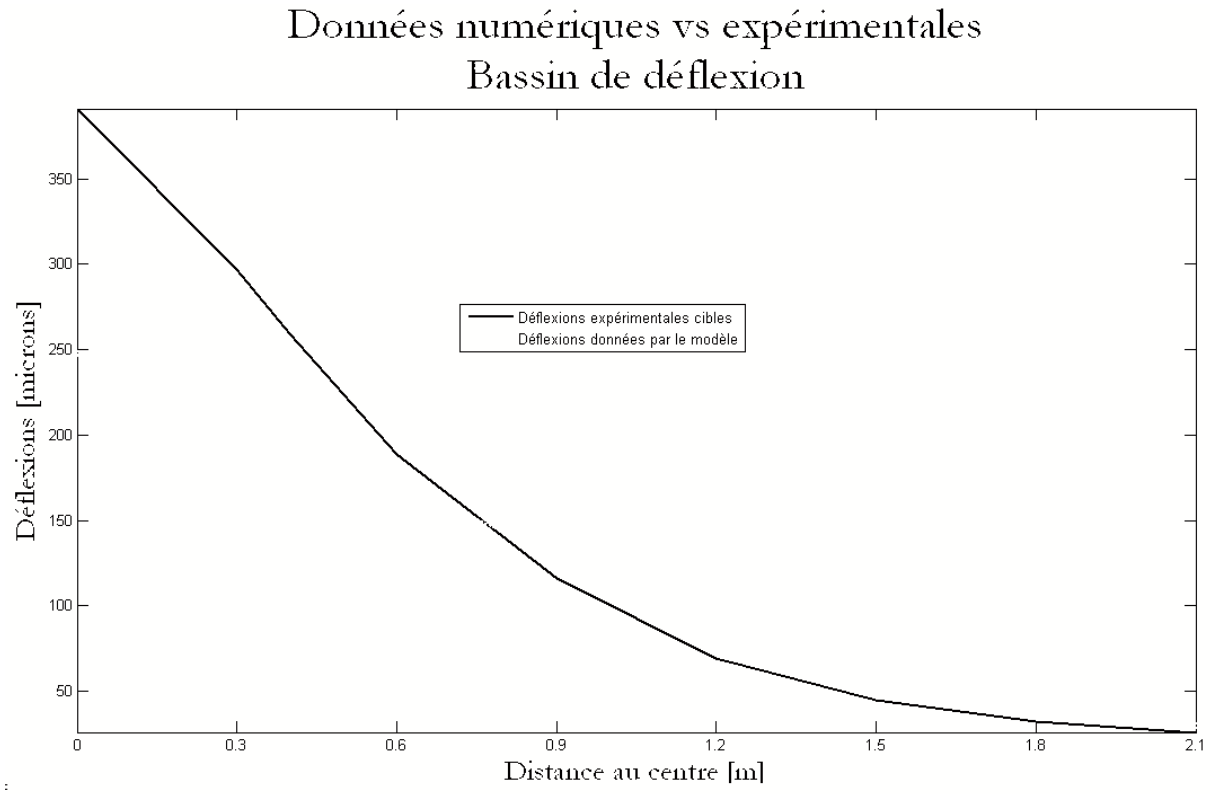

Figure 4 Direct calculation; numerical versus experimental deflection basins; S_2 structure; pseudo-static method

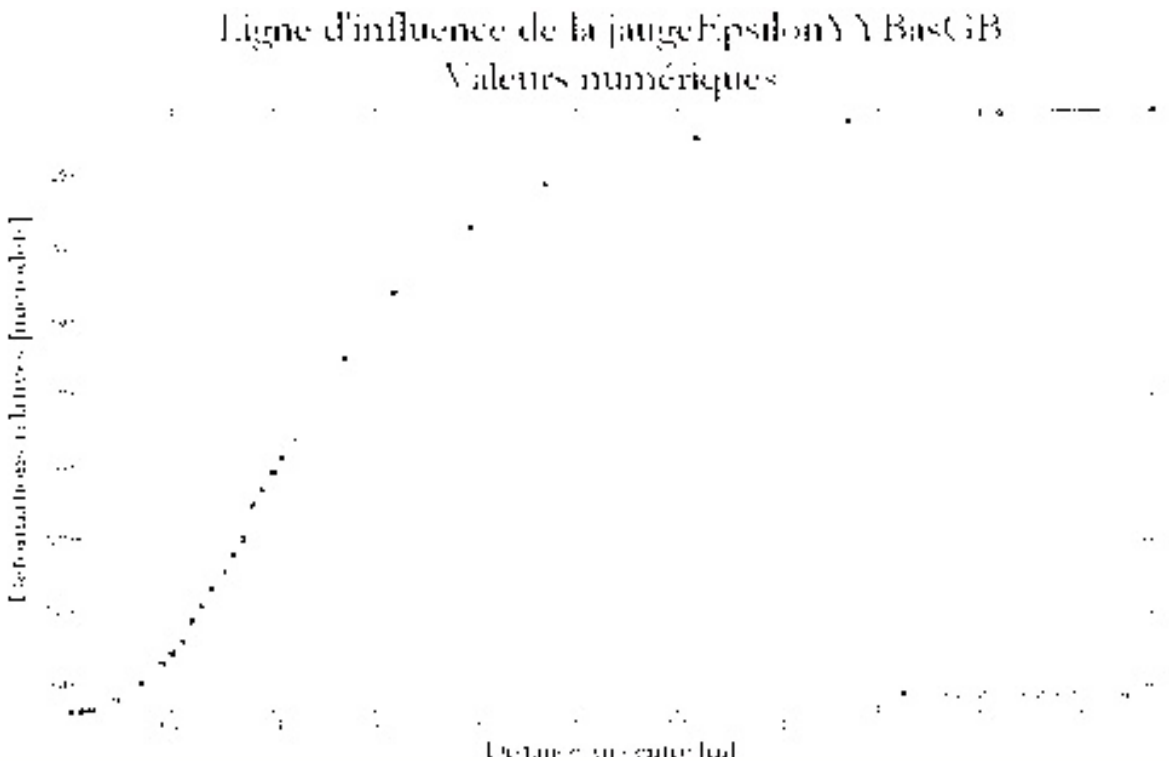

Figure 5 Direct calculation; numerical tensile strain (bottom of AC_2) basins; S_2 structure; pseudo-static method

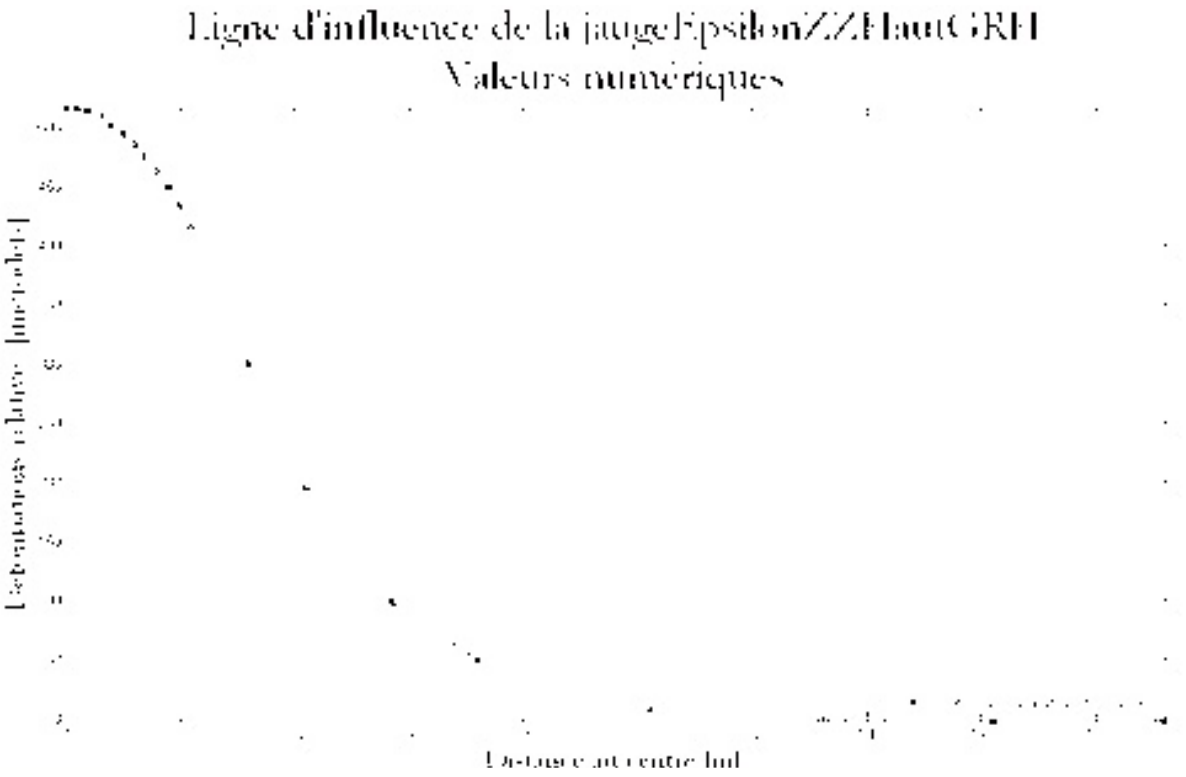

Figure 6 Direct calculation; numerical vertical strain (top of UGA) basins; S_2 structure; pseudo-static method

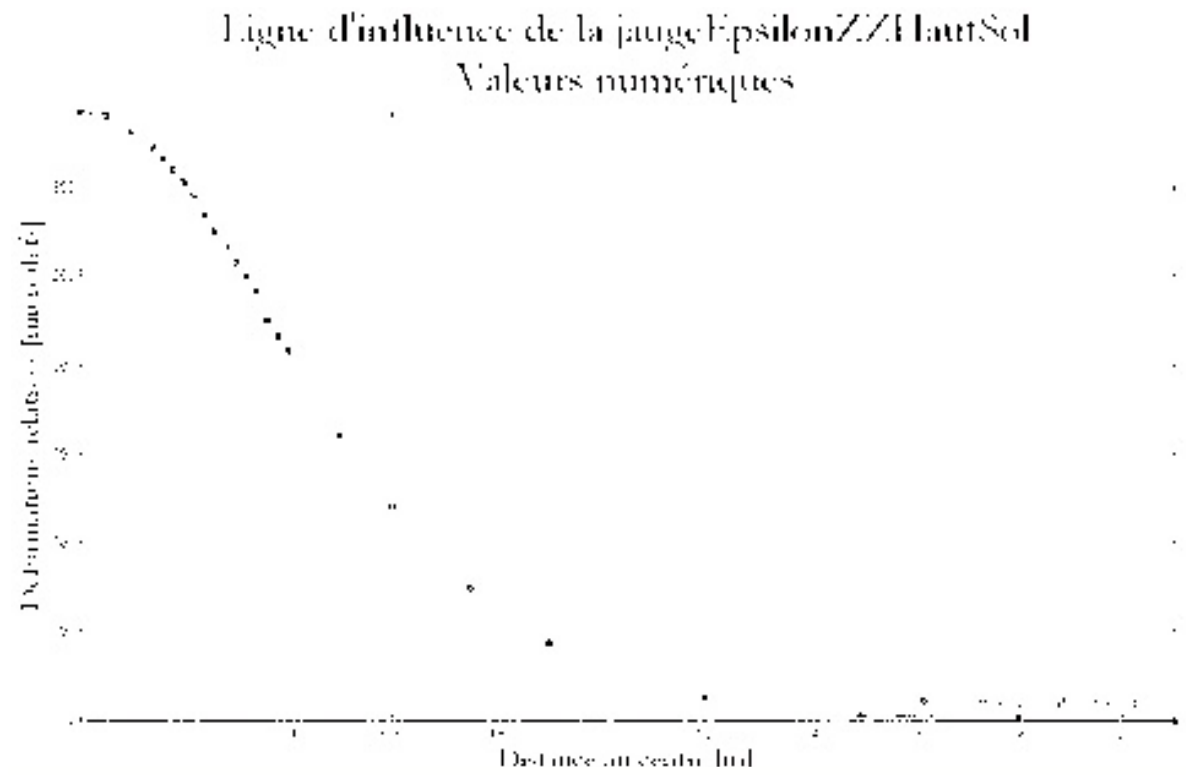

Figure 7 Direct calculation; numerical vertical strain (top of UGA) basins; S_2 structure; pseudo-static method

Opening the .ascii result file with Excel results in the following sheet:

Fichier de données :	S2_L.data								
Options du calcul :									
s déflexions de surface (géophones du HWD)									
Nombre de géophones utilisés :	9								
Numéro du géophone :	1	2	3	4	5	6	7	8	9
Distance au centre :	0	0.3	0.4	0.6	0.9	1.2	1.5	1.8	2.1
l contenant les déflexions et l'effort appliqué :	nantes6juin08								
Chaînage du point :	1								
Chute étudiée :	3								
Paramètres :									
E(BB)[MPa]	E(GB)[MPa]	E(GRH)[MPa	E(Sol)[MPa]						
6000	10000	200	120						
Pmax[kPa]=	469								
Rayon de la plaque de chargement[cm]=	22.5								
Fmax[kN]=	74.5912								
	G1	G2	G3	G4	G5	G6	G7	G8	G9
Déflexions expérimentales [microns]:	-391	-297	-259	-189	-116	-69	-45	-32	-26
Déflexions théoriques [microns]	-247.7194	-218.9044	-203.8686	-172.755	-128.8567	-92.7445	-64.9531	-44.3301	-29.3597

→ **Experimental peak deflections**

Figure 8 Direct calculation; numerical versus experimental deflection basins; S_2 structure; pseudo-static method: Result file

Results (surface deflections; dynamic method)

The following pictures are obtained when performing dynamic direct calculations. For clarity reasons, only 5 geophones are considered for deflections: G_1, G_3, G_5, G_7 and G_9.

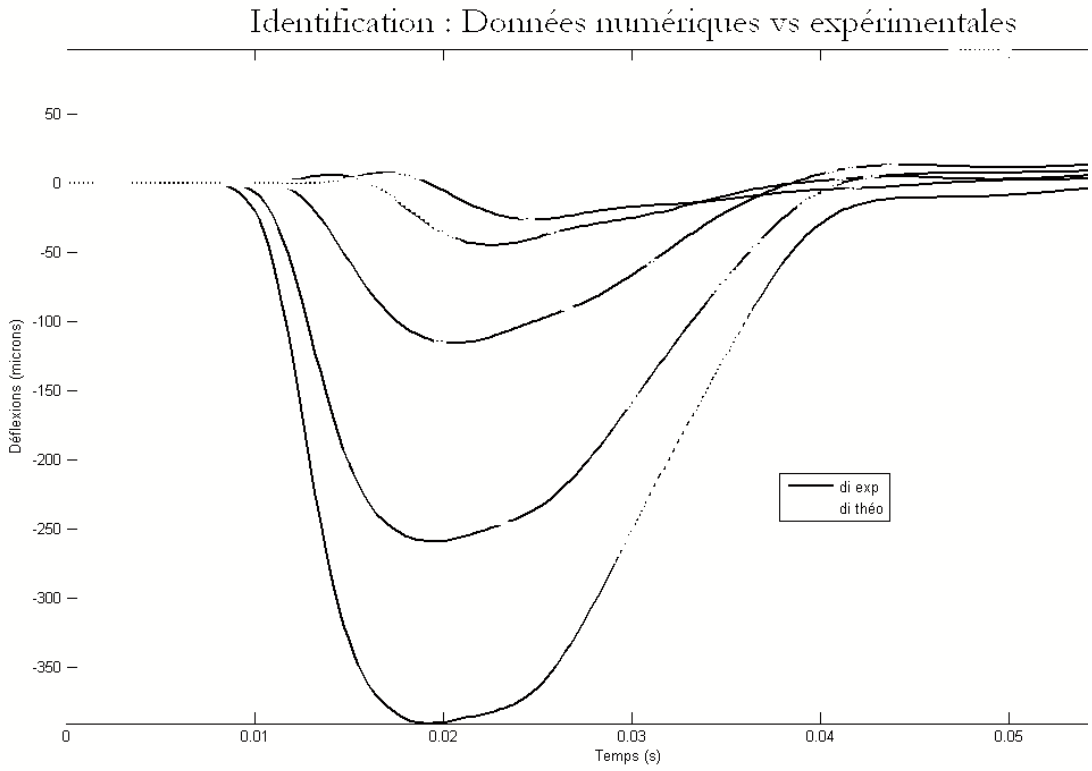

Figure 9 Direct calculation; numerical versus experimental time-related deflections; S_2 structure; dynamic method

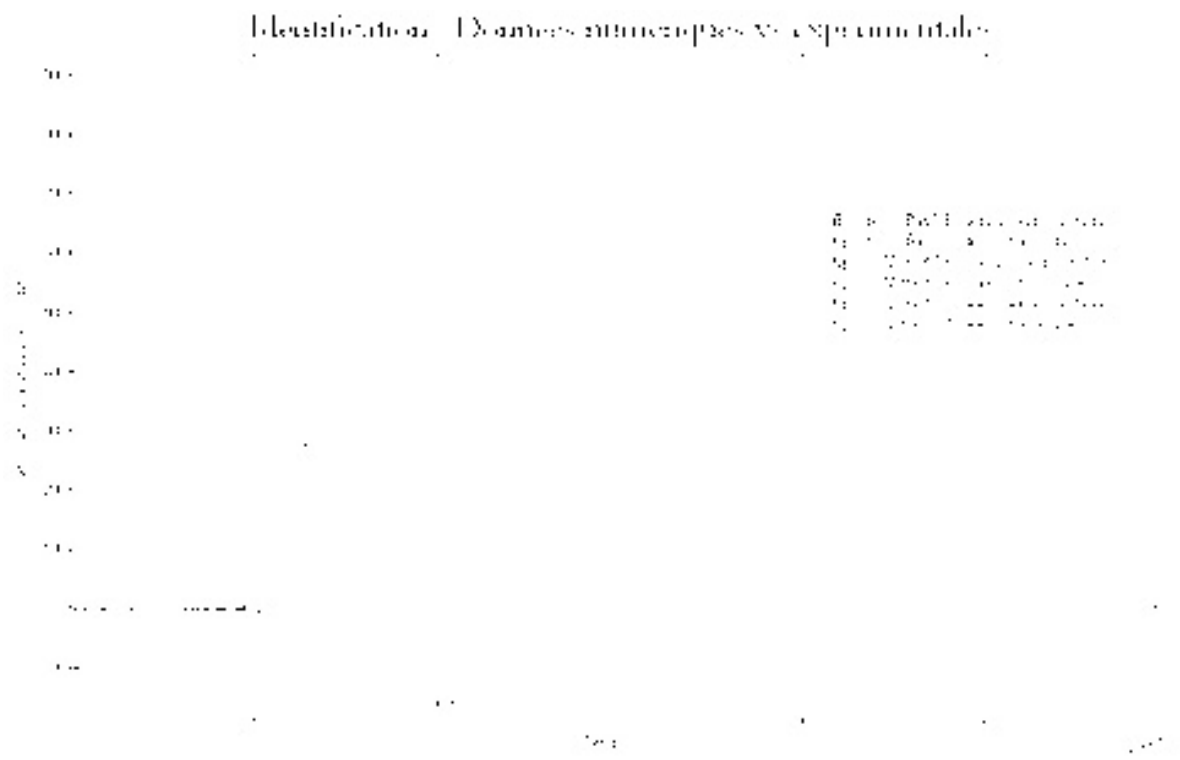

Figure 10 Direct calculation; numerical versus experimental time-related strains; S_2 structure; dynamic method

Fichier de données : S2_D.data

Calcul direct des déflexions de surface (géophones du HWD)

Nombre de géophone	9								
Numéro du géophone	1	2	3	4	5	6	7	8	9
Distance au centre :	0	0.3	0.4	0.6	0.9	1.2	1.5	1.8	2.1

Fichier expérimental c nantes6juin08

Chaînage du point :	1
Séquence de chutes	1
Chute étudiée :	3

Paramètres :

E(AC)[MPa]	E(AC)[MPa]	E(UGA)[MPa	E(Subgrade	E(Substratur	xi(%)
0.006	0.0075	0.0002	0.00012	2	4.3266

Déflexions expérimentales

t[s]	0	0.00025	0.0005	0.00075	0.001	0.00125	0.0015	0.00175	0.002	0.00
F[kN]=	1.13072	-1.84829	1.08723	-0.913273	0.978508	-0.56536	0.695828	-0.456637	0.434892	-0.543
G1[microns]	0	0.32139	0.32146	0.3187	0.31871	0.31306	0.31016	0.30155	0.29285	0.28
G2[microns]	0	0.21505	0.21392	0.20708	0.20017	0.19603	0.19185	0.18761	0.17763	0.1
G3[microns]	0	0.06937	0.060					0.00309	-0.01205	-0.02
G4[microns]	0	0.07407	0.069					0.03124	0.01783	0.00
G5[microns]	0	-0.03474	-0.042					-0.09191	-0.10316	-0.11
G6[microns]	0	-0.0503	-0.0578	-0.05995	-0.06753	-0.07519	-0.08293	-0.08803	-0.09589	-0.1
G7[microns]	0	-0.0098	-0.01274	-0.01571	-0.01593	-0.01616	-0.01916	-0.01942	-0.01691	-0.01
G8[microns]	0	0.09478	0.10215	0.10958	0.11989	0.12467	0.13512	0.14285	0.15345	0.16
G9[microns]	0	0.15372	0.16779	0.17922	0.19075	0.20517	0.21694	0.22604	0.238	0.25

Déflexions théoriques :

t[s]	0	0.00025	0.0005	0.00075	0.001	0.00125	0.0015	0.00175	0.002	0.00
F[kN]=	1.13072	-1.84829	1.08723	-0.913273	0.978508	-0.56536	0.695828	-0.456637	0.434892	-0.543
d1[microns]	0	-0.06107	-0.1653	-0.1813	-0.1507	-0.101	-0.05457	-0.02511	-0.01032	-0.02
d2[microns]	0	-0.0186	-0.07059	-0.1148	-0.1233	-0.1082	-0.08062	-0.05421	-0.03461	-0.0
d3[microns]	0	-0.009005	-0.040					0.06181	-0.04419	-0.03
d4[microns]	0	-0.001442	-0.0095					05993	-0.05149	-0.04
d5[microns]	0	0.0002427	0.00095					0.0285	-0.03322	-0.03
d6[microns]	0	9.06E-05	0.000639					000867	-0.005962	-0.01
d7[microns]	0	1.23E-05	0.0001043	0.0004628	0.001381	0.002962	0.004735	0.005847	0.005685	0.004
d8[microns]	0	1.34E-06	4.96E-06	1.11E-05	7.87E-05	0.0004127	0.001254	0.002603	0.004133	0.005
d9[microns]	0	7.93E-07	2.82E-06	-6.81E-06	-6.01E-05	-0.000155	-0.000184	4.32E-05	0.0006664	0.001

Experimental deflections

Figure 11 Direct calculation; numerical versus experimental time-related deflections; S_2 structure; dynamic method: Result file

Appendix 2.3
Backcalculation

Input parameters

```
Nom de la structure CESAR ?
S2
Nombre maximal d'itérations ?
20                                                    → Iteration maximal number
Erreur RMS normalisée cible (microns2)? (Valeur par défaut : eRMSnorm = 5 microns2 )
200                                                   → Target error
Calage de:
 (1) données réelles (option par défaut)
 (2) données simulées                                 → Simulated or real data
1
Amortissement:
 (1) rétrocalculé
 (2) fixe                                             → Fixed or backcalculated damping
1
Choix des paramètres de départ:
 (1) Entrée des données des modules et amortissement de départ
 (2) Entrée uniquement de l'amortissement
 (3) Lecture dans fichier (option par défaut)
 3
Paramètres utilisés pour le calage :
 (1) Déflexions du HWD uniquement (option par défaut)
 (2) Signaux mesurés sur jauges
 (3) Déflexions du HWD et signaux mesurés sur jauges
1
Pondération des paramètres pour le calage :
 (1) Coefficient "1" pour tous les paramètres ? (option par défaut)
 (2) Pondération par 1/Valeurs experimentales ?      → Weighting coefficients
 (3) Entrée manuelle des coefficients ?
1
Nombre de géophones ? (Valeur par défaut : 9)
9
Option par défaut: 9 géophones
Emplacement des géophones:
 (1) Valeurs par défaut (Distances au centre par défaut [cm] : 0, 30, 40, 60
 (2) Lecture dans le fichier expérimental (uniquement cas du calage sur donn
 (3) Entrée à la main

Rayon de la plaque de chargement [m]? (Valeur par défaut : 0.225m)

Rayon de la plaque = 0.225m
Fréquence de résonnance de la structure ? (Utilisée pour l'établissement de
 et le taux d'amortissement xi d'autre part ; Valeur par défaut : 6,5Hz)

Optimization terminated: first-order optimality less than OPTIONS.TolFun,
 and no negative/zero curvature detected in trust region model.
Nom du fichier expérimental (déflexions HWD) (calcul numero1) ?  (entrée pou
nantes6juin08
fichier d'etude : nantes6juin08.his
Chaînage du point ? (entrée pour afficher la liste des chaînages disponibles)
1
Chaînage du point étudié : 1
numéro de séquence ?
1
numéro de chute ?
3
```

```
Choix du pas de temps:
 (1) Lecture du fichier original
 (2) Prise en compte d'un pas de temps sur N
2
Choix de l'ensemble de la plage de temps ? (Pour gains temps calcul...)
 (1) Oui
 (2) Non
2
tmax calcul ?
 51
--------------------Nombre de pas de temps du fichier initial : 240--------------------
N=?
 3
```

→ **Choice of 1 time step over N**

```
Recalage temporel ? (Attention ! choisir un multiple de 0,25ms dans le cas des fichiers non découpés
 Valeur par défaut : 3,5ms)
3.5
```

→ **Temporal adjustment (to correct the measurement bias)**

```
--------------------intervalle de travail : [1;68]--------------------
Borne inférieure de la plage temporelle considérée pour le calage ? Pas de temps Nmin = ? (Valeur par défaut : 1)
7
Borne supérieure de la plage temporelle considérée pour le calage ? Pas de temps Nmax = ? (Valeur par défaut :68)
45
```

→ **Time frame selection for target error calculation**

Backcalculation results

Figures 12 and 13 provided by PREDIWARE show the final fittings obtained, at the close of the backcalculation procedure (i.e. when either the target error has been reached, or the maximal number of iteration) in the respective cases of the pseudo-static and dynamic with damping methods. Figure 14 depicts the stabilization of parameters (through the values X(i^{th} iteration) / X(i-1^{th} iteration) and the evolution of the error during the backcalculation process. Figure 15 focuses on the parameters evolution.

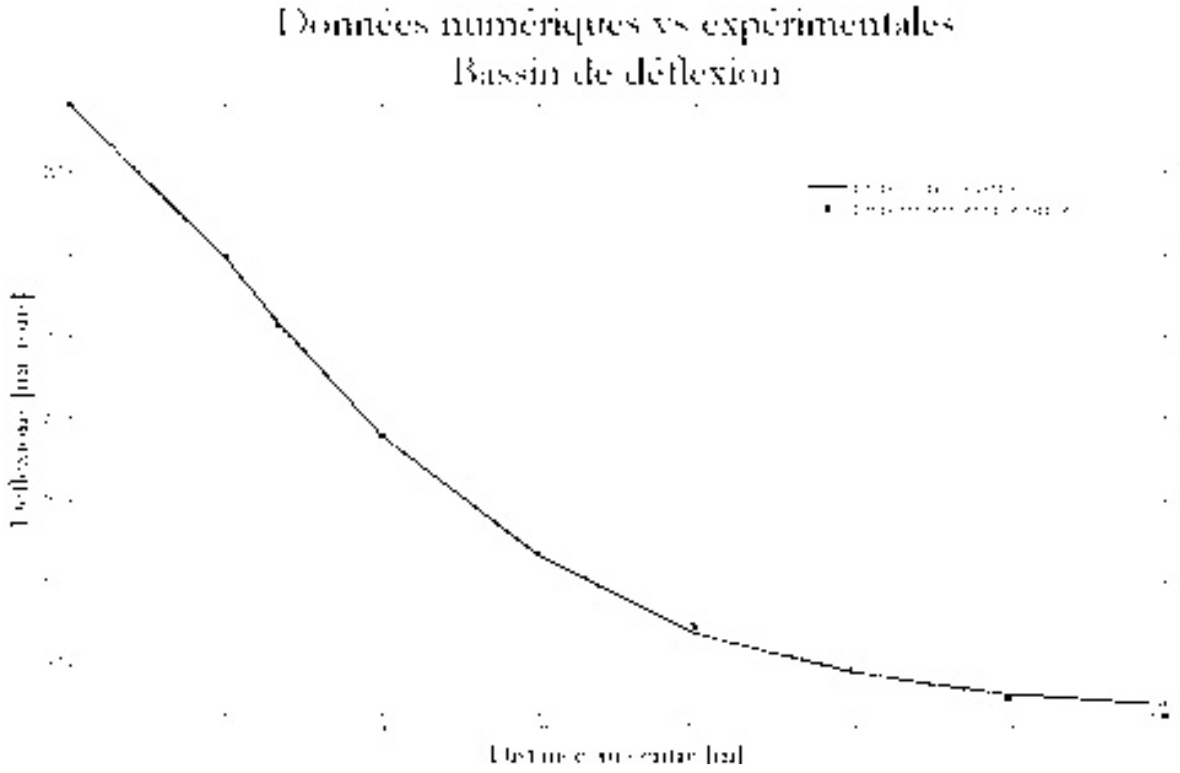

Figure 12 Backcalculation results; final fitting between numerical versus experimental deflection basins; S_2 structure; pseudo-static method

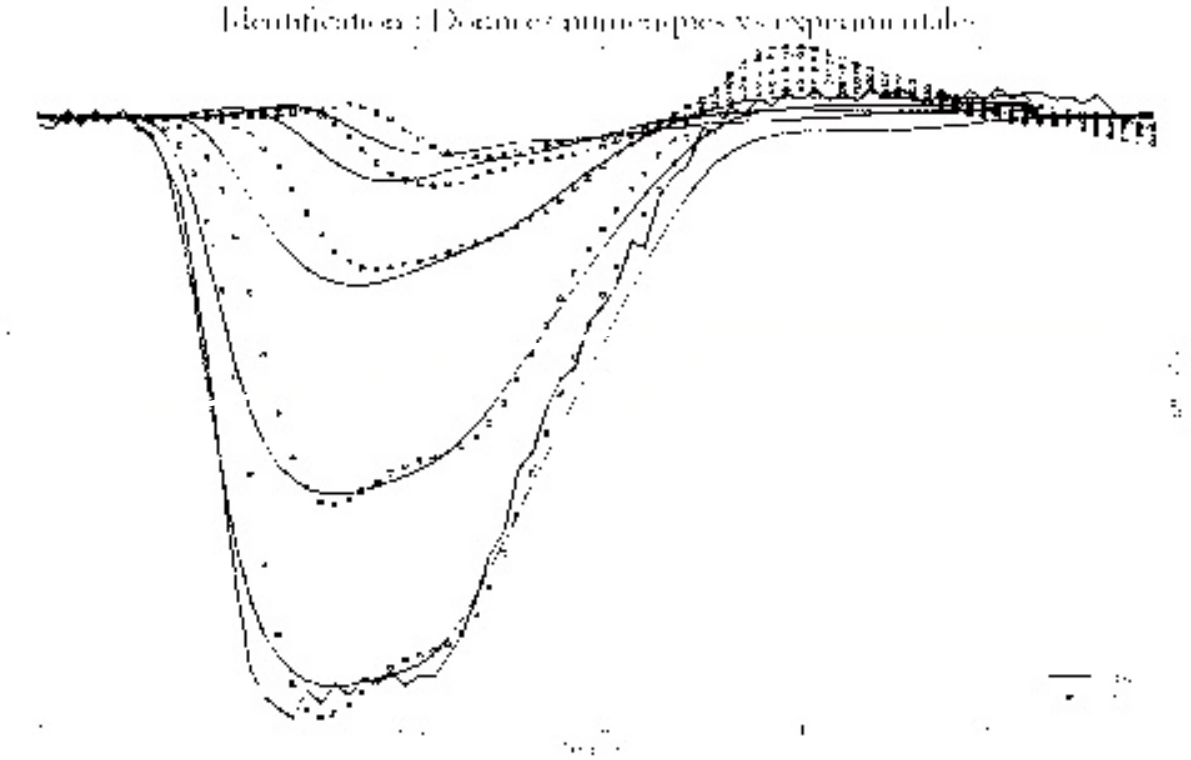

Figure 13 Backcalculation results; final fitting between numerical versus experimental time-related deflections; S_2 structure; dynamic method

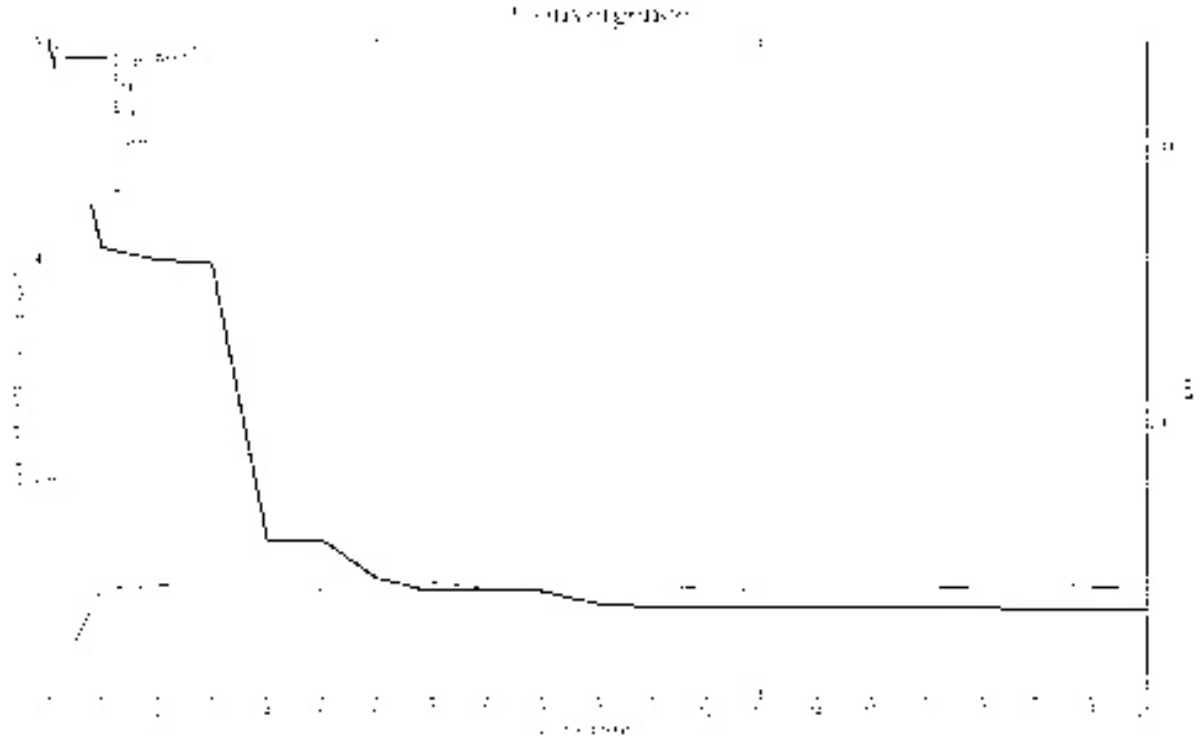

Figure 14 Backcalculation results; Stabilization of parameters and evolution of error with regard to iteration number; S_2 structure; dynamic method

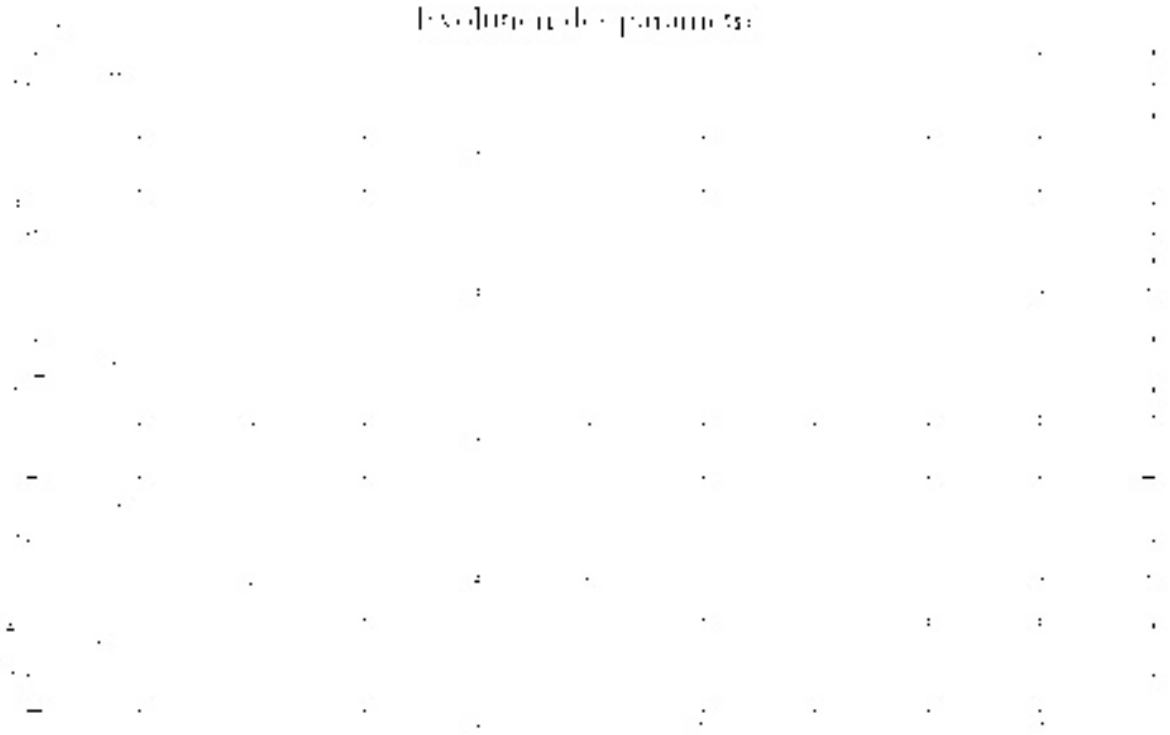

Figure 15 Backcalculation results; Evolution of parameters with regard to iteration number; S_2 structure; dynamic method

Figures 16 and 17 provide typical results files, corresponding to the pseudo-static and dynamic methods.

Fichier de données : manR6_L.data

Options du calcul :

Calage sur données réelles
Calcul inverse réalisé à partir des déflexions de surface (géophones du HWD)

Nombre de géophones u	9								
Numéro du géophone :	1	2	3	4	5	6	7	8	9
Distance au centre :	0	0.3	0.4	0.6	0.9	1.2	1.5	1.8	2.1
Coefficients de pondérat	0.33333	0.33333	0.33333	0.33333	0.33333	0.33333	0.33333	0.33333	0.33333

Fichier expérimental con nantes6juin08
Chaînage du point : 1
Chute étudiée : 3

Nombre maximal d'itératic 20
Erreur cible: 5
Evolution des paramètres

Itération	BB	GB	GRH	Sol
0	2645000000	3635000000	199000000	49000000
1	1972944405	1578846930	270252283	83915547
2	1982130084	1300051590	245166122	117227485
3	2006231566	1334382115	227673006	132460572
4	2009373819	1345412219	221602056	135192145
5	1922277139	1594466900	162727568	142272467
6	1923379990	1638066603	163935468	143794178
7	1923205223	1638507944	163933300	143823896
8	1861536034	1685355623	160889866	144524170
9	1861069014	1686727677	160902618	144536432
10	1860950121	1686875354	160900929	144537931
11	1860861180	1686952929	160898782	144538728
12	1827620718	1707575422	160583410	144634932
13	1827498009	1707851787	160588194	144636366
14	1827431584	1707930325	160588797	144636705
15	1810305684	1718335521	160536895	144664826
16	1810262978	1718402067	160538340	144665137
17	1810226303	1718444315	160538984	144665333
18	1810193707	1718468817	160539230	144665445
19	1810163616	1718491359	160539411	144665547
20	1810125382	1718505579	160539049	144665503

Fmax[kN]= 74.5912

	G1[microns]	G2[microns]	G3[microns]	G4[microns]	G5[microns]	G6[microns]	G7[microns]	G8[microns]	G9[microns]
Données expérimentales	-391	-297	-259	-189	-116	-69	-45	-32	-26
dthéo(Itération1)[microns	-549.6602	-485.3062	-451.9831	-385.1036	-292.0739	-215.0986	-154.6746	-108.5921	-74.0851
dthéo(Itération2)[microns	-465.8165	-374.9715	-333.3216	-263.7741	-183.241	-125.9201	-85.6614	-57.4943	-37.7683
dthéo(Itération3)[microns	-415.6439	-318.2591	-274.7051	-206.9612	-135.49	-89.0764	-58.7353	-38.6035	-25.0056
dthéo(Itération4)[microns	-395.3436	-299.1776	-256.3317	-190.0682	-121.5964	-78.5029	-51.1264	-33.3508	-21.5105
dthéo(Itération5)[microns	-392.9483	-296.9364	-254.1203	-187.8523	-119.5751	-76.8732	-49.9191	-32.5063	-20.9457
dthéo(Itération6)[microns	-395.9543	-301.9144	-259.3537	-190.4723	-118.1374	-73.7443	-46.74	-29.936	-19.0938
dthéo(Itération7)[microns	-391.2642	-298.4767	-256.5906	-188.5902	-117.0014	-73.0166	-46.2582	-29.6142	-18.8814
dthéo(Itération8)[microns	-391.2113	-298.4328	-256.5528	-188.5606	-116.9802	-73.0015	-46.2477	-29.6071	-18.8768
dthéo(Itération9)[microns	-391.2683	[illegible]	[illegible]	[illegible]	[illegible]	[illegible]	[illegible]	[illegible]777	-18.7103
dthéo(Itération10)[micror	-391.1959	[illegible]	[illegible]	[illegible]	[illegible]	[illegible]	[illegible]	[illegible]756	-18.7087
dthéo(Itération11)[micron	-391.1908	[illegible]	[illegible]	[illegible]	[illegible]	[illegible]	[illegible]	[illegible].375	-18.7083
dthéo(Itération12)[micror	-391.1898	-298.3221	-256.6707	-188.6554	-116.8181	-72.714	-45.3606	-29.3748	-18.7081
dthéo(Itération13)[micror	-391.2355	-298.2425	-256.7052	-188.7238	-116.8246	-72.6791	-45.9153	-29.3346	-18.6774
dthéo(Itération14)[micror	-391.2228	-298.2343	-256.6999	-188.7217	-116.8241	-72.679	-45.9153	-29.3345	-18.6773
dthéo(Itération15)[micror	-391.2195	-298.2317	-256.6981	-188.7206	-116.8235	-72.6786	-45.915	-29.3343	-18.6772
dthéo(Itération16)[micror	-391.2431	-298.1838	-256.7094	-188.7544	-116.8326	-72.6691	-45.8997	-29.32	-18.6659
dthéo(Itération17)[micror	-391.2413	-298.1826	-256.7088	-188.7542	-116.8326	-72.6691	-45.8998	-29.3201	-18.6659
dthéo(Itération18)[micror	-391.2399	-298.1816	-256.7082	-188.754	-116.8326	-72.6692	-45.8998	-29.3201	-18.6659
dthéo(Itération19)[micror	-391.2397	-298.1814	-256.7081	-188.7542	-116.8327	-72.6692	-45.8998	-29.3201	-18.6659
dthéo(Itération20)[micror	-391.2385	-298.1801	-256.7071	-188.7533	-116.832	-72.6687	-45.8995	-29.3198	-18.6657

→ **Exp. deflections**

Evolution de l'erreur RMS

Itération	eRMS
0	69628.4142
1	10998.3278
2	881.6662
3	71.0023
4	51.2323
5	44.3497
6	27.7695
7	27.7583
8	27.5968
9	27.5926
10	27.5924
11	27.5924
12	27.5732
13	27.573
14	27.5729
15	27.5679
16	27.5678
17	27.5678
18	27.5679
19	27.5677
20	27.5678

Figure 16 Storage of backcalculation results; S_2 structure; pseudo-static method

Fichier de d manR1_D.data

Options du calcul :

Calage sur données réelles
Amortissement fixé
Calcul inverse réalisé à partir des déflexions de surface (géophones du HWD)

Nombre de	9								
Numéro du	1	2	3	4	5	6	7	8	9
Distance au	0	0.3	0.4	0.6	0.9	1.2	1.5	1.8	2.1
Coefficients	0.33333	0.33333	0.33333	0.33333	0.33333	0.33333	0.33333	0.33333	0.33333

Fichier expé nantes6juin08decoup_3
Chaînage d 1
Chute étudi 3

Nombre ma 12
Erreur cible: 5

tmax / N pas	0.04875	66	0.00075

Evolution des paramètres

Itération	BB	GB	GRH	Sol
0	4.7E+09	9E+09	200000000	120000000
1	4.7E+09	9E+09	241947165	181059088
2	4.7E+09	9E+09	259969865	197017128
3	4.7E+09	9E+09	291751671	190128175
4	2.562E+09	3.53E+09	234938497	139516933
5	1.425E+09	3.53E+09	258251287	175604028
6	600383250	663330466	224563394	185634226
7	825714314	1.166E+09	222147355	185008025
8	974682641	1.539E+09	214149942	184383630
9	1.006E+09	1.59E+09	212935175	184496525
10	1.012E+09	1.597E+09	212536819	184516143
11	1.016E+09	1.611E+09	212042862	184517648
12	1.011E+09	1.616E+09	211721354	184515810

Données expérimentales

t[s]	0	0.00075	0.0015	0.00225	0.003	0.00375	0.0045	0.00525	0.006	0.00675	0.0075	0.00825
F[kN]	1.13072	1.28293	-0.761061	1.13072	-0.695828	0.630593	-0.869785	1.45689	1.97876	6.13198	9.61112	20.1355
G1[microns	0	0.28121	0.24269	0.18862	0.12432	0.05222	-0.02487	-0.11568	-0.20949	0.55963	4.56035	14.27797
G2[microns	0	0.1704	0.13965	0.10214	0.06074	0.01237	-0.02589	-0.07671	-0.15474	0.00787	1.74693	6.70795
G3[microns	0	-0.02735								614	0.54431	4.10998
G4[microns	0	0.00981								003	-0.21917	1.08307
G5[microns	0	-0.11453								175	-0.56213	-0.6892
G6[microns	0	-0.10112								093	-0.44683	-0.71828
G7[microns	0	-0.01714								135	-0.17831	-0.27274
G8[microns	0	0.16416								692	0.21534	0.21747
G9[microns	0	0.25006	0.28968	0.32199	0.35231	0.37219	0.37844	0.3847	0.38814	0.38311	0.37215	0.36904

Time-related experimental deflections

Evolution des déflexions théoriques

t[s]	0	0.00075	0.0015	0.00225	0.003	0.00375	0.0045	0.00525	0.006	0.00675	0.0075	0.00825
F[kN]	1.13072	1.28293	-0.761061	1.13072	-0.695828	0.630593	-0.869785	1.45689	1.97876	6.13198	9.61112	20.1355
d1(Itération1	0	1.01								4.826	10.09	19.85
d2(Itération'	0	0.42								3.012	6.513	13.06
d3(Itération'	0	0.264								2.302	5.143	10.39
d4(Itération'	0	0.0867								1.259	2.867	6.028
d5(Itération'	0	0.00230								0.4475	0.9053	1.939
d6(Itération'	0	-0.00554								0.2329	0.1953	0.3187
d7(Itération'	0	-0.00221								0.2121	0.09268	-0.06813
d8(Itération'	0	-0.000429	-0.004221	-0.02059	-0.05338	-0.06638	-0.01846	0.04375	0.07582	0.118	0.119	-0.01209
d9(Itération'	0	-3.37E-05	-0.000197	-0.003279	-0.02037	-0.05566	-0.07604	-0.05083	-0.01161	0.01841	0.05832	0.06029

Evolution des déflexions théoriques

t[s]	0	0.00075	0.0015	0.00225	0.003	0.00375	0.0045	0.00525	0.006	0.00675	0.0075	0.00825
F[kN]	1.13072	1.28293	-0.761061	1.13072	-0.695828	0.630593	-0.869785	1.45689	1.97876	6.13198	9.61112	20.1355
d1(Itération2	0	0.9983	0.8839	0.7308	0.8718	0.514	0.447	0.4919	1.882	4.587	9.655	19.02

Evolution des déflexions théoriques

t[s]	0	0.00075	0.0015	0.00225	0.003	0.00375	0.0045	0.00525	0.006	0.00675	0.0075	0.00825
F[kN]	1.13072	1.28293	-0.761061	1.13072	-0.695828	0.630593	-0.869785	1.45689	1.97876	6.13198	9.61112	20.1355
d1(Itération1	0	2.303	2.246	1.083	1.851	0.8614	0.2988	1.129	3.716	10.54	21.79	42.46
d2(Itération'	0	0.4341									8.985	18.44
d3(Itération'	0	0.1661	0								5.471	11.76
d4(Itération'	0	0.01314	0								1.58	4.022
d5(Itération'	0	-0.005203	-0.0								0.1946	0.1054
d6(Itération'	0	-0.001344	-0.								0.2659	0.05579
d7(Itération'	0	-0.000269	-0.00								0.3081	0.2481
d8(Itération'	0	-7.44E-05	-0.000595	-0.001667	-0.002016	-0.005692	-0.03383	-0.09885	-0.1478	-0.09543	0.05659	0.205
d9(Itération'	0	-2.57E-05	-0.000253	-0.000906	-0.000989	0.00192	0.004232	-0.01145	-0.06032	-0.1251	-0.1527	-0.0858

Evolution de l'erreur RMS

Itération	eRMS
0	1936.4055
1	2749.7839
2	3224.1021
3	3188.3393
4	910.0695
5	759.4587
6	1103.8404
7	408.3251
8	332.1144
9	330.0017
10	329.8376
11	329.5768
12	329.6336

Figure 17 Storage of backcalculation results; S_2 structure; dynamic method

Appendix 3

Mathematical resolutions

Appendix 3.1
Mathematical resolution of the Nth step of the Gauss Newton algorithm

System to be solved is:

$$\forall\ j \in [1; n+1]\ \ f_t j(\vec{E}) = \sum_{st=st\min}^{st\max} \sum_{k=1}^{m} q_k \left(w_k(\vec{E}, st) - d_k(st) \right) \times \frac{\partial w_k}{\partial E_j} = 0 \qquad \text{(Ej)}$$

A - Writing of the Nth step system:

Let $\vec{E}^{N-1}$ be the parameters set at beginning of the Nth step. One calls it reference parameters set at step N.

Each (Ej) equation is solved using the Newton method. This needs to solve at each step of the iterative process the following (S2) system:

$$\forall\ j \in [1; n+1]\ ,\ f_t j(\vec{E}) + \sum_{i=1}^{n+1} \frac{\partial f_t j(\vec{E})}{\partial E_i} dE_i = 0$$

This leads to:

$$\sum_{st=st\min}^{st\max} \sum_{k=1}^{m} q_k \left(w_k(\vec{E}, st) - d_k(st) \right) \frac{\partial w_k}{\partial E_j} + \sum_{st=st\min}^{st\max} \sum_{k=1}^{m} \sum_{i=1}^{n+1} q_k \frac{\partial w_k}{\partial E_j} \frac{\partial w_k}{\partial E_i} dE_i + \sum_{st=st\min}^{st\max} \sum_{k=1}^{m} \sum_{i=1}^{n+1} q_k \left(w_k(\vec{E}, st) - d_k(st) \right) \frac{\partial^2 w_k}{\partial E_i \partial E_j} dE_i = 0$$

$$\forall\ j \in [1; n+1].$$

When ignoring the last term (which becomes rapidly negligible due to the $\left(w_k(\vec{E}, st) - d_k(st) \right)$ factor) this can be rewritten in matrix form as:

$$S^N \cdot d\vec{E}^N = \vec{R}^N \qquad \text{(S2)}$$

where S^N is the (n+1)×(n+1) real-valued matrix whose generic (i, j) entry is:

$$S_{ij}^N = \sum_{st=st\min}^{st\max} \sum_{k=1}^{m} q_k \frac{\partial w_k}{\partial E_i} \frac{\partial w_k}{\partial E_j} \qquad (1)$$

and $\vec{R}^N$ and $d\vec{E}^N$ the (n+1)-sized real-valued column vectors whose j entries are respectively:

$$\vec{R}_j^N = -\sum_{st=st\min}^{st\max} \sum_{k=1}^{m} q_k \left(w_k(\vec{E}^N, t) - d_k(t) \right) \times \frac{\partial w_k}{\partial E_j} \qquad (2)$$

And

$$d\vec{E}_j = dE_j \quad (3)$$

S^N is called sensitivity matrix (or Hessian matrix). $\vec{R}^N$ is called remainder vector.

B - Decomposition:

S^N being a square symmetric matrix, it can be written as follows:

$$S^N = V^N D^N \left(V^N\right)^T \quad (4)$$

with V^N an orthogonal matrix ($V^N \left(V^N\right)^T = I$) and D^N a diagonal matrix.

Let σi be the terms of D.

Solution of S1 system is thus $d\vec{E}^N = V^N \left(D^N\right)^{-1} \left(V^N\right)^T \vec{R}^N$

with $\left(D^N\right)^{-1}$ the pseudo-inverse matrix related to D^N.

Thus, $d\vec{E}$ can theoretically be calculated by writing:

$$d\vec{E} = \sum_{i=1}^{n+1} \frac{v_i{}^T \vec{R}}{\sigma_i} v_i \quad (5)$$

with v_i the eigenvector of S^N corresponding to the σi eigenvalue.

Netherveless, the S matrix is ill-conditioned.
Actually, let us call Cond(S) its condition number. It is defined as the ratio between its maximal and minimal single value, i.e.:

$$\text{Cond(H)} = \max(\sigma i)/\min(\sigma i) \quad (6)$$

Numerical values obtained using Matlab on two practical cases (respectively without and with damping) are 10^7 and 10^{23}.

This implies that a regularization process is required for numerical resolution, especially in the case where damping is introduced.

The DSVD (Damped Singular Value Decomposition) method available in Matlab is here chosen.

It amounts to write:

$$d\vec{E} = \sum_{i=1}^{n+1} f_i \frac{v_i{}^T \vec{R}}{\sigma_i} v_i \quad (7)$$

with f_i a filters, expressed as:

$$f_i = \frac{\sigma_i}{\sigma_i + \lambda} \quad (8)$$

Several methods allow finding an optimal λ value. One of them is the L-curve method [Matlab]. It is retained in the thesis.

Appendix 3.2
Burmister resolution

Problem setting

In cylindrical coordinates, the compatibility equation for linear elastic behavior of a continuous medium amounts to $\Delta^2\phi(r,z)=0$, (E 1)

with Δ^2 the double Laplacian; $\Delta^2 = \left(\frac{\partial^2}{\partial r^2}+\frac{1}{r}\frac{\partial}{\partial r}+\frac{\partial^2}{\partial z^2}\right)^2$, and ϕ a stress function satisfying the equilibrium equations i.e.:

$$\sigma_z = \frac{\partial}{\partial z}\left((2-\nu)\Delta\phi(r,z)-\frac{\partial^2\phi(r,z)}{\partial z^2}\right) \quad \text{(E 2)}$$

$$\sigma_r = \frac{\partial}{\partial z}\left(\nu\,\Delta\phi(r,z)-\frac{\partial^2\phi(r,z)}{\partial r^2}\right) \quad \text{(E 3)}$$

$$\sigma_t = \frac{\partial}{\partial z}\left(\nu\,\Delta\phi(r,z)-\frac{1}{r}\frac{\partial\phi(r,z)}{\partial r}\right) \quad \text{(E 4)}$$

$$\tau_{rz} = \frac{\partial}{\partial r}\left((1-\nu)\Delta\phi(r,z)-\frac{\partial^2\phi(r,z)}{\partial z^2}\right) \quad \text{(E 5)}$$

$$w = \frac{1+\nu}{E}\left(2(1-\nu)\Delta\phi(r,z)-\frac{\partial^2\phi(r,z)}{\partial z^2}\right) \quad \text{(E 6)}$$

$$u = -\frac{1+\nu}{E}\frac{\partial^2\phi(r,z)}{\partial r\,\partial z} \quad \text{(E 7)}$$

wherer $\sigma_z,\sigma_r,\sigma_t$, τ_{rz} are respectively the vertical, radial and tangential in the horizontal plane, and shear stresses; w and u the vertical and radial displacements ; E and ν the Young's modulus and Poisson's ratio of the considered material.

The (E1) compability equation warrants that the displacements are continuous, that each bulk element is in quilibrium, and in the considered case that strains and stresses are linked by the Hooke's law.

General solution

The resolution mounts thus to the research for a stress function which satisfies the (E1) condition.

To this end a zero order Hankel transform is applied to (E1)[3] with regard to the *r* variable. When observing that $(\Delta\phi)^* = \left(\frac{d^2}{dz^2} - \alpha^2\right)\phi^*$, it amounts to solve:

$$\left(\frac{d^2}{dz^2} - \alpha^2\right)\phi^* = 0 \qquad \text{(E 1}^*\text{)}$$

The resolution phase of (E1*) is not detailed here; it results in: $\phi^*(\alpha) = Ae^{\alpha z} + Be^{-\alpha z} + Cze^{\alpha z} + Dze^{-\alpha z}$,

And thus $\phi(r,z) = \int_0^\infty \left(Ae^{\alpha z} + Be^{-\alpha z} + Cze^{\alpha z} + Dze^{-\alpha z}\right)\alpha J_0(\alpha r)d\alpha$ (E 8)

with A, B, C et D scalar numbers to be calculated from boundary conditions.

When injecting the ϕ^* expression in the (E 2*) (E 5*) (E 6*) (E 7*) Hankel transform of the (E 2) (E 5) (E 6) (E 7) equations respectively, and then applying to the solutions the inverse transform, the general following solutions are applied:

$$\sigma_{z,i} = \int_0^\infty \left(\alpha^2 \left\{\left[-A_i\alpha + C_i(1-2\nu-\alpha z)\right]e^{\alpha z} + \left[B_i\alpha + D_i(1-2\nu+\alpha z)\right]e^{-\alpha z}\right\}\right)\alpha J_0(\alpha r)d\alpha \qquad \text{(E9)}$$

$$\tau_{rz} = \int_0^\infty \left(\alpha^2 \frac{J_1(\alpha r)}{J_0(\alpha r)}\left\{\left[A_i\alpha + C_i(2\nu+\alpha z)\right]e^{\alpha z} + \left[B_i\alpha - D_i(2\nu-\alpha z)\right]e^{-\alpha z}\right\}\right)\alpha J_0(\alpha r)d\alpha \qquad \text{(E10)}$$

$$w_i = \frac{1+\nu}{E}\int_0^\infty \alpha\left\{\left[-A_i\alpha + C_i(2-4\nu-\alpha z)\right]e^{\alpha z} - \left[B_i\alpha + D_i(2-4\nu+\alpha z)\right]e^{-\alpha z}\right\}\alpha J_0(\alpha r)d\alpha \qquad \text{(E11)}$$

$$u = \frac{1+\nu}{E}\int_0^\infty \alpha\frac{J_1(\alpha r)}{J_0(\alpha r)}\left\{\left[A_i\alpha + C_i(1+\alpha z)\right]e^{\alpha z} - \left[B_i\alpha - D_i(1-\alpha z)\right]e^{-\alpha z}\right\}\alpha J_0(\alpha r)d\alpha \qquad \text{(E12)}$$

with $\sigma_{z,i}$, $\tau_{rz,i}$ w_i and u_i the stresses and displacements in the i^{th} layer (see Figure 1 below).

Boundary and interface conditions

In the case of a n-layer pavement, 4n equations are required to determine the A_i B_i C_i D_i constants.

As shown in Figure 1, 2 equations are available relative to the boundary conditions at the surface of the pavement, as well as 4 equations for each of the n-1 interfaces, and 2 conditions towards infinity.

---

[3]The Hankel transform of a *f* function is $f^*(\alpha) = \int_0^\infty f(r)rJ_0(\alpha r)dr$ and its inverse transform $f(r) = \int_0^\infty f^*(\alpha)\alpha J_0(\alpha r)d\alpha$

- At the surface, the continuities of the σ_z vertical stress and τ_{rz} shear stress are to be obeyed, what amounts to the two equations
  - $\sigma_z(r) = q(r)$ with $q(r) = p$ if $r<a$ and $q(r) = 0$ if $r>a$,
  - $\tau_{rz} = 0$

- At each interface, the first two equations still involve the σ_z and τ_{rz} continuity. The third one comes from the continuity condition of the w vertical displacement. The last one depends on the interface quality: if the two layers are fully bonded, the continuity of the radial u displacement is warranted. Otherwise, a law is to be chosen to describe the relationship between the relative radial displacement and the shear stress, the most used being of the $\tau_{zr} = k.\Delta u$ form.

Remark: the case $k = \infty$ corresponds to the « fully bonded »condition, and the cases $k=0$ to the « fully unbonded » one.

- Towards infinity, stresses are null. Accordingly, the coefficients relative to the $e^{\alpha z}$ shall be null, i.e. $A_n = C_n = 0$.

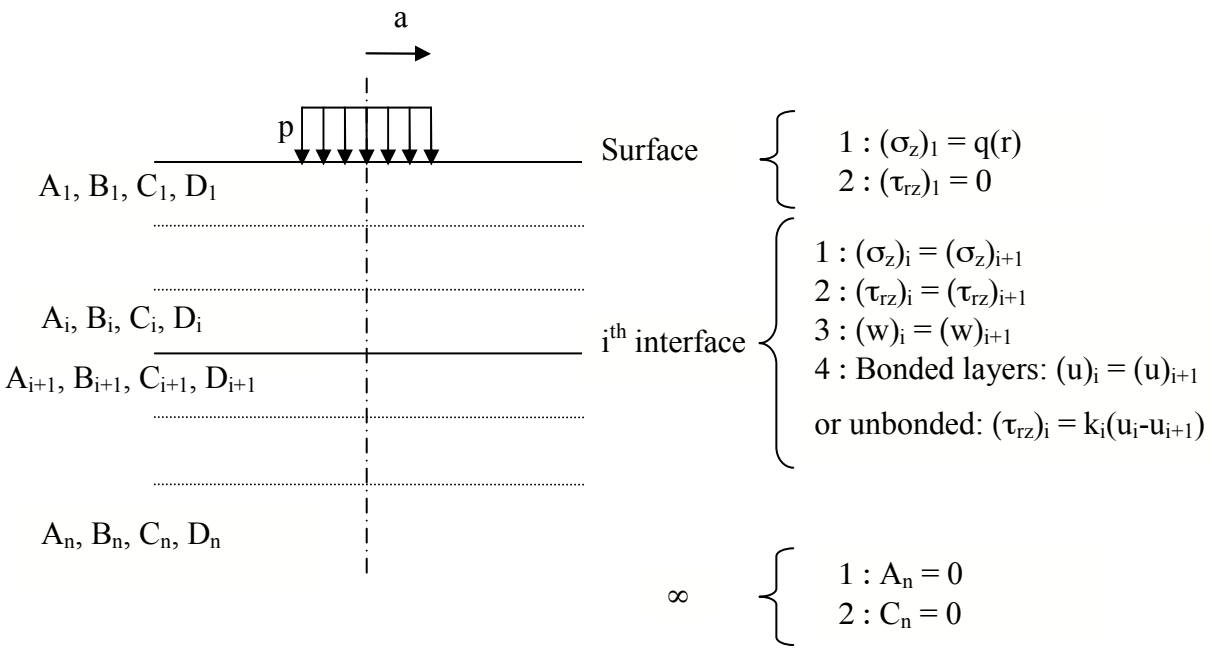

Figure 1 Burmister modelling and interface conditions

Mathematical resolution allows obtaining for each α over the integration frame, the A_i B_i C_i et D_i scalar number. It relies on the inverting of a $(4n-2)\times(4n-2)$ matrix. It is not detailed here.

Appendix 3.3
Backcalculation of pavement moduli from HWD tests
Use of the self-adjoint method in the transient domain

The possibility of introducing this method in the HWD backcalculation process is in progress.

Mathematical developments are proposed hereafter. Settling equation has been performed by Jean-Michel Piau (LCPC).

&&&

The purpose is to minimize, with regard to the Young's moduli field $E(x)$ the expression:

$$I(E) = \frac{1}{2}\int_0^T \int_\Omega p_\alpha(x)\left[u_{\alpha mes}(x,t) - u_{\alpha cal}(x,t,E)\right]^2 dx\,dt$$

with:

T = useful HWD recording frame time
t = time
Ω = elastic pavement structure (ex : multilayered) + optionally stress system (Dropped mass + buffers + load plate)
x = space variable = current point of Ω
α = displacement component (longitudinal, transverse or vertical)
$u_{\alpha mes}(x,t)$ = measured displacements in the α direction, induced by the HWD load
$u_{\alpha cal}(x,t,E)$ = numerical displacements obtained from dynamic elastic modelling (see infra the hypotheses related to the u_{cal} calculation).
p_α = function or distribution describing the weighting and loacting of the measure points
$E(x)$ = unknown moduli field in the structure

Remarks:

i) *Sum on repeated subscripts is implicit.*

ii) *Several mentioned quantities are implicitely to be considered in a vectorial or tensorial sense.*

iii) *Localizing functions allow specifying amongst others the displacement measurement locations and the recorded components; typically, for a F or HWD,*

$p_\alpha(x) = 0$ *for the longitudinal and transverse components*

$p_z(x) = \sum_{i=1}^{n} \delta_{x_i}(x)$ *for the vertical component*

with: n = *number of geophones (ex :* $n = 9$)

$\delta_{x_i}(x) =$ *Dirac distribution at the* x_i *point corresponding to the* i^{th} *geophone*

iv) in the case of the modelling of a multilayered elastic pavement, the study of the E field amounts to the determination of the E_j *modulus values related to each of the* N *layers, so that:*

$$E(x) = \sum_{j=1}^{N} E_j \, I_{C_j}(x)$$

with: $I_{C_j}(x)$ *= indicator function of the* j^{th} *layer;* $I_{C_j}(x) = 1$ *if* $x \in C_j$, $I_{C_j}(x) = 0$ *otherwise.*

v) It is here chosen to consider a problem where the only unknown are the pavement elastic moduli ; other parameters could nevertheless be considered through I, such as the Poisson's ratios, layer thicknesses, …

Hypotheses related to the u_{cal} field calculation

It is assumed that the usual hypotheses related to the elastodynamics in small deformations are respected, i.e.:

- the usual compatibility equation between the displacements field u_{cal} and the deformation field ε_{cal}
- the dynamical equilibrium between stresses, inertia forces, and external forces. The latter depend on the modelling chosen for the HWD test ; they can be null or not
- the tensorial elastic (isotropic) behaviour law of the medium, which can be written as:

$$\sigma_{cal} = E(x)N(\nu(x))\varepsilon_{cal}$$

with:
$E(x) =$ Young's moduli scalar field,
$N(\nu)\varepsilon = \Lambda(\nu)tr(\varepsilon)I + 2\mathrm{M}(\nu)\varepsilon$,
$\Lambda(\nu), \mathrm{M}(\nu) =$ Lamé coefficients at the x point, associated to the $\nu(x)$ Poisson's ratio (assumed to be known) and at the $E = 1$ value for Young's modulus.

- the boundary conditions (without effect for Ω wide enough),
- the initial conditions in terms of displacements and velocity (once more depending on the modelling).

When using the Virtual Work Principle (VWP) and the aforementioned behaviour law, the following equation (checked whatever the kinematicsly allowable $\hat{u}$ displacement is) is to be introduced for each time step:

$$\int_{\Omega} E(x)N(\nu(x))\varepsilon_{cal} : \hat{\varepsilon}\, dx + \int_{\Omega} \rho \ddot{u}_{cal} \hat{u}\, dx = 0$$

(The case where external forces are null, the shock being modelled by the initialization of the velocity field in Ω is here considered, i.e. $\dot{u}_{cal}(x,0) = \text{given value} = \dot{u}_{Fall}$ for $x \in$ Falling mass, $\dot{u}_{cal}(x,0) = 0$ elsewhere).

The resolution of this type of transient problem usually relies on the FEM method, after spacial and temporal discretizations (cf. Cesar-LCPC DYNI module).

&&&

Minimization of I by the self-adjoint states method

Resolution principle

It relies on the calculation of the δI variation in I induced by a « little » δE variation in the E field. The self-adjoint states method allows expressing δI by means of a linear form of δE. The expression of the latter appears to be a valuable guide for the construction of the δE fields trending to make I decrease.
A series of $E^{(i)}$ fields is built by computing, at each ith teration a $\delta E^{(i)}$ field, as a function of the $E^{(i-1)}$ field, and writting $E^{(i)} = E^{(i-1)} + \delta E^{(i)}$.

Initial expression of δI

By differenciation, it is obtained:

$$\delta I(E) = \int_0^T \int_\Omega p_\alpha(x)\left[u_{\alpha\, cal}(x,t,E) - u_{\alpha\, mes}(x,t)\right]\delta u_{\alpha\, cal}(x,t,E)\,dx\,dt$$

With $\delta u_{\alpha\, cal}(x,t,E)$ the variation of the $u_{\alpha\, cal}(x,t,E)$ numerical displacement field, with a $\delta E(x)$ variation in the stiffness field.

Self-adjoint definition

Let us define the self-adjoint as the « displacement » field u^* which satisfies over the $[0,T]$ time frame the « retrograde[4] » problem defined in Ω, by:

- the presence of an « external » « bulk » forces field defined as:

$$f_\alpha(x,t) = p_\alpha(x)\left[u_{\alpha\, cal}(x,t,E) - u_{\alpha\, mes}(x,t)\right]$$

- « initial » displacement conditions and null velocities at the T time:

$$u^*(x,T) = \dot{u}^*(x,T) = 0$$

[4] Retrograde problem = problem obtained by reversing the time course in the equations, i.e. by writting: $t^* = T - t$. For an elastodynamic problem, the equations are similar to those relative to the usual problem. However, the initial conditions ar relative to the displacment and velocity values at the T time.

In practice, $u*$ is computed in the same manner as u_{cal}, for instance with the César-LCPC DYNI module. When considering the $t' = T - t$ time variable, and writing $u*(x,t) = u**(x,t')$, the usual elastodynamic problem in terms of $(u**,t')$ is obtained with:

- external force field: $p_\alpha(x)\left[u_{\alpha cal}(x,t',E) - u_{\alpha mes}(x,t')\right]$

- initial conditions: $u**(x,0) = \dot{u}**(x,0) = 0$

Using the VWP, $u*$ shall satisfy the following variational equation:

$$\int_\Omega E(x)N(\nu(x))\varepsilon*:\hat{\varepsilon}\,dx + \int_\Omega \rho\ddot{u}*\hat{u}\,dx = \int_\Omega p_\alpha(x)\left[u_{\alpha cal}(x,t,E) - u_{\alpha mes}(x,t)\right]\hat{u}_\alpha\,dx$$

Rewritting of δI according to the adjoint state

When considering in the previous expression the $\delta u_{cal}(x,t,E)$ displacement virtual field, it comes:

$$\int_\Omega E(x)N(\nu(x))\varepsilon*:\delta\varepsilon_{cal}(x,t,E)\,dx + \int_\Omega \rho\ddot{u}*\delta u_{cal}(x,t,E)\,dx =$$
$$\int_\Omega p_\alpha(x)\left[u_{\alpha cal}(x,t,E) - u_{\alpha mes}(x,t)\right]\delta u_{\alpha cal}(x,t,E)\,dx$$

When integrating this expression with regard to time, over the $[0,T]$ time frame, the $\delta I(E)$ expression appears on the left, so that:

$$\delta I(E) = \int_0^T\int_\Omega E(x)N(\nu(x))\varepsilon*(x,t):\delta\varepsilon_{cal}(x,t,E)\,dxdt + \int_0^T\int_\Omega \rho\ddot{u}*(x,t)\delta u_{cal}(x,t,E)\,dxdt$$

Characterization of the $\delta u_{cal}(x,t,E)$ displacement field

The previous $\delta I(E)$ expression involves the $\delta u_{cal}(x,t,E)$ variation of the du champ de déplacement $u_{cal}(x,t,E)$ displacement field with a $\delta E(x)$ variation in the modulus.

Let us interest to the characteristic equations relative to this field, which will be required in the following for the $\delta I(E)$ transformation.

Let us differentiate the VWP expression relative to the u_{cal} field:

$$\int_\Omega E(x)N(\nu(x))\varepsilon_{cal}:\hat{\varepsilon}\,dx + \int_\Omega \rho\ddot{u}_{cal}\hat{u}\,dx = 0$$

It comes:

$$\int_\Omega E(x)N(\nu(x))\delta\varepsilon_{cal} : \hat{\varepsilon}\, dx + \int_\Omega \rho\delta\ddot{u}_{cal}\hat{u}\, dx = -\int_\Omega \delta E(x)N(\nu(x))\varepsilon_{cal} : \hat{\varepsilon}\, dx$$

Besides, by the differenciation of the initial velocity and displacment conditions:

$$\delta u_{cal}(x,0) = \delta\dot{u}_{cal}(x,0) = 0$$

Thus, the δu_{cal} calculation amounts to an elastodynamic problem with:

- occurrence of bulk forces, depending on time, of the following intensity:
$\delta E(x)N(\nu(x))\varepsilon_{cal}(x,t)$
- initial conditions null.

Let us carry on with the transformation of the $\delta I(E)$ term.

Integrating by parts with regard to time the last integral of the $\delta I(E)$ expression

Let us integrate two times by part, with regard to time, the $\delta J = \int_0^T \int_\Omega \rho\ddot{u} * \delta u_{cal}\, dx$ integral, in order to make the second temporal derivative pass from u to δu_{cal}.

It comes:

$$\delta J = -\int_0^T \int_\Omega \rho\dot{u} * \delta\dot{u}_{cal}\, dxdt + \left[\int_\Omega \rho\dot{u} * \delta u_{cal}\, dx\right]_0^T$$

Last term is null, due to the « initial » conditions checked by δu_{cal} at $t = 0$ and by $\dot{u}*$ at t = T i.e. $\delta u_{cal}(x,0) = 0$, $\dot{u}*(x,T) = 0$.

Hence, $\delta J = -\int_0^T \int_\Omega \rho\dot{u} * \delta\dot{u}_{cal}\, dxdt = \int_0^T \int_\Omega \rho u * \delta\ddot{u}_{cal}\, dxdt - \left[\int_\Omega \rho u * \delta\dot{u}_{cal}\, dx\right]_0^T$

Once more, the last term is null due to initial conditions $\delta\dot{u}_{cal}(x,0) = 0$ and $u*(x,T) = 0$.
Finally, $\delta J = \int_0^T \int_\Omega \rho u * \delta\ddot{u}_{cal}\, dxdt$, so that:

$$\delta I(E) = \int_0^T \int_\Omega E(x)N(\nu(x))\varepsilon*(x,t) : \delta\varepsilon_{cal}(x,t,E)\, dxdt + \int_0^T \int_\Omega \rho u*(x,t)\delta\ddot{u}_{cal}(x,t,E)\, dxdt$$

i.e. when permuting in the first integral the roles of $\varepsilon*$ and $\delta\varepsilon_{cal}$:

$$\delta I(E) = \int_0^T \int_\Omega E(x)N(\nu(x))\delta\varepsilon_{cal}(x,t,E) : \varepsilon*(x,t)\, dxdt + \int_0^T \int_\Omega \rho\delta\ddot{u}_{cal}(x,t,E)u*(x,t)\, dxdt$$

Let us chosen as virtual field $\hat{u}$, the $u*$ field in the VWP expression applied to the δu_{cal} field.

It comes at each time:

$$\int_\Omega E(x)N(\nu(x))\delta\varepsilon_{cal} : \varepsilon^* dx + \int_\Omega \rho\delta\ddot{u}_{cal} u^* dx = -\int_\Omega \delta E(x)N(\nu(x))\varepsilon_{cal} : \varepsilon^* dx$$

Hence, when integrating with regard to time over the $[0,T]$ time frame:

$$\delta I(E) = -\int_0^T \int_\Omega \delta E(x)N(\nu(x))\varepsilon_{cal}(x,t,E) : \varepsilon^*(x,t)\, dxdt$$

The final expression of $\delta I(E)$ as a linar form of δE is expressed as:

$$\boxed{\delta I(E) = -\int_\Omega \left[\int_0^T N(\nu(x))\varepsilon_{cal}(x,t,E) : \varepsilon^*(x,t)dt\right]\delta E(x)dx}$$

In the case of a multilayered medium, for which $E(x) = \sum_{j=1}^{N} E_j\, I_{C_j}(x)$, it comes:

$$\boxed{\delta I(E) = -\sum_{j=1}^{N} \delta E_j \int_{C_j} \left[\int_0^T N(\nu(x))\varepsilon_{cal}(x,t,E) : \varepsilon^*(x,t)dt\right]dx}$$

Use of the $\delta I(E)$ expressions

The latter allow evaluating the influence of a $\delta E(x)$ variation in the stiffness field on the I variation, and especially its variation sense.

Especially, the following choices:

$$\boxed{\delta E(x) = \Delta\lambda \int_0^T N(\nu(x))\varepsilon_{cal}(x,t,E) : \varepsilon^*(x,t)dt}$$

Or, in the case of a multilayered medium:

$$\boxed{\delta E_j = \Delta\lambda_j \int_{C_j} \left[\int_0^T N(\nu(x))\varepsilon_{cal}(x,t,E) : \varepsilon^*(x,t)dt\right]dx}$$

with $\Delta\lambda$, $\Delta\lambda_j$ positive scalar numbers, small enough, insure *a priori* the decrease in I since:

$$\boxed{\delta I(E) \approx -\Delta\lambda \int_\Omega \left[\int_0^T N(\nu(x))\varepsilon_{cal}(x,t,E) : \varepsilon^*(x,t)dt\right]^2 dx \le 0}$$

or:

$$\boxed{\delta I(E) = -\sum_{j=1}^{N} \Delta\lambda_j \left[\int_{C_j} \int_0^T N(\nu(x)) \varepsilon_{cal}(x,t,E) : \varepsilon^*(x,t) dt dx \right]^2}$$

Such choices allow minimizing $I(E)$.

Remark: the expressions of δE or δE_j can be adapted with regard to the « complexity » of $I(E)$, in order to avoid solutions correponding to local minima.

&&&

Summary of the method

Algorithmic pattern for a multilayered medium

- Initialization : choice of an initial stiffness set $E_j^{(0)}$

- Iterative loop corresponding to the (i) index, from $i = 0$; the $E_j^{(i)}$ values are assumed to be known at the beginning of the loop.

  - Calculation of the elastodynamic solution $u_{cal}{}^{(i)}(x,t,E_j^{(i)})$ over $[0,T]$
    - Taking into account the initial conditions $u_{cal}{}^{(i)}$

  - Calculation of the second member, for the $u*^{(i)}$ adjoint state calculation:

$$p_\alpha(x)\left[u^{(i)}_{\alpha_{cal}}(x,t',E) - u_{\alpha\,mes}(x,t')\right]$$

  - Calculation of the elastodynamic solution $u**^{(i)}(x,t',E_j^{(i)})$ for t' varying over the $[0,T]$ time frame
    - Taking into account the previous load and the initial conditions about $u**^{(i)}$

  - Calculation of the adjoint state: $u*^{(i)}(x,t,E_j^{(i)}) = u**^{(i)}(x,T-t,E_j^{(i)})$
  - Calculation of the quatities: $g_j^{(i)} = \int_{C_j}\left[\int_0^T N(\nu(x))\varepsilon_{cal}^{(i)} : \varepsilon*_j^{(i)}\, dt\right]dx$
  - Choice of the $\Delta\lambda_j^{(i)}$ coefficients and calculations of the corrections: $\delta E_j^{(i)} = \Delta\lambda_j^{(i)} g_j^{(i)}$
    (without sum on the *j* index)

  - Updating of the E_j values: $E_j^{(i+1)} = E_j^{(i)} + \delta E_j^{(i)}$
  - Test of the stop criteria (ex: intensity of the $\delta E_j^{(i)}$ corrections, I value,…)
  - If the test is negative, $(i) = (i)+1$ and beginning of a new loop

  - If the test is positive, displaying of the $E_j^{(i+1)}$ moduli values

  - Optional complementary calculations

- End of the algorithm

Detail of the quantities calcualtion:

$$g_j^{(i)} = \int_{C_j} \left[\int_0^T N(\nu(x))\varepsilon_{cal}^{(i)} : \varepsilon^{*(i)}_j \, dt \right] dx$$

1) Explicit expression of the $A = N(\nu)\varepsilon_{cal} : \varepsilon^*$ quantity at the P point, when knowing the σ_{cal} et σ^* stresses, as well as the E Young's modulus and ν Poisson's ratio at that point.

On the one hand: $N(\nu)\varepsilon_{cal} = \frac{1}{E}\sigma_{cal}$ (in a tensorial sense)

On the other hand: $\varepsilon^* = \frac{1+\nu}{E}\sigma^* - \frac{\nu}{E} tr(\sigma^*) I$

Hence: $A = \frac{1}{E^2}\left[(1+\nu)\sigma_{cal} : \sigma^* - \nu tr(\sigma^*) tr(\sigma_{cal})\right]$

i.e. in an axisymmetric case:

$$A = \frac{1}{E^2}\begin{bmatrix} (1+\nu)(\sigma_{cal}^{rr}\sigma^{rr\,*} + \sigma_{cal}^{\theta\theta}\sigma^{\theta\theta\,*} + \sigma_{cal}^{zz}\sigma^{zz\,*} + 2\sigma_{cal}^{rz}\sigma^{rz\,*}) \\ -\nu(\sigma_{cal}^{rr} + \sigma_{cal}^{\theta\theta} + \sigma_{cal}^{zz})(\sigma^{rr\,*} + \sigma^{\theta\theta\,*} + \sigma^{zz\,*}) \end{bmatrix}$$

2) Calculation of the quantities $B = \int_0^T N(\nu(x))\varepsilon_{cal}^{(i)} : \varepsilon^{*(i)}_j \, dt = \int_0^T A(t)dt$ from the DYNI results (and especially the stresses vectors) corresponding to the calculations of u_{cal} and u^* .

When assuming that the $[0,T]$ time frame is discretized in N time steps Δt, the calculation in a selected point is performed using the trapezia method:

$$B = \left[\frac{A(0)}{2} + A(\Delta t) + \ldots + A((N-1)\Delta t) + \frac{A(N\Delta t)}{2} \right] \Delta t$$

Hence the algorithm to obtain a values file, whose structure is similar to the one relative to a CESAR-PEGGY[5] stresses table, with one component:

[5] The DYNI result files present amongst others a comportent $VCOEL$ table providing for each time step, for each mesh element the stress tensor values at each node of the element.
.It is here chosen to create in the same manner a B_e^i vector containing for each element, the B values at each node.

Algorithm for the B_e^i table calculation

- Initialization to 0 of the B_e^i table values
- Loop relative to the N time steps: $npas$

  - If $npas = 0$ or $npas = N$, $coef = 1/2$; otherwise $coef = 1$
  - Reading of the stress vectors $VCOEL_{cal}$, $VCOEL*$ relative to the $npas$ time step of the two DYNI files

- Loop relative to the mesh elements: e
- Loop relative to the element nodes: i

  - calculation of the scalar number : $A_e^i(npas)$ (see supra)
  - calculation of: $B_e^i = B_e^i + coef \times A_e^i(npas)$

- End of the loop relative to i
  - $B_e^i = B_e^i \times \Delta t$

- End of the loop relative to e
- End of the loop relative to $npas$

3) Calculation of the scalar number $g = \int_c \left[\int_0^T N(\nu(x))\varepsilon_{cal} : \varepsilon * dt \right] dx = \int_c B(x)dx$ for a selected layer.

An integration is performed on each e element of the considered layer, and all values are summed:

$$g = \sum_e g_e$$

with: $g_e = \int_e B(x)dx = 2\pi \int_e B(r,z)rdrdz$

From the table B_e^i values, the g_e calculation usually relies on a numerical integral over the isoparametric reference element associated with the e element (typically here a reference quadrilateral with 8 nodes).

Thus, when writting[6]:

[6] Rigorously, namings could be improved: the nodes numbers of the reference element and those of the e reference are not the same

$$r = \sum_i N_e^i(\xi,\eta) r_e^i$$
$$z = \sum_i N_e^i(\xi,\eta) z_e^i$$
$$B_e(r,z) = \sum_i N_e^i(\xi,\eta) B_e^i$$

with: $N_e^i(\xi,\eta)$ = interpolation function at the i node of the e_{ref} reference element.

It is obtained:

$$g_e = 2\pi \int_{e_{ref}} \sum_i N_e^i(\xi,\eta) B_e^i \sum_j N_e^j(\xi,\eta) r_e^j J d\xi d\eta$$

with: $J = \dfrac{D(r,z)}{D(\xi,\eta)}$ = Jacobian of the variable changing $(r,z) \rightarrow (\xi,\eta)$

Hence:

$$g_e \approx 2\pi \sum_g w_g \sum_i N_e^i(\xi_g,\eta_g) B_e^i \sum_j N_e^j(\xi_g,\eta_g) r_e^j J(\xi_g,\eta_g)$$

with:

g = index of the Gauss point of the numerical integrating algorithm[7]
(ξ_g,η_g) = coordinates of the Gauss point in the reference element
w_g = integration weight associated to the g Gauss point.

Hence the following algorithm:

[7] Not to be mixed up with the g quantities to be calculated

Algorithm relative to the quantities calculation g

- Loop relative to the layers (or groups of elements): c
  - Initialization : $g = 0$

- Loop relative to the elements of the c layer : e
  - Initialization $g_e = 0$
- Loop relative to the Gauss points of the reference element: g
    - $B = 0$
    - $r = 0$
  - Loop relative to the nodes of the element: i
    - $B = B + N_e^i(\xi_g, \eta_g) B_e^i$
    - $r = r + N_e^i(\xi_g, \eta_g) r_e^i$
    - Calculation of the Jacobian
  - End of the loop relative to i
  - $g_e = g_e + 2\pi w_g BrJ(\xi_g, \eta_g)$
  - $g = g + g_e$

- End of the e loop
- End of the g loop
- End of the c loop